University of Alberta

Re-Os Geochronology of Precambrian Organic-rich Sedimentary Rocks: Systematics and Applications

by

Brian Stanley Kendall ©

A thesis submitted to the Faculty of Graduate Studies and Research
in partial fulfillment of the requirements for the degree of

Doctor of Philosophy

Dept. of Earth and Atmospheric Sciences

Edmonton, Alberta
Spring 2008

Library and
Archives Canada

Published Heritage
Branch

395 Wellington Street
Ottawa ON K1A 0N4
Canada

Bibliothèque et
Archives Canada

Direction du
Patrimoine de l'édition

395, rue Wellington
Ottawa ON K1A 0N4
Canada

Your file Votre référence
ISBN: 978-0-494-45542-5
Our file Notre référence
ISBN: 978-0-494-45542-5

NOTICE:
The author has granted a non-exclusive license allowing Library and Archives Canada to reproduce, publish, archive, preserve, conserve, communicate to the public by telecommunication or on the Internet, loan, distribute and sell theses worldwide, for commercial or non-commercial purposes, in microform, paper, electronic and/or any other formats.

The author retains copyright ownership and moral rights in this thesis. Neither the thesis nor substantial extracts from it may be printed or otherwise reproduced without the author's permission.

AVIS:
L'auteur a accordé une licence non exclusive permettant à la Bibliothèque et Archives Canada de reproduire, publier, archiver, sauvegarder, conserver, transmettre au public par télécommunication ou par l'Internet, prêter, distribuer et vendre des thèses partout dans le monde, à des fins commerciales ou autres, sur support microforme, papier, électronique et/ou autres formats.

L'auteur conserve la propriété du droit d'auteur et des droits moraux qui protège cette thèse. Ni la thèse ni des extraits substantiels de celle-ci ne doivent être imprimés ou autrement reproduits sans son autorisation.

In compliance with the Canadian Privacy Act some supporting forms may have been removed from this thesis.

While these forms may be included in the document page count, their removal does not represent any loss of content from the thesis.

Conformément à la loi canadienne sur la protection de la vie privée, quelques formulaires secondaires ont été enlevés de cette thèse.

Bien que ces formulaires aient inclus dans la pagination, il n'y aura aucun contenu manquant.

Canada

ABSTRACT

The ^{187}Re-^{187}Os radioisotope system in organic-rich shales represents a precise and accurate deposition-age geochronometer that has widespread utility for Precambrian geological timescale calibration and sedimentary basin analysis. New Re-Os ages of 643.0 ± 2.4 Ma and 657.2 ± 5.4 Ma from the Tindelpina Shale Member and Aralka Formation constrain the end of "Sturtian" glaciation in southern and central Australia, respectively. Black shales overlying Sturtian-equivalent diamictites in northwestern Tasmania yield an identical Re-Os age (640.7 ± 4.7 Ma) as the Tindelpina Shale Member. The "Sturtian" ice age is thus shown to be markedly diachronous and/or there were multiple glaciations at ca. 750-643 Ma. A Re-Os date of 1100 ± 77 Ma was obtained from Lapa Formation post-glacial shales (Brazil) overlying glacial diamictites previously ascribed to "Sturtian" glaciation.

Joint application of the Re-Os deposition-age geochronometer and the Mo isotope paleoredox proxy has tremendous potential for tracing atmosphere and ocean oxidation over geological time. New Re-Os ages of 1361 ± 21 Ma and 1417 ± 29 Ma constrain the depositional age of the Velkerri Formation, Australia. Black shales from the upper Velkerri Formation were deposited from euxinic bottom waters and have an average Mo isotope composition ($\delta^{97/95}$Mo) of 0.72 ± 0.10 ‰ that is ~ 0.8‰ lighter than present-day seawater. This reflects decreased uptake of Mo onto Mn oxides associated with the expansion of deep-sea euxinia and contraction of oxic marine deposition. A Re-Os age of 2501.1 ± 8.2 Ma for the Mt. McRae Shale (Western Australia) constrains the timing of mild shallow-ocean oxygenation prior to the 2.45-2.32 Ga Great Oxidation Event. Precambrian seawater Os isotope compositions and Re and Os abundances and

^{187}Re/^{188}Os isotope ratios are consistent with hypothesized anoxic Archean atmosphere/oceans, stratified Proterozoic oceans under a weakly to mildly oxygenated atmosphere, and fully oxygenated Late Neoproterozoic and Phanerozoic oceans.

Reconnaissance Re-Os, Mo, and Fe isotope data for the 635-551 Ma Doushantuo Formation (South China) suggest further studies will yield valuable insights regarding inter-relationships between ocean oxygenation, glaciation, and metazoan evolution.

The Re-Os and Mo isotope systematics of black shales are found to be disturbed during post-depositional hydrothermal fluid flow.

ACKNOWLEDGEMENTS

My Ph.D. research was supported by the Natural Sciences and Engineering Research Council of Canada (Canada Graduate Scholarship – Doctoral), the Alberta Ingenuity Fund (Ingenuity Ph.D. Studentship), Canadian Association of Petroleum Producers Graduate Scholarship, Dr. Roy Dean Hibbs Memorial Graduate Scholarship, GL Cumming Memorial Graduate Scholarship, and teaching assistantships from the Department of Earth and Atmospheric Sciences. This research was supported by a Natural Sciences and Engineering Research Council (NSERC) Discovery Grant to my supervisor, Dr. Robert A. Creaser. Student research grants were provided by the Geological Society of America and the Alberta Ingenuity Fund. Travel expenses to Geological Society of America and V.M. Goldschmidt conferences were funded in part by travel awards from the University of Alberta's Institute for Geophysical Research (funded by Burlington Resources Canada Ltd. and Devon Canada Corporation), the NASA Astrobiology Institute, a J Gordin Kaplan Graduate Student Award, and the Alberta Ingenuity Fund.

I greatly appreciate the opportunity given me by Rob to participate in the development and application of the Re-Os deposition-age geochronometer for Precambrian black shales. He is an excellent teacher and an ideal supervisor because he allowed me to work independently yet always kept close tabs on the research progress. I would like to thank Rob for the two memorable trips to Australia. On the first excursion, Rob and I collected black shale drill core samples in Adelaide, Alice Springs, and Canberra, Australia's capital city. In Canberra, I had the honor of meeting Rob's wonderful parents. In the bush behind his parent's house, I managed to sneak up near a wild adult male grey kangaroo, turn slowly around, and pose for a picture (taken by Rob). In Adelaide, Rob treated me to an unforgettable authentic Australian feast of crocodile, kangaroo, emu, and wallaby. The second trip to Australia was for the V.M. Goldschmidt conference where Rob's Re-Os research group attended a game of Australian Rules football. I am also grateful to Rob for funding a four month visit to the Valley of the Sun and Arizona State University to work in the laboratory of Dr. Ariel Anbar. The research visit to Arizona State University ultimately led to my securing a postdoctoral fellowship position in Ariel's lab.

In turn, I thank Ariel for the opportunity to work in his mega-sized laboratory as a visiting graduate student and his open-mindedness towards my experimentations with Mo and Fe isotopes on my Proterozoic shale samples. At Arizona State University, I got to experience a bit of mad scientist fantasy (i.e., boiling, multi-colored liquids!) by carry out sulfur extractions for degree-of-pyritization (DOP) determinations. My complaints about the heat earned me a dual thermometer-clock (calibrated for Arizona weather of course) from Ariel and his research group at the end of my visit.

During most of my time as a graduate student at the University of Alberta, Dr. David Selby was the resident post-doctoral fellow and research scientist in Rob's lab. Dave played a major role in my training in analytical protocols regarding Re-Os chemistry, and we had many invaluable discussions regarding Re-Os black shale geochronology. When I started out as a M.Sc. student, Dave was exceedingly patient with answering my inexhaustible store of questions regarding clean lab work. Dave was very easy-going and I enjoyed working with him in the clean lab.

I thank Dr. Gwyneth Gordon for her assistance with my work at Arizona State University. She was my main source of information regarding heavy stable isotope and trace metal clean lab work, and assisted me with DOP analytical protocols and Q-ICP-MS and MC-ICP-MS analyses. Drs. Gail Arnold and Laura Wasylenki helpfully answered any questions regarding their clean lab.

I thank my Ph.D. thesis defense committee members for their time, advice, and thesis comments: Dr. Robert Creaser, Dr. Larry Heaman, Dr. Thomas Chacko, Dr. Richard Walker, and Dr. Al Meldrum. I thank Richard for making the journey from Maryland to Edmonton in the heart of the Canadian winter to sit-in on my thesis defense. I would also like to acknowledge the following collaborators during my Ph.D. program: Dr. Ariel Anbar, Dr. Gail Arnold, Dr. Karem Azmy, Dr. Clive Calver, Dr. David Evans, Dr. Gwyneth Gordon, Dr. Ganqing Jiang, Dr. Martin Kennedy, Dr. Joseph Kirschvink, Timothy Raub, and Dr. Kevin Root. Dr. Martin Kennedy is thanked for his hospitality when Rob and I visited the University of California, Riverside, and for the field excursion into Death Valley. Yun Duan is thanked for discussions regarding Fe isotopes in black shales and for showing me her Fe isotope data for Devonian black shales.

Ryan Morelli was a fellow Ph.D. student under Rob, and was an excellent colleague and lab-mate. He was always willing to help out when necessary in the lab and his unselfish attitude made him a joy to work with. I wish him the best with his career.

I thank Stacey Hagen and Gayle Hatchard for their assistance with mass spectrometer analyses, Kelly Nixon and Jamie Hallowes for their assistance in the clean lab, and Dr. Antonio Simonetti and Guangcheng Chen for their assistance with trace metal analyses at the University of Alberta. Diane Caird is thanked for running X-ray diffraction analyses, and Mark Labbe and Don Resultay for assistance with sample processing.

Sample collection of Australian Proterozoic shales was assisted by the staff of the Northern Territory Geological Survey of Australia (Alice Springs, Northern Territory), Department of Primary Industries and Resources, South Australia (Glenside core library at Adelaide, South Australia), Geoscience Australia (Canberra, Australian Capital Territory), and Department of Mines and Mineral Resources, Tasmania (Hobart, Tasmania) core libraries.

Last, but not least, I would like to thank my wife Kimberly Kendall and my family for their love and support.

TABLE OF CONTENTS

Chapter 1: Introduction 1
1.1 Introduction 2
1.2 The ^{187}Re-^{187}Os system in ORS: A deposition-age geochronometer and seawater Os isotope tracer 3
1.3 Development of the Re-Os geochronometer for ORS 7
1.4 Accuracy of the Re-Os geochronometer for ORS and the ^{187}Re decay constant 10
1.5 Re-Os isotope systematics of Precambrian ORS 11
References 18

Chapter 2: Re-Os, Mo, and Fe isotope systematics of black shales from the 635 – 551 Ma Doushantuo Formation, South China 27
2.1 Introduction 28
2.2 Doushantuo and Dengying Formations, South China 33
2.3 Samples and analytical methods 36
2.4 Results 38
2.4.1 Re-Os isotopes 38
2.4.2 Trace metals 40
2.4.3 Mo and Fe isotopes 41
2.5 Discussion 41
2.5.1 Re-Os isotope systematics of organic-rich carbonates 41
2.5.2 Significance of appropriate sampling protocols for Re-Os geochronology 43
2.5.3 Importance of precise Re-Os depositional ages from the Doushantuo Formation 46
2.5.4 Depositional environment of the Doushantuo Formation in the Yangtze Gorges region: Constraints from Mo isotopes 47
2.5.5 Fe isotope systematics of the Doushantuo Formation 52
2.6 Conclusions 54
References 72

Chapter 3: Re-Os geochronology of Neoproterozoic organic-rich mudrocks from mainland Australia, King Island, and Tasmania: Constraints on the timing of "Sturtian" glaciation and implications for paleogeographic reconstructions 88
3.1 Introduction 89
3.2 Neoproterozoic diamictites in southern and central Australia, northwestern Tasmania, and southeastern King Island 95
3.2.1 Adelaide Rift Complex, South Australia 95
3.2.2 Amadeus Basin, central Australia 97
3.2.3 Northwestern Tasmania 98
3.2.4 Southeastern King Island 100
3.3 Samples and analytical methods 101
3.3.1 Amadeus Basin 102
3.3.2 Adelaide Rift Complex 103

        3.3.3 Northwestern Tasmania and southeastern King Island 105
        3.3.4 Analytical methods 106
    3.4 Results 107
        3.4.1 Trace metals 107
        3.4.2 Re-Os isotope data 108
            3.4.2.1 Amadeus Basin 108
            3.4.2.2 Adelaide Rift Complex 108
            3.4.2.3 Northwestern Tasmania and southeastern King Island 109
    3.5 Discussion 110
        3.5.1 Comparison of digestion protocols for Re-Os geochronology 110
        3.5.2 Discrepancy in the age of the Aralka Formation 114
        3.5.3 Timing of Sturtian and Areyonga post-glacial sedimentation, and correlation with northwestern Tasmania... 116
        3.5.4 Implications for global correlation of Neoproterozoic ice ages 117
        3.5.5 Implications for the Neoproterozoic paleogeographic reconstructions, and the relationship between Rodinia supercontinent breakup and Sturtian glaciation 122
        3.5.6 Evaluation of shale-hosted benthic microbial mats as deposition-age geochronometers 126
        3.5.7 Variations in the initial ^{187}Re/^{188}Os ratio in organic-rich shales 130
    3.6 Conclusions 133
    References 163

Chapter 4: Re-Os isotope systematics of Late Mesoproterozoic – Earliest Neoproterozoic organic-rich mudrocks of the Lapa Formation (Vazante Group, Brazil) and Horsethief Creek Group (Windermere Supergroup, Western Canada) 185
    4.1 Introduction 186
    4.2 Geological Setting 190
        4.2.1 Vazante Group, Brazil 190
        4.2.2 Toby Formation and Horsethief Creek Group, Western Canada 193
    4.3 Samples and analytical methods 195
        4.3.1 Lapa Formation 195
        4.3.2 Horsethief Creek Group 195
        4.3.3 Analytical Methods 196
    4.4 Results 197
        4.4.1 Lapa Formation 197
        4.4.2 Horsethief Creek Group 197
    4.5 Discussion 198
        4.5.1 A 1100 – 1000 Ma depositional age for the base of the Lapa Formation 198

4.5.2 Correlation of the Vazante and Paranoá Groups? 203
4.5.3 Re-Os isotope systematics of the Horsethief Creek Group 203
4.6 Conclusions 205
References 219

Chapter 5: Re-Os, Mo, and Fe isotope systematics of black shales from the Middle Proterozoic Wollogorang, Barney Creek, and Velkerri Formations, McArthur Basin, northern Australia 230
5.1 Introduction 231
5.2 The Wollogorang, Barney Creek, and Velkerri Formations, McArthur Basin, northern Australia 233
5.2.1 Wollogorang Formation 234
5.2.2 Barney Creek Formation 236
5.2.3 Velkerri Formation 238
5.3 Samples and analytical methods 240
5.4 Results 242
5.4.1 Elemental abundances 242
5.4.2 Re-Os, Mo, and Fe isotopes 244
5.5 Discussion 246
5.5.1 Implications of the Velkerri Formation Re-Os ages and controls on the initial ^{187}Re/^{188}Os ratio during organic-rich sediment deposition 246
5.5.1.1 Re-Os depositional ages and the Os isotope composition of Middle Proterozoic seawater 246
5.5.1.2 Variations in the ^{187}Re/^{188}Os isotope ratio in black shales 248
5.5.2 The Mo isotope composition of global seawater at 1.4 Ga 251
5.5.3 Re-Os and Mo isotope systematics in black shales resulting from post-depositional hydrothermal fluid flow 253
5.5.3.1 Re-Os isotopes 253
5.5.3.2 Mo isotopes 256
5.5.4 Redox cycling of Fe in the Middle Proterozoic (1.7 – 1.4 Ga) oceans 258
5.6 Conclusions 260
References 284

Chapter 6: Re-Os isotope systematics of Late Archean and Early Paleoproterozoic black shales, the ^{187}Os/^{188}Os isotope composition of Precambrian seawater, and the Re-Os systematics of organic-rich sedimentary rocks over geological time 298
6.1 Introduction 299
6.2 Sample details 303
6.2.1 Mt. McRae Shale 303
6.2.2 Monteville Formation and Klipput Shale Member (lower Nelani Formation) 305
6.2.3 Analytical Methods 309

6.3 Results 309
    6.3.1 Mt. McRae Shale 309
    6.3.2 Monteville Formation and Klipput Shale Member (lower Nelani Formation) 310
6.4 Discussion 310
    6.4.1 Utility of the Re-Os deposition-age geochronometer for Late Archean to Early Paleoproterozoic black shales 310
    6.4.2 The redox state of Late Archean to Paleoproterozoic seawater: Implications of the I_{Os} from Re-Os black shale isochron regressions 315
    6.4.3 Progress towards a Precambrian seawater $^{187}Os/^{188}Os$ curve 319
    6.4.4 Re-Os systematics in organic-rich shales over geological time 321
6.5 Conclusions 325
References 349

Chapter 7: Conclusions 371
7.1 Accuracy and precision of the Re-Os deposition-age geochronometer for organic-rich shales 372
7.2 Limitations of the Re-Os ORS geochronometer 373
7.3 Controls on initial $^{187}Re/^{188}Os$ isotope ratios in organic-rich shales during sediment deposition 374
7.4 Applications to Precambrian organic-rich shales 375
    7.4.1 Timing of Neoproterozoic glaciation and Rodinia breakup 375
    7.4.2 Joint applications of Re-Os geochronology, and Mo and Fe stable isotope – and trace metal – based redox proxies 376
7.5 Precambrian seawater Os isotope compositions and Re-Os systematics in ORS over geological time 377
References 379

Appendices 383
Appendix A: Analytical protocols for Re-Os isotope analysis 383
    A.1 Sample collection and preparation 383
    A.2 Purification of chemical reagents of Re and Os 384
    A.3 Re-Os chemistry 386
    A.4 Negative thermal ionization mass spectrometry (NTIMS) 388
Appendix B: Analytical protocols for Mo and Fe isotope analysis 390
    B.1 Mo and Fe isotope chemistry 390
    B.2 Multiple collector inductively coupled plasma mass spectrometry (MC-ICP-MS) 391
Appendix C: Analytical protocols for element abundance and DOP Determinations 393
    C.1 Element abundance determinations at Arizona State University 393
    C.2 Element abundance determinations at the University of

Alberta 393
C.3 DOP determinations at Arizona State University 394
Appendix D: Thesis collection 394
References 406

LIST OF TABLES

Table 2.1: Re-Os isotope data for the Doushantuo Formation, South China........... 57

Table 2.2: Mo and Fe isotope, degree-of-pyritization (DOP), and trace metal data for the Doushantuo Formation, South China.. 59

Table 3.1: Major and trace element data for the Aralka, Pertatataka, and Brachina Formations and Tindelpina Shale Member.............................. 136

Table 3.2: Enrichment factors, Fe_T/Al ratios, and DOP data for the Aralka, Pertatataka, and Brachina Formations and Tindelpina Shale Member..... 137

Table 3.3: Re-Os isotope data for the Pertatataka and Aralka Formations, Amadeus Basin, central Australia.. 138

Table 3.4: Re-Os isotope data for the Brachina Formation and Tindelpina Shale Member (Tapley Hill Formation), Adelaide Rift Complex, southern Australia.. 139

Table 3.5: Re-Os isotope data for the Julius River Member, upper Black River Dolomite, northwestern Tasmania.. 140

Table 3.6: Re-Os isotope data for the Yarra Creek Shale, City of Melbourne Bay coastal outcrop, southeastern King Island.. 141

Table 3.7: Comparison of Re-Os isotope data derived from inverse *aqua regia* and Cr^{VI}-H_2SO_4 digestions.. 142

Table 3.8: Coefficients of determination for Re and ^{192}Os abundance, and $^{187}Re/^{188}Os$ isotope ratio plotted against elemental abundances.............. 143

Table 4.1: Re-Os data for the basal Lapa Formation organic-rich shales, upper Vazante Group, east-central Brazil.. 208

Table 4.2: Re-Os data for the basal Horsethief Creek Group, lower Windermere Supergroup, Western Canada.. 209

Table 5.1: Major and trace element data for selected samples of the Wollogorang, Barney Creek, and Velkerri Formation black shales......... 263

Table 5.2: Enrichment factors, Fe_T/Al ratios, and DOP data for the Wollogorang, Barney Creek, and Velkerri Formation black shales......... 264

Table 5.3: Re-Os, Mo, and Fe isotope data for the Velkerri Formation (drill hole Urapunga-4)... 265

Table 5.4: Re-Os, Mo, and Fe isotope data for the Barney Creek Formation (drill hole McArthur 2)........ 266

Table 5.5: Re-Os, Mo, and Fe isotope data for the Wollogorang Formation (drill hole Mount Young 2)........ 267

Table 5.6: Coefficients of determination for Re, ^{192}Os, and ^{187}Re/^{188}Os plotted against elemental abundances........ 268

Table 6.1: Re-Os data for the Mt McRae Shale (drill hole ABDP 9), Hamersley Group, Western Australia........ 327

Table 6.2: Re-Os data for the Monteville Formation (drill hole GKP01) and Klipput Shale Member (drill hole GEC01), Transvaal Supergroup, South Africa........ 328

Table 6.3: Re, Os abundances and ^{187}Re/^{188}Os ratios of organic-rich sedimentary rocks over geological time........ 329

Table A.1: Blank Re abundances for CrO_3 powders........ 395

Table A.2: Comparison of Re-Os data obtained using $CHCl_3$ and CCl_4 as organic solvents during Os solvent extraction........ 396

Table A.3: Average standard isotope ratios for AB-1 (Re) and AB-2 (Os)........ 397

Table D.1: Thesis collection........ 398

LIST OF FIGURES

Figure 1.1: Summary of the major near-surface reservoirs of Os and their isotopic composition.......... 13

Figure 1.2: Re-Os isochron diagrams for the Early Mississippian Bakken Shale (North Dakota) and Late Jurassic Kimmeridge Clay (Dorset, UK).......... 14

Figure 1.3: Re-Os isochron diagrams for the Devonian-Mississippian Exshaw Formation (Western Canada Sedimentary Basin).......... 15

Figure 1.4: Re-Os isochron diagram for the Neoproterozoic Old Fort Point Formation, Windermere Supergroup, Western Canada.......... 16

Figure 1.5: Re-Os isochron diagram for Exshaw Formation black shales straddling the Devonian-Mississippian boundary.......... 17

Figure 2.1: Paleogeographic map of facies distributions during Early Doushantuo time.......... 60

Figure 2.2: Generalized stratigraphic column for the Late Neoproterozoic stratigraphy of South China.......... 61

Figure 2.3: Distribution of Doushantuo and Dengying Formation biota and the composite carbon isotope curve for the Late Neoproterozoic of South China.......... 62

Figure 2.4: Re-Os isochron diagrams for the Shibantan Member, Dengying Formation, and Upper Member 2, Doushantuo Formation.......... 63

Figure 2.5: Re-Os isochron diagrams for Member 4, Doushantuo Formation.......... 64

Figure 2.6: Mo and Fe isotope and abundance data for the Doushantuo Formation.......... 65

Figure 2.7: Re-Os isochron diagram showing the four most radiogenic samples for Member 4, Doushantuo Formation.......... 66

Figure 2.8: Molybdenum isotope composition of present-day seawater sources and sinks.......... 67

Figure 3.1: Location of sample sites and Late Neoproterozoic stratigraphic columns from the Adelaide Rift Complex and Amadeus Basin, and stratigraphic columns and $\delta^{13}C$ data for drill holes intersecting Sturtian and Areyonga glacial deposits.......... 144

Figure 3.2: Neoproterozoic rocks of Tasmania and King Island and stratigraphic columns for the Grassy and Togari Groups........................ 145

Figure 3.3: Possible correlation scheme for diamictite intervals from central and southern Australia, southeastern King Island, and northwestern Tasmania.. 146

Figure 3.4: Re-Os isochron diagram for the Aralka Formation, Amadeus Basin, central Australia.. 147

Figure 3.5: Re-Os isochron diagrams for Neoproterozoic ORS from the Adelaide Rift Complex, southern Australia.. 148

Figure 3.6: Re-Os isochron diagrams for ORS from northwestern Tasmania and southeastern King Island.. 149

Figure 3.7: Re-Os isochron diagrams for the Aralka Formation showing the inverse *aqua regia* and Cr^{VI}-H_2SO_4 regressions from Schaefer and Burgess (2003) and this study, respectively.. 150

Figure 3.8: Summary of radiometric age constraints on the timing of Neoproterozoic glaciation.. 151

Figure 3.9: Sequence stratigraphy for the Adelaide Rift Complex, South Australia.. 152

Figure 3.10: Re-Os isochron diagrams illustrating possible Re-Os systematics of shale-hosted benthic microbial mats... 153

Figure 3.11: Variation in Re and ^{192}Os abundances of Neoproterozoic ORS from central and southern Australia, northwestern Tasmania, and southeastern King Island.. 154

Figure 3.12: Geochemical diagrams illustrating variations in $^{187}Re/^{188}Os$ isotope ratio plotted against ^{192}Os, Re, Mo, and V abundance............ 155

Figure 4.1: Geology of the São Francisco Craton and the location of drill hole MASW01.. 210

Figure 4.2: Generalized stratigraphy of the Vazante Group and stratigraphic column and carbon isotope chemostratigraphy of the Lapa Formation in drill hole MASW01.. 211

Figure 4.3: Distribution of the Windermere Supergroup in the southeastern Canadian Cordillera.. 212

Figure 4.4: Stratigraphic columns for the Windermere Supergroup in the Canadian Cordillera.......... 213

Figure 4.5: Re-Os isochron diagrams for the basal Lapa Formation and basal Horsethief Creek Group.......... 214

Figure 4.6: Re-Os isochron diagram for the Lapa Formation showing the two regressions from Figure 4.5A, B, as well as 700 Ma reference isochrons with I_{Os} of 0.12, 1.06, and 1.54.......... 215

Figure 5.1: Regional geological setting of the McArthur Basin, northern Australia.......... 269

Figure 5.2: Lithostratigraphic column for the Wollogorang Formation in drill hole Mount Young 2.......... 270

Figure 5.3: Lithostratigraphic column and inferred relative water depth curve for the Barney Creek Formation and Reward Dolomite in drill hole McArthur 2.......... 271

Figure 5.4: Generalized stratigraphic column and age constraints for the Roper Group, lithostratigraphic column for the Velkerri Formation in drill hole Urapunga-4, and Mo isotope and DOP data.......... 272

Figure 5.5: Re-Os isochron diagrams for the upper and lower Velkerri Formation and Wollogorang Formation.......... 273

Figure 5.6: Molybdenum isotope compositions of the Velkerri and Wollogorang Formation black shales plotted against Mo abundance and DOP.......... 274

Figure 5.7: Iron isotope compositions plotted against DOP for the upper and lower Velkerri, Wollogorang, and Barney Creek Formations.......... 275

Figure 5.8: Variation in Re and Os abundance in the Velkerri and Wollogorang Formation black shales.......... 276

Figure 5.9: Geochemical diagrams illustrating variations in ^{187}Re/^{188}Os isotope ratio plotted against ^{192}Os, Re, Mo, and V abundance for the Velkerri and Wollogorang Formation black shales.......... 277

Figure 5.10: Re-Os isochron diagram for the Wollogorang Formation showing an increasing degree of deviation, with stratigraphic depth, from a 1730 Ma reference line with chondritic initial ^{187}Os/^{188}Os, and a comparison of the Re-Os isotope systematics of dolomite veinlets plus surrounding shale relative to adjacent shale material ≥ 4 mm from dolomite veinlets 278

Figure 6.1: Simplified geological map of the Pilbara Craton showing the extent of the Hamersley Group 334

Figure 6.2: Generalized stratigraphic column for the Hamersley Group and stratigraphy of the Mt. McRae Shale in drill hole ABDP-9 335

Figure 6.3: Geology of the Griqualand West sub-basin and its position within the Kaapvaal Craton 336

Figure 6.4: Correlations between Transvaal Supergroup strata in the Griqualand West and Transvaal Sub-basins 337

Figure 6.5: Stratigraphic columns for drill holes GKP01 and GEC01, Ghaap Group, Transvaal Supergroup 338

Figure 6.6: Re-Os isochron diagrams for the Mt. McRae Shale 339

Figure 6.7: Re-Os isochron diagrams for the Monteville Formation and Klipput Shale Member 340

Figure 6.8: Geochemical diagrams illustrating well-correlated trends between calculated individual sample I_{Os} and $^{187}Re/^{188}Os$ isotope ratio and ^{192}Os abundance for the Klipput Shale Member 341

Figure 6.9: Seawater Os isotope composition over geological time 342

Figure 6.10: Trends between Re and ^{192}Os abundance over geological time 344

Figure 6.11: Trends between Re or ^{192}Os abundance with $^{187}Re/^{188}Os$ isotope ratio over geological time 345

LIST OF PLATES

Plate 2.1: Sub-sample of whole rock H_1O_1 (finely laminated, shaly limestone), base of Member 2, Neoproterozoic Doushantuo Formation, South China.................... 68

Plate 2.2: Sub-samples of whole rocks H_1O_9 (left) and H_1O_{14} (right) (finely laminated black shale), lower to middle Member 2, Doushantuo Formation.................... 69

Plate 2.3: Sub-samples of whole rocks H_1O_{18} (left), H_1O_{20} (middle), and H_1O_{21} (right) (finely laminated black shale), Member 4, Doushantuo Formation.................... 70

Plate 2.4: Sub-samples of whole rocks H_1O_{26} (left) and H_1O_{32} (right) (dark gray bituminous limestone), Shibantan Member, Ediacaran Dengying Formation, South China.................... 71

Plate 3.1: Pyritic, dolomitic organic-rich siltstone of the Neoproterozoic Aralka Formation, drill hole Wallara-1, Amadeus Basin, central Australia........ 156

Plate 3.2: Aralka Formation and overlying Pioneer Sandstone and cap carbonate in drill hole Wallara-1.................... 157

Plate 3.3: Shale-hosted benthic microbial mat facies of the Ediacaran Pertatataka Formation, drill hole Wallara-1.................... 158

Plate 3.4: Finely-laminated, pyritic and dolomitic organic-rich shale of the Neoproterozoic Tindelpina Shale Member, basal Tapley Hill Formation (Umberatana Group), Adelaide Rift Complex, southern Australia.................... 159

Plate 3.5: Shale-hosted benthic microbial mat facies of the Ediacaran Brachina Formation (Wilpena Group), drill hole BWM1a-1, Curnamona Craton, southern Australia.................... 160

Plate 3.6: Finely-laminated, pyritic black shale from the upper Black River Dolomite (Neoproterozoic Togari Group), drill hole Forest-1, northwestern Tasmania.................... 161

Plate 3.7: Pyritic shale-hosted benthic microbial mat facies from the Neoproterozoic Yarra Creek Shale (Grassy Group), City of Melbourne Bay coastal outcrop, southeastern King Island.................... 162

Plate 4.1: Pyritic, organic-rich shales from the basal Lapa Formation (Late Mesoproterozoic to Early Neoproterozoic Vazante Group, Brazil), drill hole MASW01 216

Plate 4.2: Carbonaceous and argillaceous carbonate from the Neoproterozoic lower Horsethief Creek Group (lower Windermere Supergroup), Western Canada 217

Plate 4.3: Pyritic, organic-rich shale from the basal Horsethief Creek Group 218

Plate 5.1: Pyritic, dolomitic, thinly laminated black shale from the Late Paleoproterozoic Wollogorang Formation (Tawallah Group, McArthur Basin, northern Australia), drill hole Mount Young 2 279

Plate 5.2: Finely-laminated and pyritic black shale from the HYC Pyritic Shale Member, Late Paleoproterozoic Barney Creek Formation (McArthur Group, McArthur Basin), drill hole McArthur 2 280

Plate 5.3: Pyritic, finely-laminated black shale from the upper organic-rich interval of the Early Mesoproterozoic Velkerri Formation (Roper Group, McArthur Basin), drill hole Urapunga-4 281

Plate 5.4: Pyritic, finely-laminated black shale from the lower organic-rich interval of the Velkerri Formation, drill hole Urapunga-4 282

Plate 5.5: Wollogorang Formation black shale at 76.91-76.96 m depth with a prominent dolomite veinlet and the three sub-samples from this interval 283

Plate 6.1: Finely laminated, pyritic black shale from the Late Archean Mt. McRae Shale (drill hole ABDP-9), Hamersley Group, Mt. Bruce Supergroup, Western Australia 346

Plate 6.2: Finely laminated, pyritic black shale from the Late Archean Monteville Formation (drill hole GKP01), Campbellrand Subgroup, Ghaap Group, Transvaal Supergroup, South Africa 347

Plate 6.3: Finely laminated dark grey shale of the Early Paleoproterozoic Klipput Shale Member, lower Nelani Formation (drill hole GEC01), Koegas Subgroup, Ghaap Group, South Africa 348

LIST OF ABBREVIATIONS

λ^{187}Re	^{187}Re decay constant
DOP	Degree of pyritization
EF	Enrichment factor
Fe_{HR}/Fe_T	Highly reactive Fe to total Fe ratio
Fe_T/Al	Total Fe to Al ratio
Ga	Giga annum (billion years)
GOE	Great Oxidation Event
GSSP	Global stratotype section and point
$I_{Os(t)}$	Initial ^{187}Os/^{188}Os isotopic composition at time t
ICP-MS	Inductively coupled plasma mass spectrometry
ID-NTIMS	Isotope dilution – negative thermal ionization mass Spectrometry
ID-SIMS	Isotope dilution – secondary ion mass spectrometry
IUGS	International Union of Geological Sciences
Ma	Mega annum (million years)
MIF	Mass independent fractionation
MC-ICP-MS	Multiple collector inductively coupled plasma mass spectrometry
MSWD	Mean square of weighted deviates
NTIMS	Negative thermal ionization mass spectrometry
ORS	Organic-rich sedimentary rocks
PGE	Platinum group elements
ppb	Parts per billion

ppm	Parts per million
ppt	Parts per trillion
Q-ICP-MS	Quadrupole – inductively coupled plasma – mass Spectrometry
rho	Error correlation function (“ρ”)
SHRIMP	Sensitive high resolution ion microprobe
TOC	Total organic carbon
TIMS	Thermal ionization mass spectrometry
XAFS	X-ray absorption fine-structure spectroscopy

CHAPTER 1

Introduction

Part of this chapter has been submitted to the following source:
Kendall, B., Creaser, R.A., and Selby D., ^{187}Re-^{187}Os geochronology of Precambrian organic-rich sedimentary rocks: Geological Society (London) Special Publication, Accepted.

Note: Research contributions in each chapter that are derived in part from a published or submitted manuscript represents only the portion of the published/submitted material that is based on written work and/or research results obtained by Brian Kendall. This thesis does not report research results obtained by the co-authors.

1.1 INTRODUCTION

Accurately determining the depositional ages of sedimentary rocks has proven extremely difficult to accomplish using the conventional long-lived radioisotope systems (e.g., Rb-Sr, Sm-Nd, U-Pb, K-Ar). The U-Pb SHRIMP dating of detrital minerals such as zircon has proven useful for provenance studies and constraining the maximum depositional age (e.g., Bingen et al., 2005). However, authigenic minerals (e.g., apatite, glauconite, illite, K-feldspar, monazite) generally yield diagenetic ages that are variably younger than the depositional age of the host sedimentary rock. For example, the fine (e.g., < 0.2 μm) and coarse (1-2 μm) fractions of illite from shales often yield Rb-Sr ages that reflect diagenesis or provenance, respectively, but not the depositional age (Morton, 1985; Gorokhov et al., 2001). Diagenetic age determinations on authigenic minerals are also hampered by low closure temperatures of the applied radioisotope system, resulting in a high susceptibility to thermal resetting even during relatively low-temperature hydrothermal alteration or metamorphism (Dickin, 2005). Diagenetic xenotime is found in a wide variety of siliciclastic and volcaniclastic rocks and represents a robust U-Pb geochronometer with the potential for resolving complex geological histories within sedimentary basins (Rasmussen, 2005). However, U-Pb xenotime dates also can reflect the timing of diagenesis rather than deposition.

Currently, the most reliable method of constraining the depositional age of sedimentary rocks is by U-Pb zircon dating of interbedded tuff horizons. In the case of Phanerozoic sedimentary basins, such U-Pb ages can be used to calibrate high-resolution Phanerozoic biostratigraphic and chemostratigraphic records thereby facilitating regional and global correlations of stratigraphic successions (e.g., Lehrmann et al., 2006). However, the coarse biostratigraphic and chemostratigraphic resolution of the Precambrian rock record does not currently permit this approach, and in cases where datable ash beds are absent, the ages of Precambrian sedimentary rocks are generally only poorly constrained by radiometric dates from overlying or underlying volcanic rocks, or cross-cutting plutonic rocks.

The development of the ^{187}Re-^{187}Os radioisotope system as a reliable deposition-age geochronometer for organic-rich sedimentary rocks (ORS; total organic carbon [TOC] ≥ 0.5%) like black shales (Ravizza and Turekian, 1989; Cohen et al., 1999;

Creaser et al., 2002; Selby and Creaser, 2003, 2005a; Kendall et al., 2004) has the potential to alleviate the problems associated with radiometric calibration of the Precambrian sedimentary rock record. Improvements in sampling and analytical methodologies, combined with the high precision of isotope dilution – negative thermal ionization mass spectrometry (ID-NTIMS; Creaser et al., 1991; Völkening et al., 1991; Walczyk et al., 1991), have made it possible to obtain a Re-Os age for black shale with a precision better than ± 1% (2σ), with the absolute uncertainty comparable in some cases to the uncertainties on U-Pb ages derived from SHRIMP or laser ablation MC-ICP-MS analyses of zircons from tuffaceous beds (e.g., Kendall et al., 2004; Selby and Creaser, 2005a). Recently, the Re-Os ORS geochronometer has been successfully applied to studies regarding Phanerozoic geological timescale calibration (Oxfordian-Kimmeridgian, Devonian-Mississippian, and Frasnian-Famennian boundary; Selby and Creaser, 2005a; Turgeon et al., 2007; Selby, in press) and the timing of Neoproterozoic glaciation (Kendall et al., 2004). In addition, the initial ^{187}Os/^{188}Os value (I_{Os}) from Re-Os isochron regressions has served as a tracer for the Os isotope composition of Phanerozoic seawater (e.g., Cohen et al., 1999, 2004; Creaser et al., 2002; Selby and Creaser, 2003; Cohen, 2004; Turgeon et al., 2007; Selby, in press).

1.2 THE ^{187}Re-^{187}Os SYSTEM IN ORS: A DEPOSITION-AGE GEOCHRONOMETER AND SEAWATER Os ISOTOPE TRACER

In addition to being siderophilic and chalcophilic (e.g., Shirey and Walker, 1998), Re and Os are also "organophilic" and redox-sensitive. This geochemical behavior of Re and Os in Earth surface environments enables the ^{187}Re-^{187}Os isotope pair to be used as a deposition-age geochronometer for ORS and a tracer of paleo-seawater Os isotope composition. Under oxidizing atmospheric conditions, Re is transported to the oceans primarily by rivers as the highly soluble perrhenate anion ReO_4^- (this speciation has been recently confirmed by X-ray absorption fine-structure spectroscopy [XAFS]; Yamashita et al., 2007), displays conservative behaviour in the oceans, and has a long seawater residence time of ~ 750 k.y. (Anbar et al., 1992; Colodner et al., 1993). Typical marine oxic sediments have Re abundances (e.g., 0.1-1 ppb; Crusius et al., 1996) comparable to estimates for average continental crust (0.2-2 ppb; Esser and Turekian, 1993; Peucker-

Ehrenbrink and Jahn, 2001; Hattori et al., 2003; Sun et al., 2003a, b). Relative to average crust, however, Re is enriched in suboxic, anoxic, and euxinic sediments to a degree unmatched by any other metal (Colodner et al., 1993; Crusius et al., 1996; Morford and Emerson, 1999). Rhenium removal from suboxic, anoxic, and euxinic pore-waters occurs near the sediment-water interface ($\leq$ 1 cm) below the zones of Fe and U reduction but above the zones of sulfate reduction and Mo enrichment (Crusius et al., 1996; Nameroff et al., 2002; Morford et al., 2005). Recently, Sundby et al. (2004) suggested nearly complete Re removal from pore waters may occur at much deeper sediment depths (e.g., ~ 45 cm), but is essentially complete after ~ 10 years (precipitation rate constant of ~ 0.2 a^{-1}). Removal of Re from pore waters does not occur by particle scavenging, but rather by reductive capture whereby $Re^{VII}O_4^-$ is reduced to Re^{IV} (Colodner et al., 1993; Yamashita et al., 2007). The rate of this reduction is controlled by slow precipitation kinetics and is independent of sediment accumulation rate and sulfide concentration (Crusius and Thomson, 2000; Sundby et al., 2004; Yamashita et al., 2007).

The concentration of Os in the oceans is much lower (6.6-10.9 pg/kg; Levasseur et al., 1998; Woodhouse et al., 1999) relative to Re (7.4 ng/kg; Anbar et al., 1992), leading to a high $^{187}Re/^{188}Os$ ratio for present-day seawater (~ 3200 to 5300). Although Os may not exhibit strictly conservative behavior in the oceans (Woodhouse et al., 1999), the $^{187}Os/^{188}Os$ isotope composition of present-day seawater from the Pacific, Atlantic, and Indian oceans is nearly homogenous (~ 1.06; Sharma et al., 1997; Levasseur et al., 1998; Woodhouse et al., 1999; Peucker-Ehrenbrink and Ravizza, 2000), consistent with a seawater residence time for Os of ~ 10^4 years (Oxburgh, 1998, 2001; Levasseur et al., 1999). The dominant source of Os to the oceans today (~ 70-80%) is from weathering of the upper continental crust, and can be described as a mixture of average upper crustal material plus ~ 0.1% black shale and ~ 1.4% ultramafic material from young mafic, subduction-related crust (McDaniel et al., 2004). Recent estimates of the average $^{187}Os/^{188}Os$ for the currently eroding upper continental crust and riverine inputs are between 1.0 and 1.4 (Esser and Turekian, 1993; Peucker-Ehrenbrink and Jahn, 2001; Hattori et al., 2003) and ~ 1.54 (with a large uncertainty of > 20%; Levasseur et al., 1999), respectively (Figure 1.1). The other 20-30% of the present-day oceanic Os budget comprises unradiogenic contributions from dissolved cosmic dust (Peucker-Ehrenbrink,

1996) and the low- and high-temperature hydrothermal alteration of oceanic crust and peridotites (Ravizza et al., 1996; Sharma et al., 2000; Cave et al., 2003). Convecting and primitive upper mantle, ordinary and enstatite chondrites, ureilites (achondrites), and carbonaceous chondrites are characterized by a narrow range in $^{187}Os/^{188}Os$ of 0.126 to 0.130 (Becker et al., 2001; Meisel et al., 1996, 2001; Walker et al., 2002a, b; Rankenburg et al., 2007), whereas iron meteorites can have slightly more radiogenic Os (up to ~ 0.17; e.g., Smoliar et al., 1996; Shen et al., 1996, 1998; Shirey and Walker, 1998; Chen et al., 2002). Reductive capture of dissolved Os was first proposed as the removal mechanism into organic-rich sediments (Koide et al., 1991), but the inferred presence of soluble osmium-bearing organic complexes in seawater suggests Os may instead be incorporated into reducing sediments in direct association with organic matter (Levasseur et al., 1998). This is supported by positive correlations between ^{192}Os abundance and TOC content in recent Black Sea and Saanich Inlet organic-rich sediments (Ravizza et al., 1991; Poirier, 2006) and Phanerozoic black shales (Peucker-Ehrenbrink and Hannigan, 2000; Creaser et al., 2002). Osmium removal from seawater into reducing sediments may occur below the depth of Re enrichment (e.g., below 8 cm depth in modern Saanich Inlet sediments; Poirer, 2006). Recently, sequential extraction techniques and X-ray absorption spectroscopy applied to an experimental system comprising artificial seawater, a multi-tracer, and reducing Tokyo Bay sediment has revealed the rather complex nature of Os marine geochemistry (Yamashita et al., 2007). Osmium is likely present in seawater as an octavalent oxyanion (e.g., $HOsO_5^-$, $H_3OsO_6^-$), and may be rapidly removed to organic-rich sediments first as Os(IV), and is then further reduced to Os(III) by organic complexation.

Rhenium and Os in ORS are predominantly hydrogenous and are physically associated with organic matter (e.g., Ravizza and Turekian, 1989; Ravizza et al., 1991; Ravizza and Turekian, 1992; Ravizza and Esser, 1993; Cohen et al., 1999; Martin et al., 2000; Peucker-Ehrenbrink and Hannigan, 2000; Pierson-Wickmann et al., 2000, 2002; Creaser et al., 2002; Jaffe et al., 2002; Poirier, 2006). Rhenium and Os are present in natural hydrocarbons (Poplavko et al., 1975; Barre et al., 1995; Woodland et al., 2001; Selby and Creaser, 2005b; Selby et al., 2007a) and bitumens (Selby et al., 2005), and bulk organic matter is known to contain a large fraction of the Re and Os in shale source rocks (Ripley et al., 2001; Selby and Creaser, 2003).

The fundamental assumptions behind the Re-Os ORS geochronometer include: 1) all Re and Os in ORS are hydrogenous (i.e., negligible contributions from detrital and/or extraterrestrial particulates), 2) rapid immobilization of Re and Os in ORS following sediment deposition such that Re-Os dates reflect the timing of deposition rather than younger diagenesis, 3) homogenous I_{Os} derived from the contemporaneous seawater, and 4) negligible post-depositional mobilization of Re and Os. Obtaining a precise Re-Os date by the isochron diagram method requires a suitable range in initial $^{187}Re/^{188}Os$ such that β-decay of ^{187}Re to ^{187}Os over time generates a range in present-day $^{187}Os/^{188}Os$. The radioactive decay equation representing this process is:

$$(^{187}Os/^{188}Os)_P = (^{187}Os/^{188}Os)_I + (^{187}Re/^{188}Os)_P (e^{\lambda t} - 1) \qquad (1)$$

where $(^{187}Os/^{188}Os)_P$ and $(^{187}Re/^{188}Os)_P$ represent the present-day isotope ratios, $(^{187}Os/^{188}Os)_I$ represents the initial Os isotopic composition at the time (t) of sediment deposition, and λ represents the ^{187}Re decay constant. Although ORS may contain Re and Os concentrations ranging from average upper crustal abundances (~ 0.2-2 ppb Re and 30-50 ppt Os; Esser and Turekian, 1993; Peucker-Ehrenbrink and Jahn, 2001; Hattori et al., 2003; Sun et al., 2003a, b) to hundreds of ppb Re and tens of ppb Os (e.g., Cohen et al., 1999; Turgeon and Creaser, 2007), the high Re/Os ratios of ORS derived from seawater means that only moderate enrichments in Re are required to generate radiogenic present-day $^{187}Os/^{188}Os$ ratios for Precambrian ORS (e.g., Kendall et al., 2004). One significant challenge of Re-Os ORS geochronology concerns the first assumption, which requires an analytical methodology to release hydrogenous Os from ORS while minimizing release of detrital Re and Os that could compromise the accuracy and precision of Re-Os age determinations and the value of I_{Os} from isochron regressions (e.g., Ravizza et al., 1991). Extraterrestrial particulates are generally negligible sources of Os to ORS (< 0.2% of total Os for ORS with Os abundances greater than 150 ppt) if meteoritic fluxes are similar to Cenozoic fluxes (Cohen et al., 1999; Kendall et al., 2004).

1.3 DEVELOPMENT OF THE Re-Os GEOCHRONOMETER FOR ORS

The development of Re-Os ORS geochronology resulted from several studies on Phanerozoic shales. The pioneering study of Ravizza and Turekian (1989) on the lower Mississippian Bakken Formation (North Dakota, U.S.A.) employed a NiS fire assay to concentrate Re and Os from shale powders into insoluble sulfides that were dissolved in a Cr^{VI}-H_2SO_4 solution prior to separation and purification. For some samples, Re abundances were determined by both NiS fire assay and acid dissolution. Using the York (1966) regression and isotope dilution – secondary ion mass spectrometry (ID-SIMS), Ravizza and Turekian (1989) obtained dates of 354 ± 49 Ma ($\lambda^{187}Re = 1.52 \times 10^{-11}$ a^{-1}; Luck and Allègre, 1983) and 337 ± 46 Ma ($\lambda^{187}Re = 1.64 \times 10^{-11}$ a^{-1}; Lindner et al., 1989), nominally consistent with known biostratigraphic age constraints for the Bakken Shale (~ 360-352 Ma). Regression of the data using *Isoplot V.3.0* (Ludwig, 2003) and the value of 1.666×10^{-11} a^{-1} for $\lambda^{187}Re$ (Smoliar et al., 1996; Selby et al., 2007b) yields a Model 3 date of 323 ± 110 Ma (2σ, mean square of weighted deviates [MSWD] = 5.6; Figure 1.2A). Although the Re-Os date has a large uncertainty, it can be attributed in part to analytical uncertainties, particularly the poor precision (3-10%) for $^{187}Os/^{186}Os$ ratios measured by SIMS (Luck and Allègre, 1983). Furthermore, Ravizza and Turekian (1989) suggested that some of the scatter about the regression line resulted predominantly from disturbance of the Re-Os systematics by hydrocarbon maturation.

Using new analytical methodologies including the Carius tube technique (e.g., see Appendix A) for whole-rock digestions in inverse *aqua regia* (Shirey and Walker, 1995), improved chemical separation and purification protocols for Os (Cohen and Waters, 1996), and ID-NTIMS analysis (Creaser et al., 1991; Völkening et al., 1991; Walczyk et al., 1991), Cohen et al. (1999) provided the first relatively precise Re-Os age determinations from hydrocarbon immature, high-TOC (> 5%) Jurassic ORS from the United Kingdom. Cohen et al. (1999) obtained Re-Os dates of 207 ± 12 Ma (Model 3, MSWD = 88), 181 ± 13 Ma (Model 3, MSWD = 17), and 155.2 ± 4.3 Ma (Model 3, MSWD = 11; Figure 1.2B) for Hettangian (Blue Lias, Dorset), Toarcian (Jet Rock, Yorkshire), and Kimmeridgian (Kimmeridge Clay, Dorset) shales. Recalculation of the Cohen et al. (1999) data (which used *Isoplot V.1.0*; Ludwig, 1998) with *Isoplot V.3.0* yields identical Re-Os dates. These dates agree within uncertainty to the respective stratigraphic ages of 198.0 ± 1.5 Ma, 179.3 ± 3.7 Ma, and 152.7 ± 1.9 Ma (Gradstein et al., 2004). Cohen et al. (1999) established that sampling of stratigraphic intervals representing short intervals of geological time (e.g., ~ 500 ka for the Kimmeridgian) were required to minimize I_{Os} heterogeneity and thereby obtain precise Re-Os depositional ages. Because Barre et al. (1995) had reported high concentrations of Re and Os in crude oils and asphaltenes, Cohen et al. (1999) considered the selection of immature ORS, which have not undergone hydrocarbon maturation, as a critical factor for the order of magnitude increase in the precision of their Re-Os dates relative to Ravizza and Turekian (1989).

However, Creaser et al. (2002) evaluated the effects of hydrocarbon maturation on the Re-Os isotope systematics of immature, mature, and overmature black shales from the Devonian-Mississippian Exshaw Formation (Western Canada Sedimentary Basin). Regression of samples from all hydrocarbon maturity levels yield a Re-Os date of 358 ± 10 Ma (Model 3, MSWD = 19) for the Exshaw Formation lower black shale member (Figure 1.3A) that was in agreement with previous biostratigraphic (Late Famennian expansa to Early Tournaisian duplicata Zones), U-Pb monazite (363.3 ± 0.4 Ma from a tuff at the base of the lower black shale member; Richards et al., 2002), and U-Pb zircon (363.6 ± 1.6 Ma from the Upper expansa zone in New Brunswick, Canada; Tucker et al., 1998) age constraints. Individual regressions for immature and mature plus overmature samples yield similar Re-Os dates within 2σ uncertainties, suggesting that hydrocarbon maturation did not grossly perturb the Re-Os system in ORS in this case. High-TOC (> 5%) samples were shown to yield a superior regression (358 ± 9 Ma, Model 3, MSWD = 1.8) compared to low-TOC samples (360 ± 9 Ma, Model 3, MSWD = 8.0) suggesting that non-hydrogenous Re and Os can be liberated by inverse *aqua regia* whole-rock digestions and thus negatively impact the precision and accuracy of Re-Os ages derived from low-TOC samples.

To limit the release of detrital Re and Os from ORS matrices, a new whole-rock digestion protocol (Cr^{VI}-H_2SO_4) was developed by Selby and Creaser (2003). Using the same shale aliquots as Creaser et al. (2002), two subsets with distinctive $I_{Os\ (364\ Ma)}$ values were identified and separately regressed to yield Re-Os dates of 366.1 ± 9.6 Ma (Model 3, MSWD = 2.2; I_{Os} = 0.51 ± 0.06; Figure 1.3B) and 363.4 ± 5.6 Ma (Model 1, MSWD =

1.6; I_{Os} = 0.41 ± 0.04; Figure 1.3C). These Re-Os dates are more precise and better correlated than the Re-Os dates for the same subsets derived using the data from Creaser et al. (2002) for inverse *aqua regia* digestion (356 ± 23 Ma; MSWD = 11.1 and 356 ± 12 Ma; MSWD = 5.2, respectively). Selby and Creaser (2003) thus showed that the Cr^{VI}-H_2SO_4 medium represents a superior digestion protocol to inverse *aqua regia* for obtaining depositional age information as well as estimating the $^{187}Os/^{188}Os$ isotope composition of contemporaneous seawater.

The inverse *aqua regia* and Cr^{VI}-H_2SO_4 dissolution methods were further evaluated on Precambrian ORS by Kendall et al. (2004) using low-TOC (< 1% although original TOC content was likely much higher) slates of the Neoproterozoic Old Fort Point Formation (Windermere Supergroup, Western Canada). An imprecise Re-Os date of 634 ± 57 Ma (Model 3, MSWD = 65) was determined using inverse *aqua regia*, whereas dissolution of the same sample powders with a Cr^{VI}-H_2SO_4 medium yield a much more precise date of 607.8 ± 4.7 Ma (Model 1, MSWD = 1.2) (Figure 1.4). Although both ages are in agreement with existing U-Pb age constraints that bracket the Old Fort Point Formation between ca. 710-667 Ma and 570 Ma (Colpron et al., 2002; Lund et al., 2003; Fanning and Link 2004), the poor precision of the date derived from inverse *aqua regia* analyses reflects a variably radiogenic, detrital Os component that was dissolved by the inverse *aqua regia* solution but not by the Cr^{VI}-H_2SO_4 medium. In addition, these results suggested the potential of the Re-Os radioisotope system for providing the depositional ages of ORS was greater than previously realized. For example, neither chlorite-grade metamorphism nor low TOC content precluded a Re-Os age determination for the Old Fort Point Formation. In fact, the precision of the 607.8 ± 4.7 Ma Re-Os age (± 0.8%, 2σ) exceeded the precision of earlier Re-Os dating studies on higher-TOC rocks analyzed through either inverse *aqua regia* (Cohen et al., 1999; Creaser et al., 2002) or NiS fire assay (Ravizza and Turekian, 1989; Singh et al., 1999) (≥ 3%, 2σ).

1.4 ACCURACY OF THE Re-Os GEOCHRONOMETER FOR ORS AND THE ^{187}Re DECAY CONSTANT

An accurate and precise determination of the decay constant for ^{187}Re, together with agreement between Re-Os black shale and U-Pb zircon ages from the same rock unit, are necessary prerequisites to qualify the Re-Os system as an accurate deposition-age geochronometer for ORS. The most widely used value of λ^{187}Re ($1.666 \pm 0.005 \times 10^{-11}$ a^{-1}), determined by Smoliar et al. (1996), was calculated using the slope of Re-Os data from group IIIA iron meteorites and the Pb-Pb age of 4557.8 ± 0.4 Ma determined for angrite meteorites (Lugmair and Galer, 1992) that are assumed to form at the same time as group IIIA irons. This assumption is supported by ^{53}Mn-^{53}Cr ages for angrite and group IIIAB meteorites that constrain their formation to be within ± 5 M.y. of each other (Hutcheon and Olsen, 1991; Hutcheon et al., 1992). Although the uncertainty in λ^{187}Re was calculated to be ± 0.31% (2σ) by Smoliar et.al. (1996), the ammonium hexachloro-osmate standard used by these researchers is only stoichiometric to within ± 1.2% (Morgan et al., 1995) and thus the total uncertainty in λ^{187}Re would be ~ 1% (2σ) for spike solutions not calibrated against the particular Os standard used by Smoliar et al. (1996). Subsequent studies have yielded slightly different values for λ^{187}Re using either direct counting experiments or analyses from meteorites (Shukolyukov and Lugmair, 1997; Birck and Allègre, 1998; Shen et al., 1998). Recently, Selby et al. (2007b) intercalibrated the Re-Os molybdenite and U-Pb zircon geochronometers using eleven magmatic-hydrothermal ore deposits spanning ca. 2700 M.y. of Earth history, and calculated values of $1.6668 \pm 0.0034 \times 10^{-11}$ a^{-1} (using U decay constants from Jaffey et al., 1971) and $1.6689 \pm 0.0031 \times 10^{-11}$ a^{-1} (using λ^{238}U from Jaffey et al., 1971, and λ^{235}U from Schoene et al., 2006) for λ^{187}Re that are nominally higher (0.1-0.2 %) than the value determined by Smoliar et al. (1996), but within calculated uncertainty.

To establish the utility of the Re-Os ORS geochronometer for geological timescale calibration, Selby and Creaser (2005a) studied black shales from the Devonian-Mississippian (D-M) boundary of the Exshaw Formation at its type section of Jura Creek (~ 80 km west of Calgary, Alberta, Canada). Here, the D-M boundary is constrained to an interval of 2.9 m based on conodont biostratigraphy, and has been tentatively placed at the contact between non-calcareous and calcareous black shales of the Exshaw

Formation's lower black shale member. Black shales obtained along a 10 cm stratigraphic interval straddling this boundary yield a Re-Os age of 361.3 ± 2.4 Ma (Model 1, including a λ^{187}Re uncertainty of ± 0.35%, MSWD = 1.2; Figure 1.5) that agrees to within ~ 0.2% of a recent calibration (360.7 ± 0.7 Ma) for the D-M boundary based on interpolation of U-Pb zircon dates from New Brunswick, Canada, and Germany (Trapp et al., 2004). The excellent agreement between the Re-Os black shale and U-Pb zircon ages thus demonstrates the utility of the Re-Os ORS geochronometer for accurately constraining the timing, duration, and rate of geological events and processes.

1.5 Re-Os ISOTOPE SYSTEMATICS OF PRECAMBRIAN ORS

This thesis evaluates the Re-Os isotope systematics of Precambrian ORS ranging in age between the Late Archean Eon (~ 2.6 Ga) and the Ediacaran Period (~ 0.55 Ga). The main focus is on application of the Re-Os radioisotope system as a geochronometer, but this work also includes assessment of the limitations of the ORS geochronometer, the suitability of ORS rock types other than black shale for geochronology, and the implications of Re-Os systematics in ORS concerning the evolution of Earth's atmosphere and ocean redox chemistry over geological time. In addition, some Precambrian black shales were also analyzed for Mo and Fe isotopes, and elemental and Fe-based redox proxies (e.g., degree-of-pyritization [DOP]) with the aim of providing constraints on the redox state of local and/or global deep ocean waters during sediment deposition, and the nature of Mo and Fe geochemical cycles in Earth's early oceans.

Chapter 2 represents a reconnaissance study of the Re-Os, Mo, and Fe isotope systematics of the 635-551 Ma Doushantuo Formation (Yangtze Gorges region, South China). The utility of organic-rich carbonates for geochronology is also assessed using the overlying ca. 551-542 Ma Dengying Formation.

Rhenium-Os geochronology of post-glacial ORS overlying previously undated Neoproterozoic diamictites in Australia is the major theme of Chapter 3. New Re-Os depositional ages from central and southern Australia (Aralka Formation and Tindelpina Shale Member, basal Tapley Hill Formation, respectively) and northwestern Tasmania (upper Black River Dolomite) provide critical tests regarding the synchronicity of the "Sturtian" glaciation, and the relationship between Rodinia continental breakup and

"Sturtian" glaciation. Shale-hosted benthic microbial mats stratigraphically overlying "Marinoan" glacial deposits in central and southern Australia (Pertatataka and Brachina Formations, respectively) and southeastern King Island (Yarra Creek Shale) are evaluated for their utility as Re-Os deposition-age geochronometers. The Re-Os abundance and isotope systematics of the Aralka Formation and Tindelpina Shale Member are compared with trace metal data to determine the mechanism(s) controlling variation in initial ^{187}Re/^{188}Os during organic-rich sediment deposition.

Chapter 4 examines the complex Re-Os isotope systematics of two undated post-glacial black shales from Brazil (Lapa Formation, Vazante Group) and western Canada (lower Horsethief Creek Group), and attempts to provide age information on underlying diamictites that are regarded as correlatives of a global "Sturtian" glaciation.

A combined Re-Os, Mo, and Fe isotope study was carried out on Middle Proterozoic shales (Velkerri, Barney Creek, and Wollogorang Formations) from the McArthur Basin, northern Australia, and is presented in Chapter 5. This work provides new depositional age constraints for the Velkerri Formation and a precise estimate of the Mo isotope composition of global seawater at 1.4 Ga. The robustness of the Re-Os, Mo, and Fe isotope systems during post-depositional hydrothermal fluid flow is evaluated using the 1.73 Ga Wollogorang Formation. As in Chapter 2, trace metal data from the Velkerri and Wollogorang Formations are compared with Re and Os abundance and isotope data to elucidate controls on the fractionation of Re from Os during organic-rich sediment deposition.

In Chapter 6, the first precise and accurate Re-Os ORS age is presented for an Archean black shale (2.5 Ga Mt. McRae Shale, western Australia). Mixing relationships between detrital and hydrogenous Re and Os, and their effect on depositional age determinations, are evaluated on Late Archean and Early Paleoproterozoic shales (Monteville Formation and Klipput Shale Member, lower Nelani Formation, South Africa). Reviews of the Os isotope composition of Precambrian seawater and the Re-Os abundance and isotope systematics of ORS over geological time are presented, and provide insights into the evolution of the marine Re and Os geochemical cycle over time and their relationship with the multi-stage evolution of Earth's atmosphere and ocean redox state.

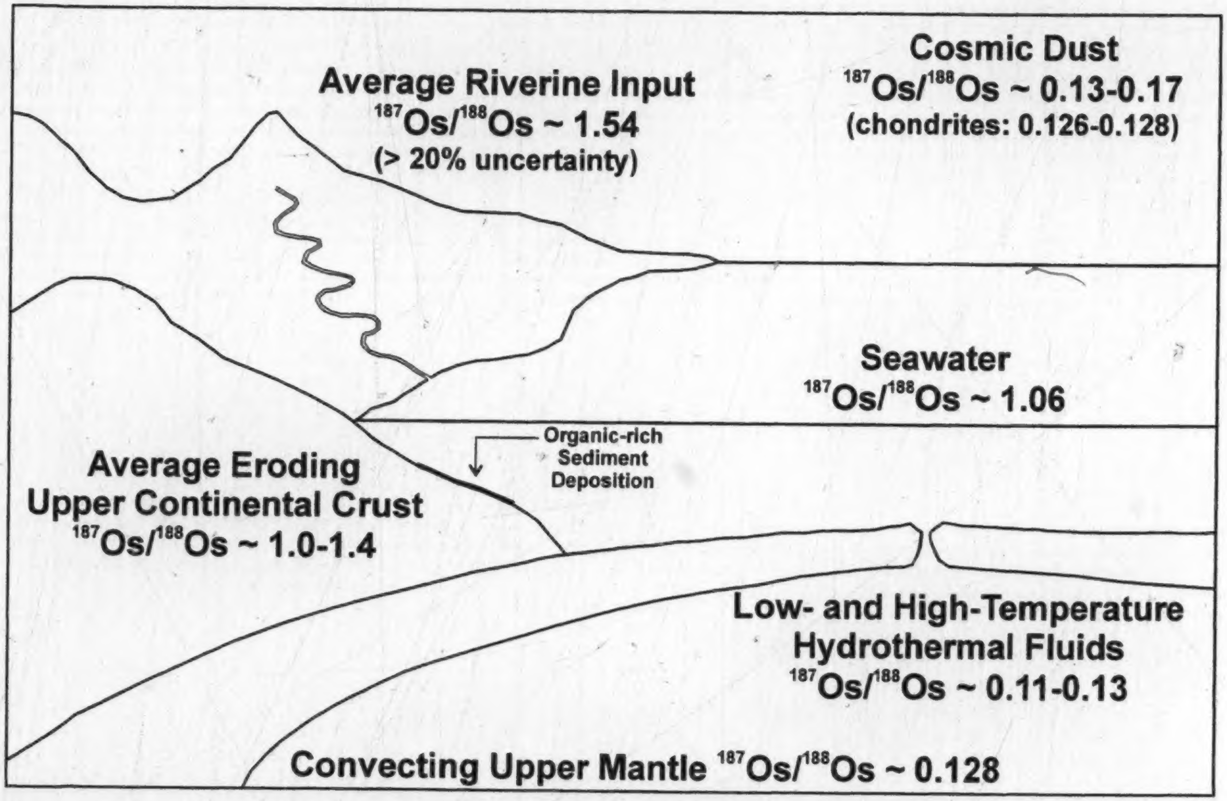
Average Riverine Input
^{187}Os/^{188}Os ~ 1.54
(> 20% uncertainty)
Cosmic Dust
^{187}Os/^{188}Os ~ 0.13-0.17
(chondrites: 0.126-0.128)
Seawater
^{187}Os/^{188}Os ~ 1.06
Organic-rich Sediment Deposition
Average Eroding Upper Continental Crust
^{187}Os/^{188}Os ~ 1.0-1.4
Low- and High-Temperature Hydrothermal Fluids
^{187}Os/^{188}Os ~ 0.11-0.13
Convecting Upper Mantle ^{187}Os/^{188}Os ~ 0.128

Figure 1.1: Summary of the major near-surface reservoirs of Os and their isotopic composition. The dominant source of Os to the oceans today is from eroding upper continental crust (~ 70-80%), with subordinate contributions from hydrothermal fluids and dissolution of cosmic dust (~ 20-30%). See text for sources of data. Modified from Peucker-Ehrenbrink and Ravizza (2000).

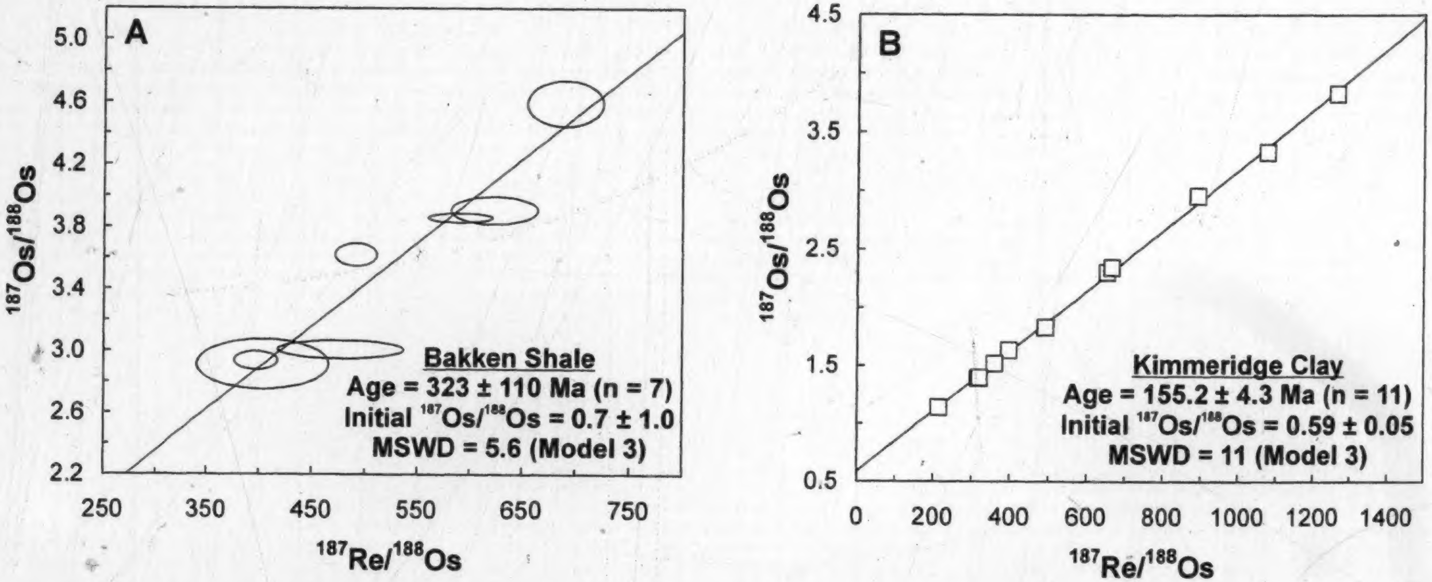

Figure 1.2: Re-Os isochron diagrams. (A) Early Mississippian Bakken Shale, North Dakota (Ravizza and Turekian, 1989). Conversion of $^{187}Re/^{186}Os$ and $^{187}Os/^{186}Os$ isotope ratios to $^{187}Re/^{188}Os$ and $^{187}Os/^{188}Os$ were made using $^{186}Os/^{188}Os = 0.11983$. Input errors used measured 2σ uncertainties quoted by Ravizza and Turekian (1989). (B) Late Jurassic Kimmeridge Clay, Dorset, UK (Cohen et al., 1999). Blanket uncertainties of 1.0% and 0.4% were used for $^{187}Re/^{188}Os$ and $^{187}Os/^{188}Os$, respectively. Data points are shown by squares for clarity. Both regressions were calculated using *Isoplot V.3.0.* (Ludwig, 2003) and the current value for ^{187}Re (1.666×10^{-11} a^{-1}; Smoliar et al., 1996). Note the order of magnitude improvement in precision of the Re-Os age obtained by Cohen et al. (1999) relative to the study of Ravizza and Turekian (1989).

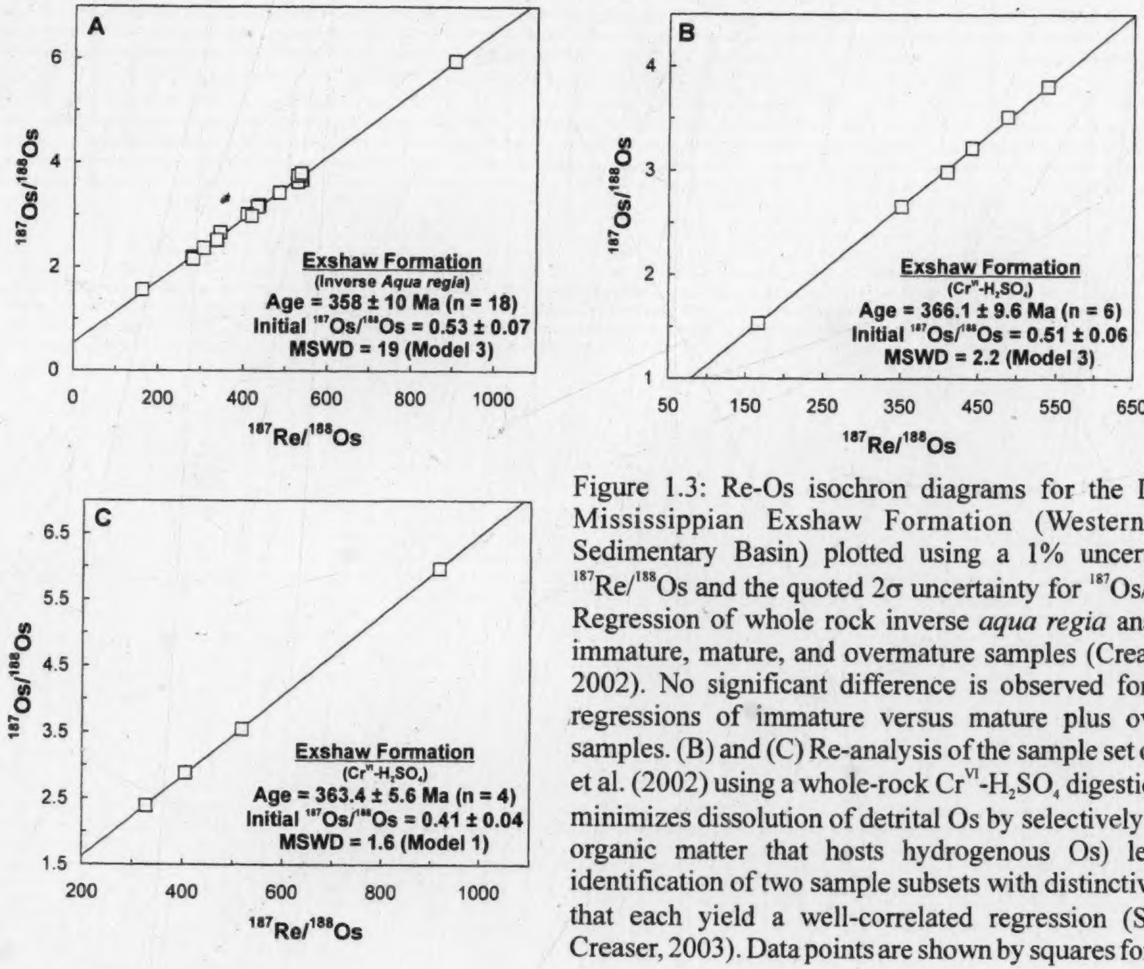

Figure 1.3: Re-Os isochron diagrams for the Devonian-Mississippian Exshaw Formation (Western Canada Sedimentary Basin) plotted using a 1% uncertainty for $^{187}Re/^{188}Os$ and the quoted 2σ uncertainty for $^{187}Os/^{188}Os$. (A) Regression of whole rock inverse *aqua regia* analyses for immature, mature, and overmature samples (Creaser et al., 2002). No significant difference is observed for separate regressions of immature versus mature plus overmature samples. (B) and (C) Re-analysis of the sample set of Creaser et al. (2002) using a whole-rock Cr^{VI}-H_2SO_4 digestion (which minimizes dissolution of detrital Os by selectively attacking organic matter that hosts hydrogenous Os) led to the identification of two sample subsets with distinctive $I_{Os\ (364\ Ma)}$ that each yield a well-correlated regression (Selby and Creaser, 2003). Data points are shown by squares for clarity.

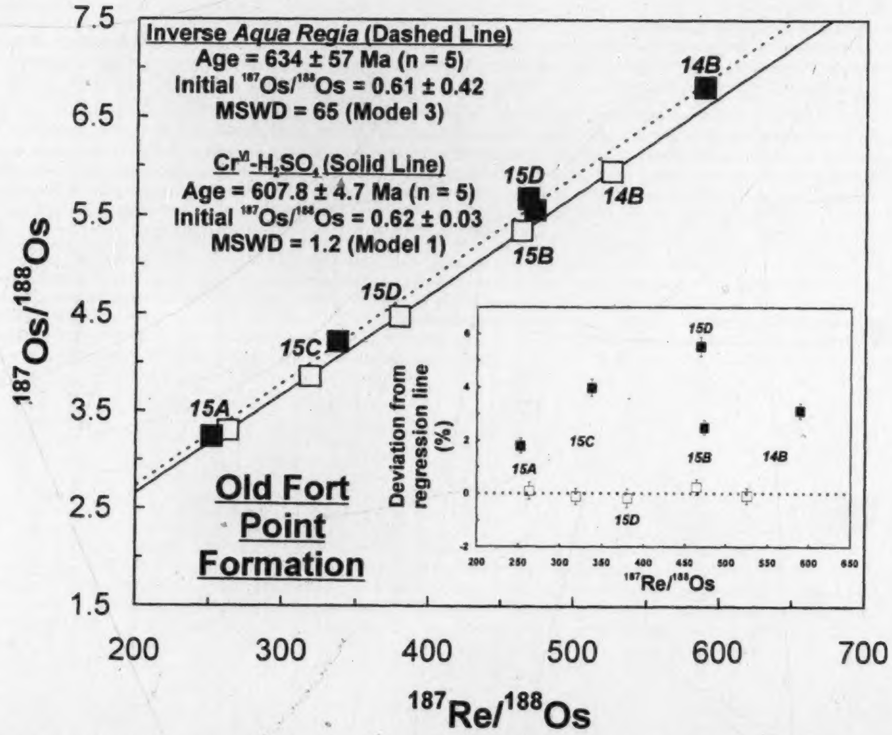

Figure 1.4: Re-Os isochron diagram for the Neoproterozoic Old Fort Point Formation, Windermere Supergroup, Western Canada (Kendall et al., 2004). Regression of inverse *aqua regia* analyses (filled squares; dashed regression line) yields an imprecise Model 3 date whereas regression of Cr^{VI}-H$_2$SO$_4$ digestion analyses (open squares; solid regression line) yields a precise Model 1 age. The inset diagram shows the deviation of each point from the Cr^{VI}-H$_2$SO$_4$ best-fit regression line. Regression used measured 2σ uncertainties for both ^{187}Re/^{188}Os and ^{187}Os/^{188}Os, and, for the first time, the error correlation function rho (ρ) (Ludwig, 1980). Data points are shown by squares for clarity.

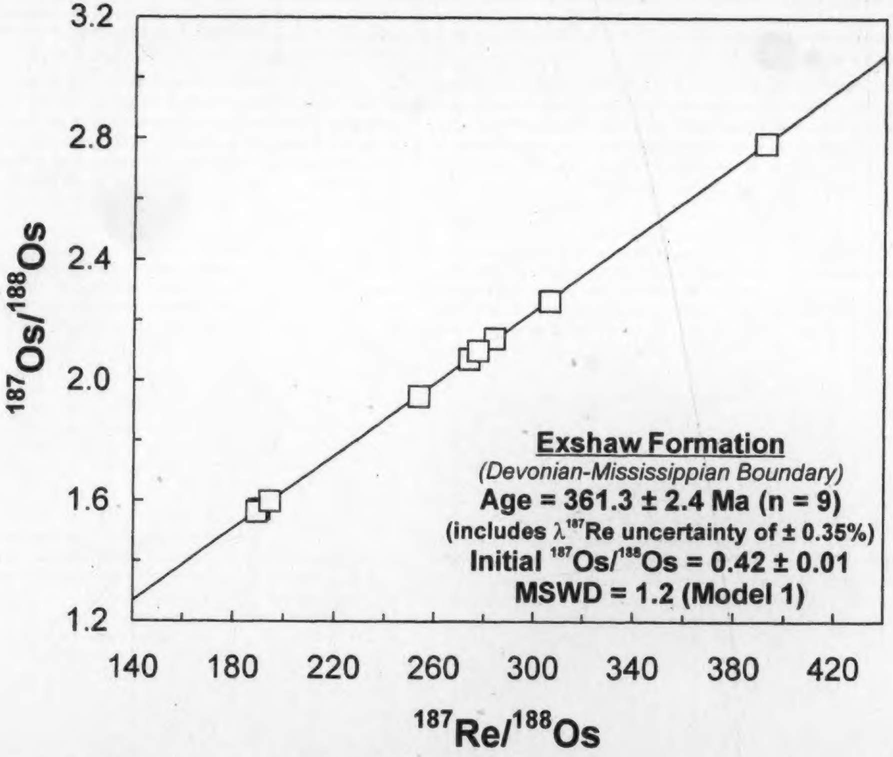

Figure 1.5: Re-Os isochron diagram for Exshaw Formation black shales straddling the Devonian-Mississippian boundary (Selby and Creaser, 2005a). The excellent agreement (to within 0.2%) between the Exshaw Formation Re-Os age and the interpolated U-Pb zircon age of 360.7 ± 0.7 Ma (Trapp et al., 2004) for the Devonian-Mississippian boundary demonstrates the accuracy of the Re-Os deposition-age geochronometer. Data points are shown by squares for clarity.

REFERENCES

Anbar, A.D., Creaser, R.A., Papanastassiou, D.A., and Wasserburg, G.J., 1992, Rhenium in seawater: confirmation of generally conservative behaviour: Geochimica et Cosmochimica Acta, v. 56, p. 4099-4103.

Barre, A.B., Prinzhofer, A., and Allegre, C.J., 1995, Osmium isotopes in the organic matter of crude oil and asphaltenes: Terra Abstracts, v. 7, p. 1999.

Becker, H., Morgan, J.W., Walker, R.J., MacPherson, G.J., and Grossman, J.N., 2001, Rhenium-osmium systematics of calcium-aluminum-rich inclusions in carbonaceous chondrites: Geochimica et Cosmochimica Acta, v. 65, p. 3379-3390.

Bingen, B., Griffin, W.L., Torsvik, T.H., and Saeed, A., 2005, Timing of late Neoproterozoic glaciation on Baltica constrained by detrital zircon geochronology in the Hedmark Group, south-east Norway: Terra Nova, v. 17, p. 250-258.

Birck, J.-L., and Allègre, C.-J., 1998, Rhenium 187 – osmium 187 in iron meteorites and the strange origin of the Kodaikanal meteorite: Meteoritic Planetary Science, v. 33, p. 647-653.

Cave, R.R., Ravizza, G.E., German, C.R., Thomson, J., and Nesbitt, R.W., 2003, Deposition of osmium and other platinum-group elements beneath the ultramafic-hosted Rainbow hydrothermal plume: Earth and Planetary Science Letters, v. 210, p. 65-79.

Chen, J.H., Papanastassiou, D.A., and Wasserburg, G.J., 2002, Re-Os and Pd-Ag systematics in Group IIIAB irons and in pallasites: Geochimica et Cosmochimica Acta, v. 66, p. 3793-3810.

Cohen, A.S., 2004, The rhenium-osmium isotope system: applications to geochronological and paleoenvironmental problems: Journal of the Geological Society, London, v. 161, p. 729-734.

Cohen, A.S., and Waters, F.G., 1996, Separation of osmium from geological materials by solvent extraction for analysis by thermal ionization mass spectrometry: Analytical Chimica Acta, v. 332, p. 269-375.

Cohen, A.S., Coe, A.L., Bartlett, J.M., and Hawkesworth, C.J., 1999, Precise Re-Os ages of organic-rich mudrocks and the Os isotope composition of Jurassic seawater: Earth and Planetary Science Letters, v. 167, p. 159-173.

Cohen, A.S., Coe, A.L., Harding, S.M., and Schwark, L., 2004, Osmium isotope evidence for the regulation of atmospheric CO_2 by continental weathering: Geology, v. 32, p. 157-160.

Colodner, D., Sachs, J., Ravizza, G., Turekian, K., Edmond, J., and Boyle, E. 1993, The geochemical cycle of rhenium: a reconnaissance: Earth and Planetary Science Letters, v. 117, p. 205-221.

Colpron, M., Logan, J.M., and Mortensen, J.K., 2002, U-Pb zircon age constraint for late Neoproterozoic rifting and initiation of the lower Paleozoic passive margin of western Laurentia: Canadian Journal of Earth Sciences, v. 39, p. 133-143.

Creaser, R.A., Papanastassiou, D.A., and Wasserburg, G.J., 1991, Negative thermal ion mass spectrometry of osmium, rhenium, and iridium: Geochimica et Cosmochimica Acta, v. 55, p. 397-401.

Creaser, R.A., Sannigrahi, P., Chacko, T., and Selby, D. 2002, Further evaluation of the Re-Os geochronometer in organic-rich sedimentary rocks: a test of hydrocarbon maturation effects in the Exshaw Formation, Western Canada Sedimentary Basin: Geochimica et Cosmochimica Acta, v. 66, p. 3441-3452.

Crusius, J., and Thomson, J., 2000, Comparative behavior of authigenic Re, U, and Mo during reoxidation and subsequent long-term burial in marine sediments: Geochimica et Cosmochimica Acta, v. 64, p. 2233-2242.

Crusius, J., Calvert, S., Pedersen, T., and Sage, D., 1996, Rhenium and molybdenum enrichments in sediments as indicators of oxic, suboxic, and sulfidic conditions of deposition: Earth and Planetary Science Letters, v. 145, p. 65-78.

Dickin, A.P., 2005, Radiogenic Isotope Geology, 2nd edition: Cambridge, Cambridge University Press.

Esser, B.K., and Turekian, K.K., 1993, The osmium isotopic composition of the continental crust: Geochimica et Cosmochimica Acta, v. 57, p. 3093-3104.

Fanning, C.M., and Link, P.K., 2004, U-Pb SHRIMP ages of Neoproterozoic (Sturtian) glaciogenic Pocatello Formation, southeastern Idaho: Geology, v. 32, p. 881-884.

Gorokhov, I.M., Siedlecka, A., Roberts, D., Melnikov, N.N., and Turchenko, T.L., 2001, Rb-Sr dating of diagenetic illite in Neoproterozoic shales, Varanger Peninsula, northern Norway: Geological Magazine, v. 138, p. 541-562.

Gradstein, F.M., Ogg, J.G., and Smith, A.G., 2004, A Geologic Time Scale 2004: Cambridge, Cambridge University Press.

Hattori, Y., Suzuki, K., Honda, M., and Shimizu, H., 2003, Re-Os isotope systematics of the Taklimakan Desert sands, moraines and river sediments around the Taklimakan Desert, and of Tibetan soils: Geochimica et Cosmochimica Acta, v. 67, p. 1195-1205.

Hutcheon, I.D., and Olsen, E., 1991, Cr isotopic composition of differentiated meteorites: A search for ^{53}Mn: Lunar and Planetary Sciences, v. 22, p. 605-606.

Hutcheon, I.D., Olsen, E., Zipfel, J., and Wasserburg, G.J., 1992, Cr isotopic composition of differentiated meteorites: Evidence for ^{53}Mn: Lunar and Planetary Sciences, v. 23, p. 565-566.

Jaffe, L.A., Peucker-Ehrenbrink, B., and Petsch, S.T., 2002, Mobility of rhenium, platinum group elements and organic carbon during black shale weathering: Earth and Planetary Science Letters, v. 198, p. 339-353.

Jaffey, A.H., Flynn, K.F., Glendenin, L.E., Bentley, W.C., and Essling, A.M., 1971, Precision measurement of half-lives and specific activities of ^{235}U and ^{238}U: Physics Reviews, v. 4, p. 1889-1906.

Kendall, B.S., Creaser, R.A., Ross, G.M., and Selby, D., 2004, Constraints on the timing of Marinoan "Snowball Earth" glaciation by ^{187}Re-^{187}Os dating of a Neoproterozoic, post-glacial black shale in Western Canada: Earth and Planetary Science Letters, v. 222, p. 729-740.

Koide, M., Goldberg, E.D., Niemeyer, S., Gerlach, D., Hodge, V., Bertine, K.K., and Padova, A., 1991, Osmium in marine sediments: Geochimica et Cosmochimica Acta, v. 55, p. 1641-1648.

Lehrmann, D.J., Ramezani, J., Bowring, S.A., Martin, M.W., Montgomery, P., Enos, P., Payne, J.L., Orchard, M.J., Hongmei, W., and Jiayong, W., 2006, Timing of recovery from the end-Permian extinction: geochronologic and biostratigraphic constraints from south China: Geology, v. 34, p. 1053-1056.

Levasseur, S., Birck, J.-L., and Allègre, C.J., 1998, Direct measurement of femtomoles of osmium and the ^{187}Os/^{186}Os ratio in seawater: Science, v. 282, p. 272-274.

Levasseur, S., Birck, J.-L., and Allègre, C.J., 1999, The osmium riverine flux and the oceanic mass balance of osmium: Earth and Planetary Science Letters, v. 174, p. 7-23.

Lindner, M., Leich, D.A., Russ, G.P., Bazan, J.M., and Borg, R.J., 1989, Direct determination of the half-life of ^{187}Re: Geochimica et Cosmochimica Acta, v. 53, p. 1597-1606.

Luck, J.-M., and Allègre, C.J., 1983, ^{187}Re-^{187}Os systematics in meteorites and cosmochemical consequences: Nature, v. 302, p. 130-132.

Ludwig, K., 1998, Isoplot/Ex, version 1: A geochronological toolkit for Microsoft Excel: Geochronology Center Berkeley.

Ludwig, K., 2003, Isoplot/Ex, version 3: A geochronological toolkit for Microsoft Excel: Geochronology Center Berkeley.

Lugmair, G.W., and Galer, S.J.G., 1992, Age and isotopic relationships among angrites Lewis Cliff 86010 and Angra dos Reis: Geochimica et Cosmochimica Acta, v. 56, p. 1673-1694.

Lund, K., Aleinikoff, J.N., Evans, K.V., and Fanning, C.M., 2003, SHRIMP U-Pb geochronology of Neoproterozoic Windermere Supergroup, central Idaho: Implications for rifting of western Laurentia and synchroneity of Sturtian glacial deposits: Geological Society of America Bulletin, v. 115, p. 349-372.

Martin, C.E., Peucker-Ehrenbrink, B., Brunskill, G.J., and Szymczak, R., 2000, Sources and sinks of unradiogenic osmium runoff from Papua New Guinea: Earth and Planetary Science Letters, v. 183, p. 261-274.

McDaniel, D.K., Walker, R.J., Hemming, S.R., Horan, M.F., Becker, H., and Grauch, R.I., 2004, Sources of osmium to the modern oceans: new evidence from the ^{190}Pt-^{186}Os system: Geochimica et Cosmochimica Acta, v. 68, p. 1243-1252.

Meisel, T., Walker, R.J., and Morgan, J.W., 1996, The osmium isotopic composition of the Earth's primitive upper mantle: Nature, v. 383, p. 517-520.

Meisel, T., Walker, R.J., Irving, A.J., and Lorand, J.-P., 2001, Osmium isotopic compositions of mantle xenoliths: a global perspective: Geochimica et Cosmochimica Acta, v. 65, p. 1311-1323.

Morford, J.L., and Emerson, S., 1999, The geochemistry of redox sensitive trace metals in sediments: Geochimica et Cosmochimica Acta, v. 63, p. 1735-1750.

Morford, J.L., Emerson, S.R., Breckel, E.J., and Kim, S.H., 2005, Diagenesis of oxyanions (V, U, Re, and Mo) in pore waters and sediments from a continental margin: Geochimica et Cosmochimica Acta, v. 69, p. 5021-5032.

Morgan, J.W., Horan, M.F., Walker, R.J., and Grossman, J.N., 1995, Rhenium-osmium concentration and isotope systematics in group IIAB iron meteorites: Geochimica et Cosmochimica Acta, v. 59, p. 2331-2344.

Morton, J.P., 1985, Rb-Sr dating of diagenesis and source age of clays in Upper Devonian black shales of Texas: Geological Society of America Bulletin, v. 96, p. 1043-1049.

Nameroff, T.J., Balistrieri, L.S., and Murray, J.W., 2002, Suboxic trace metal geochemistry in the eastern tropical North Pacific: Geochimica et Cosmochimica Acta, v. 66, p. 1139-1158.

Oxburgh, R., 1998, Variations in the osmium isotope composition of seawater over the past 200,000 years: Earth and Planetary Science Letters, v. 159, p. 183-191.

Oxburgh, R., 2001, Residence time of osmium in the oceans: Geochemistry, Geophysics, Geosystems, Paper #2000GC000104.

Peucker-Ehrenbrink, B., 1996, Accretion of extraterrestrial matter during the last 80 million years and its effect on the marine osmium isotope record: Geochimica et Cosmochimica Acta, v. 60, p. 3187-3196.

Peucker-Ehrenbrink, B., and Hannigan, R.E., 2000, Effects of black shale weathering on the mobility of rhenium and platinum group elements: Geology, v. 28, p. 475-478.

Peucker-Ehrenbrink, B., and Ravizza, G., 2000, The marine osmium isotope record: Terra Nova, v. 12, p. 205-219.

Peucker-Ehrenbrink, B., and Jahn, B.-M., 2001, Rhenium-osmium isotope systematics and platinum group element concentrations: loess and the upper continental crust: Geochemistry Geophysics Geosystems, v. 2, Paper 2001GC000172.

Pierson-Wickmann, A.-C., Reisberg, L., and France-Lanord, C., 2000, The Os isotopic composition of Himalayan river bedloads and bedrocks: importance of black shales: Earth and Planetary Science Letters, v. 176, p. 203-218.

Pierson-Wickmann, A.-C., Reisberg, L., and France-Lanord, C., 2002, Behavior of Re and Os during low-temperature alteration: results from Himalayan soils and altered black shales: Geochimica et Cosmochimica Acta, v. 66, p. 1539-1548.

Poirier, A., 2006, Re-Os and Pb isotope systematics in reduced fjord sediments from Saanich Inlet (Western Canada): Earth and Planetary Science Letters, v. 249, p. 119-131.

Poplavko, Y.M., Ivanov, V.V., Karasik, T.G., Miller, A.D., Fadeyeva, V.A., Orekhov, V.S., Taliyev, S.D., and Tarkhov, Y.A., 1975, On the concentration of rhenium in petroleum, petroleum bitumens and oil shales: Geochemistry International, v. 11, p. 969-972.

Rankenburg, K., Brandon, A.D., and Humayun, M., 2007, Osmium isotope systematics of ureilites: Geochimica et Cosmochimica Acta, v. 71, p. 2402-2413.

Rasmussen, B., 2005, Radiometric dating of sedimentary rocks: the application of diagenetic xenotime geochronology: Earth-Science Reviews, v. 68, p. 197-243.

Ravizza, G., and Turekian, K.K., 1989, Application of the ^{187}Re-^{187}Os system to black shale geochronometry: Geochimica et Cosmochimica Acta, v. 53, p. 3257-3262.

Ravizza, G., and Turekian, K.K., 1992, The osmium isotopic composition of organic-rich marine sediments: Earth and Planetary Science Letters, v. 110, p. 1-6.

Ravizza, G., and Esser, B.K., 1993, A possible link between the seawater osmium isotope record and weathering of ancient sedimentary organic matter: Chemical Geology, v. 107, p. 255-258.

Ravizza, G., Turekian, K.K., and Hay, B.J., 1991, The geochemistry of rhenium and osmium in recent sediments from the Black Sea: Geochimica et Cosmochimica Acta, v. 55, p. 3741-3752.

Ravizza, G., Martin, C.E., German, C.R., and Thompson, G., 1996, Os isotopes as tracers in seafloor hydrothermal systems: Metalliferous deposits from the TAG hydrothermal area, 26°N Mid-Atlantic Ridge: Earth and Planetary Science Letters, v. 138, p. 105-119.

Richards, B.C., Ross, G.M., and Utting, J., 2002, U-Pb geochronology, lithostratigraphy and biostratigraphy of tuff in the upper Famennian to Tournaisian Exshaw Formation: Evidence for a mid-Paleozoic magmatic arc on the northwestern margin of North America, *in* Hills, L.V., et al., eds., Carboniferous and Permian of the World: Canadian Society of Petroleum Geologists Memoir, v. 19, p. 158-207.

Ripley, E.M., Park, Y.-R., Lambert, D.D., and Frick, L.R., 2001, Re-Os isotopic composition and PGE contents of Proterozoic carbonaceous argillites, Virginia Formation, Northeastern Minnesota: Organic Geochemistry, v. 32, p. 857-866.

Schoene, B., Crowley, J.L., Condon, D.J., Schmitz, M.D., and Bowring, S.A., 2006, Reassessing the uranium decay constants for geochronology using ID-TIMS U-Pb data: Geochimica et Cosmochimica Acta, v. 70, p. 426-445.

Selby, D., Direct rhenium-osmium age of the Oxfordian-Kimmeridgian boundary, Staffin Bay, Isle of Skye, UK and the Late Jurassic geologic timescale: Norwegian Journal of Geology, in press.

Selby, D., and Creaser, R.A., 2003, Re-Os geochronology of organic-rich sediments: an evaluation of organic matter analysis methods: Chemical Geology, v. 200, p. 225-240.

Selby, D., and Creaser, R.A., 2005a, Direct radiometric dating of the Devonian-Mississippian time-scale boundary using the Re-Os black shale geochronometer: Geology, v. 33, p. 545-548.

Selby, D., and Creaser, R.A., 2005b, Direct radiometric dating of hydrocarbon deposits using rhenium-osmium isotopes: Science, v. 308, p. 1293-1295.

Selby, D., Creaser, R.A., Dewing, K., and Fowler, M., 2005, Evaluation of bitumen as a ^{187}Re-^{187}Os geochronometer for hydrocarbon maturation and migration: a case study from the Polaris MVT deposit, Canada: Earth and Planetary Science Letters, v. 235, p. 1-15.

Selby, D., Creaser, R.A., and Fowler, M.G., 2007a, Re-Os elemental and isotopic systematics in crude oils: Geochimica et Cosmochimica Acta, v. 71, p. 378-386.

Selby, D., Creaser, R.A., Stein, H.J., Markey, R.J., and Hannah, J.L., 2007b, Assessment of the ^{187}Re decay constant by cross calibration of Re-Os molybdenite and U-Pb zircon chronometers in magmatic ore systems: Geochimica et Cosmochimica Acta, v. 71, p. 1999-2013.

Sharma, M., Papanastassiou, D.A., and Wasserburg, G.J., 1997, The concentration and isotopic composition of osmium in the oceans: Geochimica et Cosmochimica Acta, v. 61, p. 3287-3299.

Sharma, M., Wasserburg, G.J., Hofmann, A.W., and Butterfield, D.A., 2000, Osmium isotopes in hydrothermal fluids from the Juan de Fuca Ridge: Earth and Planetary Science Letters, v. 179, p. 139-152.

Shen, J.J., Papanastassiou, D.A., and Wasserburg, G.J., 1996, Precise Re-Os determinations and systematics of iron meteorites: Geochimica et Cosmochimica Acta, v. 60, p. 2887-2900.

Shen, J.J., Papanastassiou, D.A., and Wasserburg, G.J., 1998, Re-Os systematics in pallasite and mesosiderite metal: Geochimica et Cosmochimica Acta, v. 62, p. 2715-2723.

Shirey, S.B., and Walker, R.J., 1995, Carius tube digestion for low-blank rhenium-osmium analysis: Analytical Chemistry, v. 67, p. 2136-2141.

Shirey, S.B., and Walker, R.J., 1998, The Re-Os isotope system in cosmochemistry and high temperature geochemistry: Annual Reviews of Earth and Planetary Sciences, v. 26, p. 423-500.

Shukolyukov, A., and Lugmair, G.W., 1997, The ^{53}Mn-^{53}Cr isotope system in the Omolon pallasite and the half-life of ^{187}Re: Lunar and Planetary Sciences Abstracts, v. 28, p. 1315-1316.

Singh, S.K., Trivedi, J.R., and Krishnaswami, S., 1999, Re-Os isotope systematics in black shales from the Lesser Himalaya: their chronology and role in the ^{187}Os/^{188}Os evolution of seawater: Geochimica et Cosmochimica Acta, v. 63, p. 2381-2392.

Smoliar, M.I., Walker, R.J., and Morgan, J.W., 1996, Re-Os ages of Group IIA, IIIA, IVA, and IVB iron meteorites: Science, v. 271, p. 1099-1102.

Sun, W., Arculus, R.J., Bennett, V.C., Eggins, S.M., and Binns, R.A., 2003a, Evidence for rhenium enrichment in the mantle wedge from submarine arc-like volcanic glasses (Papua New Guinea): Geology, v. 31, p. 845-848.

Sun, W., Bennett, V.C., Eggins, S.M., Kamenetsky, V.S., and Arculus, R.J., 2003b, Enhanced mantle-to-crust rhenium transfer in undegassed arc magmas: Nature, v. 422, p. 294-297.

Sundby, B., Martinez, P., and Gobeil, C., 2004, Comparative geochemistry of cadmium, rhenium, uranium, and molybdenum in continental margin sediments: Geochimica et Cosmochimica Acta, v. 68, p. 2485-2493.

Trapp, E., Kaufmann, B., Mezger, K., Korn, M., and Weyer, D., 2004, Numerical calibration of the Devonian-Mississippian boundary: Two new U-Pb isotope dilution-thermal ionization mass spectrometry single-zircon ages from Hasselbachtal (Sauerland, Germany): Geology, v. 32, p. 857-860.

Tucker, R.D., Bradley, D.C., Ver Straeten, C.A., Harris, A.G., Erbert, J.R., and McCutcheon, S.R., 1998, New U-Pb zircon ages and the duration and division of Devonian time: Earth and Planetary Science Letters, v. 158, p. 175-186.

Turgeon, S.C., and Creaser, R.A., 2007, Widespread Os isotope evidence for a magmatic pulse at the onset of Oceanic Anoxic Event 2: Geochimica et Cosmochimica Acta, v. 71 (15; supplement 1), p. A1042.

Turgeon, S.C., Creaser, R.A., and Algeo, T.J., 2007, Re-Os depositional ages and seawater Os estimates for the Frasnian-Famennian boundary: Implications for weathering rates, land plant evolution, and extinction mechanisms: Earth and Planetary Science Letters, v. 261, p. 649-661.

Völkening, J., Walczyk, T., and Heumann, K.G., 1991, Osmium isotope ratio determinations by negative thermal ionization mass spectrometry: International Journal of Mass Spectrometry and Ion Processes, v. 105, p. 147-159.

Walczyk, T., Hebeda, E.H., and Heumann, K.G., 1991, Osmium isotope ratio measurements by negative thermal ionization mass spectrometry (NTI-MS): Improvement in precision and enhancement in emission by introducing oxygen or Freon into the ion source: Fresenius' Journal of Analytical Chemistry, v. 341, p. 537-541.

Walker, R.J., Horan, M.F., Morgan, J.W., Becker, H., Grossman, J.N., and Rubin, A.E., 2002a, Comparative ^{187}Re-^{187}Os systematics of chondrites: implications regarding early solar system processes: Geochimica et Cosmochimica Acta, v. 66, p. 4187-4201.

Walker, R.J., Prichard, H.M., Ishiwatari, A., and Pimentel, M., 2002b, The osmium isotopic composition of convecting upper mantle deduced from ophiolite chromites: Geochimica et Cosmochimica Acta, v. 66, p. 329-345.

Woodhouse, O.B., Ravizza, G., Falkner, K.K., Statham, P.J., and Peucker-Ehrenbrink, B., 1999, Osmium in seawater: vertical profiles of concentration and isotopic composition in the eastern Pacific Ocean: Earth and Planetary Science Letters, v. 173, p. 223-233.

Woodland, S.J., Ottley, C.J., Pearson, D.G., and Swarbrick, R.E., 2001, Microwave digestion of oils for analysis of platinum group and rare earth elements by ICP-MS, *in* Plasma Source Mass Spectrometry: Special Publication Royal Society of Chemistry, p. 17-24.

Yamashita, Y., Takahashi, Y., Haba, H., Enomoto, S., and Shimizu, H., 2007, Comparison of reductive accumulation of Re and Os in seawater-sediment systems: Geochimica et Cosmochimica Acta, v. 71, p. 3458-3475.

York, D., 1966, Least-squares fitting of a straight line: Canadian Physics, v. 44, p. 1079-1086.

CHAPTER 2

Re-Os, Mo, and Fe Isotope Systematics of Black Shales from the 635 – 551 Ma Doushantuo Formation, South China

Part of this chapter has been submitted to the following source:
Kendall, B., Creaser, R.A., and Selby D., ^{187}Re-^{187}Os geochronology of Precambrian organic-rich sedimentary rocks: Geological Society (London) Special Publication, Accepted.

2.1 INTRODUCTION

In March 2004, the International Union of Geological Sciences (IUGS) formally added the Ediacaran Period to the geological timescale (Knoll et al., 2004, 2006). The initial global stratotype point and section (GSSP) for the Ediacaran Period (located at Enorama Creek, Flinders Ranges, South Australia) lies at the base of the Nuccaleena Formation cap carbonate. The end of the Ediacaran Period coincides with the Precambrian-Cambrian boundary (~ 542 Ma; Amthor et al., 2003). Although a direct radiometric age constraint for the initial GSSP of the Ediacaran Period is absent, the underlying glaciogenic Elatina Formation has been correlated (on the basis of pre-glacial negative $\delta^{13}C$ excursions and cap carbonate litho- and chemo-stratigraphy; Hoffman et al., 1998; Kennedy et al., 1998; McKirdy et al., 2001; Hoffman and Schrag, 2002; Zhou et al., 2004; Halverson et al., 2005; Halverson, 2006) with ca. 635 Ma glacial deposits in Namibia (Ghaub Formation; Hoffmann et al., 2004), and South China (Nantuo Formation; Condon et al., 2005; Yin et al., 2005; Zhang et al., 2005). Alternatively, the Elatina Formation has been correlated with younger (ca. 582-575 Ma) glacial deposits from Tasmania (Croles Hill Diamictite) and King Island (Cottons Breccia) and may have been deposited during the < 1 M.y. long Gaskiers glaciation at ca. 580 Ma (Bowring et al., 2003; Calver et al., 2004). Thus, the Ediacaran Period is between ~ 35 M.y. and ~ 90 M.y. in duration.

Concerning the Earth's paleontological record, the Ediacaran Period bridges the predominantly unicellular prokaryotic and eukaryotic life of the Precambrian with the diverse and complex multicellular organisms characteristic of the Phanerozoic Eon. The name of the period is derived from the spectacular exposures at Ediacara Hills, South Australia, of dominantly soft-bodied, macroscopic metazoans (Ediacara Biota; Sprigg, 1947). These organisms represent the first unambiguous large animals to appear in the fossil record. Some biota and trace fossils may represent primitive members of animal clades (e.g., bilaterians and cnidarians; Narbonne, 1998; Knoll and Carroll, 1999; Bottjer and Clapham, 2006; Jensen et al., 2006), but some have no Phanerozoic analogues (e.g., rangeomorphs; Narbonne, 2004). Early animal evolution in the Neoproterozoic occurred during a time following Rodinia supercontinent breakup and during Gondwana/Pan-African amalgamation (Derry et al., 1992; Kaufman et al., 1993; Kaufman and Knoll, 1995; Jacobsen and Kaufman, 1999; Walter et al., 2000; Squire et al., 2006), multiple episodes of global or near-global glaciation ("Snowball" or "Slushball" Earth; Harland, 1964; Kirschvink, 1992; Hoffman et al., 1998; Kennedy et al., 1998; Hyde et al., 2000; Hoffman and Schrag, 2002), a bolide impact (Acraman event, southern Australia; Grey et al., 2003), a possible major decrease in ocean salinity (Knauth, 2006), and one or more increases in atmosphere and ocean oxygen abundances (Knoll et al., 1986; Knoll, 1991; Derry et al., 1992; Des Marais et al., 1992; Canfield and Teske, 1996; Hurtgen et al., 2005; Fike et al., 2006; Kennedy et al., 2006; Canfield et al., 2007). These events had far-reaching, but poorly understood, effects on the radiation and diversification of macroscopic metazoans.

Molecular clocks yield conflicting information regarding eukaryotic kingdom (Paleoproterozoic to Early Mesoproterozoic, or Late Mesoproterozoic to Early Neoproterozoic) and animal phyla (Late Mesoproterozoic to Early Neoproterozoic or Late Neoproterozoic/Ediacaran) diversification times (Hedges et al., 2006 and references therein). Recently, biomarkers diagnostic of demosponges have been discovered in the Huqf Supergroup (Oman; Love et al., 2006). The oldest known fossils that may represent Ediacaran-type fauna are preserved as simple, low-diversity cm-scale rings and discs in the Twitya Formation of the Windermere Supergroup (Mackenzie Mountains, Canada; Hofmann et al., 1990). In both cases, the host stratigraphic units lie between glacial intervals suggested to be correlative with the "Sturtian" (e.g., 750-685 Ma) and "Marinoan" (e.g., 635 Ma Ghaub-Nantuo) glaciations (see Chapter 3). In South China, the first direct evidence for multicellular animal life in the fossil record is preserved as part of a diverse and unique fossil assemblage in the Doushantuo Formation (bracketed between 635.2 ± 0.6 Ma and 551.1 ± 0.6 Ma by U-Pb zircon ages from ash beds at its base and top; Condon et al., 2005) that includes protists, simple spheroidal and complex acanthomorphic acritarchs (Zhang et al., 1998; Xiao, 2004a; Zhou et al., 2007), multicellular algae (Xiao et al., 1998a, 2002; Xiao, 2004a), fungi (Yuan et al., 2005), and micrometazoans such as sponges (Li et al., 1998), cnidarians (Xiao et al., 2000; Chen et al., 2002; Xiao et al., 2002), and bilaterians (Chen et al., 2004a). This assemblage may also include the oldest known animal eggs and embryos (Xiao et al., 1998a, 2007; Xiao and Knoll, 2000; Chen et al., 2006; Hagadorn et al., 2006; Yin et al., 2007; see Bailey et al., 2007, for an alternative interpretation as giant sulfur-oxidizing bacteria). Recently, acanthomorphic acritarchs have been shown to host cleavage stage animal embryos, suggesting the acritarchs are egg cysts (Yin et al., 2007). Identical acritarchs are preserved in dolomitic shales just above a 632.5 ± 0.5 Ma ash bed (U-Pb zircon age; Condon et al., 2005), suggesting stem-group animals may have flourished in the Neoproterozoic oceans immediately following the meltback of the ca. 635 Ma Nantuo/Ghaub glaciation (Hagadorn et al., 2006; Yin et al., 2007). Pb-Pb dating of phosphorites suggests the most diverse fossil assemblages preserved in the upper Doushantuo Formation have an age between 576 ± 14 Ma and 599.3 ± 4.2 Ma (Barfod et al., 2002; Chen et al., 2004b). However, Condon et al. (2005) question the accuracy of these radiometric ages, and instead suggest a maximum age of ca. 580 Ma for the diverse fossil assemblages based on interpretation of a karstic sequence boundary in the middle Doushantuo Formation (at the Weng'an locality) as a manifestation of glacio-eustatic sea-level fall associated with the Gaskiers glaciation.

The first unequivocal macroscopic Ediacaran metazoans (Mistaken Point assemblage) are preserved in the ca. 575 Ma Drook Formation (Conception Group, Avalon Peninsula, Newfoundland) (U-Pb zircon age from an ash bed; Bowring et al., 2003; Narbonne and Gehling, 2003). Diverse Ediacaran fauna are also preserved in the overlying Briscal and Mistaken Point Formations (Conception Group) and Trepassey and Fermeuse Formations (St. John's Group) (Clapham and Narbonne, 2002; Narbonne, 2004; Gehling and Narbonne, 2007). Volcanic ash near the top of the Mistaken Point Formation buried these organisms at 565 ± 3 Ma (U-Pb zircon age; Benus, 1988). During late Ediacaran time, faunal assemblages reached their peak diversity (Bottjer and Clapham, 2006), with the first establishment of motile and burrowing forms (including the oldest known bilaterian, *Kimberella*) by 555.3 ± 0.3 Ma (U-Pb zircon age from an ash bed, Zimnie Gory section, White Sea region, Russia; Martin et al., 2000; Grazhdankin, 2004). An U-Pb zircon age of 548.8 ± 1 Ma for an ash bed in the Hoogland Member (Kuibis Subgroup, Namibia) represents a minimum age for small Ediacaran-type biomineralized fossils (e.g., *Cloudina*) (Grotzinger et al., 1995). Together with age constraints from the White Sea region, the most diverse Ediacaran metazoans likely span at least 12 million years prior to the Precambrian-Cambrian boundary. The appearance of

Kimberella (and other planktonic bilaterians with guts), algae with resistant cell wall biopolymers, planktonic animals with guts, small shelly fossils (Rothman et al., 2003), and Ediacaran-type trace fossils (Jensen et al., 2006) may be associated with one or more negative carbon isotope excursions that is preserved in strata from South China (Jiang et al., 2007; Zhou and Xiao, 2007), Namibia (Saylor et al., 1998), South Australia (Calver, 2000), western United States (Corsetti and Kaufman, 2003; Kaufman et al., 2007), Oman (Fike et al., 2006; Le Guerroué et al., 2006a, b), and possibly Norway (Melezhik et al., 2005) and India (Kaufman et al., 2006). These excursions may reflect oxidation of a large dissolved deep-ocean organic carbon reservoir (Rothman et al., 2003; Jiang et al., 2007) that in turn may have been followed by ocean anoxia, elevated organic carbon burial, and concomitant deep ocean oxygenation (Condon et al., 2005; Fike et al., 2006; Jiang et al., 2007).

The Doushantuo Formation represents a critical stratigraphic interval for characterizing the paleoenvironmental conditions under which some of the earliest animals thrived. Presently, the chronology of the upper Doushantuo Formation diverse fossil assemblages with respect to well-dated sections elsewhere (e.g., Mistaken Point assemblage, Newfoundland) remains poorly constrained. Radiometric calibration of the Doushantuo Formation and other Ediacaran sections (e.g., Australia) are ultimately required for evaluating: 1) the ca. 580 Ma Gaskiers glaciation as a stimulus for Ediacaran metazoan diversification (Narbonne and Gehling, 2003), 2) the ca. 635 Ma Nantuo/Ghaub glaciation (Hoffman and Schrag, 2002), Acraman bolide impact (of unknown age; Grey et al., 2003), and evolution of grazing eumetazoans (Peterson et al., 2004; Peterson and Butterfield, 2005) as explanations for the radiation of "Doushantuo-Pertatataka" acanthomorphic acritarchs, and 3) the Gaskiers glaciation (Xiao, 2004b; Xiao et al., 2004), evolution of Ediacaran metazoans (Huntley et al., 2006; Zhou et al., 2007), and shallow water anoxia (Jiang et al., 2007) as explanations for the demise of "Doushantuo-Pertatataka" acritarchs. In addition, the timing and duration of the Ediacaran negative carbon isotope excursion(s) (and its relationship to the Gaskiers glaciation; Halverson et al., 2005; Halverson, 2006) is poorly constrained, and has been estimated on the basis of U-Pb zircon age constraints, sediment accumulation rates, and thermal subsidence modelling to be between 1-2 and 10-11 M.y. (Saylor et al., 1998;

Condon et al., 2005), or as long as 50 M.y. (Le Guerroué et al., 2006b). The Doushantuo Formation contains abundant organic-rich shale horizons in its lower (Member 2) and upper (Member 4) sections. Selby and Creaser (2005) have demonstrated that black shales can yield Re-Os depositional ages that are both precise and accurate. Thus, Re-Os depositional age determinations on the Doushantuo Formation black shales have the potential to address the above issues as well as provide an improved radiometric calibration of the Ediacaran rock record.

Recent application of Fe redox proxies (e.g., degree-of-pyritization [DOP] and highly reactive iron to total iron ratios [Fe_{HR}/Fe_T]) to deep-sea marine sediments deposited before, during, and after the Gaskiers glaciation suggests the deep ocean became oxidizing after the end of glaciation and was followed within 5 M.y. by the appearance of Ediacaran biota (Canfield et al., 2007). However, Fe redox proxies do not uniquely determine if the post-Gaskiers oxygenation event was a local or global phenomenon. Carbon and sulfur isotope data from Oman point towards the possibility of multiple oxygenation events during late Neoproterozoic/Ediacaran time (Fike et al., 2006). However, radiometric age constraints and the geobiological record are insufficient for reliable global correlations between Oman and other Ediacaran sections, and significant intra- and inter-continental variability is present in the Ediacaran chemostratigraphic record (e.g., Kaufman and Knoll, 1995; Kaufman et al., 1997; Calver and Lindsay, 1998; Saylor et al., 1998; Calver, 2000; Corsetti and Kaufman, 2003; Halverson et al., 2005; Fike et al., 2006; Kaufman et al., 2006; Le Guerroué et al., 2006a, b; Jiang et al., 2007; Zhou and Xiao, 2007). Accordingly, neither study has uniquely constrained the temporal evolution of the atmosphere and ocean redox state during the Late Neoproterozoic Era.

Molybdenum and iron isotopes in euxinic black shales show excellent promise as ocean paleoredox proxies. Black shales may record the Mo isotope composition of contemporaneous seawater if Mo uptake from the immediately overlying euxinic water column and pore waters is quantitative (Barling et al., 2001; Arnold et al., 2004). Fractionation of seawater Mo isotopes relative to lithogenic sources occurs predominantly in association with adsorption of isotopically light Mo onto Mn nodules in oxic environments (Barling et al., 2001; Siebert et al., 2003; Barling and Anbar, 2004).

Recent studies suggest much smaller Mo isotope fractionation occurs upon Mo uptake into reducing sediments in anoxic/non-sulfidic environments (Poulson et al., 2006). Consequently, the ocean Mo isotope budget is sensitive to the redox state (e.g., oxic versus euxinic) of the global deep oceans (Barling et al., 2001; Siebert et al., 2003; Arnold et al., 2004). Bulk and pyrite Fe isotope analyses of modern sediments and ancient black shales have shown that Fe isotopes can be used to recognize ancient euxinia within sedimentary basins, and may track the nature of Fe redox cycling within ocean basins over geological time (Rouxel et al., 2005; Yamaguchi et al., 2005; Archer and Vance, 2006; Severmann et al., 2006a, b; Duan et al., 2006, 2007). Thus, the Mo and Fe isotope and trace metal redox proxies, together with improved radiometric age constraints for the Doushantuo Formation, holds tremendous potential for an improved understanding of the link between the evolution of primitive animal life and the timing and nature of Ediacaran-age carbon isotope excursions, ocean and atmosphere oxygenation, and glaciation. In this chapter, preliminary Re-Os radioisotope, Mo and Fe stable isotope, and trace metal data are presented for the Doushantuo Formation.

2.2 DOUSHANTUO AND DENGYING FORMATIONS, SOUTH CHINA

Late Neoproterozoic strata of the 635-551 Ma Doushantuo and 551-542 Ma Dengying Formations were deposited on a passive continental margin located on the southeastern portion of the Yangtze Block (Jiang et al., 2003a). In the Yangtze Gorges area, the Doushantuo Formation comprises up to 250 m of unmetamorphosed phosphorites, carbonates, and fine-grained, organic-rich siliciclastic sedimentary rocks that were deposited in the shallow-water Western Hubei platform (Figure 2.1; Wang et al., 1998; Xiao et al., 1998a; Zhang et al., 1998; Jiang et al., 2003a; Zhu et al., 2003; Zhou and Xiao, 2007). The Western Hubei platform was surrounded by the deep-water Hunan – Guangxi (HG) basin. Numerous studies based on carbon isotope chemostratigraphy have been carried out on the Doushantuo and overlying dolomitic Dengying Formations, and is summarized by Zhou and Xiao (2007) who, along with Jiang et al. (2007), have produced updated composite carbonate carbon isotope curves based on data from shallow-water platform sections on the Yangtze Block.

Recently, two main schemes have been utilized for subdividing the Doushantuo Formation into four informal members: Members 1 through 4 (based on lithology; Wang et al., 1998; Zhu et al., 2003; Zhou and Xiao, 2007) and Lower Dolomite Member, Lower Sequence, Upper Sequence, and Miaohe Member (based on sequence stratigraphy; Jiang et al., 2003a; Condon et al., 2005) (Figure 2.2). The basal Member 1 is equivalent to the Lower Dolomite Member (~ 5 m thick), and represents the post-glacial cap carbonate to the disconformably underlying glaciogenic Nantuo Formation. Distinctive sedimentary structures (e.g., aragonite fans, sheet cracks, tepee-like structures, and methane-seep related stromatactis-like structures; Jiang et al., 2003b, 2006; Zhou et al., 2004) and geochemical features (e.g., upward decreasing $\delta^{13}C_{carb}$ isotope excursion to values less than –5‰; referred to as "EN1" and "N1" in Zhou and Xiao, 2007 and Jiang et al., 2007, respectively) of Member 1 are similar to other cap carbonates above glacial diamictites (e.g., Ghaub and Elatina Formations) suggested to represent the product of a near-global ("Slushball Earth") or global ("Snowball" Earth) glaciation that ended at ca. 635 Ma (Kennedy et al., 1998; Hoffman and Schrag, 2002; Hoffmann et al., 2004; Condon et al., 2005). Paleomagnetic data from Member 1 also suggests deposition took place at equatorial paleo-latitudes (3.0±4.5°N; Macouin et al., 2004).

Subdivision of the middle Doushantuo Formation using sequence stratigraphy is based on a sequence boundary that separates the transgressive Lower and Upper Sequences. In the Yangtze Gorges region, each sequence comprises a basal black shale and phosphorite interval that is gradually overlain by dolomitic micrite (Jiang et al., 2003a; Condon et al., 2005). In the alternative lithological subdivision, Member 2 comprises 150 m of black shale with thin interbeds of dolomite, and contains abundant chert nodules at multiple stratigraphic horizons. The postulated sequence boundary in the Yangtze Gorges region may be near the top of Member 2, but is not well-defined (Zhou and Xiao, 2007). The stratigraphically overlying Member 3 is composed predominantly of 80 m of dolostone interbedded with thin chert layers (Wang et al., 1998; Zhu et al., 2003; Zhou and Xiao, 2007). Acanthomorphic acritarchs, sponge spicules, multicellular macroscopic and red algae, and possible animal embryos are present in chert nodules of Member 2, but the most diverse assemblages are preserved in chert nodules and horizons of Member 3 (Zhang et al., 1998; Xiao, 2004a; Zhou and Xiao, 2007; Yin et al., 2007;

Zhou et al., 2007). The appearance of Member 2 fossils coincides broadly with a positive carbon isotope excursion ("EP1"; $\delta^{13}C_{carb} > +5‰$; Zhou and Xiao, 2007) (Figure 2.3). An excursion to negative values occurs near the interface of Members 2 and 3 ("EN2" and "N2"; to –5‰), and is followed by a positive excursion ("EP2"; up to ~ +5‰) (Jiang et al., 2007; Zhou and Xiao, 2007).

At proximal sections such as Weng'an, the Doushantuo Formation above the cap carbonate is much thinner and contains a lower phosphorite bed (1-5 m thick) and upper phosphorite bed (6-12 m thick) sandwiched by dolomite (up to 4 m thick) (Chen et al., 2003; Chen et al., 2004b). A subaerial karstic unconformity present at the top of the dolomite layer may correspond to the sequence boundary between the Lower and Upper Sequences (Xiao et al., 1998a; Condon et al., 2005). Whereas the upper phosphorite bed preserves diverse fossil assemblages (including animal eggs and embryos; Zhang et al., 1998; Xiao et al., 1998a, 2000; 2007; Li et al., 1998; Xiao and Knoll, 2000; Chen et al., 2002, 2004a, 2006; Yuan et al., 2005; Hagadorn et al., 2006), the lower phosphorite bed is barren. This observation likely reflects taphonomic bias because rare-earth-element data (e.g., Ce anomalies) suggests the lower and upper phosphorite beds were deposited under anoxic and oxic conditions, respectively (Chen et al., 2003; Zhou et al., 2007).

A sequence boundary between Members 3 and 4 in the Yangtze Gorges region (Wang et al., 1998) may represent a potentially long-lived hiatus, and may be correlative with a karstic subaerial exposure surface just below the Doushantuo-Dengying contact at Weng'an (Zhou and Xiao, 2007). The uppermost Doushantuo Formation is represented by the fossiliferous Member 4 (up to 20 m thick; also equivalent to the Miaohe Member) which comprises siliceous, organic-rich (TOC reaching > 10%; Jiang et al., 2007) black shale deposited in a quiet-water, restricted (possibly lagoonal), subtidal environment (Wang et al., 1998; Xiao et al., 1998b). Member 4 may form the lower part of a third transgressive sequence that ends in the overlying Dengying Formation (e.g., Condon et al., 2005). This member is not observed in proximal sections such as at Weng'an. Carbonaceous compression fossils of prokaryotes, macroscopic multicellular algae, and metazoans (cnidarians) on Miaohe Member shales have been described as a Burgess-Shale-type taphonomic window into latest Neoproterozoic biology (Xiao et al., 2002). "Doushantuo-Pertatataka" acritarchs are not present in Member 4 (Zhou et al., 2007). An excursion to negative $\delta^{13}C_{carb}$ values ($< -5‰$) begins at the top of Member 3 ("EN3" and "N3"), continues in Member 4, and ends with a transition back to positive values in the basal Dengying Formation (Jiang et al., 2007; Zhou and Xiao, 2007).

Conformably overlying the Doushantuo Formation in the Yangtze Gorges region is the 240-850 m thick Dengying Formation that is subdivided into the lower Hamajing (light gray dolostone with thin chert layers), middle Shibantan (dark gray limestone), and upper Baimatuo Members (light gray dolostone) (Wang et al., 1998; Zhu et al., 2003; Zhou and Xiao, 2007). Macroscopic Ediacaran metazoan fossils, vendotaenid algae and horizontal trace fossils similar to *Planolites* occur in the Shibantan Member (e.g., Sun, 1986; Xiao et al., 2005), and Ediacaran-type small shelly fossils (*Cloudina*-like tubular fossils; Bengtson and Zhao, 1992; Hua et al., 2005) and *Skolithus*-like trace fossils (Wang et al., 1998) are present in the Baimatuo Member. Disconformably overlying the Baimatuo Member are phosphatic dolostones of the basal Cambrian Tianzhushan Member (Yanjiahe Formation; equivalent to Zhujiaqing Formation) that contain Early Cambrian small shelly fossils and *Micrhystridium*-like acritarchs (Qian et al., 1979; Ding et al., 1992; Zhou and Xiao, 2007). A positive carbon isotope excursion ("EP3"; $> +5‰$) in the lower Dengying Formation is followed upsection by a slightly positive $\delta^{13}C$ plateau ($\sim +2.5‰$). The carbon isotope curve of the Ediacaran Period in South China closes with a marked negative $\delta^{13}C_{carb}$ excursion ("EN4" and "N4"; +3‰ to $< -10‰$) just below the Precambrian-Phanerozoic boundary (Jiang et al., 2007; Zhou and Xiao, 2007).

2.3 SAMPLES AND ANALYTICAL METHODS

Unmetamorphosed outcrop samples of the Doushantuo and Dengying Formations were obtained in collaboration with Dr. Ganqing Jiang (University of Nevada) and Dr. Martin Kennedy (University of California, Riverside). The samples are from the Jijiapo outcrop section that is less than 20 km from the outcrop sections containing ash beds sampled for U-Pb zircon geochronology (these sections are within the Yangtze Gorges region; Condon et al., 2005; Yin et al., 2005; Zhang et al., 2005; Zhou and Xiao, 2007). Doushantuo Formation samples include a whole-rock sample (H_1O_1; dark-colored, finely-laminated shaly limestone; Plate 2.1) from the base of Member 2, three finely-laminated black shale samples from the lower (H_1O_4) to middle (H_1O_9, H_1O_{14}) Member 2 (Plate

2.2), and two finely-laminated black shale samples (H_1O_{16}-A, B) containing abundant disseminated pyrite from the top of Member 2. From each of these whole rocks, sub-samples ranging in size from 4 g to 18 g were processed to fine powder. Four samples of very black finely-laminated shale from Member 4 (from stratigraphically lowest to highest over a ~ 3.5 m interval: H_1O_{18}, H_1O_{19}, H_1O_{20}, H_1O_{21}) were sub-sampled into fractions of $\leq$ 10 g and $\geq$ 20 g of material (Plate 2.3). Disseminated and framboidal pyrite are clearly visible in H_1O_{18}, H_1O_{19}, H_1O_{20}, but not in H_1O_{21}; the latter sample is the most organic-rich shale based on color. The Doushantuo Formation samples appear fresh and devoid of secondary alteration. Single sub-samples of bituminous gray to dark gray limestone (ranging between 6 g and 22 g of material) were also prepared from four samples of the Shibantan Member, Dengying Formation (from stratigraphically lowest to highest: H_1O_{26}, H_1O_{32}, H_1O_{33}, H_1O_{36}). Sample H_1O_{32} contains abundant thin organic-rich laminae. Diagenetic carbonate veinlets are visible in samples H_1O_{26} and H_1O_{36} (Plate 2.4).

Protocols for metal-free processing of organic-rich sedimentary rocks (ORS) to produce powdered samples, subsequent chemical digestion, separation, and purification of Re and Os, and isotopic analysis by isotope dilution – negative thermal ionization mass spectrometry (ID-NTIMS) are described in Appendix A. Chemical digestion, separation, purification, and isotopic analysis of Mo and Fe by multiple collector – inductively coupled plasma – mass spectrometry (MC-ICP-MS) was carried out following the methods outlined in Appendix B. In addition, trace metal abundances of sample powders were determined by quadrupole – inductively coupled plasma – mass spectrometry (Q-ICP-MS) (Appendix C.1). Sample degree-of-pyritization (DOP) was determined following the protocols outlined in Appendix C.3.

Except for some sub-samples from whole rocks H_1O_4, H_1O_9, and H_1O_{14}, all sub-samples were analyzed for their Re and Os isotope composition. Total Re procedural blanks based on Cr^{VI}-H_2SO_4 digestions using batches of CrO_3 from Fisher Scientific and Fluka Chemika were unacceptably high at ~ 73 pg (n = 1) and 60.1 ± 5.2 pg (1σ, n = 3), respectively. This Re contamination represented at least a few percent of the Re present in samples, with the exception of the Re-rich shales of Member 4. In contrast, blank Os abundances for the Fisher Scientific and Fluka Chemika CrO_3 were acceptably low, and averaged 0.65 ± 0.17 pg (1σ, $n = 4$) and 0.39 ± 0.03 pg (1σ, $n = 2$), respectively, with blank $^{187}Os/^{188}Os$ of 0.19 ± 0.06 (1σ, $n = 4$) and 0.22 ± 0.08 (1σ, $n = 2$), respectively. Low procedural Re blank abundances (< 1 pg) from anion exchange column chromatography of purified 4N H_2SO_4 solutions suggests most of the background Re contamination is derived from these CrO_3 powders. Attempts were made to purify CrO_3 solutions through chelation of Re by organic solvents dissolved in chloroform, but this approach was not successful (see Appendix A for further details). Ultimately, batches of Fluka Chemika CrO_3 with acceptably low Re procedural blanks (5 pg to 20 pg) were identified and used for Re-Os digestions of black shales described in subsequent chapters in this thesis (except Horsethief Creek Group shales and carbonates [Chapter 4] studied prior to study of the Doushantuo and Dengying Formations).

Trace metal abundances and Fe isotope compositions were determined for selected sub-samples from Members 2 and 4 of the Doushantuo Formation. Molybdenum isotope compositions and metal abundances were obtained from the same $HF\text{-}HNO_3\text{-}HCl$ acid digestion (Appendix B) whereas Fe isotope analyses were derived from a separate acid digestion. Molybdenum and Fe isotope data are reported using the conventional per-mil delta (δ) notation:

$$\delta R_{sample}\ (‰) = [R_{sample}/R_{standard} - 1] \times 1000 \qquad (1)$$

where R = isotope ratio ($\delta^{97/95}Mo$ or $\delta^{56/54}Fe$). Sample $\delta^{97/95}Mo$ is reported relative to the Johnson Matthey Specpure® Mo plasma standard (Lot #802309E; RochMo2) which has an identical Mo isotopic composition as the RochMo standard (Lot #7024991) used at the University of Rochester (Anbar et al., 2001; Barling et al., 2001; Arnold et al., 2004). Iron isotope analyses are reported as $\delta^{56/54}Fe$ relative to the IRMM-014 standard (Taylor et al., 1992).

2.4 RESULTS

2.4.1 Re-Os Isotopes

Rhenium and Os isotope data for the Doushantuo and Dengying Formations are presented in Table 2.1, and trace metal, DOP, and Mo and Fe isotope analyses for Member 2 black shales of the Doushantuo Formation are presented in Table 2.2. The shaly limestone sample from the base of Member 2 (H_1O_1) has low Re (~ 0.3-0.4 ppb) and Os (47-55 ppt) abundances that are comparable to average crustal values (~ 0.2-2 ppb Re and 30-50 ppt Os; Esser and Turekian 1993; Peucker-Ehrenbrink and Jahn 2001; Hattori et al., 2003; Sun et al., 2003a, b). All four sub-samples yield low and uniform ^{187}Re/^{188}Os (31-44) and ^{187}Os/^{188}Os (0.85-0.91) isotope ratios that do not enable a meaningful regression. Bituminous limestone from the Shibantan Member of the Dengying Formation also contains low Re abundances (0.1-0.7 ppb) comparable to average crust, but has lower Os abundances (5-21 ppt), and a wide range in ^{187}Re/^{188}Os (74-626) and ^{187}Os/^{188}Os (0.74-5.21) isotope ratios. Regression of the Shibantan Member Re-Os isotope data yields an imprecise date of 459 ± 230 Ma (2σ, n = 4, Mean Square of Weighted Deviates [MSWD] = 192, Model 3, initial ^{187}Os/^{188}Os [I_{Os}] = 0.5 ± 1.3) (Figure 2.4A).

Member 2 black shales are moderately enriched in Re (2.6-5.3 ppb) and Os (78-157 ppt) abundances relative to average crust, whereas Member 4 black shales are highly enriched in Re (30-566 ppb) and Os (1.14-8.24 ppb). Isotope ratios for ^{187}Re/^{188}Os and ^{187}Os/^{188}Os are between 117 and 236, and between 1.8 and 3.0, respectively, for Member 2, and between 169 and 617, and between 2.4 and 6.8, respectively, for Member 4. Duplicate analyses of ≥ 20 g aliquots of Member 4 shale show excellent reproducibility in Re and Os abundances (< 3% variation), and ^{187}Re/^{188}Os and ^{187}Os/^{188}Os isotope ratios (< 2% variation), suggesting that any nugget effect is generally absent from these aliquots. In contrast, for ≤ 10 g aliquots of Member 4 shale, larger variations are observed in Re and Os abundances (up to 4% for most samples), and ^{187}Re/^{188}Os (up to 16%) and ^{187}Os/^{188}Os (up to 8%) isotope ratios. Regression of the isotope data for upper Member 2 (H_1O_{16}) and Member 4 black shales yields Re-Os dates of 583 ± 55 Ma (n = 13, MSWD = 41, Model 3, I_{Os} = 0.65 ± 0.18; Figure 2.4B) and 598 ± 16 Ma (n = 31, MSWD = 275, Model 3, I_{Os} = 0.65 ± 0.13; Figure 2.5A), respectively. Separate regressions of the ≤ 10 g and ≥ 20 g aliquots from Member 4 yield Model 3 Re-Os dates of 590 ± 20 Ma (n = 21, MSWD = 360, Model 3, I_{Os} = 0.69 ± 0.16; Figure 2.5B) and 623 ± 13 Ma (n = 10, MSWD = 16, Model 3, I_{Os} = 0.51 ± 0.10; Figure 2.5C), respectively.

2.4.2 Trace Metals

The Fe redox proxies (e.g., DOP, Fe_T/Al, and Fe_{HR}/Fe_T where Fe_T = total Fe and Fe_{HR} = highly reactive iron) have become one of the most widely used paleoredox indicators of ancient local euxinia in sedimentary basins. For example, DOP values between 0 and 0.45, between 0.45 and 0.75, and between 0.75 and 1 are interpreted to record oxidizing, suboxic to anoxic (non-sulfidic), and euxinic bottom water conditions, respectively, although the boundary between these fields is probably transitional (Raiswell et al., 1988). In the absence of high siliciclastic sedimentation rates, elevated Fe_T/Al ratios (two to three times greater relative to typical marine sediments deposited under oxygenated bottom waters) and DOP values are typically preserved in sediments overlain by euxinic bottom waters. This reflects highly reactive iron enrichment associated with water-column scavenging of Fe during syngenetic pyrite formation (Canfield et al., 1996; Raiswell and Canfield, 1996; Lyons, 1997; Wijsman et al., 2001; Lyons et al., 2003; Raiswell and Anderson, 2005; Lyons and Severmann, 2006). Black shales may also be strongly enriched in redox-sensitive elements (such as Cr, V, U, Ni, Co, Cu, Zn, Mo, and Re) whose degree of enrichment may be useful for assessing the paleoredox state of overlying bottom waters (e.g., Piper, 1994; Calvert and Pedersen, 1996; Crusius et al., 1996; Algeo and Maynard, 2004; Tribovillard et al., 2006).

With the exception of Re, black shales from Member 2 are depleted in redox-sensitive metals relative to average shale abundances (see Table 2.2). Despite the depletion of elements considered to be of "strong euxinic affinity" (Mo, U, and V; Algeo and Maynard, 2004; Tribovillard et al., 2006), high DOP values are observed for four of five Member 2 shales (0.61-0.72), and Fe_T/Al ratios (0.9-1.0) are elevated above average shale (0.55) by nearly a factor of two. Manganese abundances are also strongly depleted, consistent with an absence of oscillating redox conditions (Calvert and Pedersen, 1996), and Fe abundances are low. Thus, Member 2 shales may have been deposited from anoxic/non-sulfidic or euxinic bottom waters depleted in redox-sensitive metals. In contrast, Member 4 black shales are strongly enriched in Mo, U, and V, and are characterized by highly elevated DOP values (0.95-0.96), unambiguously suggesting deposition from euxinic bottom waters. Fe_T/Al ratios (0.45-0.69) are not significantly elevated above average shale values, but may reflect enhanced reactivity of the detrital Fe fraction (Anderson and Raiswell, 2004).

2.4.3 Mo and Fe Isotopes

Member 4 black shales show a wide range in Mo abundance (57-355 ppm) and $\delta^{97/95}$Mo (–0.37‰ to +0.89‰). Sub-sample H_1O_{21}-3 has the highly positive $\delta^{97/95}$Mo value whereas the other four sub-samples have near-zero or negative $\delta^{97/95}$Mo. Excluding sub-sample H_1O_{21}-3, there is an inverse correlation between $\delta^{97/95}$Mo and Mo abundance ($R^2 = 0.89$) for the remaining four sub-samples (Figure 2.6A). Similar relationships are observed between $\delta^{97/95}$Mo and many other redox-sensitive metals, such as Pb ($R^2 = 0.99$), U ($R^2 = 0.94$), Re ($R^2 = 0.85$), Cu ($R^2 = 0.81$), V ($R^2 = 0.80$), and Cr ($R^2 = 0.70$).

Excluding sub-sample H_1O_4-2 (anomalously low DOP of 0.21), Fe abundance and $\delta^{56/54}$Fe are well-correlated for Member 2 shales ($R^2 = 0.91$) (Figure 2.6B). The $\delta^{56/54}$Fe of Member 2 and Member 4 shales range between +0.13‰ and +0.32‰, and between +0.26‰ to +0.38‰, respectively. Of the Member 4 black shales, sub-sample H_1O_{21}-3 is notably lighter in $\delta^{56/54}$Fe (+0.26 ± 0.04‰) relative to the other four sub-samples, which define a narrow range in heavy $\delta^{56/54}$Fe (+0.35‰ to +0.38‰).

2.5 DISCUSSION

2.5.1 Re-Os Isotope Systematics of Organic-rich Carbonates

Both the organic-rich shaly limestone from the base of Member 2 (H_1O_1) and the bituminous limestones from the Dengying Formation have low abundances of Re (0.1-0.7 ppb) and Os (5-55 ppt) that are comparable to, or less than, average crustal abundances. Widom et al. (2004) also reported comparable abundances of Re (0.1-1.0 ppb) and Os (5-50 ppt) for most samples of organic-rich Ordovician limestones from the Serpent Mound cryptoexplosion structure (Ohio, USA). Unlike black shales, organic-rich carbonates do not appear to be appreciably enriched in hydrogenous Re and Os over average upper crustal values. This may reflect insufficiently reducing conditions in the overlying water column for reductive capture of Re and Os, limited organic complexation of Re and Os, and/or post-depositional mobilization.

The Re-Os date of 459 ± 230 Ma for the Dengying Formation overlaps U-Pb age constraints that bracket this rock unit between 551.1 ± 0.6 Ma (U-Pb zircon age from ash bed in the uppermost Doushantuo Formation; Condon et al., 2005) and 538.2 ± 1.5 Ma (U-Pb SHRIMP zircon age from Lower Cambrian tuff, Meischucun section; Jenkins et al., 2002), but is associated with a large degree of scatter (MSWD = 192). Analytical artefacts such as large blank corrections (up to ~ 10% for Os; more than ~ 10% for Re), and small-scale post-depositional mobility and/or decoupling of Re from Os present within ≤ 10 g sample aliquots (see section 2.5.2) may explain the observed scatter. Additional possibilities include a probable large detrital Re and Os component and large-scale post-depositional mobility (e.g., diagenetic fluid flow as evidenced from carbonate veinlets in H_1O_{26} and H_1O_{36}). The latter can be tested by calculating sample I_{Os} using independent age constraints (e.g., U-Pb zircon dates). Sample I_{Os} values should fall between maximum values of ~ 1.0-1.5 (currently eroding upper continental crust and average riverine input; Esser and Turekian, 1993; Levasseur et al., 1999; Peucker-Ehrenbrink and Jahn, 2001; Hattori et al., 2003) and a minimum value of ~ 0.12 (unradiogenic seawater Os sourced from hydrothermal alteration of mafic/ultramafic rocks and cosmic dust at ca. 551-542 Ma; Meisel et al., 2001, Walker et al., 2002a, b). Calculated $I_{Os\ (551\text{-}542\ Ma)}$ for samples H_1O_{26} and H_1O_{32} are 0.59-0.62 and 0.39-0.40, respectively. The difference may reflect a change in seawater Os isotope composition during the > 100 m difference in stratigraphic position between these samples. Calculated $I_{Os\ (632\ Ma)}$ for H_1O_1 (basal Member 2) is between 0.44 and 0.56. These observations suggest that large-scale post-depositional mobilization of Re and/or Os in these organic-rich carbonate samples may not have been significant. Widom et al. (2004) advocate a similar conclusion for the Serpent Mound limestones, which yield Re-Os dates of 485 ± 35 Ma (I_{Os} = 0.54 ± 0.15) and 443 ± 34 Ma (I_{Os} = 0.53 ± 0.04) for whole-rock and leachable fractions, respectively, that are in general agreement with independent biostratigraphic age constraints of ~ 472-445 Ma. The slightly older whole-rock Re-Os age was suggested to reflect the presence of a radiogenic detrital Os component. Consequently, the leachate Re-Os date may represent a good approximation of the depositional age of the Serpent Mound limestones, and the I_{Os} value from the isochron regression may reflect the Os isotope composition of local Ordovician seawater (Widom et al., 2004).

However, samples H_1O_{33} and H_1O_{36} from the Dengying Formation have near-zero and negative $I_{Os\ (551\text{-}542\ Ma)}$, respectively. The latter suggests significant post-depositional mobility of Re and/or Os during diagenesis. Both samples are also lighter in color and have exceptionally low Os abundances relative to H_1O_1, H_1O_{26}, H_1O_{32}, and the Serpent Mound carbonates. Thus, the generally low hydrogenous component of Re and Os in organic-rich carbonates, together with the potential for open-system behaviour of Re and Os during diagenesis, indicates that attempts at Re-Os carbonate geochronology should be approached with caution.

2.5.2 Significance of Appropriate Sampling Protocols for Re-Os Geochronology

One critical aspect of Re-Os ORS geochronology concerns the protocol for selecting and sampling appropriate material. This is not simply a matter of targeting ORS that have not been significantly affected by post-depositional processes such as weathering, metamorphism, diagenesis, and hydrothermal fluid flow. For example, Selby and Creaser (2004) showed that the required aliquant size for obtaining reproducible and accurate Re-Os ages for molybdenite depends critically on the molybdenite grain size and age, and that small aliquant sizes can result in inaccurate and/or non-reproducible Re-Os molybdenite ages. Similarly, it is necessary to determine carefully the optimal sampling strategies to avoid the generation of erroneous and/or imprecise Re-Os dates from ORS. The reliability of Re and Os isotope analyses can ideally be checked by replicate analyses of the same sample aliquot. Even if a nugget effect exists in a powder aliquot, coupled variations in $^{187}Re/^{188}Os$ and $^{187}Os/^{188}Os$ isotope ratios will still result in reproducible sample I_{Os} with the added benefit of introducing additional variation along Re-Os isochrons (Creaser et al., 2002; Kendall et al., 2004). Post-depositional mobilization of Re and Os and/or a randomly distributed component of detrital Os (with variable I_{Os}) in powder aliquots will result in scattered Re-Os isotope systematics for replicate analyses. However, it is important to distinguish, for example, between small-scale post-depositional mobility and/or decoupling of Re and Os in otherwise pristine ORS, and large-scale mobility resulting from some major post-depositional geological disturbance such as weathering, metamorphism, and diagenetic/hydrothermal fluid flow. Here, the importance of powder aliquot size on the reproducibility of Re-Os abundances and isotope ratios is demonstrated using the Member 4 black shales of the Doushantuo Formation. A precise U-Pb zircon age of 551.1 ± 0.6 Ma from an ash bed < 1 m below the Doushantuo-Dengying contact constrains the depositional age of Member 4.

Replicate analyses of the ≥ 20 g powder aliquots from Member 4 show excellent reproducibility of Re and Os abundances, $^{187}Re/^{188}Os$ and $^{187}Os/^{188}Os$ isotope ratios, and $I_{Os\ (551\ Ma)}$, whereas the ≤ 10 g aliquots do not. Similarly, one 18 g aliquot (H_1O_{16}-A-1) of shale from Member 2 showed good reproducibility in Re and Os abundances and isotope ratios for two analyses, and $I_{Os\ (632\text{-}551\ Ma)}$ for all three analyses (e.g., a nugget effect), but a smaller 10 g aliquot (subsample H_1O_{16}-B-1) did not. These observations are independent of sample powder aliquant size used for Carius Tube dissolution (0.2-0.8 g). The black shales show no obvious secondary alteration from weathering or diagenetic/hydrothermal fluid flow (e.g., quartz/carbonate veinlets are absent), and are unmetamorphosed. Thus, the contrast in reproducibility between the ≥ 20 g and ≤ 10 g Member 4 subsets likely results from small-scale post-depositional mobilization and/or decoupling of Re and Os that is not sufficiently homogenized in the ≤ 10 g aliquot subset.

Although the Re-Os date of 623 ± 13 Ma (MSWD = 16) derived from the ≥ 20 g aliquot subset of Member 4 is more precise than the Re-Os dates obtained using the combined dataset (598 ± 16 Ma, MSWD = 275) or the ≤ 10 g aliquot subset (590 ± 20 Ma, MSWD = 360), all three Re-Os dates are significantly older than the U-Pb zircon age of 551.1 ± 0.6 Ma from the ash bed within Member 4 (Condon et al., 2005). In addition, the 623 ± 13 Ma date is older than the Pb-Pb phosphorite ages of 599.3 ± 4.2 Ma (Barfod et al., 2002) and 576 ± 14 Ma (Chen et al., 2004b) for the upper phosphorite bed at Weng'an (i.e., Upper Sequence or Member 3) that stratigraphically underlies Member 4. This age discrepancy is suggested to reflect I_{Os} heterogeneity related to the temporal evolution of seawater Os isotope composition.

In the Yangtze Gorges area, the Doushantuo Formation is typically ~ 250 m thick, but represents a duration of > 80 M.y. Consequently, average sedimentation rates during Doushantuo time may have been quite slow, although at least two sequence boundaries are present within the Doushantuo Formation (Xiao et al., 1998a; Wang et al., 1998;

Jiang et al., 2003a; Condon et al., 2005; Zhou and Xiao, 2007). Assuming relatively uniform sedimentation rates, the sampled stratigraphic interval of 3.5 m from Member 4 could represent > 1 M.y. Because of the relatively short seawater residence time of Os (~ 10^4 years; Oxburgh, 1998, 2001; Levasseur et al., 1999), it is plausible that the Os isotope composition of seawater changed during the time period encompassed by the sampled stratigraphic interval. Of the ≥ 20 g aliquot subset, sub-samples H_1O_{18}-3, H_1O_{19}-3, and H_1O_{20}-4 and their replicate analyses have similar $I_{Os\ (551\ Ma)}$ (1.16-1.19) values and together yield a Model 1 Re-Os isochron date of 543 ± 24 Ma (n = 6, MSWD = 0.51; I_{Os} = 1.26 ± 0.22) (Figure 2.7) that overlaps the U-Pb zircon age of 551.1 ± 0.6 Ma for Member 4 (Condon et al., 2005). However, both analyses of sample H_1O_{20}-5 do not plot on this isochron, and have less radiogenic $I_{Os\ (551\ Ma)}$ values of 1.05-1.09 suggesting a possible change in seawater Os isotope composition is recorded within whole rock H_1O_{20} (volume: 80 cm^3). The stratigraphically highest sub-sample H_1O_{21}-3 has the lowest $I_{Os\ (551\ Ma)}$ values (0.73-0.77) and is characterized by a significantly less radiogenic Os isotope composition compared to the other ≥ 20 g aliquots. Thus, this one sub-sample exerted a large effect on the ≥ 20 g aliquot regression that yields an erroneously old age estimate of 623 ± 13 Ma. The Member 4 Re-Os data demonstrates that a deceptively attractive date can be obtained for a sample suite with heterogeneous I_{Os}, especially when there is a large, but skewed, distribution in $^{187}Re/^{188}Os$ and $^{187}Os/^{188}Os$ isotope ratios. Because of the potentially slow sedimentation rates for some condensed black shale sequences (e.g., < 2 m/Ma; Arthur and Sageman 1994), a thin stratigraphic sampling interval is required to ensure homogenous I_{Os}. Sampling strategies should take into account any available information regarding sediment accumulation rates. Recent studies have successfully produced precise Model 1 Re-Os dates for shales from stratigraphic intervals ranging from 10 cm to a few meters, and by using powder aliquots comprising > 20 g of powdered shale (e.g., Kendall et al., 2004; Selby and Creaser, 2005; see Chapters 3, 5, and 6).

Although imprecise, the upper Member 2 Re-Os date of 583 ± 55 Ma is consistent with U-Pb zircon age constraints that bracket the Doushantuo Formation between 635.2 ± 0.6 Ma and 551.1 ± 0.6 Ma (Condon et al., 2005) and with the Pb-Pb phosphorite dates from Member 3. As was the case for Member 4, the Member 2 black shales show no signs of secondary alteration and are unmetamorphosed. Initial Os isotope heterogeneity resulting from temporal variations in seawater Os isotope composition is not likely to account for the observed scatter because the Re-Os isotope data derive from two whole-rock samples from approximately the same stratigraphic horizon. Because the Re-Os data for the upper Member 2 was derived by analysis of powdered aliquots comprising < 12 g material (except for H_1O_{16}-A-1), the large degree of scatter associated with the Re-Os date likely results from decoupling of Re and Os and/or small-scale post-depositional mobility. Rejection of four analyses that account for most of the excess scatter results in an improved Re-Os date of 583 ± 22 Ma (n = 9, Model 3, MSWD = 3.9, I_{Os} = 0.67 ± 0.08) that may represent a loose constraint for the depositional age of upper Member 2.

2.5.3 Importance of Precise Re-Os Depositional Ages from the Doushantuo Formation

The Doushantuo Formation black shales have the potential to yield precise Re-Os depositional ages that would be essential for radiometric calibration of the Late Neoproterozoic/Ediacaran rock record. Condon et al. (2005) suggested the subaerial exposure surface in the middle Doushantuo Formation at Weng'an may reflect glacio-eustatic sea-level fall associated with the ca. 580 Ma Gaskiers glaciation. A negative $\delta^{13}C_{carb}$ excursion ("EN2") near the top of Member 2 in the Yangtze Gorges region could potentially be related to the Weng'an subaerial exposure surface (Zhou and Xiao, 2007). Alternatively, the timing of Gaskiers glaciation may correlate with the sequence boundary between Members 3 and 4 in the Yangtze Gorges region, as well as the karstic subaerial exposure surface just below the Doushantuo-Dengying contact at Weng'an (Xiao, 2004b, Xiao et al., 2004; Zhou and Xiao, 2007). The latter interpretation is consistent with Pb-Pb phosphorite age constraints that bracket the upper phosphorite bed between 599.3 ± 4.2 Ma and 576 ± 14 Ma (Barfod et al., 2002; Chen et al., 2004b). Thus, either the Pb-Pb phosphorite ages are inaccurate (because of diagenetic effects, incorporation of detrital Pb into leaching solutions, or initial Pb isotope heterogeneity from sampling over meters of section; Condon et al., 2005) or the middle Doushantuo Formation subaerial exposure surface and/or negative carbon isotope excursion are not related to the Gaskiers glaciation (e.g., the excursion may represent a diagenetic artefact, restricted basin conditions, or upwelling of ^{13}C-depleted deep water formed by oxidation of a deep-ocean dissolved organic carbon [DOC] reservoir; Bristow et al., 2006; Jiang et al., 2007). The imprecise Re-Os age of 583 ± 22 Ma for upper Member 2 cannot distinguish between these two hypotheses, nor can it aid in distinguishing among possible explanations (Gaskiers glaciation, metazoan evolution, or the development of shallow-water anoxia) for the demise of the "Doushantuo-Pertatataka" acanthomorphic acritarchs prior to the deposition of Member 4.

The Re-Os black shale geochronometer also has the potential to precisely establish the chronology of the diverse Member 3 (Upper Sequence) fossil assemblages relative to other well-dated fossiliferous sections, such as the Mistaken Point assemblage of Newfoundland (Bowring et al., 2003; Narbonne and Gehling, 2003). Member 3 comprises predominantly dolostone and may not be amenable to Re-Os geochronology, but its age can be bracketed by precise Re-Os black shale ages from the top of Member 2 and the base of Member 4. The Re-Os ages would also serve as a test for the robustness of the Pb-Pb phosphorite ages and may provide further constraints on the timing and duration of the "EN2/N2" and "EN3/N3" (Jiang et al., 2007; Zhou and Xiao, 2007) negative carbon isotope excursion (currently estimated between 1 and 50 Myr; Saylor et al., 1998; Condon et al., 2005; Le Guerroué et al., 2006b). The end of the "EN3/N3" excursion is recorded in Member 4 and the base of the overlying Dengying Formation, and dated at 551.1 ± 0.6 Ma (Condon et al., 2005). However, the timing of the onset of the excursion remains uncertain. If the Pb-Pb phosphorite age of 576 ± 14 Ma from the top of the upper phosphorite bed at Weng'an (Chen at al., 2004b) is correct, the duration of the "EN3/N3" excursion was potentially long-lived (between 10 and 40 M.y.), suggesting a significant hiatus between Members 3 and 4.

2.5.4 Depositional Environment of the Doushantuo Formation in the Yangtze Gorges Region: Constraints From Mo Isotopes

The Mo isotope composition of Mo- and organic-rich shales deposited from euxinic bottom waters may be useful for distinguishing between deposition in a marine basin at least partially connected to the open ocean, and a severely restricted or isolated basin. Molybdenum is principally supplied to the oceans today via rivers (with subordinate inputs from low-temperature ridge-flank hydrothermal fluids; Wheat et al., 2002), and is present in oxygenated seawater as the soluble molybdate anion (MoO_4^{2-}), which has a residence time of ~ 800 k.y. (e.g., Emerson and Huested, 1991; Morford and Emerson, 1999). Principal sedimentary sinks for Mo and recent estimates for their output fluxes include Mn oxides (0.9×10^{-8} mol Mo y^{-1}), suboxic/anoxic continental margin sediments (0.7×10^{-8} mol Mo y^{-1}), and euxinic sediments (0.4×10^{-8} mol Mo y^{-1}) (Siebert et al., 2006). Present-day euxinic depositional environments account for < 0.3% of the present-day ocean floor, but ~ 20% of the Mo removal flux, thus highlighting the redox-sensitive nature of Mo (Bertine and Turekian, 1973; Emerson and Huested, 1991; Crusius et al., 1996). Lithogenic material (e.g., organic-poor clastic sedimentary rocks, granites, and basalts) has an average $\delta^{97/95}$Mo near 0‰ (Siebert et al., 2003). Present-day riverine $\delta^{97/95}$Mo is assumed to be near 0‰ as well, but has yet to be determined precisely. Some minor variation in riverine $\delta^{97/95}$Mo over geological time may result from oxidative weathering of isotopically variable, high-Mo sources such as black shales (Barling et al., 2001; Arnold et al., 2004; Siebert et al., 2005; this study; see Chapter 5) and molybdenites (Barling et al., 2001; Wieser and de Laeter, 2003; Pietruszka et al., 2006; Malinovsky et al., 2007; Hannah et al., 2007) (Figure 2.8). However, the uniformity of seawater $\delta^{97/95}$Mo over the last 60 Ma (as recorded in Fe-Mn crusts; Siebert et al., 2003) and the absence of correlated molybdenite $\delta^{97/95}$Mo – age variations over the last 2.7 Ga of Earth history (Hannah et al., 2007) suggests riverine $\delta^{97/95}$Mo remained generally constant over geological time.

Global present-day seawater $\delta^{97/95}$Mo is fractionated relative to riverine $\delta^{97/95}$Mo by preferential adsorption of isotopically light Mo into authigenic Mn oxides ($\Delta^{97/95}Mo_{SW\text{-}oxic}$ ~ 2‰; Barling et al., 2001; Siebert et al., 2003) (see Figure 2.8). Experimental determination of the fractionation factor for Mo adsorption onto Mn oxides suggests a remarkably similar offset of ~1.8‰ between adsorbed and dissolved Mo, suggesting this process to be the principal isotope fractionation mechanism responsible for the heavy global present-day seawater $\delta^{97/95}$Mo value of ~ 1.5‰ (Barling and Anbar, 2004). Thus, a decrease in the extent of oxic Mo deposition in ancient oceans should result in a corresponding decrease in global seawater $\delta^{97/95}$Mo. Smaller fractionations in Mo isotopes are also known to occur in association with diagenetic Mo sulfide formation, and also result in lighter Mo isotope compositions of anoxic/non-sulfidic sediments ($\Delta^{97/95}Mo_{SW\text{-}anoxic}$ ~ 0.5‰) relative to seawater (Nägler et al., 2005; Poulson et al., 2006; Siebert et al., 2006), but likely play a much smaller role in the global Mo isotope budget. Euxinic black shales may record variations in global seawater $\delta^{97/95}$Mo over geological time. When dissolved H_2S concentrations in bottom waters become sufficiently high (> 10 μM) to activate the geochemical "switchpoint" of Mo (MoS_4^{2-}, rather than MoO_4^{2-}, is present in solution; Helz et al., 1996; Erickson and Helz, 2000; Zheng et al., 2000), then quantitative uptake of Mo into euxinic black shales may occur if the Mo recharge time to deep waters from oxic surface waters is sufficiently slow (Algeo and Lyons, 2006) and [H_2S] is sufficiently high (> ~ 100 μM). Under these conditions, euxinic black shales can preserve the Mo isotope composition of contemporaneous global seawater if the local water column is well-mixed with the global ocean relative to the long Mo ocean residence time (e.g., as is observed for Recent euxinic sediments of the semi-restricted Black Sea; Barling et al., 2001; Arnold et al., 2004).

The Member 4 black shales from the Doushantuo Formation have high and invariant DOP values (0.95-0.96) and are strongly enriched in Mo, U and V, suggesting deposition from euxinic bottom waters. Thus, these shales likely record the Mo isotope composition of the overlying water column. However, four of five samples have Mo isotope compositions that are near-zero or negative ($\delta^{97/95}$Mo between –0.37‰ and +0.11‰). If the overlying water column was well-mixed with respect to the ca. 551 Ma global ocean, then the Mo isotope data suggest a completely anoxic global ocean with minimal or negligible fractionation of Mo isotopes associated with Mn oxide deposition. However, this interpretation conflicts with the high Mo abundances of the Member 4 shales (57-355 ppm; comparable to Phanerozoic shales; Anbar et al., 2007), which suggests abundant dissolved Mo in oxic waters. A significant oceanic anoxic event and associated elevated organic carbon burial rates at ca. 551 Ma is suggested to follow the oxidation of a deep-ocean DOC reservoir (Rothman et al., 2003; Jiang et al., 2007). However, such low $\delta^{97/95}$Mo seawater compositions are not observed for Phanerozoic global oceanic anoxic events (Arnold et al., 2004; Gordon et al., 2006; Pearce et al., 2006). Indeed, the disappearance of the DOC reservoir is linked to a rise in atmospheric and ocean oxygen concentrations (e.g., Condon et al., 2005; Fike et al., 2006).

Alternatively, Member 4 may have been deposited in an isolated, euxinic basin such that riverine Mo and euxinic sediments represent the dominant input and output Mo fluxes, respectively. In this scenario, the low $\delta^{97/95}$Mo may approximate riverine $\delta^{97/95}$Mo. However, the suggested global magnitude of the upper Doushantuo – Dengying negative $\delta^{13}C_{carb}$ excursion (Jiang et al., 2007; Zhou and Xiao, 2007) argues against complete isolation of the Western Hubei platform from the global ocean. A strong inverse correlation between $\delta^{97/95}$Mo and Mo abundance ($R^2 = 0.89$) (and other redox-sensitive metals) for the four low $\delta^{97/95}$Mo samples suggests a third possibility. Member 4 may have been deposited in a basin that was only semi-restricted, but the seawater $\delta^{97/95}$Mo signature was overprinted by a large riverine influx of redox-sensitive metals to the Western Hubei platform, such as from weathering of a nearby Cu or Mo porphyry or base metal ore deposit (e.g., Evans, 1993). Sample H_1O_{18}-3, which contains the highest Mo abundance (355 ppm) and the most negative $\delta^{97/95}$Mo (–0.37‰), may approximate the end-member Mo-rich riverine source. Declining metal abundances up-section may reflect drawdown of seawater metal inventories associated with prolonged euxinia. Member 4 black shales contain clay minerals whose chemistry is also consistent with deposition from a relatively open-marine rather than in an isolated basin (Bristow et al., 2006).

A significant change in seawater $\delta^{97/95}$Mo (from 0.1‰ to 0.9‰) and ^{187}Os/^{188}Os isotope composition (from 1.05-1.18 to 0.73-0.77 based on calculated $I_{Os\ (551\ Ma)}$ from ≥ 20 g aliquots) between deposition of whole rocks H_1O_{20} and H_1O_{21} may represent a change in basin paleohydrographic conditions (e.g., more open-marine conditions) and/or a shift in the riverine Mo input flux and/or isotopic composition. Identical DOP values for these two samples indicate continued euxinic marine conditions. Although more data are obviously needed, the $\delta^{97/95}$Mo of ~ 0.9‰ potentially represents global seawater $\delta^{97/95}$Mo at 551 Ma being lighter than present-day seawater by ~ 0.6‰ (assuming similar global riverine $\delta^{97/95}$Mo at 551 Ma and today). Thus, ca. 551 Ma seawater $\delta^{97/95}$Mo may be slightly heavier than Middle Proterozoic seawater (~ 0.7-0.8‰; Arnold et al., 2004; see Chapter 5), and may be similar to early Cambrian seawater (based on black shale and sulfide $\delta^{97/95}$Mo data from the Yangtze Gorges region; Lehmann et al., 2007). Relative to the present-day oceans, the ca. 551 Ma global ocean, if deposited during a significant anoxic event (Jiang et al., 2007), was probably characterized by decreased uptake of Mo onto Mn oxides associated with expanded deep sea anoxia and euxinia relative to oxic and suboxic marine deposition.

Interestingly, the abundances of most redox-sensitive metals from Member 2 shales are depleted relative to average shale despite their generally high DOP values (0.61-0.72) and elevated Fe_T/Al ratios (0.9-1.0). Similar observations were noted by Bristow et al. (2006). Because of the inferred slow sedimentation rates for the Doushantuo Formation (~ 250 m of strata over > 80 M.y.), the low abundances of redox-sensitive elements are not likely the product of sedimentary dilution. Based on the low redox-sensitive metal abundances, presence of Mg-rich clay minerals, and limited $\delta^{34}S$ fractionation (10-15‰) between carbonate-associated sulphate and pyrite, Bristow et al. (2006) suggested Member 2 shales in the Yangtze Gorges region accumulated in an alkaline lake or restricted basin. In contrast, Member 2 shales from slope/basinal sections south of the Yangtze Gorges region contain clay minerals indicative of normal marine chemistry, consistent with a connection to the global ocean.

Ultimately, a better understanding of the paleohydrographic and paleoredox conditions during Doushantuo Formation deposition requires a detailed Mo isotope chemostratigraphic profile through Member 2 and 4 from multiple sections that record deposition in platform, slope, and deep basin environments. Euxinic, slope/basinal black shales may record the Mo isotope composition of contemporaneous global seawater. When anchored by Re-Os shale and U-Pb zircon ages, a Mo isotope chemostratigraphic profile through the Doushantuo Formation may trace the chronology of oxidation of Late Neoproterozoic/Ediacaran oceans because increasing deep ocean oxygen concentrations would shift seawater $\delta^{97/95}Mo$ to more positive values. The Mo isotope data may provide an independent test of proposed mechanisms for Ediacaran ocean oxygenation, such as remineralization of a deep-ocean DOC reservoir (Rothman et al., 2003; Fike et al., 2006; Jiang et al., 2007), increasing clay mineral deposition resulting from the evolution of primitive land plants (Kennedy et al., 2006), elevated primary productivity and associated organic carbon burial following the Gaskiers glaciation (Canfield et al., 2007) and during Pan-African/Gondwana amalgamation (Derry et al., 1992; Kaufman et al., 1993; Kaufman and Knoll, 1995; Jacobsen and Kaufman, 1999; Walter et al., 2000).

2.5.5 Fe Isotope Systematics of the Doushantuo Formation

Archean to Phanerozoic igneous rocks and organic carbon-poor clastic sedimentary rocks, and present-day weathering products (e.g., soil, marine sediments, aerosols, and riverine particulate loads) are characterized by $\delta^{56/54}$Fe values near 0‰ (Beard et al., 2003a, b; Yamaguchi et al., 2005). In contrast, modern organic-rich sediments and ancient black shales are characterized by bulk and pyrite Fe isotope compositions that are fractionated relative to this baseline (Matthews et al., 2004; Yamaguchi et al., 2005; Rouxel et al., 2005; Archer and Vance, 2006; Duan et al., 2006; Fehr et al., 2006; Severmann et al., 2006a). Bulk and pyrite Fe isotope compositions from black shales may thus reflect the nature of marine Fe redox cycling in ancient sedimentary basins, and may also be useful for recognition of local euxinia, especially when used in conjunction with other iron-based paleoredox proxies such as DOP, Fe_{HR}/Fe_T, and Fe_T/Al (Duan et al., 2006; Severmann et al., 2006a).

Severmann et al. (2006c) and Staubwasser et al. (2006) have demonstrated that fractionation of Fe isotopes associated with microbial dissimilatory Fe(III) reduction occurs during early diagenesis in modern suboxic marine sediments from the California and Arabian Sea continental margins. This process results in the production of pore waters with isotopically light Fe ($\delta^{56/54}$Fe as low as ~ –3‰; Severmann et al., 2006c), as well as increasingly lower $\delta^{56/54}$Fe for reactive Fe(III) in Fe-Mn crusts and nodules towards the sediment-water interface (as low as –0.8‰; Levasseur et al., 2004; Staubwasser et al., 2006). In contrast, Fe cycling via bacterial sulfate reduction appears to generate isotopically heavier pore fluids ($\delta^{56/54}$Fe up to ~ +0.4‰) at depth below the zone of dissimilatory Fe(III) reduction (Severmann et al., 2006c). Transport of the benthic $Fe(II)_{aq}$ flux from suboxic continental shelf sediments to basin floors via the iron shuttle can result in highly reactive Fe enrichments in euxinic sediments (Wijsman et al., 2001; Anderson and Raiswell, 2004; Raiswell and Anderson, 2005; Lyons and Severmann, 2006). Recent studies suggest the isotopically light Fe isotope signature of the Fe shuttle is recorded in modern euxinic sediments and ancient euxinic black shales (Duan et al., 2006; Severmann et al., 2006a, b). A negative correlation between bulk $\delta^{56/54}$Fe and DOP consistent with shelf-to-basin transport of an isotopically light benthic $Fe(II)_{aq}$ flux was observed for Recent sediments of the Black Sea (Severmann et al., 2006a) and the

Devonian Oatka Creek and Geneseo Formations from the eastern U.S.A. (Duan et al., 2006). Highly variable and negative bulk and pyrite $\delta^{56/54}$Fe from Archean black shales Rouxel et al., 2005; Yamaguchi et al., 2005; Archer and Vance, 2006) contrast with lower amplitude variations from present-day organic-rich sediments and Phanerozoic black shales (Matthews et al., 2004; Fehr et al., 2006; Severmann et al., 2006a, b). These differences may reflect changes in the nature of Fe redox cycling over geological time (e.g., limited fractionation associated with a decreased Fe[II]$_{aq}$ pool in pervasively oxygenated Phanerozoic oceans; Rouxel et al., 2005).

Euxinic Member 4 shales have strongly positive $\delta^{56/54}$Fe (+0.26‰ to +0.38‰) that contrasts with the negative values of euxinic Recent Black Sea sediments and euxinic black shales from the Oatka Creek Formation (Duan et al., 2006; Severmann et al., 2006a). Most Member 4 shales have $\delta^{56/54}$Fe (+0.35‰ to +0.38‰) similar to that of pore fluids derived from the zone of bacterial sulfate reduction in the Santa Barbara Basin (Severmann et al., 2006c). One possibility is that the $\delta^{56/54}$Fe of Member 4 shales reflects isotopically heavy Fe(II)$_{aq}$ entering the semi-restricted Western Hubei platform from the surrounding deeper water Yangtze continental margin, which may have been characterized by extensive bacterial sulfate reduction and organic-rich sediment deposition (e.g., Jiang et al., 2007; Zhou and Xiao, 2007). The complementary light Fe reservoir may then be buried in deeper-water organic-rich shales. A decrease in $\delta^{56/54}$Fe between deposition of whole rocks H_1O_{20} and H_1O_{21} (from 0.35-0.38‰ to 0.26‰) is in line with similar shifts in seawater Mo and ^{187}Os/^{188}Os isotopes. The significance of the decreased $\delta^{56/54}$Fe of Fe(II)$_{aq}$ is not presently clear, but could reflect an increasing importance of dissimilatory Fe(III) reduction on the Yangtze continental margin.

The $\delta^{56/54}$Fe of anoxic/non-sulfidic Member 2 (+0.13‰ to +0.32‰) shales have similar $\delta^{56/54}$Fe as suboxic shales from the Geneseo Formation (up to +0.30‰; Duan et al., 2006). However, deposition of Member 2 may have occurred in a low-sulfate restricted basin/alkaline lake environment with low seawater metal inventories (Bristow et al., 2006) rather than an open marine or semi-restricted environment. Iron abundance and $\delta^{56/54}$Fe are well-correlated for those Member 2 shales with elevated DOP (~ 0.6-0.7), but the significance of this correlation is not clear. If the basin was completely isolated, sulfur availability was limited, and anoxic/non-sulfidic depositional conditions prevailed, then the heavy $\delta^{56/54}$Fe reflects isotopic exchange reactions during authigenic mineral formation, perhaps involving isotopically heavy dissolved $Fe(II)_{aq}$ (> 0‰) (Severmann et al., 2006a, c). Alternatively, Member 2 shales were deposited under generally euxinic conditions with quantitative Fe uptake, with a limited connection to open marine waters. In this case, the $\delta^{56/54}$Fe could represent bottom water $\delta^{56/54}$Fe, which was heavy because of widespread bacterial sulfate reduction on the Yangtze continental margin.

The above discussion is highly speculative, but an understanding of Fe isotope fractionations in the natural marine environment is still in its infancy, and an improved knowledge of fractionation factors, especially for pyrite (e.g., such as between the FeS precursor and pyrite), is required for interpreting $\delta^{56/54}$Fe of ancient black shales (Severmann et al., 2006c). Further comparison of bulk $\delta^{56/54}$Fe for black shales of the Doushantuo Formation across a platform-to-basin transect, and determination of $\delta^{56/54}$Fe from different Fe fractions by selective chemical extraction techniques (e.g., pyrite Fe; Poulton and Canfield, 2005; Duan et al., 2006; Severmann et al., 2006c) are required to understand the nature of Fe redox cycling on the Yangtze passive margin between 635 and 551 Ma.

2.6 CONCLUSIONS

Preliminary Re-Os isotope data from black shales of the 635-551 Ma Doushantuo Formation (Yangtze Gorges region, South China) yield Re-Os dates of 583 ± 55 Ma (upper Member 2) and 598 ± 16 Ma (Member 4). The poor precisions for these dates (MSWD = 41 and 275, respectively) reflect small-scale post-depositional mobility and/or decoupling of Re and Os within small (≤ 10 g) powder aliquots rather than large-scale post-depositional mobility. The Member 2 Re-Os date is broadly consistent with U-Pb zircon age constraints from ash beds that bracket the depositional age of the Doushantuo Formation between ca. 635 and 551 Ma. However, both the Re-Os date of 598 ± 16 Ma, as well as the 623 ± 13 Ma (MSWD = 16) date derived from ≥ 20 g aliquots of Member 4, are erroneously older than the U-Pb zircon age of 551.1 ± 0.6 Ma obtained from an ash bed near the top of Member 4 (Condon et al., 2005). This discrepancy is suggested to reflect initial Os isotope heterogeneity resulting from temporal evolution of local seawater Os isotope composition during Member 4 deposition. Because the Doushantuo

Formation is not metamorphosed, precise and accurate Re-Os depositional ages are potentially forthcoming for Member 2 and 4 black shales. Organic-rich shale intervals should be sampled over limited stratigraphic intervals (< 0.5 m because sedimentation rates during deposition of Doushantuo Formation black shales was likely slow, perhaps < 5 m/Ma) at multiple horizons within Member 2 and 4. This may enable significant improvements in calibration of the Late Neoproterozoic/Ediacaran rock record. Organic-rich carbonates from the overlying Dengying Formation contain low abundances of Re and Os, and show some evidence for post-depositional mobilization of Re and Os, probably during diagenesis. Hence, organic-rich carbonates may have limited utility for Re-Os geochronology.

Member 4 shales are enriched in Mo (57-355 ppm) and have elevated degree-of-pyritization (DOP) values (0.95-0.96) that are consistent with deposition from euxinic bottom water conditions. However, Mo isotope data from most Member 4 shales have near-zero or negative $\delta^{97/95}$Mo signatures (–0.37‰ to +0.11‰) comparable to lithogenic/riverine $\delta^{97/95}$Mo (~ 0‰). The Mo isotope data, together with clay mineralogy and light stable isotope data (e.g., Bristow et al., 2006), are most consistent with a semi-restricted environment for the Western Hubei platform during deposition of Member 4. Positive $\delta^{56/54}$Fe values (+0.26‰ to +0.38‰) for the Member 4 black shales may reflect sequestration of isotopically heavy seawater $Fe(II)_{aq}$ entering the Western Hubei platform from continental margin regions dominated by extensive bacterial sulfate reduction and organic-rich sediment deposition.

Slope and basinal sections of the Doushantuo Formation may have been deposited from a water column that was well-mixed with respect to the global ocean (Bristow et al., 2006). Thus, application of the Mo and Fe isotope and metal redox proxies (including DOP) to Mo- and organic-rich shales from these sections has the potential to provide important constraints on the redox state of Late Neoproterozoic/Ediacaran global deep ocean waters (cf. Arnold et al., 2004) as well as the nature of diagenetic Fe redox cycling on the Yangtze passive margin. Application of Re-Os black shale geochronology and the Mo isotope paleoredox proxy to the Doushantuo Formation holds potential for an improved understanding of the relationships between early animal evolution, the timing and nature of Ediacaran-age carbon isotope excursions, the Gaskiers glaciation, and the timing of ocean and atmosphere oxygenation.

Table 2.1 Re-Os isotope data for the Doushantuo Formation, South China.

Sample	Aliquot Mass (g)	Aliquant Mass (g)*	Re (ppb)	Os (ppt)	^{192}Os (ppt)	^{187}Re/^{188}Os	^{187}Os/^{188}Os	rho	I_{Os}†
Doushantuo Formation, Member 2									
H_1O_1-1	17.8	1.18	0.39 ± 0.01	54.8 ± 0.2	20.6 ± 0.1	37.33 ± 0.56	0.8943 ± 0.0056	0.317	0.50
replicate		1.47	0.30 ± 0.01	46.8 ± 0.9	17.5 ± 0.7	33.68 ± 1.46	0.9149 ± 0.0524	0.671	0.56
replicate		1.50	0.32 ± 0.01	48.3 ± 1.0	18.1 ± 0.7	35.55 ± 1.52	0.9142 ± 0.0523	0.678	0.54
H_1O_1-2	15.9	1.51	0.39 ± 0.01	47.0 ± 0.9	17.6 ± 0.7	44.23 ± 2.05	0.9112 ± 0.0521	0.627	0.44
H_1O_1-3	10.3	1.51	0.30 ± 0.01	50.8 ± 1.0	19.2 ± 0.8	30.96 ± 1.33	0.8496 ± 0.0485	0.672	0.52
H_1O_1-4	17.5	1.49	0.35 ± 0.01	50.4 ± 1.0	18.9 ± 0.8	36.39 ± 1.55	0.8924 ± 0.0510	0.676	0.51
H_1O_4-1	3.6	0.99	3.48 ± 0.02	106.9 ± 0.7	34.3 ± 0.2	202.31 ± 1.72	2.3395 ± 0.0200	0.597	0.20 to 0.47
H_1O_5-1	11.1	1.23	2.56 ± 0.01	77.6 ± 0.5	24.8 ± 0.2	205.74 ± 1.65	2.3764 ± 0.0197	0.662	0.20 to 0.48
H_1O_{16}-A-1	17.6	0.98	3.56 ± 0.02	120.7 ± 0.6	38.1 ± 0.1	185.74 ± 1.07	2.4838 ± 0.0104	0.560	0.52 to 0.77
replicate		1.19	3.80 ± 0.02	122.3 ± 0.8	38.2 ± 0.2	198.04 ± 1.39	2.5984 ± 0.0189	0.606	0.50 to 0.77
replicate		1.19	3.70 ± 0.02	120.8 ± 0.8	37.7 ± 0.2	195.01 ± 1.38	2.5974 ± 0.0191	0.608	0.53 to 0.80
H_1O_{16}-A-2	11.1	1.21	3.81 ± 0.02	107.3 ± 0.7	32.5 ± 0.2	233.36 ± 1.69	2.9236 ± 0.0219	0.631	0.45 to 0.77
H_1O_{16}-A-3	10.1	1.23	3.20 ± 0.01	94.4 ± 0.6	28.8 ± 0.2	221.18 ± 1.65	2.8342 ± 0.0218	0.644	0.49 to 0.79
H_1O_{16}-A-4	6.6	1.23	2.97 ± 0.01	149.0 ± 0.8	50.4 ± 0.3	117.34 ± 0.81	1.8175 ± 0.0134	0.562	0.56 to 0.74
H_1O_{16}-A-5	8.1	1.20	5.30 ± 0.02	157.1 ± 1.0	48.7 ± 0.3	218.51 ± 1.46	2.6646 ± 0.0190	0.585	0.37 to 0.67
H_1O_{16}-A-6	6.1	1.22	2.61 ± 0.01	82.6 ± 0.6	25.8 ± 0.2	200.99 ± 1.69	2.5843 ± 0.0244	0.634	0.46 to 0.73
H_1O_{16}-A-7	5.1	1.17	3.61 ± 0.02	101.4 ± 0.7	30.4 ± 0.2	235.79 ± 1.78	3.0001 ± 0.0236	0.646	0.50 to 0.83
H_1O_{16}-B-1	9.7	1.18	3.60 ± 0.02	109.9 ± 0.7	33.9 ± 0.2	211.52 ± 1.58	2.7313 ± 0.0210	0.618	0.49 to 0.78
H_1O_{16}-B-2	5.7	1.18	2.77 ± 0.01	87.9 ± 0.6	27.5 ± 0.2	199.88 ± 1.65	2.5655 ± 0.0227	0.656	0.45 to 0.72
H_1O_{16}-B-3	4.1	1.23	3.97 ± 0.02	125.5 ± 0.8	39.0 ± 0.2	202.44 ± 1.43	2.6533 ± 0.0199	0.606	0.51 to 0.79
Doushantuo Formation, Member 4									
H_1O_{18}-1	7.0	0.81	284.41 ± 1.14	4418.4 ± 16.9	1026.9 ± 1.2	550.97 ± 2.30	6.0788 ± 0.0110	0.195	1.00
replicate		0.80	275.38 ± 1.10	4510.1 ± 15.2	1048.6 ± 0.9	522.45 ± 2.13	6.0743 ± 0.0086	0.140	1.26
H_1O_{18}-2	10.4	0.78	565.95 ± 2.26	8234.7 ± 32.8	1836.9 ± 2.3	612.26 ± 2.57	6.6343 ± 0.0125	0.205	0.99
H_1O_{18}-3	39.8	0.78	402.35 ± 1.60	6225.1 ± 23.9	1413.7 ± 1.6	566.22 ± 2.34	6.3985 ± 0.0114	0.186	1.18
replicate		0.50	392.22 ± 1.56	6093.9 ± 24.1	1387.1 ± 1.5	562.52 ± 2.32	6.3655 ± 0.0120	0.149	1.18
H_1O_{19}-1	7.8	0.80	388.52 ± 1.55	5970.6 ± 22.5	1387.9 ± 1.7	556.92 ± 2.32	6.0771 ± 0.0107	0.193	0.94
replicate		0.15	374.73 ± 1.50	6007.3 ± 21.4	1398.3 ± 1.5	533.12 ± 2.20	6.0583 ± 0.0096	0.170	1.14
H_1O_{19}-2	6.6	0.80	392.16 ± 1.57	5654.4 ± 23.2	1264.2 ± 1.7	617.10 ± 2.60	6.6189 ± 0.0132	0.212	0.93
replicate		0.15	381.80 ± 1.53	5641.9 ± 32.8	1256.1 ± 3.3	604.69 ± 2.88	6.6769 ± 0.0258	0.367	1.10
replicate		0.79	384.57 ± 1.53	5715.4 ± 19.2	1264.8 ± 1.1	604.89 ± 2.46	6.7631 ± 0.0091	0.137	1.18
H_1O_{19}-3	20.5	0.78	335.93 ± 1.34	5539.5 ± 21.2	1302.4 ± 1.4	513.12 ± 2.12	5.9227 ± 0.0109	0.181	1.19
replicate		0.58	338.91 ± 1.35	5577.7 ± 18.3	1311.9 ± 1.1	513.92 ± 2.09	5.9172 ± 0.0080	0.129	1.18
H_1O_{20}-1	4.8	0.79	160.31 ± 0.64	2426.9 ± 9.9	558.2 ± 0.8	571.35 ± 2.42	6.2219 ± 0.0127	0.224	0.95
replicate		0.26	154.73 ± 0.62	2489.7 ± 11.9	579.2 ± 0.9	531.48 ± 2.28	6.0667 ± 0.0169	0.201	1.17
H_1O_{20}-2	5.9	0.78	105.69 ± 0.42	1776.3 ± 7.3	433.9 ± 0.6	484.54 ± 2.06	5.4170 ± 0.0118	0.229	0.95
replicate		0.30	102.42 ± 0.41	1833.9 ± 8.8	461.4 ± 0.9	441.61 ± 1.96	5.0412 ± 0.0154	0.272	0.97
H_1O_{20}-3	5.5	0.80	181.41 ± 0.72	2756.8 ± 11.3	629.3 ± 0.8	573.51 ± 2.41	6.3271 ± 0.0128	0.204	1.04
replicate		0.25	178.81 ± 0.72	2809.1 ± 13.1	647.2 ± 1.1	549.62 ± 2.39	6.1976 ± 0.0183	0.256	1.13
replicate		0.80	179.73 ± 0.72	2767.8 ± 9.1	633.2 ± 0.5	564.62 ± 2.30	6.2948 ± 0.0083	0.128	1.09
H_1O_{20}-4	22.0	0.82	167.29 ± 0.67	2660.7 ± 16.2	614.9 ± 1.6	541.20 ± 2.58	6.1555 ± 0.0267	0.331	1.18
replicate		0.54	165.81 ± 0.66	2654.6 ± 6.9	614.5 ± 0.6	536.84 ± 2.20	6.1346 ± 0.0086	0.159	1.18
H_1O_{20}-5	32.8	0.78	117.44 ± 0.47	1945.4 ± 10.4	464.0 ± 1.0	503.58 ± 2.26	5.7320 ± 0.0201	0.270	1.09
replicate		0.54	118.57 ± 0.47	1972.8 ± 7.1	473.7 ± 0.5	497.93 ± 2.06	5.6414 ± 0.0093	0.184	1.05
H_1O_{21}-1	8.9	0.67	33.76 ± 0.14	1185.5 ± 3.9	368.5 ± 0.5	182.28 ± 0.77	2.6444 ± 0.0056	0.180	0.96
replicate		0.60	40.89 ± 0.16	1230.4 ± 5.6	385.9 ± 1.0	210.78 ± 1.01	2.5529 ± 0.0103	0.360	0.61
replicate		0.75	39.09 ± 0.16	1205.9 ± 3.7	377.0 ± 0.5	206.27 ± 0.86	2.5846 ± 0.0046	0.192	0.68

Table 2.1 Continued

Sample	Aliquot Mass (g)	Aliquant Mass (g)*	Re (ppb)	Os (ppt)	^{192}Os (ppt)	^{187}Re/^{188}Os	^{187}Os/^{188}Os	rho	I_{Os}†
H_1O_{21}-2	4.6	0.53	32.88 ±0.13	1138.8 ±3.6	358.2 ±0.5	182.60 ±0.78	2.5224 ±0.0051	0.210	0.84
replicate		0.62	34.52 ±0.14	1175.4 ±4.4	373.2 ±0.7	184.00 ±0.81	2.4290 ±0.0071	0.246	0.73
replicate		0.74	30.44 ±0.12	1139.8 ±3.3	359.2 ±0.4	168.59 ±0.70	2.5037 ±0.0043	0.187	0.95
H_1O_{21}-3	32.2	0.49	37.09 ±0.15	1175.9 ±4.2	367.7 ±0.6	200.68 ±0.87	2.5825 ±0.0065	0.279	0.73
replicate		0.46	36.59 ±0.15	1181.5 ±4.8	369.3 ±0.8	197.08 ±0.89	2.5864 ±0.0082	0.312	0.77
Dengying Formation									
H_1O_{28}-1	17.2	1.30	0.73 ±0.01	21.3 ±0.2	6.7 ±0.1	219.77 ±4.26	2.6173 ±0.0513	0.834	0.59 to 0.62
H_1O_{32}-1	22.4	1.22	0.37 ±0.01	17.5 ±0.2	6.1±0.1	119.44 ±2.65	14869 ±0.0288	0.680	0.39 to 0.40
H_1O_{33}-1	11.2	1.26	0.06 ±0.01	4.5 ±0.1	17 ±0.1	73.51±7.39	0.7381±0.0540	0.594	0.06 to 0.07
H_1O_{36}-1	5.5	1.25	0.40 ±0.01	5.2 ±0.2	13 ±0.1	625.51±55.58	5.2062 ±0.4674	0.967	−0.56 to −0.47

Uncertainties are quoted at the 2σ level.

*Used for individual Re-Os analysis.

†I_{Os} = initial ^{187}Os/^{188}Os ratio calculated at 632 Ma (H_1O_1; based on the U-Pb zircon age of 632.5 ±0.5 Ma from an ash bed 5 m above the base of Member 2; Condon et al., 2005), 632-551Ma (H_1O_4, H_1O_8, H_1O_{10}; younger age is based on the U-Pb zircon age of 551.1±0.6 Ma from an ash bed < 1m below the Doushantuo-Dengying contact; Condon et al., 2005), 551Ma (Member 4), and 551-542 Ma (Dengying Formation; younger age is based on the U-Pb zircon age of 542.0 ±0.3 Ma for the Precambrian-Cambrian boundary; Amthor et al., 2003).

Table 2.2. Mo and Fe isotope, Degree-Of-Pyritization (DOP), and trace metal data for the Doushantuo Formation, South China.

Sample	Mo	$\delta^{97/95}$Mo (‰)	n*	Fe	$\delta^{56/54}$Fe (‰)	n*	DOP	Fe_T/Al	Al	Ti	V	Cr	Mn	Co	Ni	Cu	Zn	Pb	U
Member 2																			
H_1O_4-2	0.9			10215	0.18 ±0.03	3	0.21	0.91	21057	2918	42	24	260	5.4	24	30	44	4.1	1.1
H_1O_9-2	1.2			9800	0.18 ±0.07	3	0.61	1.0	9412	1271	23	15	230	4.7	19	19	32	2.1	1.0
H_1O_{14}-1	1.2			4810	0.13 ±0.03	3	0.65	1.1	4476	606	14	11	148	2.8	15	13	15	1.4	0.89
H_1O_{16}-A-1	0.7			15415	0.32 ±0.03	2	0.68	0.92	15735	2403	33	27	218	7.7	27	31	46	4.7	1.9
H_1O_{16}-B-1	0.8			17174	0.29 ±0.01	3	0.72	1.2	14690	2071	31	24	214	7.0	25	29	40	4.1	1.8
Member 4																			
H_1O_{18}-3	355	−0.37 ±0.06	3	27869	0.38 ±0.02	3	0.95	0.69	40480	3216	1314	125	124	14	104	122	347	59	15
H_1O_{19}-3	97	−0.10 ±0.05	3	21474	0.36 ±0.02	3	0.95	0.45	47299	2529	1196	123	138	11	119	110	719	47	12
H_1O_{20}-4	70	0.11±0.09	4	23728	0.35 ±0.01	3	0.96	0.61	39155	2778	868	88	304	13	76	71	36	38	8.1
H_1O_{20}-5	57	0.08 ±0.01	3	23295	0.38 ±0.04	3	0.95	0.60	38792	2533	695	71	240	12	47	54	33	35	7.1
H_1O_{21}-3	131	0.69 ±0.04	3	23383	0.26 ±0.04	3	0.95	0.61	38381	2211	205	51	297	14	39	63	67	24	30
Average Shale	1.3	~0		~46000	~0			0.55	88900	~4700	130	90	850	19	68	45	95	22	3.7

Concentrations in ppm. Uncertainties for Mo and Fe isotope data are quoted at the 2σ level. Average shale data from Wedepohl (1971, 1991).

*Number of replicate Mo or Fe isotope mass spectrometer analyses.

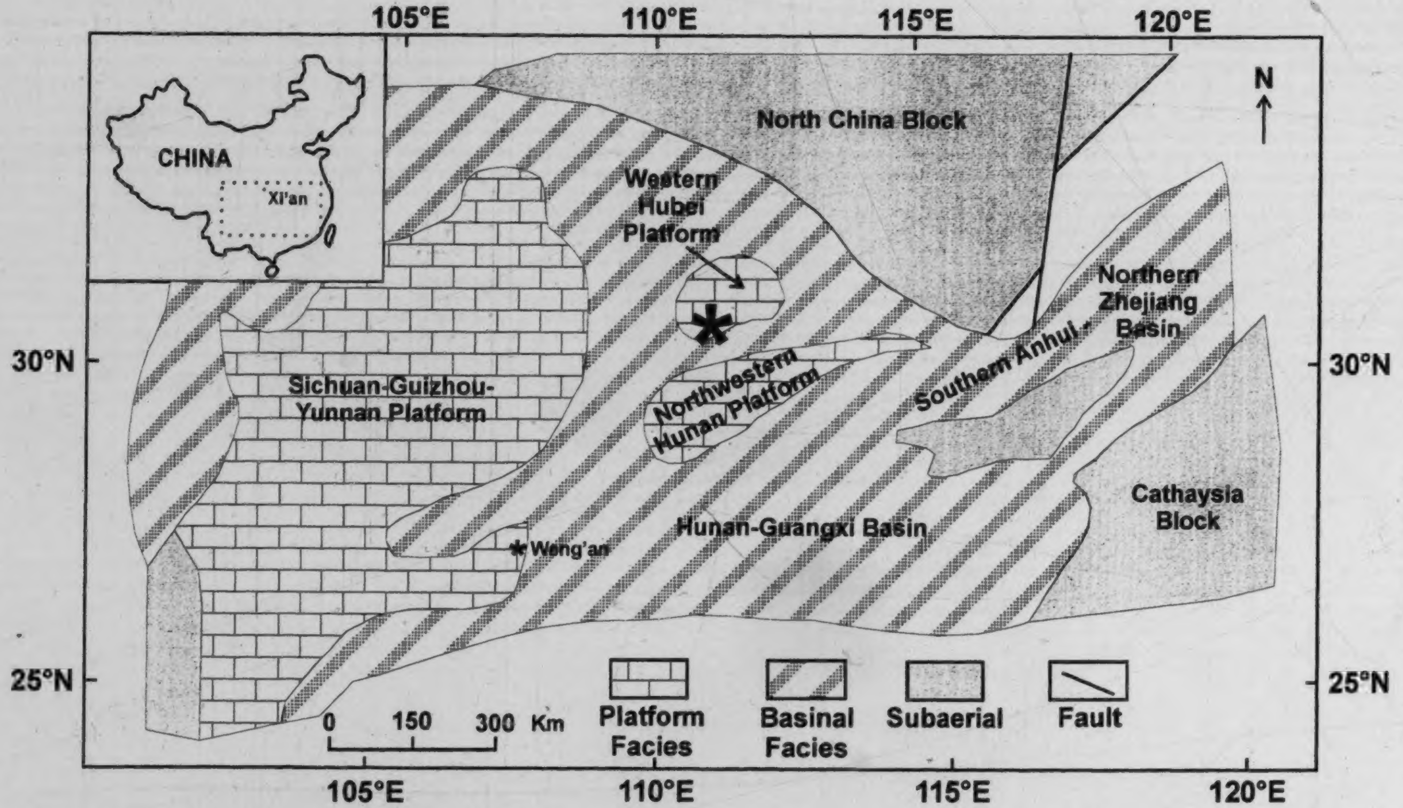
105°E
110°E
115°E
120°E
30°N
25°N
N
CHINA
Xi'an
North China Block
Western Hubei Platform
Sichuan-Guizhou-Yunnan Platform
Northwestern Hunan Platform
Southern Anhui
Northern Zhejiang Basin
Hunan-Guangxi Basin
Cathaysia Block
Weng'an
0
150
300 Km
Platform Facies
Basinal Facies
Subaerial
Fault

Figure 2.1: Paleogeographic map of facies distributions during Early Doushantuo time. The asterisk marks the location of the Yangtze Gorges region (including the Jijiapo platform section). Modified from Zhou and Xiao (2007).

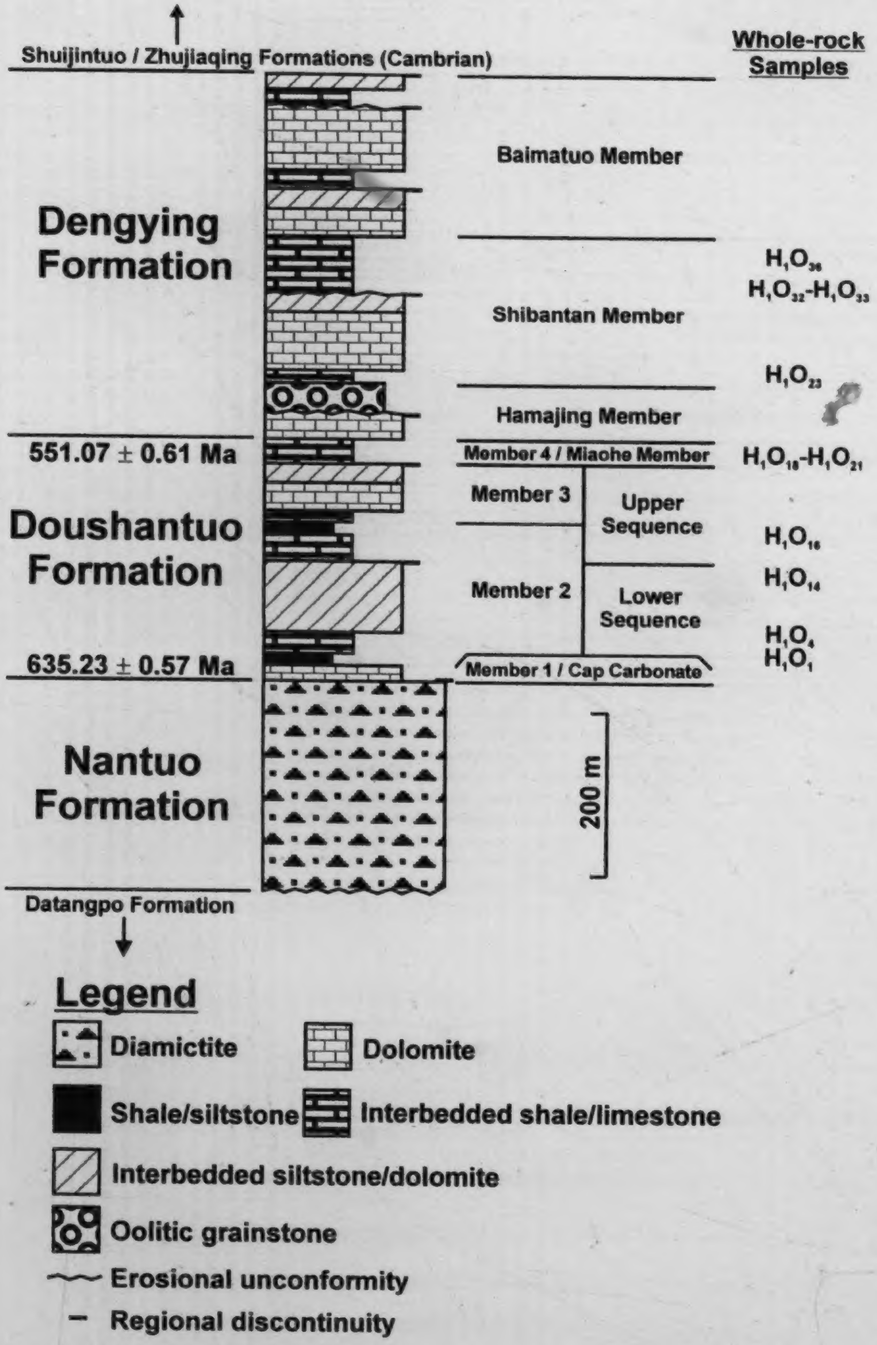
Shuijintuo / Zhujiaqing Formations (Cambrian)
Whole-rock Samples
Dengying Formation
Baimatuo Member
Shibantan Member
Hamajing Member
551.07 ± 0.61 Ma
Member 4 / Miaohe Member
Doushantuo Formation
Member 3
Upper Sequence
Member 2
Lower Sequence
635.23 ± 0.57 Ma
Member 1 / Cap Carbonate
Nantuo Formation
200 m
Datangpo Formation
H1O36
H1O32-H1O33
H1O23
H1O18-H1O21
H1O16
H1O14
H1O4
H1O1
Legend
Diamictite
Dolomite
Shale/siltstone
Interbedded shale/limestone
Interbedded siltstone/dolomite
Oolitic grainstone
Erosional unconformity
Regional discontinuity

Figure 2.2: Generalized stratigraphic column for the Late Neoproterozoic stratigraphy of South China. The two informal member subdivisions of the Doushantuo Formation and the stratigraphic position of whole rock samples are shown on the right. Modified from Jiang et al. (2003a).

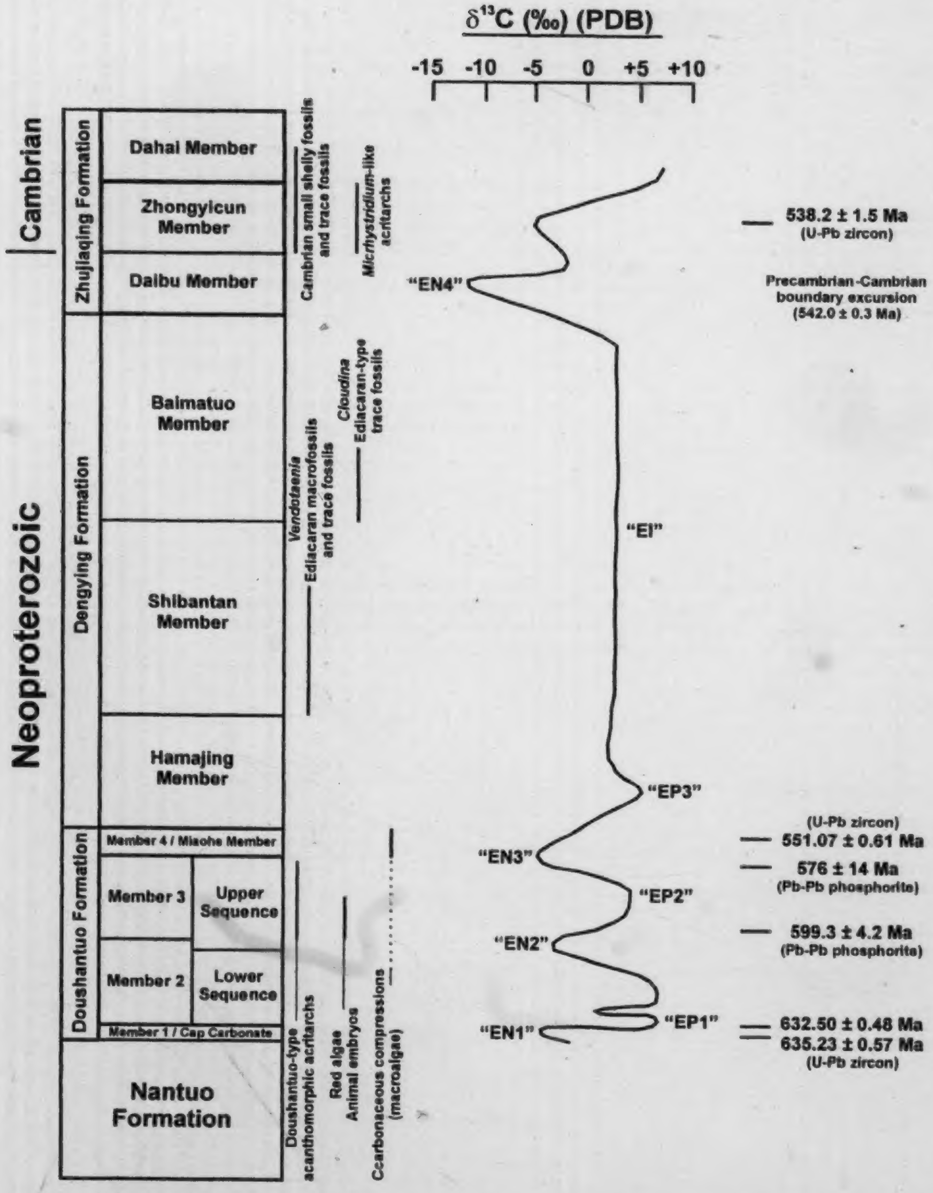

Figure 2.3: Distribution of Doushantuo and Dengying Formation biota and the composite carbon isotope curve for the Late Neoproterozoic of South China. U-Pb zircon ages for the Doushantuo Formation from Condon et al. (2005), Pb-Pb phosphorite ages from Barfod et al. (2002) and Chen et al. (2004b), Precambrian-Cambrian boundary age from Amthor et al. (2003), and Early Cambrian age from Jenkins et al. (2002). Modified from Zhou and Xiao (2007).

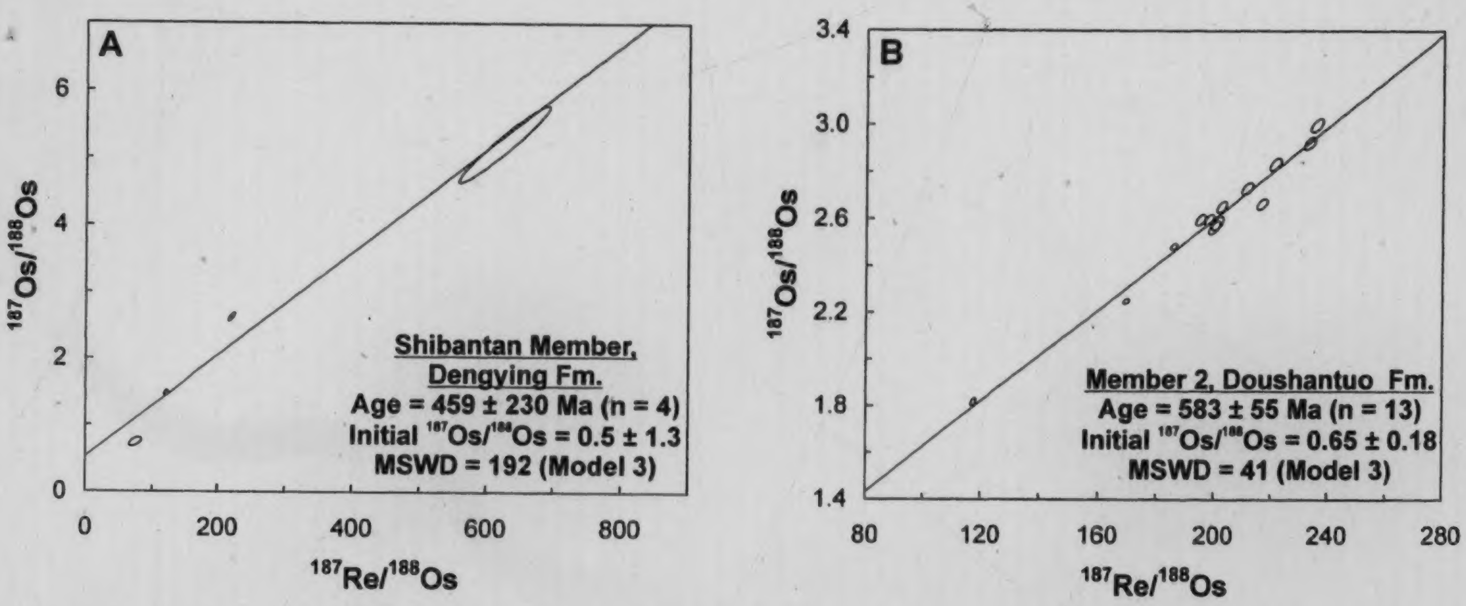

Figure 2.4: Re-Os isochron diagrams. (A) Shibantan Member, Dengying Formation. (B) Upper Member 2, Doushantuo Formation.

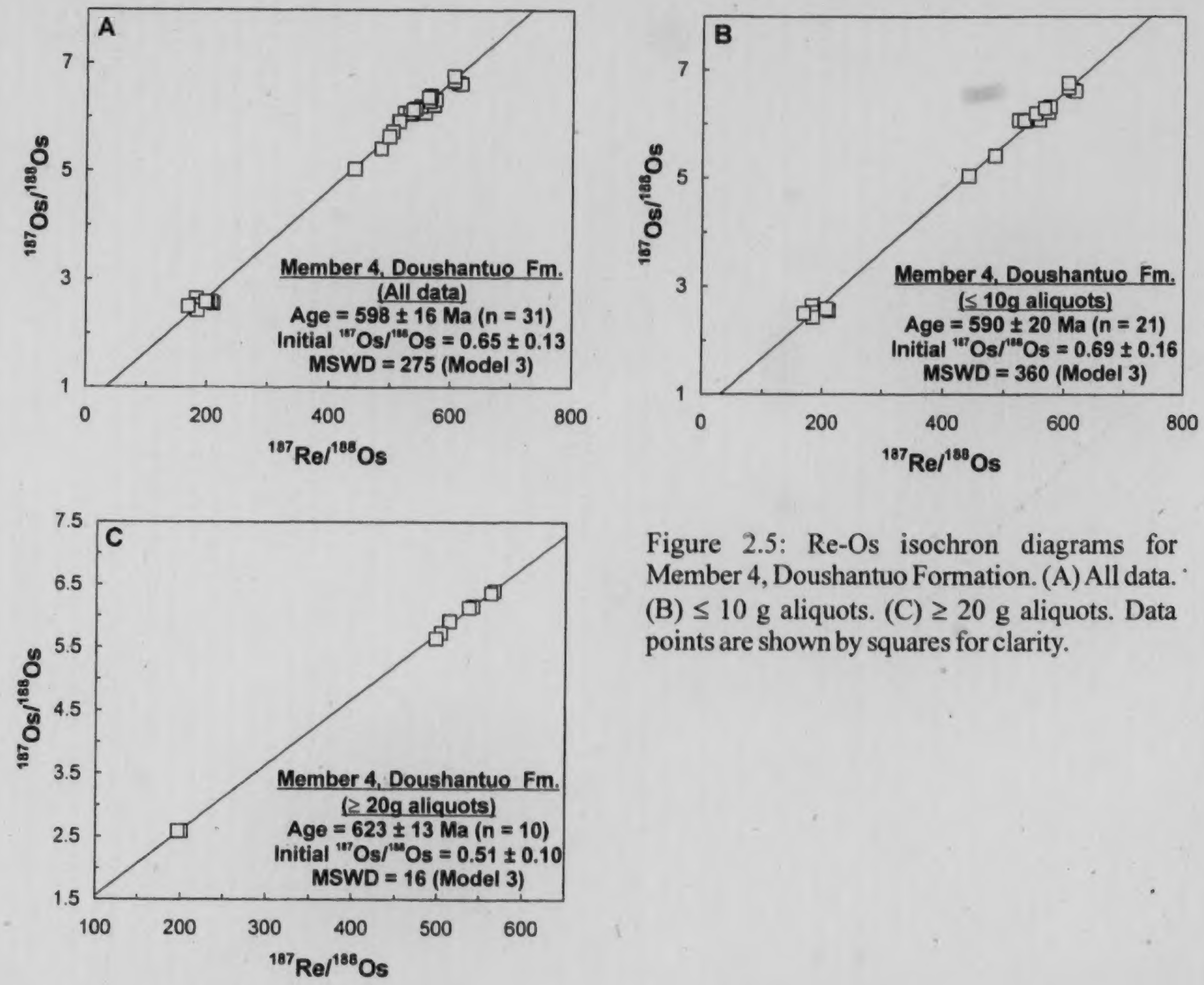

Figure 2.5: Re-Os isochron diagrams for Member 4, Doushantuo Formation. (A) All data. (B) ≤ 10 g aliquots. (C) ≥ 20 g aliquots. Data points are shown by squares for clarity.

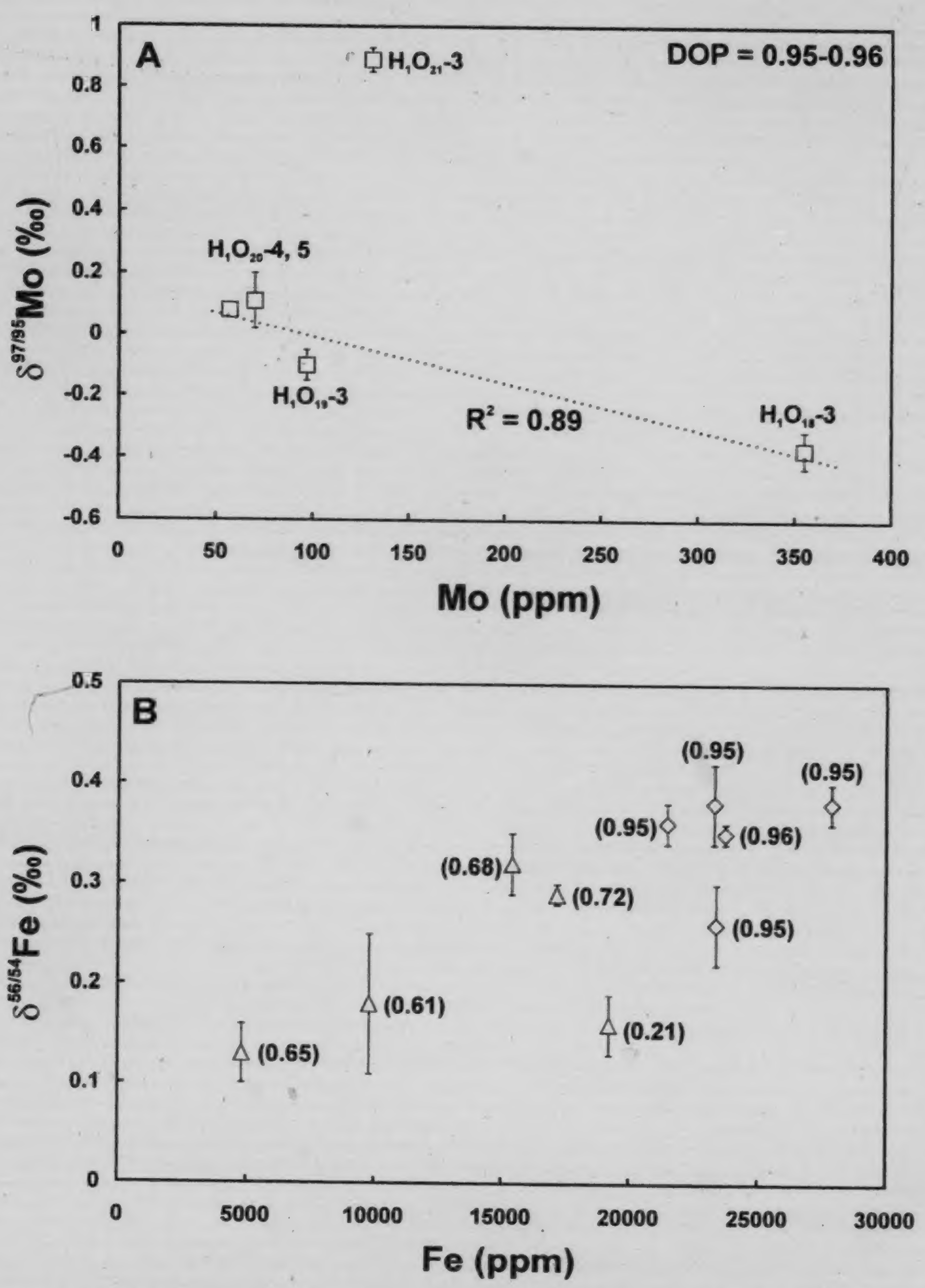

Figure 2.6: Mo and Fe isotope and abundance data for the Doushantuo Formation. (A) Mo abundance versus Mo isotope composition for Member 4. (B) Fe abundance versus Fe isotope composition for Member 2 (triangles) and Member 4 (diamonds). DOP values are given in brackets.

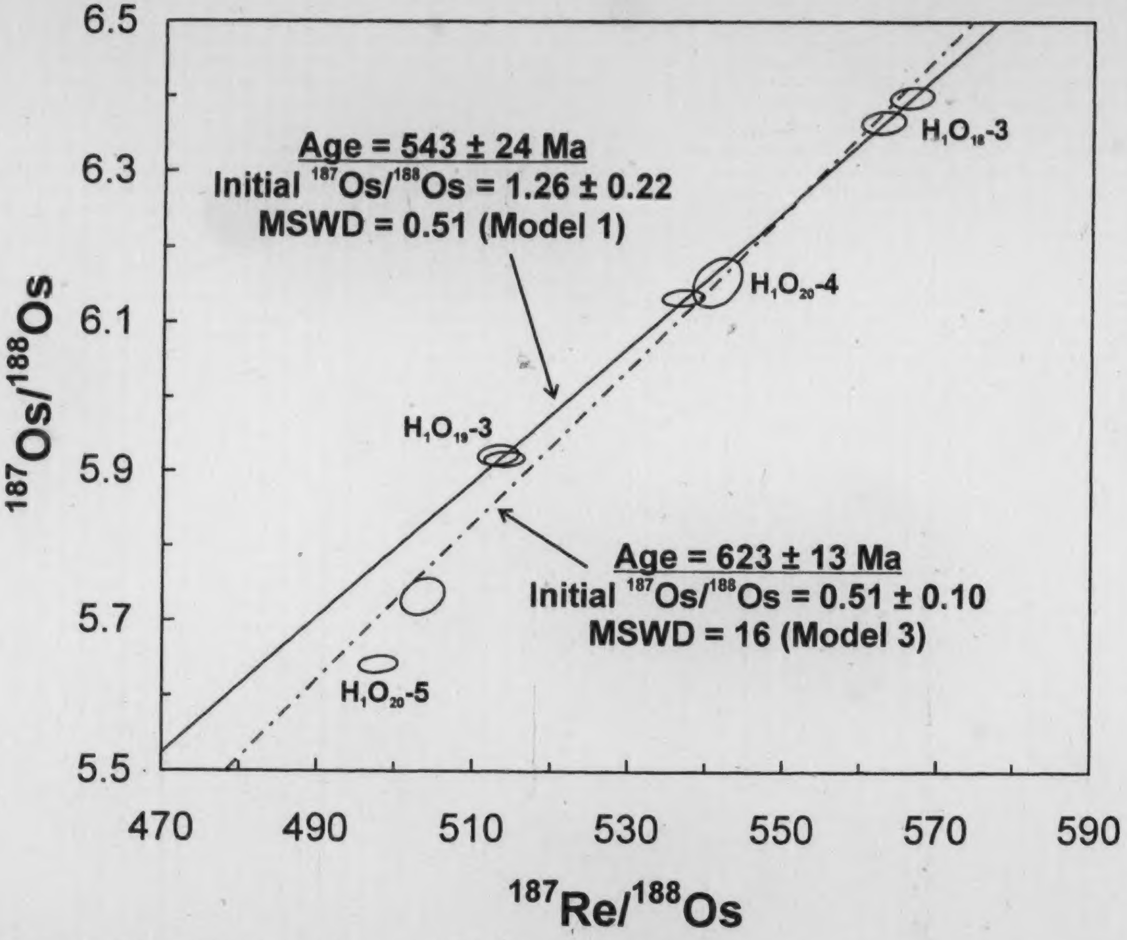

Figure 2.7: Re-Os isochron diagram showing the four most radiogenic samples (≥ 20 g aliquots only) for Member 4, Doushantuo Formation.

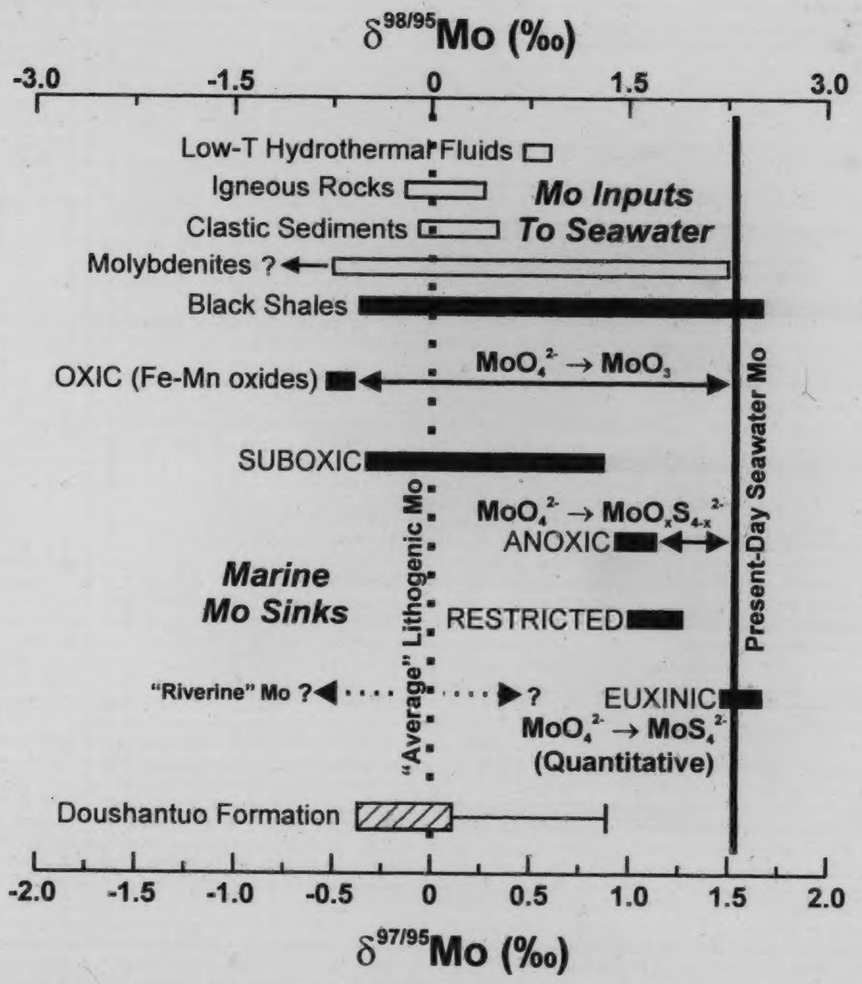

Figure 2.8: Molybdenum isotope composition of present-day seawater sources and sinks. The range in Mo isotope composition for molybdenites is uncertain given difficulties in comparing data from laboratories employing different in-house solution standards. See text for discussion. Mo isotope data from Member 4 of the Doushantuo Formation is shown for comparison. Data sources: Low-temperature hydrothermal fluids: McManus et al. (2002); "Continental/lithogenic source" (igneous rocks, clastic sediments, molybdenites, black shales): Barling et al. (2001), Siebert et al. (2003, 2005), Arnold et al. (2004), Nägler et al. (2005), Pietruszka et al. (2006), Malinovsky et al. (2007), Hannah et al. (2007), this study; Fe-Mn oxides: Barling et al. (2001), Siebert et al. (2003); Suboxic sediments: Siebert et al. (2006); Anoxic sediments: Poulson et al. (2006); Restricted basin sediments: Arnold et al. (2004); Nägler et al. (2005); Euxinic sediments: Barling et al. (2001); Arnold et al. (2004).

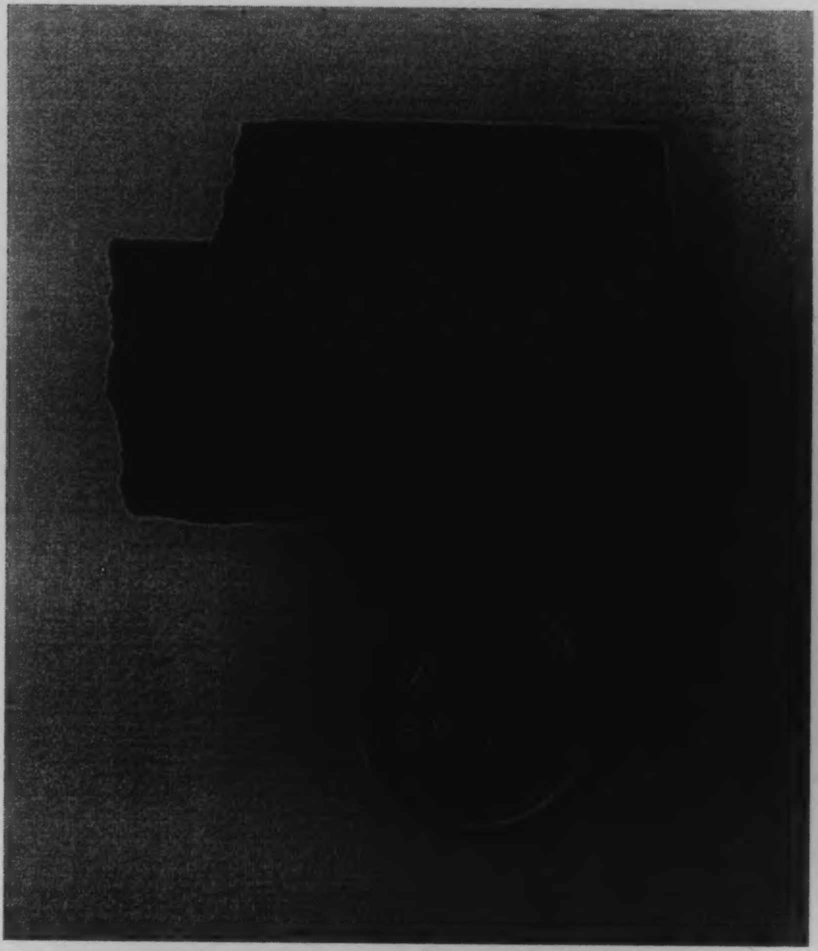

Plate 2.1: Sub-sample of whole-rock H_1O_1 (finely laminated, shaly limestone), base of Member 2, Neoproterozoic Doushantuo Formation, South China.

Plate 2.2: Sub-samples of whole rocks H_1O_9 (left) and H_1O_{14} (right) (finely laminated black shale), lower to middle Member 2, Doushantuo Formation.

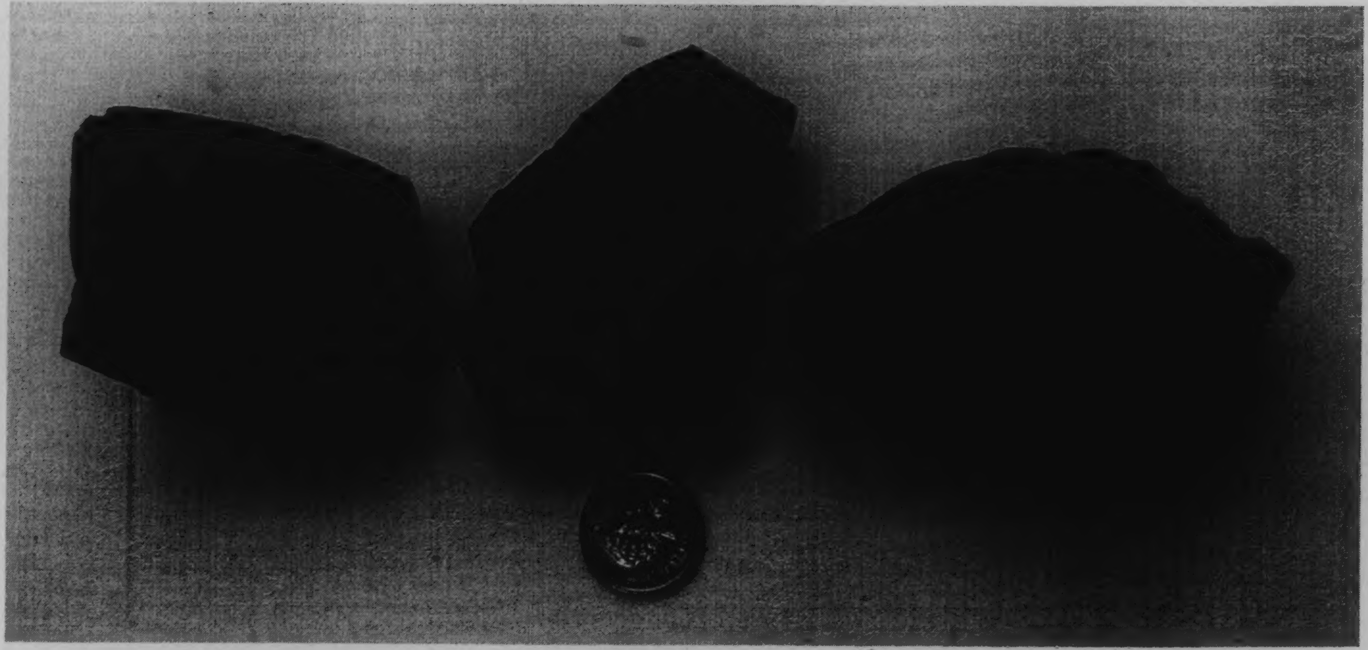

Plate 2.3: Sub-samples of whole rocks H_1O_{18} (left), H_1O_{20} (middle), and H_1O_{21} (right) (finely laminated black shale), Member 4, Doushantuo Formation.

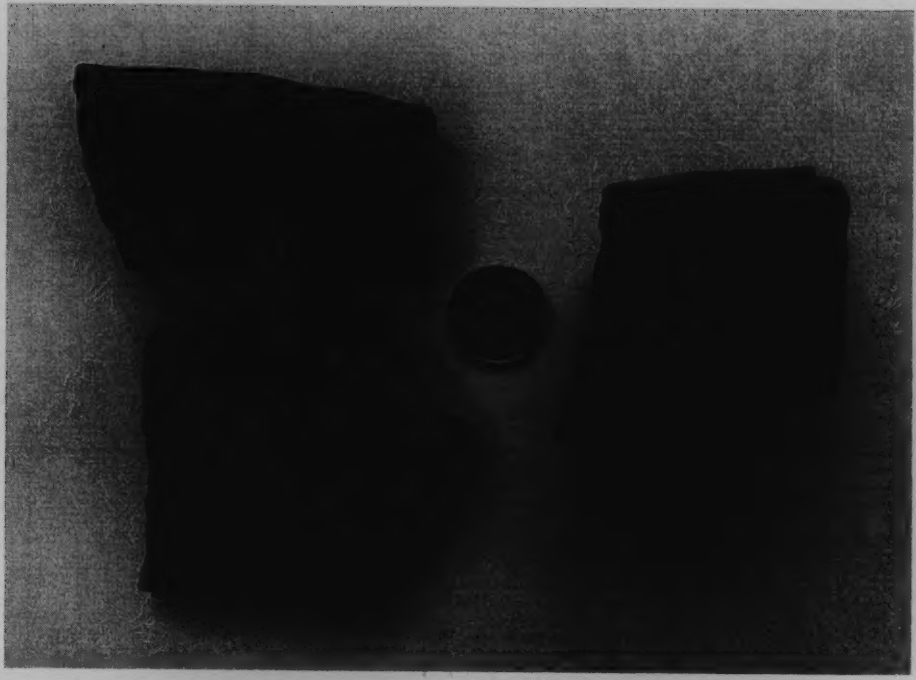

Plate 2.4: Sub-samples of whole rocks H_1O_{26} (left) and H_1O_{32} (right) (dark gray bituminous limestone), Shibantan Member, Ediacaran Dengying Formation, South China. Darker bands in H_1O_{32} are organic-rich laminae.

REFERENCES

Algeo, T.J., and Maynard, J.B., 2004, Trace-element behavior and redox facies in core shales of Upper Pennsylvanian Kansas-type cyclothems: Chemical Geology, v. 206, p. 289-318.

Algeo, T.J., and Lyons, T.W., 2006, Mo – total organic carbon covariation in modern anoxic marine environments: implications for analysis of paleoredox and paleohydrographic conditions: Paleoceanography, v. 21, paper PA1016.

Amthor, J.E., Grotzinger, J.P., Schröder, S., Bowring, S.A., Ramezani, J., Martin, M.W., and Matter, A., 2003, Extinction of *Cloudina* and *Namacalathus* at the Precambrian-Càmbrian boundary in Oman: Geology, v. 31, p. 431-434.

Anbar, A.D., Knab, K.A., and Barling, J., 2001, Precise determination of mass-dependent variations in the isotopic composition of molybdenum using MC-ICPMS: Analytical Chemistry, v. 73, p. 1425-1431.

Anbar, A.D., Duan, Y., Lyons, T.W., Arnold, G.L., Kendall, B., Creaser, R.A., Kaufman, A.J., Gordon, G.W., Scott, C., Garvin, J., and Buick, R., 2007, A whiff of oxygen before the Great Oxidation Event?: Science, v. 317, p. 1903-1906.

Anderson, T.F., and Raiswell, R., 2004, Sources and mechanisms for the enrichment of highly reactive iron in euxinic Black Sea sediments: American Journal of Science, v. 304, p. 203-233.

Archer, C., and Vance, D., 2006, Coupled Fe and S isotope evidence for Archean microbial Fe(III) and sulfate reduction: Geology, v. 34, p. 153-156.

Arnold, G.L., Anbar, A.D., Barling, J., and Lyons, T.W., 2004, Molybdenum isotope evidence for widespread anoxia in Mid-Proterozoic oceans: Science, v. 304, p. 87-90.

Arthur, M.A., and Sageman, B.B., 1994, Marine black shales: Depositional mechanisms and environments of ancient deposits: Annual Reviews in Earth and Planetary Sciences, v. 22, p. 499-551.

Bailey, J.V., Joye, S.B., Kalanetra, K.M., Flood, B.E., and Corsetti, F.A., 2007, Evidence of giant sulphur bacteria in Neoproterozoic phosphorites: Nature, v. 445, p. 198-201.

Barling, J., and Anbar, A.D., 2004, Molybdenum isotope fractionation during adsorption by manganese oxides: Earth and Planetary Science Letters, v. 217, p. 315-329.

Barling, J., Arnold, G.L., and Anbar, A.D, 2001, Natural mass-dependent variations in the isotopic composition of molybdenum: Earth and Planetary Science Letters, v. 193, p. 447-457.

Barfod, G.H., Albarède, F., Knoll, A.H., Xiao, S., Télouk, P., Frei, R., and Baker, J., 2002, New Lu-Hf and Pb-Pb age constraints on the earliest animal fossils: Earth and Planetary Science Letters, v. 201, p. 203-212.

Beard, B.L., Johnson, C.M., Skulan, J.L., Nealson, K.H., Cox, L., and Sun, H., 2003a, Application of Fe isotopes to tracing the geochemical and biological cycling of Fe: Chemical Geology, v. 195, p. 87-117.

Beard, B.L., Johnson, C.M., Von Damm, K.L., and Poulson, R.L., 2003b, Iron isotope constraints on Fe cycling and mass balance in oxygenated Earth oceans: Geology, v. 31, p. 629-632.

Bengtson, S., and Zhao, Y., 1992, Predatorial borings in Late Precambrian mineralized exoskeletons: Science, v. 257, p. 367-369.

Benus, A. P., 1988, Sedimentological context of a deep-water Ediacaran fauna (Mistaken Point, Avalon Zone, eastern Newfoundland), *in* Landing, E., et al., eds., Trace fossils, small shelly fossils and the Precambrian-Cambrian boundary: New York State Museum and Geological Survey Bulletin, v. 463, p. 8-9.

Bertine, K.K., and Turekian, K.K., 1973, Molybdenum in marine deposits: Geochimica et Cosmochimica Acta, v. 37, p. 1415-1434.

Bottjer, D.J., and Clapham, M.E., 2006, Evolutionary paleoecology of Ediacaran benthic marine animals, *in* Xiao, S., and Kaufman, A.J., eds., Neoproterozoic Geobiology and Paleobiology: Springer, New York, p. 91-114.

Bowring, S.A., Myrow, P., Landing, E., and Ramenzani, J., 2003, Geochronological constraints on Terminal Neoproterozoic events and the rise of metazoans: Geophysical Research Abstracts, v. 5, p. 13,219.

Bristow, T.F., Kennedy, M.J., Jiang, G., and Derrowski, A., 2006, Do geochemical records from the Doushantuo Formation record a marine signal?: Geological Society of America Abstracts With Programs, v. 38 (7), p. 57.

Calver, C.R., 2000, Isotope stratigraphy of the Ediacarian (Neoproterozoic III) of the Adelaide Rift Complex, Australia, and the overprint of water column stratification: Precambrian Research, v. 100, p. 121-150.

Calver, C.R., and Lindsay, J.F., 1998, Ediacarian sequence and isotope stratigraphy of the Officer Basin, South Australia: Australian Journal of Earth Sciences, v. 45, p. 513-532.

Calver, C.R., Black, L.P., Everard, J.L., and Seymour, D.B., 2004, U-Pb zircon age constraints on Late Neoproterozoic glaciation in Tasmania: Geology, v. 32, p. 893-896.

Calvert, S.E., and Pedersen, T.F., 1996, Sedimentary geochemistry and manganese: Implications for the environment of formation of manganiferous black shales: Economic Geology, v. 91, p. 36-47.

Canfield, D.E., and Teske, A., 1996, Late Proterozoic rise in atmospheric oxygen concentration inferred from phylogenetic and sulphur-isotope studies: Nature, v. 382, p. 127-132.

Canfield, D.E., Lyons, T.W., and Raiswell, R., 1996, A model for iron deposition to euxinic Black Sea sediments: American Journal of Science, v. 296, p. 818-834.

Canfield, D.E., Poulton, S.W., and Narbonne, G.M., 2007, Late-Neoproterozoic deep-ocean oxygenation and the rise of animal life: Science, v. 315, p. 92-95.

Chen, J., Oliveri, P., Gao, F., Dornbos, S.Q., Li, C.-W., Bottjer, D.J., and Davidson, E.H., 2002, Precambrian animal life: Probable developmental and adult cnidarians forms from Southwest China: Developmental Biology, v. 2[illegible], p. 182-196.

Chen, D.F., Dong, W.Q., Qi, L., Chen, G.Q., and Chen, X.P., 2003, Possible REE constraints on the depositional and diagenetic constraints environment of Doushantuo Formation phosphorites containing the earliest metazoan fauna: Chemical Geology, v. 201, p. 103-118.

Chen, J.-Y., Bottjer, D.J., Oliveri, P., Dornbos, S.Q., Gao, F., Ruffins, S., Chi, H., Li, C-W., and Davidson, E.H., 2004a, Small bilaterian fossils from 40 to 55 million years before the Cambrian: Science, v. 305, p. 218-222.

Chen, D.F., Dong, W.Q., Zhu, B.Q., and Chen, X.P., 2004b, Pb-Pb ages of Neoproterozoic Doushantuo phosphorites in South China: Constraints on early metazoan evolution and glaciation events: Precambrian Research, v. 132, p. 123-132.

Chen, J.-Y., Bottjer, D.J., Davidson, E.H., Dornbos, S.Q., Gao, X., Yang, Y.-H., Li, C.-W., Li, G., Wang, X.-Q., Xian, D.-C., Wu, H.-J., Hwu, Y.-K., and Tafforeau, P., 2006, Phosphatized polar lobe-forming embryos from the Precambrian of Southwest China: Science, v. 312, p. 1644-1646.

Clapham, M.E., and Narbonne, G.M., 2002, Ediacaran epifaunal tiering: Geology, v. 30, p. 627-630.

Condon, D., Zhu, M., Bowring, S., Wang, W., Yang, A., and Jin, Y, 2005, U-Pb ages from the Neoproterozoic Doushantuo Formation, China: Science, v. 308, p. 95-98.

Corsetti, F.A., and Kaufman, A.J., 2003, Stratigraphic investigations of carbon isotope anomalies and Neoproterozoic ice ages in Death Valley, California: Geological Society of America Bulletin, v. 115, p. 916-932.

Creaser, R.A., Sannigrahi, P., Chacko, T., and Selby, D. 2002, Further evaluation of the Re-Os geochronometer in organic-rich sedimentary rocks: a test of hydrocarbon maturation effects in the Exshaw Formation, Western Canada Sedimentary Basin: Geochimica et Cosmochimica Acta, v. 66, p. 3441-3452.

Crusius, J., Calvert, S., Pedersen, T., and Sage, D., 1996, Rhenium and molybdenum enrichments in sediments as indicators of oxic, suboxic, and sulfidic conditions of deposition: Earth and Planetary Science Letters, v. 145, p. 65-78.

Derry, L.A., Kaufman, A.J., and Jacobsen, S.B., 1992, Sedimentary cycling and environmental change in the Late Proterozoic: Evidence from stable and radiogenic isotopes: Geochimica et Cosmochimica Acta, v. 56, p. 1317-1329.

Des Marais, D.J., Strauss, H., Summons, R.E., and Hayes, J.M., 1992, Carbon isotope evidence for the stepwise oxidation of the Proterozoic environment: Nature, v. 359, p. 605-608.

Ding, L., Li, Y., and Chen, H., 1992, Discovery of *Micrhystridium regulare* from Sinian-Cambrian boundary strata in Yichang, Hubei, and its stratigraphic significance: Acta Micropaleontologica Sinica, v. 9, p. 303-309.

Duan, Y., Anbar, A.D., Gordon, G., Severmann, S., Lyons, T.W., and Sageman, B., 2006, Investigation of iron isotope systematics in Middle Devonian anoxic basins. Astrobiology Science Conference 2006 abstract, Washington, D.C.

Duan, Y., Anbar, A.D., Arnold, G.L., Gordon, G.W., Severmann, S., and Lyons, T.W., 2007, The iron isotope variations in the ~ 2.5 Ga Mt. McRae Shale: Geological Society of America Abstracts With Programs, v. 39 (6), p. 449.

Emerson, S.R., and Huested, S.S., 1991, Ocean anoxia and the concentrations of molybdenum and vanadium in seawater: Marine Chemistry, v. 34, p. 177-196.

Erickson, B.E., and Helz, G.R., 2000, Molybdenum (VI) speciation in sulfidic waters: stability and lability of thiomolybdates: Geochimica et Cosmochimica Acta, v. 64, p. 1149-1158.

Esser, B.K., and Turekian, K.K., 1993, The osmium isotopic composition of the continental crust: Geochimica et Cosmochimica Acta, v. 57, p. 3093-3104.

Evans, A.M., 1993, Ore geology and industrial minerals: An introduction (3rd edition): Blackwell Science, UK.

Fehr, M.A., Andersson, P.S., and Hålenius, U., 2006, Iron isotopes in sedimentary pyrites from the Baltic Sea: Geochimica et Cosmochimica Acta, v. 70 (18; supplement 1), p. A168.

Fike, D.A., Grotzinger, J.P., Pratt, L.M., and Summons, R.E., 2006, Oxidation of the Ediacaran ocean: Nature, v. 444, p. 744-747.

Gehling, J.G., and Narbonne, G.M., 2007, Spindle-shaped Ediacara fossils from the Mistaken Point assemblage, Avalon Zone, Newfoundland: Canadian Journal of Earth Sciences, v. 44, p. 367-387.

Gordon, G.W., Anbar, A.D., Macleod K., and Lyons, T., 2006, Evaluation of the Mo isotope paleoredox proxy in Late Cretaceous ocean sediments: Geochimica et Cosmochimica Acta, v. 70 (18; supplement 1), p. A209.

Grazhdankin, D., 2004, Patterns of distribution in the Ediacaran biotas: facies versus biogeography and evolution: Paleobiology, v. 30, p. 203-221.

Grey, K., Walter, M.R., and Calver, C.R., 2003, Neoproterozoic biotic diversification: Snowball Earth or aftermath of the Acraman impact?: Geology, v. 31, p. 459-462.

Grotzinger, J.P., Bowring, S.A., Saylor, B.Z., and Kaufman, A.J., 1995, Biostratigraphic and geochronologic constraints on early animal evolution: Science, v. 270, p. 598-604.

Hagadorn, J.W., Xiao, S., Donoghue, P.C.J., Bengtson, S., Gostling, N.J., Pawlowska, M., Raff, E.C., Raff, R.A., Turner, F.R., Chongyu, Y., Zhou, C., Yuan, X., McFeely, M.B., Stampanoni, M., and Nealson, K.H., 2006, Cellular and subcellular structure of Neoproterozoic animal embryos: Science, v. 314, p. 291-294.

Harland, W.B., 1964, Critical evidence for a great infra-Cambrian glaciation: Geologische Rundschau, v. 54, p. 45-61.

Halverson, G.P., 2006, A Neoproterozoic chronology, *in* Xiao, S., and Kaufman, A.J., eds., Neoproterozoic Geobiology and Paleobiology: Springer, New York, p. 231-271.

Halverson, G.P., Hoffman, P.F., Schrag, D.P., Maloof, A.C., and Rice, A.H.N., 2005, Toward a Neoproterozoic composite carbon-isotope record: Geological Society of America Bulletin, v. 117, p. 1181-1207.

Hannah, J.L., Stein, H.J., Wieser, M.E., de Laeter, J.R., and Varner, M.D., 2007, Molybdenum isotope variations in molybdenite: Vapor transport and Rayleigh fractionation of Mo: Geology, v. 35, p. 703-706.

Hattori, Y., Suzuki, K., Honda, M., and Shimizu, H., 2003, Re-Os isotope systematics of the Taklimakan Desert sands, moraines and river sediments around the Taklimakan Desert, and of Tibetan soils: Geochimica et Cosmochimica Acta, v. 67, p. 1195-1205.

Hedges, S.B., Battistuzzi, F.U., and Blair, J.E., 2006, Molecular timescale of evolution in the Proterozoic, *in* Xiao, S., and Kaufman, A.J., eds., Neoproterozoic Geobiology and Paleobiology: Springer, New York, p. 199-229.

Helz, G.R., Miller, C.V., Charnock, J.M., Mosselmans, J.F.W., Pattrick, R.A.D., Garner, C.D., and Vaughan, D.J., 1996, Mechanism of molybdenum removal from the sea and its concentration in black shales: EXAFS evidence: Geochimica et Cosmochimica Acta, v. 60, p. 3631-3642.

Hoffman, P.F., and Schrag, D.P., 2002, The snowball Earth hypothesis: Testing the limits of global change: Terra Nova, v. 14, p. 129-155.

Hoffman, P.F., Kaufman, A.J., Halverson, G.P., and Schrag, D.P., 1998, A Neoproterozoic snowball Earth: Science, v. 281, p. 1342-1346.

Hoffmann, K.-H., Condon, D.J., Bowring, S.A., and Crowley, J.L., 2004, U-Pb zircon date from the Neoproterozoic Ghaub Formation, Namibia: Constraints on Marinoan glaciation: Geology, v. 32, p. 817-820.

Hofmann, H.J., Narbonne, G.M., and Aitken, J.D., 1990, Ediacaran remains from intertillite beds in northwestern Canada: Geology, v. 18, p. 1199-1202.

Hua, H., Chen, Z., Yuan, X., Zhang, L., and Xiao, S., 2005, Skeletogenesis and asexual reproduction in the earliest biomineralizing animal *Cloudina*: Geology, v. 33, p. 277-280.

Huntley, J.W., Xiao, S., and Kowalewski, M., 2006, On the morphological history of Proterozoic and Cambrian acritarchs, *in* Xiao, S., and Kaufman, A.J., eds., Neoproterozoic Geobiology and Paleobiology: Springer, New York, p. 23-56.

Hurtgen, M.T., Arthur, M.A., and Halverson, G.P., 2005, Neoproterozoic sulfur isotopes, the evolution of microbial sulfur species, and the burial efficiency of sulfide as sedimentary pyrite: Geology, v. 33, 41-44.

Hyde, W.T., Crowley, T.J., Baum, S.K., and Peltier, W.R., 2000, Neoproterozoic 'snowball Earth' simulations with a coupled climate/ice-sheet model: Nature, v. 405, p. 425-429.

Jacobsen, S.B., and Kaufman, A.J., 1999, The Sr, C and O isotopic composition of Neoproterozoic seawater: Chemical Geology, v. 361, p. 37-57.

Jenkins, R.J.F., Cooper, J.A., and Compston, W., 2002, Age and biostratigraphy of Early Cambrian tuffs from SE Australia and southern China: Geological Society [London], v. 159, p. 645-648.

Jensen, S., Droser, M.L., and Gehling, J.G., 2006, A critical look at the Ediacaran trace fossil record, *in* Xiao, S., and Kaufman, A.J., eds., Neoproterozoic Geobiology and Paleobiology: Springer, New York, p. 115-157.

Jiang, G., Sohl, L.E., and Christie-Blick, N., 2003a, Neoproterozoic stratigraphic comparison of the Lesser Himalaya (India) and Yangtze block (South China): Paleogeographic implications: Geology, v. 31, p. 917-920.

Jiang, G., Kennedy, M.J., and Christie-Blick, N., 2003b, Stable isotopic evidence for methane seeps in Neoproterozoic postglacial cap carbonates: Nature, v. 426, p. 822-826.

Jiang, G., Kennedy, M.J., Christie-Blick, N., Wu, H., and Zhang, S., 2006, Stratigraphy, sedimentary structures, and textures of the Late Neoproterozoic Doushantuo cap carbonate in South China: Journal of Sedimentary Research, v. 76, p. 978-995.

Jiang, G., Kaufman, A.J., Christie-Blick, N., Zhang, S., and Wu, H., 2007, Carbon isotope variability across the Ediacaran Yangtze platform in South China: Implications for a large surface-to-deep ocean $\delta^{13}C$ gradient: Earth and Planetary Science Letters, v. 261, p. 303-320.

Kaufman, A.J., and Knoll, A.H., 1995, Neoproterozoic variations in the C-isotopic composition of seawater: Stratigraphic and biogeochemical implications: Precambrian Research, v. 73, p. 27-49.

Kaufman, A.J., Jacobsen, S.B., and Knoll, A.H., 1993, The Vendian record of Sr and C isotopic variations in seawater: Implications for tectonics and paleoclimate: Earth and Planetary Science Letters, v. 120, p. 409-430.

Kaufman, A.J., Knoll, A.H., and Narbonne, G.M., 1997, Isotopes, ice ages, and Terminal Proterozoic Earth history: Proceedings of the National Academy of Sciences, v. 94, p. 6600-6605.

Kaufman, A.J., Jiang, G., Christie-Blick, N., Banerjee, D.M., and Rai, V., 2006, Stable isotope record of the Terminal Neoproterozoic Krol platform in the Lesser Himalayas of northern India: Precambrian Research, v. 147, p. 156-185.

Kaufman, A.J., Corsetti, F.A., and Varni, M.A., 2007, The effect of rising atmospheric oxygen on carbon and sulfur isotope anomalies in the Neoproterozoic Johnnie Formation, Death Valley, USA: Chemical Geology, v. 237, p. 47-63.

Kendall, B.S., Creaser, R.A., Ross, G.M., and Selby, D., 2004, Constraints on the timing of Marinoan "Snowball Earth" glaciation by ^{187}Re-^{187}Os dating of a Neoproterozoic, post-glacial black shale in Western Canada: Earth and Planetary Science Letters, v. 222, p. 729-740.

Kennedy, M.J., Runnegar, B., Prave, A.R., Hoffmann, K.-H., and Arthur, M.A., 1998, Two or four Neoproterozoic glaciations?: Geology, v. 26, p.1059-1063.

Kennedy, M., Droser, M., Mayer, L.M., Pevear, D., Mrofka, D., 2006, Late Precambrian oxygenation; inception of the clay mineral factory: Science, v. 311, p. 1446-1449.

Kirschvink, J.L., 1992, Late Proterozoic low-latitude global glaciation: The Snowball Earth, *in* Schopf, J.W., and Klein, C., eds., The Proterozoic biosphere: Cambridge University Press, p. 51-52.

Knauth, L.P., 2006, Temperature and salinity history of the Precambrian ocean: Implications for the course of microbial evolution: Palaeogeography, Palaeoclimatology, Palaeoecology, v. 219, p. 53-69.

Knoll, A.H., 1991, End of the Proterozoic Eon: Scientific American, v. 265, p. 64-73.

Knoll, A.H., and Carroll, S.B., 1999, Early animal evolution: Emerging views from comparative biology and geology: Science, v. 284, p. 2129-2137.

Knoll, A.H., Hayes, J.M., Kaufman, A.J., Swett, K., and Lambert, I.B., 1986, Secular variation in carbon isotope ratios from Upper Proterozoic successions of Svalbard and East Greenland: Nature, v. 321, p. 832-838.

Knoll, A.H., Walter, M.R., Narbonne, G.M., and Christie-Blick, N., 2004, A new period for the geologic time scale: Science, v. 305, p. 621-622.

Knoll, A.H., Walter, M.R., Narbonne, G.M., and Christie-Blick, N., 2006, The Ediacaran Period: A new addition to the geologic time scale: Lethaia, v. 39, p. 13-30.

Le Guerroué, E., Allen, P.A., and Cozzi, A., 2006a, Chemostratigraphic and sedimentological framework of the largest negative carbon isotopic excursion in Earth history: The Neoproterozoic Shuram Formation (Nafun Group, Oman): Precambrian Research, v. 146, p. 68-92.

Le Guerroué, E., Allen, P.A., Cozzi, A., Etienne, J.L., and Fanning, M., 2006b, 50 Myr recovery from the largest negative δ^{13}C excursion in the Ediacaran ocean: Terra Nova, v. 18, p. 147-153.

Lehmann, B., Nägler, T.F., Holland, H.D., Wille, M., Mao, J., Pan, J., Ma, D., and Dulski, P., 2007, Highly metalliferous carbonaceous shale and Early Cambrian seawater: Geology, v. 35, p. 403-406.

Levasseur, S., Birck, J.-L., and Allègre, C.J., 1999, The osmium riverine flux and the oceanic mass balance of osmium: Earth and Planetary Science Letters, v. 174, p. 7-23.

Levasseur, S., Frank, M., Hein, J.R., and Halliday, A.N., 2004, The global variation in the iron isotope composition of marine hydrogenetic ferromanganese deposits: Implications for seawater chemistry?: Earth and Planetary Science Letters, v. 224, p. 91-105.

Li, C.-W., Chen, J.-Y., and Hua, T.-E., 1998, Precambrian sponges with cellular structures: Science, v. 279, p. 879-882.

Love, G.D., Fike, D.A., Grosjean, E., Stalvies, C., Grotzinger, J., Bradley, A.S., Bowring, S., Condon, D., and Summons, R.E., 2006, Constraining the timing of basal metazoan radiation using molecular biomarkers and U-Pb isotope dating: Geochimica et Cosmochimica Acta, v. 70 (18; supplement 1), p. A371.

Lyons, T.W., 1997, Sulfur isotope trends and pathways of iron sulfide formation in the upper Holocene sediments of the anoxic Black Sea: Geochimica et Cosmochimica Acta, v. 61, p. 3367-3382.

Lyons, T.W., and Severmann, S., 2006, A critical look at iron paleoredox proxies: New insights from modern euxinic marine basins: Geochimica et Cosmochimica Acta, v. 70, p. 5698-5722.

Lyons, T.W., Werne, J.P., Hollander, D.J., and Murray, R.W., 2003, Contrasting sulfur geochemistry and Fe/Al and Mo/Al ratios across the last oxic-to-anoxic transition in the Cariaco Basin, Venezuela: Chemical Geology, v. 195, p. 131-157.

Macouin, M., Besse, J., Ader, M., Gilder, S., Yang, Z., Sun, Z., and Agrinier, P., 2004, Combined paleomagnetic and isotopic data from the Doushantuo carbonates, South China: Implications for the "snowball" Earth hypothesis: Earth and Planetary Science Letters, v. 224, p. 387-398.

Malinovsky, D., Hammarlund, D., Ilyashuk, B., Martinsson, O., and Gelting, J., 2007, Variations in the isotopic composition of molybdenum in freshwater lake systems: Chemical Geology, v. 236, p. 181-198.

Martin, M.W., Grazhdankin, D.V., Bowring, S.A., Evans, D.A.D., Fedonkin, M.A., and Kirschvink, J.L., 2000, Age of Neoproterozoic bilatarian body and trace fossils, White Sea, Russia: Implications for Metazoan evolution: Science, v. 288, p. 841-845.

Matthews, A., Morgans-Bell, H.S., Emmanuel, S., Jenkyns, H.C., Erel, Y., and Halicz, L., 2004, Controls on iron-isotope fractionation in organic-rich sediments

(Kimmeridge Clay, Upper Jurassic, southern England): Geochimica et Cosmochimica Acta, v. 68, p. 3107-3123.

McKirdy, D.M., Burgess, J.M., Lemon, N.M., Yu, X., Cooper, A.M., Gostin, V.A., Jenkins, R.J.F., and Both, R.A., 2001, A chemostratigraphic overview of the late Cryogenian interglacial sequence in the Adelaide Fold-Thrust Belt, South Australia: Precambrian Research, v. 106, p. 149-186.

Meisel, T., Walker, R.J., Irving, A.J., and Lorand, J.-P., 2001, Osmium isotopic compositions of mantle xenoliths: a global perspective: Geochimica et Cosmochimica Acta, v. 65, p. 1311-1323.

Melezhik, V.A., Fallick, A.E., and Pokrovsky, B.G., 2005, Enigmatic nature of thick sedimentary carbonates depleted in ^{13}C beyond the canonical mantle value: the challenges to our understanding of the terrestrial carbon cycle: Precambrian Research, v. 137, v. 131-165.

Morford, J.L., and Emerson, S., 1999, The geochemistry of redox sensitive trace metals in sediments: Geochimica et Cosmochimica Acta, v. 63, p. 1735-1750.

Nägler, T.F., Siebert, C., Lüshcen, H., and Böttcher, M.E., 2005, Sedimentary Mo isotope record across the Holocene fresh-brackish water transition of the Black Sea: Chemical Geology, v. 219, p. 283-295.

Narbonne, G.M., 1998, The Ediacara biota: A Terminal Neoproterozoic experiment in the evolution of life: GSA Today, v. 8 (2), p. 1-6.

Narbonne, G.M., 2004, Modular construction of early Ediacaran complex life forms: Science, v. 305, p. 1141-1144.

Narbonne, G.M., and Gehling, J.G., 2003, Life after snowball: The oldest complex Ediacaran fossils: Geology, v. 31, p. 27-30.

Oxburgh, R., 1998, Variations in the osmium isotope composition of seawater over the past 200,000 years: Earth and Planetary Science Letters, v. 159, p. 183-191.

Oxburgh, R., 2001, Residence time of osmium in the oceans: Geochemistry, Geophysics, Geosystems, Paper #2000GC000104.

Pearce, C.R., Cohen, A.S., Coe, A.L., and Burton, K.W., 2006, Changes in the extent of marine anoxia during the Early Jurassic: Evidence from molybdenum isotopes: Geochimica et Cosmochimica Acta, v. 70 (18; supplement 1), p. A476.

Peterson, K.J., and Butterfield, N.J., 2005, Origin of the Eumetazoa: Testing ecological predictions of molecular clocks against the Proterozoic fossil record: Proceedings of the National Academy of Sciences, v. 102, p. 9547-9552.

Peterson, K.J., Lyons, J.B., Nowak, K.S., Takacs, C.M., Wargo, M.J., and McPeek, M.A., 2004, Estimating metazoan divergence times with a molecular clock: Proceedings of the National Academy of Sciences, v. 101, p. 6536-6541.

Peucker-Ehrenbrink, B., and Jahn, B.-M., 2001, Rhenium-osmium isotope systematics and platinum group element concentrations: loess and the upper continental crust: Geochemistry Geophysics Geosystems, v. 2, Paper 2001GC000172.

Pietruszka, A.J., Walker, R.J., and Candela, P.A., 2006, Determination of mass-dependent molybdenum isotopic variations by MC-ICP-MS: An evaluation of matrix effects: Chemical Geology, v. 225, p. 121-136.

Piper, D.Z., 1994, Seawater as the source of minor elements in black shales, phosphorites and other sedimentary rocks: Chemical Geology, v. 114, p. 95-114.

Poulson, R.L., Siebert, C., McManus, J., and Berelson, W.M., 2006, Authigenic molybdenum isotope signatures in marine sediments: Geology, v. 34, p. 617-620.

Poulton, S.W., and Canfield, D.E., 2005, Development of a sequential extraction procedure for iron: Implications for iron partitioning in continentally derived particulates: Chemical Geology, v. 214, p. 209-221.

Qian, Y., Chen, M., and Chen, Y., 1979, Hyolithids and other small shelly fossils from the Lower Cambrian Huangshandong Formation in the eastern part of the Yangtze Gorge: Acta Paleontologica Sinica, v. 18, p. 207-232.

Raiswell, R., and Canfield, D.E., 1996, Rates of reaction between silicate iron and dissolved sulfide in Peru Margin sediments: Geochimica et Cosmochimica Acta, v. 60, p. 2777-2787.

Raiswell, R., and Anderson, T.F., 2005, Reactive iron enrichment in sediments deposited beneath euxinic bottom waters: Constraints on supply by shelf recycling, *in* McDonald, I., et al., eds., Mineral deposits and Earth evolution: Geological Society Special Publication 248, p. 179-194.

Raiswell, R., Buckley, F., Berner, R.A., and Anderson, T.F., 1988, Degree of pyritization of iron as a paleoenvironmental indicator of bottom-water oxygenation: Journal of Sedimentary Petrology, v. 58, p. 812-819.

Rothman, D.H., Hayes, J.M., and Summons, R.E., 2003, Dynamics of the Neoproterozoic carbon cycle: Proceedings of the National Academy of Sciences, v. 100, p. 8124-8129.

Rouxel, O.J., Bekker, A., and Edwards, K.J., 2005, Iron isotope constraints on the Archean and Paleoproterozoic ocean redox state: Science, v. 307, p. 1088-1091.

Saylor, B.Z., Kaufman, A.J., Grotzinger, J.P., and Urban, F., 1998, A composite reference section for Terminal Proterozoic strata of southern Namibia: Journal of Sedimentary Research, v. 68, p. 1223-1235.

Selby, D., and Creaser, R.A., 2004, Macroscale NTIMS and microscale LA-MC-ICP-MS Re-Os isotopic analysis of molybdenite: Testing spatial restrictions for reliable Re-Os age determinations, and implications for the decoupling of Re and Os within molybdenite: Geochimica et Cosmochimica Acta, v. 68, p. 3897-3908.

Selby, D., and Creaser, R.A., 2005, Direct radiometric dating of the Devonian-Mississippian time-scale boundary using the Re-Os black shale geochronometer: Geology, v. 33, p. 545-548.

Severmann, S., Lyons, T., Anbar, A., Gordon, G., and McManus, J., 2006a, The isotopic expression of iron shuttling in the euxinic Black Sea basin and implications for the rise of oxygen in the early atmosphere: Geological Society of America Abstracts With Programs, v. 38 (7), p. 124.

Severmann, S., Lyons, T.W., Duan, Y., Anbar, A., Gordon, G., and McManus, J., 2006b, The isotopic expression of Fe shuttling in modern and ancient euxinic sediments: implications for the rise of oxygen: Geochimica et Cosmochimica Acta, v. 70 (18; supplement 1), p. A572.

Severmann, S., Johnson, C.M., Beard, B.L., and McManus, J., 2006c, The effect of early diagenesis on the Fe isotope compositions of porewaters and authigenic minerals in continental margin sediments: Geochimica et Cosmochimica Acta, v. 70, p. 2006-2022.

Siebert, C., Nägler, T.F., von Blanckenburg, F., and Kramers, J.D., 2003, Molybdenum isotope records as a potential new proxy for paleoceanography: Earth and Planetary Science Letters, v. 211, p. 159-171.

Siebert, C., Kramers, J.D., Meisel, T., Morel, P., and Nägler, T.F., 2005, PGE, Re-Os, and Mo isotope systematics in Archean and early Proterozoic sedimentary systems as proxies for redox conditions of the early Earth: Geochimica et Cosmochimica Acta, v. 69, p. 1787-1801.

Siebert, C., McManus, J., Bice, A., Poulson, R., and Berelson, W.M., 2006, Molybdenum isotope signatures in continental margin sediments: Earth and Planetary Science Letters, v. 241, p. 723-733.

Sprigg, R.G., 1947, Early Cambrian (?) jellyfishes from the Flinders Ranges, South Australia: Royal Society of South Australia Transactions, v. 71, p. 212-224.

Squire, R.J., Campbell, I.H., Allen, C.M., and Wilson, C.J.L., 2006, Did the Transgondwanan Supermountain trigger the explosive radiation of animals on Earth?: Earth and Planetary Science Letters, v. 250, p. 116-133.

Staubwasser, M., Von Blanckenburg, F., and Schoenberg, R., 2006, Iron isotopes in the early marine diagenetic iron cycle: Geology, v. 34, p. 629-632.

Sun, W., 1986, Late Precambrian pennatulids (sea pens) from the eastern Yangtze Gorge, China: Paracharnia gen. nov.: Precambrian Research, v. 31, p. 361-375.

Sun, W., Arculus, R.J., Bennett, V.C., Eggins, S.M., and Binns, R.A., 2003a, Evidence for rhenium enrichment in the mantle wedge from submarine arc-like volcanic glasses (Papua New Guinea): Geology, v. 31, p. 845-848.

Sun, W., Bennett, V.C., Eggins, S.M., Kamenetsky, V.S., and Arculus, R.J., 2003b, Enhanced mantle-to-crust rhenium transfer in undegassed arc magmas: Nature, v. 422, p. 294-297.

Taylor, P.D.P., Maeck, R., and De Bièvre, P., 1992, Determination of the absolute isotopic composition and atomic weight of a reference sample of natural iron: International Journal of Mass Spectrometry and Ion Processes, v. 121, p. 111-125.

Tribovillard, N., Algeo, T.J., Lyons, T., and Riboulleau, A., 2006, Trace metals as paleoredox and paleoproductivity proxies: An update: Chemical Geology, v. 232, p. 12-32.

Walker, R.J., Horan, M.F., Morgan, J.W., Becker, H., Grossman, J.N., and Rubin, A.E., 2002a, Comparative ^{187}Re-^{187}Os systematics of chondrites: implications regarding early solar system processes: Geochimica et Cosmochimica Acta, v. 66, p. 4187-4201.

Walker, R.J., Prichard, H.M., Ishiwatari, A., and Pimentel, M., 2002b, The osmium isotopic composition of convecting upper mantle deduced from ophiolite chromites: Geochimica et Cosmochimica Acta, v. 66, p. 329-345.

Walter, M.R., Veevers, J.J., Calver, C.R., Gorjan, P., and Hill, A.C., 2000, Dating the 840-544 Ma Neoproterozoic interval by isotopes of strontium, carbon, and sulfur in seawater, and some interpretative models: Precambrian Research, v. 100, p. 371-433.

Wang, X., Erdtmann, B.-D., Chen, X., and Mao, X., 1998, Integrated sequence-, bio- and chemo-stratigraphy of the Terminal Proterozoic to lowermost Cambrian "black rock series" from central South China: Episodes, v. 21, p. 178-189.

Wedepohl, K.H., 1971, Environmental influences on the chemical composition of shales and clays, *in* Ahrens, L.H., et al., eds., Physics and chemistry of the Earth, volume 8: Pergamon, Oxford, UK, p. 305-333.

Wedepohl, K.H., 1991, The composition of the upper Earth's crust and the natural cycles of selected metals. Metals in natural raw materials. Natural resources, *in* Merian, E., ed., Metals and their compounds in the environment: VCH, Weinheim, Germany, p. 3-17.

Wheat, C.G., Motil, M.J., and Rudnicki, M., 2002, Trace element and REE composition of a low-temperature ridge-flank hydrothermal spring: Geochimica et Cosmochimica Acta, v. 66, p. 3693-3705.

Widom, E., Gaddis, S.J., and Wells, N.E., Jr., 2004, Re-Os isotope systematics in carbonates from Serpent Mound, Ohio: Implications for Re-Os dating of crustal rocks and the osmium isotopic composition of Ordovician seawater: Geochemistry, Geophysics, Geosystems, v. 5, Paper #2002GC000444.

Wieser, M.E., and de Laeter, J.R., 2003, A preliminary study of isotope fractionation in molybdenites: International Journal of Mass Spectrometry, v. 225, p. 177-183.

Wijsman, J.W.M., Middleburg, J.J., and Heip, C.H.R., 2001, Reactive iron in Black Sea sediments: Implications for iron cycling: Marine Geology, v. 172, p. 167-180.

Xiao, S., 2004a, New multicellular algal fossils and acritarchs in Doushantuo chert nodules (Neoproterozoic; Yangtze Gorges, South China): Journal of Paleontology, v. 78, p. 393-401.

Xiao, S., 2004b, Neoproterozoic glaciations and the fossil record, *in* Jenkins, G.S., et al., eds., The extreme Proterozoic: Geology, geochemistry, and climate: American Geophysical Union Geophysical Monograph 146, p. 199-214.

Xiao, S., and Knoll, A.H., 2000, Phosphatized animal embryos from the Neoproterozoic Doushantuo Formation at Weng'an, Guizhou, South China: Journal of Paleontology, v. 74, p. 767-788.

Xiao, S., Zhang, Y., and Knoll, A.H., 1998a, Three-dimensional preservation of algae and animal embryos in a Neoproterozoic phosphorite: Nature, v. 391, p. 553-558.

Xiao, S., Knoll, A.H., and Yuan, X., 1998b, Morphological reconstruction of Miaohephyton bifurcatum, a possible brown alga from the Doushantuo Formation (Neoproterozoic), South China, and its implications for stramenopile evolution: Journal of Paleontology, v. 72, p. 1072-1086.

Xiao, S., Yuan, X., and Knoll, A.H., 2000, Eumetazoan fossils in Terminal Proterozoic phosphorites: Proceedings of the National Academy of Sciences, v. 97, p. 13,684-13,689.

Xiao, S., Yuan, X., Steiner, M., and Knoll, A.H., 2002, Macroscopic carbonaceous compressions in a Terminal Proterozoic shale: A systematic reassessment of the Miaohe Biota, South China: Journal of Paleontology, v. 76, p. 347-376.

Xiao, S., Bao, H., Wang, H., Kaufman, A.J., Zhou, C., Li, G., Yuan, X., and Ling, H., 2004, The Neoproterozoic Quruqtagh Group in eastern Chinese Tianshan: Evidence for a post-Marinoan glaciation: Precambrian Research, v. 130, p. 1-26.

Xiao, S., Shen, B., Zhou, C., Xie, G., and Yuan, X., 2005, A uniquely preserved Ediacaran fossil with direct evidence for a quilted bodyplan: Proceedings of the National Academy of Sciences, v. 102, p. 10,227-10,232.

Xiao, S., Hagadorn, J.W., Zhou, C., and Yuan, X., 2007, Rare helical spheroidal fossils from the Doushantuo Lagerstätte: Ediacaran animal embryos come of age?: Geology, v. 35, p. 115-118.

Yamaguchi, K.E., Johnson, C.M., Beard, B.L., and Ohmoto, H., 2005, Biogeochemical cycling of iron in the Archean-Paleoproterozoic Earth: Constraints from iron isotope variations in sedimentary rocks from the Kaapvaal and Pilbara Cratons: Chemical Geology, v. 218, p. 135-169.

Yin, C., Tang, F., Liu, Y., Gao, L., Liu, P., Xing, Y., Yang, Z., Wan, Y., and Wang, Z., 2005, U-Pb zircon age from the base of the Ediacaran Doushantuo Formation in the Yangtze Gorges, South China: Constraint on the age of Marinoan glaciation: Episodes, v. 28, p. 48-49.

Yin, L., Zhu, M., Knoll, A.H., Yuan, X., Zhang, J., and Hu, J., 2007, Doushantuo embryos preserved inside diapauses egg cysts: Nature, v. 446, p. 661-663.

Yuan, X., Xiao, S., and Taylor, T.N., 2005, Lichen-like symbiosis 600 million years ago: Science, v. 308, p. 1017-1020.

Zhang, S., Jiang, G., Zhang, J., Song, B., Kennedy, M.J., and Christie-Blick, N., 2005, U-Pb sensitive high-resolution ion microprobe ages from the Doushantuo Formation in south China: Constraints on late Neoproterozoic glaciations: Geology, v. 33, p. 473-476.

Zhang, Y., Yin, L., Xiao, S., and Knoll, A.H., 1998, Permineralized fossils from the Terminal Proterozoic Doushantuo Formation, South China: The Paleontological Society Memoir 50, p. 1-52.

Zheng, Y., Anderson, R.F., Van Geen, A., and Kuwabara, J., 2000, Authigenic molybdenum formation in marine sediments: A link to pore water sulfide in the Santa Barbara Basin: Geochimica et Cosmochimica Acta, v. 64, p. 4165-4178.

Zhou, C., and Xiao, S., 2007, Ediacaran $\delta^{13}C$ chemostratigraphy of South China: Chemical Geology, v. 237, p. 89-108.

Zhou, C., Tucker, R., Xiao, S., Peng, Z., Yuan, X., and Chen, Z., 2004, New constraints on the ages of Neoproterozoic glaciations in South China: Geology, v. 32, p. 437-440.

Zhou, C.M., Xie, G.W., McFadden, K.A., Xiao, S.H., and Yuan, X.L., 2007, The diversification and extinction of Doushantuo-Pertatataka acritarchs in South China: Causes and biostratigraphic significance: Geological Journal, v. 42, p. 229-262.

Zhu, M., Zhang, J., Steiner, M., Yang, A., Li, G., and Erdtmann, B.D., 2003, Sinian-Cambrian stratigraphic framework for shallow- to deep-water environments of the Yangtze Platform: An integrated approach: Progress in Natural Science, v. 13, p. 951-960.

CHAPTER 3

Re-Os Geochronology of Neoproterozoic Organic-rich Mudrocks from Mainland Australia, King Island, and Tasmania: Constraints on the Timing of "Sturtian" Glaciation and Implications for Paleogeographic Reconstructions

Part of this chapter is published in the following source:
Kendall, B., Creaser, R.A., and Selby, D., 2006, Re-Os geochronology of postglacial black shales in Australia: Constraints on the timing of "Sturtian" glaciation: Geology, v. 34, p. 729-732.

3.1 INTRODUCTION

The significance of Neoproterozoic glaciation on the evolution and diversification of macroscopic animals is a subject of considerable interest (e.g., Baker, 2006). Paleomagnetic data from six Neoproterozoic glacial deposits (or overlying cap carbonates) yield paleolatitude estimates of 30° or less, including two equatorial determinations (Schmidt and Williams, 1995; Park, 1997; Sohl et al., 1999; Trindade et al., 2003; Macouin et al., 2004; Huang et al., 2005; Kilner et al., 2005). Together with geological evidence for glaciomarine deposition (e.g., dropstones in mudstones, and tidal rhythmites; Williams, 2004; Williams and Schmidt, 2004), the paleomagnetic data suggest the presence of low-latitude Neoproterozoic marine ice sheets at sea-level. Cap carbonates containing unusual sedimentary structures (e.g., pseudo-teepee and stromatactis-like structures, vertical "tubestones", sheet cracks, aragonite/barite crystal fans) and negative carbon isotope excursions ($\delta^{13}C_{carb}$ to $\leq -5‰$) often abruptly overlie glaciogenic diamictites. Carbonate precipitation is suggested to occur on rapid (< 10 k.y.) or prolonged (> 100 k.y.) timescales, and from seawater with unusual but poorly understood chemistry (e.g., Williams, 1979; Fairchild, 1993; Grotzinger and Knoll, 1995; Kennedy, 1996; Hoffman et al., 1998a, b, 2007; Kennedy et al., 1998, 2001a; James et al., 2001; Hoffman and Schrag, 2002; Jiang et al., 2003, 2006; Ridgwell et al., 2003; Noguiera et al., 2003; Ridgwell and Kennedy, 2004; Allen and Hoffman, 2005; Corsetti and Grotzinger, 2005; Gammon et al., 2005; Shields, 2005; Fairchild and Kennedy, 2007; Vieira et al., 2007). In some cases, negative $\delta^{13}C_{carb}$ excursions precede the onset of glaciation (Hoffman et al., 1998a, b; Brasier and Shields, 2000; Walter et al., 2000; McKirdy et al., 2001; Halverson et al., 2002, 2005; Hoffman and Schrag, 2002; Schrag et al., 2002; Halverson, 2006). The origin of these large-scale fluctuations in the Neoproterozoic carbon cycle associated with glaciation continues to be actively debated (see the reviews by Hoffman and Schrag, 2002; Shields, 2005; Fairchild and Kennedy, 2007). Large accumulations of iron formation, last seen in the rock record at ca. 1.8 Ga (at which time the deep oceans are suggested to have changed from anoxic to oxic, suboxic, or euxinic; see Chapter 5) are associated with some Neoproterozoic glacial deposits (e.g., Young, 1988; Kirschvink, 1992). Glaciation occurred during and following breakup of a postulated equatorial supercontinent (Rodinia) whose paleogeographic configuration remains poorly constrained because of insufficient geochronological and paleomagnetic constraints (Trindade and Macouin, 2007). Neoproterozoic glaciation occurred during a time of increasing atmosphere and ocean oxygenation (Knoll et al., 1986; Knoll, 1991; Derry et al., 1992; Des Marais et al., 1992; Kaufman et al., 1993; Kaufman and Knoll, 1995; Canfield and Teske, 1996; Hurtgen et al., 2005; Fike et al., 2006; Kennedy et al., 2006; Canfield et al., 2007). The first unequivocal large animals (Ediacaran fauna) appeared in the fossil record ~ 5 M.y. after the final Neoproterozoic glaciation at ca. 580 Ma (Bowring et al., 2003; Narbonne and Gehling, 2003), and the first motile and burrowing forms appeared in another ~ 20 M.y. (Martin et al., 2000).

In addition to the controversy surrounding cap carbonates and carbon isotope excursions, spirited discussion has ensued regarding the significance of climate modelling studies of Neoproterozoic glaciation (e.g., Jenkins, 2004 and references therein; Donnadieu et al., 2004a, b; Pollard and Kasting, 2004; Peltier et al., 2004; Pierrehumbert, 2004, 2005; Goodman, 2006; Goddéris et al., 2007; Le Hir et al., 2007) and sedimentary features and geochemical weathering proxies during glacial and inter-glacial periods (McMechan, 2000; Condon et al., 2002; Leather et al., 2002; Maloof et al., 2002; Dobrzinski et al., 2004; Williams, 2004; Williams and Schmidt, 2004; James et al., 2005; Arnaud and Eyles, 2006; Rieu et al., 2007). The association between Rodinia breakup, deposition of iron formation, and glaciation (Young, 1988, 1995, 2002; Kirschvink, 1992; Eyles, 1993; Crowell, 1999; Hoffman and Schrag, 2002; Goddéris et al., 2003; Donnadieu et al., 2004a; Eyles and Januszczak, 2004; Li et al., 2004; Goddéris et al., 2007) as well as the synchronicity or diachronicity of ice ages based on geochronological data (Brasier et al., 2000; Lund et al., 2003; Calver et al., 2004; Fanning and Link, 2004; Hoffmann et al., 2004; Kendall et al., 2004; Zhou et al., 2004; Condon et al., 2005; this study) is an ongoing topic of discussion. Biomarker and paleontological evidence for a detrimental effect of extreme low-latitude glaciation on the diversity and complexity of ecosystems is controversial (Corsetti et al., 2003, 2006; Grey et al., 2003; McMenamin, 2004; Xiao, 2004; Olcott et al., 2005). The significance of biogeochemical perturbations of carbon, sulfur, strontium, and other elements during and following glaciation is also not well understood (Hoffman et al., 1998a, b; Kennedy et al., 1998, 2001b; Jacobsen and Kaufman, 1999; Walter et al., 2000; James et al., 2001;

Halverson et al., 2002; Hurtgen et al., 2002, 2005, 2006; Higgins and Schrag, 2003; Kasemann et al., 2005). Even the geological evidence for glaciation in diamictites, the temporal relationship between cap carbonates and glaciation, and the reliability of the paleomagnetic record has been questioned (e.g., Eyles, 1993; Eyles and Januszczak, 2004). Ultimately, the sum of this research is a vigorous debate regarding the origin, timing, number, duration, and severity of Neoproterozoic glaciation. Contrasting interpretations of the geological, geochemical, paleontological, and paleomagnetic records have resulted in four main competing hypotheses that attempt to explain the origin of Neoproterozoic glacial deposits (Fairchild and Kennedy, 2007):

1. The "Snowball Earth" hypothesis (Kirschvink, 1992; Hoffman et al., 1998a, b; Hoffman and Schrag, 2002) suggests that one or more global glaciations, each lasting 3-30 M.y. (a recent estimate based on Ir anomalies in cap carbonates suggests ~ 12 M.y.; Bodiselitsch et al., 2005) and characterized by average surface temperatures of –50°C (based on climate modelling, e.g., Jenkins and Smith, 1999), resulted from a runaway ice albedo feedback. This catastrophic climate state was reversed only by the slow build-up of volcanically-derived atmospheric CO_2 under conditions of reduced hydrological cycle activity and continental silicate weathering, and isolation of the ocean from the atmosphere. Upon reaching some critical threshold of atmospheric CO_2 abundance (possibly between 0.1 and 0.3 bar; Caldeira and Kasting, 1992; Le Hir et al., 2007), rapid deglaciation occurs and is followed by a transient greenhouse climate state until re-equilibration of ocean and atmosphere CO_2 levels.
2. The "Slushball Earth" hypothesis (Harland, 1964; Hyde et al., 2000; Baum and Crowley, 2001; Peltier et al., 2004) represents a near-global glaciation whereby marine ice sheets advance into tropical paleolatitudes, but do not undergo runaway ice sheet growth. A "slushball Earth" would have actively functioning hydrological cycles and significant expanses of ice-free equatorial regions, thus allowing for less stressful climatic conditions on eukaryotic life.
3. The presence of both glacial and non-glacial diamictites within Neoproterozoic rift basin successions indicates at least a partial tectonic

control on the timing and spatial distribution of glacial deposition (e.g., Schermerhorn, 1974; Young, 1988, 1995, 2002; Eyles, 1993; Brookfield, 1994; Crowell, 1999). Thus, Eyles and Januszczak (2004) proposed the "zipper-rift" hypothesis whereby the protracted breakup of the supercontinent Rodinia resulted in widespread, but regional and diachronous glaciation that took place primarily on uplifted rift margins. Glaciomarine deposition between ca. 750 and 610 Ma occurred in conjunction with diachronous rifting along western and eastern Laurentia, respectively.

4. Perhaps the most unique explanation proposed to explain low-latitude Neoproterozoic glaciation is the "high orbital obliquity" hypothesis of Williams (1975, 1993, 2004) and Williams and Schmidt (2004). This hypothesis suggests preferential development of ice sheets at low latitudes would be a natural consequence of a Precambrian Earth with an orbital obliquity > 54° because the large tilt of the Earth's spin axis relative to the ecliptic plane would result in greater annual solar insolation at the poles relative to the equator. However, this hypothesis has been weakened considerably by the recent suggestion of a low orbital obliquity and geocentric-axial-dipole magnetic field for the last 2.25 Ga based on the paleomagnetic record for evaporite deposition (Evans, 2006).

Distinguishing among these hypotheses ultimately requires more rigorous geochronological and paleomagnetic control on the Neoproterozoic rock record than currently exists (Evans, 2000; Trindade and Macouin, 2007).

In the absence of a well-defined chrono- and bio-stratigraphic Neoproterozoic framework, various global correlation schemes have been erected on the basis of lithostratigraphy and carbon and strontium (and to a lesser extent, sulfur) isotope chemostratigraphy (Kaufman et al., 1991, 1993, 1997; Derry et al., 1992; Kaufman and Knoll, 1995; Kennedy et al., 1998; Jacobsen and Kaufman, 1999; Gorjan et al., 2000, 2003; Walter et al., 2000; Hurtgen et al., 2005; Halverson et al., 2005; Halverson, 2006). In particular, the "Sturtian" and "Marinoan" (Elatina) glacial deposits of southern Australia (Adelaide Rift Complex) have served as marker horizons for these global correlation schemes. Distinctive geological (presence or absence of iron formation associated with diamictites, and cap carbonate petrology) and geochemical (post-cap carbonate $^{87}Sr/^{86}Sr$ values; shape and magnitude of negative $\delta^{13}C$ excursions in cap carbonates) features associated with the glacial intervals in Australia and other continents have been interpreted as evidence for global or near-global "Sturtian" and "Marinoan" ice ages (Kennedy et al., 1998; Hoffman et al., 1998a, b; Hoffman and Schrag, 2002; Halverson et al., 2005; Halverson, 2006). Recently, direct U-Pb zircon age determinations for some glacial deposits have led to a new general consensus for three major Neoproterozoic glaciations at approximately 580 Ma ("Gaskiers"; Bowring et al., 2003), 635 Ma ("Marinoan"; Hoffmann et al., 2004), and 712-685 Ma ("Sturtian"; Brasier et al., 2000; Allen et al., 2002; Lund et al., 2003).

Nevertheless, the number, timing, extent, and duration of glaciation remain uncertain because of a general paucity of suitable material for radiometric dating of most Neoproterozoic glacial deposits. For example, direct radiometric age constraints for the southern Australia glacial intervals are particularly poor, comprising U-Pb zircon ages of 802 ± 10 Ma (Rook Tuff; Callanna Group; Fanning et al., 1986) and 777 ± 7 Ma (Boucaut Volcanics, basal Burra Group; Preiss, 2000) from volcanic rocks > 6 km below Sturtian glacial deposits (see Figure 3.9), and imprecise Rb-Sr whole-rock shale dates from the Sturtian postglacial Tapley Hill Formation (750 ± 53 Ma), interglacial Enorama Shale and Trezona Formation (690 ± 21 Ma), and Elatina postglacial Brachina Formation (601 ± 68 Ma) (McKirdy et al., 2001 and references therein). A detrital zircon grain from the Marino Arkose Member (located stratigraphically between the Sturtian and Elatina glacial deposits) and tuffaceous zircons from the Early Cambrian Heatherdale Shale yield U-Pb sensitive high-resolution ion microprobe (SHRIMP) ages of 655 ± 17 Ma (Ireland et al., 1998) and 526 ± 4 Ma (Cooper et al., 1992) that provide loose maximum and minimum age constraints for Elatina glaciation. Other dates from post-Elatina rocks include a Rb-Sr determination of 588 ± 35 Ma from the Yarloo Shale on the Stuart Shelf (Bunyeroo Formation equivalent; Preiss, 2000) and a single zircon U-Pb SHRIMP determination of 556 ± 24 Ma from the lower Pound Subgroup (Ireland et al., 1998). The Elatina Formation has been correlated with the Croles Hill Diamictite, northwestern Tasmania (maximum age of 582 ± 4 Ma), and Cottons Breccia, southeastern King Island (minimum age of 575 ± 3 Ma) (U-Pb SHRIMP zircon ages on associated igneous rocks;

Calver et al., 2004). Alternatively, the Elatina Formation may be correlative with glaciogenic diamictites of the Ghaub Formation, Namibia (direct U-Pb zircon age constraint of 635.51 ± 0.54 Ma from an intercalated ash bed; Hoffmann et al., 2004) and the Nantuo Formation, South China (minimum U-Pb zircon age constraint of 635.23 ± 0.57 Ma from an ash bed within the overlying cap carbonate; Condon et al., 2005) Hoffman et al., 1998; Kennedy et al., 1998; McKirdy et al., 2001; Hoffman and Schrag, 2002; Zhou et al., 2004; Halverson et al., 2005; Halverson, 2006). A three-point Re-Os date of 592 ± 14 Ma obtained for organic-rich siltstones (Aralka Formation) separating the otherwise undated Areyonga (possible Sturtian-equivalent) and Olympic (possible Elatina-equivalent) glacial deposits in central Australia (Schaefer and Burgess, 2003) has been challenged because it is not consistent with global correlation schemes (Hoffmann et al., 2004).

Precise age constraints for the Australian Neoproterozoic successions are clearly required to test proposed global correlation schemes and the synchronicity of ice ages. Here, I present new Re-Os depositional ages from post-glacial organic-rich mudrocks in southern and central Australia, and northwestern Tasmania that are used to: 1) constrain the timing of glacial rocks used for global correlation of a putative global "Sturtian" ice age, thus allowing an evaluation of the proposed global correlation schemes, 2) confirm previous correlations of "Sturtian"-age diamictites between southern Australia and northwestern Tasmania, and 3) evaluate the temporal relationship between supercontinent breakup and Sturtian glaciation in southern Australia. In addition, the utility of shale-hosted benthic microbial mats for Re-Os geochronology is evaluated on post-glacial rocks overlying the Elatina and Olympic Formations (southern and central Australia), and the Cottons Breccia (southeastern King Island). Trace metal data obtained for selected shales is also used to evaluate controls on the fractionation of Re from Os during organic-rich sediment deposition.

3.2 NEOPROTEROZOIC DIAMICTITES IN SOUTHERN AND CENTRAL AUSTRALIA, NORTHWESTERN TASMANIA, AND SOUTHEASTERN KING ISLAND

3.2.1 Adelaide Rift Complex, South Australia

Two discrete intervals of glaciogenic diamictite occur at the top and base of the Umberatana Group (lower Heysen Supergroup) throughout the Adelaide Rift Complex of southern Australia (Figure 3.1). The Sturt – Appila – Pualco – Bolla Bollana – Merinjina Tillites and Wilyerpa – Lyndhurst Formations (Yudnamutana Subgroup) represent the waxing and waning stages of the older Sturtian glaciation, respectively, and rest unconformably upon Burra Group sedimentary rocks (upper Warrina Supergroup; Young and Gostin, 1988; Preiss, 1990; Preiss et al., 1998). Evidence for glacial deposition includes dropstones and polished and striated clasts from two diamictite – mudstone intervals in the extensional Yudnamutana Trough and other sections of the North Flinders Zone. Here, the Sturtian glacial succession reaches maximum thicknesses of 6 km, and was deposited largely by sediment gravity flows contemporaneously with two glacial depositional cycles (Coats, 1981; Preiss, 1990, 1993; Young and Gostin, 1988, 1989, 1990, 1991). In the extensional Baratta Trough (eastern Adelaide Rift Complex and Central Flinders Zone), dropstones and striated clasts within a thick succession of diamictite, conglomerate, breccia, sandstone, and mudstone indicate contemporaneous rainout of glacial debris and sediment gravity flows during deposition of the Pualco Tillite and overlying Wilyerpa Formation (Eyles et al., 2007). Tidal rhythmites from the Pualco Tillite and paleomagnetic data from the Officer Basin may indicate low-latitude Sturtian glaciomarine deposition (Pisarevsky et al., 2001; Williams and Schmidt, 2004). Sturtian glacial deposition is suggested to be synchronous with continental rifting associated with opening of the Proto-Pacific Ocean (Powell et al., 1994; Preiss, 2000; Li and Powell, 2001). Massive and laminated ironstones and ironstone-rich diamictites of the Braemer Ironstone Facies and Holowilena Ironstone are associated with the Pualco Tillite and overlying interglacial sediments (Benda Siltstone) (Preiss, 1990, 1993, 2000; Lottermoser and Ashley, 2000). Locally, Sturtian glacial deposits may be capped by fine-grained organic-rich carbonates containing anastomosing, rhythmic laminae, and negative

$\delta^{13}C$ values at their base that become increasingly positive upsection (Preiss et al., 1978; Preiss and Forbes, 1981; Preiss, 1993; Kennedy, 1996; Kennedy et al., 1998; Walter et al., 2000; McKirdy et al., 2001).

Overlying the Sturtian glacial deposits are dolomitic siltstones and shales of the Tapley Hill Formation, deposited during widespread postglacial transgression. Pyritic, organic-rich dolomitic mudrocks of the Tindelpina Shale Member mark the base of the post-glacial interval (Preiss and Forbes, 1981; Preiss, 2000; McKirdy et al., 2001). Continental separation along the Adelaidean margin is suggested to commence during Sturtian postglacial times, followed by sag-phase sedimentation (Brighton Limestone and Lower Upalinna Subgroup), renewed marine transgression (Upper Upalinna Subgroup), and a regression that preceded the Elatina ("Marinoan") glaciation (Yerelina Subgroup) (Preiss et al., 1998; Preiss, 2000; Li and Powell, 2001; McKirdy et al., 2001).

The top and bottom of the 100-500 m thick Elatina Formation in the northeastern, central, and western Adelaide Rift Complex comprises tillite with polished, striated and faceted clasts, and dropstone-bearing muddy diamictite, respectively, that indicates deposition under glacial conditions. In the North Flinders Zone and southeastern Adelaide Rift Complex, the glaciogenic Yerelina Subgroup exceeds 1500 m in thickness (Preiss, 1990, 1993; Lemon and Gostin, 1990; Schmidt and Williams, 1995). Tidal rhythmites and paleomagnetic evidence for multiple paleomagnetic field polarity reversals, suggests that grounded marine ice sheets and glaciers may have existed near the paleoequator for several hundreds of thousands to millions of years during Elatina Formation deposition (Embleton and Williams, 1986; Schmidt et al., 1991; Schmidt and Williams, 1995; Sohl et al., 1999). The base of the Elatina Formation cap carbonate (Nuccaleena Formation) at Enorama Creek (Flinders Ranges, South Australia) represents the global stratotype section and point (GSSP) for the recently ratified Ediacaran Period (Knoll et al., 2004, 2006). The Nuccaleena Formation is succeeded by fine-grained sandstones, siltstones, and shales of the Brachina Formation (Calver, 2000), which contains shale-hosted fossil benthic microbial mats (Logan et al., 1999).

3.2.2 Amadeus Basin, Central Australia

As for the Adelaide Rift Complex, the Amadeus Basin in central Australia contains two distinctive glacial intervals. The older Areyonga Formation is up to 500 m thick and is capped by dark grey dolomite that is lithologically and geochemically (including a basal negative $\delta^{13}C$ excursion) similar to Sturtian cap carbonates. Accordingly, the Areyonga and Sturtian glacial deposits have been considered correlatives (Preiss et al., 1978; Preiss and Forbes, 1981; Walter et al., 1995, 2000; Kennedy, 1996; Kennedy et al., 1998). The Areyonga Formation is separated from the underlying Bitter Springs Formation by an erosional unconformity that may reflect a change in tectonic regime from anorogenic subsidence to foreland basin (Lindsay, 1989, 2002; Lindsay et al., 2005). Glacial deposition was contemporaneous with tectonically induced faulting in the Amadeus Basin associated with fragmentation of the Australian intracratonic Centralian Superbasin into four distinct, but interconnected, foreland sub-basins (Amadeus, Officer, Ngalia, and Georgina Basins) with uplifted basement blocks between them (Walter et al., 1995; Lindsay, 2002). Evidence for glacial deposition in the Areyonga Formation includes an abundance of extrabasinal clasts and rare striated clasts, as well as massive diamictites, thin sandstones and boulder surfaces interpreted as ice-marginal and sub-glacial drainage deposits. Glacial debris may have been shed from small ice caps located on the uplifted basement between the Amadeus and Ngalia Basins (Lindsay, 1989).

Organic-rich dolomitic siltstones of the Aralka Formation overlie Areyonga diamictites and are lithologically similar to the Tindelpina Shale Member in the Adelaide Rift Complex (Preiss and Forbes, 1981; Walter et al., 1995). A hiatus of unknown duration separates the Aralka Formation from the overlying glaciogenic Olympic Formation (~ 200 m thick) (Preiss et al., 1978; Preiss and Forbes, 1981; Walter et al., 1995) and may be associated with renewed uplift of basin margins that facilitated the development of local ice caps (Lindsay, 2002). The Olympic Formation is only preserved in the northeastern Amadeus Basin, and its equivalent lithostratigraphic unit to the west is the non-glacial Pioneer Sandstone (Preiss et al., 1978). Evidence for a glaciogenic influence on deposition of the Olympic Formation includes a diamictite unit containing striated and faceted clasts, together with dropstone-bearing horizons (Field, 1991).

Correlation of the Elatina and Olympic Formation glacial deposits is based on the presence of similar pinkish cap dolomites that contain similar negative $\delta^{13}C$ excursions (that become increasingly negative upsection) and petrological features (e.g., crystal fans, tepee-like structures, and sheet cracks) (Preiss et al., 1978; Williams, 1979; Preiss and Forbes, 1981; Walter et al., 1995; 2000; Kennedy, 1996; Kennedy et al., 1998). In addition, the fine-grained siliciclastics of the Pertatataka Formation overlying the Olympic Formation includes shale-hosted microbial mats that are remarkably similar to those observed in the Brachina Formation in South Australia (Walter et al., 1995; Logan et al., 1999). Organic carbon isotope chemostratigraphy and the similar stratigraphic position above distinctive pinkish cap carbonates suggest more-or-less synchronous deposition of these microbial-mat bearing shales in the Adelaide Rift Complex and the Amadeus Basin (Walter et al., 1995; Logan et al., 1999; Calver, 2000).

3.2.3 Northwestern Tasmania

Possible correlatives of the Adelaidean Neoproterozoic succession may be present in the Togari Group of northwestern Tasmania (Calver, 1998; Calver and Walter, 2000; Calver et al., 2004). In the Smithton Synclinorium (Figure 3.2), an unconformity separates unmetamorphosed and gently deformed strata of the Togari Group from the underlying, predominantly siliciclastic Rocky Cape Group. Locally, the coarse-grained Forest Conglomerate defines the base of the Togari Group, and is overlain by 600 m of stromatolitic dolomites, organic-rich chert and shale, and diamictite of the Black River Dolomite. A number of lines of evidence suggest the ≤ 200 m thick diamictites of the Julius River Member (upper Black River Dolomite) are correlative with Sturtian diamictites (Figure 3.3; Calver, 1998). Iron formation is associated with both Sturtian diamictites (Preiss, 1990, 1993; Lottermoser and Ashley, 2000) and Julius River Member correlatives in western Tasmania (Calver, 1998). Dolomite clasts within the Julius River Member contain the stromatolite *Baicalia burra* (Griffin and Preiss, 1976; Calver, 1998), which is also found in the Adelaidean Skillogalee Dolomite (Burra Group) underlying Sturtian glacial deposits (Belperio, 1990; Preiss, 1990). Least-altered $^{87}Sr/^{86}Sr$ values of ~ 0.7063 from the Black River Dolomite (e.g., pre-dating the Late Neoproterozoic/Cambrian rise in $^{87}Sr/^{86}Sr$ associated with Gondwana/Pan-African orogenesis; Asmerom et al., 1991; Derry et al., 1992; Kaufman et al., 1993; Jacobsen and Kaufman, 1999; Walter et al., 2000; Shields, 2007), and the lithological (e.g., stromatolitic dolostones and organic-rich chert) and carbon isotope similarities (e.g., $\delta^{13}C$ ~ +2‰ to +6‰) of the Skillogalee Dolomite and middle/lower Black River Dolomite carbonates support their correlation (Schidlowski et al., 1975; Veizer and Hoefs, 1976; Belperio, 1990; Calver, 1998). Evidence of a glacial influence in the Julius River Member is not compelling because the diamictite comprises sub-rounded clasts composed only of dolomite surrounded by a fine-grained, dolomitic mudstone matrix (Calver, 1998). Overlying the Julius River Member near the top of the Black River Dolomite are organic-rich, pyritic shales with subordinate carbonate that are reminiscent of the basal Tindelpina Shale Member in the Adelaide Rift Complex (Calver, 1998; Calver and Walter, 2000). A conspicuous cap carbonate does not appear to be present above the Julius River Member (Calver, 1998). The Black River Dolomite is succeeded by the 1 km-thick Kannunah Subgroup that comprises a basal unit of fine-grained siliciclastics and volcaniclastic arenites (Keppel Creek Formation) overlain by rhyodacite and diamictite (250 m thick Croles Hill Diamictite). The latter contains a wide variety of igneous and sedimentary clast lithologies as well as thin, fine-grained dropstone-bearing intervals that suggest a possible glacial imprint during deposition. However, the Croles Hill Diamictite is not known to have a distinctive cap carbonate, but is instead overlain by 10-50 m of red mudstone and more than 200 m of tholeiitic basalt (Spinks Creek Volcanics) (Calver et al, 2004).

Correlation between the Neoproterozoic successions of the Adelaide Rift Complex and the Togari Group is hampered in part by a paucity of reliable radiometric age constraints. Possible correlatives of the Rocky Cape Group in the highly deformed Arthur Metamorphic Complex were intruded by syn-orogenic granitoids at 777 ± 7 Ma (U-Pb SHRIMP zircon). The magmatic activity and unconformity between the Rocky Cape and Togari Groups are associated with the Wickham Orogeny (Turner et al., 1998). Other relevant age constraints for the basal Togari Group (e.g., pre-Black River Dolomite) are from correlatives southeast of the Arthur Metamorphic Complex (Burnie and Oonah Formations), and include a K-Ar detrital muscovite date of 708 ± 6 Ma (Turner, 1993) plus a K-Ar biotite date of 711 ± 16 Ma from the syn-depositional Cooee

Dolerite (McDougall and Leggo, 1965). The Croles Hill Diamictite has a maximum age of 582 ± 4 Ma (U-Pb SHRIMP zircon date from underlying rhyodacite; Calver et al., 2004). Dolerite dykes (Rocky Cape Dyke Swarm) intruding the Rocky Cape Group are geochemically similar to the Spink Creek Volcanics and have K-Ar ages of 588 ± 8 and 600 ± 8 Ma that indirectly constrain the age of the Spink Creek Volcanics (Brown, 1986).

3.2.4 Southeastern King Island

The Neoproterozoic succession on eastern King Island commences with a 6-7 km thick un-named unit of weakly metamorphosed siltstones, shales, and subordinate sandstone (Calver and Walter, 2000; Meffre et al., 2004) that may be correlative with the Rocky Cape Group of northwestern Tasmania (Calver and Walter, 2000) (see Figure 3.2). This un-named unit may be in part correlative with high-grade metamorphosed and deformed sedimentary rocks from western King Island intruded by granitoids at 760 ± 12 Ma (U-Pb SHRIMP zircon age) during the Wickham Orogeny (Turner et al., 1998). Although field relationships between western and southeastern King Island are poorly understood, an unconformity is suggested to occur between the basal un-named unit and the overlying Grassy Group, and may be associated with the Wickham Orogeny (Calver and Walter, 2000). On southeastern King Island, the slightly metamorphosed, tilted but otherwise relatively undeformed Grassy Group (Calver and Walter, 2000; Meffre et al., 2004) comprises a basal siliciclastic unit (sandstone-siltstone-conglomerate) (Waldron and Brown, 1993) that is overlain by the ca. 100 m thick Cottons Breccia. The latter unit comprises two diamictite successions (containing diverse sedimentary and rare basement clast lithologies as well as dropstone-bearing intervals suggestive of a glacial influence on deposition) separated by an interval of volcaniclastic sandstone (Jago, 1974; Calver and Walter, 2000; Preiss, 2000). The Cumberland Creek Dolostone (Meffre et al., 2004) and Cottons Breccia have been correlated with the Nuccaleena and Elatina Formations, respectively, on the basis of similar lithology (e.g., pinkish dolomites with teepee-like structures) and geochemistry (e.g., decreasing $\delta^{13}C$ trend up-section; Calver and Walter, 2000; Preiss, 2000) of the cap carbonates. In addition, the 100-200 m thick, multi-colored Yarra Creek Shale contains fossil benthic microbial mats in its middle part that are also remarkably similar to those observed in the Brachina and Pertatataka Formations (Logan et al., 1999; Calver and Walter, 2000). Intruding the upper part of the un-named basal siltstone-shale-sandstone succession, the Cottons Breccia, Cumberland Creek Dolostone, and Yarra Creek Shale are fine-grained andesitic and amygdaloidal sills of the 10-150 m thick Grimes Intrusive Suite (Calver et al., 2004; Meffre et al., 2004). Conformably overlying the Yarra Creek Shale are tholeiitic pillow lavas, breccias, and peperites of the City of Melbourne Volcanics (> 20-40 m thick). These in turn are overlain by the picrites and breccias of the Shower Droplet Volcanics (200-300 m thick), and the tholeiitic Bold Head Volcanics (300 m thick) (Meffre et al., 2004).

Calver et al. (2004) obtained a U-Pb SHRIMP zircon age of 575 ± 3 Ma for the sills of the Grimes Intrusive Suite. The amygdaloidal texture of the sills and the textural relationships at the contact between the sills and enclosing sedimentary rocks indicate intrusion occurred at shallow depth prior to lithification of the Yarra Creek Shale (Calver et al., 2004; Meffre et al., 2004). Accordingly, Calver et al. (2004) suggest the U-Pb age of ca. 575 Ma represents a close minimum age constraint for the Cottons Breccia. A similar, but less precise, Sm-Nd age of 579 ± 16 Ma was obtained for the picrites and basalts of the Shower Droplet and Bold Head Volcanics, respectively (Meffre et al., 2004). Correlation of the Grassy Group with the upper part of the Togari Group (see Figures 3.2 and 3.3) is suggested based on their similar lithostratigraphy (e.g., diamictite overlain by shale and volcanic rocks) and U-Pb age constraints for the Cottons Breccia and Croles Hill Diamictite (Calver and Walter, 2000; Calver et al., 2004).

3.3 SAMPLES AND ANALYTICAL METHODS

Drill core samples of organic-rich mudrocks were obtained from:

1. the Aralka and Pertatataka Formations (drill hole Wallara-1, Amadeus Basin, Northern Territory Geological Survey of Australia core library at Alice Springs, Northern Territory)
2. the Tindelpina Shale Member (drill holes Blinman-2 and SCYW-1a) and Brachina Formation (drill hole BWM1a-1) (Adelaide Rift Complex, Department of Primary Industries and Resources, South Australia, Glenside core library at Adelaide, South Australia)

3. the upper Black River Dolomite (drill hole Forest-1, northwestern Tasmania, Department of Mines and Mineral Resources, Tasmania core library at Hobart, Tasmania, obtained in collaboration with Clive Calver)
4. the Yarra Creek Shale (City of Melbourne Bay coastal outcrop exposure, southeastern King Island, obtained in collaboration with Clive Calver).

Kerogen atomic H/C ratios are ≥ 0.4 in the sampled drill cores from the Amadeus Basin and Adelaide Rift Complex (Calver, 2000; McKirdy et al., 2001; Schaefer and Burgess, 2003), suggesting minimal thermal alteration (e.g., temperatures below 300°C; Hayes et al., 1983). Similar information is not available for the Neoproterozoic successions of northwestern Tasmania and King Island. However, the Togari Group succession in drill hole Forest-1 is considered to be virtually unmetamorphosed (Turner et al., 1998), and carbonates and shales preserve minimally altered $\delta^{13}C_{carb}$, $\delta^{13}C_{org}$, and $^{87}Sr/^{86}Sr$ values (based on geochemical screening of samples and parallel variations in carbon and organic carbon isotope compositions; Calver, 1998). Lower greenschist-facies metamorphism is suggested for the Grassy Group on eastern King Island based on the metamorphic mineral assemblage (prehnite, chlorite, actinolite, epidote, and sericite) of volcanic rocks (Meffre et al., 2004).

3.3.1 Amadeus Basin

In drill hole Wallara-1, diamictites of the 152 m thick Areyonga Formation (Lindsay et al., 2005) are capped by a thin (~ 1 m) laminated grey dolostone, and are overlain by the dolomitic, organic-rich siltstones (TOC = 0.5-1.0 %; Schaefer and Burgess, 2003) of the Aralka Formation (Plate 3.1). The sampled interval from the Aralka Formation (depth 1298.2-1300.2 m) occurs 7-9 m stratigraphically above the conformable contact with the underlying Areyonga Formation diamictites (depth ~ 1307 m; Gorjan et al., 2000) (see Figure 3.1). An abrupt contact exists between the Aralka Formation and the overlying Pioneer Sandstone (non-glacial Olympic Formation equivalent; Preiss et al., 1978) (Plate 3.2). Accordingly, the very thin stratigraphic thickness of the Aralka Formation preserved in drill hole Wallara-1 (~ 27 m) may not result from a condensed section, but rather reflect the presence of a lacuna unconformity between the Aralka Formation and the Pioneer Sandstone (~ 1281 m depth), meaning that only the lowermost Aralka Formation strata are preserved in this drill hole (e.g., Logan et al., 1999; Gorjan et al., 2000) not the uppermost part as portrayed in Figure 4 of Schaefer and Burgess (2003). The Pioneer Formation in Wallara-1 comprises a thin interval (~ 8 m thick) of coarse-grained sandstone and conglomerate capped by buff-to-pink dolostone with parallel– or ripple – laminated mudstone. Overlying this cap dolostone are fine-grained siliciclastics of the ~ 525 m thick Pertatataka Formation that contains shale-hosted benthic microbial mat intervals in its lower part (Plate 3.3). The microbial mat facies are hosted in light-colored, organic-poor shale (TOC ~ 0.1%) and are represented by cm- to mm-thick beds of grey shale (TOC up to 0.7%) containing thin (< 50 μm) anastomosing layers of dark brown organic matter surrounded by pyrite framboids. The host organic-poor shale encloses thin mm-scale rip-up clasts of darker microbial mat material. Relative to the enclosing, organic-poor shale, kerogen and pyrite from the organic-rich microbial mat material are strongly depleted in ^{13}C and ^{34}S, respectively, suggesting that organic matter was dominantly sourced from benthic (rather than planktonic) material. Together with an abundance of > C_{20} even-carbon numbered n-alkanes and mid-chain methyl alkanes, the carbon and sulfur isotope data are best explained by the presence of non-photosynthetic sulfide-oxidising bacteria within the microbial mats. These micro-organisms require dissolved oxygen for their metabolism. Sediment deposition by low-density turbidity currents and hemi-planktonic processes took place in the relatively shallow oxygenated waters (< 150 m) of the mid-continental shelf at, or below, storm wave base (Logan et al., 1999). Samples of the Pertatataka Formation were obtained from depths 1175.9-1177.4 m in Wallara-1. For the shale-hosted microbial mats studied in this work (Pertatataka and Brachina Formations and Yarra Creek Shale), only organic-rich beds of microbial mat material were extracted for Re-Os isotope analysis because the lighter-colored shale may represent deposition under oxidizing conditions.

3.3.2 Adelaide Rift Complex

Dolomitic, organic-rich shales (total organic carbon [TOC] = 0.5-1.0 %; McKirdy et al., 2001) were sampled from the base of the Tindelpina Shale Member (lowermost Tapley Hill Formation). The Tindelpina Shale Member samples were obtained from two drill holes located ~ 160 km apart (Blinman-2, Central Flinders Zone, depth 1610.0-1610.9 m; and SCYW-1a, Stuart Shelf, depth 1369.3-1370.1 m) (Plate 3.4). The Blinman-2 and SCYW-1a samples are 7-8 m and 3-4 m above the contact with the underlying Sturtian glacial deposits (see Figure 3.1), respectively, which appears conformable in both drill cores (Gorjan et al., 2000). A distinctive cap carbonate litho-facies is not discernable at the contact between the Tindelpina Shale Member and the underlying glaciogenic Wilyerpa Formation in the Blinman-2 core (depth 1618 m; McKirdy et al., 2001). Instead, a gradual transition from coarse- to fine-grained strata occurs between ~ 1618 m and 1610 m, and is followed up-section by grey to dark grey mudstone with interspersed medium- to coarse-grained clasts, and occasional stratigraphic horizons of breccia (e.g., Eyles et al., 2007). In the SCYW-1a core, the contact between the Sturt/Appila glaciogenic diamictites and the Tindelpina Shale Member occurs at ~ 1373 m (Gorjan et al., 2000; Walter et al., 2000) and is marked by the appearance of dolomitic siltstones, and dark grey laminated siltstones and shales. A negative $\delta^{13}C_{carb}$ excursion (also seen for $\delta^{13}C_{org}$ in SCYW-1a) at the base of the Tindelpina Shale Member in Blinman-2 is immediately followed by increasingly more positive $\delta^{13}C$ values up-section (Walter et al., 2000; McKirdy et al., 2001), a trend considered typical of Sturtian post-glacial "cap carbonate sequences" (Kennedy et al., 1998; Halverson et al., 2005). The samples from both drill holes are located stratigraphically beneath the most negative $\delta^{13}C$ values.

Shale-hosted benthic microbial mats occur within the middle part of the ~ 75 m thick Brachina Formation in drillhole BWM1a-1 on the Curnamona Craton east of the Adelaide Rift Complex. Lithologically, these shales are similar to those of the Pertatataka Formation, but the darker, microbial mat-bearing intervals are characterized by a lower TOC content of 0.2-0.3 % (Calver, 2000). Samples from the Brachina Formation were obtained from 157.4-158.4 m depth (Plate 3.5), and lie ~ 64-65 m above the contact (located at ~ 222 m depth) with the underlying 11 m thick buff-to-pink colored Nuccaleena Formation cap carbonate.

3.3.3 Northwestern Tasmania and Southeastern King Island

In the Forest-1 drill core from northwestern Tasmania, the Julius River Member is 130 m thick and comprises two diamictite units sandwiched by a thin ~ 15 m interval of limestone with subordinate organic-rich shale (see Figure 3.2). Fine-grained organic-rich dolostone caps the Julius River Member, and is not considered lithologically similar to cap carbonates occurring above either Sturtian or Elatina glacial deposits (Calver, 1998). The succeeding ~ 40 m of strata comprises pyritic black shale with subordinate carbonate, and is lithologically similar to the basal Tindelpina Shale Member (Calver and Walter, 2000). Overlying the black shales are fine-grained volcaniclastic mudstones that grade up-section into volcaniclastic sandstones (Keppel Creek Formation, Kanunnah Subgroup) (Calver, 1998; Calver and Walter, 2000). Two intervals of finely laminated pyritic black shale were sampled at 835.58-835.87 m and 828.11-828.58 m and are located 1 m and 8 m above the contact with the underlying Julius River Member diamictites, respectively (Plate 3.6). XRD analysis of one sample from the 835.58-835.87 m interval reveals a mineral assemblage comprising quartz + feldspar + muscovite + dolomite + kaolinite + pyrite, suggesting the black shales are unmetamorphosed.

On southeastern King Island, the Yarra Creek Shale is well-exposed at a coastal outcrop at the City of Melbourne Bay and comprises multi-colored (red, yellow-brown, gray-green, and black) shale. Red shale from near the base is lithologically similar to the lower Brachina Formation in the Adelaide Rift Complex. In the middle of the section is a > 16 m interval of pyritic black shale interbedded and interlaminated with gray-green shale (see Figure 3.3). This interval is similar to the shale-hosted benthic microbial mat successions of the Brachina and Pertatataka Formations (Logan et al., 1999; Calver, 2000), including the presence of thin, anastomosing layers and rip-up clasts of black shale within the lighter-colored host shale (Calver and Walter, 2000). A 4 cm thick interval of black shale with abundant framboidal pyrite was sampled along strike for ~ 3 m (Plate 3.7). In addition to pyrite, the mineralogy of the black shale includes quartz + feldspar + muscovite + chlorite, consistent with thermal alteration no higher than chlorite-grade metamorphism.

3.3.4. Analytical Methods

Powder aliquot sizes for Australian Neoproterozoic ORS ranged from 20 g to > 100 g. Protocols for metal-free processing of organic-rich sedimentary rocks (ORS) to produce powdered samples, subsequent chemical digestion, separation, and purification of Re and Os, and isotopic analysis by isotope dilution – negative thermal ionization mass spectrometry (ID-NTIMS) are described in Appendix A. Major and trace metal abundances were determined by quadrupole – inductively coupled plasma – mass spectrometry (Q-ICP-MS) (Appendix C.2). Sample degree-of-pyritization (DOP) was determined following the protocols outlined in Appendix C.3.

During the early part of this study, standard high-temperature (240°C) Cr^{VI}-H_2SO_4 digestions for Re-Os isotope analysis were carried out on ORS from the Adelaide Rift Complex and Amadeus Basin. Near the end of the thesis work, an experiment was carried out whereby black shales from the upper Black River Dolomite were digested at 240°C and at the lower temperature of 80°C. As described further below, the Re-Os isotope data obtained using both temperatures produced identical Re-Os ages (within 2σ uncertainties) for the Black River Dolomite shales. Subsequently, only low-temperature Cr^{VI}-H_2SO_4 digestions were carried out for the Yarra Creek Shale. Inverse *aqua regia* analyses (see section 3.5.1) were also obtained for some samples of the Aralka Formation and Tindelpina Shale Member for the purpose of evaluating the effect of the detrital Os budget on the Re-Os isotope systematics in these samples. Average total procedural blanks for Cr^{VI}-H_2SO_4 digestions of ORS from the Aralka, Pertatataka, and Brachina Formations, and Tindelpina Shale Member were 10.6 ± 2.2 pg (1σ, n = 6) and 0.26 ± 0.13 pg (1σ, n = 5) for Re and Os, respectively, with blank $^{187}Os/^{188}Os$ of 0.17 ± 0.05 (1σ, n = 5). For digestions of the Yarra Creek Shale and Black River Dolomite ORS, total procedural blanks were 10.8 ± 1.5 pg (1σ, n = 9) and 0.12 ± 0.05 pg (1σ, n = 8) for Re and Os, respectively, with blank $^{187}Os/^{188}Os$ of 0.24 ± 0.08 (1σ, n = 8).

3.4 RESULTS

3.4.1 Trace Metals

Elemental abundances for the Aralka Formation and Tindelpina Shale Member, and one sample each from the Brachina and Pertatataka Formations, are presented in Table 3.1. Enrichment factors (EF) were calculated for each element using the following formula:

$$EF = (\text{element}/\text{Al})_{\text{sample}} / (\text{element}/\text{Al})_{\text{average shale}} \qquad (1)$$

where average shale data is from Wedepohl (1971, 1991). Elemental EF and Fe_T/Al ratios are presented in Table 3.2 together with DOP determinations on selected samples (see section 2.4.2 for a brief summary). This data is used to place constraints on the paleoredox state of bottom waters during sediment deposition.

With the exception of Re and Pb (EF up to 11), redox-sensitive metal abundances in the Aralka Formation and Tindelpina Shale Member are not appreciably enriched relative to average shale. Some samples are enriched in Mn, CaO, and MgO, reflecting relatively larger carbonate content. The Fe_T/Al ratios of the Aralka Formation (0.7-0.9) and Tindelpina Shale Member (0.5-0.6) are moderately elevated or similar to average shale (0.55), respectively. Both shales have moderate DOP values ranging between 0.42 and 0.73, and have low TOC content (0.5-1.0%; McKirdy et al., 2001; Schaefer and Burgess, 2003). These observations are most consistent with deposition of the Aralka Formation and Tindelpina Shale Member from suboxic to anoxic/non-sulfidic bottom waters. Two individual analyses for shale-hosted microbial mat material from the Brachina and Pertatataka Formations reveal an absence of redox-sensitive metal enrichment as well as low DOP values of 0.38 and 0.48 that may indicate weakly oxygenated to suboxic conditions within the organic-rich microbial mat layers. Given that carbon and sulfur isotope geochemistry and molecular biomarkers suggests the microbial mats were comprised (at least in part) of sulfide-oxidising bacteria, the overlying bottom water column was probably oxygenated (Logan et al., 1999).

3.4.2 Re-Os Isotope Data

3.4.2.1 Amadeus Basin

Four samples of organic-rich benthic microbial mat material from the Pertatataka Formation are characterized by Re (0.9-1.1 ppb) and Os (75-98 ppt) abundances (Table 3.3) similar to the average upper continental crust abundances for these elements (~ 0.2-2 ppb Re, 30-50 ppt Os; Esser and Turekian, 1993; Peucker-Ehrenbrink and Jahn, 2001; Hattori et al., 2003; Sun et al., 2003a, b). Despite sampling over ~ 1.5 m of stratigraphy, there is unfortunately a highly restricted range in ^{187}Re/^{188}Os (~ 68-69) and ^{187}Os/^{188}Os (1.83-1.91) isotope ratios that does not permit a meaningful regression for the Pertatataka Formation. In contrast, Re and Os abundances in the Aralka Formation are moderately elevated relative to average crustal values and range from 4.1 to 5.9 ppb, and 82 to 151 ppt, respectively. The ^{187}Re/^{188}Os and ^{187}Os/^{188}Os isotope ratios range between 252 and 447, and 3.59 and 5.75, respectively. Replicate analyses of two samples (BK-04-WALLARA-1A and 5A) show excellent reproducibility in Re and Os abundances and ^{187}Re/^{188}Os and ^{187}Os/^{188}Os isotope ratios. Regression of the Aralka Formation isotope data yields a Re-Os date of 657.2 ± 5.4 Ma (2σ, $n = 10$, Mean Square of Weighted Deviates [MSWD] = 1.2, Model 1, probability of fit = 0.33, initial ^{187}Os/^{188}Os [I_{Os}] = 0.82 ± 0.03) (Figure 3.4). If a λ^{187}Re uncertainty of ± 0.31% (2σ) (Smoliar et al., 1996; Selby et al., 2007) is propagated together with the uncertainty from the slope of the regression, the Re-Os date for the Aralka Formation is 657.2 ± 5.9 Ma.

3.4.2.2 Adelaide Rift Complex

The Tindelpina Shale Member contains similar abundances of Os (93-145 ppt) to the Aralka Formation but displays a greater range in Re content (1.7-10.0 ppb) and ^{187}Re/^{188}Os (102-1010) and ^{187}Os/^{188}Os (2.06-11.83) isotope ratios (Table 3.4). Although Os abundances for shales from the Blinman-2 and SCYW-1a drill cores are broadly similar, the Blinman-2 samples contain lower Re abundances (1.7-4.7 ppb), and ^{187}Re/^{188}Os (102-234) and ^{187}Os/^{188}Os (2.06-3.47) isotope ratios relative to the SCYW-1a drill core samples (Re = 5.6-10.0 ppb; ^{187}Re/^{188}Os = 551-1010; ^{187}Os/^{188}Os = 6.87-11.83). A replicate analysis of BK-04-BLINMAN-5 shows excellent reproducibility in Re and

Os abundances, and $^{187}Re/^{188}Os$ and $^{187}Os/^{188}Os$ isotope ratios. Replicate analyses suggest a minor to pronounced nugget effect is present within the powdered aliquots of BK-04-BLINMAN-7 and BK-04-SCYW-1a-3-4, respectively, but in both cases, the replicate analyses yield similar calculated $I_{Os\ (643\ Ma)}$. Regression of the Blinman-2 and SCYW-1a Re-Os isotope data yields Model 1 dates of 645.1 ± 4.8 Ma (n = 11, MSWD = 1.2, probability of fit = 0.30, I_{Os} = 0.95 ± 0.01; Figure 3.5A) and 647 ± 10 Ma (n = 4, MSWD = 0.79, probability of fit = 0.46, I_{Os} = 0.89 ± 0.12; Figure 3.5B), respectively, that are equivalent within 2σ uncertainties. Combining the two data sets for the Tindelpina Shale Member yields a Re-Os date of 643.0 ± 2.4 Ma (n = 15, MSWD = 1.1, Model 1, probability of fit = 0.35, I_{Os} = 0.95 ± 0.01; Figure 3.5C), or a Re-Os date of 643.0 ± 3.1 Ma if the uncertainty on $\lambda^{187}Re$ is included.

Four samples of the Brachina Formation organic-rich microbial mat material contain Re and Os abundances of 2.0-5.6 ppb and 107-130 ppt, respectively, with $^{187}Re/^{188}Os$ and $^{187}Os/^{188}Os$ isotope ratios ranging between 113 and 328, and 2.31 and 4.65, respectively. Three samples were analyzed in replicate, and show excellent reproducibility in Re and Os abundances and $^{187}Re/^{188}Os$ and $^{187}Os/^{188}Os$ isotope ratios. However, regression of the Re-Os isotope data for the Brachina Formation yields an imprecise date of 647 ± 30 Ma (n = 7, MSWD = 34, Model 3, I_{Os} = 1.14 ± 0.12; Figure 3.5D).

3.4.2.3 Northwestern Tasmania and Southeastern King Island

Of the Neoproterozoic shales from the Australian region, the black shales overlying the Julius River Member (upper Black River Dolomite) in northwestern Tasmania contain the highest Re (19-102 ppb) and Os (328-1800 ppt) abundances (Table 3.5). Shales from 835.58-835.87 m depth in drill hole Forest-1 are characterized by elevated and variable $^{187}Re/^{188}Os$ (533-832) and $^{187}Os/^{188}Os$ (6.74-9.95) isotope ratios. Regression of the Re-Os data from this interval derived from the standard high temperature (240°C, 48 h) and the lower temperature (80°C, 48 h) Cr^{VI}-H_2SO_4 shale digestions yields precise Model 1 dates of 642.7 ± 6.9 Ma (n = 11, MSWD = 0.69, probability of fit = 0.72, I_{Os} = 0.98 ± 0.08; Figure 3.6A) and 639.3 ± 6.4 Ma (n = 8, MSWD = 1.3, probability of fit = 0.25, I_{Os} = 1.02 ± 0.07; Figure 3.6B), respectively, that are equivalent within 2σ uncertainties. The excellent agreement in Re-Os abundance and isotope data between low-temperature and high-temperature analyses of the same sample powders (e.g., samples RC06-FOR-01-C, C3, D2, E, and E2; a nugget effect is likely present within RC06-FOR-01-D) and the excellent reproducibility of two low-temperature analyses of sample RC06-FOR-01-D2 suggests complete digestion and equilibration of sample and spike Re and Os occurs during the 80°C digestion. Combining both Re-Os isotope data sets for the upper Black River Dolomite shales yields a precise date of 640.7 ± 4.7 Ma (n = 19, MSWD = 0.91, Model 1, probability of fit = 0.56, I_{Os} = 1.00 ± 0.05) (Figure 3.6C), or a Re-Os date of 640.7 ± 5.2 Ma if the uncertainty on λ^{187}Re is included. Five black shale samples from a second stratigraphic interval in Forest-1 (828.11-828.58 m) have higher Re (94-102 ppb) and Os (1675-1800 ppt) abundances, but a severely limited range in ^{187}Re/^{188}Os (390-418) and ^{187}Os/^{188}Os (6.07-6.20) isotope ratios precludes a meaningful regression.

The organic-rich microbial mats from the Yarra Creek Shale contain higher Re (11.9-15.8 ppb) and Os (294-330 ppt) abundances relative to the microbial mat facies of the Brachina and Pertatataka Formations (Table 3.6). Despite a suitable range in ^{187}Re/^{188}Os (284-462) and ^{187}Os/^{188}Os (4.12-6.30) isotope ratios, the Re-Os isotope data yield an imprecise date of 704 ± 86 Ma (2σ, n = 11, MSWD = 125, Model 3, I_{Os} = 0.91 ± 0.55). Two samples (RC06-KI-01-B and H) account for a significant fraction of the scatter in this regression. Exclusion of these samples yields a Re-Os date of 636 ± 53 Ma (n = 9, MSWD = 30, Model 3, I_{Os} = 1.34 ± 0.33) (Figure 3.6D).

3.5 DISCUSSION

3.5.1 Comparison of Digestion Protocols for Re-Os Geochronology

Extraterrestrial particulates are generally negligible sources of Os to organic-rich sedimentary rocks (< 0.2% of total Os for ORS with Os abundances greater than 150 ppt) if meteoritic fluxes are similar to Cenozoic fluxes (Cohen et al., 1999; Kendall et al., 2004). For shales with low Os abundances, however, the terrestrial particulate Os fraction may not be negligible relative to the hydrogenous fraction. For example, Ravizza et al. (1991) demonstrated that mixing of detrital and hydrogenous Re and Os may result in Re-

Os dates that are erroneously younger or older than the true depositional age. Creaser et al. (2002) observed a positive correlation between TOC content and I_{Os}, and a negative correlation between I_{Os} and "common Os" (^{192}Os) abundance (normalized to TOC content) for Exshaw Formation black shales (Western Canada Sedimentary Basin) and attributed these relationships to mixing of hydrogenous and unradiogenic particulate Os released during inverse *aqua regia* digestion. High-TOC (> 5%) samples were shown to yield a superior regression (358 ± 9 Ma, Model 3, MSWD = 1.8) compared to low-TOC samples (360 ± 9 Ma, Model 3, MSWD = 8.0) suggesting that non-hydrogenous Os can be liberated by inverse *aqua regia* whole-rock digestions and thus negatively impact the precision and accuracy of Re-Os ages derived from low-TOC samples. Subsequently, Selby and Creaser (2003) developed the Cr^{VI}-H_2SO_4 whole-rock Carius Tube digestion protocol that minimizes the release of detrital Re and Os from silicate matrices by selectively attacking organic matter, thus releasing predominantly hydrogenous Re and Os into solution. Inverse *aqua regia* (from Creaser et al., 2002) and Cr^{VI}-H_2SO_4 (from Selby and Creaser, 2003) digestions of the same Exshaw Formation powder aliquots yield similar Re (typically < 100 ppb) and Os (typically < 1 ppb) abundances and ^{187}Re/^{188}Os and ^{187}Os/^{188}Os isotope ratios, suggesting that only small amounts of detrital Re and Os reside in the silicate matrices of these black shales. Nevertheless, two subsets with distinctive $I_{Os\ (364\ Ma)}$ values were identified from the Cr^{VI}-H_2SO_4 analyses and separately regressed to yield Re-Os dates of 366.1 ± 9.6 Ma (Model 3, MSWD = 2.2; I_{Os} = 0.51 ± 0.06) and 363.4 ± 5.6 Ma (Model 1, MSWD = 1.6; I_{Os} = 0.41 ± 0.04). These Re-Os dates are more precise and better correlated than the Re-Os dates for the same subsets derived using the data from Creaser et al. (2002) for inverse *aqua regia* digestion (356 ± 23 Ma; MSWD = 11.1 and 356 ± 12 Ma; MSWD = 5.2, respectively) (Selby and Creaser, 2003).

Similarly, Re (≤ 15 ppb) and Os (≤ 250 ppt) abundances from low-TOC (~ 0.5%) shale powder aliquots of the Neoproterozoic Old Fort Point Formation (Windermere Supergroup, Western Canada) were broadly similar for the two digestion protocols (Kendall et al., 2004). However, the Cr^{VI}-H_2SO_4 analysis had lower ^{187}Re/^{188}Os and ^{187}Os/^{188}Os isotope ratios relative to the corresponding inverse *aqua regia* analysis for most samples. Significantly, the regression for the subset of Re-Os isotope data from

Cr^{VI}-H_2SO_4 digestion was better correlated (Model 1 age of 607.8 ± 4.7 Ma, MSWD = 1.2, I_{Os} = 0.62 ± 0.03) relative to the data derived from inverse *aqua regia* digestion (Model 3 age of 634 ± 57 Ma, MSWD = 65, I_{Os} = 0.61 ± 0.42). All of the inverse *aqua regia* analyses plotted above the regression line derived from Cr^{VI}-H_2SO_4 analyses, consistent with the liberation of a radiogenic detrital component of Os by the inverse *aqua regia* medium, but not by the Cr^{VI}-H_2SO_4 solution. The variable deviations from the ~ 608 Ma Cr^{VI}-H_2SO_4 regression line, combined with a wide range in $I_{Os\ (608\ Ma)}$ values for the *aqua regia* analyses, suggested the detrital Os component was apparently not homogenous over a 50-cm sampled stratigraphic interval. This may have reflected changes in the Os isotope composition and/or magnitude of the detrital Os flux to the Old Fort Point Formation during deposition. Thus, the Cr^{VI}-H_2SO_4 medium represents a superior digestion protocol to inverse *aqua regia* for obtaining depositional age information as well as estimating the $^{187}Os/^{188}Os$ isotope composition of contemporaneous seawater (Selby and Creaser, 2003; Kendall et al., 2004).

Further comparison of the Re-Os isotope systematics derived from these two digestion protocols was attempted here by comparing Re-Os and X-ray diffraction (XRD) data for individual samples of the Aralka Formation (sample BK-04-WALLARA-5A) and Tindelpina Shale Member (sample BK-04-BLINMAN-5). Both samples have similar mineral assemblages consisting of quartz + feldspar + muscovite + calcite/dolomite + pyrite/marcasite + rutile ± chlorite (Aralka Formation) ± siderite (Tindelpina Shale Member). The residues left behind after Cr^{VI}-H_2SO_4 and inverse *aqua regia* digestions were collected, dried, and weighed, and were found to account for 73-86 % and 56-65 % of the original sample powder, respectively (the residue from one sample of the higher-TOC Exshaw Formation accounted for 94% and 38%, respectively, Selby and Creaser, 2003). XRD analysis of the residues from Cr^{VI}-H_2SO_4 dissolution identified quartz + feldspar + anhydrite + gypsum ± rutile (Tindelpina Shale Member) whereas the inverse *aqua regia* residues contained only quartz + feldspar. Selby and Creaser (2003) also identified calcite/dolomite and muscovite in the Exshaw Formation residue from Cr^{VI}-H_2SO_4 digestion. These observations could represent evidence for a harsher acid attack on silicate minerals by the inverse *aqua regia* medium. However, anhydrite, gypsum, and calcite/dolomite may have precipitated from the Cr^{VI}-H_2SO_4 solution during sample digestion, and thus may account at least partially for the larger residue weight left behind after Cr^{VI}-H_2SO_4 dissolution.

Hydrogenous Re and Os associated with the organic matter of ORS should be fully oxidized and equilibrated with spike Re and Os following a Cr^{VI}-H_2SO_4 Carius Tube digestion at 240°C. Full support for this assumption is provided, for example, by the reproducibility of replicate analyses and identical Model 1 Re-Os dates (within 2σ uncertainties) derived from low-temperature (80°C) and conventional high-temperature (240°C) Cr^{VI}-H_2SO_4 digestion of the black shales from the upper Black River Dolomite. Thus, an inverse *aqua regia* digestion of the residue left behind after Cr^{VI}-H_2SO_4 digestion should liberate only the remaining detrital Re and Os fraction from the silicate matrix. The $I_{Os\ (657\ Ma)}$ values for the whole-rock Cr^{VI}-H_2SO_4 digestion and inverse *aqua regia* analysis of the Cr^{VI}-H_2SO_4 digestion residue from BK-04-WALLARA-5 are similar (0.83 and 0.85, respectively), suggesting broadly similar Os isotope compositions for the detrital and hydrogenous fractions of the Aralka Formation (Table 3.7). In contrast, the whole-rock Cr^{VI}-H_2SO_4 digestion and the residue from BK-04-BLINMAN-5 have distinctive $I_{Os\ (643\ Ma)}$ values of 0.93-0.95 and 0.22, respectively, suggesting the detrital and hydrogenous fractions of the Tindelpina Shale Member have distinctive $^{187}Os/^{188}Os$ isotope compositions. The Os concentration of the unradiogenic detrital end-member is ~ 12 ppt, or ~ 10.5% of the Os concentration determined from Cr^{VI}-H_2SO_4 digestion, and thus represents a significant fraction of the total Os budget in this aliquant. However, a whole-rock inverse *aqua regia* analysis from a separate aliquant of BK-04-BLINMAN-5 yields slightly higher $^{187}Re/^{188}Os$ and $^{187}Os/^{188}Os$ isotope ratios (~ 3-4%), but appreciably lower Re (~ 6%) and Os (~ 9-10%) abundances. The calculated $I_{Os\ (643\ Ma)}$ from the inverse *aqua regia* digestion (0.98) is inconsistent with the unradiogenic $I_{Os\ (643\ Ma)}$ from the residue. Either a nugget effect is present within this powder aliquot or sample and spike were not fully equilibrated during inverse *aqua regia* digestion of the residue material.

Rhenium (1.3 to 18.4 ppt) and Os (2.3 to 11.9 ppt) abundances in the two Cr^{VI}-H_2SO_4 residues are less than their estimated upper continental crust abundances of ~ 0.2-2 ppb and 30-50 ppt, respectively (Esser and Turekian, 1993; Peucker-Ehrenbrink and Jahn, 2001; Hattori et al., 2003; Sun et al., 2003a, b). This suggests some fraction of the detrital Re and Os is dissolved by the Cr^{VI}-H_2SO_4 medium (Ravizza et al., 1991) or that detrital Re and Os abundances in shales are variable and sometimes lower than crustal values. Either way, the determination of precise Model 1 ages for low-TOC rocks (~ 0.5-1%) of the Aralka Formation (657.2 ± 5.4 Ma, MSWD = 1.2), Tindelpina Shale Member (643.0 ± 2.4 Ma, MSWD = 1.2), and Old Fort Point Formation (607.8 ± 4.7 Ma, MSWD = 1.2) (Kendall et al., 2004) clearly indicates that Cr^{VI}-H_2SO_4 digestions of organic-rich sedimentary rocks can yield precise Re-Os dates. The accuracy of Re-Os shale ages and the decay constant for ^{187}Re is well-established based on cross-calibration with the U-Pb zircon chronometer (Selby and Creaser, 2005, Selby et al., 2007). In addition, a U-Pb SHRIMP zircon age of ca. 658 Ma obtained from a tuffaceous bed within the glaciogenic Sturtian Merinjina Formation (North Flinders Zone; Fanning and Link, 2006) agrees well with the ca. 643 Ma Re-Os age from the overlying Sturtian post-glacial Tindelpina Shale Member. The excellent agreement between the Re-Os dates for the Tindelpina Shale Member and upper Black River Dolomite (640.7 ± 4.7 Ma, MSWD = 0.91) is in accord with previous correlation of these rock units based on litho-, chemo-, and bio-stratigraphy (e.g., Calver, 1998; Calver and Walter, 2000). These observations strongly support the utility of the Re-Os black shale geochronometer for providing precise and accurate depositional ages.

3.5.2 Discrepancy in the Age of the Aralka Formation

Using the inverse *aqua regia* dissolution protocol, Schaefer and Burgess (2003) reported Re-Os dates of 592 ± 14 Ma (n = 3, MSWD << 1, $I_{Os} = 0.91 \pm 0.07$) and 623 ± 18 Ma (n = 7, MSWD = 5.2, $I_{Os} = 0.78 \pm 0.10$) for the Aralka Formation. Because the seven samples defining the 623 ± 18 Ma date spanned a stratigraphic interval of ~ 10 m that could potentially be characterized by heterogeneous I_{Os}, Schaefer and Burgess (2003) suggested the regression defined by the three samples in closest stratigraphic proximity (~ 1.6 m) represented the best estimate of the true depositional age. However, a significantly older Re-Os date of 657.2 ± 5.4 Ma (MSWD = 1.2, $I_{Os} = 0.82 \pm 0.03$) has been obtained in this study by Cr^{VI}-H_2SO_4 digestion of ten samples derived from a ~ 2 m stratigraphic interval within the larger 10 m interval sampled by Schaefer and Burgess (2003) (see Figure 3.1).

To determine if the reason for this age discrepancy was simply the nature of the digestion mediums used (as suggested by Kendall et al., 2004), three of the Aralka Formation samples (BK-04-WALLARA-1A, 2A, 5A) were re-analyzed using inverse *aqua regia*. The initial analyses used ~ 1.44-1.48 g of shale powder for Carius Tube digestion, and plot near the ca. 623 Ma isochron of Schaefer and Burgess (2003) (Figure 3.7). However, replicate analyses for BK-04-WALLARA-1A and 5A using the same amount of sample powder were not reproducible in terms of Re and Os abundances, $^{187}Re/^{188}Os$ and $^{187}Os/^{188}Os$ isotope ratios, and $I_{Os\ (657\ Ma)}$. Subsequently, replicate analyses used 0.50-0.54 g of powder for inverse *aqua regia* digestion, and these data plot near the ca. 657 Ma isochron defined by the Cr^{VI}-H_2SO_4 analyses. In addition, the ~ 0.50-0.54 g inverse *aqua regia* analyses have broadly similar Re and Os abundances, $^{187}Re/^{188}Os$ and $^{187}Os/^{188}Os$ isotope ratios, and $I_{Os\ (657\ Ma)}$ to the Cr^{VI}-H_2SO_4 analyses from the same powder aliquots. Regression of the 0.50-0.54 g *aqua regia* subset from this study yields a Model 1 Re-Os date of 657 ± 15 Ma (MSWD = 0.7; $I_{Os} = 0.87 \pm 0.09$) that is statistically equivalent to the ca. 657 Ma age obtained using Cr^{VI}-H_2SO_4 digestion. In addition, the residue from Cr^{VI}-H_2SO_4 digestion of BK-04-WALLARA-5A plots near the I_{Os} intercept on the isochrons derived from the Schaefer and Burgess (2003) and the Cr^{VI}-H_2SO_4 Re-Os data (this study). The residue has a calculated $I_{Os\ (657\ Ma)}$ of 0.85 broadly similar to the range in calculated $I_{Os\ (657\ Ma)}$ values for all Cr^{VI}-H_2SO_4 analyses (0.81-0.84), but is more radiogenic than calculated $I_{Os\ (657\ Ma)}$ values of 0.47-0.71 from the data of Schaefer and Burgess (2003). The similar ages derived here using the two dissolution mediums, together with the Re-Os data for the residue, suggests the detrital component in the Aralka Formation is negligible and/or has similar or slightly more radiogenic I_{Os} (Table 3.7) as the hydrogenous Os fraction. Accordingly, the discrepancy between the Re-Os data derived by Schaefer and Burgess (2003) and Cr^{VI}-H_2SO_4 digestion (this study) may relate to incomplete sample-spike equilibration during inverse *aqua regia* digestion of large (e.g., 1.4-1.5 g) aliquant fractions. In contrast, reproducible Re-Os data diagnostic of complete sample-spike equilibration during Cr^{VI}-H_2SO_4 digestions was obtained for the Aralka Formation using up to 1.5 g of sample. Because sample details were not provided by Schaefer and Burgess (2003), further comparison with the data reported here is not possible.

3.5.3 Timing of Sturtian and Areyonga Post-glacial Sedimentation, and Correlation with Northwestern Tasmania

The similarity of the individual Tindelpina Shale Member Re-Os dates and I_{Os} values for the Blinman-2 (645.1 ± 4.8 Ma; I_{Os} = 0.95 ± 0.01) and SCYW-1a (647 ± 10 Ma; I_{Os} = 0.89 ± 0.12) drill cores is consistent with the inferred synchronicity of the sampled shales suggested by their stratigraphic position beneath postglacial $\delta^{13}C$ excursions. Thus, the pooled Re-Os age of 643.0 ± 2.4 Ma is considered the most precise estimate of the depositional age for the Tindelpina Shale Member. Because of the close stratigraphic proximity of the sampled shales to the conformably underlying diamictites, the Re-Os ages provide tight minimum age constraints for the end of the Sturtian and Areyonga glaciations. Correlation of the postglacial fine-grained sediments of the Aralka Formation and Tindelpina Shale Member is a key feature of Australian intra-continental correlation schemes, and is suggested to reflect widespread melting of ice sheets after the end of Sturtian and Areyonga glaciation (Preiss and Forbes, 1981; Walter et al., 1995; Preiss, 2000). This correlation is based on lithological and geochemical similarities of the organic-rich cap carbonates overlying Sturtian and Areyonga glacial deposits (Preiss et al., 1978; Preiss and Forbes, 1981; Walter et al., 1995, 2000; Kennedy, 1996; Kennedy et al., 1998). However, both the combined Tindelpina Shale Member Re-Os age of 643.0 ± 2.4 Ma and the Blinman-2 Re-Os age of 645.1 ± 4.8 Ma are younger (given 2σ uncertainties) than the Aralka Formation Re-Os age of 657.2 ± 5.4 Ma. These data suggest diachronous deglaciation and post-glacial sedimentation, or synchronous deglaciation but different sediment accumulation rates for the Aralka Formation compared to the Tindelpina Shale Member. The latter scenario would require very slow sedimentation rates for the Tindelpina Shale Member relative to the Aralka Formation to explain the observed Re-Os ages. However, this seems unlikely given the ~ 1600 m and ~ 100 m thickness of the Tapley Hill Formation and Tindelpina Shale Member, respectively, in Blinman-2, and the ~ 27 m thickness of the Aralka Formation in Wallara-1. Alternatively, the end of the Sturtian and Areyonga glaciations was synchronous, but the onset of post-glacial sedimentation was diachronous because of differences in depositional environment between the Tapley Hill Formation (developing passive margin) and Aralka Formation (intracratonic basin) (Walter et al., 1995; Preiss, 2000; Li and Powell, 2001; Lindsay, 2002). However, this requires a significant hiatus between the Wilyerpa Formation and Tindelpina Shale Member to explain the younger Blinman-2 Re-Os age. No obvious hiatus is observed, although this could reflect the deepwater environment of deposition recorded in this core (McKirdy et al., 2001). If the end of the Sturtian and Areyonga glaciations was indeed diachronous, the timing of glaciation in southern and central Australia may have still overlapped, considering the great thickness of Sturtian glacial deposits (e.g., ~ 6 km in the North Flinders Zone; Young and Gostin, 1988, 1989, 1990, 1991). For example, the U-Pb zircon age of ca. 658 Ma from the Merinjina Formation (Fanning and Link, 2006), a waxing phase of the Sturtian glaciation (Preiss et al., 1998), overlaps the Aralka Formation Re-Os age.

The Re-Os age of 640.7 ± 4.7 Ma for the organic-rich shales of the upper Black River Dolomite is equivalent (within 2σ uncertainties) to the Re-Os age of 643.0 ± 2.4 Ma for the Tindelpina Shale Member. Because the upper Black River Dolomite age was obtained ~ 1 m above the contact with the underlying Julius River Member diamictites, the Re-Os shale ages suggest the Julius River Member is a Sturtian-correlative, consistent with previous lithological, chemostratigraphic, and biostratigraphic evidence (Calver, 1998; Calver and Walter, 2000). The Skillogalee Dolomite is also suggested to be a correlative of the Black River Dolomite carbonates underlying Julius River Member diamictites (Calver, 1998). Because the Skillogalee Dolomite is separated from the Sturtian glacial deposits by ~ 2-3 km of sedimentary rocks, a major unconformity is likely present at the base of the Julius River Member and is correlative with the unconformity separating Sturtian glacial deposits from the underlying Burra Group (Preiss, 1990, 2000; Calver, 1998).

3.5.4 Implications for Global Correlation of Neoproterozoic Ice Ages

Previous radiometric age constraints for the "Sturtian" ice age on other continents include U-Pb zircon ages of 684 ± 4 Ma and 685 ± 7 Ma for the Edwardsburg Formation (central Idaho; Lund et al., 2003) and 711.8 ± 1.6 Ma for the Ghubrah Formation (Oman; Allen et al., 2002). Both ages were obtained on volcanic rocks intercalated with glaciogenic diamictite. Other glacial intervals are radiometrically constrained between U-Pb zircon dates of 667 ± 5 Ma and 709 ± 5 Ma (Scout Mountain

Member, Pocatello Formation, southern Idaho; Fanning and Link, 2004), 663 ± 4 Ma and 761 ± 8 Ma (Changan and Tiesiao Formations, southern China; Zhou et al., 2004), 727 ± 10 Ma and 755 ± 15 Ma (Baiyisi Formation, northwestern China; Huang et al., 2005; Xu et al., 2005), 735 ± 5 Ma and 765 ± 5 Ma (Grand Conglomerat, northwestern Zambia; Key et al., 2001), 741 ± 6 Ma and 771 ± 6 Ma (Kaigas Formation, southwestern Namibia; Frimmel et al., 1996, 2001). U-Pb zircon age constraints of 746 ± 2 Ma and 755 ± 18 Ma (detrital zircon) also provide a maximum age constraint on glaciogenic deposits of the Chuos Formation (northern Namibia; Hoffman et al., 1996) and the Rapitan Group (Mackenzie Mountains, N.W.T., Canada; Ross and Villeneuve, 1997). Significantly, the minimum Re-Os age constraints of 643.0 ± 2.4 Ma and 657.2 ± 5.4 Ma for the Sturtian and Areyonga glaciations, together with the U-Pb SHRIMP zircon age of ca. 658 Ma for the Merinjina Formation (Fanning and Link, 2006) suggest they are not likely to be correlative with most of the above ca. 685–750 Ma glacial intervals (Figure 3.8). However, some overlap in ages cannot be ruled out because the duration of Sturtian and Areyonga glaciation is not known. The onset of Sturtian glaciation may be contemporaneous with the erosional unconformity at the base of Sturtian glacial deposits. For example, Preiss (2000) mention rare dropstones in the Mintaro Shale (Belair Subgroup) below the unconformity. A U-Pb zircon age of 663 ± 4 Ma from an ash bed within the rhodochrosite cap carbonate of the Tiesiao Formation (South China; Zhou et al., 2004) overlaps the basal Aralka Formation age, indicating possible synchronicity of glaciation during Areyonga and Tiesiao deposition, and possible overlap with Sturtian glaciation. However, the most significant observation from the present geochronologic database is that the end of the ''Sturtian'' ice age was likely markedly diachronous worldwide, and/or there were multiple glaciations between ca. 750 Ma and 643 Ma.

Global correlations of ''Marinoan'' (e.g., including the Elatina Formation) glacial deposits are based in part on pre-glacial negative $\delta^{13}C$ excursions (Trezona anomaly) and cap carbonate litho- and chemostratigraphy (e.g., Hoffman et al., 1998a, b; Kennedy et al., 1998; Walter et al., 2000; McKirdy et al., 2001; Halverson et al., 2002, 2005; Hoffman and Schrag, 2002; Schrag et al., 2002; Halverson, 2006). Precise age constraints for this ice age include U-Pb zircon ages of 635.51 ± 0.54 Ma and 635.23 ± 0.57 Ma from ash beds within the upper Ghaub Formation in Namibia (Hoffmann et al., 2004) and the

Nantuo cap carbonate (Doushantuo Formation) in southern China (Condon et al., 2005), respectively. Although not strictly dating the same geological event (i.e., glacial versus post-glacial deposition), these ages suggest the possibility of a worldwide ''Marinoan'' glaciation terminating synchronously at ~ 635 Ma. The Tindelpina Shale Member Re-Os age of 643.0 ± 2.4 Ma does not necessarily refute the prevailing "Marinoan" correlation scheme, although accepting an age of 635 Ma for the undated Elatina Formation glacial deposits requires high sedimentation rates to accommodate ~ 4 km of inter-glacial strata in the Central Flinders Zone (Preiss et al., 1998). Based on Ir anomalies in cap carbonates from the eastern Congo craton, Bodiselitsch et al. (2005) estimate the duration of "Marinoan" glaciation to be 12 M.y., but permit a minimum duration of 3 M.y. if extraterrestrial input fluxes to the Earth were an order of magnitude higher than the Cenozoic. An age of ca. 643 Ma for Sturtian deglaciation places a time constraint of << 8 M.y. for the duration of a "Marinoan" snowball Earth glaciation ending synchronously at ca. 635 Ma. However, the assumptions of an exclusively extraterrestrial origin for the Ir as well as simple re-deposition from a (melted) static ice sheet is questionable (Fairchild and Kennedy, 2007), and thus the time constraint suggested by Bodiselitsch et al. (2005) require testing through acquisition of additional PGE data from other Neoproterozoic glacial intervals.

Alternatively, Calver et al. (2004) suggest the Marinoan glaciation in southern Australia is correlative with the 580 Ma Gaskiers glaciation (eastern Canada) based on correlation of the Elatina Formation with the Croles Hill Diamictite and Cottons Breccia. At first glance, this scenario would appear to be more compatible with the 643 Ma Tindelpina Shale Member age. However, the correlation of younger diamictite units between southern Australia, northwestern Tasmania, and southeastern King Island is controversial. In southeastern King Island, sills of the Grimes Intrusive Suite (U-Pb SHRIMP zircon age of 575 ± 3 Ma intrude the Cottons Breccia, Cumberland Creek Dolostone cap carbonate, and post-glacial Yarra Creek Shale (Calver et al., 2004). The similarity of the petrology (pinkish dolostone with tepee-like structures) and geochemistry (e.g., upward decreasing $\delta^{13}C$ values) of the Cumberland Creek Dolostone and the Nuccaleena Formation does support correlation of the Elatina Formation and Cottons Breccia (Calver and Walter, 2000; Preiss, 2000). The Yarra Creek Shale may have been only partially consolidated at the time of sill intrusion (Meffre et al., 2004), but it remains unclear if emplacement of the Grimes Intrusive Suite quickly followed the end of glaciation or is significantly younger. In northwestern Tasmania, the Croles Hill Diamictite has a maximum age of 582 ± 4 Ma (U-Pb SHRIMP zircon date from underlying rhyodacite) (Calver et al., 2004). However, correlation of the Croles Hill Diamictite with the Cottons Breccia and Elatina Formation of southern Australia remains questionable in the absence of a distinctive cap carbonate (and concomitant $\delta^{13}C$ isotope data) above the Croles Hill Diamictite. Imprecise Re-Os dates of 647 ± 30 Ma and 704 ± 86 Ma for the Brachina Formation and Yarra Creek Shale, respectively, do not help to resolve these questions. Consequently, an age of either 635 or 580 Ma for the Elatina Formation (and Cottons Breccia) remains compatible with current geochronological data.

Paleomagnetic and sedimentological (e.g., dropstone-bearing intervals and tidal rhythmites) studies suggest that Neoproterozoic glaciomarine deposition occurred at low latitudes in some instances (in contrast to the mid- and high-latitude Phanerozoic glaciations), thus implying unusually severe glaciations (Schmidt and Williams, 1995; Park, 1997; Sohl et al., 1999; Trindade et al., 2003; Macouin et al., 2004; Williams, 2004; Williams and Schmidt, 2004; Huang et al., 2005; Kilner et al., 2005). Available radiometric age constraints for Neoproterozoic glaciation permit the possibility of a global or near-global ice age (of unknown duration) at ca. 750 Ma (Baiyisi–Grand Conglomerat–Kaigas), ca. 712 Ma (Ghubrah–Scout Mountain) and ca. 635 Ma (Ghaub–Nantuo). However, the new Re-Os age constraints for the Sturtian and Areyonga glacial deposits, together with U-Pb age constraints of ca. 685 Ma for the Edwardsburg Formation, provide compelling geochronological evidence for diachronous and/or multiple episodes of glaciation between ca. 750 and 643 Ma, thus ruling out a simple tripartite ("Sturtian"–"Marinoan"–"Gaskiers") division of all Neoproterozoic glacial deposits (see Figure 3.8). Radiometric age constraints for Neoproterozoic glaciogenic deposits also negate use of cap carbonate types for global correlation schemes. "Sturtian"-type cap carbonates (e.g., Kennedy et al., 1998) occur above the ca. 712 Ma Ghubrah Formation (Brasier et al., 2000), > 663 Ma Tiesiao Formation (Zhou et al., 2004), > 657 Ma Aralka Formation and the ca. 658-643 Ma Sturtian glacial deposits (Preiss et al., 1978; Preiss and Forbes, 1981; Kennedy, 1996), and thus do not represent useful chronostratigraphic marker horizons. Similarly, Corsetti and Lorentz (2006) showed that "Marinoan"-type cap carbonates span a time interval of up to 100 M.y. Indeed, the Ghubrah Formation, containing a "Sturtian"-type cap carbonate, may have been deposited synchronously with the Scout Mountain Member, containing a "Marinoan"-type cap carbonate (Corsetti and Lorentz, 2006). Thus, I support the suggestion of Corsetti and Lorentz (2006) that the terms "Sturtian" and "Marinoan" no longer be used to describe episodes of global or near-global Neoproterozoic glaciation.

Plate tectonics exerts a significant control on the spatial distribution of glaciomarine deposition and can result in diachronous glaciation (Schermerhorn, 1974; Young, 1988, 1995, 2002; Eyles, 1993; Crowell, 1999; Eyles and Januszczak, 2004). For example, the Sturtian and Edwardsburg diamictites of Australia and western Laurentia, respectively, may have been products of local ice sheet growth on uplifted rift margins during or subsequent to Rodinia breakup (Preiss, 2000; Lund et al., 2003; Eyles and Januszczak, 2004). Geological evidence (e.g., thick diamictite successions interspersed with coarse- and fine-grained strata, including intercalated dropstone-free and dropstone-bearing intervals suggesting significant meltwater fluxes from wet-based glaciers) for actively functioning hydrological cycles and oscillatory waxing and waning of Neoproterozoic ice sheets is well-documented not only from the Sturtian glacial deposits of southern Australia (Young and Gostin, 1988, 1989, 1990, 1991; Eyles et al., 2007), but also from the Mount Vreeland Formation (western Canada; McMechan, 2000), Fiq Member (Ghadir Manquil Formation, Oman; Leather et al., 2002), Port Askaig Formation (Arnaud and Eyles, 2006), Chuos and Ghaub Formations (Namibia), Kingston Peak Formation (southwestern United States), Blässkrans Formation (Namibia), and the Southern Highland Group (Ireland-Scotland) (Condon et al., 2002). Sedimentary structures such as tidal rhythmites in the Elatina and Sturtian glacial deposits also suggest unfrozen oceans during glaciation (e.g., Schmidt and Williams, 1995; Williams, 2004; Williams and Schmidt, 2004). Recently, chemical weathering indices (chemical and mineral indices of alteration) from the Fiq Formation suggests climatic oscillation of cold glacial and warm-humid inter-glacial periods (Rieu et al., 2007). Thus, at least some Neoproterozoic glaciations probably resembled those of the Pleistocene Epoch (Leather et al., 2002) although active debate continues regarding the possibility of multi – million year "Snowball" or "Slushball" Earth Neoproterozoic glaciations.

3.5.5 Implications for the Neoproterozoic Paleogeographic Reconstructions, and the Relationship Between Rodinia Supercontinent Breakup and Sturtian Glaciation

Neoproterozoic rocks of the Adelaide Rift Complex may record at least five major rift events (Preiss, 2000), but the significance of each event with regards to breakup of the Mesoproterozoic-Neoproterozoic Rodinia supercontinent and opening of the Paleo-Pacific Ocean remains disputed (e.g., Bond et al., 1984; Lindsay et al., 1987; Powell et al., 1994; Veevers et al., 1997; Preiss, 2000; Li and Powell, 2001). The timing of the first three phases of rifting are broadly constrained by U-Pb zircon and baddeleyite ages on coeval volcanic rocks. The oldest rift episode is represented by the 827 ± 9 Ma Little Broken Hill gabbro (easternmost Adelaide Rift Complex) and the 827 ± 6 Ma Gairdner Dyke Swarm (Gawler Craton and Stuart Shelf), whose co-genetic equivalents likely include the Beda Volcanics (Stuart Shelf) and Wooltana Volcanics (Arkaroola Subgroup, Callana Group; Adelaide Rift Complex) (Wingate et al., 1998). The Gairdner Dyke Swarm is suggested to originate from mantle plume activity that initiated development of the Centralian Superbasin following thermal subsidence (Zhao et al., 1994; Wingate et al., 1998; Lindsay, 2002). Stratigraphically above the Wooltana Volcanics in the Adelaidean succession is the 802 ± 10 Ma Rook Tuff (Curdimurka Subgroup, Callana Group; Fanning et al., 1986), which may mark a discrete younger rift episode. The first two phases of rifting may be intracratonic and associated with NE-SW crustal extension. A north-south trending rift zone along the Torrens Hinge Zone is associated with extrusion of the 777 ± 7 Ma Boucaut Volcanics (basal Burra Group) and the first major marine inundation of the Adelaidean basin (Preiss, 2000). Volcanism is apparently not coeval with the fourth rift episode, but deposition of the thick Sturtian diamictites in NW- and E-W trending half-grabens (e.g., Yudnamutana Trough) at the southwestern (Baratta Trough) and northwestern (North Flinders Zone) margins of the Curnamona Craton suggest renewed NE-SW directed rifting (Preiss, 2000). A major sea-level rise following the Sturtian glaciation is suggested by Preiss (2000) and Li and Powell (2001) to record the onset of continental separation associated with Rodinia breakup. If the temporal and spatial distribution of magmatic activity is reasonably well preserved in the rock record, then the timing of proposed continental separation (ca. 643 Ma Tindelpina Shale Member) and Sturtian glaciation (ca. 658-643 Ma) post-dates by more than 100 M.y. the ca. 827-777 Ma magmatic activity in the Adelaide Rift Complex. These observations render it possible that the main phase of continental rifting and separation pre-dated Sturtian glacial/post-glacial sedimentation.

The continental block(s) adjoining eastern Australia-Antarctica within the Rodinia supercontinent is a matter of extensive debate. Numerous paleogeographic reconstructions have placed eastern Australia against northwestern (SWEAT; Southwest US – East Antarctica; Dalziel, 1991, 1997; Moores, 1991; Hoffman, 1991; Weil et al., 1998), western (AUSWUS; Australia – Western US; Brookfield, 1993; Karlstrom et al., 1999; Burrett and Berry, 2000), and southern (AUSMEX; Australia – Mexico; Wingate et al., 2002; Pisarevsky et al., 2003) Laurentia. Alternative reconstructions place South China (e.g., Li et al., 1995, 1999, 2002) or Siberia (Sears and Price, 2003) between Laurentia and eastern Australia. A paleopole from 1070 ± 6 Ma sills of the Bangemall Basin (western Australia) lies 30-40° away from the apparent polar wander path of Laurentia between 1100 and 1020 Ma, and permits the AUSMEX, but not the SWEAT or AUSWUS, configurations (Wingate et al., 2002). Paleomagnetic data from the Mundine Wells Dyke Swarm suggest significant separation of Laurentia from Australia by 755 ± 3 Ma (U-Pb SHRIMP age from zircon and baddeleyite; Wingate and Giddings, 2000). In addition, recent paleomagnetic data suggests South China was adjoined to the northwestern or western margin of Australia between middle Neoproterozoic and middle Devonian time (Macouin et al., 2004; Yang et al., 2004). A possible breakup between Australia and Siberia-Laurentia is suggested to have occurred in the early Neoproterozoic (Sears and Price, 2003), but geological dissimilarities render a western Laurentia – Siberia connection problematic (Pisarevsky et al., 2003), and Siberia may have instead had a proximal location near northern Laurentia (Gladkochub et al., 2006). Pisarevsky et al. (2003) place the paleomagnetically unconstrained Rio de la Plata craton next to Australia – eastern Antarctica in their reconstruction, and suggest these cratonic blocks began to separate at ca. 827 Ma (contemporaneous with the Gairdner Dyke Swarm). This event may have been followed by a northerly shift in the locus of rifting at ca. 780 Ma that led to separation of Australia and Laurentia. None of these reconstructions advocate a major phase of continental breakup at ca. 658-643 Ma.

If the AUSMEX connection is valid at all, then continental separation and concomitant marine inundation may have occurred earlier during deposition of the middle Burra Group (Woolshed Flat Shale to Saddleworth Formation; "Torrensian 3" of Preiss, 2000) (Figure 3.9). This interval is interpreted by Preiss (2000) to represent the first major marine inundation of the Adelaide Rift Complex. Maximum flooding conditions may be represented by two intervals in the fine-grained, organic-rich Auburn Dolomite Member (Saddleworth Formation). This was followed by renewed crustal uplift and marine flooding (Belair Subgroup; uppermost Burra Group), and widespread regional erosion associated with the onset of Sturtian glaciation (Preiss, 2000). Deposition of thick diamictite units by sediment gravity flow processes and ice-rafting in deep marine basins during the Sturtian glaciation (Coats, 1981; Preiss, 1990, 1993; Young and Gostin, 1988, 1989, 1990, 1991; Eyles et al., 2007) may be associated with uplift and crustal extension without necessarily resulting in calving of cratonic blocks from the Australian margin. This may explain the lack of rift-related magmatic activity associated with Sturtian glacial deposition.

A thick pile (up to 6 km) of intrusive and volcanic rocks in eastern South Australia, western New South Wales, western Victoria, King Island, and Tasmania form offset linear segments hundreds of kilometres in length, are associated with distinctive gravity and magnetic anomalies, and the volcanics have similar geochemistry (alkaline basalts, rift tholeiites, and picrites). They also bear a remarkable geometric similarity to the northwestern Australian volcanic passive margin (Direen and Crawford, 2003). U-Pb zircon and Sm-Nd age constraints for volcanic rocks of the Kanunnah Subgroup (582 ± 4 Ma; Calver et al., 2004) and Rocky Cape Dyke Swarm (588 ± 8 Ma and 600 ± 8 Ma; Brown, 1986) on northwestern Tasmania, Grassy Group on southeastern King Island (575 ± 3 Ma and 579 ± 16 Ma; Calver et al., 2004; Meffre et al., 2004), and Mt. Arrowsmith Volcanics (586 ± 7 Ma; Crawford et al., 1997) on western New South Wales suggests development of an Adelaidean passive margin after ca. 600-570 Ma. A Rb-Sr age of 586 ± 30 Ma from pre-Wonoka Formation strata in the Adelaide Rift Complex is suggested to date the end of Adelaidean intra-basinal fluid flow (Foden et al., 2001) and the onset of rift-related canyon incision (Williams and Gostin, 2000). Mafic volcanism in the Officer Basin (Table Hill Volcanics) is also broadly of the same age (e.g., Rb-Sr whole-rock date of 563 ± 40 Ma; Walter et al., 1995). Breakup may be associated with renewed mantle plume activity in southern Australia (Williams and Gostin, 2000). Direen and Crawford (2003) suggest this younger rifting event at ca. 600-570 Ma may have obscured or removed the evidence for the main pulse of magmatic activity associated with Rodinia breakup.

Significant uncertainty surrounds the tectonic relationships between western Tasmania, King Island, and southeastern Australia during the Neoproterozoic (e.g., Calver and Walter, 2000; Preiss, 2000). The ca. 777-760 Ma Wickham Orogeny is suggested to represent a period of deformation, magmatism, and metamorphism affecting King Island and western Tasmania (Turner et al., 1998), but in the Adelaide Rift Complex, similarly aged rocks in the basal Burra Group record crustal extension (Preiss, 2000). Western Tasmania and King Island may have represented fragments of a separate microcontinent that did not collide with Australia until the early phase of the ca. 510-490 Ma Tyennan-Ross-Delamarian orogenies. Alternatively, granitic magmatism may have been associated with crustal extension and pre-dated the metamorphism and deformation that in turn could be associated with the accretion of Cambrian volcanic island arcs during the Tyennan-Ross-Delamarian orogenies (Preiss, 2000). This is the preferred interpretation because identical Re-Os ages for the Tindelpina Shale Member and upper Black River Dolomite, together with the presence of *Baicalia burra* in Julius River Member carbonate clasts and the Skillogalee Dolomite (Griffin and Preiss, 1976; Preiss, 1990; Belperio, 1990) suggest northwestern Tasmania represented a southernmost link of the Adelaide Rift Complex (Calver, 1998; Calver and Walter, 2000) during Torrensian and Sturtian time. Litho- and chemo-stratigraphic similarities between the diamictite, cap carbonates, and post-glacial microbial mat – bearing shales of the Grassy Group on southeastern King Island with the Adelaide Rift Complex, together with correlations with the Togari Group, suggest a tectonic affinity between southeastern Australia, King Island, and western Tasmania during the Sturtian and Elatina glaciation (Calver and Walter, 2000). Lithological and chemostratigraphic dissimilarities between the Ediacaran Smithton Dolomite (northwestern Tasmania), the predominantly siliciclastic Wilpena

Group (Adelaide Rift Complex), and absence of similarly-aged rocks on King Island suggests possible rifting of western Tasmania and King Island from southeastern Australia after ca. 600-570 Ma (Calver, 1998; Calver and Walter, 2000). An earlier rifting event for western Tasmania relative to King Island is possible (Calver and Walter, 2000), but initiation of mafic volcanism in western Tasmania may not significantly precede that of King Island in view of the ca. 643 Ma age (rather than 700 Ma as originally assumed) of Sturtian post-glacial sedimentation.

Consideration of the geological history of the Adelaidean succession suggests a long period of episodic crustal extension and rifting between ca. 827 and 580 Ma followed by the onset of convergent tectonics associated with the ca. 510-490 Ma Delamarian Orogeny. Evidence for rift-related magmatism is associated only with pre-Sturtian (ca. 827, 802, and 777 Ma) and post-Elatina (ca. 600-570 Ma) deposition. Both events could be associated with continental separation and the formation of passive margins (Direen and Crawford, 2003), and it remains inconclusive which event is directly related to Rodinia supercontinent breakup. Ultimately, evaluation of the position of eastern Australia-Antarctica within Rodinia will require significant improvements in the quality of Neoproterozoic apparent polar wander paths (Pisarevsky et al., 2003).

3.5.6 Evaluation of Shale-hosted Benthic Microbial Mats as Deposition-Age Geochronometers

Prior to the onset of intense bioturbation in Cambrian-Ordovician times, the subtidal siliciclastic seafloors of Neoproterozoic oceans may have been populated by benthic microbial mats (Hagadorn and Bottjer, 1997, 1999; Gehling, 1999; Logan et al., 1999; Seilacher, 1999, Bottjer et al., 2000; Noffke et al., 2002; Grazhdankin, 2004; Bottjer, 2005; Bottjer and Clapham, 2006). Benthic microbial mats may facilitate the formation of organic-rich shales by creating a strong reducing environment within the substrate despite the presence of an overlying oxygenated water column (Schieber, 1986). The organic-rich mat material from the Brachina Formation and Yarra Creek Shale are enriched in Re (2-16 ppb) and Os (105-330 ppt). Accordingly, Proterozoic microbial mat facies merit consideration as potential Re-Os deposition-age geochronometers. However, the Re-Os dates for the microbial mat facies of the Brachina Formation (647 ± 30 Ma) and Yarra Creek Shale (704 ± 86 Ma) are associated with a large degree of scatter (MSWD = 34 and 125, respectively). Temporal evolution of paleo-seawater Os isotope composition during deposition of the ~ 1 m sampled stratigraphic interval from the Brachina Formation is one possible explanation for the scatter. This is difficult to evaluate given the uncertainty on the depositional age of the Brachina Formation, which may be as old as 635 Ma (Hoffmann et al., 2004; Condon et al., 2005) or as young as 580 Ma (Calver et al., 2004), and the absence of constraints on sedimentation rate. However, this process is not likely to explain the scattered Re-Os isotope systematics in the Yarra Creek Shale, which has a sampled stratigraphic interval of only ~ 4 cm. Thus, the scatter in the Re-Os systematics of the microbial mat facies more likely results from post-depositional mobilization of Re and/or Os.

Because the Brachina Formation samples were obtained from drill core, and Yarra Creek Shale outcrop samples contain abundant unaltered pyrite, weathering is not the likely cause of the observed scatter. No evidence of hydrothermal or diagenetic fluid flow (e.g., carbonate veinlets) is present in either sample set. Thermal alteration of the Brachina Formation is minimal based on kerogen H/C ratios and preservation of primary or near-primary $\delta^{13}C_{carb}$ and $\delta^{13}C_{org}$ values (Calver, 2000). Metamorphic mineral assemblages in the Grassy Group suggest the Yarra Creek Shale may have undergone lower greenschist facies (chlorite-grade) metamorphism (Meffre et al., 2004). Although Kendall et al. (2004) obtained precise depositional age information from the similarly metamorphosed Old Fort Point Formation, Kendall (2003) suggested post-depositional mobilization of Re and Os associated with thermal breakdown of organic matter may begin to occur above ~ 300-350°C (see Chapter 4). Thus, thermal alteration of the Re-Os isotope systematics in the Yarra Creek Shale cannot be conclusively ruled out.

Alternatively, the scattered Re-Os isotope systematics of the microbial mats may reflect diagenetic re-distribution during percolation of oxygenated bottom waters into the mats. Sulfide-oxidizing bacteria require a thin transitional zone (e.g., a few mm thick) between overlying oxygenated waters and underlying anoxic, H_2S-bearing sediments (Williams and Reimers, 1983). Kerogen isolated from the Pertatataka Formation microbial mats show evidence of oxidation and in-situ biodegradation by heterotrophic bacteria (Logan et al., 1999). In suboxic organic-rich sediments with sufficiently slow sedimentation rates (< 50-100 m/Ma), Re may be mobilized quantitatively by overlying oxygenated bottom waters and re-immobilized below the oxidation front over a depth range of ~ 0.5-3 m (Colodner et al., 1992; Crusius and Thomson, 2000, 2003). In addition, some fraction of Re may be lost to the overlying water column. Significant overlap between oxidation fronts and re-immobilization peaks is caused by the upward propagation of oxidation fronts over time. The mobility of Os during subaqueous weathering is not known, but studies on subaerial weathering of black shales (Peucker-Ehrenbrink and Hannigan, 2000; Jaffe et al., 2002; Pierson-Wickmann et al., 2002) suggest that Os will probably also be mobilized by oxidizing bottom waters.

Thus, sedimentation rates during deposition of the Australian Early Ediacaran microbial mats may have been sufficiently slow to allow subaqueous oxidative weathering and diagenetic mobilization of Re and Os in the microbial mat material. Because the host and microbial mat shale have very low TOC contents (< 1%; Logan et al., 1999), a significant fraction of the oxidized Re and Os may not have been re-immobilized below oxidation fronts, but rather was lost to the overlying water column (cf. Crusius and Thomson, 2000, 2003). The degree of disturbance to Re-Os isotope systematics is difficult to evaluate, however, given the uncertainty in the ages of the Brachina Formation and Yarra Creek Shale. If the Brachina Formation and Yarra Creek Shale are only slightly younger than ca. 635 Ma (e.g., Hoffmann et al., 2004; Condon et al., 2005), then sample $I_{Os\ (635\ Ma)}$ values would range between 1.10 and 1.18, between 1.12 and 1.24, and between 1.09 and 1.66 for the Pertatataka Formation, Brachina Formation and Yarra Creek Shale, respectively (see Tables 3.3, 3.4, and 3.6). Exclusion of two outliers yields a narrower range of between 1.27 and 1.41 for the Yarra Creek Shale. These compositions are broadly equivalent to the estimated $^{187}Os/^{188}Os$ ratio of the currently eroding upper continental crust (~ 1.0-1.4; Esser and Turekian, 1993; Peucker-Ehrenbrink and Jahn, 2001; Hattori et al., 2003) and average riverine input (~ 1.54; Levasseur et al., 1999), and could potentially reflect dominance of the ocean Os input fluxes by riverine Os during deglaciation. If correct, this interpretation suggests primary, but imprecise, depositional age information can be preserved by benthic microbial mats (Figure 3.10A). Alternatively, if these shales were deposited shortly after the end of a ca. 580 Ma glaciation (as suggested by Calver et al., 2004), then sample $I_{Os\ (580\ Ma)}$ values would range between 1.16 and 1.25, between 1.22 and 1.50, and between 1.36 and 2.06 for the Pertatataka Formation, Brachina Formation and Yarra Creek Shale, respectively. The upper range of values is significantly higher than eroding upper continental crust, suggesting significant disturbance of the Re-Os system. Following diagenetic re-immobilization and final closure of the Re-Os isotope system, a positively correlated variation between $^{187}Re/^{188}Os$ and $^{187}Os/^{188}Os$, reflecting differences in Re and Os diffusion rates (e.g., greater mobility of Re relative to Os as observed during subaerial oxidative weathering; Jaffe et al., 2002; Pierson-Wickmann et al., 2002), may have resulted in erroneously old ages for the Brachina Formation and Yarra Creek Shale (Figure 3.10B). If correct, then organic-rich benthic microbial mat material would be both imprecise and inaccurate as a deposition-age geochronometer.

Recently, Miller (2004) obtained Model 3 Re-Os dates of 381.4 ± 4.3 Ma (MSWD = 16, $I_{Os} = 0.26 \pm 0.02$) and 458 ± 14 Ma (MSWD = 660, $I_{Os} = 0.44 \pm 0.06$) from rapidly deposited, high-TOC (typically > 5% and up to ~ 60%), carbonate-hosted algal laminites of the Devonian Keg River Formation and Ordovician Yeoman Formation (western Canada), respectively. Both Re-Os dates are broadly equivalent to radiometric and biostratigraphic age constraints for the studied rock units. The Keg River Formation contains Re (21-224 ppb) and Os (0.47-2.32 ppb) abundances comparable to those of Phanerozoic black shales and was deposited from anoxic and hyper-saline bottom waters. Notwithstanding possible minor post-depositional mobility (MSWD = 16), anoxic, rapidly deposited carbonate-hosted algal laminites may represent viable deposition-age geochronometers. Miller (2004) suggest the low Re and Os abundances (typically < 1 ppb and < 0.1 ppb, respectively) in the Yeoman Formation laminites reflects slow diffusion rates across the sediment-water interface, and rapid deposition within a relatively shallow water, hyper-saline, oxidizing environment. Small-scale Re and Os mobilization during oxidative subaqueous weathering may have resulted in an imprecise (MSWD = 660), yet accurate (within 2σ uncertainties) Re-Os date for the Yeoman Formation. An alternative or additional possibility in view of the low Re and Os abundances is a significant detrital Os component with heterogeneous I_{Os}.

3.5.7 Variations in the Initial ^{187}Re/^{188}Os Ratio in Organic-rich Shales

A sample suite of organic-rich shales with homogenous I_{Os} and a sufficiently large range in initial ^{187}Re/^{188}Os isotope ratio is required for obtaining precise Re-Os depositional ages by the isochron method. However, the mechanism(s) controlling the range in initial ^{187}Re/^{188}Os of ORS is not well understood. This problem results from a limited understanding of the nature of the host phase(s) of Re and Os in these rocks. The possibility of multiple and/or separate host phases for Re and Os in shales has only been indirectly inferred from the greater overall reproducibility of Re relative to Os abundances in some powder aliquots (Creaser et al., 2002; Kendall et al., 2004), and preferential leaching of Re relative to Os by a HF-BF_3 acid attack employed for isolation of organic matter from shale source rocks (Selby and Creaser, 2003). A suitable spread in ^{187}Re/^{188}Os isotope ratios was previously obtained from stratigraphic intervals ranging from ~ 10 cm (representing ~ 43,100 years; Selby and Creaser, 2005) to several meters (representing millions of years; e.g., Cohen et al., 1999). In this study, large ranges in ^{187}Re/^{188}Os isotope ratio were generated from stratigraphic intervals ranging between 4 cm (^{187}Re/^{188}Os = 284-462; Yarra Creek Shale) and 2 m (^{187}Re/^{188}Os = 252-447; Aralka Formation). The upper Black River Dolomite shale interval containing high abundances of Re and Os have a narrower range in isotope ratios (828.05-828.60 m depth in Forest-1; ^{187}Re/^{188}Os = 479-499) compared to the second interval with lower Re and Os abundances (835.58-835.87 m depth; ^{187}Re/^{188}Os = 533-832). These observations suggest elemental fractionation of Re from Os during uptake into organic-rich sediments may not result solely from temporal fluctuations in seawater Re and Os abundances.

Rhenium and ^{192}Os abundance data from all Australian Neoproterozoic shales show a positive correlation that likely reflects a general trend of increasing enrichment in black shales with declining redox potential in bottom waters (Figure 3.11). For individual stratigraphic intervals, the correlated Re-^{192}Os variations range from moderately negative (Yarra Creek Shale and Brachina Formation), weakly positive (Tindelpina Shale Member), and strongly positive (Aralka Formation, Black River Dolomite, and Pertatataka Formation). Shale-hosted benthic microbial mats represent a distinctive type of ORS, and thus the negative correlations between Re and ^{192}Os abundance observed for the Yarra Creek Shale and Brachina Formation are probably not typical of ORS in general, but could be representative of microbial mat material. The Pertatataka Formation deviates from this observation, but these mats also do not show appreciable enrichment of Re and Os beyond average crustal abundances.

Some interesting observations can be made from perusal of scatter plots for ^{187}Re/^{188}Os isotope ratios and either ^{192}Os or Re abundance for the Australian Neoproterozoic shales characterized by a large range in ^{187}Re/^{188}Os (Figure 3.12A, B). With the exception of the Aralka Formation, Re abundance and ^{187}Re/^{188}Os isotope ratios are well-correlated (R^2 between 0.6 and 1.0), whereas the relationship between ^{192}Os abundance and ^{187}Re/^{188}Os isotope ratio ranges from a weak positive ($R^2 = 0.30$ for the Black River Dolomite) to a strong negative ($R^2 = 0.77$ for the Yarra Creek Shale). The generally well-correlated variations between Re abundance and ^{187}Re/^{188}Os ($R^2 = 0.60$ for all samples in Figure 3.12B) may suggest Re sequestration plays a dominant role for primary ^{187}Re/^{188}Os variations, but for individual shale intervals, the nature of the depositional environment can also be significant. For example, the Aralka Formation exhibits a weak inverse correlation between ^{187}Re/^{188}Os isotope ratio and Re abundance ($R^2 = 0.15$), but ^{187}Re/^{188}Os isotope ratio and ^{192}Os abundance are well-correlated ($R^2 = 0.82$). Declining ^{192}Os abundances with depth in Wallara-1 may correspond to declining Os fluxes to the Aralka Formation organic-rich sediments. The well-correlated positive and inverse trends between ^{187}Re/^{188}Os and Re or ^{192}Os abundance, respectively, observed for the Yarra Creek Shale may represent an artefact of diagenetic remobilization of Re and Os. Nevertheless, the generally good correlation between ^{187}Re/^{188}Os isotope ratio and Re abundance, and the absence of a similar correlation between ^{187}Re/^{188}Os isotope ratio and ^{192}Os abundance, represents further indirect evidence that Re and Os are sequestered into ORS through different mechanisms.

Cross-plots of major and trace metal abundances with Re and ^{192}Os abundances, and ^{187}Re/^{188}Os isotope ratios, were employed to try and elucidate the dominant control(s) on ^{187}Re/^{188}Os isotope variations in the Aralka Formation and the Tindelpina Shale Member (Blinman-2 samples). The trace metal abundance and DOP data suggest suboxic to anoxic/non-sulfidic bottom water conditions during deposition. To avoid the development of spurious correlations, elemental abundances were not normalized to Al (Van der Weijden, 2002). The Aralka Formation shows predominantly negative correlations between ^{187}Re/^{188}Os isotope ratio and metal abundance (e.g., Figure 3.12C, D). Molybdenum abundance appears to be decoupled from Re and ^{192}Os abundance ($R^2 \sim 0.35$). Well-correlated positive trends are observed between ^{192}Os and redox-sensitive trace metal abundance ($R^2 > 0.75$ for V, Cr, Ni, Cu, Pb, and U) in the Aralka Formation. In comparison, these particular trace metals show good ($R^2 > 0.5$), but consistently poorer correlations with Re abundance, consistent with observed negative correlations between ^{187}Re/^{188}Os isotope ratio and metal abundance (R^2 of ~ 0.5-0.8). Together with declining ^{192}Os, but variable Re, abundances with stratigraphic depth, these observations suggest temporal variation in seawater Os abundance and/or the flux of Os-complexing organic matter to accumulating sediments controlled a large proportion of the variation in ^{187}Re/^{188}Os isotope ratio during deposition of the Aralka Formation. With the exception of Pb (removed rapidly from anoxic waters as insoluble Pb sulfide; Morse and Luther, 1999), the other metals (V, Cr, Ni, Cu, U) are known to be associated with organic matter in anoxic/non-sulfidic sediments (Algeo and Maynard, 2004). Both Re and Os are associated with the organic matter in shales (Ripley et al., 2001; Selby and Creaser, 2003), but only Os may be present as dissolved organo-metallic complexes in seawater (Levasseur et al., 1998) or complexed rapidly into organic matter following reductive capture (Yamashita et al., 2007). In contrast, slow precipitation kinetics associated with reductive capture may instead dominate the removal of Re from the overlying suboxic or anoxic/non-sulfidic bottom waters into underlying sediments (Crusius and Thomson, 2000; Sundby et al., 2004; Yamashita et al., 2007) although a large fraction of the Re is ultimately also incorporated into organic complexes (Ripley et al., 2001; Selby and Creaser, 2003).

A number of good correlations are observed between ^{187}Re/^{188}Os isotope ratio ($R^2 \geq 0.5$) and Re abundance ($R^2 \geq 0.6$) with trace metal abundance (V, Cr, Ni, Zn, As, Mo, and Pb) for the Tindelpina Shale Member. In contrast, moderate to poor correlations are consistently observed between these metals and ^{192}Os abundance ($R^2 < 0.5$). The TOC contents (~ 0.5-1.0 %; McKirdy et al., 2001; Schaefer and Burgess, 2003) and ^{192}Os abundances (~ 20-43 ppt) are broadly similar for both shales, but Re and Mo abundances in the Tindelpina Shale Member are distinctly lower. Significantly, the range in Re abundance in the Tindelpina Shale Member is much greater than that of Os, whereas the opposite is true for the Aralka Formation. Variations in seawater Re abundance together with precipitation kinetics associated with the reductive capture of Re (and other trace metals; Morse and Luther, 2001; Crusius and Thomson, 2000; Sundby et al., 2004; Yamashita et al., 2007) may have been the dominant control on ^{187}Re/^{188}Os isotope variation in the Tindelpina Shale Member. The lack of variation in ^{187}Re/^{188}Os in the Pertatataka Formation may reflect relatively uniform fluxes of Re and Os to the microbial mats. In contrast, the strongly elevated and variable Re (94-102 ppb) and ^{192}Os (390-418 ppt) abundances, yet uniform ^{187}Re/^{188}Os, of one interval from the upper Black River Dolomite (828.11-828.58 m) suggests parallel variations in the rate of Re and Os sequestration during deposition from euxinic bottom waters. The cause of such coupled sequestration is not known, but could reflect similar reductive capture rates and/or host phases for Re and Os (see Chapter 5).

3.6 CONCLUSIONS

New Re-Os depositional ages of 657.2 ± 5.4 Ma (MSWD = 1.2) and 643.0 ± 2.4 Ma (MSWD = 1.1) for the Aralka Formation (Amadeus Basin, central Australia) and Tindelpina Shale Member (Adelaide Rift Complex, southern Australia) provide precise minimum age constraints for the end of Areyonga and Sturtian glaciation, respectively, which may have been diachronous. In addition, both the Areyonga and Sturtian glacial deposits are at least partially younger than other ca. 685-750 Ma Neoproterozoic glacial deposits previously regarded as possible correlatives. Thus, the "Sturtian" ice age was markedly diachronous, and/or there were multiple episodes of glaciation between ca. 750 and 643 Ma. This observation suggests that not all Neoproterozoic glacial deposits may result from "Slushball" or "Snowball" Earth glaciations. Instead, some Neoproterozoic glacial deposits may reflect glaciomarine deposition in deep marine basins bordering faulted and/or uplifted rift margins during episodes of crustal extension and/or continental breakup. Paleomagnetic data suggest the AUSMEX (Australia – Mexico) Rodinia connection between eastern Antarctica – Australia, if valid at all, was likely terminated prior to ca. 755 Ma (Wingate and Giddings, 2000). Sturtian glacial and post-glacial deposition (ca. 658-643 Ma) significantly post-dates ca. 827-777 Ma magmatic activity in the Adelaide Rift Complex associated with Rodinia continental breakup. Thus, marine inundation associated with the onset of continental separation and passive margin formation likely pre-dates Sturtian glaciation, and may be represented by sandstone and fine-grained siliciclastic and carbonate strata in the middle Burra Group ("Torrensian 3" of Preiss, 2000). Sturtian glaciation itself was probably associated with a period of crustal extension and uplift, but this event did not result in a major phase of continental breakup.

The Re-Os age for the Tindelpina Shale Member is identical (within 2σ uncertainties) to a Re-Os age of 640.7 ± 4.7 Ma (MSWD = 0.91) for black shales overlying diamictites of the Julius River Member (Black River Dolomite, Togari Group, northwestern Tasmania). Consistent with previous litho-, chemo-, and bio-stratigraphic evidence, the Re-Os ages suggests correlation between the Sturtian and Julius River Member diamictites. Western Tasmania was thus likely connected to southeastern Australia during Sturtian glacial/post-glacial sedimentation. Litho- and chemo-stratigraphic similarities of cap carbonates and post-glacial shales above the Adelaidean Elatina Formation and Cottons Breccia (Grassy Group, southeastern King Island) (Calver and Walter, 2000) suggest a continued tectonic affinity between southeastern Australia, King Island, and western Tasmania through the Elatina glaciation.

Imprecise Re-Os dates of 647 ± 30 Ma (MSWD = 34) and 705 ± 86 Ma (MSWD = 120) were obtained from shale-hosted fossil benthic microbial mats of the Brachina Formation (Adelaide Rift Complex) and Yarra Creek Shale (Grassy Group, southeastern King Island), respectively. Subaqueous weathering by oxygenated bottom waters has likely resulted in post-depositional mobilization of Re and Os in the organic-rich microbial mat material. Because both microbial mat – bearing shales overlie glacial deposits (Elatina Formation and Cottons Breccia, respectively) of uncertain age (e.g., 635 Ma or 580 Ma), the degree of post-depositional mobility is not known. Nevertheless, shale-hosted benthic microbial mats are not precise deposition-age geochronometers.

An initial attempt has been made to constrain the mechanism(s) controlling the variation in initial ^{187}Re/^{188}Os isotope ratio during organic-rich deposition from suboxic to anoxic/non-sulfidic bottom waters through comparison of major and trace metal abundances with Re and common Os (^{192}Os) abundances and present-day ^{187}Re/^{188}Os isotope ratios. Analysis of the Aralka Formation and Tindelpina Shale Member suggests the initial ^{187}Re/^{188}Os isotope ratio in shales deposited from suboxic to anoxic/non-sulfidic bottom waters can be controlled by temporal variations in the flux of Os-bearing organic complexes to accumulating sediments, or by the slow precipitation kinetics of Re, in addition to seawater Re and Os abundances.

Table 3.1 Major and trace element data for the Aralka, Pertatataka, and Brachina Formations and Tindelpina Shale Member.

Core Depth (m)	Al_2O_3	TiO_2	Fe_2O_3	MgO	CaO	Na_2O	K_2O	V	Cr	Mn	Co	Ni	Cu	Zn	As	Rb	Sr	Zr	Mo	Ba	Pb	U
Aralka Formation, Drillhole Wallara-1																						
BK-04-WALLARA-1A	11.17	1.07	6.62	3.83	2.52	1.29	2.92	192	75	578	23	46	51	93	13	142	99	206	4.8	254	117	4.5
BK-04-WALLARA-1B	11.52	1.05	6.51	3.76	2.46	1.30	3.06	187	72	566	22	45	50	107	12	140	97	206	4.7	498	128	4.3
BK-04-WALLARA-2A	12.07	1.10	6.21	3.73	2.30	1.38	3.12	175	69	544	19	40	45	85	8.8	145	95	214	5.1	429	115	3.8
BK-04-WALLARA-2B	12.02	1.11	6.43	3.74	2.31	1.41	3.14	174	69	541	20	41	47	92	11	145	95	213	5.0	414	117	3.8
BK-04-WALLARA-3	10.49	0.93	6.04	6.12	6.55	1.23	2.60	144	57	1318	17	32	36	129	13	120	99	180	4.8	347	89	3.2
BK-04-WALLARA-4A	8.66	0.83	6.04	7.32	8.98	1.10	2.22	114	50	2136	17	38	33	51	14	102	96	160	4.2	272	80	2.9
BK-04-WALLARA-4B	12.38	1.14	6.55	3.65	2.29	1.45	3.13	156	66	569	21	40	46	66	10	145	89	214	5.0	395	109	3.5
BK-04-WALLARA-5A	8.55	0.81	5.88	7.87	10.33	1.05	2.10	109	46	2595	17	28	31	57	5.5	98	139	149	4.0	244	75	2.7
Tindelpina Shale Member, Drillholes Blinman-2 and SCYW-1a																						
BK-04-BLINMAN-1	11.56	0.85	5.61	5.52	8.92	0.75	3.82	181	75	645	15	43	37	18	44	172	55	163	2.7	240	44	4.1
BK-04-BLINMAN-3	11.67	0.86	5.50	5.21	8.68	0.77	3.96	180	73	631	16	42	43	16	32	173	52	165	2.6	238	41	3.9
BK-04-BLINMAN-4	11.46	0.86	5.30	4.14	6.74	0.89	3.79	167	68	520	17	32	51	14	22	171	46	185	2.4	235	30	4.2
BK-04-BLINMAN-5	12.02	0.90	5.16	3.84	6.21	0.90	4.18	178	71	481	15	27	38	14	21	181	44	178	2.2	255	26	4.4
BK-04-BLINMAN-6	12.24	0.82	5.23	4.13	6.55	0.86	4.13	179	69	536	15	26	38	14	20	187	45	165	2.1	262	25	4.2
BK-04-BLINMAN-7	11.65	0.87	5.05	4.30	6.91	0.87	3.86	189	75	550	15	44	35	17	26	178	48	170	2.9	246	45	3.9
BK-04-BLINMAN-9	11.59	0.84	5.08	4.14	6.55	0.87	3.85	189	77	539	15	43	35	17	38	179	47	174	3.1	247	45	3.9
BK-04-BLINMAN-10	10.85	0.85	5.09	3.78	6.37	0.89	3.83	188	74	528	15	43	35	17	34	175	46	167	2.8	247	43	3.8
BK-04-BLINMAN-11	11.26	0.84	5.14	4.06	6.39	0.89	3.70	188	75	532	15	45	37	17	34	176	47	167	2.9	243	47	3.9
BK-04-SCYW1a-3-4	14.56	1.51	5.99	2.72	0.74	1.22	5.32	195	72	516	31	51	57	81	22	205	92	265	4.1	359	195	4.8
BK-04-SCYW1a-5	15.33	1.51	6.34	2.47	0.44	1.25	5.53	202	79	467	42	63	62	39	32	219	88	269	3.2	366	221	4.8
BK-04-SCYW1a-6-7	15.51	1.38	5.53	2.34	0.22	1.06	5.67	183	70	413	40	58	62	38	22	215	87	257	4.3	391	191	5.7
Pertatataka Formation, Drillhole Wallara-1																						
BK-04-WP-2	3.41	0.99	8.76	2.96	1.44	1.42	3.09	165	81	1042	37	63	76	249	29	123	99	117	3.7	317	141	3.8
Brachina Formation, Drillhole BWM 1a-1																						
BK-04-BWM 1a-1-5	3.21	0.99	5.62	2.81	1.04	0.93	4.22	183	78	505	24	47	26	189	79	176	78	141	3.7	324	51	5.1
Average Shale	16.7	0.78	6.90	2.60	2.20	1.60	3.60	130	90	850	19	68	45	95	10	140	300	160	1.3	580	22	3.7

Oxide and trace metal concentrations in weight percent and ppm, respectively. Average shale data from Wedepohl (1971, 1991).

Table 3.2. Enrichment factors, Fe_T/Al ratios, and DOP data for the Araka, Pertatataka, and Brachina Formations and Tindelpina Shale Member.

Core Depth (m)	Ti	Fe	Mg	Ca	Na	K	V	Cr	Mn	Co	Ni	Cu	Zn	As	Rb	Sr	Zr	Mo	Ba	Re	Pb	U	Fe_T/Al	DOP
Araka Formation, Drillhole Wallara-1																								
BK-04-WALLARA-1A	2.0	1.4	2.2	1.7	1.2	1.2	2.2	1.2	1.0	1.9	1.0	1.7	1.4	1.9	1.5	0.49	1.9	5.4	0.65	8.1	7.9	1.8	0.78	
BK-04-WALLARA-1B	2.0	1.4	2.1	1.6	1.2	1.2	2.0	1.2	0.97	1.7	0.96	1.6	1.6	1.8	1.4	0.47	1.9	5.1	1.2	7.9	8.4	1.7	0.75	0.58
BK-04-WALLARA-2A	2.0	1.2	2.0	1.4	1.2	1.2	1.8	1.1	0.89	1.4	0.82	1.4	1.2	1.3	1.4	0.44	1.9	5.3	1.0	7.2	7.2	1.4	0.68	
BK-04-WALLARA-2B	2.0	1.3	2.0	1.4	1.3	1.2	1.8	1.1	0.89	1.5	0.84	1.4	1.3	1.6	1.4	0.44	1.9	5.3	0.99	7.5	7.3	1.4	0.71	
BK-04-WALLARA-3	1.9	1.4	3.7	4.7	1.3	1.1	1.7	1.0	2.5	1.5	0.75	1.3	2.1	2.0	1.4	0.52	1.8	5.8	0.95	6.5	6.4	1.4	0.76	
BK-04-WALLARA-4A	2.0	1.7	5.3	7.8	1.4	1.2	1.7	1.1	4.9	1.8	1.1	1.4	1.0	2.7	1.4	0.62	1.9	6.1	0.90	8.6	6.9	1.5	0.92	
BK-04-WALLARA-4B	2.0	1.3	1.9	1.4	1.3	1.2	1.6	1.0	0.90	1.5	0.79	1.4	0.91	1.4	1.4	0.40	1.8	5.0	0.91	8.0	6.6	1.3	0.70	
BK-04-WALLARA-5A	2.0	1.7	5.6	9.1	1.3	1.1	1.6	1.0	6.0	1.8	0.80	1.3	1.1	1.1	1.3	0.90	1.8	5.9	0.82	8.6	6.6	1.4	0.91	0.42
Tindelpina Shale Member, Drillholes Blinman-2 and SCYW-1a																								
BK-04-BLINMAN-1	1.6	1.2	3.0	5.8	0.70	1.5	2.0	1.2	1.1	1.2	0.92	1.2	0.27	6.6	1.8	0.26	1.5	2.9	0.60	5.5	2.9	1.6	0.84	
BK-04-BLINMAN-3	1.6	1.1	2.8	5.6	0.71	1.6	1.9	1.2	1.1	1.2	0.88	1.4	0.24	4.6	1.7	0.25	1.5	2.8	0.58	5.1	2.7	1.5	0.82	
BK-04-BLINMAN-4	1.6	1.1	2.3	4.4	0.84	1.5	1.8	1.1	0.89	1.3	0.70	1.7	0.21	3.2	1.8	0.22	1.7	2.6	0.59	3.4	2.0	1.7	0.61	
BK-04-BLINMAN-5	1.6	1.0	2.0	3.9	0.81	1.6	1.9	1.1	0.79	1.1	0.55	1.2	0.21	2.9	1.8	0.20	1.6	2.3	0.61	2.9	1.6	1.7	0.57	
BK-04-BLINMAN-6	1.4	1.0	2.1	4.0	0.76	1.6	1.8	1.0	0.86	1.1	0.52	1.2	0.20	2.8	1.8	0.20	1.4	2.1	0.61	2.3	1.5	1.5	0.56	
BK-04-BLINMAN-7	1.6	1.0	2.3	4.5	0.80	1.5	2.0	1.2	0.93	1.2	0.93	1.1	0.25	3.9	1.8	0.23	1.5	3.2	0.60	6.1	2.9	1.5	0.57	0.59
BK-04-BLINMAN-9	1.6	1.1	2.3	4.2	0.81	1.5	2.1	1.2	0.92	1.2	0.92	1.1	0.26	5.6	1.8	0.22	1.6	3.4	0.61	6.8	2.9	1.5	0.58	
BK-04-BLINMAN-10	1.7	1.1	2.2	4.4	0.88	1.6	2.2	1.3	0.96	1.3	0.98	1.2	0.27	5.3	1.9	0.24	1.6	3.3	0.65	5.9	3.0	1.6	0.62	
BK-04-BLINMAN-11	1.6	1.1	2.3	4.3	0.87	1.5	2.1	1.2	0.93	1.2	0.98	1.2	0.27	5.2	1.8	0.23	1.6	3.2	0.62	6.3	3.1	1.5	0.60	
BK-04-SCYW1a-3-4	2.2	0.99	1.2	0.38	0.91	1.7	1.7	0.92	0.70	1.9	0.87	1.5	0.96	2.6	1.7	0.35	1.9	3.6	0.71	11	10	1.5	0.54	
BK-04-SCYW1a-5	2.1	0.99	1.0	0.22	0.88	1.7	1.7	0.95	0.60	2.5	1.0	1.5	0.44	3.6	1.7	0.32	1.8	2.6	0.68	6.2	11	1.4	0.55	
BK-04-SCYW1a-6-7	1.9	0.86	0.95	0.11	0.74	1.7	1.5	0.84	0.52	2.3	0.91	1.5	0.43	2.4	1.6	0.31	1.7	3.5	0.72	11	9.3	1.7	0.47	0.73
Pertatataka Formation, Drillhole Wallara-1																								
BK-04-WP-2	1.5	1.4	1.3	0.74	1.1	0.98	1.4	1.0	1.4	2.3	1.1	1.9	2.9	3.4	1.0	0.38	0.84	3.2	0.62	1.3	7.3	1.2	0.80	0.48
Brachina Formation, Drillhole BWM1a-1																								
BK-04-BWM1a-1-5	1.8	1.2	1.5	1.2	0.85	1.7	2.0	1.2	0.85	1.9	0.99	0.82	2.5	12	1.8	0.37	1.3	3.9	0.79	7.9	3.3	2.0	0.63	0.38

Enrichment factors calculated using average shale data from Wedepohl (1971, 1991) except for Re (1 ppb; Crusius et al., 1996).

Re enrichment factors calculated using the Re abundance data from Tables 3.3 and 3.4.

Table 3.3. Re-Os isotope data for the Pertatataka and Aralka Formations, Amadeus Basin, central Australia.

Sample	Depth (m)	Re (ppb)	Os (ppt)	^{192}Os (ppt)	^{187}Re/^{188}Os	^{187}Os/^{188}Os	rho	$I_{Os\,(580\,Ma)}$*	$I_{Os\,(635\,Ma)}$*	$I_{Os\,(657\,Ma)}$*
Pertatataka Formation, Drillhole Wallara-1										
BK-04-WP-2	1175.93-1175.95	1.14 ± 0.01	98.0 ± 0.6	33.1 ± 0.2	68.38 ± 0.46	1.8255 ± 0.0139	0.507	1.16	1.10	
BK-04-WP-7	1176.11-1176.12	0.97 ± 0.01	84.9 ± 0.5	28.5 ± 0.1	68.08 ± 0.45	1.9086 ± 0.0130	0.476	1.25	1.18	
BK-04-WP-8	1177.25-1177.27	0.86 ± 0.01	74.8 ± 0.4	25.1 ± 0.1	68.20 ± 0.44	1.8795 ± 0.0117	0.453	1.22	1.15	
BK-04-WP-11	1177.36-1177.40	0.95 ± 0.01	82.1 ± 0.4	27.6 ± 0.1	68.58 ± 0.42	1.8734 ± 0.0097	0.438	1.21	1.14	
Aralka Formation, Drillhole Wallara-1										
BK-04-WALLARA-1A	1298.20-1298.25	5.41 ± 0.02	145.9 ± 0.7	41.0 ± 0.1	262.10 ± 1.23	3.7170 ± 0.0125	0.525			0.83
replicate		5.41 ± 0.02	145.3 ± 0.7	40.9 ± 0.1	263.41 ± 1.20	3.7149 ± 0.0129	0.436			0.82
BK-04-WALLARA-1B	1298.20-1298.25	5.45 ± 0.02	151.3 ± 1.1	43.0 ± 0.2	251.98 ± 1.61	3.5941 ± 0.0281	0.543			0.82
BK-04-WALLARA-2A	1299.00-1299.05	5.18 ± 0.02	125.3 ± 0.7	33.9 ± 0.1	304.28 ± 1.54	4.1659 ± 0.0164	0.596			0.82
BK-04-WALLARA-2B	1299.00-1299.05	5.40 ± 0.02	128.8 ± 0.8	34.6 ± 0.1	309.84 ± 1.56	4.2277 ± 0.0206	0.473			0.82
BK-04-WALLARA-3	1299.50-1299.60	4.08 ± 0.02	95.3 ± 0.6	25.3 ± 0.1	319.98 ± 1.96	4.3602 ± 0.0256	0.661			0.84
BK-04-WALLARA-4A	1300.10-1300.15	4.42 ± 0.02	85.7 ± 0.6	20.9 ± 0.1	421.90 ± 2.38	5.4732 ± 0.0292	0.603			0.83
BK-04-WALLARA-4B	1300.10-1300.15	5.86 ± 0.02	116.5 ± 0.7	28.8 ± 0.1	405.02 ± 1.96	5.2661 ± 0.0223	0.479			0.81
BK-04-WALLARA-5A	1300.20-1300.25	4.38 ± 0.02	81.8 ± 0.6	19.5 ± 0.1	447.17 ± 3.28	5.7469 ± 0.0421	0.746			0.83
replicate		4.36 ± 0.02	81.8 ± 0.6	19.5 ± 0.1	443.99 ± 2.71	5.7200 ± 0.0354	0.625			0.83

All data were obtained by Cr^{VI}-H_2SO_4 whole rock digestion at 240°C. Uncertainties are quoted at the 2_σ level.

*I_{Os} = initial ^{187}Os/^{188}Os ratio calculated using the age in brackets.

Table 3.4. Re-Os isotope data for the Brachina Formation and Tindelpina Shale Member (Tapley Hill Formation), Adelaide Rift Complex, southern Australia.

Sample	Depth (m)	Re (ppb)	Os (ppt)	^{192}Os (ppt)	^{187}Re/^{188}Os	^{187}Os/^{188}Os	rho	$I_{Os\,(580\,Ma)}$*	$I_{Os\,(635\,Ma)}$*	$I_{Os\,(643\,Ma)}$*
Brachina Formation, Drillhole BWM1a-1										
BK-04-BWM1a-1-1	157.37-157.40	2.20 ± 0.01	106.7 ± 0.6	33.2 ± 0.1	131.42 ± 0.70	2.6205 ± 0.0130	0.462	1.34	1.22	
BK-04-BWM1a-1-2	157.43-157.46	2.04 ± 0.01	108.7 ± 0.5	34.7 ± 0.1	116.75 ± 0.62	2.3818 ± 0.0115	0.463	1.25	1.14	
replicate		2.03 ± 0.01	111.5 ± 0.7	35.8 ± 0.2	112.75 ± 0.76	2.3149 ± 0.0196	0.518	1.22	1.12	
BK-04-BWM1a-1-4	158.29-158.31	4.87 ± 0.02	126.6 ± 0.9	33.9 ± 0.2	285.42 ± 1.73	4.2745 ± 0.0302	0.529	1.50	1.24	
replicate		4.80 ± 0.02	126.5 ± 0.8	34.1 ± 0.1	280.00 ± 1.57	4.2076 ± 0.0256	0.505	1.49	1.23	
BK-04-BWM1a-1-5	158.32-158.35	5.56 ± 0.02	129.9 ± 1.1	33.8 ± 0.2	327.62 ± 2.14	4.6462 ± 0.0386	0.527	1.47	1.16	
replicate		5.48 ± 0.02	130.0 ± 1.1	33.9 ± 0.2	322.01 ± 2.10	4.6061 ± 0.0368	0.545	1.48	1.18	
Tindelpina Shale Member, Drillhole Blinman-2										
BK-04-BLINMAN-1	1609.98-1610.01	3.80 ± 0.01	120.0 ± 0.8	35.1 ± 0.2	215.67 ± 1.33	3.2820 ± 0.0237	0.545			0.96
BK-04-BLINMAN-3	1610.05-1610.06	3.47 ± 0.01	115.5 ± 0.6	34.3 ± 0.1	201.12 ± 1.03	3.1175 ± 0.0145	0.524			0.95
BK-04-BLINMAN-4	1610.07-1610.08	2.32 ± 0.01	105.1 ± 0.6	33.3 ± 0.2	138.56 ± 0.86	2.4548 ± 0.0167	0.585			0.96
BK-04-BLINMAN-5	1610.10-1610.12	2.05 ± 0.01	113.6 ± 0.6	37.2 ± 0.1	109.51 ± 0.60	2.1324 ± 0.0120	0.460			0.95
replicate		2.05 ± 0.01	112.2 ± 0.9	36.8 ± 0.3	110.80 ± 0.99	2.1238 ± 0.0273	0.559			0.93
BK-04-BLINMAN-6	1610.13-1610.14	1.69 ± 0.01	99.6 ± 0.5	32.9 ± 0.1	102.31 ± 0.55	2.0560 ± 0.0101	0.466			0.95
BK-04-BLINMAN-7	1610.76-1610.77	4.25 ± 0.02	125.6 ± 0.8	36.1 ± 0.2	234.04 ± 1.34	3.4728 ± 0.0219	0.527			0.95
replicate		4.21 ± 0.02	128.5 ± 1.0	37.3 ± 0.2	224.76 ± 1.61	3.3713 ± 0.0317	0.553			0.95
BK-04-BLINMAN-9	1610.80-1610.82	4.66 ± 0.02	144.6 ± 0.8	42.1 ± 0.2	220.16 ± 1.16	3.3389 ± 0.0180	0.486			0.97
BK-04-BLINMAN-10	1610.84-1610.87	3.83 ± 0.02	120.1 ± 0.8	35.1 ± 0.2	217.17 ± 1.34	3.3061 ± 0.0223	0.556			0.97
BK-04-BLINMAN-11	1610.88-1610.90	4.25 ± 0.02	127.7 ± 0.8	36.9 ± 0.2	228.77 ± 1.27	3.4120 ± 0.0204	0.504			0.95
BK-04-SCYW1a-3-4	1369.33-1369.42	9.12 ± 0.03	124.4 ± 1.2	23.3 ± 0.1	778.66 ± 5.39	9.3713 ± 0.0775	0.594			0.99
replicate		9.03 ± 0.03	135.1 ± 1.0	27.6 ± 0.1	649.82 ± 3.81	7.9300 ± 0.0480	0.577			0.93
BK-04-SCYW1a-5	1370.00-1370.05	5.63 ± 0.02	92.5 ± 0.9	20.3 ± 0.1	551.24 ± 4.19	6.8705 ± 0.0642	0.613			0.93
BK-04-SCYW1a-6-7	1370.06-1370.14	9.95 ± 0.04	119.9 ± 1.0	19.6 ± 0.1	1010.00 ± 6.20	11.8317 ± 0.0771	0.597			0.95

All data were obtained by Cr^{VI}-H_2SO_4 whole rock digestion at 240°C. Uncertainties are quoted at the 2σ level.

*I_{Os} = initial ^{187}Os/^{188}Os ratio calculated using the age in brackets.

Table 3.5. Re-Os isotope data for the Julius River Member, upper Black River Dolomite, northwestern Tasmania.

Sample	Depth (m)	Re (ppb)	Os (ppt)	^{192}Os (ppt)	^{187}Re/^{188}Os	^{187}Os/^{188}Os	rho	I_{Os}*
Drillhole Forest-1, 835.58-835.87 m								
RC06-FOR-01-A-HighT	835.84-835.87	33.01 ± 0.11	440.7 ± 3.4	80.8 ± 0.3	812.73 ± 4.12	9.7250 ± 0.0538	0.518	0.97
RC06-FOR-01-B-HighT	835.77-835.79	39.20 ± 0.13	524.9 ± 4.0	96.3 ± 0.4	809.73 ± 4.04	9.7128 ± 0.0534	0.500	0.99
RC06-FOR-01-B2-HighT	835.79-835.84	31.30 ± 0.10	448.0 ± 2.6	87.7 ± 0.2	710.13 ± 2.91	8.6322 ± 0.0303	0.389	0.98
RC06-FOR-01-B2-LowT		31.32 ± 0.10	445.2 ± 2.7	87.0 ± 0.2	716.20 ± 3.04	8.6538 ± 0.0331	0.419	0.94
RC06-FOR-01-C-HighT	835.70-835.72	31.78 ± 0.11	424.7 ± 3.7	78.0 ± 0.3	810.34 ± 4.43	9.6873 ± 0.0675	0.491	0.96
RC06-FOR-01-C-LowT		32.32 ± 0.11	430.2 ± 3.0	78.7 ± 0.2	816.65 ± 3.64	9.7570 ± 0.0440	0.431	0.96
RC06-FOR-01-C2-HighT	835.72-835.74	31.96 ± 0.11	453.4 ± 3.9	88.0 ± 0.3	722.85 ± 3.71	8.7741 ± 0.0618	0.421	0.99
RC06-FOR-01-C3-HighT	835.74-835.77	33.90 ± 0.11	447.2 ± 3.2	81.0 ± 0.2	832.18 ± 3.63	9.9297 ± 0.0467	0.382	0.97
RC06-FOR-01-C3-LowT		33.87 ± 0.11	447.7 ± 2.5	81.0 ± 0.2	831.51 ± 3.28	9.9481 ± 0.0297	0.373	0.99
RC06-FOR-01-D-HighT	835.65-835.68	27.47 ± 0.09	402.0 ± 2.8	80.5 ± 0.2	678.89 ± 3.02	8.2679 ± 0.0400	0.398	0.96
RC06-FOR-01-D-LowT		28.18 ± 0.09	401.3 ± 2.4	78.2 ± 0.2	716.86 ± 3.00	8.7005 ± 0.0315	0.416	0.98
RC06-FOR-01-D2-HighT	835.68-835.70	21.52 ± 0.07	347.8 ± 2.2	75.2 ± 0.2	569.25 ± 2.54	7.0957 ± 0.0319	0.437	0.96
replicate		21.41 ± 0.07	345.3 ± 2.0	74.6 ± 0.2	571.22 ± 2.35	7.1144 ± 0.0262	0.382	0.96
RC06-FOR-01-D2-LowT		21.15 ± 0.07	342.9 ± 1.9	74.2 ± 0.2	566.91 ± 2.37	7.0857 ± 0.0256	0.412	0.98
replicate		21.48 ± 0.07	348.1 ± 2.1	75.2 ± 0.2	568.29 ± 2.50	7.1123 ± 0.0298	0.439	0.99
RC06-FOR-01-E-HighT	835.58-835.62	28.38 ± 0.09	400.9 ± 3.3	77.7 ± 0.3	726.43 ± 3.68	8.7836 ± 0.0573	0.438	0.96
RC06-FOR-01-E-LowT		28.35 ± 0.09	403.6 ± 3.1	78.4 ± 0.3	719.03 ± 3.59	8.7446 ± 0.0514	0.468	1.00
RC06-FOR-01-E2-HighT	835.62-835.65	19.45 ± 0.07	327.9 ± 2.5	72.7 ± 0.3	532.66 ± 2.68	6.7435 ± 0.0431	0.440	1.01
RC06-FOR-01-E2-LowT		19.62 ± 0.07	329.7 ± 1.9	73.0 ± 0.2	534.79 ± 2.24	6.7580 ± 0.0260	0.397	1.00
Drillhole Forest-1, 828.11-828.58 m								
RC06-FOR-02-B-LowT	828.11-828.15	93.80 ± 0.31	1675.4 ± 8.4	389.6 ± 0.8	478.97 ± 1.87	6.0720 ± 0.0186	0.342	0.91
RC06-FOR-02-D-LowT	828.23-828.27	95.16 ± 0.32	1687.8 ± 8.6	392.6 ± 0.8	482.22 ± 1.90	6.0678 ± 0.0192	0.349	0.87
RC06-FOR-02-G-LowT	828.37-828.40	100.40 ± 0.34	1751.1 ± 8.0	404.7 ± 0.7	493.57 ± 1.86	6.1558 ± 0.0158	0.316	0.84
RC06-FOR-02-H-LowT	828.48-828.50	98.37 ± 0.33	1701.9 ± 7.9	392.0 ± 0.7	499.24 ± 1.89	6.2021 ± 0.0163	0.314	0.83
RC06-FOR-02-I-LowT	828.55-828.58	101.52 ± 0.34	1800.0 ± 9.1	417.7 ± 0.8	483.46 ± 1.88	6.0988 ± 0.0186	0.332	0.89

Data were obtained by Cr^{VI}-H_2SO_4 whole rock digestion at 240°C (HighT) or 80°C (LowT). Uncertainties are quoted at the 2σ level.

*I_{Os} = initial ^{187}Os/^{188}Os ratio calculated at 643 Ma.

Table 3.6. Re-Os isotope data for the Yarra Creek Shale, City of Melbourne Bay coastal outcrop, southeastern King Island.

Sample	Re (ppb)	Os (ppt)	^{192}Os (ppt)	^{187}Re/^{188}Os	^{187}Os/^{188}Os	rho	$I_{Os\ (580\ Ma)}$*	$I_{Os\ (635\ Ma)}$*
RC06-KI-01-A	15.83 ± 0.05	296.6 ± 1.7	68.2 ± 0.2	461.76 ± 1.95	6.2263 ± 0.0235	0.412	1.74	1.32
RC06-KI-01-A2	15.36 ± 0.05	299.5 ± 1.7	69.7 ± 0.2	438.71 ± 1.82	6.0684 ± 0.0228	0.383	1.81	1.40
RC06-KI-01-B	15.72 ± 0.05	313.3 ± 2.0	71.6 ± 0.2	436.73 ± 1.96	6.3049 ± 0.0300	0.420	2.06	1.66
RC06-KI-01-C	14.04 ± 0.05	308.8 ± 2.1	77.0 ± 0.3	362.86 ± 1.75	5.1568 ± 0.0286	0.452	1.63	1.30
RC06-KI-01-D	14.91 ± 0.05	301.8 ± 1.5	72.2 ± 0.1	410.74 ± 1.60	5.6896 ± 0.0171	0.343	1.70	1.32
RC06-KI-01-E	13.75 ± 0.05	294.1 ± 1.9	71.8 ± 0.2	381.14 ± 1.71	5.4265 ± 0.0281	0.386	1.73	1.37
RC06-KI-01-E2	12.85 ± 0.04	295.9 ± 1.8	74.4 ± 0.2	343.70 ± 1.49	5.0547 ± 0.0241	0.366	1.72	1.40
RC06-KI-01-F	11.89 ± 0.04	305.9 ± 1.7	80.1 ± 0.2	295.51 ± 1.24	4.5545 ± 0.0189	0.367	1.69	1.41
RC06-KI-01-G	12.56 ± 0.04	299.7 ± 1.6	77.5 ± 0.2	322.30 ± 1.35	4.6961 ± 0.0188	0.372	1.57	1.27
RC06-KI-01-G2	12.74 ± 0.04	296.2 ± 2.1	75.7 ± 0.3	334.78 ± 1.63	4.8466 ± 0.0315	0.391	1.60	1.29
RC06-KI-01-H	12.79 ± 0.04	329.5 ± 1.5	89.4 ± 0.2	284.43 ± 1.11	4.1196 ± 0.0125	0.335	1.36	1.09

All data were obtained by Cr^{VI}-H_2SO_4 whole rock digestion at 80°C. Uncertainties are quoted at the 2_σ level.

*I_{Os} = initial ^{187}Os/^{188}Os ratio calculated using the age in brackets.

Table 3.7. Comparison of Re-Os isotope data derived from inverse *aqua regia* and Cr^{VI}-H_2SO_4 digestions.

Sample	Method*	Aliquant Mass (g)	Re (ppb)	Os (ppt)	^{192}Os (ppt)	^{187}Re/^{188}Os	^{187}Os/^{188}Os	rho	I_{Os}†
Aralka Formation									
BK-04-WALLARA-1A	Cr^{VI}-H_2SO_4	1.06	5.41 ± 0.02	145.9 ± 0.7	41.0 ± 0.1	262.10 ± 1.23	3.7170 ± 0.0125	0.525	0.83
	Cr^{VI}-H_2SO_4-rpt	1.48	5.41 ± 0.02	145.3 ± 0.7	40.9 ± 0.1	263.41 ± 1.20	3.7149 ± 0.0129	0.436	0.82
	IAR	1.45	6.01 ± 0.02	145.0 ± 0.7	40.8 ± 0.1	293.02 ± 1.30	3.7190 ± 0.0127	0.331	0.49
	IAR-rpt	1.46	5.36 ± 0.02	148.1 ± 0.8	41.8 ± 0.2	255.03 ± 1.38	3.6755 ± 0.0166	0.642	0.87
	IAR-rpt	0.54	5.33 ± 0.02	146.7 ± 1.7	41.4 ± 0.6	256.18 ± 3.68	3.6721 ± 0.0660	0.747	0.85
BK-04-WALLARA-2A	Cr^{VI}-H_2SO_4	1.02	5.18 ± 0.02	125.3 ± 0.7	33.9 ± 0.1	304.28 ± 1.54	4.1659 ± 0.0164	0.596	0.82
	IAR	1.46	5.12 ± 0.02	176.1 ± 0.8	54.7 ± 0.2	186.27 ± 0.91	2.6518 ± 0.0097	0.561	0.60
	IAR-rpt	0.50	4.88 ± 0.02	122.5 ± 1.3	33.4 ± 0.5	291.15 ± 4.14	4.0802 ± 0.0611	0.885	0.88
BK-04-WALLARA-5A	Cr^{VI}-H_2SO_4	0.99	4.38 ± 0.02	81.8 ± 0.6	19.5 ± 0.1	447.17 ± 3.28	5.7469 ± 0.0421	0.746	0.83
	Cr^{VI}-H_2SO_4-rpt	1.49	4.36 ± 0.02	81.8 ± 0.6	19.5 ± 0.1	443.99 ± 2.71	5.7200 ± 0.0354	0.625	0.83
	IAR	1.48	4.67 ± 0.02	87.5 ± 0.6	22.0 ± 0.1	421.86 ± 2.14	5.0383 ± 0.0254	0.421	0.40
	IAR-rpt	1.44	4.34 ± 0.02	85.5 ± 0.7	19.7 ± 0.2	437.89 ± 3.77	6.2048 ± 0.0517	0.843	1.39
	IAR-rpt	0.52	4.44 ± 0.02	84.3 ± 1.2	20.2 ± 0.4	436.58 ± 9.32	5.7034 ± 0.1241	0.946	0.88
	IAR-rpt	0.51	4.18 ± 0.02	79.8 ± 0.9	19.2 ± 0.2	434.01 ± 4.48	5.6272 ± 0.0742	0.677	0.85
	Cr^{VI}-H_2SO_4-res	0.87	11.6 ± 2.3 ppt	2.3 ± 0.1	0.8 ± 0.1	27.26 ± 6.45	1.1466 ± 0.1803	0.432	0.85
Tindelpina Shale Member									
BK-04-BLINMAN-5	Cr^{VI}-H_2SO_4	1.44	2.05 ± 0.01	113.6 ± 0.6	37.2 ± 0.1	109.51 ± 0.60	2.1324 ± 0.0120	0.460	0.95
	Cr^{VI}-H_2SO_4-rpt	1.38	2.05 ± 0.01	112.2 ± 0.9	36.8 ± 0.3	110.80 ± 0.99	2.1238 ± 0.0273	0.559	0.93
	IAR	0.57	1.93 ± 0.01	103.6 ± 1.1	33.6 ± 0.5	114.16 ± 1.68	2.2067 ± 0.0438	0.683	0.98
	Cr^{VI}-H_2SO_4-res	1.00	1.3 ± 2.0 ppt	11.9 ± 0.5	4.9 ± 0.4	0.52 ± 0.82	0.2234 ± 0.0275	0.038	0.22

Inverse *aqua regia* blanks ranged between 1.6 and 5.4 pg for Re, between 0.5 and 2.3 pg for Os, with blank ^{187}Os/^{188}Os between 0.17 and 0.21.

All whole rock digestions were carried out at 240°C. All uncertainties are quoted at the 2σ level.

*rpt, IAR, and res denote replicate, inverse *aqua regia* , and residue analysis by IAR, respectively.

†I_{Os} = initial ^{187}Os/^{188}Os isotope ratio calculated at 657 Ma (Aralka Formation) and 643 Ma (Tindelpina Shale Member).

Table 3.8. Coefficients of determination for Re and ^{192}Os abundance, and ^{187}Re/^{188}Os isotope ratio plotted against elemental abundances.

	Re		^{192}Os		^{187}Re/^{188}Os	
	Aralka	Tindelpina*	Aralka	Tindelpina*	Aralka	Tindelpina*
Al	0.65	0.37 (I)	0.51	0.01 (I)	0.37 (I)	0.46 (I)
Ti	0.77	0.00	0.57	0.03	0.37 (I)	0.01 (I)
Fe	0.82	0.03 (I)	0.70	0.21 (I)	0.38 (I)	0.00
Mg	0.77 (I)	0.04	0.73 (I)	0.05 (I)	0.51	0.09
Ca	0.74 (I)	0.03	0.73 (I)	0.07 (I)	0.53	0.09
Na	0.66	0.02 (I)	0.39	0.05	0.26 (I)	0.05 (I)
K	0.70	0.51 (I)	0.63	0.03 (I)	0.46 (I)	0.58 (I)
V	0.55	0.59	0.93	0.34	0.81 (I)	0.50
Cr	0.65	0.92	0.89	0.45	0.71 (I)	0.83
Mn	0.64 (I)	0.12	0.71 (I)	0.04 (I)	0.58	0.20
Co	0.79	0.00	0.81	0.05 (I)	0.45 (I)	0.00
Ni	0.60	0.92	0.76	0.13	0.49 (I)	0.99
Cu	0.76	0.24 (I)	0.89	0.25 (I)	0.61 (I)	0.18 (I)
Zn	0.00	0.83	0.26	0.17	0.60 (I)	0.87
As	0.00	0.60	0.11	0.16	0.19 (I)	0.60
Rb	0.71	0.13 (I)	0.67	0.02	0.49 (I)	0.23 (I)
Sr	0.25 (I)	0.17	0.22 (I)	0.02 (I)	0.22	0.26
Zr	0.72	0.12 (I)	0.64	0.02	0.47 (I)	0.19 (I)
Mo	0.34	0.98	0.36	0.39	0.40 (I)	0.90
Ba	0.28	0.17 (I)	0.32	0.01	0.27 (I)	0.25 (I)
Pb	0.69	0.96	0.91	0.19	0.67 (I)	0.99
U	0.52	0.68 (I)	0.98	0.06 (I)	0.80 (I)	0.74 (I)

(I) denotes inverse correlation. To avoid spurious correlations, sample elemental abundances were not normalized to Al abundances.

*Based only on data from drillhole Blinman-2.

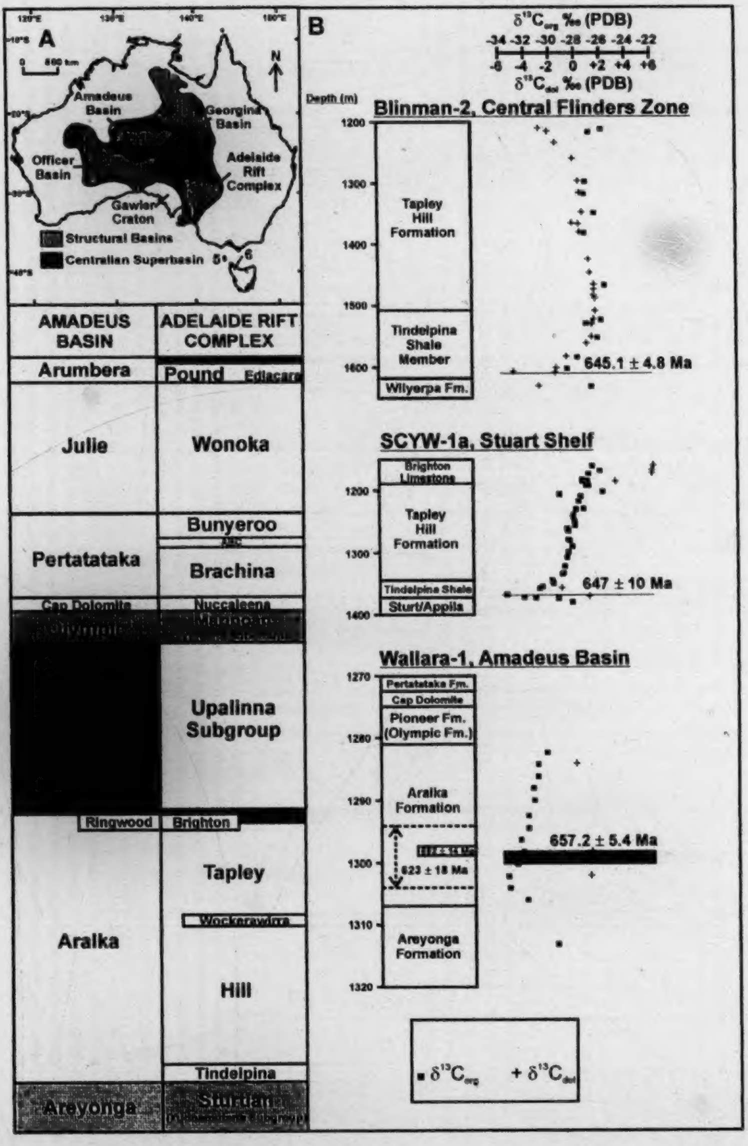

Figure 3.1: (A) Location of sample sites and stratigraphic columns showing proposed correlations of Neoproterozoic strata between the Adelaide Rift Complex and Amadeus Basin (from Walter et al., 2000). Sample sites denoted by numbers: 1: Wallara-1, 2: SCYW-1a, 3: Blinman-2, 4: BWM1a-1, 5: City of Melbourne Bay coastal outcrop, 6: Forest-1. (B) Stratigraphic columns and $\delta^{13}C$ data for drill holes intersecting Sturtian and Areyonga glacial deposits (from Walter et al., 2000; McKirdy et al., 2001). Re-Os ages and sampling intervals (shaded regions) in the chemostratigraphic profiles are from this study; Re-Os ages shown in the Wallara-1 stratigraphic column (representing sampled intervals of 1294-1304 m and 1297.3-1298.9 m) are from Schaefer and Burgess (2003).

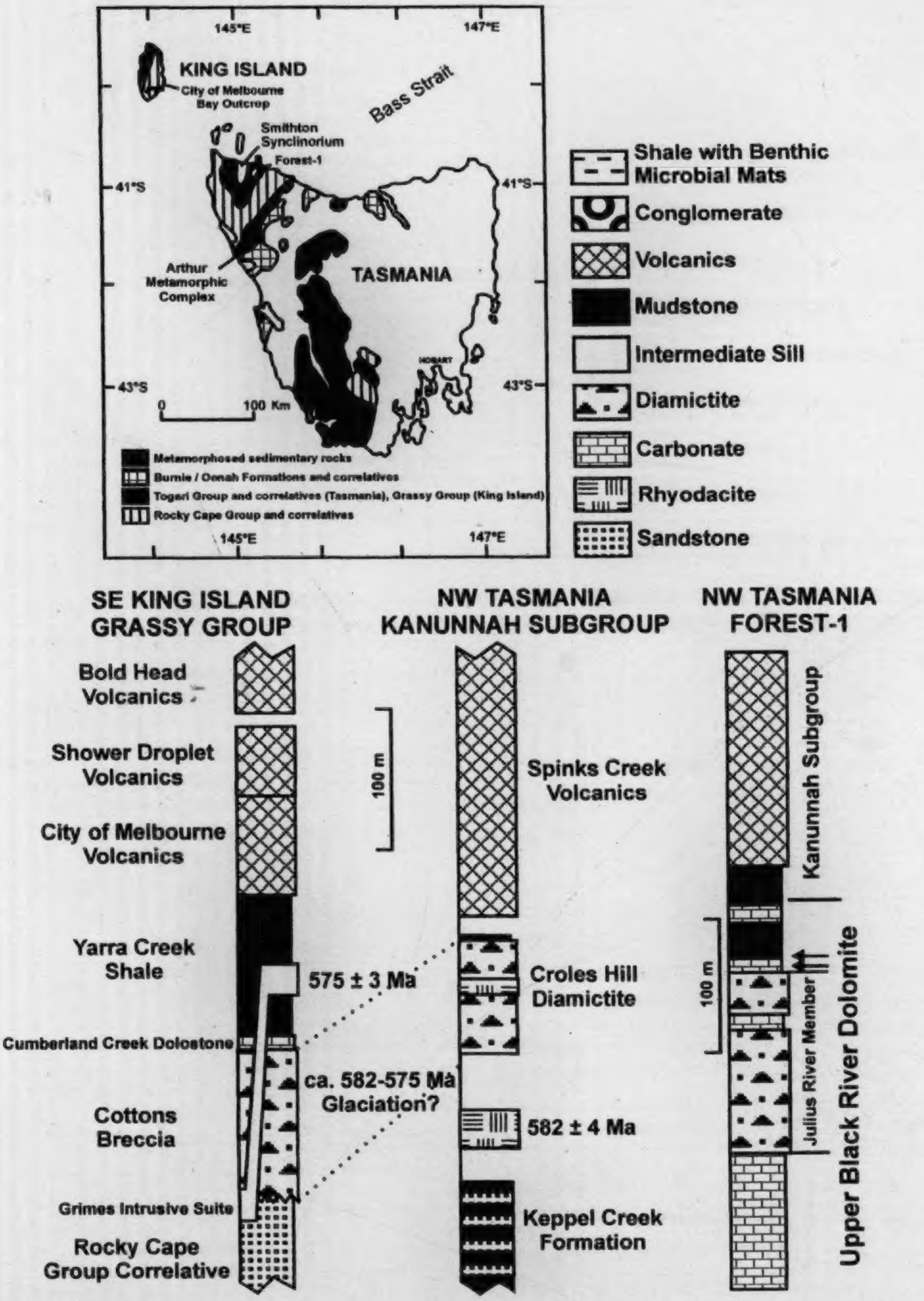
145°E
147°E
KING ISLAND
City of Melbourne Bay Outcrop
Bass Strait
Smithton Synclinorium
Forest-1
41°S
Arthur Metamorphic Complex
TASMANIA
HOBART
43°S
0
100 Km
Metamorphosed sedimentary rocks
Burnie / Oonah Formations and correlatives
Togari Group and correlatives (Tasmania), Grassy Group (King Island)
Rocky Cape Group and correlatives
Shale with Benthic Microbial Mats
Conglomerate
Volcanics
Mudstone
Intermediate Sill
Diamictite
Carbonate
Rhyodacite
Sandstone
SE KING ISLAND GRASSY GROUP
Bold Head Volcanics
Shower Droplet Volcanics
City of Melbourne Volcanics
Yarra Creek Shale
Cumberland Creek Dolostone
Cottons Breccia
Grimes Intrusive Suite
Rocky Cape Group Correlative
575 ± 3 Ma
ca. 582-575 Ma Glaciation?
100 m
NW TASMANIA KANUNNAH SUBGROUP
Spinks Creek Volcanics
Croles Hill Diamictite
582 ± 4 Ma
Keppel Creek Formation
NW TASMANIA FOREST-1
Kanunnah Subgroup
100 m
Julius River Member
Upper Black River Dolomite

Figure 3.2: Neoproterozoic rocks of Tasmania and King Island (top; modified from Calver and Walter, 2000) and stratigraphic columns for the Grassy (left) and Togari (middle, right) Groups (modified from Calver, 1998 and Calver et al., 2004). Note suggested correlation between Cottons Breccia and Croles Hill Diamictite. Arrows denote sampled stratigraphic intervals in Forest-1.

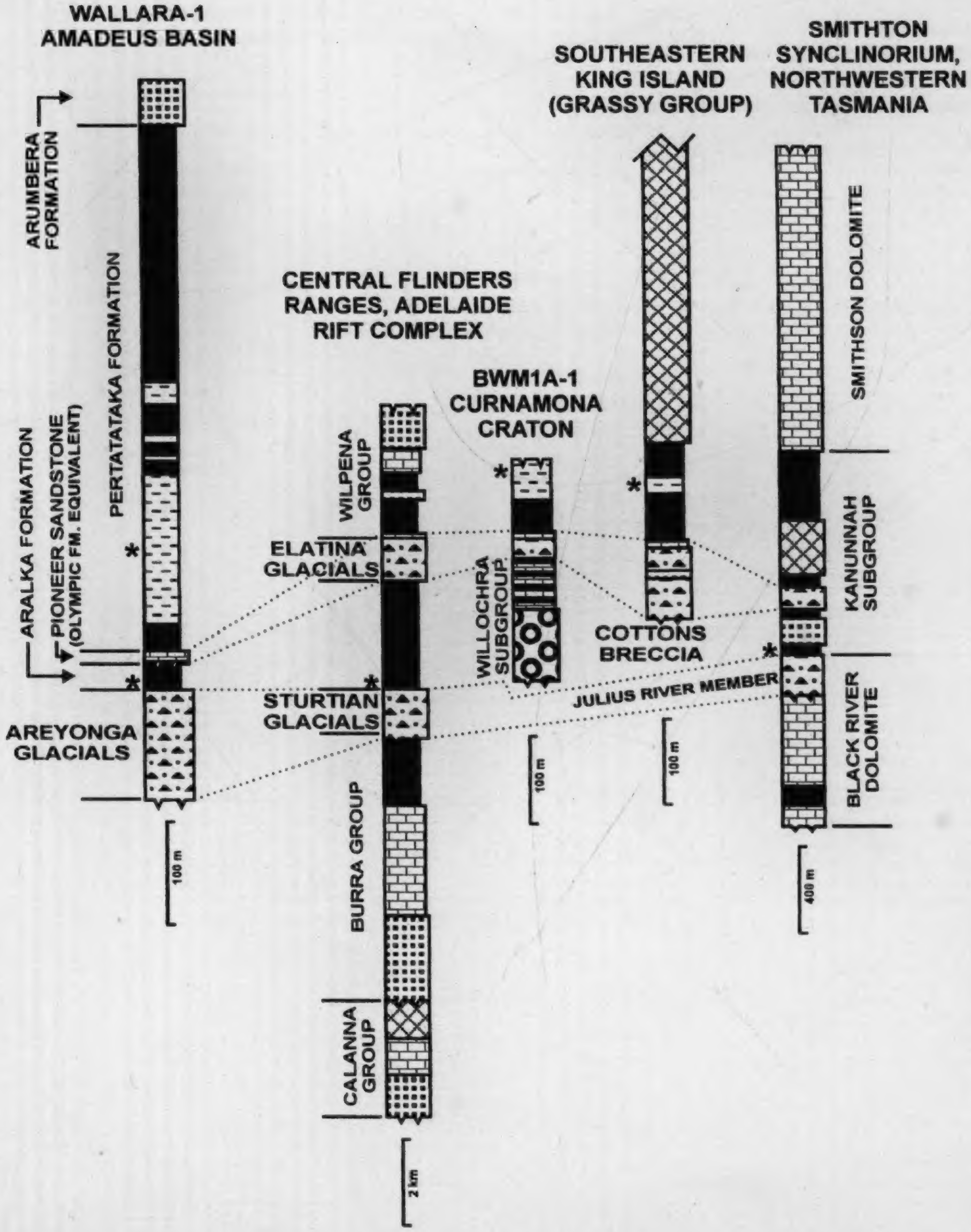
WALLARA-1
AMADEUS BASIN
ARUMBERA FORMATION
PERTATATAKA FORMATION
ARALKA FORMATION
PIONEER SANDSTONE (OLYMPIC FM. EQUIVALENT)
AREYONGA GLACIALS
100 m
CENTRAL FLINDERS RANGES, ADELAIDE RIFT COMPLEX
WILPENA GROUP
ELATINA GLACIALS
STURTIAN GLACIALS
BURRA GROUP
CALANNA GROUP
2 km
BWM1A-1
CURNAMONA CRATON
WILLOCHRA SUBGROUP
100 m
SOUTHEASTERN KING ISLAND (GRASSY GROUP)
COTTONS BRECCIA
100 m
JULIUS RIVER MEMBER
SMITHTON SYNCLINORIUM, NORTHWESTERN TASMANIA
SMITHSON DOLOMITE
KANUNNAH SUBGROUP
BLACK RIVER DOLOMITE
400 m

Figure 3.3: Possible correlation scheme for diamictite intervals from central and southern Australia, southeastern King Island, and northwestern Tasmania (from Calver and Walter, 2000). Stratigraphic columns modified after Logan et al. (1999) and Calver and Walter (2000). Asterisks denote stratigraphic horizons sampled for Re-Os isotope analysis. See Figure 3.2 for legend.

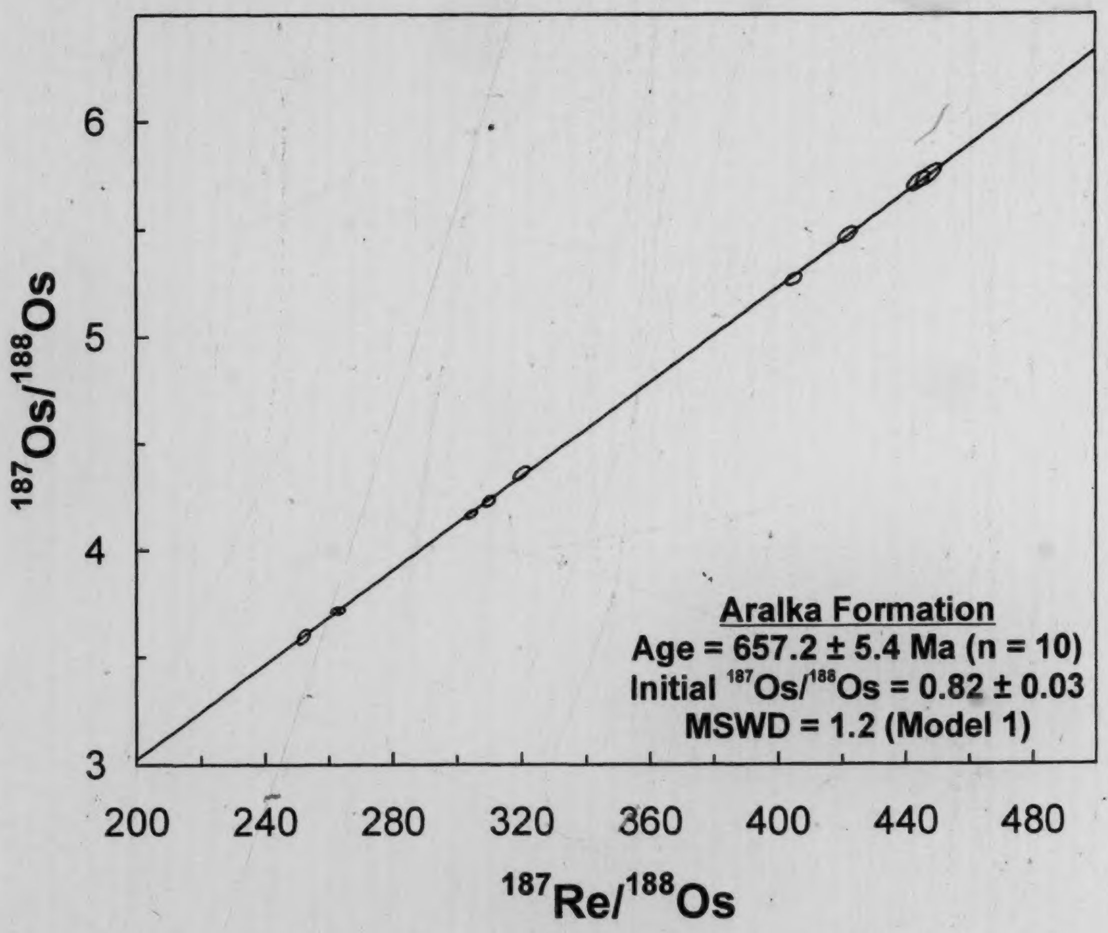

Figure 3.4: Re-Os isochron diagram for the Aralka Formation, Amadeus Basin, central Australia.

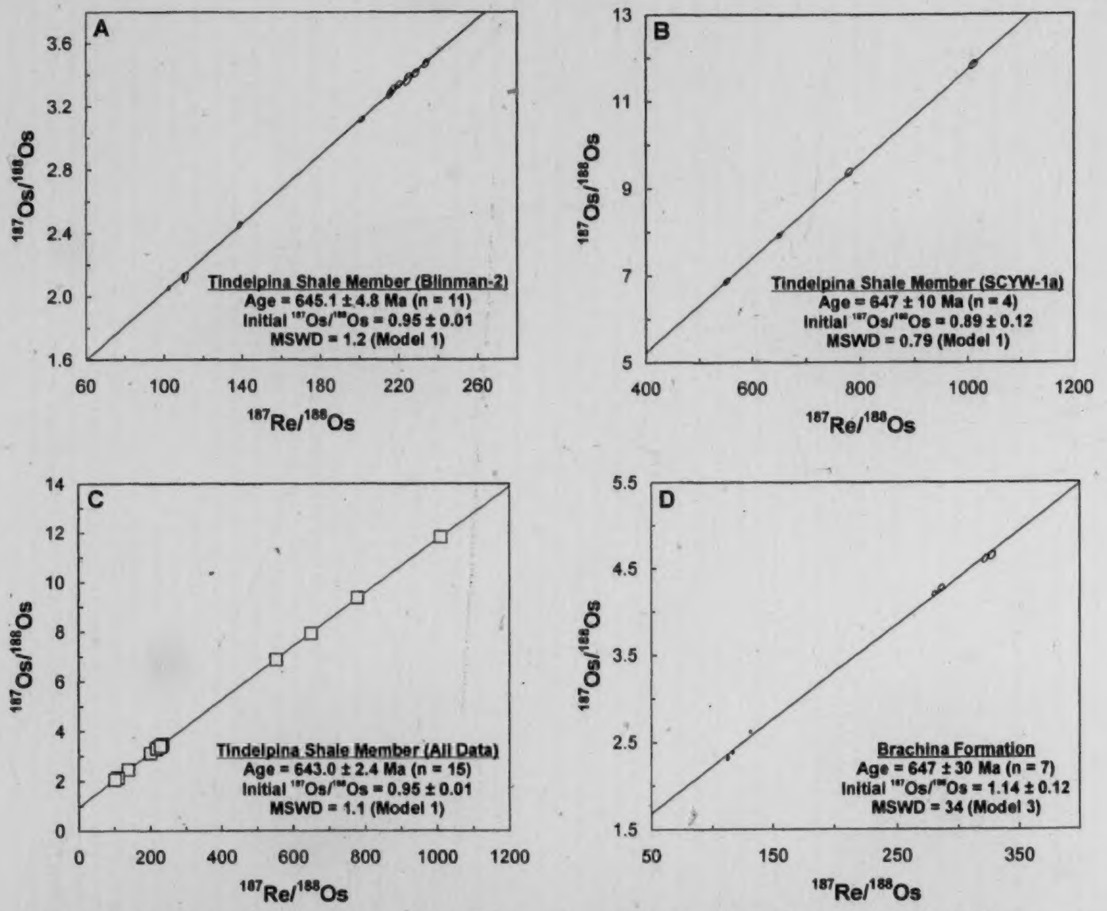

Figure 3.5: Re-Os isochron diagrams for Neoproterozoic ORS from the Adelaide Rift Complex, southern Australia. (A) Tindelpina Shale Member, Blinman-2 drill core. (B) Tindelpina Shale Member, SCYW-1a drill core. (C) Tindelpina Shale Member, all data. Squares were used instead of error ellipses for clarity. (D) Brachina Formation.

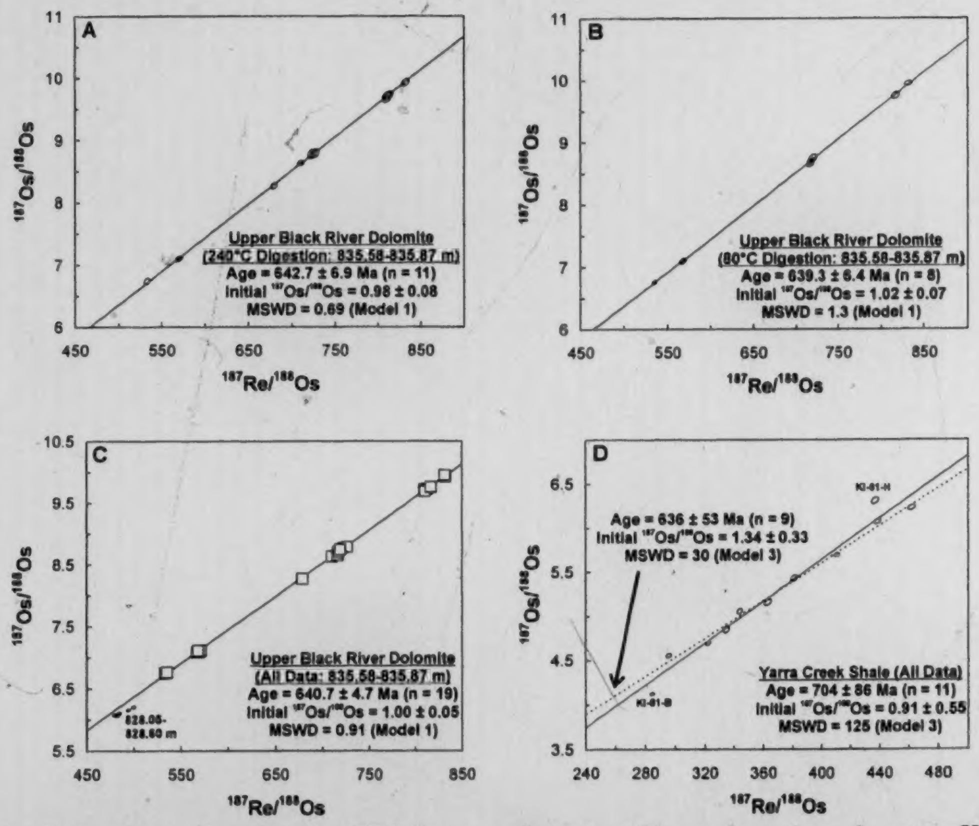

Figure 3.6: Re-Os isochron diagrams for ORS from northwestern Tasmania and southeastern King Island. (A) Upper Black River Dolomite (high-temperature digestion). (B) Upper Black River Dolomite (low temperature digestion). (C) Upper Black River Dolomite (all data). Squares were used instead of error ellipses for clarity. For comparison, samples from 828.05-828.60 m are shown. (D) Yarra Creek Shale (low temperature digestion). Samples KI-01-B and KI-01-H account for a significant proportion of the scatter and exclusion of these samples yields a better-correlated regression with significantly lower MSWD (dashed regression line).

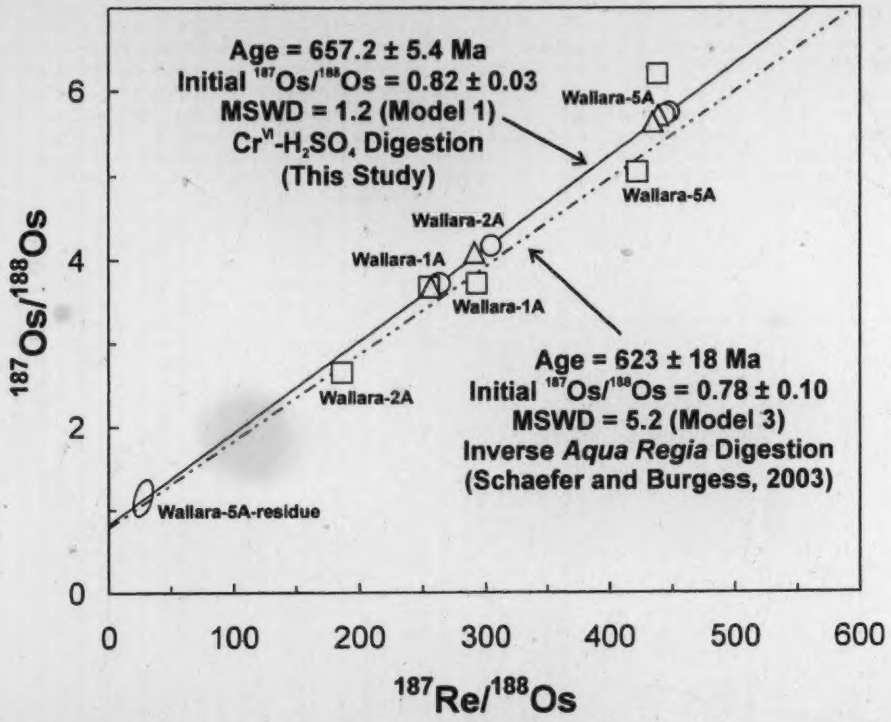

Figure 3.7: Re-Os isochron diagram for the Aralka Formation showing the inverse *aqua regia* and Cr^{VI}-H_2SO_4 regressions from Schaefer and Burgess (2003) and this study, respectively. For clarity, only data for samples BK-04-Wallara-1A, 2A, and 5A are shown. Circles - Cr^{VI}-H_2SO_4 analyses, triangles – inverse *aqua regia* analyses using an aliquant size of ~ 0.5 g, squares – inverse *aqua regia* analyses using an aliquant size of ~ 1.4-1.5 g. Regression of the ~ 0.5 g inverse *aqua regia* subset yields a Model 1 Re-Os date (not shown) of 657 ± 15 Ma (MSWD = 0.7; I_{Os} = 0.87 ± 0.09) that is equivalent within 2σ uncertainties to the Cr^{VI}-H_2SO_4 isochron age. The inverse *aqua regia* analysis of the residue from Cr^{VI}-H_2SO_4 digestion of sample BK-04-Wallara-5A provides an estimate of the detrital Re-Os isotope systematics in the Aralka Formation.

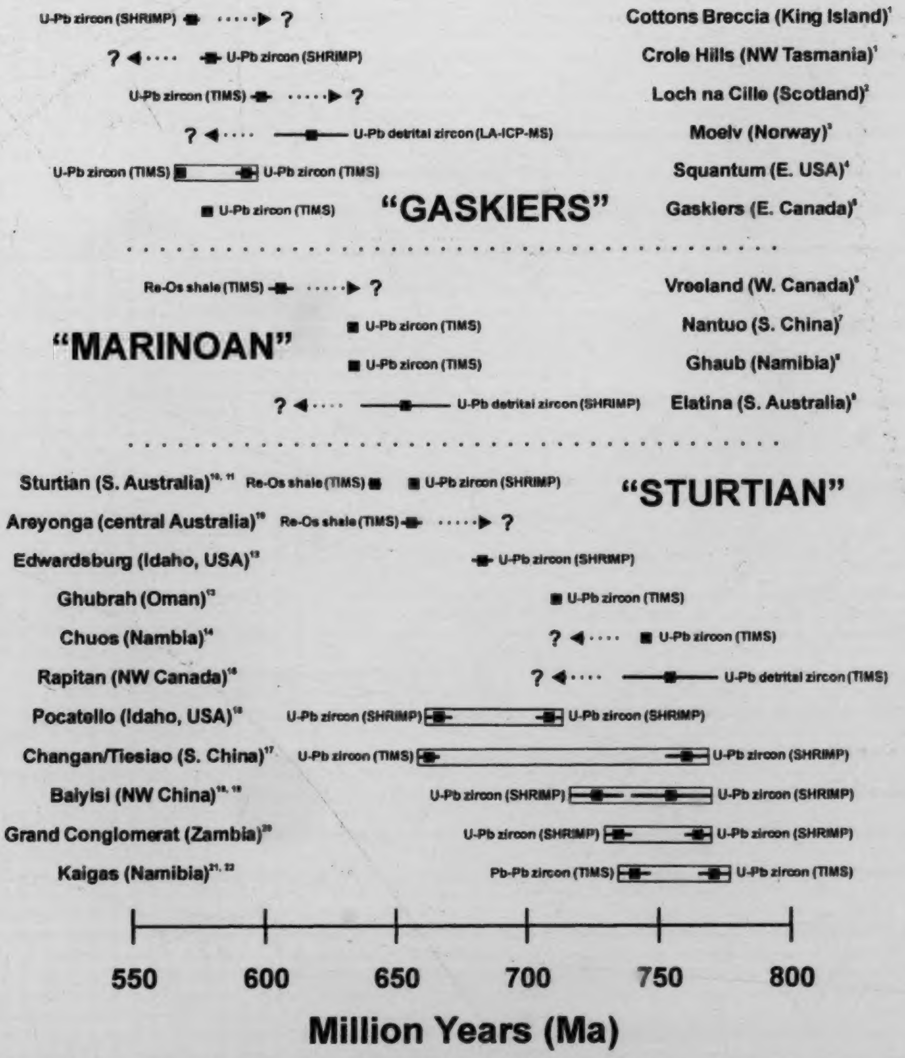

Figure 3.8: Summary of radiometric age constraints on the timing of Neoproterozoic glaciation. Rb-Sr ages are excluded because detrital and authigenic considerations hamper the determination of reliable depositional ages. Note the large spread in ages for putative "Sturtian" glacial deposits. Boxes enclose minimum and maximum age constraints. Sources of data: 1 – Calver et al. (2004), 2 – Dempster et al. (2002), 3 – Bingen et al. (2005), 4 – Thompson and Bowring (2000), 5 – Bowring et al. (2003), 6 – Kendall et al. (2004), 7 – Condon et al. (2005), 8 – Hoffmann et al. (2004), 9 – Ireland et al. (1998), 10 – This study, 11 – Fanning and Link (2006), 12 – Lund et al. (2003), 13 – Allen et al. (2002), 14 – Hoffman et al. (1996), 15 – Ross and Villeneuve (1997), 16 – Fanning and Link (2004), 17 – Zhou et al. (2004), 18 – Huang et al. (2005), 19 – Xu et al. (2005), 20 – Key et al. (2001), 21 – Frimmel et al. (1996), 22 – Frimmel et al. (2001).

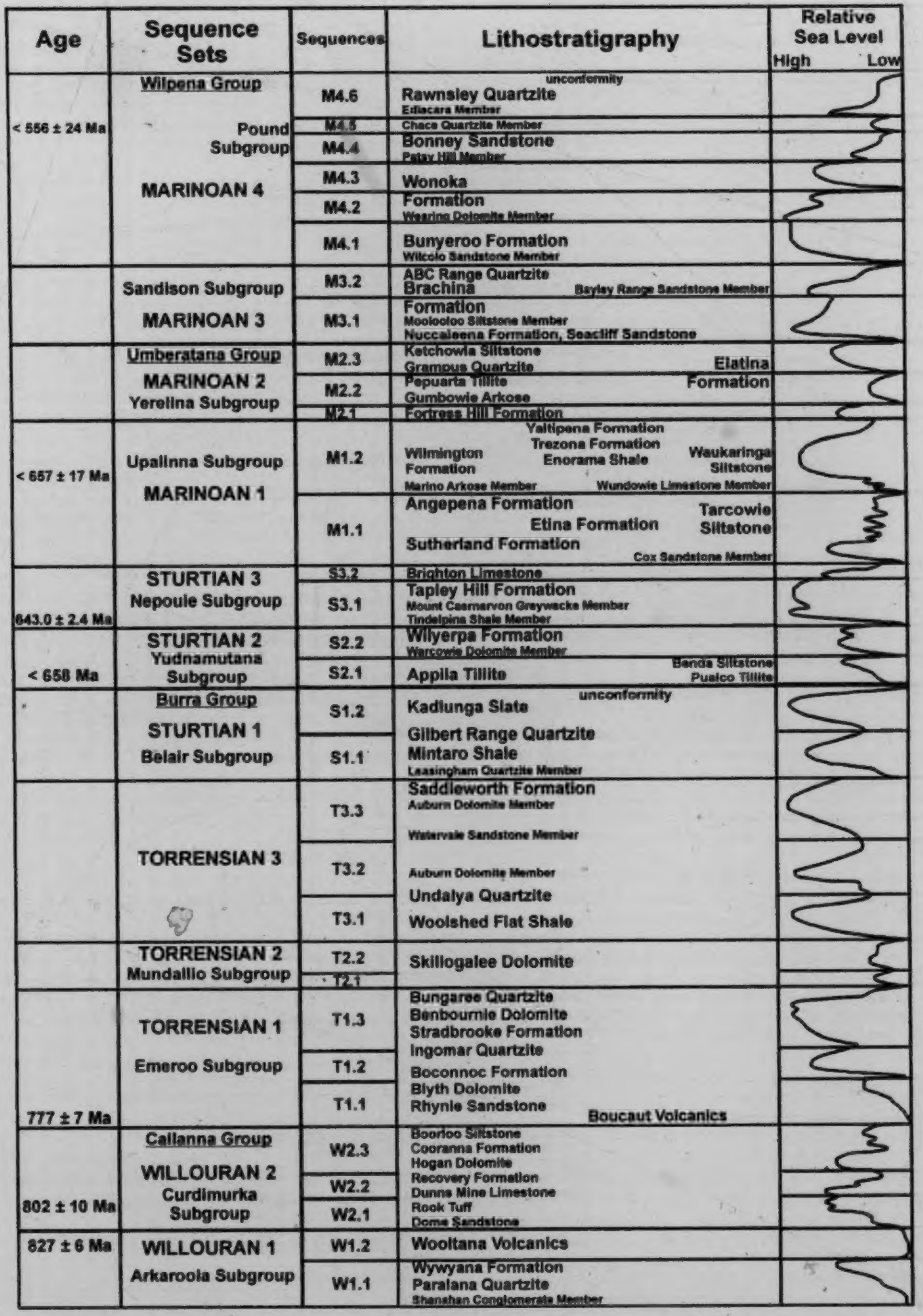

Age	Sequence Sets	Sequences	Lithostratigraphy	Relative Sea Level High Low
< 556 ± 24 Ma	Wilpena Group Pound Subgroup MARINOAN 4	M4.6	unconformity Rawnsley Quartzite Ediacara Member	
		M4.5	Chace Quartzite Member	
		M4.4	Bonney Sandstone Patsy Hill Member	
		M4.3	Wonoka	
		M4.2	Formation Wearing Dolomite Member	
		M4.1	Bunyeroo Formation Wilcolo Sandstone Member	
	Sandison Subgroup MARINOAN 3	M3.2	ABC Range Quartzite Brachina Bayley Range Sandstone Member	
		M3.1	Formation Moolooloo Siltstone Member Nuccaleena Formation, Seacliff Sandstone	
	Umberatana Group MARINOAN 2 Yerelina Subgroup	M2.3	Ketchowla Siltstone Grampus Quartzite Elatina	
		M2.2	Pepuarta Tillite Gumbowie Arkose Formation	
		M2.1	Fortress Hill Formation	
< 657 ± 17 Ma	Upalinna Subgroup MARINOAN 1	M1.2	Yaltipena Formation Trezona Formation Enorama Shale Wilmington Formation Waukaringa Siltstone Marino Arkose Member Wundowie Limestone Member	
		M1.1	Angepena Formation Tarcowie Siltstone Etina Formation Sutherland Formation Cox Sandstone Member	
643.0 ± 2.4 Ma	STURTIAN 3 Nepouie Subgroup	S3.2	Brighton Limestone	
		S3.1	Tapley Hill Formation Mount Caernarvon Greywacke Member Tindelpina Shale Member	
< 658 Ma	STURTIAN 2 Yudnamutana Subgroup	S2.2	Wilyerpa Formation Warcowie Dolomite Member	
		S2.1	Appila Tillite Benda Siltstone Pualco Tillite	
	Burra Group STURTIAN 1 Belair Subgroup	S1.2	unconformity Kadlunga Slate	
		S1.1	Gilbert Range Quartzite Mintaro Shale Leasingham Quartzite Member	
	TORRENSIAN 3	T3.3	Saddleworth Formation Auburn Dolomite Member Watervale Sandstone Member	
		T3.2	Auburn Dolomite Member Undalya Quartzite	
		T3.1	Woolshed Flat Shale	
	TORRENSIAN 2 Mundallio Subgroup	T2.2	Skillogalee Dolomite	
		T2.1		
777 ± 7 Ma	TORRENSIAN 1 Emeroo Subgroup	T1.3	Bungaree Quartzite Benbournie Dolomite Stradbrooke Formation Ingomar Quartzite	
		T1.2	Boconnoc Formation	
		T1.1	Blyth Dolomite Rhynie Sandstone Boucaut Volcanics	
802 ± 10 Ma	Callanna Group WILLOURAN 2 Curdimurka Subgroup	W2.3	Boorloo Siltstone Cooranna Formation Hogan Dolomite	
		W2.2	Recovery Formation Dunns Mine Limestone	
		W2.1	Rook Tuff Dome Sandstone	
827 ± 6 Ma	WILLOURAN 1 Arkaroola Subgroup	W1.2	Wooltana Volcanics	
		W1.1	Wywyana Formation Paralana Quartzite Shanahan Conglomerate Member	

Figure 3.9: Sequence stratigraphy for the Adelaide Rift Complex, South Australia (modified from Preiss, 2000). Age constraints from Fanning et al. (1986), Ireland et al. (1998), Wingate et al. (1998), Preiss (2000), Fanning and Link (2006), and this study.

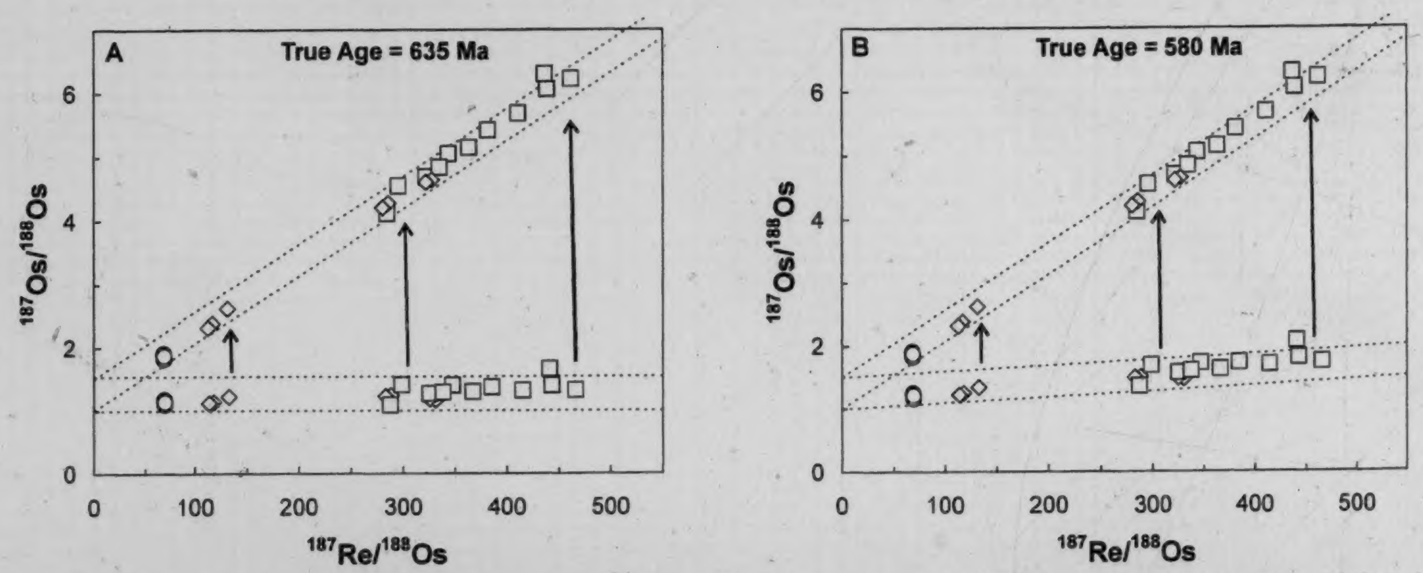

Figure 3.10: Re-Os isochron diagrams illustrating possible Re-Os systematics of shale-hosted benthic microbial mats. (A) Diagenetic mobilization of Re and Os on a limited scale during subaqueous oxidative weathering results in accurate but imprecise Re-Os dates. (B) Differential diffusion rates of Re and Os may result in a positive slope following final closure of the Re-Os isotope system during diagenesis, thus yielding erroneously old and imprecise Re-Os dates. Squares – Yarra Creek Shale, diamonds – Brachina Formation, circles – Pertatataka Formation.

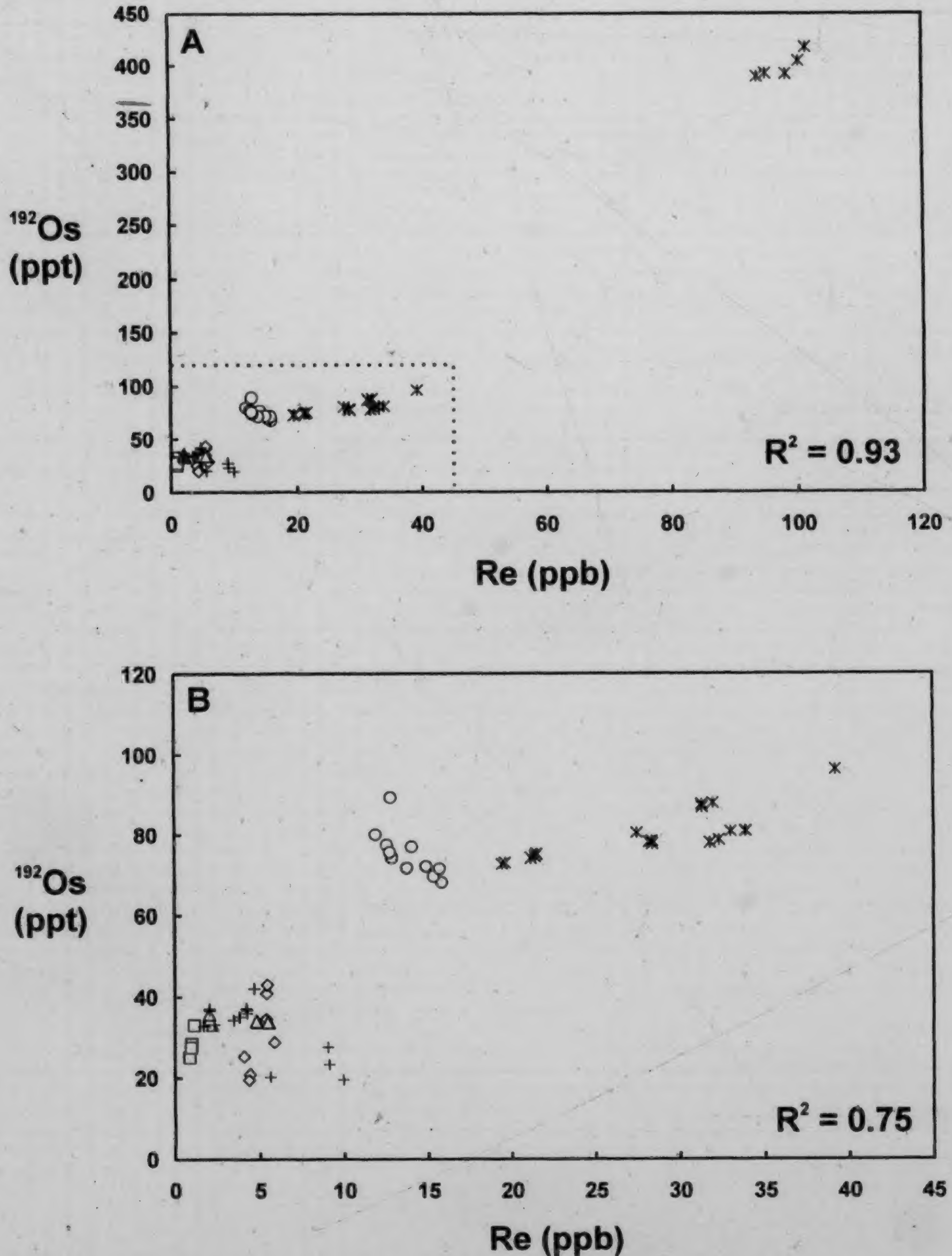

Figure 3.11: Variation in Re and ^{192}Os abundances of Neoproterozoic ORS from central and southern Australia, northwestern Tasmania, and southeastern King Island. Enclosed region within (A) is shown in (B). Asterisks – Upper Black River Dolomite, circles – Yarra Creek Shale, pluses – Tindelpina Shale Member, squares – Pertatataka Formation, diamonds – Aralka Formation, triangles – Brachina Formation.

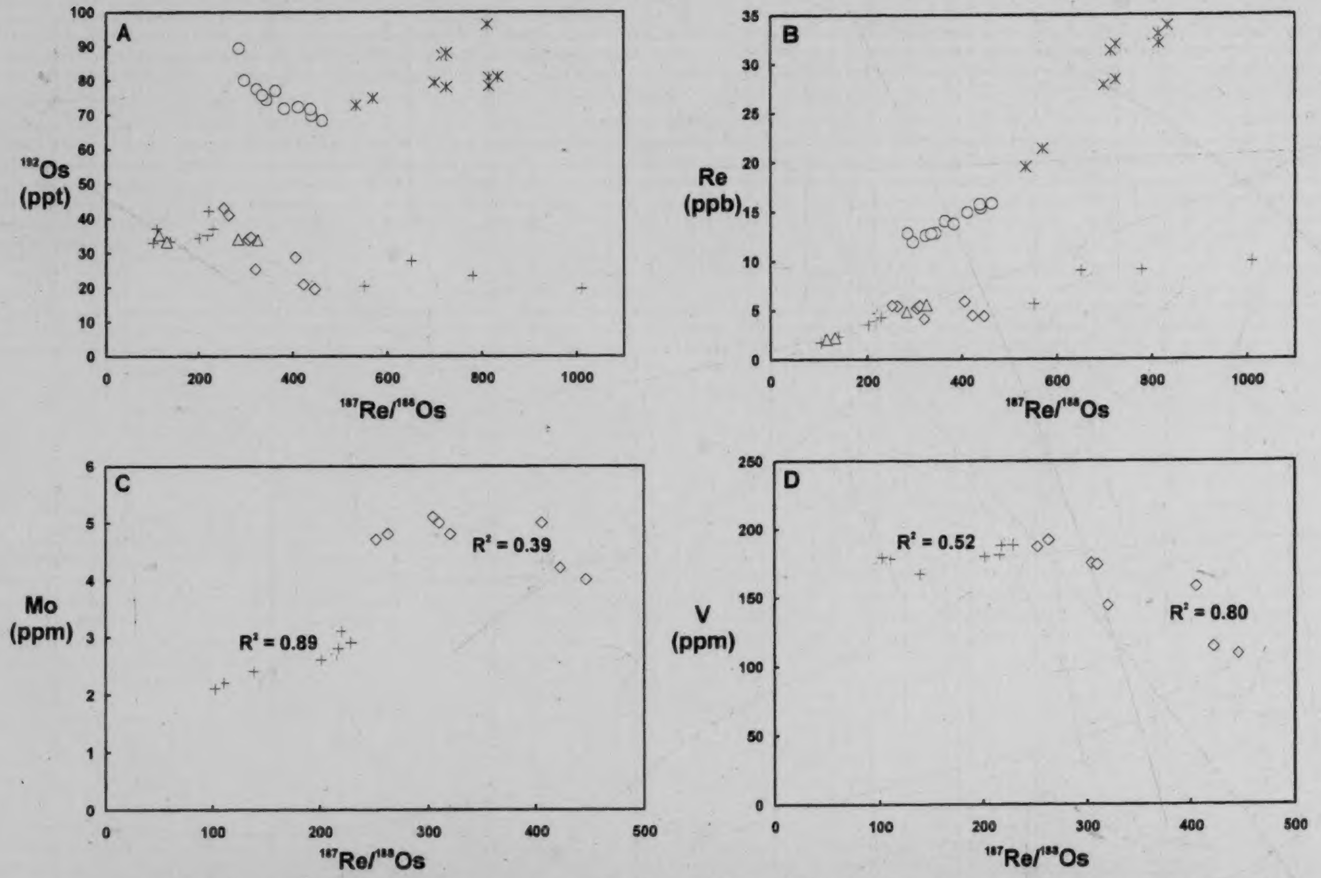

Figure 3.12: Geochemical diagrams illustrating variations in ^{187}Re/^{188}Os isotope ratio plotted against (A) ^{192}Os, (B) Re, (C) Mo, and (D) V abundance. Symbols are the same as in Figure 3.11. Replicate analyses were averaged. Coefficients of determination for the Aralka Formation and Tindelpina Shale Member (Blinman-2 data only) are shown in (C) and (D).

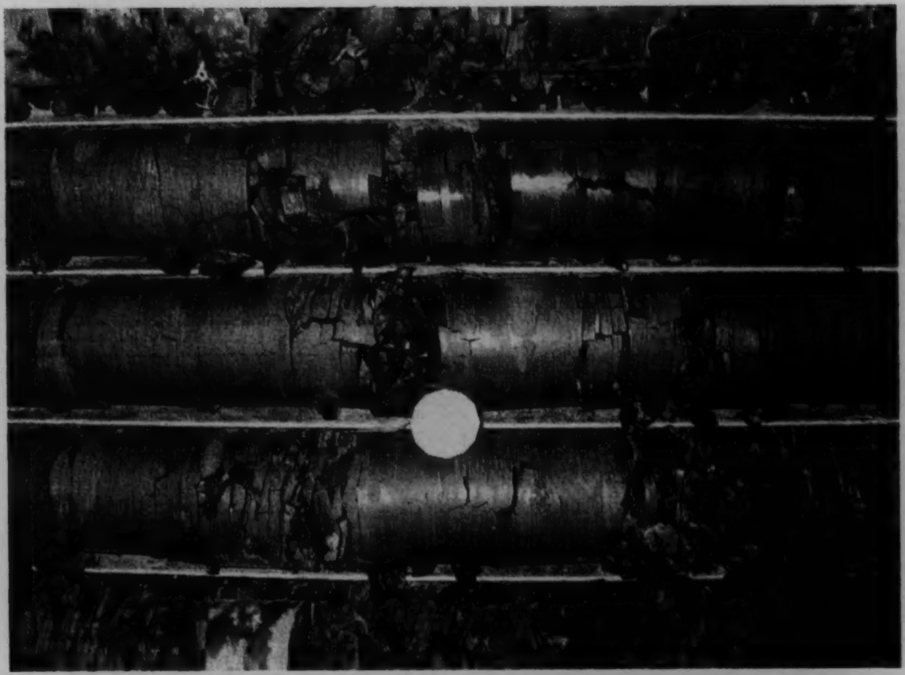

Plate 3.1: Pyritic, dolomitic organic-rich siltstone of the Neoproterozoic Aralka Formation, drill hole Wallara-1, Amadeus Basin, central Australia.

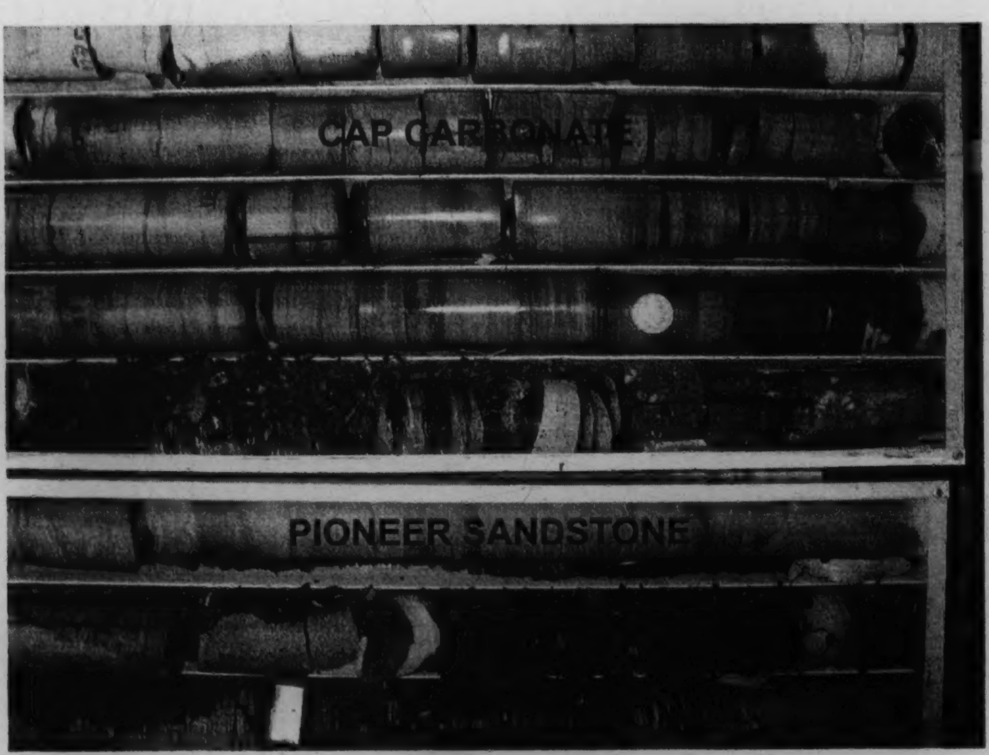
CAP CARBONATE
PIONEER SANDSTONE

Plate 3.2: Aralka Formation and overlying Pioneer Sandstone and cap carbonate in drill hole Wallara-1. Vertical black bar represents the abrupt contact between the Aralka Formation and Pioneer Sandstone.

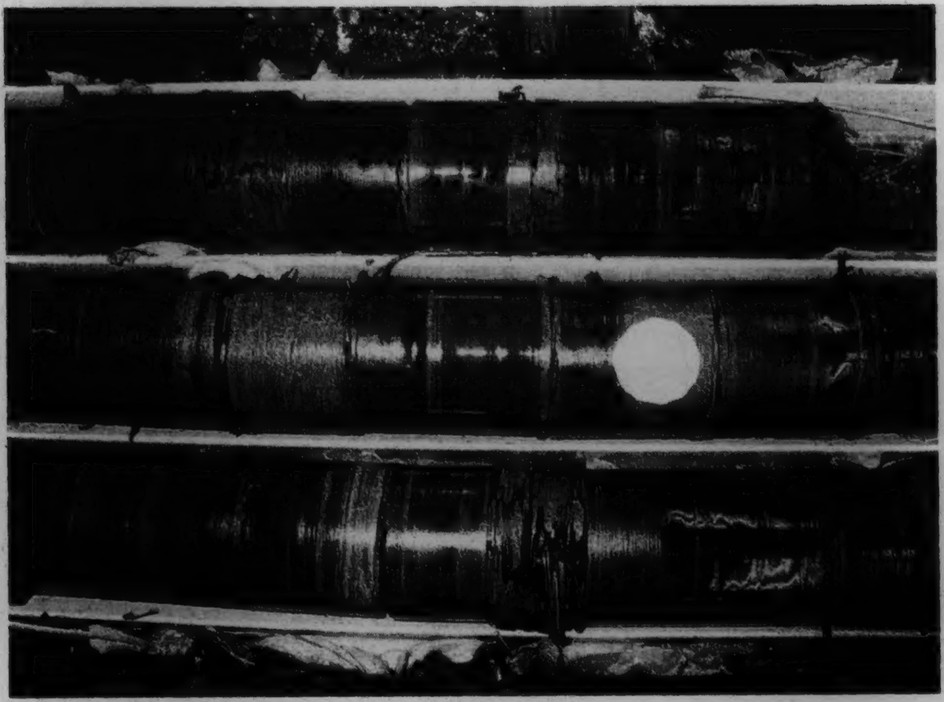

Plate 3.3: Shale-hosted benthic microbial mat facies of the Ediacaran Pertatataka Formation, drill hole Wallara-1.

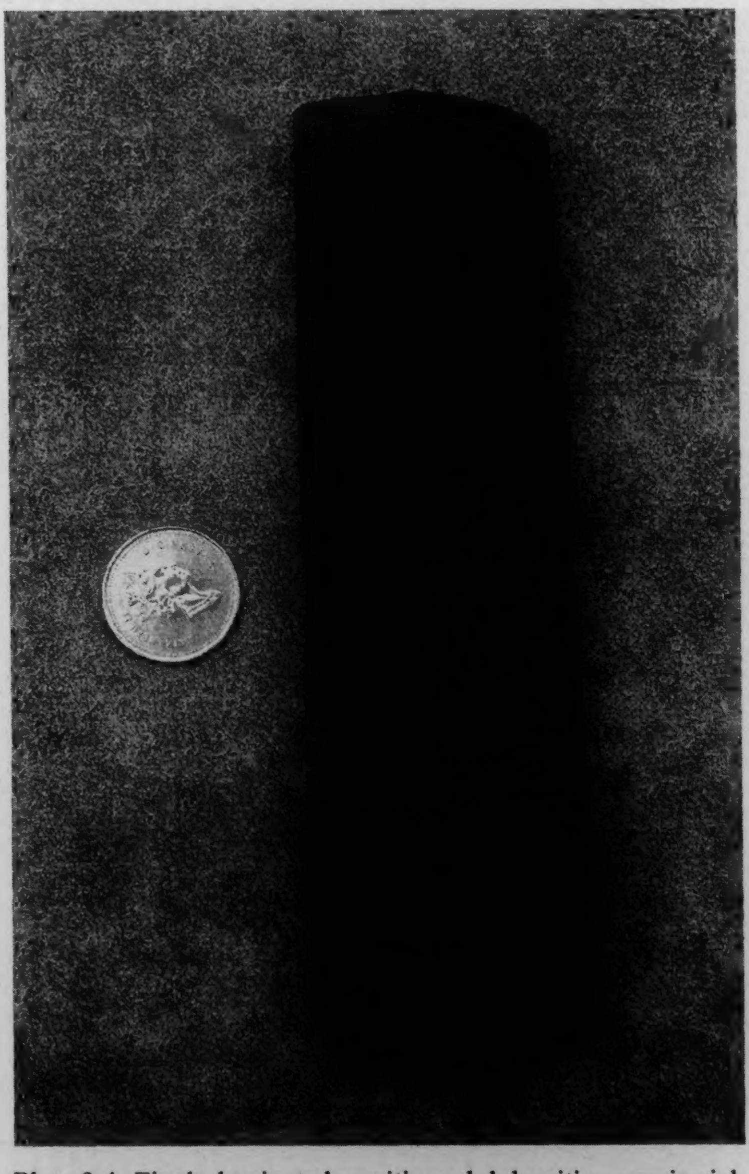

Plate 3.4: Finely laminated, pyritic and dolomitic organic-rich shale of the Neoproterozoic Tindelpina Shale Member, basal Tapley Hill Formation (Umberatana Group), Adelaide Rift Complex, southern Australia. Numbers refer to samples (BK-04-Blinman-1 to 6 (1609.98-1610.14 m). Note that light-colored material between intervals 4 and 5 was omitted during sampling.

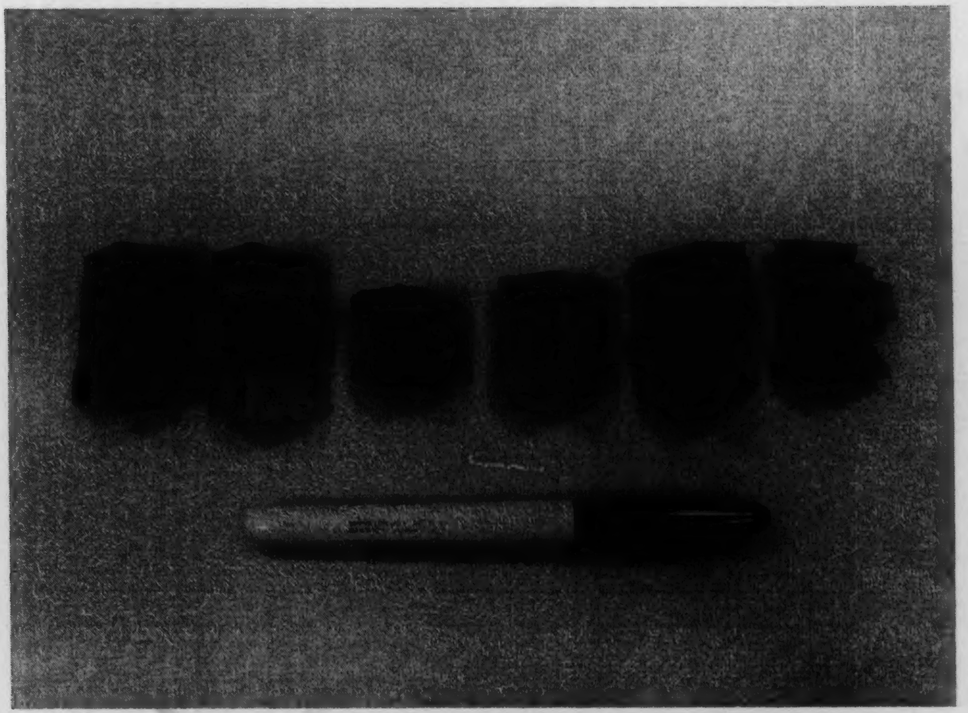

Plate 3.5: Shale-hosted benthic microbial mat facies of the Ediacaran Brachina Formation (Wilpena Group), drill hole BWM1a-1, Curnamona Craton, southern Australia. From left to right, samples BK-04-BWM1a-1-1 to 6. All light-colored material was removed (e.g., BK-04-BWM1a-1-2) prior to Re-Os analysis. Samples BK-04-BWM1a-1-3 and 6 were not analyzed.

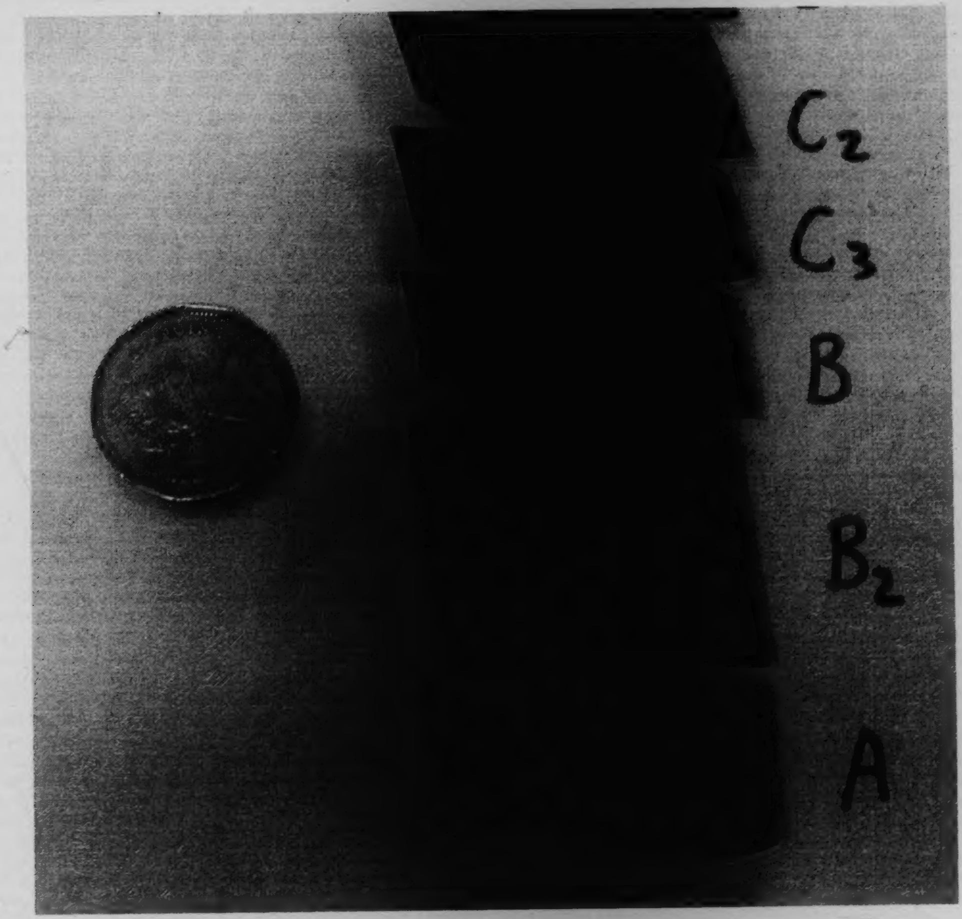

Plate 3.6: Finely laminated, pyritic black shale from the upper Black River Dolomite (Neoproterozoic Togari Group), drill hole Forest-1 (835.72-835.87 m), northwestern Tasmania.

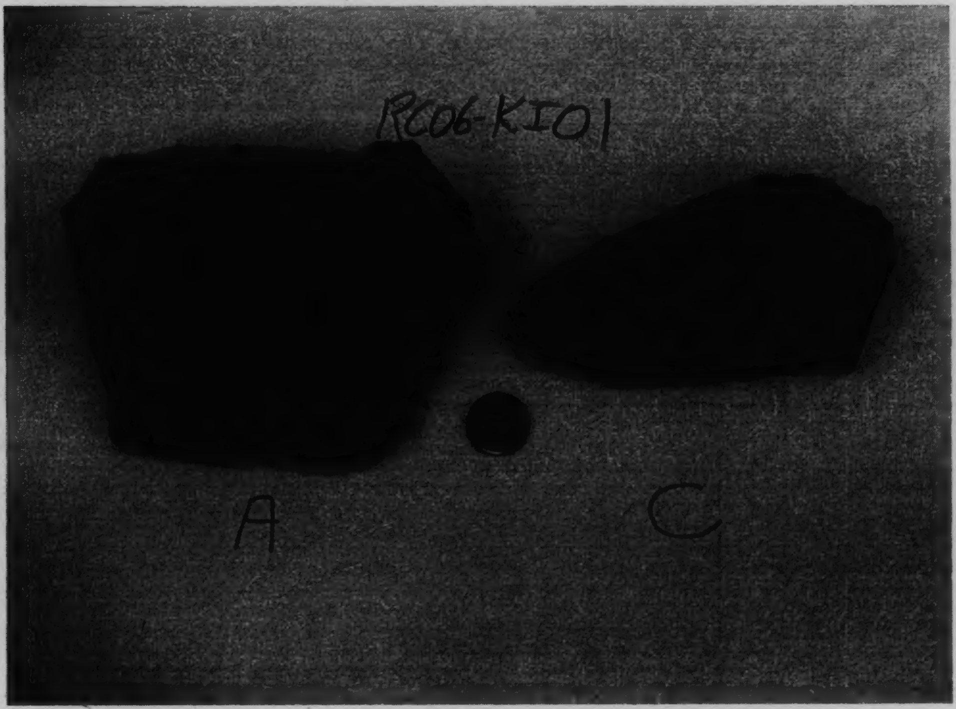

Plate 3.7: Pyritic shale-hosted benthic microbial mat facies from the Neoproterozoic Yarra Creek Shale (Grassy Group), City of Melbourne Bay coastal outcrop, southeastern King Island. Note the contrasting organic-rich black and organic-poor green shale.

REFERENCES

Algeo, T.J., and Maynard, J.B., 2004, Trace-element behavior and redox facies in core shales of Upper Pennsylvanian Kansas-type cyclothems: Chemical Geology, v. 206, p. 289-318.

Allen, P.A., Bowring, S.A., Leather, J., Brasier, M., Cozzi, A., Grotzinger, J.P., McCarron, G., and Amthor, J.J., 2002, Chronology of Neoproterozoic glaciations: New insights from Oman: International Sedimentological Congress, 16th, Johannesburg, South Africa, July 8-12, 2002, Abstract Volume, p. 7-8.

Allen, P.A., and Hoffman, P.F., 2005, Extreme winds and waves in the aftermath of a Neoproterozoic glaciation: Nature, v. 433, p. 123-127.

Arnaud, E., and Eyles, C.H., 2006, Neoproterozoic environmental change recorded in the Port Askaig Formation, Scotland: Climatic and tectonic controls: Sedimentary Geology, v. 183, p. 99-124.

Asmerom, Y., Jacobsen, S.B., Knoll, A.H., Butterfield, N.J., and Swett, K., 1991, Strontium isotopic variations of Neoproterozoic seawater: Implications for crustal evolution: Geochimica et Cosmochimica Acta, v. 55, p. 2883-2894.

Baker, M.E., 2006, The genetic response to snowball Earth: Role of HSP90 in the Cambrian Explosion: Geobiology, v. 4, p. 11-14.

Baum, S.K., and Crowley, T.J., 2001, GCM response to Late Precambrian (~ 590 Ma) ice-covered continents: Geophysical Research Letters, v. 28, p. 583-586.

Belperio, A.P., 1990, Palaeoenvironmental interpretations of the Late Proterozoic Skillogalee Dolomite in the Willouran Ranges, South Australia, *in* Jago, J.B., and Moore, P.S., eds., The evolution of a Late Precambrian – Early Palaeozoic rift complex: The Adelaide Geosyncline: Geological Society of Australia Special Publication 16, p. 85-104.

Bingen, B., Griffin, W.L., Torsvik, T.H., and Saeed, A., 2005, Timing of Late Neoproterozoic glaciation on Baltica constrained by detrital zircon geochronology in the Hedmark Group, south-east Norway: Terra Nova, v. 17, p. 250-258.

Bodiselitsch, B., Koeberi, C., Master, S., and Reimold, W.U., 2005, Estimating duration and intensity of Neoproterozoic snowball glaciations from Ir anomalies: Science, v. 308, p. 239-242.

Bond, G.C., Nickeson, P.A., and Kominz, M.A., 1984, Breakup of a supercontinent between 625 Ma and 555 Ma: New evidence and implications for continental histories: Earth and Planetary Science Letters, v. 70, p. 325-345.

Bottjer, D.J., 2005, Geobiology and the fossil record: Eukaryotes, microbes, and their interactions: Palaeogeography, Palaeoclimatology, Palaeoecology, v. 219, p. 5-21.

Bottjer, D.J., and Clapham, M.E., 2006, Evolutionary paleoecology of Ediacaran benthic marine animals, *in* Xiao, S., and Kaufman, A.J., eds., Neoproterozoic Geobiology and Paleobiology: Springer, New York, p. 91-114.

Bottjer, D.J., Hagadorn, J.W., and Dornbos, S.Q., 2000, The Cambrian substrate revolution: GSA Today, v. 10 (9), p. 1-7.

Bowring, S.A., Myrow, P., Landing, E., and Ramenzani, J., 2003, Geochronological constraints on Terminal Neoproterozoic events and the rise of metazoans: Geophysical Research Abstracts, v. 5, Abstract #13,219.

Brasier, M.D., and Shields, G., 2000, Neoproterozoic chemostratigraphy and correlation of the Port Askaig glaciation, Dalradian Supergroup of Scotland: Geological Society (London) Journal, v. 157, p. 909-914.

Brasier, M., McCarron, G., Tucker, R., Leather, J., Allen, P., and Shields, G., 2000, New U-Pb zircon dates for the Neoproterozoic Ghubrah glaciation and for the top of the Huqf Supergroup, Oman: Geology, v. 28, p. 175-178.

Brookfield, M.E., 1993, Neoproterozoic Laurentia-Australia fit: Geology, v. 21, p. 683-686.

Brookfield, M.E., 1994, Problems in applying preservation, facies and sequence models to Sinian (Neoproterozoic) glacial sequences in Australia and Asia: Precambrian Research, v. 70, p. 113-143.

Brown, A.V., 1986, Geology of the Dundas – Mt Lindsay – Mt Ramsay area: Geological Survey of Tasmania Bulletin 62.

Burrett, C., and Berry, R., 2000, Proterozoic Australia – Western United States (AUSWUS) fit between Laurentia and Australia: Geology, v. 28, p. 103-106.

Caldiera, K., and Kasting, J.F., 1992, Susceptibility of the early Earth to irreversible glaciation caused by carbon dioxide clouds: Nature, v. 359, p. 226-228.

Calver, C.R., 1998, Isotope stratigraphy of the Neoproterozoic Togari Group, Tasmania: Australian Journal of Earth Sciences, v. 45, p. 865-874.

Calver, C.R., 2000, Isotope stratigraphy of the Ediacarian (Neoproterozoic III) of the Adelaide Rift Complex, Australia, and the overprint of water column stratification: Precambrian Research, v. 100, p. 121-150.

Calver, C.R., and Walter, M.R., 2000, The Late Neoproterozoic Grassy Group of King Island, Tasmania: Correlation and palaeogeographic significance: Precambrian Research, v. 100, p. 299-312.

Calver, C.R., Black, L.P., Everard, J.L., and Seymour, D.B., 2004, U-Pb zircon age constraints on Late Neoproterozoic glaciation in Tasmania: Geology, v. 32, p. 893-896.

Canfield, D.E., and Teske, A., 1996, Late Proterozoic rise in atmospheric oxygen concentration inferred from phylogenetic and sulphur-isotope studies: Nature, v. 382, p. 127-132.

Canfield, D.E., Poulton, S.W., and Narbonne, G.M., 2007, Late-Neoproterozoic deep-ocean oxygenation and the rise of animal life: Science, v. 315, p. 92-95.

Coats, R.P., 1981, Late Proterozoic (Adelaidean) tillites of the Adelaide Geosyncline, *in* Hambrey, M.J., and Harland, W.B., eds., Earth's pre-Pleistocene glacial record: Cambridge, United Kingdom, Cambridge University Press, p. 537-548.

Cohen, A.S., Coe, A.L., Bartlett, J.M., and Hawkesworth, C.J., 1999, Precise Re-Os ages of organic-rich mudrocks and the Os isotope composition of Jurassic seawater: Earth and Planetary Science Letters, v. 167, p. 159-173.

Colodner, D.C., Boyle, E.A., Edmond, J.M., and Thomson, J., 1992, Post-depositional mobility of platinum, iridium, and rhenium in marine sediments: Nature, v. 358, p. 402-404.

Condon, D.J., Prave, A.R., and Benn, D.I., 2002, Neoproterozoic glacial-rainout intervals: Observations and implications: Geology, v. 30, p. 35-38.

Condon, D., Zhu, M., Bowring, S., Wang, W., Yang, A., and Jin, Y, 2005, U-Pb ages from the Neoproterozoic Doushantuo Formation, China: Science, v. 308, p. 95-98.

Cooper, J.A., Jenkins, R.J.F., Compston, W., and Williams, I.S., 1992, Ion-probe zircon dating of a mid-Early Cambrian tuff in South Australia: Geological Society (London) Journal, v. 149, p. 185-192.

Corsetti, F.A., and Grotzinger, J.P., 2005, Origin and significance of tube structures in Neoproterozoic post glacial cap carbonates: example from the Noonday Dolomite, Death Valley, United States: Palaios, v. 20, p. 348-387.

Corsetti, F.A., and Lorentz, N.J., 2006, On Neoproterozoic cap carbonates as chronostratigraphic markers, *in* Xiao, S., and Kaufman, A.J., eds., Neoproterozoic Geobiology and Paleobiology: Springer, New York, p. 273-294.

Corsetti, F.A., Awramik, S.M., and Pierce, D., 2003, A complex microbiota from snowball Earth times: Microfossils from the Neoproterozoic Kingston Peak Formation, Death Valley, USA: Proceedings of the National Academy of Sciences, v. 100, p. 4399-4404.

Corsetti, F.A., Olcott, A.N., and Bakermans, C., 2006, The biotic response to Neoproterozoic snowball Earth: Palaeogeography, Palaeoclimatology, Palaeoecology, v. 232, p. 114-130.

Crawford, A.J., Stevens, B.P.J., and Fanning, M., 1997, Geochemistry and tectonic setting of some Neoproterozoic and Early Cambrian volcanics in western New South Wales: Australian Journal of Earth Sciences, v. 44, p. 831-852.

Creaser, R.A., Sannigrahi, P., Chacko, T., and Selby, D., 2002, Further evaluation of the Re-Os geochronometer in organic-rich sedimentary rocks: a test of hydrocarbon maturation effects in the Exshaw Formation, Western Canada Sedimentary Basin: Geochimica et Cosmochimica Acta, v. 66, p. 3441-3452.

Crowell, J.C., 1999, Pre-Mesozoic ice ages: Their bearing on understanding the climate system: Geological Society of America Memoir 192.

Crusius, J., and Thomson, J., 2000, Comparative behavior of authigenic Re, U, and Mo during reoxidation and subsequent long-term burial in marine sediments: Geochimica et Cosmochimica Acta, v. 64, p. 2233-2242.

Crusius, J. and Thomson, J., 2003, Mobility of authigenic rhenium, silver, and selenium during postdepositional oxidation in marine sediments: Geochimica et Cosmochimica Acta, v. 67, p. 265-273.

Crusius, J., Calvert, S., Pedersen, T., and Sage, D., 1996, Rhenium and molybdenum enrichments in sediments as indicators of oxic, suboxic, and sulfidic conditions of deposition: Earth and Planetary Science Letters, v. 145, p. 65-78.

Dalziel, I.W.D., 1991, Pacific margins of Laurentia and East Antarctica-Australia as a conjugate rift-pair: Evidence and implications for an Eocambrian supercontinent: Geology, v. 19, p. 598-601.

Dalziel, I.W.D., 1997, Neoproterozoic-Paleozoic geography and tectonics: Review, hypothesis, environmental speculation: Geological Society of America Bulletin, v. 109, p. 16-42.

Dempster, T.J., Rogers, G., Tanner, P.W.G., Bluck, B.J., Muir, R.J., Redwood, S.D., Ireland, T.R., and Paterson, B.A., 2002, Timing of deposition, orogenesis and glaciation within the Dalradian rocks of Scotland: Constraints from U-Pb zircon ages: Geological Society [London] Journal, v. 159, p. 83-94.

Derry, L.A., Kaufman, A.J., and Jacobsen, S.B., 1992, Sedimentary cycling and environmental change in the Late Proterozoic: Evidence from stable and radiogenic isotopes: Geochimica et Cosmochimica Acta, v. 56, p. 1317-1329.

Des Marais, D.J., Strauss, H., Summons, R.E., and Hayes, J.M., 1992, Carbon isotope evidence for the stepwise oxidation of the Proterozoic environment: Nature, v. 359, p. 605-608.

Direen, N.G., and Crawford, A.J., 2003, Fossil seaward-dipping reflector sequences preserved in southeastern Australia: A 600 Ma volcanic passive margin in eastern Gondwanaland: Geological Society (London) Journal, v. 160, p. 985-990.

Dobrzinski, N., Bahlburg, H., Strauss, H., and Zhang, Q., 2004, Geochemical climate proxies applied to the Neoproterozoic glacial succession on the Yangtze Platform, South China, *in* Jenkins, G.S., et al., eds., The extreme Proterozoic: Geology, geochemistry, and climate: American Geophysical Union Geophysical Monograph 146, p. 13-32.

Donnadieu, Y., Goddéris, Y., Ramstein, G., Nédélec, A., and Meert, J., 2004a, A 'snowball Earth' climate triggered by continental break-up through changes in runoff: Nature, v. 428, p. 303-306.

Donnadieu, Y., Ramstein, G., Goddéris, Y., and Fluteau, F., 2004b, Global tectonic setting and climate of the Late Neoproterozoic: A climate-geochemical coupled study, *in* Jenkins, G.S., et al., eds., The extreme Proterozoic: Geology, geochemistry, and climate: American Geophysical Union Geophysical Monograph 146, p. 79-89.

Embleton, B.J.J., and Williams, G.E., 1986, Low palaeolatitude of deposition for late Precambrian periglacial varvities in South Australia: Implications for Palaeoclimatology: Earth and Planetary Science Letters, v. 79, p. 419-430.

Esser, B.K., and Turekian, K.K., 1993, The osmium isotopic composition of the continental crust: Geochimica et Cosmochimica Acta, v. 57, p. 3093-3104.

Evans, D.A.D., 2000, Stratigraphic, geochronological, and paleomagnetic constraints upon the Neoproterozoic climatic paradox: American Journal of Science, v. 300, p. 347-433.

Evans, D.A.D., 2006, Proterozoic low orbital obliquity and axial-dipolar geomagnetic field from evaporite palaeolatitudes: Nature, v. 444, p. 51-55.

Eyles, C.H., Eyles, N., and Grey, K., 2007, Palaeoclimate implications from deep drilling of Neoproterozoic strata in the Officer Basin and Adelaide Rift Complex of Australia; a marine record of wet-based glaciers: Palaeogeography, Palaeoclimatology, Palaeoecology, v. 248, p. 291-312.

Eyles, N., 1993, Earth's glacial record and its tectonic setting: Earth-Science Reviews, v. 35, p. 1-248.

Eyles, N., and Januszczak, N., 2004, 'Zipper-rift': A tectonic model for Neoproterozoic glaciations during the breakup of Rodinia after 750 Ma: Earth-Science Reviews, v. 65, p. 1-73.

Fairchild, I.J., 1993, Balmy shores and icy wastes: The paradox of carbonates associated with glacial deposits in Neoproterozoic times, *in* Wright, V.P., ed., Sedimentology Review, v. 1, p. 1-16.

Fairchild, I.J., and Kennedy, M.J., 2007, Neoproterozoic glaciation in the Earth system: Geological Society (London) Journal, v. 164, p. 895-921.

Fanning, C.M., and Link, P.K., 2004, U-Pb SHRIMP ages of Neoproterozoic (Sturtian) glaciogenic Pocatello Formation, southeastern Idaho: Geology, v. 32, p. 881-884.

Fanning, C.M., and Link, P., 2006, Constraints on the timing of the Sturtian glaciation from southern Australia; i.e. for the true Sturtian: Geological Society of America Abstracts With Programs, v. 38 (7), p. 115.

Fanning, C.M., Ludwig, K.R., Forbes, B.G., and Preiss, W.V., 1986, Single and multiple grain U-Pb zircon analyses for the early Adelaidean Rook Tuff, Willouran Ranges, South Australia: Geological Society of Australia Abstracts, v. 15, p. 71-72.

Field, B.D., 1991, Paralic and periglacial facies and contemporaneous deformation of the Late Proterozoic Olympic Formation, Pioneer Sandstone and Gaylad Sandstone, Amadeus Basin, central Australia, *in* Korsch, R.J., and Kennard, J.M., eds., Geological and geophysical studies in the Amadeus Basin, Central Australia: Australian Bureau of Mineral Resources Bulletin, v. 236, p. 127-136.

Fike, D.A., Grotzinger, J.P., Pratt, L.M., and Summons, R.E., 2006, Oxidation of the Ediacaran ocean: Nature, v. 444, p. 744-747.

Foden, J., Barovich, K., Jane, M., and O'Halloran, G., 2001, Sr-isotopic evidence for Late Neoproterozoic rifting in the Adelaide Geosyncline at 586 Ma: Implications for a Cu ore forming fluid flux: Precambrian Research, v. 106, p. 291-308.

Frimmel, H.E., Klötzli, U.S., and Siegfried, P.R., 1996, New Pb-Pb single zircon age constraints on the timing of Neoproterozoic glaciation and continental break-up in Namibia: Journal of Geology, v. 104, p. 459-469.

Frimmel, H.E., Zartman, R.E., and Späth, A., 2001, The Richtersveld Igneous Complex, South Africa: U-Pb zircon and geochemical evidence for the beginning of Neoproterozoic continental breakup: Journal of Geology, v. 109, p. 493-508.

Gammon, P.R., McKirdy, D.M., and Smith, H.D., 2005, The timing and environment of teepee formation in a Marinoan cap carbonate: Sedimentary Geology, v. 177, p. 195-208.

Gehling, J.G., 1999, Microbial mats in Terminal Proterozoic siliciclastics: Ediacaran death masks: Palaios, v. 14, p. 40-57.

Gladkochub, D.P., Wingate, M.T.D., Pisarevsky, S.A., Donskaya, T.V., Mazukabzov, A.M., Ponomarchuk, V.A., and Stanevich, A.M., 2006, Mafic intrusions in southwestern Siberia and implications for a Neoproterozoic connection with Laurentia: Precambrian Research, v. 147, p. 260-278.

Goddéris, Y., Donnadieu, Y., Nédélec, A., Dupré, B., Dessert, C., Grard, A., Ramstein, G., and Francois, L.M., 2003, The Sturtian 'snowball' glaciation: Fire and ice: Earth and Planetary Science Letters, v. 211, p. 1-12.

Goddéris, Y., Donnadieu, Y, Dessert, C., Dupré, B., Fluteau, F., Francois, L.M., Meert, J., Nédélec, A., and Ramstein, G., 2007, Coupled modeling of global carbon cycle and climate in the Neoproterozoic: links between Rodinia breakup and major glaciations: Comptes Rendus Geoscience, v. 339, p. 212-222.

Goodman, J.C., 2006, Through thick and thin: Marine and meteoric ice in a "Snowball Earth" climate: Geophysical Research Letters, v. 33, paper 2006GL026840.

Gorjan, P., Veevers, J.J., and Walter, M.R., 2000, Neoproterozoic sulfur-isotope variation in Australia and global implications: Precambrian Research, v. 100, p. 151-179.

Gorjan, P., Walter, M.R., and Swart, R., 2003, Global Neoproterozoic (Sturtian) post-glacial sulfide-sulfur isotope anomaly recognised in Namibia: Journal of African Earth Sciences, v. 36, p. 89-98.

Grazhdankin, D., 2004, Patterns of distribution in the Ediacaran biotas: facies versus biogeography and evolution: Paleobiology, v. 30, p. 203-221.

Grey, K., Walter, M.R., and Calver, C.R., 2003, Neoproterozoic biotic diversification: Snowball Earth or aftermath of the Acraman impact?: Geology, v. 31, p. 459-462.

Griffin, B.J., and Preiss, W.V., 1976, The significance and provenance of stromatolitic clasts in a probable late Precambrian diamictite in north-western Tasmania: Papers and Proceedings of the Royal Society of Tasmania, v. 110, p. 111-127.

Grotzinger, J.P., and Knoll, A.H., 1995, Anomalous carbonate precipitates: Is the Precambrian the key to the Permian?: Palaios, v. 10, p. 578-596.

Hagadorn, J.W., and Bottjer, D.J., 1997, Wrinkle structures: Microbially mediated sedimentary structures common in subtidal siliciclastic settings at the Proterozoic-Phanerozoic transition: Geology, v. 25, p. 1047-1050.

Hagadorn, J.W., and Bottjer, D.J., 1999, Restriction of a Late Neoproterozoic biotope: Suspect-microbial structures and trace fossils at the Vendian-Cambrian transition: Palaios, v. 14, p. 73-85.

Halverson, G.P., Hoffman, P.F., Schrag, D.P., and Kaufman, A.J., 2002, A major perturbation of the carbon cycle before the Ghaub glaciation (Neoproterozoic) in Namibia: Prelude to snowball Earth?: Geochemistry, Geophysics, Geosystems, v. 3, paper 2001GC000244.

Halverson, G.P., Hoffman, P.F., Schrag, D.P., Maloof, A.C., and Rice, A.H.N., 2005, Toward a Neoproterozoic composite carbon-isotope record: Geological Society of America Bulletin, v. 117, p. 1181-1207.

Harland, W.B., 1964, Critical evidence for a great infra-Cambrian glaciation: Geologische Rundschau, v. 54, p. 45-61.

Hattori, Y., Suzuki, K., Honda, M., and Shimizu, H., 2003, Re-Os isotope systematics of the Taklimakan Desert sands, moraines and river sediments around the Taklimakan Desert, and of Tibetan soils: Geochimica et Cosmochimica Acta, v. 67, p. 1195-1205.

Hayes, J.M., Kaplan, I.R., and Wedeking, K.W., 1983, Precambrian organic geochemistry, preservation of the record, *in* Schopf, J.W., ed., Earth's earliest biosphere: Its origin and evolution: Princeton University Press, Princeton, New Jersey, p. 93-134.

Higgins, J.A., and Schrag, D.P., 2003, Aftermath of a snowball Earth: Geochemistry, Geophysics, Geosystems: Paper #2002GC000403.

Hoffman, P.F., 1991, Did the breakout of Laurentia turn Gondwanaland inside-out?: Science, v. 252, p. 1409-1412.

Hoffman, P.F., and Schrag, D.P., 2002, The snowball Earth hypothesis: Testing the limits of global change: Terra Nova, v. 14, p. 129-155.

Hoffman, P.F., Hawkins, D.P., Isachsen, C.E., and Bowring, S.A., 1996, Precise U-Pb zircon ages for Early Damaran magmatism in the Summas Mountains and Welwitschia Inlier, northern Damara belt, Namibia: Communications of the Geological Survey of Namibia, v. 11, p. 47-52.

Hoffman, P.F., Kaufman, A.J., Halverson, G.P., and Schrag, D.P., 1998a, A Neoproterozoic snowball Earth: Science, v. 281, p. 1342-1346.

Hoffman, P.F., Kaufman, A.J., and Halverson, G.P., 1998b, Comings and goings of global glaciations on a Neoproterozoic tropical platform in Namibia: GSA Today, v. 8 (5), p. 1-9.

Hoffman, P.F., Halverson, G.P., Domack, E.W., Husson, J.M., Higgins, J.A., and Schrag, D.P., 2007, Are basal Ediacaran (635 Ma) post-glacial "cap dolostones" diachronous?: Earth and Planetary Science Letters, v. 258, p. 114-131.

Hoffmann, K.-H., Condon, D.J., Bowring, S.A., and Crowley, J.L., 2004, U-Pb zircon date from the Neoproterozoic Ghaub Formation, Namibia: Constraints on Marinoan glaciation: Geology, v. 32, p. 817-820.

Huang, B., Xu, B., Zhang, C., Li, Y., and Zhu, R., 2005, Paleomagnetism of the Baiyisi volcanic rocks (ca. 740 Ma) of Tarim, northwest China: A continental fragment of Neoproterozoic Western Australia?: Precambrian Research, v. 142, p. 83-92.

Hurtgen, M.T., Arthur, M.A., Suits, N.S., and Kaufman, A.J., 2002, The sulfur isotopic composition of Neoproterozoic seawater sulfate: Implications for a snowball Earth?: Earth and Planetary Science Letters, v. 203, p. 413-429.

Hurtgen, M.T., Arthur, M.A., and Halverson, G.P., 2005, Neoproterozoic sulfur isotopes, the evolution of microbial sulfur species, and the burial efficiency of sulfide as sedimentary pyrite: Geology, v. 33, 41-44.

Hurtgen, M.T., Halverson, G.P., Arthur, M.A., and Hoffman, P.F., 2006, Sulfur cycling in the aftermath of a 635-Ma snowball glaciation: Evidence for a syn-glacial sulfidic deep ocean: Earth and Planetary Science Letters, v. 245, p. 551-570.

Hyde, W.T., Crowley, T.J., Baum, S.K., and Peltier, W.R., 2000, Neoproterozoic 'snowball Earth' simulations with a coupled climate/ice-sheet model: Nature, v. 405, p. 425-429.

Ireland, T.R., Flöttmann, T., Fanning, C.M., Gibson, G.M., and Preiss, W.V., 1998, Development of the early Paleozoic Pacific margin of Gondwana from detrital-zircon ages across the Delamarian orogeny: Geology, v. 26, p. 243-246.

Jacobsen, S.B., and Kaufman, A.J., 1999, The Sr, C and O isotopic evolution of Neoproterozoic seawater: Chemical Geology, v. 161, p. 37-57.

Jaffe, L.A., Peucker-Ehrenbrink, B., and Petsch, S.T., 2002, Mobility of rhenium, platinum group elements and organic carbon during black shale weathering: Earth and Planetary Science Letters, v. 198, p. 339-353.

Jago, J.B., 1974, The origin of the Cottons Breccia, King Island, Tasmania: Transactions of the Royal Society of South Australia, v. 98, p. 13-28.

James, N.P., Narbonne, G.M., and Kyser, T.K., 2001, Late Neoproterozoic cap carbonates: Mackenzie Mountains, northwestern Canada: Precipitation and global glacial meltdown: Canadian Journal of Earth Sciences, v. 38, p. 1229-1262.

James, N.P., Narbonne, G.M., Dalrymple, R.W., and Kyser, T.K., 2005, Glendonites in Neoproterozoic low-latitude, interglacial, sedimentary rocks, northwest Canada: Insights into the Cryogenian ocean and Precambrian cold-water carbonates: Geology, v. 33, p. 9-12.

Jenkins, G.S., 2004, A review of Neoproterozoic climate modeling studies, *in* Jenkins, G.S., et al., eds., The extreme Proterozoic: Geology, geochemistry, and climate: American Geophysical Union Monograph 146, p. 73-78.

Jenkins, G.S., and Smith, S.R., 1999, GCM simulations of Snowball Earth conditions during the late Proterozoic: Geophysical Research Letters, v. 26, p. 2263-2266.

Jiang, G., Kennedy, M.J., and Christie-Blick, N., 2003, Stable isotopic evidence for methane seeps in Neoproterozoic postglacial cap carbonates: Nature, v. 426, p. 822-826.

Jiang, G., Kennedy, M.J., Christie-Blick, N., Wu, H., and Zhang, S., 2006, Stratigraphy, sedimentary structures, and textures of the Late Neoproterozoic Doushantuo cap carbonate in South China: Journal of Sedimentary Research, v. 76, p. 978-995.

Karlstrom, K.E., Williams, M.L., McLelland, J., Geissman, J.W., and Åhäll, K.-I., 1999, Refining Rodinia: Geologic evidence for the Australia-Western U.S. connection in the Proterozoic: GSA Today, v. 9 (10), p. 1-7.

Kasemann, S.A., Hawkesworth, C.J., Prave, A.R., Fallick, A.E., and Pearson, P.N., 2005, Boron and calcium isotope composition in Neoproterozoic carbonate rocks from Namibia: Evidence for extreme environmental change: Earth and Planetary Science Letters, v. 231, p. 73-86.

Kaufman, A.J., and Knoll, A.H., 1995, Neoproterozoic variations in the C-isotopic composition of seawater: Stratigraphic and biogeochemical implications: Precambrian Research, v. 73, p. 27-49.

Kaufman, A.J., Hayes, J.M., Knoll, A.H., and Germs, G.J.B., 1991, Isotopic compositions of carbonates and organic carbon from upper Proterozoic successions in Namibia: Stratigraphic variation and the effects of diagenesis and metamorphism: Precambrian Research, v. 49, p. 301-327.

Kaufman, A.J., Jacobsen, S.B., and Knoll, A.H., 1993, The Vendian record of Sr and C isotopic variations in seawater: Implications for tectonics and paleoclimate: Earth and Planetary Science Letters, v. 120, p. 409-430.

Kaufman, A.J., Knoll, A.H., and Narbonne, G.M., 1997, Isotopes, ice ages, and terminal Proterozoic Earth history: Proceedings of the National Academy of Sciences, v. 94, p. 6600-6605.

Kendall, B.S., 2003, Evaluation of the Re-Os geochronometer in organic-rich mudrocks as a method for constraining the absolute ages of Neoproterozoic glaciogenic deposits: M.Sc, Thesis, University of Alberta.

Kendall, B.S., Creaser, R.A., Ross, G.M., and Selby, D., 2004, Constraints on the timing of Marinoan "Snowball Earth" glaciation by ^{187}Re-^{187}Os dating of a Neoproterozoic, post-glacial black shale in Western Canada: Earth and Planetary Science Letters, v. 222, p. 729-740.

Kennedy, M.J., 1996, Stratigraphy, sedimentology, and isotopic geochemistry of Australian Neoproterozoic cap dolostones: Deglaciation, δ^{13}C excursions, and carbonate precipitation: Journal of Sedimentary Research, v. 66, p. 1050-1064.

Kennedy, M.J., Runnegar, B., Prave, A.R., Hoffmann, K.-H., and Arthur, M.A., 1998, Two or four Neoproterozoic glaciations?: Geology, v. 26, p.1059-1063.

Kennedy, M.J., Christie-Blick, N., and Sohl, L.E., 2001a, Are Proterozoic cap carbonates and isotopic excursions a record of gas hydrate destabilization following Earth's coldest intervals?: Geology, v. 29, p. 443-446.

Kennedy, M.J., Christie-Blick, N., and Prave, A.R., 2001b, Carbon isotopic composition of Neoproterozoic glacial carbonates as a test of paleoceanographic models for snowball Earth phenomena: Geology, v. 29, p. 1135-1138.

Kennedy, M., Droser, M., Mayer, L.M., Pevear, D., Mrofka, D., 2006, Late Precambrian oxygenation; inception of the clay mineral factory: Science, v. 311, p. 1446-1449.

Key, R.M., Liyungu, A.K., Njamu, F.M., Somwe, V., Banda, J., Mosley, P.N., and Armstrong, R.A., 2001, The western arm of the Lufilian Arc in NW Zambia and its potential for copper mineralization: Journal of African Earth Sciences, v. 33, p. 503-528.

Kilner, B., Niocaill, C.M., and Brasier, M., 2005, Low-latitude glaciation in the Neoproterozoic of Oman: Geology, v. 33, p. 413-416.

Kirschvink, J.L., 1992, Late Proterozoic low-latitude global glaciation: The Snowball Earth, *in* Schopf, J.W., and Klein, C., eds., The Proterozoic biosphere: Cambridge University Press, p. 51-52.

Knoll, A.H., 1991, End of the Proterozoic Eon: Scientific American, v. 265, p. 64-73.

Knoll, A.H., Hayes, J.M., Kaufman, A.J., Swett, K.,. and Lambert, I.B., 1986, Secular variation in carbon isotope ratios from Upper Proterozoic successions of Svalbard and East Greenland: Nature, v. 321, p. 832-838.

Knoll, A.H., Walter, M.R., Narbonne, G.M., and Christie-Blick, N., 2004, A new period for the geologic time scale: Science, v. 305, p. 621-622.

Knoll, A.H., Walter, M.R., Narbonne, G.M., and Christie-Blick, N., 2006, The Ediacaran Period: A new addition to the geologic time scale: Lethaia, v. 39, p. 13-30.

Le Hir, G., Ramstein, G., Donnadieu, Y., Pierrehumbert, R.T., 2007, Investigating plausible mechanisms to trigger a deglaciation from a hard Snowball Earth: Comptes Rendus Geoscience, v. 339, p. 274-287.

Leather, J., Allen, P.A., Brasier, M.D., and Cozzi, A., 2002, Neoproterozoic snowball Earth under scrutiny: Evidence from the Fiq glaciation of Oman: Geology, v. 30, p. 891-894.

Lemon, N.M., and Gostin, V.A., 1990, Glacigenic sediments of the Late Proterozoic Elatina Formation and equivalents, Adelaide Geosyncline, South Australia, *in* Jago, J.B., and Moore, P.S., eds., The evolution of a Late Precambrian – Early Palaeozoic Rift Complex: The Adelaide Geosyncline: Geological Society of Australia Special Publication 16, p. 149-163.

Levasseur, S., Birck, J.-L., and Allègre, C.J., 1998, Direct measurement of femtomoles of osmium and the ^{187}Os/^{186}Os ratio in seawater: Science, v. 282, p. 272-274.

Levasseur, S., Birck, J.-L., and Allègre, C.J., 1999, The osmium riverine flux and the oceanic mass balance of osmium: Earth and Planetary Science Letters, v. 174, p. 7-23.

Li, Z.X., and Powell, C.M., 2001, An outline of the palaeogeographic evolution of the Australasian region since the beginning of the Neoproterozoic: Earth-Science Reviews, v. 53, p. 237-277.

Li, Z.X., Zhang, L., and Powell, C.M., 1995, South China in Rodinia: Part of the missing link between Australia-East Antarctica and Laurentia?: Geology, v. 23, p. 407-410.

Li, Z.X., Li, X.H., Kinny, P.D., and Wang, J., 1999, The breakup of Rodinia: Did it start with a mantle plume beneath South China?: Earth and Planetary Science Letters, v. 173, p. 171-181.

Li, Z.X., Li, X.H., Zhou, H., and Kinny, P.D., 2002, Grenvillian continental collision in south China: New SHRIMP U-Pb zircon results and implications for the configuration of Rodinia: Geology, v. 30, p. 163-166.

Li, Z.X., Evans, D.A.D., and Zhang, S., 2004, A 90° spin on Rodinia: Possible causal links between the Neoproterozoic supercontinent, superplume, true polar wander and low-latitude glaciation: Earth and Planetary Science Letters, v. 220, p. 409-421.

Lindsay, J.F., 1989, Depositional controls on glacial facies associations in a basinal setting, Late Proterozoic, Amadeus Basin, central Australia: Palaeogeography, Palaeoclimatology, Palaeoecology, v. 73, p. 205-232.

Lindsay, J.F., 2002, Supersequences, superbasins, supercontinents – Evidence from the Neoproterozoic – Early Palaeozoic basins of central Australia: Basin Research, v. 14, p. 207-223.

Lindsay, J.F., Korsch, R.J., and Wilford, J.R., 1987, Timing the breakup of a Proterozoic supercontinent: Evidence from Australian intracratonic basins: Geology, v. 15, p. 1061-1064.

Lindsay, J.F., Kruse, P.D., Green, O.R., Hawkins, E., Brasier, M.D., Cartlidge, J., and Corfield, R.M., 2005, The Neoproterozoic-Cambrian record in Australia: A stable isotope study: Precambrian Research, v. 143, p. 113-133.

Logan, G.A., Calver, C.R., Gorjan, P., Summons, R.E., Hayes, J.M., and Walter, M.R., 1999, Terminal Proterozoic mid-shelf benthic microbial mats in the Centralian Superbasin and their environmental significance: Geochimica et Cosmochimica Acta, v. 63, p. 1345-1358.

Lottermoser, B.G., and Ashley, P.M., 2000, Geochemistry, petrology and origin of Neoproterozoic ironstones in the eastern part of the Adelaide Geosyncline, South Australia: Precambrian Research, v. 101, p. 49-67.

Lund, K.L., Aleinikoff, J.N., Evans, K.V., and Fanning, C.M., 2003, SHRIMP U-Pb geochronology of Neoproterozoic Windermere Supergroup, central Idaho: Implications for rifting of western Laurentia and synchroneity of Sturtian glacial deposits: Geological Society of America Bulletin, v. 115, p. 349-372.

Macouin, M., Besse, J., Ader, M., Gilder, S., Yang, Z., Sun, Z., and Agrinier, P., 2004, Combined paleomagnetic and isotopic data from the Doushantuo carbonates, South China: Implications for the "snowball" Earth hypothesis: Earth and Planetary Science Letters, v. 224, p. 387-398.

Maloof, A.C., Kellogg, J.B., and Anders, A.M., 2002, Neoproterozoic sand wedges: Crack formation in frozen soils under diurnal forcing during a Snowball Earth: Earth and Planetary Science Letters, v. 204, p. 1-15.

Martin, M.W., Grazhdankin, D.V., Bowring, S.A., Evans, D.A.D., Fedonkin, M.A., and Kirschvink, J.L., 2000, Age of Neoproterozoic bilatarian body and trace fossils, White Sea, Russia: Implications for Metazoan evolution: Science, v. 288, p. 841-845.

McDougall, I., and Leggo, P.J., 1965, Isotopic age determinations on granitic rocks from Tasmania: Geological Society (Australia) Journal, v. 12, p. 295-332.

McKirdy, D.M., Burgess, J.M., Lemon, N.M., Yu, X., Cooper, A.M., Gostin, V.A., Jenkins, R.J.F., and Both, R.A., 2001, A chemostratigraphic overview of the late Cryogenian interglacial sequence in the Adelaide Fold-Thrust Belt, South Australia: Precambrian Research, v. 106, p. 149-186.

McMechan, M.E., 2000, Vreeland diamictites – Neoproterozoic glaciogenic slope deposits, Rocky Mountains, northeast British Columbia: Bulletin of Canadian Petroleum Geology, v. 48, p. 246-261.

McMenamin, M.A.S., 2004, Climate, paleoecology and abrupt change during the Late Proterozoic: A consideration of causes and effects, *in* Jenkins, G.S., et al., eds., The extreme Proterozoic: Geology, geochemistry, and climate: American Geophysical Union Geophysical Monograph 146, p. 215-229.

Meffre, S., Direen, N.G., Crawford, A.J., and Kamenetsky, V., 2004, Mafic volcanic rocks on King Island, Tasmania: Evidence for 579 Ma break-up in east Gondwana: Precambrian Research, v. 135, p. 177-191.

Miller, C.A., 2004, Re-Os dating of algal laminites: Reduction-enrichment of metals in the sedimentary environment and evidence of new geoporphyrins: M.Sc. Thesis, University of Saskatchewan.

Moores, E.M., 1991, Southwest U.S. – East Antarctic (SWEAT) connection: A hypothesis: Geology, v. 19, p. 425-428.

Morse, J.W., Luther III, G.W., 1999, Chemical influences on trace metal-sulfide interactions in anoxic sediments: Geochimica et Cosmochimica Acta, v. 63, p. 3373-3378.

Narbonne, G.M., and Gehling, J.G., 2003, Life after snowball: The oldest complex Ediacaran fossils: Geology, v. 31, p. 27-30.

Noffke, N., Knoll, A.H., and Grotzinger, J.P., 2002, Sedimentary controls on the formation and preservation of microbial mats in siliciclastic deposits: A case study from the Upper Neoproterozoic Nama Group, Namibia: Palaios, v. 17, p. 533-544.

Nogueira, A.C.R., Riccomini, C., Sial, A.N., Moura, C.A.V., and Fairchild, T.R., 2003, Soft-sediment deformation at the Neoproterozoic Puga cap carbonate (southwestern Amazon Craton, Brazil): Confirmation of rapid icehouse to greenhouse transition in snowball Earth: Geology, v. 31, p. 613-616.

Olcott, A.N., Sessions, A.L., Corsetti, F.A., Kaufman, A.J., and de Oliviera, T.F., 2005, Biomarker evidence for photosynthesis during Neoproterozoic glaciation: Science, v. 310, p. 471-474.

Park, J.K., 1997, Paleomagnetic evidence for low-latitude glaciation during deposition of the Neoproterozoic Rapitan Group, Mackenzie Mountains, N.W.T., Canada: Canadian Journal of Earth Sciences, v. 34, p. 34-49.

Peltier, W.R., Tarasov, L., Vettoretti, G., and Solheim, L.P., 2004, Climate dynamics in deep time: Modeling the "Snowball bifurcation" and assessing the plausibility of its occurrence, *in* Jenkins, G.S., et al., eds., The extreme Proterozoic: Geology, geochemistry, and climate: American Geophysical Union Geophysical Monograph 146, p. 107-124.

Peucker-Ehrenbrink, B., and Hannigan, R.E., 2000, Effects of black shale weathering on the mobility of rhenium and platinum group elements: Geology, v. 28, p. 475-478.

Peucker-Ehrenbrink, B., and Jahn, B.-M., 2001, Rhenium-osmium isotope systematics and platinum group element concentrations: loess and the upper continental crust: Geochemistry Geophysics Geosystems, v. 2, Paper 2001GC000172.

Pierrehumbert, R.T., 2004, High levels of atmospheric carbon dioxide necessary for the termination of global glaciation: Nature, v. 429, p. 646-649.

Pierrehumbert, R.T., 2005, Climate dynamics of a hard snowball Earth: Journal of Geophysical Research, v. 110, paper 2004JD005162.

Pierson-Wickmann, A.-C., Reisberg, L., and France-Lanord, C., 2002, Behavior of Re and Os during low-temperature alteration: Results from Himalayan soils and altered black shales: Geochimica et Cosmochimica Acta, v. 66, p. 1539-1548.

Pisarevsky, S.A., Li, Z.X., Grey, K., and Stevens, M.K., 2001, A palaeomagnetic study of Empress 1A, a stratigraphic drillhole in the Officer Basin: Evidence for a low-latitude position of Australia in the Neoproterozoic: Precambrian Research, v. 110, p. 93-108.

Pisarevsky, S.A., Wingate, M.T.D., Powell, C.M., Johnson, S., and Evans, D.A.D., 2003, Models of Rodinia assembly and fragmentation, *in* Yoshida, M., et al., eds., Proterozoic East Gondwana: Supercontinent assembly and breakup: Geological Society (London) Special Publications 206, p. 35-55.

Pollard, D., and Kasting, J.F., 2004, Climate-ice sheet simulations of Neoproterozoic glaciation before and after collapse to Snowball Earth, *in* Jenkins, G.S., et al., eds., The extreme Proterozoic: Geology, geochemistry, and climate: American Geophysical Union Geophysical Monograph 146, p. 91-105.

Powell, C.A., Preiss, W.V., Gatehouse, C.C., Krapez, B., and Li, Z.X., 1994, South Australian record of a Rodinian epicontinental basin and its mid-Neoproterozoic breakup (~ 700 Ma) to form the Palaeo-Pacific Ocean: Tectonophysics, v. 237, p. 113-140.

Preiss, W.V., 1990, A stratigraphic and tectonic overview of the Adelaide Geosyncline, South Australia, *in* Jago, J.B., and Moore, P.S., eds., The evolution of a late Precambrian – early Paleozoic rift complex: The Adelaide Geosyncline: Geological Society of Australia Special Publication 16, p. 1-33.

Preiss, W.V. (compiler), 1993, Neoproterozoic, *in* Drexel, J.F., et al., eds., The Geology of South Australia. Volume 1, The Precambrian: South Australia Department of Mines and Energy, Geological Survey of South Australia Bulletin 54, p. 170-203.

Preiss, W.V., 2000, The Adelaide Geosyncline of South Australia and its significance in Neoproterozoic continental reconstruction: Precambrian Research, v. 100, p. 21-63.

Preiss, W.V., and Forbes, B.G., 1981, Stratigraphy, correlation, and sedimentary history of Adelaidean (Late Proterozoic) basins in Australia: Precambrian Research, v. 15, p. 255-304.

Preiss, W.V., Walter, M.R., Coats, R.P., and Wells, A.T., 1978, Lithological correlations of Adelaidean glaciogenic rocks in parts of the Amadeus Basin, Ngalia, and Georgina Basins: BMR Journal of Australian Geology and Geophysics, v. 3, p. 43-53.

Preiss, W.V., Dyson, I.A., Reid, P.W., and Cowley, W.M., 1998, Revision of lithostratigraphic classification of the Umberatana Group: Mines and Energy South Australia Journal, v. 9, p. 36-42.

Ravizza, G., Turekian, K.K., and Hay, B.J., 1991, The geochemistry of rhenium and osmium in recent sediments from the Black Sea: Geochimica et Cosmochimica Acta, v. 55, p. 3741-3752.

Rigwell, A., and Kennedy, M., 2004, Secular changes in the importance of neritic carbonate deposition as a control on the magnitude and stability of Neoproterozoic ice ages, *in* Jenkins, G.S., et al., eds., The extreme Proterozoic: Geology, geochemistry, and climate: American Geophysical Union Geophysical Monograph, v. 146, p. 55-72.

Ridgwell, A.J., Kennedy, M.J., and Caldeira, K., 2003, Carbonate deposition, climate stability, and Neoproterozoic ice ages: Science, v. 302, p. 859-862.

Rieu, R., Allen, P.A., Plötze, M., and Pettke, T., 2007, Climatic cycles during a Neoproterozoic "snowball" glacial epoch: Geology, v. 35, p. 299-302.

Ripley, E.M., Park, Y.-R., Lambert, D.D., and Frick, L.R., 2001, Re-Os isotopic composition and PGE contents of Proterozoic carbonaceous argillites, Virginia Formation, Northeastern Minnesota: Organic Geochemistry, v. 32, p. 857-866.

Ross, G.M., and Villeneuve, M.E., 1997, U-Pb geochronology of stranger stones in Neoproterozoic diamictites, Canadian Cordillera: Implications for provenance and ages of deposition: Radiogenic Age and Isotopic Studies, Report 10, Geological Survey of Canada Current Research, 1997-F, p. 141-155.

Schaefer, B.F., and Burgess, J.M., 2003, Re-Os isotopic age constraints on deposition in the Neoproterozoic Amadeus Basin: Implications for the 'Snowball Earth': Geological Society (London) Journal, v. 160, p. 825-828.

Schermerhorn, L.J.G., 1974, Late Precambrian mixtites: Glacial and/or non-glacial?: American Journal of Science, v. 274, p. 673-824.

Schidlowski, M., Eichmann, R., and Junge, C., 1975, Precambrian sedimentary carbonates: Carbon and oxygen isotope geochemistry and implications for the terrestrial oxygen budget: Precambrian Research, v. 2, p. 1-69.

Schieber, J., 1986, The possible role of benthic microbial mats during the formation of carbonaceous shales in shallow Mid-Proterozoic basins: Sedimentology, v. 33, p. 521-536.

Schmidt, P.W., and Williams, G.E., 1995, The Neoproterozoic climatic paradox: Equatorial palaeolatitude for Marinoan glaciation near sea level in South Australia: Earth and Planetary Science Letters, v. 134, p. 107-124.

Schmidt, P.W., Williams, G.E., and Embleton, B.J.J., 1991, Low palaeolatitude of Late Proterozoic glaciation: Early timing of remanence in haematite of the Elatina Formation, South Australia: Earth and Planetary Science Letters, v. 105, p. 355-367.

Schrag, D.P., Berner, R.A., Hoffman, P.F., and Halverson, G.P., 2002, On the initiation of a snowball Earth: Geochemistry, Geophysics, Geosystems, v. 3, paper 2001GC000219.

Sears, J.W., and Price, R.A., 2003, Tightening the Siberian connection to western Laurentia: Geological Society of America Bulletin, v. 115, p. 943-953.

Seilacher, A., 1999, Biomat-related lifestyles in the Precambrian: Palaios, v. 14, p. 86-93.

Selby, D., and Creaser, R.A., 2003, Re-Os geochronology of organic-rich sediments: an evaluation of organic matter analysis methods: Chemical Geology, v. 200, p. 225-240.

Selby, D., and Creaser, R.A., 2005, Direct radiometric dating of the Devonian-Mississippian time-scale boundary using the Re-Os black shale geochronometer: Geology, v. 33, p. 545-548.

Selby, D., Creaser, R.A., Stein, H.J., Markey, R.J., and Hannah, J.L., 2007, Assessment of the ^{187}Re decay constant by cross calibration of Re-Os molybdenite and U-Pb zircon chronometers in magmatic ore systems: Geochimica et Cosmochimica Acta, v.71, p. 1999-2013.

Shields, G.A., 2005, Neoproterozoic cap carbonates: A critical appraisal of existing models and the plumeworld hypothesis: Terra Nova, v. 17, p. 299-310.

Shields, G.A., 2007, A normalised seawater strontium isotope curve and the Neoproterozoic-Cambrian chemical weathering event: eEarth Discuss, v. 2, p. 69-84.

Smoliar, M.I., Walker, R.J., and Morgan, J.W., 1996, Re-Os ages of Group IIA, IIIA, IVA, and IVB iron meteorites: Science, v. 271, p. 1099-1102.

Sohl, L.E., Christie-Blick, N., and Kent, D.V., 1999, Paleomagnetic polarity reversals in Marinoan (ca. 600 Ma) glacial deposits of Australia: Implications for the duration of low-latitude glaciation in Neoproterozoic time: Geological Society of America Bulletin, v. 111, p. 1120-1139.

Sun, W., Arculus, R.J., Bennett, V.C., Eggins, S.M., and Binns, R.A., 2003a, Evidence for rhenium enrichment in the mantle wedge from submarine arc-like volcanic glasses (Papua New Guinea): Geology, v. 31, p. 845-848.

Sun, W., Bennett, V.C., Eggins, S.M., Kamenetsky, V.S., and Arculus, R.J., 2003b, Enhanced mantle-to-crust rhenium transfer in undegassed arc magmas: Nature, v. 422, p. 294-297.

Sundby, B., Martinez, P., and Gobeil, C., 2004, Comparative geochemistry of cadmium, rhenium, uranium, and molybdenum in continental margin sediments: Geochimica et Cosmochimica Acta, v. 68, p. 2485-2493.

Thompson, M.D., and Bowring, S.A., 2000, Age of the Squantum 'tillite', Boston Basin, Massachusetts: U-Pb zircon constraints on Terminal Neoproterozoic glaciation: American Journal of Science, v. 300, p. 630-655.

Trindade, R.I.F., and Macouin, M., 2007, Palaeolatitude of glacial deposits and palaeogeography of Neoproterozoic ice ages: Comptes Rendus Geoscience, v. 339, p. 200-211.

Trindade, R.I.F., Font, E., D'Agrella-Filho, M.S., Nogueira, A.C.R., and Riccomini, C., 2003, Low-latitude and multiple geomagnetic reversals in the Neoproterozoic Puga cap carbonate, Amazon Craton: Terra Nova, v. 15, p. 441-446.

Turner, N.J., 1993, K-Ar geochronology in the Arthur Metamorphic Complex, Ahrberg Group and Oonah Formation, Corinna District: Mineral Resources Tasmania Report 1993/12.

Turner, N.J., Black, L.P., and Kamperman, M., 1998, Dating of Neoproterozoic and Cambrian orogenies in Tasmania: Australian Journal of Earth Sciences, v. 45, p. 789-806.

Van der Weijden, C.H., 2002, Pitfalls of normalization of marine geochemical data using a common divisor: Marine Geology, v. 184, p. 167-187.

Veevers, J.J., Walter, M.R., and Scheibner, E., 1997, Neoproterozoic tectonics of Australia-Antarctica and Laurentia and the 560 Ma birth of the Pacific Ocean reflect the 400 M.y. Pangean supercycle: Journal of Geology, v. 105, p. 225-242.

Veizer, J., and Hoefs, J., 1976, The nature of $^{18}O/^{16}O$ and $^{13}C/^{12}C$ secular trends in sedimentary carbonate rocks: Geochimica et Cosmochimica Acta, v. 40, p. 1387-1397.

Vieira, L.C., Trindade, R.I.F., Nogueira, A.C.R., and Ader, M., 2007, Identification of a Sturtian cap carbonate in the Neoproterozoic Sete Lagoas carbonate platform, Bambuí Group, Brazil: Comptes Rendus Geoscience, v. 339, p. 240-258.

Waldron, H.M., and Brown, A.V., 1993, Geological setting and petrochemistry of Eocambrian-Cambrian volcano-sedimentary rock sequences from southeast King Island, Tasmania: Mineral Resources Tasmania Report 1993/28.

Walter, M.R., Veevers, J.J., Calver, C.R., and Grey, K., 1995, Neoproterozoic stratigraphy of the Centralian Superbasin, Australia: Precambrian Research, v. 73, p. 173-195.

Walter, M.R., Veevers, J.J., Calver, C.R., Gorjan, P., and Hill, A.C., 2000, Dating the 840-544 Ma Neoproterozoic interval by isotopes of strontium, carbon, and sulfur in seawater, and some interpretative models: Precambrian Research, v. 100, p. 371-433.

Wedepohl, K.H., 1971, Environmental influences on the chemical composition of shales and clays, *in* Ahrens, L.H., et al., eds., Physics and chemistry of the Earth, volume 8: Pergamon, Oxford, UK, p. 305-333.

Wedepohl, K.H., 1991, The composition of the upper Earth's crust and the natural cycles of selected metals. Metals in natural raw materials. Natural resources, *in* Merian, E., ed., Metals and their compounds in the environment: VCH, Weinheim, Germany, p. 3-17.

Weil, A.B., Van der Voo, R., Niocaill, C.M., and Meert, J.G., 1998, The Proterozoic supercontinent Rodinia: Paleomagnetically derived reconstructions for 1100 to 800 Ma: Earth and Planetary Science Letters, v. 154, p. 13-24.

Williams, G.E., 1975, Late Precambrian glacial climate and the Earth's obliquity: Geological Magazine, v. 112, p. 441-465.

Williams, G.E., 1979, Sedimentology, stable-isotope geochemistry and paleoenvironment of dolostones capping late Precambrian glacial sequences in Australia: Geological Society (Australia) Journal, v. 26, p. 377-386.

Williams, G.E., 1993, History of the Earth's obliquity: Earth-Science Reviews, v. 34, p. 1-45.

Williams, G.E., 2004, The paradox of Proterozoic glaciomarine deposition, open seas and strong seasonality near the palaeo-equator: Global implications, *in* Eriksson, P.G., et al., eds., The Precambrian Earth: Tempos and events: Developments in Precambrian Geology 12, Elsevier Amsterdam, p. 448-459.

Williams, G.E., and Gostin, V.A., 2000, Mantle plume uplift in the sedimentary record: Origin of kilometre-deep canyons within late Neoproterozoic successions, South Australia: Geological Society (London) Journal, v. 157, p. 759-768.

Williams, G.E., and Schmidt, P.W., 2004, Neoproterozoic glaciation: Reconciling low paleolatitudes and the geologic record, *in* Jenkins, G.S., et al., eds., The extreme Proterozoic: Geology, geochemistry, and climate: American Geophysical Union Geophysical Monograph 146, p. 145-159.

Williams, L.A., and Reimers, C., 1983, Role of bacterial mats in oxygen-deficient marine basins and coastal upwelling regimes: Preliminary report: Geology, v. 11, p. 267-269.

Wingate, M.T.D., and Giddings, J.W., 2000, Age and palaeomagnetism of the Mundine Well dyke swarm, Western Australia: Implications for an Australia-Laurentia connection at 755 Ma: Precambrian Research, v. 100, p. 335-357.

Wingate, M.T.D., Campbell, I.H., Compston, W., and Gibson, G.M., 1998, Ion microprobe U-Pb ages for Neoproterozoic basaltic magmatism in south-central Australia and implications for the breakup of Rodinia: Precambrian Research, v. 87, p. 135-159.

Wingate, M.T.D., Pisarevsky, S.A., and Evans, D.A.D., 2002, Rodinia connections between Australia and Laurentia: no SWEAT, no AUSWUS?: Terra Nova, v. 14, p. 121-128.

Xiao, S., 2004, Neoproterozoic glaciations and the fossil record, *in* Jenkins, G.S., et al., eds., The extreme Proterozoic: Geology, geochemistry, and climate: American Geophysical Union Geophysical Monograph 146, p. 199-214.

Xu, B., Jian, P., Zheng, H., Zou, H., Zhang, L., Liu, D., 2005, U-Pb zircon geochronology and geochemistry of Neoproterozoic volcanic rocks in the Tarim Block of northwest China: Implications for the breakup of Rodinia supercontinent and Neoproterozoic glaciations: Precambrian Research, v. 136, p. 107-123.

Yamashita, Y., Takahashi, Y., Haba, H., Enomoto, S., and Shimizu, H., 2007, Comparison of reductive accumulation of Re and Os in seawater-sediment systems: Geochimica et Cosmochimica Acta, v. 71, p. 3458-3475.

Yang, Z., Sun, Z., Yang, T., and Pei, J., 2004, A long connection (750-380 Ma) between South China and Australia: Paleomagnetic constraints: Earth and Planetary Science Letters, v. 220, p. 423-434.

Young, G.M., 1988, Proterozoic plate tectonics, glaciation, and iron-formations: Sedimentary Geology, v. 58, p. 127-144.

Young, G.M., 1995, Are Neoproterozoic glacial deposits preserved on the margins of Laurentia related to the fragmentation of two supercontinents?: Geology, v. 23, p. 153-156.

Young, G.M., 2002, Stratigraphic and tectonic settings of Proterozoic glaciogenic rocks and banded-iron formations: Relevance to the snowball Earth debate: Journal of African Earth Sciences, v. 35, p. 451-466.

Young, G.M., and Gostin, V.A., 1988, Stratigraphy and sedimentology of Sturtian glacigenic deposits in the western part of the North Flinders Basin, South Australia: Precambrian Research, v. 39, p. 151-170.

Young, G.M., and Gostin, V.A., 1989, An exceptionally thick upper Proterozoic (Sturtian) glacial succession in the Mount Painter area, South Australia: Geological Society of America Bulletin, v. 101, p. 834-845.

Young, G.M., and Gostin, V.A., 1990, Sturtian glacial deposition in the vicinity of the Yankaninna Anticline, North Flinders Basin, South Australia: Australian Journal of Earth Sciences, v. 37, p. 447-458.

Young, G.M., and Gostin, V.A., 1991, Late Proterozoic (Sturtian) succession of the North Flinders Basin, South Australia: An example of temperate glaciation in an active rift setting: Geological Society of America Special Paper 261, p. 207-222.

Zhao, J., McCulloch, M.T., and Korsch, R.J., 1994, Characterisation of a plume-related ~ 800 Ma magmatic event and its implications for basin formation in central-southern Australia: Earth and Planetary Science Letters, v. 121, p. 349-367.

Zhou, C., Tucker, R., Xiao, S., Peng, Z., Yuan, X., and Chen, Z., 2004, New constraints on the ages of Neoproterozoic glaciations in South China: Geology, v. 32, p. 437-440.

CHAPTER 4

Re-Os Isotope Systematics of Late Mesoproterozoic – Earliest Neoproterozoic Organic-rich Mudrocks of the Lapa Formation (Vazante Group, Brazil) and Horsethief Creek Group (Windermere Supergroup, Western Canada)

Part of this chapter is published in the following source:
Azmy, K., Kendall, B., Creaser, R.A., Heaman, L., Misi, A., and de Oliveira, T.F., Global correlation of the Vazante Group, São Francisco Basin, Brazil: Re-Os and U-Pb radiometric age constraints: Precambrian Research, Accepted.

4.1 INTRODUCTION

Global and regional correlation of the Neoproterozoic rock record is significantly hampered by a sparse paleontological record and a general paucity of suitable igneous material for precise U-Pb zircon age determinations. Consequently, efforts at establishing a composite Neoproterozoic timescale have been based largely on chemostratigraphy (primarily $\delta^{13}C$ and $^{87}Sr/^{86}Sr$ from well-preserved carbonates, and to a lesser extent $\delta^{34}S_{sulfate}$ and $^{34}S_{sulfide}$ from carbonates and shales) and identification of distinctive glaciogenic diamictite – cap carbonate pairs (Kaufman et al., 1991, 1993, 1997; Derry et al., 1992; Kaufman and Knoll, 1995; Kennedy et al., 1998; Jacobsen and Kaufman, 1999; Gorjan et al., 2000, 2003; Walter et al., 2000; Hurtgen et al., 2005; Halverson et al., 2005; Halverson, 2006), with radiometric calibration limited to a small number of precise U-Pb zircon ages. The Neoproterozoic geochronological database suggests that diamictite – cap carbonate pairs cannot be unambiguously used as chronostratigraphic marker horizons because cap carbonates with similar lithological and geochemical characteristics (e.g., "Marinoan" and "Sturtian"-type; Kennedy et al., 1998) span over 50-100 M.y. (Corsetti and Lorentz, 2006; see Chapter 3). Similarly, carbon isotope chemostratigraphic profiles can exhibit a significant degree of scatter even within a single cratonic block and require numerical calibration by independent radiometric and/or biostratigraphic tie points to be useful for global correlation schemes (e.g., Melezhik et al., 2001; Shen et al., 2005; Jiang et al., 2007; Zhou and Xiao, 2007). Thus far, Sr isotopes show limited promise (e.g., elevated $^{87}Sr/^{86}Sr$ above 0.7080 after ca. 600 Ma associated with Gondwana/Pan-African amalgamation) (Asmerom et al., 1991; Derry et al., 1992; Kaufman et al., 1993; Kaufman and Knoll, 1995; Jacobsen and Kaufman, 1999; Walter et al., 2000; Melezhik et al., 2001) and the resolution of the S isotope record is too coarse for chemostratigraphy. Consequently, precise and reliable radiometric age determinations remain a high priority for calibration of the Neoproterozoic geological timescale.

Owing to a lack of radiometric age control, the timing of Neoproterozoic glaciation on many continents remains uncertain. In South America, Neoproterozoic strata are preserved in the São Francisco Craton, Amazon Craton (and Paraguay Belt), and Rio de la Plata Craton, and in adjoining craton margins (Misi et al., 2007). From the São Francisco Craton, cap carbonates overlying glaciogenic rocks are known from the southern São Francisco Basin (Carrancas – Macaúbas – Jequitaí diamictites and overlying Sete Lagoas Formation, Bambuí Group; Peryt et al., 1990; Misi et al., 2007; Vieira et al., 2007), Irecê and Una-Utinga Basins (Bebedouro diamictites and overlying pink dolostones ["Unit C"]; Una Group; Misi et al., 2007), and the external zone of the adjoining Brasilia Fold Belt on the western margin of the craton (Santo Antônio do Bonito and Poco Verde – Morro do Calcario – Lapa Formation diamictites at the base and top of the Vazante Group, respectively, and the overlying Lapa Formation cap carbonate; Brody et al., 2004; Olcott et al., 2005; Azmy et al., 2006) (Figure 4.1), and are suggested to be correlative with the "Sturtian" glaciation. Glaciogenic diamictites of the Puga Formation and overlying "Marinoan"-type cap carbonates (basal Araras and Corumbá Groups) from the southeastern Amazon craton are suggested to be correlative with the "Marinoan" glaciation (de Alvarenga and Trompette, 1992; Boggiani et al., 2003; Nogueira et al., 2003, 2007; Trindade et al., 2003; de Alvarenga et al., 2004; Font et al., 2006; Misi et al., 2007; de Alvarenga et al., in press). Global and regional correlations of South American Neoproterozoic successions typically rely upon comparison of least-altered carbonate $^{87}Sr/^{86}Sr$ and $\delta^{13}C$ chemostratigraphic trends with composite Neoproterozoic chemostratigraphic profiles (e.g., Iyer et al., 1995; Misi and Veizer, 1998; Azmy et al., 2001, 2006; Misi et al., 2007).

Most age constraints are from the Bambuí Group in the southern São Francisco Basin and the correlative Una Group in the Irecê and Una-Utinga Basins. A Pb-Pb carbonate age of 740 ± 22 Ma (MSWD = 0.66) may provide a close estimate of the depositional age for the Sete Lagoas Formation (Babinski and Kaufman, 2003). The stratigraphically underlying glaciogenic Macaúbas Group is younger than ca. 900 Ma based on U-Pb SHRIMP detrital zircon ages from within the glacial deposits (Pedrosa-Soares et al., 2000), and a U-Pb zircon and baddeleyite age of 906 ± 2 Ma (from a dike cross-cutting the older Espinhaco Supergroup (Machado et al., 1989 as cited in Babinski et al., 1999). Other radiometric dates are from Rb-Sr, K-Ar, and Pb-Pb whole-rock and mineral dating of fine-grained sedimentary rocks and carbonates. These include various Rb-Sr (between 932 ± 30 Ma and 667 ± 30 Ma) and K-Ar (901 ± 21 Ma and 876 ± 20 Ma) dates for the glacial Bebedouro Formation that underlies the Una Group (Macedo, 1982 as cited in Misi and Veizer, 1998; Macedo and Bonhomme, 1984 as cited in

Fairchild et al., 1996), ca. 800 Ma, and between 774 ± 20 Ma and 514 ± 33 Ma for the Salitre Formation of the Una Group (Macedo and Bonhomme, 1984 as cited in Azmy et al., 2001; Trindade et al., 2004). Rb-Sr whole-rock and clay mineral, and K-Ar clay mineral ages for Bambuí Group sedimentary rocks from the southern part of the São Francisco Basin (Minas Gerais State, Brazil) range between 695 ± 12 Ma and 560 ± 40 Ma, and between 662 ± 18 Ma and ca. 478 Ma, respectively (Babinski et al., 1999 and references therein). The Rb-Sr and K-Ar ages are widely considered to reflect partial or complete resetting of isotope systematics during the ca. 640-560 Ma Pan-African – Brasiliano Orogeny (Chemale et al., 1993; Martins-Neto et al., 2001; Pedrosa-Soares et al., 2001; da Silva et al., 2005). Pb-Pb carbonate ages of 686 ± 69 Ma, 565 ± 89 Ma, and 521 ± 53 Ma (Babinski et al., 1999), and a galena Pb-Pb date of 650 ± 50 Ma (Iyer et al., 1992) have also been obtained from the Bambuí Group. The 686 ± 69 Ma age (derived from undeformed carbonates in the central part of the basin) represents a minimum depositional age for the Sete Lagoas Formation, but younger carbonate ages reflect Pb isotope resetting during fluid flow associated with late-stage tectonic deformation and granitic plutonism at ca. 530-500 Ma (Babinski et al., 1999; D'Agrella-Filho et al., 2000; Pedrosa-Soares et al., 2001; Trindade et al., 2004).

The age of the Vazante Group and its stratigraphic position relative to the better-known Bambuí Group is uncertain. A Rb-Sr whole-rock date of 600 ± 50 Ma obtained for fine-grained sedimentary rocks of the upper Vazante Group (formerly the "Vazante Formation") again likely reflects isotopic homogenization during the Brasiliano Orogeny (Amaral and Kawashita, 1967 as cited in Azmy et al., 2001). Cloud and Dardenne (1973) noted the similarity of columnar stromatolites in the Lagamar Formation of the Vazante Group to *Conophyton metula* Kirichenko stromatolites observed in Middle Riphean (ca. 1400-1050 Ma; Raaben, 2005; Ronkin et al., 2006) assemblages in Russia. Both *Conophyton metula* and *Conophyton cylindricus* Maslov stromatolites are now well known from the Vazante Group, but the genus *Conophyton* is presently regarded as characteristic of both Mesoproterozoic and Neoproterozoic carbonates (Dardenne, 2005; Dardenne et al., 2005). In contrast, the Bambuí Group contains *Gymnosolenide* stromatolites, consistent with a Neoproterozoic age (Karfunkel and Hoppe, 1988; Fairchild et al., 1996). Azmy et al. (2006) suggest that the upper Vazante Group diamictites and basal Lapa Formation are correlative with the Chuos Formation and Rasthof Formation cap carbonate (maximum age of 746 ± 2 Ma; Hoffman et al., 1996), respectively, on the basis of similar least-altered $^{87}Sr/^{86}Sr$ values of ~ 0.7068 (Azmy et al., 2001; Yoshioka et al., 2003; Halverson et al., 2005). Such low $^{87}Sr/^{86}Sr$ values are not observed in the Bambuí Group ($^{87}Sr/^{86}Sr$ ~ 0.7074-0.7075; Misi and Veizer, 1998; Misi et al., 2007). In addition, Vazante Group carbonates have moderately positive $\delta^{13}C$ values (< +4‰) (Misi et al., 2007) that contrast with highly positive values (e.g., > + 10‰) observed in the Bambuí Group (Iyer et al., 1995). Some support for correlation between the Vazante and Bambuí (and Una) Groups is suggested by their broad lithostratigraphic similarities (glaciogenic diamictite overlain by carbonate sequences), presence of Pb-Zn mineralization, and new $^{87}Sr/^{86}Sr$ isotope data for the upper Vazante (0.7076-0.7079) and Una (0.7075-0.7078) Groups (Misi et al., 2005, 2007 and references therein).

In contrast to the São Francisco craton, C and Sr isotope and biostratigraphic data are not available for the siliciclastic-dominated lower Windermere Supergroup of the southeastern Canadian Cordillera. Sparse radiometric age constraints provide poor geochronological control for the glaciogenic Toby Formation and intercalated magmatic rocks (Irene Formation). The Windermere Supergroup is older than a U-Pb zircon age of 569.6 ± 5.3 Ma from volcanic rocks of the unconformably overlying Hamill – Gog Group (Colpron et al., 2002). A minimum age constraint for the Toby Formation is provided by a Re-Os black shale age of 607.8 ± 4.7 Ma from the Old Fort Point Formation (Kendall et al., 2004), a post-glacial fine-grained marker unit interpreted as a deep-water equivalent of carbonates capping diamictites of a younger Windermere glaciation (Ross and Murphy, 1988; Ross et al., 1995). The Huckleberry Volcanics (northeastern United States) represents the lithostratigraphic equivalent of the Irene Formation and has a Sm-Nd whole-rock age of 762 ± 44 Ma (Devlin et al., 1988). A U-Pb zircon age of 736 +23/-17 Ma for granitic gneisses unconformably underlying possible equivalents of the Toby Formation (McDonough and Parrish, 1991) may provide a maximum age on the timing of glaciation. Similar U-Pb zircon ages of 740 ± 36 Ma (Parrish and Scammell, 1988) and 728 +9/-7 Ma (Evenchick et al., 1984) are also known from granitic gneisses unconformably underlying the Windermere Supergroup in British Columbia (Ross et al., 1995). The Toby Formation may be correlative with other basal Windermere diamictites preserved along the margin of western Laurentia, such as the Rapitan Group of the Mackenzie Mountains, northwest Canada (maximum age of 755 ± 18 Ma from U-Pb zircon dating of a leucogranite dropstone in the Sayunei Formation; Ross and Villeneuve, 1997), Edwardsburg Formation of Idaho (U-Pb SHRIMP zircon ages of 685 ± 7 Ma and 684 ± 4 Ma from felsic volcanic rocks interbedded with glaciogenic diamictites; Lund et al., 2003), and the Scout Mountain Member of the Pocatello Formation, Idaho (upper diamictite unit bracketed between U-Pb SHRIMP zircon ages of 709 ± 5 Ma and 667 ± 5 Ma from tuffaceous beds; Fanning and Link, 2004). These age constraints loosely bracket the Toby Formation between 750 and 607 Ma.

Both the Lapa Formation and the lower Horsethief Creek Group are associated with glaciogenic diamictites that are suggested to be correlative with other radiometrically dated glacial deposits assigned to the "Sturtian" glaciation (see Chapter 3). Thus, precise Re-Os depositional age constraints from both rock units would further test the concept of a putative global "Sturtian" glaciation. Here, I evaluate complex Re-Os isotope systematics preserved in the Lapa Formation and lower Horsethief Creek Group. The Lapa Formation black shales are suggested to preserve primary depositional age information for the associated glaciogenic diamictites, whereas the Re-Os data from organic-rich shales and argillaceous carbonates of the Horsethief Creek Group are equivocal, and do not provide reliable age information.

4.2 GEOLOGICAL SETTING

4.2.1 Vazante Group, Brazil

Basement rocks in the São Francisco craton comprise Archean to Paleoproterozoic granite-greenstone belts and medium- to high-grade metamorphic rocks that are overlain by Mesoproterozoic volcaniclastic, siliciclastic, and subordinate carbonate rocks of the Espinhaco and Chapada Diamantina Groups (Chemale et al., 1993; Azmy et al., 2001; Misi et al., 2005). Stratigraphic relationships at the base of the Vazante Group are uncertain. The Mesoproterozoic to Neoproterozoic (ca. 1170-900 Ma) Paranoá Group comprises mudrocks, quartzites, and minor carbonates and is considered the youngest stratigraphic unit underlying diamictites in the Brasilia Fold Belt (Karfunkel and Hoppe, 1988). The Paranoá Group contains abundant *Conophyton, Baicalia, and Jacutophyton* stromatolites (Fairchild et al., 1996) that are also present in the dolomites of the upper Vazante Group (Azmy et al., 2001). The latter was considered to be a possible equivalent of the Paranoá Group (Fairchild et al., 1996), but as described above, litho- and chemo-stratigraphy suggest the Vazante Group may be correlative with the younger Bambuí Group (Azmy et al., 2001, 2006; Misi et al., 2005, 2007, and references therein). The paleogeographic setting of the Vazante Group is poorly known, and may have been a passive margin environment or a Early-Middle Neoproterozoic foreland basin developed during the onset of early Brasiliano orogenesis associated with closing of the Brazilides Ocean (Dardenne, 2000; da Silva et al., 2005; Azmy et al., 2006 and references therein). The Bambuí (comprising fine-grained carbonates, mudrocks, and subordinate arkosic sandstones) and Paranoá Groups are suggested to record deposition in a restricted epicontinental sea in a foreland basin and an open marine platform, respectively (Santos et al., 2000).

Predominantly carbonate rocks of the Vazante Group are exposed ~ 300 km along the external zone of the Brasilia Fold Belt at the western margin of the São Francisco craton in east-central Brazil (Azmy et al., 2006; see Figure 4.1). The present lithostratigraphic subdivision of the ~ 5000 m thick Vazante Group (e.g., Dardenne, 2001; Azmy et al., 2001, 2006; Misi et al., 2007) includes the ~ 250 m thick basal Santo Antônio do Bonito Formation (Misi et al., 2007) that contains possible glaciogenic diamictite ("D1") in its uppermost part (Dardenne, 2001) and is overlain by feldspathic sandstone (Azmy et al., accepted; Figure 4.2A). Overlying units of the lower and middle Vazante Group include ~ 1000 m of rhythmites and carbonate fluorapatites (Rocinha Formation), ~ 250 m of predominantly stromatolitic carbonate with subordinate conglomerate (Lagamar Formation), and > 1000 m of dark-colored slate with interbedded carbonate lenses (Serra do Garrote Formation) (Azmy et al., 2006; Misi et al., 2007). The upper Vazante Group comprises ~ 1600 m of stromatolitic dolostone, organic-rich mudrocks, rhythmic marls, and carbonate diamictite (Serra do Poço Verde Formation) and ~ 300 m of carbonate diamictite and stromatolitic dolostone (Morro do Calcário Formation) (Azmy et al., 2001, 2006; Olcott et al., 2005; Misi et al., 2007). In the Paracatú region, evidence for a glacial influence during deposition of the Serra do Poço

Verde Formation rests upon the presence of dropstones and the identification of the cold-water carbonate mineral glendonite (a pseudomorph after ikaite) within organic-rich mudrocks (Brody et al., 2004; Olcott et al., 2005). Despite the uncertainty regarding the absolute age of the Serra do Poço Verde Formation, biomarker analysis of extractable hydrocarbons from organic-rich shales has been used to evaluate ecological conditions during a putative ca. 740-700 Ma glaciation (Olcott et al., 2005). Pb-Zn mineralization is present within the middle Serra do Poço Verde (Lower Pamplona Member) and Morro do Calcário Formations (e.g., Vazante and Morro Agudo deposits; Misi et al., 2005) just below a sequence boundary that marks the top of the Vazante Group (Misi et al., 2007). A low $^{87}Sr/^{86}Sr$ isotope value of 0.7061 obtained from the Morro do Calcário Formation was suggested to reflect "Sturtian" glacial seawater (Azmy et al., 2001).

A diamictite unit ("DII") at the base of the 900 m thick Lapa Formation rests upon an unconformity (Misi et al., 2005), is associated with iron formation (Brody et al., 2004; Azmy et al., 2006), and may be overlain by a cap carbonate (Azmy et al., 2006). The DII diamictite is overlain by 10 m of dropstone-bearing organic-rich mudrocks interpreted to represent post-glacial deposition (Brody et al., 2004; Azmy et al., 2006). In turn, the mudrocks are overlain by predominantly fine-grained, rhythmically bedded and laminated mudstone and dolomite, and microbialaminites with subordinate stromatolitic dolostone (Azmy et al., 2001, 2006; Figure 4.2B). Near the base of the dolostone unit in drill hole MASW01 is a pronounced negative $\delta^{13}C_{carb}$ excursion (typically to –5‰, with one sample reaching –8‰; Figure 4.2C). Although the negative $\delta^{13}C_{carb}$ excursion has a coarse stratigraphic resolution (a dozen samples over 100 m of stratigraphy), the most negative $\delta^{13}C_{carb}$ values occur at the base and are succeeded by increasingly positive values upsection. On the basis of these observations, the basal Lapa Formation is suggested to be a "Sturtian" cap carbonate litho-facies (Azmy et al., 2001, 2006). A second negative $\delta^{13}C_{carb}$ excursion occurs in organic-rich mudrocks near the top of the Lapa Formation, but is not associated with diamictite or any evidence for glaciation (Azmy et al., 2006).

Metamorphism of the Vazante Group associated with the Pan-African – Brasiliano orogeny ranges from virtually unmetamorphosed to lower greenschist facies along the margin of the São Francisco craton to amphibolite-granulite facies near the

Brasilia Fold Belt (Dardenne, 2001; Azmy et al., 2001, 2006 and references therein). The Lapa Formation from the relatively unmetamorphosed sections of the Vazante Group is characterized by well-preserved dolomite textures (e.g., fabric-retentive argillaceous dolomites). Dolomite fluid inclusions from the upper Vazante Group suggests deep burial temperatures above 120-130°C (Azmy et al., 2001), but carbon isotope compositions of carbonates and organic matter do not appear to show correlated variations that could be ascribed to thermally-induced carbon isotope exchange (Azmy et al., 2006).

4.2.2 Toby Formation and Horsethief Creek Group, Western Canada

In the southeastern Canadian Cordillera (Figure 4.3), the Neoproterozoic Windermere Supergroup comprises up to 9 km of siliciclastic and subordinate carbonate and volcanic rocks deposited within a rift zone that evolved into a west-facing passive margin (Ross, 1991; Ross et al., 1995) or within a 2500 km long intracontinental rift system (Colpron et al., 2002). The Windermere succession is unconformably underlain and overlain by the Mesoproterozoic Belt-Purcell Supergroup and the Late Neoproterozoic – Paleozoic Hamill – Gog Groups, respectively (Ross et al., 1995; Colpron et al., 2002). Paleomagnetic data from middle Neoproterozoic rocks along western Laurentia, including the glaciogenic Rapitan Group (Mackenzie Mountains, N.W.T.), suggests deposition occurred at tropical to equatorial paleolatitudes (Park, 1997; Weil et al., 2006 and references therein).

Near the base of the Windermere Supergroup in the southeastern Canadian Cordillera, the partly glaciogenic Toby Formation occurs intercalated with, and is overlain by, sills and mafic volcanic rocks of the Irene Formation, and is unconformably underlain by siliciclastics of the Mount Nelson Formation (Ross et al., 1995) (Figure 4.4). Locally, a thin carbonate unit is found above the Toby Formation, and may represent a cap carbonate (Ross et al., 1995). The Toby Formation is up to 2500 m thick and is composed dominantly of massive diamictite with subordinate conglomerate, sandstone, and mudstone that partly reflects an origin by subaqueous sediment gravity flows during syn-depositional tectonism (Aalto, 1971; Glover and Price, 1976; Lis and Price, 1976; Root, 1987). Evidence for glaciomarine deposition includes dropstones within a lower siltstone member, local occurrence of striated clasts within an upper diamictite member, and rare extrabasinal igneous and metamorphic basement clast types (Aalto, 1971; Eisbacher, 1981, 1985). Deposition within a tectonically active rift environment is inferred for the Toby Formation on the basis of evidence for magmatic activity (Aalto, 1971; Glover and Price, 1796; Leclair, 1982), large-scale normal faulting (Lis and Price, 1976; Root, 1987), and large facies changes (Root, 1987). Rifting was suggested to be associated with Rodinia breakup along the northwestern margin of Laurentia and opening of the proto-Pacific Ocean (Ross, 1991; Ross et al., 1995; Colpron et al., 2002).

Overlying sedimentary rocks of the middle Windermere Supergroup comprise predominantly feldspathic sandstones and granule conglomerates ("grits") with mudrocks and subordinate carbonates (lower Horsethief Creek, Kaza, and middle Miette Groups) that were deposited in a large (> 50,000 km^2) northwest-trending longitudinal, basinal turbidite system (Ross et al., 1989, 1995). The > 5 km thick Horsethief Creek Group in the Purcell Mountains conformably overlies the Toby Formation (Poulton and Simony, 1980; Pell and Simony, 1987). Correlations among the Horsethief Creek Group (Selkirk, Purcell, and southern Cariboo Mountains), Kaza Group and overlying Cariboo Group (Cariboo Mountains), and Miette Group (Rocky Mountains) are hampered by structural complexities and metamorphism in the southern Canadian Cordillera (Ross and Murphy, 1988; Ross et al., 1995). However, a widespread, fine-grained marker unit (Old Fort Point Formation) occurs within the lower Horsethief Creek Group, middle Kaza Group, and middle Miette Group and represents a break in coarse-grained clastic sediment deposition associated with an eustatic sea-level rise following the meltback of the second Windermere glaciation (Ross and Murphy, 1988).

In the southern Canadian Cordillera, the Windermere Supergroup is preserved in the Omineca Crystalline Belt and in the western part of the Rocky Mountain Fold and Thrust Belt (Ross et al., 1995). Metamorphism, deformation, and magmatism affecting the Windermere Supergroup are Early Jurassic to Eocene in age, and related to the Mesozoic collision of two large composite allochthonous terranes with western Laurentia (e.g., Monger et al., 1982; Brown et al., 1986; Gabrielse and Yorath, 1991; Greenwood et al., 1991). Metamorphism reached upper amphibolite facies in parts of the Omineca Belt (e.g., Greenwood et al., 1991), but lower-greenschist facies rocks are preserved in the Purcell Mountains (Root, 1987). Widespread circulation of meteoric water (to depths of

15 km) was associated with Eocene extensional and strike slip faulting in the southern Omineca Belt (Nesbitt and Muehlenbachs, 1989, 1995, 1997). Fluid inclusions from quartz ± carbonate veins in chlorite- and biotite-grade rocks from the northern and central Purcell Mountains have homogenization temperatures of between 150°C and 240°C and between 230°C and 300°C, respectively (Nesbitt and Muehlenbachs, 1995).

4.3 SAMPLES AND ANALYTICAL METHODS

4.3.1 Lapa Formation

Pyritic, organic-rich shale samples from drill core MASW01 (Plate 4.1) were obtained from a ~ 15 m stratigraphic interval (depth: 924-939 m) near the base of the Lapa Formation within the DII diamictite (Azmy et al., 2006; see Figure 4.2B). The sampled stratigraphic interval occurs well below the onset of a negative $\delta^{13}C_{carb}$ excursion (at ~ 865 m depth). Although the stratigraphy in MASW01 is essentially undeformed (Azmy et al., 2006), vein-rich horizons, sheared surfaces, and folded carbonate veins are present within the mudrocks at 924-939 m depth, suggesting post-depositional hydrothermal fluid flow within the shales. Thus, carbonate veins were carefully avoided during sample preparation. Pyrite is present as both framboids and disseminations, and as aggregates associated with veinlets. X-ray diffraction (XRD) reveals a mineral assemblage comprising quartz + muscovite/illite + pyrite ± feldspar ± rutile, consistent with metamorphism of the basal Lapa Formation being no higher than chlorite-grade. A second stratigraphic interval of dark gray shale associated with the negative $\delta^{13}C$ excursion near the top of MASW01 was also sampled at depths 211-217 m.

4.3.2 Horsethief Creek Group

Fine-grained relatively organic-poor, argillaceous carbonate (Plate 4.2) and pyritic, organic-rich shale (Plate 4.3) whole-rock samples from the basal Horsethief Creek Group were obtained from a highway roadcut (~ 50 cm stratigraphic interval) near the Panorama ski area, Purcell Mountains, southeastern British Columbia (50°27′41″ N, 116°14′20″ W; see Figure 4.3). The contact with the underlying Toby Formation is not exposed at this roadcut. Both shale and carbonate whole-rocks show clear evidence of fluid flow in the form of carbonate veinlets up to 1 cm thick. Metamorphic mineral assemblages of slates in the Delphine Creek area ~ 10-30 km to the west typically comprise muscovite + chlorite + quartz ± chloritoid, with biotite-grade metamorphic rocks located to the southwest (Root, 1987). XRD analysis of samples BK-HG-02-51B (argillaceous carbonate) and BK-HG-02-50B (organic-rich shale) reveal a mineral assemblage of calcite + muscovite + smectite + pyrite, and quartz + dolomite + muscovite + gypsum + calcite + pyrite, respectively. Roadcut strata are folded and display well-developed cleavage.

4.3.3 Analytical Methods

Powder aliquots of the basal Lapa Formation and Horsethief Creek Group comprise between 21 g and 192 g, and between 18 g and 68 g of material, respectively. One small organic-rich shale sample (~ 6 g) from the Horsethief Creek Group (BK-HG-02-50D) was also prepared from material directly adjacent to a carbonate veinlet. Protocols for metal-free processing of organic-rich sedimentary rocks (ORS) to produce powdered samples, subsequent chemical digestion, separation, and purification of Re and Os, and isotopic analysis by isotope dilution – negative thermal ionization mass spectrometry (ID-NTIMS) are described in Appendix A. Rhenium-Os isotope analysis of the Horsethief Creek Group shales and carbonates represented the initial phase of the thesis research. At that time, suitable CrO_3 powders with low Re blanks had not yet been identified (see Chapter 2), and a large Re procedural blank correction (~ 73 pg) from a Cr^{VI}-H_2SO_4 solution derived from Fisher Scientific CrO_3 was applied to all Horsethief Creek Group analyses. This Re blank correction was ~ 4-6 % of sample Re for organically-lean argillaceous carbonates, but < 0.3% for organic-rich shale samples. Osmium procedural blanks from Fisher Scientific CrO_3 averaged 0.65 ± 0.17 pg with blank $^{187}Os/^{188}Os$ of 0.19 ± 0.06 (1σ, n = 4). Chemical digestion of the Lapa Formation organic-rich shales was carried out using Cr^{VI}-H_2SO_4 solutions prepared from Fluka Chemika CrO_3 (Lots #447647/1 and 1177884). Average total procedural blanks for Re and Os from these solutions was 7.8 ± 2.2 pg and 0.36 ± 0.20 pg, respectively, with blank $^{187}Os/^{188}Os$ of 0.26 ± 0.11 (1σ, n = 8).

4.4 RESULTS

4.4.1 Lapa Formation

Rhenium and Os data for the Lapa Formation are presented in Table 4.1. Eight of eleven samples from 924-939 m depth in MASW01 show moderate enrichment in Re (3.1-16.9 ppb) and Os (113-490 ppt) abundances. Three of these samples, plus the dark grey shales from 211-217 m depth, are strongly depleted in Re (0.1-0.9 ppb) and Os (26-54 ppt) and their abundances are comparable to estimated average present-day eroding upper continental crust (~ 0.2-2 ppb Re and 30-50 ppt Os; Esser and Turekian, 1993; Peucker-Ehrenbrink and Jahn, 2001; Hattori et al., 2003; Sun et al., 2003a, b). The $^{187}Re/^{188}Os$ and $^{187}Os/^{188}Os$ isotope ratios range from 21 to 281 and from 1.21 to 5.51, respectively. Regression of the Re-Os isotope data from 924-939 m depth yields an imprecise Re-Os date of 993 ± 46 Ma (2σ, n = 11, Mean Square of Weighted Deviates [MSWD] = 35, Model 3, initial $^{187}Os/^{188}Os$ [I_{Os}] = 0.75 ± 0.16; Figure 4.5A). Excluding the three Re- and Os-poor samples yields a marginally older Re-Os date of 1100 ± 77 Ma (n = 8, MSWD = 16, Model 3, I_{Os} = 0.33 ± 0.30; Figure 4.5B) that may reflect minimal accumulation of hydrogenous (e.g., seawater-derived) Re and Os in these three samples.

4.4.2 Horsethief Creek Group

Five argillaceous carbonate samples from the Horsethief Creek Group have Re (1.2-2.0 ppb) and Os (31-39 ppt) abundances similar to average upper crust, whereas three organic-rich shale samples are enriched in Re (25-33 ppb) and Os (367-471 ppt) (Table 4.2). A large range in $^{187}Re/^{188}Os$ and $^{187}Os/^{188}Os$ isotope ratios is observed, but can be subdivided into two narrow groups on the basis of lithology. The argillaceous carbonates have $^{187}Re/^{188}Os$ and $^{187}Os/^{188}Os$ isotope ratios of 368-408 and 4.65-5.22, respectively, whereas the organic-rich shales have elevated isotope ratios of 621-715 for $^{187}Re/^{188}Os$ and 7.40-8.37 for $^{187}Os/^{188}Os$. Separate regressions of the shale and carbonate subsets yields highly imprecise and overlapping Model 3 Re-Os dates of 629 ± 260 Ma (n = 5, MSWD = 49, I_{Os} = 0.8 ± 3.0) and 743 ± 300 Ma (n = 7, MSWD = 9.6, I_{Os} = 0.1 ± 2.0), respectively. Regression of all Re-Os isotope data for the Horsethief Creek Group yields an imprecise date of 616 ± 20 Ma (n = 12, MSWD = 21, Model 3, I_{Os} = 0.96 ± 0.18; Figure 4.5C).

4.5 DISCUSSION

4.5.1 A 1100 – 1000 Ma Depositional Age for the base of the Lapa Formation

Multiple studies have shown that the process of hydrocarbon maturation and migration does not adversely affect the Re-Os isotope systematics of shale source rocks (Creaser et al., 2002; Selby and Creaser, 2003, 2005; see Chapter 5). Kendall et al. (2004) obtained a Re-Os age of 607.8 ± 4.7 Ma (MSWD = 1.2) for a chlorite-grade, low TOC (~ 0.5%) post-glacial black shale in the Old Fort Point Formation, which is in agreement with existing age constraints that bracketed this shale between ca. 710-667 Ma (age constraints for the first Windermere glaciation in Idaho; Lund et al., 2003; Fanning and Link, 2004) and ca. 570 Ma (Colpron et al., 2002). However, the robustness of the Re-Os deposition-age geochronometer during prograde metamorphism remains unknown. The Re-Os isotope systematics of ORS are known to be disturbed by hydrothermal fluid flow (ca. 1730 Ma Wollogorang Formation, McArthur Basin, northern Australia; Chapter 5).

A large degree of scatter (MSWD = 35) is observed for the Re-Os regression of the samples from the basal Lapa Formation shales (924-939 m depth in MASW01) associated with the DII diamictite at the top of the Vazante Group. Such scatter may result from detrital Os with variable I_{Os}, I_{Os} heterogeneity resulting from temporal evolution of seawater Os isotope composition, and/or post-depositional mobilization of Re and Os. The effect of detrital Os on the Os-poor samples (33-54 ppt; similar to average present-day upper continental crust) may be significant. However, the Cr^{VI}-H_2SO_4 digestion medium has successfully allowed the generation of Model 1 Re-Os ages for rocks with 0.5-1.0% TOC and containing Re and Os abundances as low as ~ 2 ppb and ~ 80 ppt, respectively (Kendall et al., 2004, Chapter 3). Thus, the MSWD of 16 for the regression defined by the eight samples with higher Re and Os abundances (> 3 ppb and > 100 ppt, respectively) is not likely to be explained solely by a component of detrital Os. The Re-Os date (1100 ± 77 Ma) and I_{Os} (0.33 ± 0.30) for the regression defined by these eight samples marginally overlaps the age (993 ± 46 Ma) and I_{Os} (0.75 ± 0.16) derived from regression of the whole dataset. This may reflect a component of detrital Os that is more radiogenic than the hydrogenous Os in the low-Os samples (thus resulting in a younger date), as the Cr^{VI}-H_2SO_4 digestion medium may partially dissolve detrital mineral phases from shale matrices (Ravizza et al., 1991). Consequently, the Re-Os age of 1100 ± 77 Ma may represent the more appropriate age estimate for the basal Lapa Formation because it is defined by samples with greater hydrogenous enrichment of Re and Os.

Because of the large sampling interval (~ 15 m) represented by this regression, it is conceivable that I_{Os} heterogeneity derived from variations in seawater Os isotope composition may be one explanation for the observed scatter because of the short residence time of Os in present-day seawater (~ 10^4 years; Oxburgh, 1998, 2001; Levasseur et al., 1999). The sedimentation rate of the Lapa Formation shales is unknown. However, two sample subsets from depths 930.35-932.35 m and 935.10-937.10 m, each representing a stratigraphic interval of ~ 2 m, should represent deposition from seawater with a more homogeneous Os isotope composition (unless sedimentation rates were anomalously low). Coherent Re-Os isochrons with Model 1 ages diagnostic of homogeneous I_{Os} have been obtained for ~ 1-2 m stratigraphic intervals from Neoproterozoic shales in Australia (see Chapter 3). Three of the four samples from the 935.10-937.10 m interval are the Re- and Os-poor samples (see Table 4.1), and it is difficult to distinguish I_{Os} heterogeneity derived from temporal evolution of seawater Os isotopes versus that derived from detrital Os. The three samples from the 930.35-932.35 m interval show a very limited range in $^{187}Re/^{188}Os$ and $^{187}Os/^{188}Os$ isotope ratios (which ultimately motivated sampling over a larger stratigraphic interval). Nevertheless, variation in $I_{Os\ (1100\ Ma)}$ (0.31-0.39) for the three 930.35-932.35 m samples is not significantly different from the entire observed variation (0.25-0.39) for the eight Re- and Os-enriched samples. Thus, temporal evolution in seawater Os isotope composition during deposition of the sampled stratigraphic interval may not fully account for the complex Re-Os isotope systematics in the Lapa Formation.

It is possible that some post-depositional mobilization of Re and Os has occurred in the basal Lapa Formation shales. Weathering is not a likely cause because drill core samples were used for analysis and Lapa Formation argillaceous dolomites are generally fabric-retentive, suggesting excellent petrographic preservation (Azmy et al., 2006). The XRD analysis (quartz + muscovite/illite + pyrite ± feldspar ± rutile) suggests metamorphism of the basal Lapa Formation in MASW01 related to the Brasiliano/Pan-African orogeny was no greater than the lowermost greenschist facies (e.g., chlorite-grade slates; Dardenne, 2001; Azmy et al., 2001, 2006) and the drill core strata are relatively undeformed (Azmy et al., 2006). Abundant carbonate veins observed in the drill core suggest some hydrothermal fluid flow has occurred through the Lapa Formation at this locality. In view of evidence for resetting of Pb-Pb isotope systematics and remagnetization of Bambuí Group carbonates during late-stage (ca. 530-500 Ma) Brasiliano deformation and magmatism (Babinski et al., 1999; D'Agrella-Filho et al., 2000; Pedrosa-Soares et al., 2001; Trindade et al., 2004), material with abundant carbonate veins was avoided during sampling so as to minimize Re and Os disturbance by hydrothermal fluids. Nevertheless, the scatter in the Re-Os regressions for the Lapa Formation implies that there might have been some mobilization of Re and Os by fluid flow.

Three lines of evidence suggest that the overall disturbance of Re and Os isotope systematics may be relatively minor such that ~ 1000-1100 Ma may be considered a reasonable depositional age for the basal Lapa Formation. The I_{Os} from the regression defined by the eight Re- and Os-enriched samples (0.33 ± 0.30) lies between reasonable minimum and maximum values of ~ 0.12 (e.g., chondritic or mantle compositions at ca. 1000-1100 Ma; Walker et al., 2002a, b) and ~ 1.0-1.5 (e.g., present-day estimated average for currently eroding upper continental crust and riverine inputs; Esser and Turekian, 1993; Levasseur et al., 1999; Peucker-Ehrenbrink and Jahn, 2001; Hattori et al., 2003), respectively, that could represent possible seawater Os isotope compositions at ca. 1000-1100 Ma. In contrast, in Chapter 5 I show that the Wollogorang Formation black shales affected by hydrothermal fluid flow yield an anomalously high I_{Os} of 3.5 ± 1.5, as well as a significantly younger Re-Os "date" (1359 ± 150 Ma; MSWD = 86) relative to the accepted depositional age of ca. 1730 Ma for this black shale (based on U-Pb SHRIMP zircon dates from interbedded tuffaceous green claystone layers; Page et al., 2000). Secondly, an absence of detrital zircons yielding concordant U-Pb ages younger than ca. 1000 Ma (Azmy et al., accepted) is generally consistent with the Re-Os dates for the basal Lapa Formation. Finally, the presence of *Conophyton metula* Kirichenko in the Lagamar Formation is consistent with a late Mesoproterozoic to early Neoproterozoic age for the Vazante Group (Cloud and Dardenne, 1973; Dardenne, 2005; Dardenne et al., 2005). *Conophyton* stromatolites are also found in the Paranoá Group whose age is loosely constrained between 1170 and 950 Ma based on Rb-Sr and U-Pb dates (Fairchild et al., 1996 and references therein). Accordingly, the Vazante Group is older than the Bambuí Group for which a Pb-Pb carbonate age of 740 ± 22 Ma (Sete Lagoas Formation; Babinski and Kaufman, 2003) and the presence of *Gymnosolenide* stromatolites suggest a Neoproterozoic age (Karfunkel and Hoppe, 1988; Fairchild et al., 1996).

The basal Lapa Formation is characterized by a negative $\delta^{13}C$ excursion (to ≤ –5‰) and overlies a dropstone-bearing diamictite unit that contains iron formation (Brody et al., 2004; Olcott et al., 2005; Azmy et al., 2006). In conjunction with a single Sr isotope signature of ~ 0.7068, the basal Lapa Formation was suggested to be correlative with the Rasthof Formation cap carbonate on the Congo Craton, Namibia (Azmy et al., 2001, 2006). The Rasthof Formation cap carbonate, together with the underlying Chuos Formation diamictites, are constrained to be younger than a U-Pb zircon age of 746 ± 2 Ma from volcanic rocks in the underlying Ombombo Subgroup (Hoffman et al., 1996). If the Lapa – Rasthof correlation is indeed correct, then a large scale perturbation of the Re-Os systematics in the basal Lapa Formation shales (e.g., associated with 640-560 Ma Pan African – Brasiliano orogenesis) is required to explain the significantly older Re-Os dates of ca. 1000-1100 Ma (Figure 4.6). Such a large perturbation requires loss of Re relative to Os (or gain of Os relative to Re) to explain the erroneously old date. The wide range in Re and Os abundances and isotope ratios is not consistent with large-scale homogenization by metamorphism, particularly if restricted to lowermost greenschist facies. It is also difficult to explain how systematic redistribution of Re and Os can yield a relatively coherent isochron (e.g., MSWD = 16 for the eight Re- and Os-enriched samples) corresponding to a date that is erroneously ~ 250-400 Ma older without significantly changing the I_{Os} of the regression (e.g., as was documented for the Wollogorang Formation). Finally, the hydrothermal remobilization of Re and Os in the Wollogorang Formation resulted in an erroneously younger, rather than older, age (see Chapter 5).

Thus, the most reasonable interpretation for the Re-Os isotope results is that the Lapa Formation has an age of ca. 1000-1100 Ma, and that the glacial deposits of the basal Lapa Formation and Vazante Group are not correlative with the "Sturtian" ice age (ca. 750-643 Ma; see Chapter 3). Thus, the diamictite horizons in the Vazante Group may record evidence of late Mesoproterozoic to earliest Neoproterozoic glaciations in which case the record of negative carbon isotope excursions in carbonates capping diamictites may be represented in each of the three Eras of the Proterozoic Eon (e.g., see Bekker et al., 2005 for a Paleoproterozoic example). Similar U-Pb zircon ages have not been obtained for glaciogenic diamictites on other continents, and the Vazante Group glaciogenic diamictites may only represent a regional glaciation. If correct, the new Re-Os age constraints for the Lapa Formation provide further support to the hypothesis that diamictite – cap carbonate pairs do not represent chronostratigraphic marker horizons (Corsetti and Lorentz, 2006; see Chapter 3).

Dating of the youngest detrital zircon fraction in a sedimentary rock establishes a maximum age constraint on the timing of deposition, which may or may not closely approximate the true depositional age. U-Pb zircon results provide additional and consistent depositional age constraints that support the Re-Os age estimates. The youngest detrital U-Pb zircon results from the basal Lapa Formation shales and the feldspathic sandstones above the Santo Antônio do Bonito Formation provide maximum depositional age estimates of 988 ± 15 Ma and 1000 ± 25 Ma, respectively (Azmy et al., in review). These U-Pb ages are equivalent within 2σ analytical uncertainties, suggesting the Vazante Group is no older than ca. 1000 Ma, which is generally consistent with the Re-Os estimates of ca. ~ 1000-1100 Ma. The Re-Os date of 1100 ± 77 Ma derived from the eight samples with higher Re and Os abundances is only marginally older (given 2σ analytical uncertainties) than the youngest U-Pb detrital zircon age (988 ± 15 Ma) for the basal Lapa Formation shales. This is consistent with relatively minor disturbance of Re-Os systematics in these shales by post-depositional processes. If correct, then the syn-diagenetic to epigenetic Pb-Zn mineralization in the middle Serra do Poço Verde and Morro do Calcário Formations (Misi et al., 2005, 2007) may represent a discrete ore-forming event from the mineralization preserved in the Bambuí Group and correlatives (Misi et al., 2007).

4.5.2 Correlation of the Vazante and Paranoá Groups?

Available radiometric age constraints for the Paranoá Group are sparse, but include a maximum age constraint of 1170 ± 24 Ma (Rb-Sr date from metavolcanics that are interpreted to represent the timing of metamorphism in the underlying Araí Group) and minimum age constraints of 906 ± 2 Ma (U-Pb zircon and baddeleyite date from a dike cross-cutting the Espinhaco Supergroup, the upper part of which may be correlative with the Paranoá Group; Machado et al. 1989 as cited in Babinski et al., 1999). Diamictite facies and Pb-Zn mineralization similar to those of the carbonate-rich Vazante Group have not been described from the siliciclastic-dominated Paranoá Group. Considering the available radiometric age constraints, however, it is possible the Paranoá and Vazante Groups were deposited at least partly synchronously, consistent with a number of geochemical and biostratigraphic similarities between them. *Conophyton metula* and *Conophyton cylindricus* stromatolites (as well as *Baicalia* and *Jacutophyton* stromatolites) are present in both Vazante and Paranoá Group carbonates, and are distinct from the *Gymnosolenide* stromatolites of the Bambuí Group (Karfunkel and Hoppe, 1988; Fairchild et al., 1996; Dardenne, 2005; Dardenne et al., 2005). Upper Paranoá Group carbonates have slightly positive $\delta^{13}C_{carb}$ values between 0 and +2‰ (Santos et al., 2000) that are somewhat reminiscent of the Vazante Group carbonates (moderately positive $\delta^{13}C_{carb} < +4‰$), but distinct from the highly positive values ($\delta^{13}C_{carb} > +10‰$) of some Bambuí Group carbonates (Iyer et al., 1995; Misi et al., 2007). An absence of volcanic ash layers within the Vazante Group supports an open marine (e.g., passive margin) depositional environment, similar to that inferred for the Paranoá Group (Santos et al., 2000), rather than a foreland basin associated with younger Brasiliano orogenesis (Dardenne, 2000; Azmy et al., 2006 and references therein).

4.5.3 Re-Os Isotope Systematics of the Horsethief Creek Group

The Model 3 Re-Os date of 616 ± 20 Ma (MSWD = 21) derived from the organic-rich shales and argillaceous carbonates of the Horsethief Creek Group may be erroneously young if the underlying Toby Formation is correlative with other radiometrically dated diamictites of the first Windermere glaciation (e.g., an age between 750 and 667 Ma; Ross et al., 1995; Ross and Villeneuve, 1997; Lund et al., 2003;

Fanning and Link, 2004). Instead, the Re-Os date for the Horsethief Creek Group overlaps the Re-Os depositional age of 607.8 ± 4.7 Ma for the Old Fort Point Formation (Kendall et al., 2004), which is interpreted as a lithostratigraphic equivalent of cap carbonates overlying diamictites of the second Windermere glaciation in the central and northern Canadian Cordillera (Ross et al., 1995). Thus, the Re-Os date of 616 ± 20 Ma may reflect significant post-depositional mobility of Re and Os during chlorite-grade metamorphism and/or hydrothermal fluid flow associated with Mesozoic and Cenozoic orogenesis in the Southern Canadian Cordillera. For example, a highly imprecise Re-Os date of 457 ± 84 Ma (n = 6, Model 3, MSWD = 212, I_{Os} = 1.55 ± 0.65) was obtained for Late Neoproterozoic (upper Miette Group) chlorite-grade, organic-rich slates (containing 7-13 ppb Re and 143-178 ppt Os) in the northern Selwyn Ranges (recalculated from Kendall, 2003). This Re-Os date was based on samples obtained from a highway roadcut located ~ 74 km and 60 km west of Jasper, Alberta and the Old Fort Point Formation sampling locality, respectively (and located a few kilometres northeast of the first occurrences of chloritoid-bearing Miette Group phyllites; McDonough and Simony, 1988). Five of the six analyses define a well-fitted regression corresponding to a Re-Os date of 472 ± 18 Ma (Model 3, MSWD = 5.7, I_{Os} = 1.40 ± 0.14). Despite the absence of independent radiometric age constraints for the Upper Miette Group and given the lack of evidence for an Ordovician metamorphic event, the Re-Os isotope data suggest partial resetting of isotope systematics during chlorite-grade metamorphism, resulting in an erroneously young (and meaningless) date and elevated I_{Os}. A mechanism enabling an apparently systematic re-distribution of Re and Os and preservation of a well-correlated trend between $^{187}Re/^{188}Os$ and $^{187}Os/^{188}Os$ isotope systematics is not known (Kendall, 2003). Nevertheless, a similar interpretation could be invoked to explain the ca. 616 Ma age and relatively high I_{Os} (0.96 ± 0.18, similar to the value of ~ 1.06 for present-day seawater; Sharma et al., 1997; Levasseur et al., 1998; Woodhouse et al., 1999; Peucker-Ehrenbrink and Ravizza, 2000) for the Horsethief Creek Group.

However, the Re-Os isotope data for the three organic-rich shale and five argillaceous carbonate samples define two discrete narrow groupings on a Re-Os isochron diagram. Low Os (< 40 ppt) abundances suggest a possibly significant detrital Os component in the argillaceous carbonates. Accordingly, an alternative explanation for the ca. 616 Ma Re-Os date for the Horsethief Creek Group is preservation of distinctive I_{Os} in the carbonate and shale subsets. For example, calculated sample I_{Os} at 685 Ma (e.g., age of the glaciogenic Edwardsburg Formation, Idaho; Lund et al., 2003) for the carbonates and shales is 0.44-0.61 and 0.09-0.28, respectively, and may reflect a radiogenic detrital Os component in the carbonates. The distinct $I_{Os\ (685\ Ma)}$ may also reflect a change in the contemporaneous seawater Os isotope composition. It should also be kept in mind the Re-Os isotope system in organic-rich carbonates is more susceptible to post-depositional mobilization of Re and Os relative to organic-rich shales (see Chapter 2). Unfortunately, separate regressions of the shale and carbonate subsets yield highly imprecise and overlapping Model 3 Re-Os dates (629 ± 260 Ma, MSWD = 49; and 743 ± 300 Ma, MSWD = 9.6), respectively, that do not enable clear contrasts to be distinguished between them. However, the scatter associated with the shale regression does suggest some post-depositional mobility of Re and Os. One sample of organic-rich shale obtained immediately adjacent to a carbonate veinlet (BK-02-HG-50D) contains a broadly similar Re and Os abundance, but appreciably lower ^{187}Re/^{188}Os and ^{187}Os/^{188}Os isotope ratio (see Table 4.2) relative to the other two shale samples. Calculated sample $I_{Os\ (715\ Ma)}$ values for the organic-rich shale analyses are negative, suggesting significant post-depositional disturbance to Re-Os isotope systematics if the Horsethief Creek Group is older than 715 Ma. Ultimately, the Horsethief Creek Group Re-Os isotope data do not yield unambiguous depositional age information or constrain the degree of post-depositional mobility associated with chlorite-grade metamorphism or fluid flow.

4.6 CONCLUSIONS

The Re-Os isotope systematics of organic-rich shales (basal Lapa Formation) associated with glaciogenic diamictites at the top of the Vazante Group (east-central Brazil), suggest that although minor post-depositional mobility of Re and Os may have occurred during fluid flow and/or chlorite-grade metamorphism, primary depositional age information is still preserved. A Re-Os date of 1100 ± 77 Ma (MSWD = 16) is defined by Lapa Formation shales containing hydrogenous enrichment of Re and Os, and together with U-Pb detrital zircon age constraints, the basal Lapa Formation is suggested to be ca. 1100-1000 Ma. Stromatolite biostratigraphy supports these age estimates and indicate the

Vazante Group is older than the Neoproterozoic Bambuí Group but possibly partly correlative with the Mesoproterozoic to earliest Neoproterozoic Paranoá Group. Glaciogenic diamictites in the Vazante Group are not correlative with "Sturtian" (ca. 750-643 Ma) glacial deposits, do not have known time-equivalent correlatives on other continents, and may represent a late Mesoproterozoic to earliest Neoproterozoic regional glaciation. Accordingly, the Re-Os shale and U-Pb zircon age constraints on the Lapa Formation cast doubt on the significance of photosynthetic and eukaryotic biomarker data from the Serra do Poço Verde Formation (Olcott et al., 2005) for evaluating ecological complexity and diversity during a putative ca. 740-700 Ma "Snowball Earth" glaciation. However, the interpretation by Olcott et al. (2005) concerning a complex ecosystem flourishing in a stratified photic zone (oxic surface water and euxinic deep water) is consistent with hypotheses of stratified Mesoproterozoic ocean basins under conditions of lower atmospheric pO_2 relative to the Phanerozoic (e.g., Arnold et al., 2004). The ca. 1100-1000 Ma diamictite – cap carbonate pair preserved at the top of the Vazante Group suggests such lithostratigraphic associations, together with negative carbon isotope excursions, may be represented in each of the three Eras of the Proterozoic Eon. In addition, the new age constraints for the Lapa Formation provide support to a growing body of geochronological evidence suggesting diamictite – cap carbonate pairs do not represent chronostratigraphic marker horizons (Corsetti and Lorentz, 2006; see Chapter 3).

A Re-Os date of 616 ± 20 Ma (MSWD = 21) was obtained for argillaceous carbonates and organic-rich shales of the Horsethief Creek Group that overlies glaciogenic diamictites of the Toby Formation (Windermere Supergroup, western Canada). This date is younger than previous radiometric age constraints for the timing of the first Windermere glaciation in western Laurentia (ca. 750-667 Ma). Because of a narrow range in Re and Os isotope ratios associated with the carbonate and shale subsets, unambiguous depositional age information and constraints on the degree of post-depositional mobility of Re and Os from the Horsethief Creek Group is not forthcoming. Nevertheless, some minor post-depositional mobility of Re and Os has occurred in the Lapa Formation and Horsethief Creek Group shales, suggesting the Re-Os geochronometer may not generally yield precise depositional age information from ORS affected by hydrothermal fluid flow and/or chlorite-grade metamorphism.

Table 4.1. Re-Os data for the basal Lapa Formation organic-rich shales, upper Vazante Group, east-central Brazil.

Sample (depths in m)	Re (ppb)	Os (ppt)	^{192}Os (ppt)	^{187}Re/^{188}Os	^{187}Os/^{188}Os	rho	$I_{Os\ (993\ Ma)}$*	$I_{Os\ (1100\ Ma)}$*
MASW01-211.00-213.00-1	0.28 ± 0.01	30.4 ± 0.4	10.3 ± 0.2	54.37 ± 1.56	1.8055 ± 0.0588	0.575	0.90	0.80
MASW01-213.00-215.00-1	0.13 ± 0.01	35.0 ± 0.3	12.7 ± 0.2	20.74 ± 0.77	1.2072 ± 0.0186	0.344	0.86	0.82
MASW01-215.00-217.00-1	0.15 ± 0.01	25.8 ± 0.3	9.0 ± 0.2	33.84 ± 1.28	1.5897 ± 0.0376	0.492	1.03	0.96
MASW01-924.00-930.35-1	4.72 ± 0.02	182.5 ± 1.5	51.7 ± 0.4	181.81 ± 1.64	3.6392 ± 0.0356	0.732	0.61	0.28
MASW01-930.35-932.35-1	3.09 ± 0.01	115.2 ± 0.8	31.7 ± 0.2	194.08 ± 1.45	3.9777 ± 0.0296	0.730	0.74	0.39
MASW01-930.35-932.35-2	3.12 ± 0.01	112.6 ± 0.9	30.6 ± 0.2	202.60 ± 1.63	4.0964 ± 0.0360	0.704	0.72	0.35
MASW01-930.35-932.35-3	3.82 ± 0.01	135.6 ± 1.0	36.8 ± 0.2	206.42 ± 1.45	4.1256 ± 0.0297	0.685	0.68	0.31
MASW01-933.10-935.10-1	11.53 ± 0.04	341.4 ± 2.9	82.8 ± 0.5	277.24 ± 2.04	5.5144 ± 0.0480	0.631	0.89	0.39
MASW01-934.35-936.35-1	13.47 ± 0.05	425.2 ± 2.9	107.6 ± 0.5	249.13 ± 1.50	4.9710 ± 0.0307	0.607	0.82	0.36
MASW01-935.10-937.10-1A	0.37 ± 0.01	35.1 ± 0.4	11.8 ± 0.2	62.59 ± 1.56	1.8498 ± 0.0391	0.702	0.81	0.69
MASW01-935.10-937.10-1B	0.36 ± 0.01	33.4 ± 0.4	11.2 ± 0.2	64.47 ± 1.75	1.9084 ± 0.0479	0.699	0.83	0.72
MASW01-935.10-937.10-2	16.85 ± 0.06	489.7 ± 3.5	119.3 ± 0.5	260.90 ± 1.63	5.4486 ± 0.0341	0.561	0.76	0.25
MASW01-935.10-937.10-3	0.91 ± 0.01	54.3 ± 0.5	[illegible].1 ± 0.2	106.17 ± 1.61	2.5032 ± 0.0364	0.805	0.73	0.54
MASW01-937.10-939.10-1	3.41 ± 0.01	119.1 ± 1.0	32.0 ± 0.3	211.59 ± 1.94	4.2295 ± 0.0420	0.751	0.70	0.32

Uncertainties are quoted at the 2σ level.

*I_{Os} = initial ^{187}Os/^{188}Os isotope ratio calculated assuming the age in brackets.

Table 4.2. Re-Os data for the basal Horsethief Creek Group, lower Windermere Supergroup, Western Canada.

Sample	Lithology	Re (ppb)	Os (ppt)	^{192}Os (ppt)	^{187}Re/^{188}Os	^{187}Os/^{188}Os	rho	$I_{Os\ (665\ Ma)}$*	$I_{Os\ (616\ Ma)}$*
BK-HG-02-50A	shale	32.05 ± 0.11	456.4 ± 2.2	91.3 ± 0.2	698.48 ± 2.63	8.2848 ± 0.0202	0.367	0.27	1.08
replicate		32.87 ± 0.11	468.6 ± 2.3	96.1 ± 0.2	680.64 ± 2.57	7.8976 ± 0.0203	0.363	0.09	0.88
replicate		32.94 ± 0.11	470.5 ± 2.4	96.5 ± 0.2	678.84 ± 2.61	7.8861 ± 0.0229	0.357	0.09	0.88
BK-HG-02-50B	shale	26.25 ± 0.09	367.1 ± 1.8	73.0 ± 0.2	715.27 ± 2.83	8.3710 ± 0.0223	0.458	0.16	0.99
BK-HG-02-50C	carbonate	1.65 ± 0.01	34.5 ± 0.4	8.9 ± 0.1	367.52 ± 5.54	4.6549 ± 0.0762	0.840	0.44	0.86
BK-HG-02-50D	shale	25.11 ± 0.08	379.9 ± 2.1	80.5 ± 0.2	620.87 ± 2.54	7.4043 ± 0.0260	0.408	0.28	1.00
BK-HG-02-50E	carbonate	1.55 ± 0.01	31.1 ± 0.4	7.8 ± 0.1	395.28 ± 6.65	5.0586 ± 0.0944	0.837	0.52	0.98
BK-HG-02-51A	carbonate	1.83 ± 0.01	36.2 ± 0.4	9.1 ± 0.1	400.72 ± 4.54	5.0597 ± 0.0585	0.848	0.46	0.93
replicate		1.88 ± 0.01	38.4 ± 0.4	9.7 ± 0.1	386.81 ± 5.42	5.0492 ± 0.0785	0.822	0.61	1.06
replicate		1.89 ± 0.01	37.4 ± 0.5	9.3 ± 0.1	404.79 ± 5.91	5.2180 ± 0.0861	0.814	0.57	1.04
BK-HG-02-51B	carbonate	2.00 ± 0.01	39.2 ± 0.5	9.8 ± 0.1	407.73 ± 5.63	5.1563 ± 0.0788	0.824	0.48	0.95
BK-HG-02-51C	carbonate	1.58 ± 0.01	31.5 ± 0.4	7.9 ± 0.1	397.74 ± 6.56	5.0652 ± 0.0914	0.845	0.50	0.96

Uncertainties are quoted at the 2σ level.

*I_{Os} = initial ^{187}Os/^{188}Os isotope ratio calculated using the age in brackets.

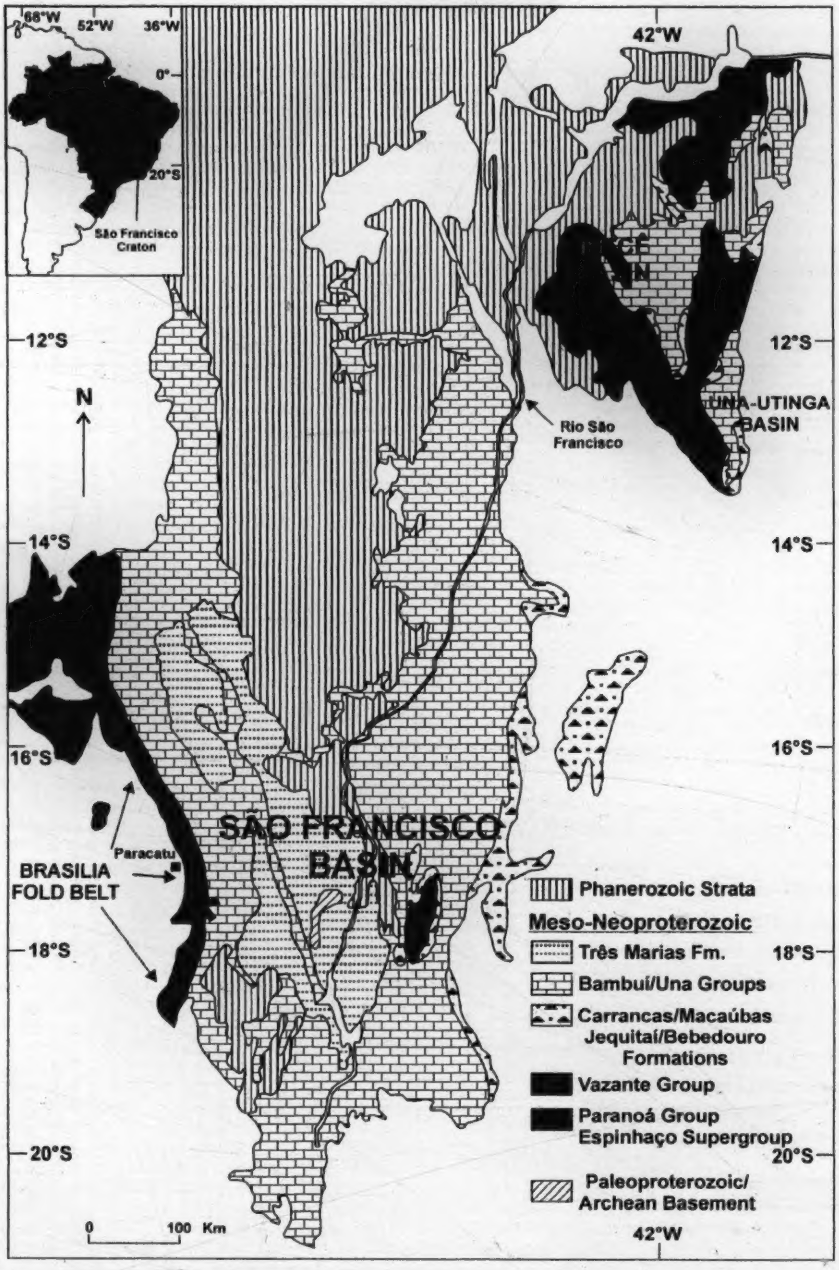
68°W
52°W
36°W
0°
20°S
São Francisco Craton
42°W
12°S
12°S
N
Rio São Francisco
UNA-UTINGA BASIN
14°S
14°S
16°S
16°S
Paracatu
BRASILIA FOLD BELT
SÃO FRANCISCO BASIN
18°S
18°S
20°S
20°S
0
100 Km
42°W
▥ Phanerozoic Strata
Meso-Neoproterozoic
Três Marias Fm.
Bambuí/Una Groups
Carrancas/Macaúbas Jequitaí/Bebedouro Formations
■ Vazante Group
■ Paranoá Group Espinhaço Supergroup
▨ Paleoproterozoic/ Archean Basement

Figure 4.1: Geology of the São Francisco Craton and the location of drill hole MASW01 (asterisk). Modified from Misi et al. (2005).

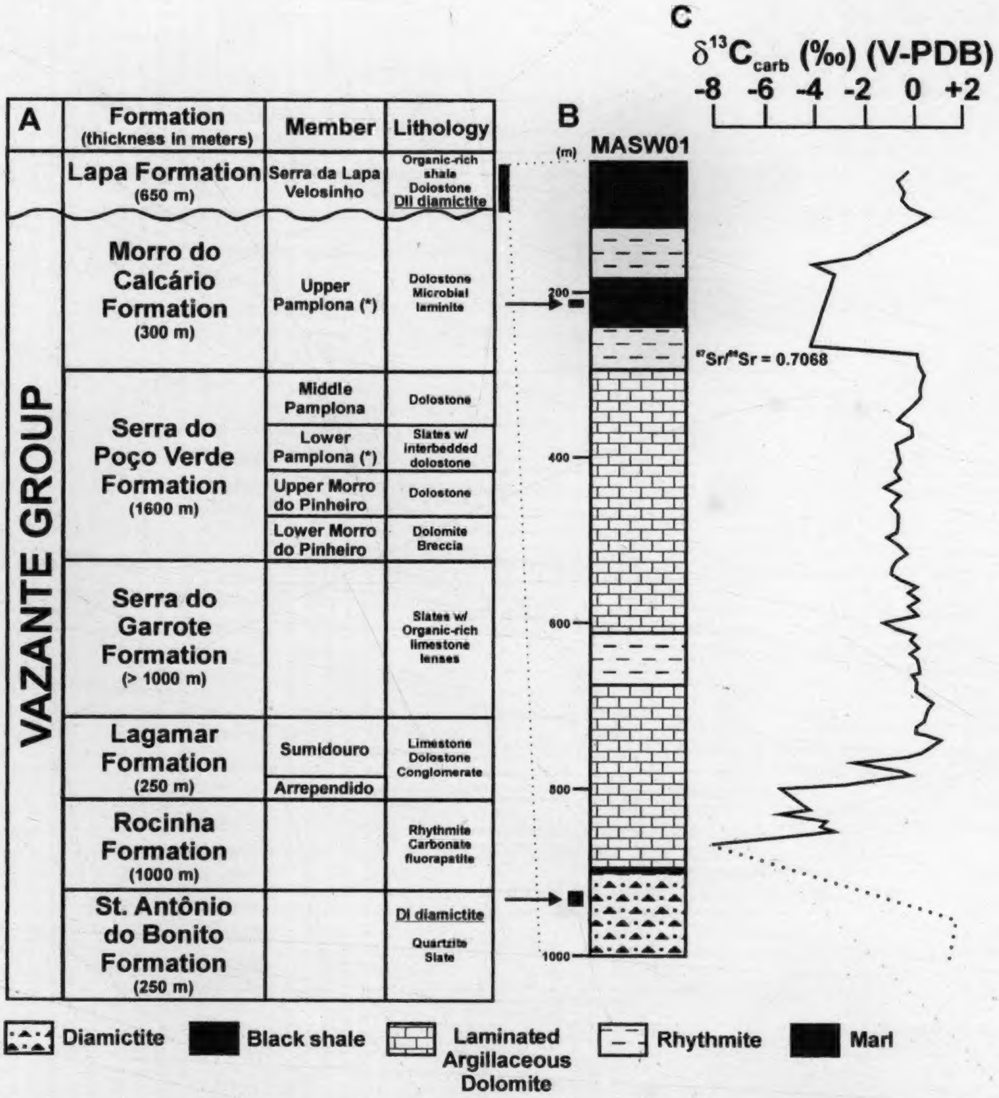

Figure 4.2: (A) Generalized stratigraphy of the Vazante Group (modified from Azmy et al., 2006; lithologies other than diamictites from Misi et al., 2007). Asterisks denote horizons of Pb-Zn mineralization. Diamictite intervals are also known from the Morro do Calcário and Serra do Poço Verde Formations (Brody et al., 2004; Olcott et al., 2005). (B) Stratigraphic column and (C) carbon isotope chemostratigraphy of the Lapa Formation in drill hole MASW01, including the position of stratigraphic intervals sampled for Re-Os analysis (modified from Azmy et al., 2006).

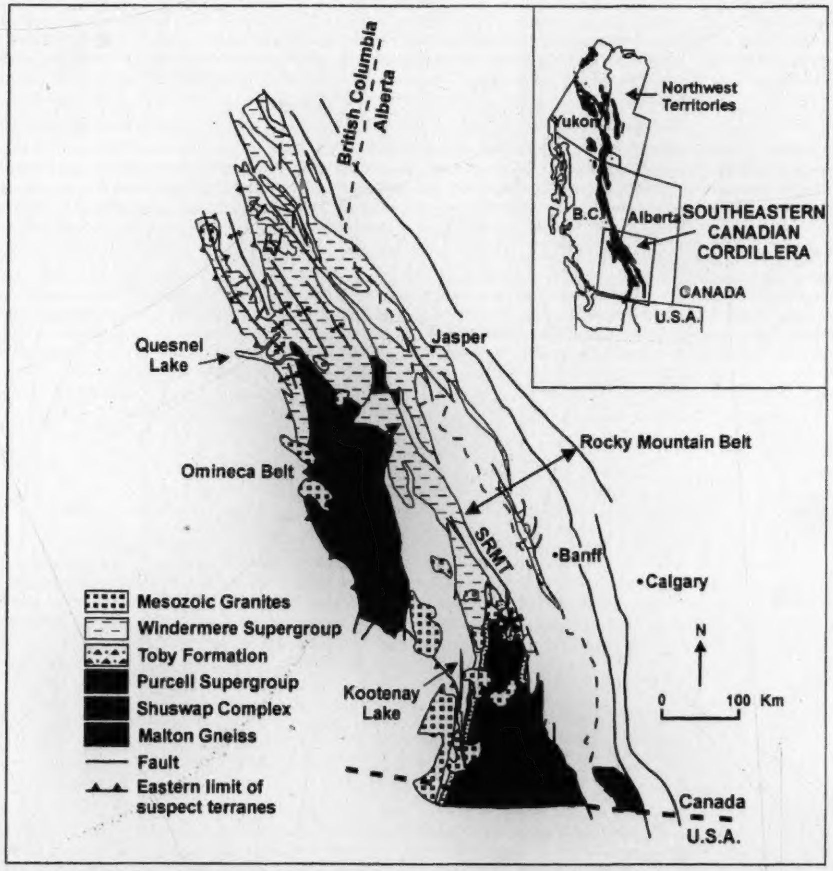
British Columbia
Alberta
Northwest Territories
Yukon
B.C.
Alberta
SOUTHEASTERN CANADIAN CORDILLERA
CANADA
U.S.A.
Jasper
Quesnel Lake
Rocky Mountain Belt
Omineca Belt
SRMT
•Banff
•Calgary
N
0
100 Km
Kootenay Lake
Canada
U.S.A.
Mesozoic Granites
Windermere Supergroup
Toby Formation
Purcell Supergroup
Shuswap Complex
Malton Gneiss
Fault
Eastern limit of suspect terranes

Figure 4.3: Distribution of the Windermere Supergroup in the southeastern Canadian Cordillera (modified from Ross et al., 1995). Sampling locality for the Horsethief Creek Group (50°27′41″ N, 116°14′20″ W) is denoted by the asterisk. SRMT = Southern Rocky Mountain Trench.

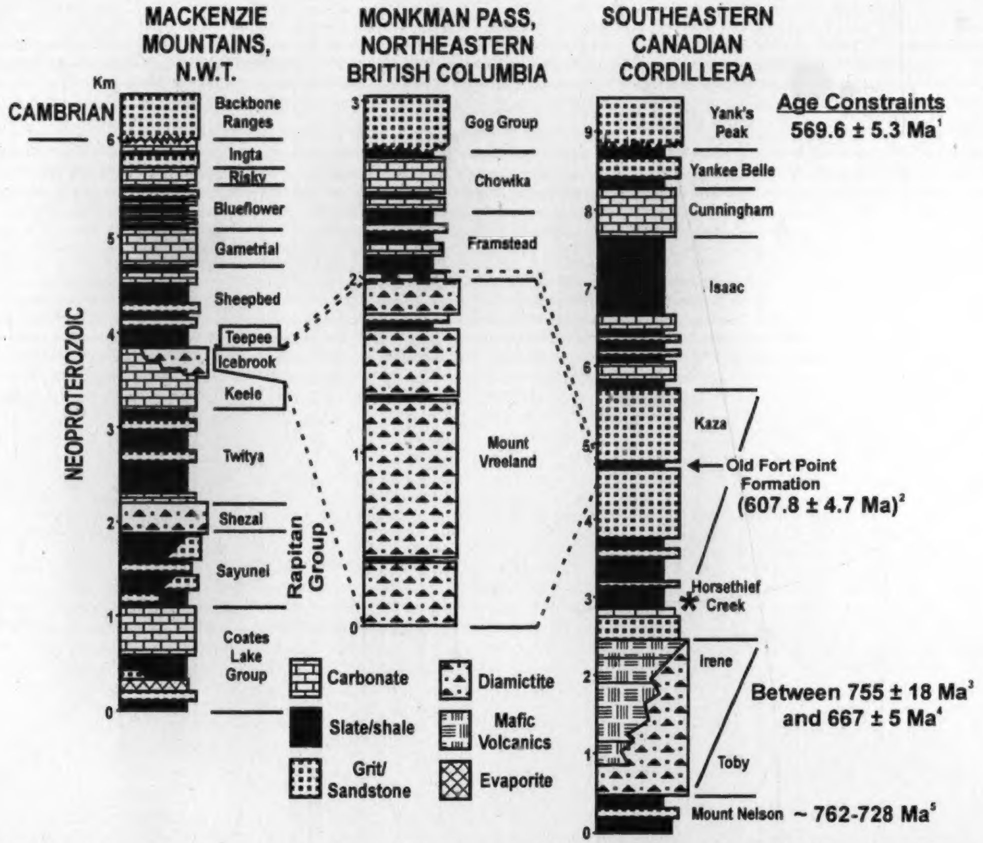
MACKENZIE MOUNTAINS, N.W.T.
MONKMAN PASS, NORTHEASTERN BRITISH COLUMBIA
SOUTHEASTERN CANADIAN CORDILLERA
Km
CAMBRIAN
NEOPROTEROZOIC
0
1
2
3
4
5
6
Backbone Ranges
Ingta
Risky
Blueflower
Gametrial
Sheepbed
Teepee
Icebrook
Keele
Twitya
Shezal
Sayunei
Coates Lake Group
Rapitan Group
Gog Group
Chowika
Framstead
Mount Vreeland
7
8
9
Yank's Peak
Yankee Belle
Cunningham
Isaac
Kaza
Old Fort Point Formation
Horsethief Creek
Irene
Toby
Mount Nelson
Age Constraints
569.6 ± 5.3 Ma^1
(607.8 ± 4.7 Ma)^2
Between 755 ± 18 Ma^3 and 667 ± 5 Ma^4
~ 762-728 Ma^5
Carbonate
Slate/shale
Grit/ Sandstone
Diamictite
Mafic Volcanics
Evaporite

Figure 4.4: Stratigraphic columns for the Windermere Supergroup in the Canadian Cordillera (modified from Ross et al., 1995). Dashed lines show the suggested correlations among glacial and post-glacial strata associated with the second Windermere glaciation. Asterisk denotes sampled stratigraphic interval from the Horsethief Creek Group. Age constraints from: 1 – Colpron et al. (2002), 2 – Kendall et al. (2004), 3 – Ross and Villeneuve (1997), 4 – Fanning and Link (2004), 5 – summarized by Ross et al. (1995).

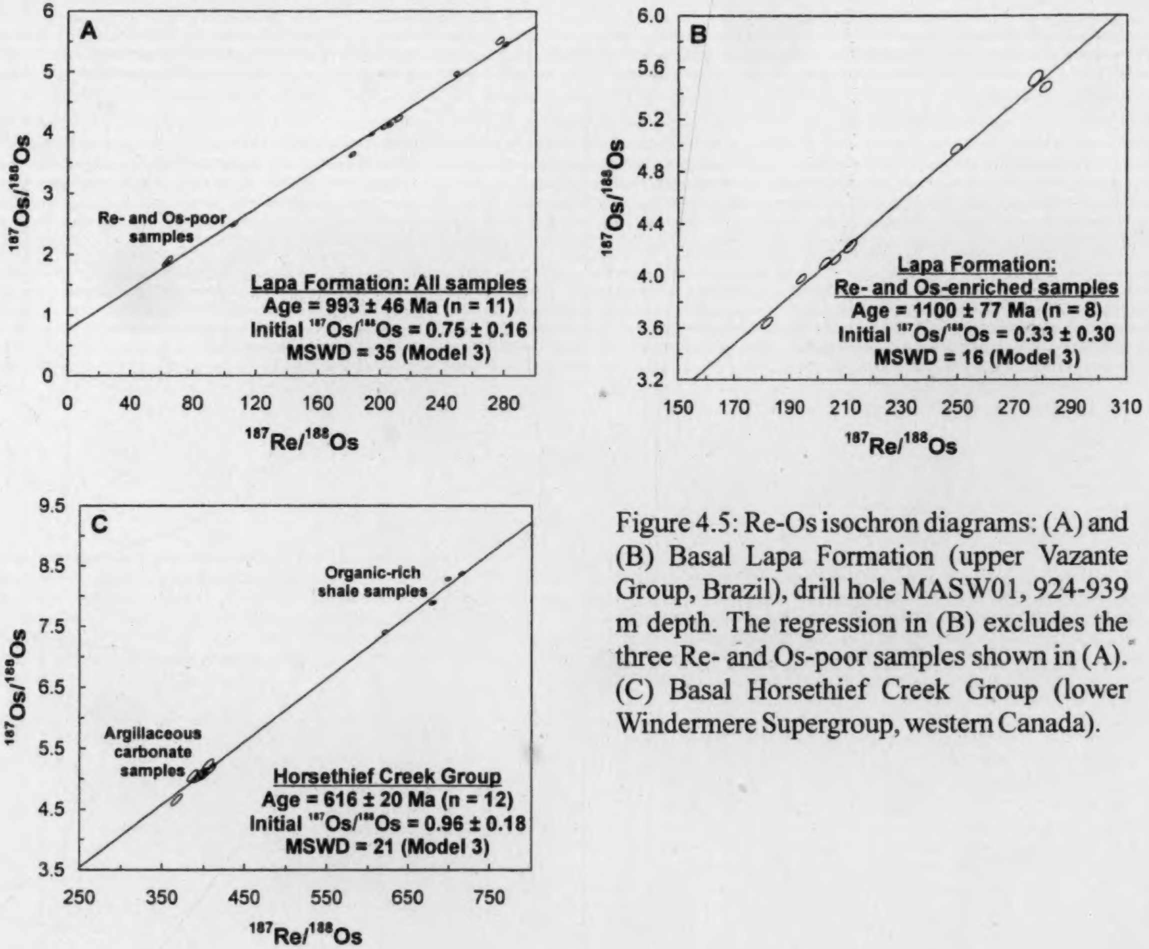

Figure 4.5: Re-Os isochron diagrams: (A) and (B) Basal Lapa Formation (upper Vazante Group, Brazil), drill hole MASW01, 924-939 m depth. The regression in (B) excludes the three Re- and Os-poor samples shown in (A). (C) Basal Horsethief Creek Group (lower Windermere Supergroup, western Canada).

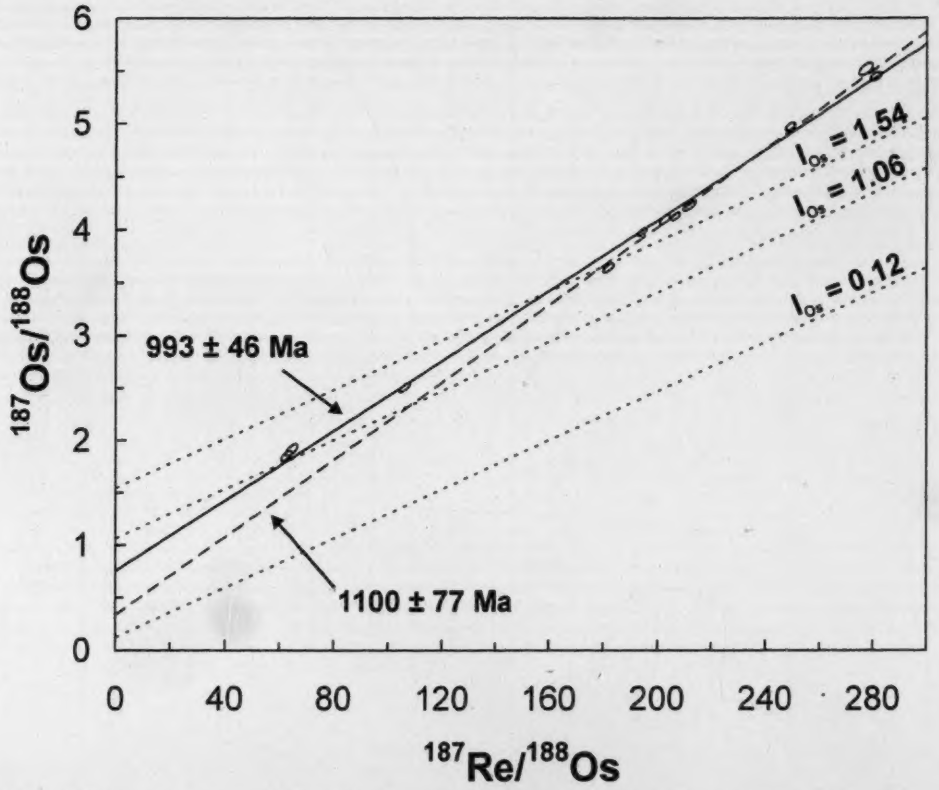

Figure 4.6: Re-Os isochron diagram for the Lapa Formation showing the two regressions from Figure 4.5A, B, as well as 700 Ma reference isochrons with I_{Os} of 0.12 (chondritic/mantle Os at ca. 1000-1100 Ma; Walker et al., 2002a, b), 1.06 (present-day seawater; Sharma et al., 1997; Levasseur et al., 1998; Woodhouse et al., 1999; Peucker-Ehrenbrink and Ravizza, 2000), and 1.54 (average present-day riverine input; Levasseur et al., 1999). If the Lapa Formation is a "Sturtian" post-glacial shale (e.g., between 750 and 643 Ma), there must have been a significant loss of Re relative to Os (or gain of Os relative to Re) to explain the erroneously old Re-Os date.

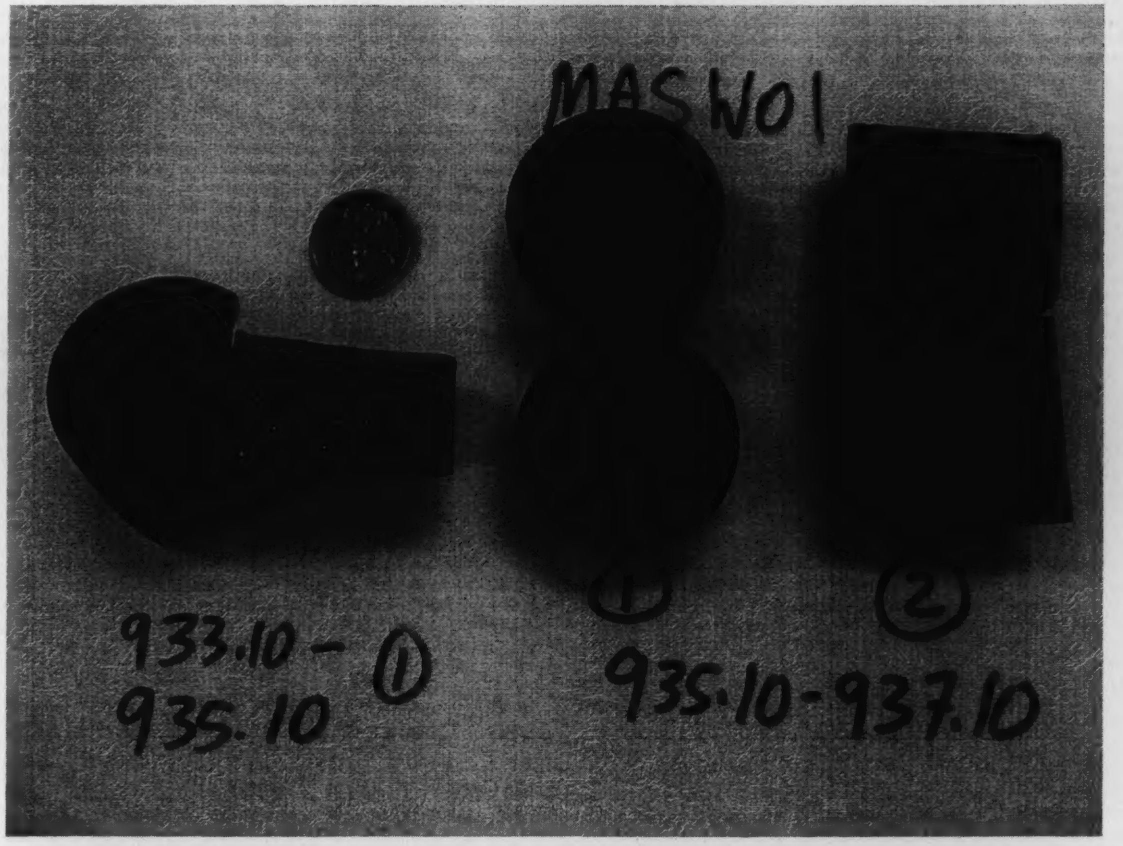
MASW01
933.10 - ①
935.10
①
②
935.10-937.10

Plate 4.1: Pyritic, organic-rich shales from the basal Lapa Formation (Late Mesoproterozoic to Early Neoproterozoic Vazante Group, Brazil), drill hole MASW01. Note the sheared surface in MASW01-933.10-935.10-1 (left) and small-scale folding in MASW01-935.10-937.10-2 (right).

Plate 4.2: Carbonaceous and argillaceous carbonate (sample BK-HG-02-51A) from the Neoproterozoic lower Horsethief Creek Group (lower Windermere Supergroup), Western Canada.

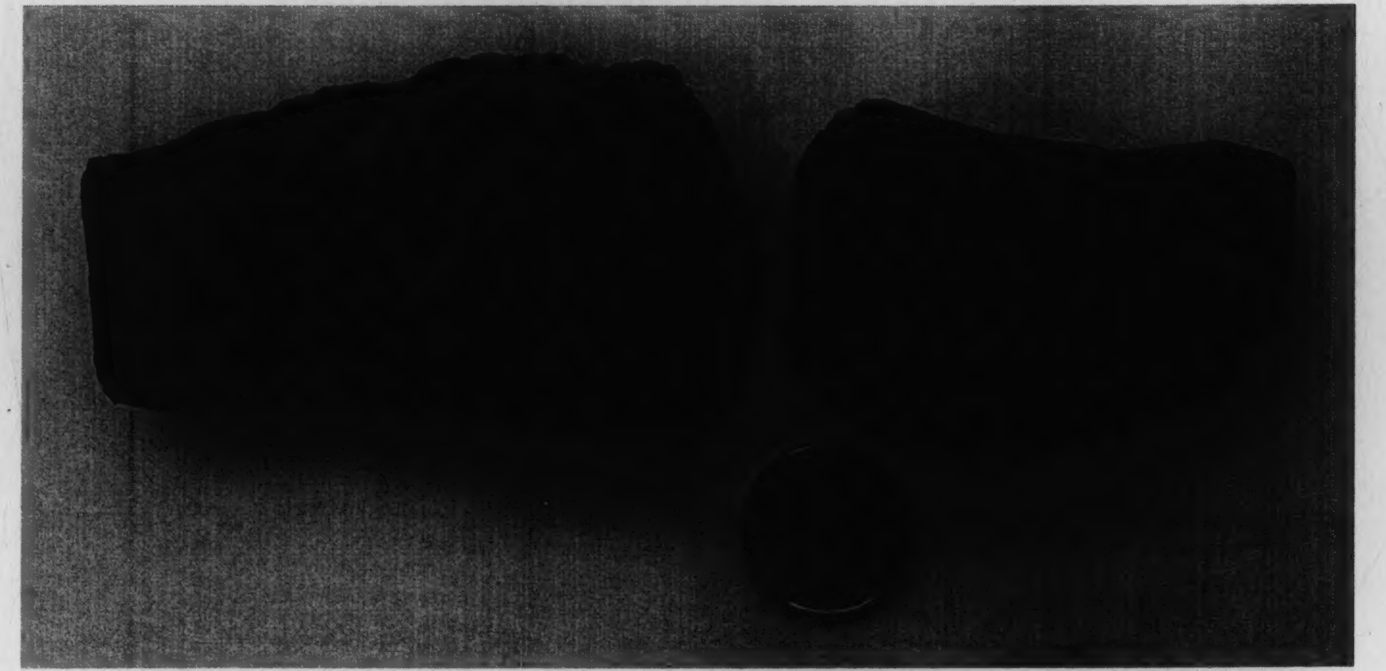

Plate 4.3: Pyritic, organic-rich shale from the basal Horsethief Creek Group. Specimens shown are part of BK-HG-02-050A (left) and BK-HG-02-050B (right). Note carbonate veinlets.

REFERENCES

Aalto, K.R., 1971, Glacial marine sedimentation and stratigraphy of the Toby Conglomerate (Upper Proterozoic), southeastern British Columbia, northwestern Idaho and northeastern Washington: Canadian Journal of Earth Sciences, v. 8, p. 753-787.

Arnold, G.L., Anbar, A.D., Barling, J., and Lyons, T.W., 2004, Molybdenum isotope evidence for widespread anoxia in Mid-Proterozoic oceans: Science, v. 304, p. 87-90.

Asmerom, Y., Jacobsen, S.B., Knoll, A.H., Butterfield, N.J., and Swett, K., 1991, Strontium isotopic variations of Neoproterozoic seawater: Implications for crustal evolution: Geochimica et Cosmochimica Acta, v. 55, p. 2883-2894.

Azmy, K., Veizer, J., Misi, A., de Oliveira, T.F., Sanches, A.L., and Dardenne, M.A., 2001, Dolomitization and stratigraphy of the Vazante Formation, São Francisco Basin, Brazil: Precambrian Research, v. 112, p. 303-329.

Azmy, K., Kaufman, A.J., Misi, A., and de Oliveira, T.F., 2006, Isotope stratigraphy of the Lapa Formation, São Francisco Basin, Brazil: Implications for Late Neoproterozoic glacial events in South America: Precambrian Research, v. 149, p. 231-248.

Azmy, K., Kendall, B., Creaser, R.A., Heaman, L., Misi, A., and de Oliveira, T.F., Global correlation of the Vazante Group, São Francisco Basin, Brazil: Re-Os and U-Pb radiometric age constraints: Precambrian Research, accepted.

Babinski, M., and Kaufman, A.J., 2003, First direct dating of a Neoproterozoic post-glaciogenic cap carbonate: IV South American Symposium on Isotope Geology, Short Papers, v. 1, p. 321-323.

Babinski, M., Van Schmus, W.R., and Chemale, F., Jr., 1999, Pb-Pb dating and Pb isotope geochemistry of Neoproterozoic carbonate rocks from the São Francisco Basin, Brazil: Implications for the mobility of Pb isotopes during tectonism and metamorphism: Chemical Geology, v. 160, p. 175-199.

Bekker, A., Kaufman, A.J., Karhu, J.A., and Eriksson, K.A., 2005, Evidence for Paleoproterozoic cap carbonates in North America: Precambrian Research, v. 137, p. 167-206.

Boggiani, P.C., Sial, A.N., Babinski, M., and Ferreira, V.P., 2003, New carbon isotopic data from the Corumbá Group as a contribution to a composite section for the Neoproterozoic III in South America, *in* Frimmel, H.E., ed., III International Colloquium Vendian-Cambrian of W-Gondwana, Programme and Extended Abstracts, Cape Town, p. 13-16.

Brody, K.B., Kaufman, A.J., Eigenbrode, J.L., and Cody, G.D., 2004, Biomarker geochemistry of a post-glacial Neoproterozoic succession in Brazil: Geological Society of America Abstracts With Programs, v. 36 (5), p. 477.

Brown, R.L., Journeay, J.M., Lane, L.S., Murphy, D.C., and Rees, C.J., 1986, Obduction, backfolding, and piggyback thrusting in the metamorphic hinterland of the southeastern Canadian Cordillera: Journal of Structural Geology, v. 8, p. 255-268.

Chemale, F., Jr., Alkmim, F.F., and Endo, I., 1993, Late Proterozoic tectonism in the interior of the São Francisco craton, *in* Findlay, R.H., et al., eds., Gondwana eight – Assembly, evolution, and dispersal: Proceedings of the Eighth Gondwana Symposium, A.A. Balkema, Rotterdam, Brookfield, p. 29-42.

Cloud, P., and Dardenne, M., 1973, Proterozoic age of the Bambuí Group in Brazil: Geological Society of America Bulletin, v. 84, p. 1673-1676.

Colpron, M., Logan, J.M., and Mortensen, J.K., 2002, U-Pb zircon age constraint for late Neoproterozoic rifting and initiation of the lower Paleozoic passive margin of western Laurentia: Canadian Journal of Earth Sciences, v. 39, p. 133-143.

Corsetti, F.A., and Lorentz, N.J., 2006, On Neoproterozoic cap carbonates as chronostratigraphic markers, *in* Xiao, S., and Kaufman, A.J., eds., Neoproterozoic Geobiology and Paleobiology: Springer, New York, p. 273-294.

Creaser, R.A., Sannigrahi, P., Chacko, T., and Selby, D., 2002, Further evaluation of the Re-Os geochronometer in organic-rich sedimentary rocks: a test of hydrocarbon maturation effects in the Exshaw Formation, Western Canada Sedimentary Basin: Geochimica et Cosmochimica Acta, v. 66, p. 3441-3452.

D'Agrella-Filho, M.S., Babinski, M., Trindade, R.I.F., Van Schmus, W.R., and Ernesto, M., 2000, Simultaneous remagnetization and U-Pb isotope resetting in Neoproterozoic carbonates of the São Francisco craton, Brazil: Precambrian Research, v. 99, p. 179-196.

Dardenne, M.A., 2000, The Brasilia Fold Belt, *in* Cordani, U.G., et al., eds., Tectonic Evolution of South America: 31st International Geological Congress, Rio de Janeiro, p. 231-263.

Dardenne, M.A., 2001, Lithostratigraphic sedimentary sequences of the Vazante Group: IGCP 450 Proterozoic sediment-hosted base metal deposits of western Gondwana (Abstract), Belo Horizonte, Brazil, p. 48-50.

Dardenne, M.A., 2005, *Conophyton* of Cabeludo, Vazante Group, State of Minas Gerais – Dolomitic constructions by cyanobacteria in the Proterozoic, *in* Winge, M., et al., eds., Geological and palaeontological sites of Brazil, SIGEP 073.

Dardenne, M.A., Campos, J.E.G., and Campos Neto, M.C., 2005, Columnar stromatolites in the Sumidouro of the Carrapato River, Lagamar, State of Minas Gerais – Record of columnar dolomitic constructions by cyanobacteria in the Proterozoic of Brazil, *in* Winge, M., et al., eds., Geological and palaeontological sites of Brazil, SIGEP 074, p. 1-8.

da Silva, L.C., McNaughton, N.J., Armstrong, R., Hartmann, L.A., and Fletcher, I.R., 2005, The Neoproterozoic Mantiqueira Province and its African connections: A zircon-based U-Pb geochronologic subdivision for the Brasiliano/Pan-African system of orogens: Precambrian Research, v. 136, p. 203-240.

de Alvarenga, C.J.S., and Trompette, R., 1992, Glacially influenced sedimentation in the Later Proterozoic of the Paraguay Belt (Mato Grosso, Brazil): Palaeogeography, Palaeoclimatology, Palaeoecology, v. 92, p. 85-105.

de Alvarenga, C.J.S., Santos, R.V., and Dantas, E.L., 2004, C-O-Sr isotopic stratigraphy of cap carbonates overlying Marinoan-age glacial diamictites in the Paraguay Belt, Brazil: Precambrian Research, v. 131, p. 1-21.

de Alvarenga, C.J.S., Dardenne, M.A., Santos, R.V., Brod, E.R., Gioia, S.M.C.L., Sial, A.N., Dantas, E.L., and Ferreira, V.P., Isotope stratigraphy of Neoproterozoic cap carbonates in the Araras Group, Brazil: Gondwana Research, in press.

Derry, L.A., Kaufman, A.J., and Jacobsen, S.B., 1992, Sedimentary cycling and environmental change in the Late Proterozoic: Evidence from stable and radiogenic isotopes: Geochimica et Cosmochimica Acta, v. 56, p. 1317-1329.

Devlin, W.J., Bruekner, H.K., and Bond, G.C., 1988, New isotopic data and a preliminary age for volcanics near the base of the Windermere Supergroup, northeastern Washington, U.S.A.: Canadian Journal of Earth Sciences, v. 25, p. 1906-1911.

Eisbacher, G.E., 1981, Sedimentary tectonics and glacial record in the Windermere Supergroup, Mackenzie Mountains, Northwest Territories: Geological Survey of Canada Paper 80-27.

Eisbacher, G.E., 1985, Late Proterozoic rifting, glacial sedimentation, and sedimentary cycles in the light of Windermere deposition, western Canada: Palaeogeography, Palaeoclimatology, Palaeoecology, v. 51, p. 231-254.

Esser, B.K., and Turekian, K.K., 1993, The osmium isotopic composition of the continental crust: Geochimica et Cosmochimica Acta, v. 57, p. 3093-3104.

Evenchick, C.A., Parrish, R.R., and Gabrielse, H., 1984, Precambrian gneiss and Late Proterozoic sedimentation in north-central British Columbia: Geology, v. 12, p. 233-237.

Fairchild, T.R., Schopf, J.W., Shen-Miller, J., Guimarães, E.M., Edwards, M.D., Lagstein, A., Li, X., Pabst, M., de Melo-Filho, L.S., 1996, Recent discoveries of Proterozoic microfossils in south-central Brazil: Precambrian Research, v. 80, p. 125-152.

Fanning, C.M., and Link, P.K., 2004, U-Pb SHRIMP ages of Neoproterozoic (Sturtian) glaciogenic Pocatello Formation, southeastern Idaho: Geology, v. 32, p. 881-884.

Font, E., Nédélec, A., Trindade, R.I.F., Macouin, M., and Charrière, A., 2006, Chemostratigraphy of the Neoproterozoic Mirassol d' Oeste cap dolostones (Mato Grosso, Brazil): An alternative model for Marinoan cap dolostone formation: Earth and Planetary Science Letters, v. 250, p. 89-103.

Gabrielse, H., and Yorath, C.J., 1991, Tectonic synthesis, Chapter 18, *in* Gabrielse, H., and Yorath, C.J., eds., Geology of the Cordilleran orogen in Canada, Geology of Canada volume 4: Geological Survey of Canada, p. 677-705.

Glover, J.K., and Price, R.A., 1976, Stratigraphy and structure of the Windermere Supergroup, southern Kootenay Arc, British Columbia: Current Research, Part B, Geological Survey of Canada Paper 76-1B, p. 21-23.

Gorjan, P., Veevers, J.J., and Walter, M.R., 2000, Neoproterozoic sulfur-isotope variation in Australia and global implications: Precambrian Research, v. 100, p. 151-179.

Gorjan, P., Walter, M.R., and Swart, R., 2003, Global Neoproterozoic (Sturtian) post-glacial sulfide-sulfur isotope anomaly recognised in Namibia: Journal of African Earth Sciences, v. 36, p. 89-98.

Greenwood, H.J., Woodsworth, G.J., Read, P.B., Ghent, E.D., Evenchick, C.A., 1991, Metamorphism, Chapter 16, *in* Gabrielse, H., and Yorath, C.J., eds., Geology of the Cordilleran orogen in Canada, Geology of Canada volume 4: Geological Survey of Canada, p. 533-570.

Halverson, G.P., 2006, A Neoproterozoic chronology, *in* Xiao, S., and Kaufman, A.J., eds., Neoproterozoic Geobiology and Paleobiology: Springer, New York, p. 231-271.

Halverson, G.P., Hoffman, P.F., Schrag, D.P., Maloof, A.C., and Rice, A.H.N., 2005, Toward a Neoproterozoic composite carbon-isotope record: Geological Society of America Bulletin, v. 117, p. 1181-1207.

Hattori, Y., Suzuki, K., Honda, M., and Shimizu, H., 2003, Re-Os isotope systematics of the Taklimakan Desert sands, moraines and river sediments around the Taklimakan Desert, and of Tibetan soils: Geochimica et Cosmochimica Acta, v. 67, p. 1195-1205.

Hoffman, P.F., Hawkins, D.P., Isachsen, C.E., and Bowring, S.A., 1996, Precise U-Pb zircon ages for early Damaran magmatism in the Summas Mountains and Welwitschia Inlier, northern Damara belt, Namibia: Communications of the Geological Survey of Namibia, v. 11, p. 47-52.

Hurtgen, M.T., Arthur, M.A., and Halverson, G.P., 2005, Neoproterozoic sulfur isotopes, the evolution of microbial sulfur species, and the burial efficiency of sulfide as sedimentary pyrite: Geology, v. 33, 41-44.

Iyer, S.S., Hoefs, J., and Krouse, H.R., 1992, Sulfur and lead isotope geochemistry of galenas from the Bambuí Group, Minas Gerais, Brazil – Implications for ore genesis: Economic Geology, v. 87, p. 437-443.

Iyer, S.S., Babinski, M., Krouse, H.R., and Chemale, F., Jr., 1995, Highly ^{13}C-enriched carbonate and organic matter in the Neoproterozoic sediments of the Bambuí Group, Brazil: Precambrian Research, v. 73, p. 271-282.

Jacobsen, S.B., and Kaufman, A.J., 1999, The Sr, C and O isotopic evolution of Neoproterozoic seawater: Chemical Geology, v. 161, p. 37-57.

Jiang, G., Kaufman, A.J., Christie-Blick, N., Zhang, S., and Wu, H., 2007, Carbon isotope variability across the Ediacaran Yangtze platform in South China: Implications for a large surface-to-deep ocean δ^{13}C gradient: Earth and Planetary Science Letters, v. 261, p. 303-320.

Karfunkel, J., and Hoppe, A., 1988, Late Proterozoic glaciation in central-eastern Brazil: Synthesis and model: Palaeogeography, Palaeoclimatology, Palaeoecology, v. 65, p. 1-21.

Kaufman, A.J., and Knoll, A.H., 1995, Neoproterozoic variations in the C-isotopic composition of seawater: Stratigraphic and biogeochemical implications: Precambrian Research, v. 73, p. 27-49.

Kaufman, A.J., Hayes, J.M., Knoll, A.H., and Germs, G.J.B., 1991, Isotopic compositions of carbonates and organic carbon from upper Proterozoic successions in Namibia: Stratigraphic variation and the effects of diagenesis and metamorphism: Precambrian Research, v. 49, p. 301-327.

Kaufman, A.J., Jacobsen, S.B., and Knoll, A.H., 1993, The Vendian record of Sr and C isotopic variations in seawater: Implications for tectonics and paleoclimate: Earth and Planetary Science Letters, v. 120, p. 409-430.

Kaufman, A.J., Knoll, A.H., and Narbonne, G.M., 1997, Isotopes, ice ages, and terminal Proterozoic Earth history: Proceedings of the National Academy of Sciences, v. 94, p. 6600-6605.

Kendall, B.S., 2003, Evaluation of the Re-Os geochronometer in organic-rich mudrocks as a method for constraining the absolute ages of Neoproterozoic glaciogenic deposits: Unpublished M.Sc. Thesis, University of Alberta.

Kendall, B.S., Creaser, R.A., Ross, G.M., and Selby, D., 2004, Constraints on the timing of Marinoan "Snowball Earth" glaciation by ^{187}Re-^{187}Os dating of a Neoproterozoic, post-glacial black shale in Western Canada: Earth and Planetary Science Letters, v. 222, p. 729-740.

Kennedy, M.J., Runnegar, B., Prave, A.R., Hoffmann, K.-H., and Arthur, M.A., 1998, Two or four Neoproterozoic glaciations?: Geology, v. 26, p.1059-1063.

Leclair, A.D., 1982, Preliminary results on the stratigraphy, structure, and metamorphism of central Kootenay Arc rocks, southeastern British Columbia: Current Research, Part A, Geological Survey of Canada Paper 82-1A, p. 45-49.

Levasseur, S., Birck, J.-L., and Allègre, C.J., 1998, Direct measurement of femtomoles of osmium and the ^{187}Os/^{186}Os ratio in seawater: Science, v. 282, p. 272-274.

Levasseur, S., Birck, J.-L., and Allègre, C.J., 1999, The osmium riverine flux and the oceanic mass balance of osmium: Earth and Planetary Science Letters, v. 174, p. 7-23.

Lis, M.G., and Price, R.A., 1976, Large-scale block faulting during deposition of the Windermere Supergroup (Hadrynian) in southeastern British Columbia: Current Research, Part A, Geological Survey of Canada Paper 76-1A, p. 135-136.

Lund, K.L., Aleinikoff, J.N., Evans, K.V., and Fanning, C.M., 2003, SHRIMP U-Pb geochronology of Neoproterozoic Windermere Supergroup, central Idaho: Implications for rifting of western Laurentia and synchroneity of Sturtian glacial deposits: Geological Society of America Bulletin, v. 115, p. 349-372.

Martins-Neto, M.A., Pedrosa-Soares, A.C., and Lima, S.A.A., 2001, Tectono-sedimentary evolution of sedimentary basins from Late Paleoproterozoic to Late Neoproterozoic in the São Francisco craton and Aracuaí fold belt, eastern Brazil: Sedimentary Geology, v. 141-142, p. 343-370.

McDonough, M.R., and Simony, P.S., 1988, Stratigraphy and structure of the late Proterozoic Miette Group, northern Selwyn Range, Rocky Mountains, British Columbia: Current Research, Part D, Geological Survey of Canada Paper 88-1D, p. 105-113.

McDonough, M.R., and Parrish, R.R., 1991, Proterozoic gneisses of the Malton Complex, near Valemount, British Columbia: U-Pb ages and Nd isotopic signatures: Canadian Journal of Earth Sciences, v. 28, p. 1202-1216.

Melezhik, V.A., Gorokhov, I.M., Kuznetsov, A.B., and Fallick, A.E., 2001, Chemostratigraphy of Neoproterozoic carbonates: Implications for 'blind dating': Terra Nova, v. 13, p. 1-11.

Misi, A., and Veizer, J., 1998, Neoproterozoic carbonate sequences of the Una Group, Irecê Basin, Brazil: Chemostratigraphy, age and correlations: Precambrian Research, v. 89, p. 87-100.

Misi, A., Iyer, S.S.S., Coelho, C.E.S., Tassinari, C.C.G., Franca-Rocha, W.J.S., Cunha, I.A., Gomes, A.S.R., de Oliveira, T.F., Teixeira, J.B.G., and Filho, V.M.C., 2005, Sediment hosted lead-zinc deposits of the Neoproterozoic Bambuí Group and correlative sequences, São Francisco Craton, Brazil: A review and a possible metallogenic evolution model: Ore Geology Reviews, v. 26, p. 263-304.

Misi, A., Kaufman, A.J., Veizer, J., Powis, K., Azmy, K., Boggiani, P.C., Gaucher, C., Teixeira, J.B.G., Sanches, A.L., and Iyer, S.S.S., 2007, Chemostratigraphic correlation of Neoproterozoic successions in South America: Chemical Geology, v. 237, p. 143-167.

Monger, J.W.H., Price, R.A., and Tempelman-Kluit, D.J., 1982, Tectonic accretion and the origin of the two major metamorphic and plutonic welts in the Canadian Cordillera: Geology, v. 10, p. 70-75.

Nesbitt, B.E., and Muehlenbachs, K., 1989, Origins and movement of fluids during deformation and metamorphism in the Canadian Cordillera: Science, v. 245, p. 733-736.

Nesbitt, B.E., and Muehlenbachs, K., 1995, Geochemical studies of the origins and effects of synorogenic crustal fluids in the southern Omineca Belt of British Columbia, Canada: Geological Society of America Bulletin, v. 107, p. 1033-1050.

Nesbitt, B.E., and Muehlenbachs, K., 1997, Paleo-hydrogeology of Late Proterozoic units of southeastern Canadian Cordillera: American Journal of Science, v. 297, p. 359-392.

Nogueira, A.C.R., Riccomini, C., Sial, A.N., Moura, C.A.V., and Fairchild, T.R., 2003, Soft-sediment deformation at the base of the Neoproterozoic Puga cap carbonate (southwestern Amazon Craton, Brazil): Confirmation of rapid icehouse to greenhouse transition in snowball Earth: Geology, v. 31, p. 613-616.

Nogueira, A.C.R., Riccomini, C., Sial, A.N., Moura, C.A.V., Trindade, R.I.F., and Fairchild, T.R., 2007, Carbon and strontium isotope fluctuations and paleoceanographic changes in the late Neoproterozoic Araras carbonate platform, southern Amazon craton, Brazil: Chemical Geology, v. 237, p. 168-190.

Olcott, A.N., Sessions, A.L., Corsetti, F.A., Kaufman, A.J., and de Oliviera, T.F., 2005, Biomarker evidence for photosynthesis during Neoproterozoic glaciation: Science, v. 310, p. 471-474.

Oxburgh, R., 1998, Variations in the osmium isotope composition of seawater over the past 200,000 years: Earth and Planetary Science Letters, v. 159, p. 183-191.

Page, R.W., Jackson, M.J., and Krassay, A.A., 2000, Constraining sequence stratigraphy in north Australian basins: SHRIMP U-Pb zircon geochronology between Mt Isa and McArthur River: Australian Journal of Earth Sciences, v. 47, p. 431-459.

Park, J.K., 1997, Paleomagnetic evidence for low-latitude glaciation during deposition of the Neoproterozoic Rapitan Group, Mackenzie Mountains, N.W.T., Canada: Canadian Journal of Earth Sciences, v. 34, p. 34-39.

Parrish, R.R., and Scammell, R.J., 1988, The age of the Mount Copeland syenite gneiss and its metamorphic zircons, Monashee Complex, southeastern British Columbia, *in* Radiogenic age and isotopic studies: Report 2: Geological Survey of Canada, Paper 88-2, p. 21-28.

Pedrosa-Soares, A.C., Cordani, U.G., and Nutman, A., 2000, Constraining the age of Neoproterozoic glaciation in eastern Brazil: First U-Pb (SHRIMP) data of detrital zircons: Revista Brasileira de Geociencias., v. 30, p. 58-61.

Pedrosa-Soares, A.C., Noce, C.M., Wiedemann, C.M., and Pinto, C.P., 2001, The Aracuaí – West-Congo Orogen in Brazil: An overview of a confined orogen formed during Gondwanaland assembly: Precambrian Research, v. 110, p. 307-323.

Pell, J., and Simony, P.S., 1987, New correlations of Hadrynian strata, south-central British Columbia: Canadian Journal of Earth Sciences, v. 24, p. 302-313.

Peryt, T.M., Hoppe, A., Bechstadt, T., Koster, J., Pierre, C., and Richter, D.K., 1990, Late Proterozoic aragonitic cement crusts, Bambuí Group, Minas-Gerais, Brazil: Sedimentology, v. 37, p. 279-286.

Peucker-Ehrenbrink, B., and Ravizza, G., 2000, The marine osmium isotope record: Terra Nova, v. 12, p. 205-219.

Peucker-Ehrenbrink, B., and Jahn, B.-M., 2001, Rhenium-osmium isotope systematics and platinum group element concentrations: loess and the upper continental crust: Geochemistry Geophysics Geosystems, v. 2, Paper 2001GC000172.

Poulton, T.P., and Simony, P.S., 1980, Stratigraphy, sedimentology, and regional correlation of the Horsethief Creek Group (Hadrynian, Late Precambrian) in the northern Purcell and Selkirk Mountains, British Columbia: Canadian Journal of Earth Sciences, v. 17, p. 1708-1724.

Raaben, M.E., 2005, On subdivisions of the Upper Riphean: Stratigraphy and Geological Correlation, v. 13, p. 143-158.

Ravizza, G., Turekian, K.K., and Hay, B.J., 1991, The geochemistry of rhenium and osmium in recent sediments from the Black Sea: Geochimica et Cosmochimica Acta, v. 55, p. 3741-3752.

Root, K.G., 1987, Geology of the Delphine Creek area, southeastern British Columbia: Implications for Paleozoic and Proterozoic of the Cordilleran divergent margin: Unpublished Ph.D. Thesis, University of Calgary.

Ronkin, Y., Sindern, S., Kramm, U., Maslov, A., Lepikhina, O., and Popova, O., 2006, The age of the Lower-Middle Riphean boundary on South Urals is 1350 ± 10 Ma or older? European Geosciences Union Geophysical Research Abstracts 8, #03579.

Ross, G.M., 1991, Tectonic setting of the Windermere Supergroup revisited: Geology, v. 19, p. 1125-1128.

Ross, G.M., and Murphy, D.C., 1988, Transgressive stratigraphy, anoxia, and regional correlations within the late Precambrian Windermere grit of the southern Canadian Cordillera: Geology, v. 16, p. 139-143.

Ross, G.M., and Villeneuve, M.E., 1997, U-Pb geochronology of stranger stones in Neoproterozoic diamictites, Canadian Cordillera: Implications for provenance and ages of deposition, *in* Radiogenic age and isotopic studies, Report 10: Geological Survey of Canada, Current Research 1997-F, p. 141-155.

Ross, G.M., McMechan, H., and Hein, F., 1989, Proterozoic history: Birth of the miogeocline, *in* Ricketts, B.D., ed., The western Canada sedimentary basin: Canadian Society of Petroleum Geologists, Calgary, Alberta, Canada, p. 79-104.

Ross, G.M., Bloch, J.D., and Krouse, H.R., 1995, Neoproterozoic strata of the southern Canadian Cordillera and the isotopic evolution of seawater sulfate: Precambrian Research, v. 73, p. 71-99.

Santos, R.V., de Alvarenga, C.J.S., Dardenne, M.A., Sial, A.N., and Ferreira, V.P., 2000, Carbon and oxygen isotope profiles across Meso-Neoproterozoic limestones from central Brazil: Bambuí and Paranoá Groups: Precambrian Research, v. 104, p. 107-122.

Selby, D., and Creaser, R.A., 2003, Re-Os geochronology of organic-rich sediments: an evaluation of organic matter analysis methods: Chemical Geology, v. 200, p. 225-240.

Selby, D., and Creaser, R.A., 2005, Direct radiometric dating of the Devonian-Mississippian time-scale boundary using the Re-Os black shale geochronometer: Geology, v. 33, p. 545-548.

Sharma, M., Papanastassiou, D.A., and Wasserburg, G.J., 1997, The concentration and isotopic composition of osmium in the oceans: Geochimica et Cosmochimica Acta, v. 61, p. 3287-3299.

Shen, Y., Zhang, T., and Chu, X., 2005, C-isotopic stratification in a Neoproterozoic postglacial ocean: Precambrian Research, v. 137, p. 243-251.

Sun, W., Arculus, R.J., Bennett, V.C., Eggins, S.M., and Binns, R.A., 2003a, Evidence for rhenium enrichment in the mantle wedge from submarine arc-like volcanic glasses (Papua New Guinea): Geology, v. 31, p. 845-848.

Sun, W., Bennett, V.C., Eggins, S.M., Kamenetsky, V.S., and Arculus, R.J., 2003b, Enhanced mantle-to-crust rhenium transfer in undegassed arc magmas: Nature, v. 422, p. 294-297.

Trindade, R.I.F., Font, E., D'Agrella-Filho, M.S., Nogueira, A.C.R., and Riccomini, C., 2003, Low-latitude and multiple geomagnetic reversals in the Neoproterozoic Puga cap carbonate, Amazon craton: Terra Nova, v. 15, p. 441-446.

Trindade, R.I.F., D'Agrella-Filho, M.S., Babinski, M., Font, E., and Brito Neves, B.B., 2004, Paleomagnetism and geochronology of the Bebedouro cap carbonate: Evidence for continental-scale Cambrian remagnetization in the São Francisco Craton, Brazil: Precambrian Research, v. 128, p. 83-103.

Vieira, L.C., Trindade, R.I.F., Nogueira, A.C.R., and Ader, M., 2007, Identification of a Sturtian cap carbonate in the Neoproterozoic Sete Lagoas carbonate platform, Bambuí Group, Brazil: Comptes Rendus Geoscience, v. 339, p. 240-258.

Walker, R.J., Horan, M.F., Morgan, J.W., Becker, H., Grossman, J.N., and Rubin, A.E., 2002a, Comparative ^{187}Re-^{187}Os systematics of chondrites: implications regarding early solar system processes: Geochimica et Cosmochimica Acta, v. 66, p. 4187-4201.

Walker, R.J., Prichard, H.M., Ishiwatari, A., and Pimentel, M., 2002b, The osmium isotopic composition of convecting upper mantle deduced from ophiolite chromites: Geochimica et Cosmochimica Acta, v. 66, p. 329-345.

Walter, M.R., Veevers, J.J., Calver, C.R., Gorjan, P., and Hill, A.C., 2000, Dating the 840-544 Ma Neoproterozoic interval by isotopes of strontium, carbon, and sulfur in seawater, and some interpretative models: Precambrian Research, v. 100, p. 371-433.

Weil, A.B., Geissman, J.W., and Ashby, J.M., 2006, A new paleomagnetic pole for the Neoproterozoic Uinta Mountain Supergroup, Central Rocky Mountain states, USA: Precambrian Research, v. 147, p. 234-259.

Woodhouse, O.B., Ravizza, G., Falkner, K.K., Statham, P.J., and Peucker-Ehrenbrink, B., 1999, Osmium in seawater: vertical profiles of concentration and isotopic composition in the eastern Pacific Ocean: Earth and Planetary Science Letters, v. 173, p. 223-233.

Yoshioka, H., Asahara, Y., Tojo, B., and Kawakami, S., 2003, Systematic variations in C, O, and Sr isotopes and elemental concentrations in Neoproterozoic carbonates in Namibia: Implications for a glacial to interglacial transition: Precambrian Research, v. 124, p. 69-85.

Zhou, C., and Xiao, S., 2007, Ediacaran $\delta^{13}C$ chemostratigraphy of South China: Chemical Geology, v. 237, p. 89-108.

CHAPTER 5

Re-Os, Mo, and Fe Isotope Systematics of Black Shales from the Middle Proterozoic Wollogorang, Barney Creek, and Velkerri Formations, McArthur Basin, Northern Australia

Part of this chapter is in preparation for submission:
Kendall, B., Creaser, R.A., Anbar, A.D. and Gordon, G.W., Re-Os and Mo isotope systematics of black shales from the Middle Proterozoic Velkerri and Wollogorang Formations, McArthur Basin, northern Australia: Geochimica et Cosmochimica Acta.

5.1 INTRODUCTION

Accumulating geological and geochemical evidence suggests there may have been a five-stage history of atmosphere and ocean oxygenation. The stages include: 1) a pre-biotic Hadean and Archean atmosphere and oceans with negligible oxygen abundances (~ 10^{-12} present-day atmosphere levels [PAL]; Goldblatt et al., 2006), 2) an anoxic Archean atmosphere (< 10^{-5} PAL; Pavlov and Kasting, 2002; Goldblatt et al., 2006) and oceans following the evolution of oxygenic photosynthesis, 3) a weakly to moderately oxygenated atmosphere (10^{-5} to > 10^{-2} PAL; Farquhar and Wing, 2003) and surface oceans following the Great Oxidation Event 2.45-2.32 Ga (Bekker et al., 2004), but with continued deep sea anoxia, 4) stratified Proterozoic oceans after ca. 1.8 Ga, with oxygenated surface waters and euxinic deep waters that terminated banded iron formation deposition (Canfield, 1998), and 5) oxygenated Latest Proterozoic and Phanerozoic atmosphere (i.e., 0.5 < PAL < 2; Lasaga and Ohmoto, 2002) and deep oceans after ca. 580 Ma (Fike et al., 2006; Canfield et al., 2007) with the exception of restricted basins of limited areal extent. Acceptance of all aspects of this model is not universal. For example, the alternative Dimroth-Ohmoto hypothesis suggests the atmosphere and oceans have been oxygenated since ca. 3.8 Ga (Ohmoto, 2004; Ohmoto et al., 2006). Nevertheless, geochemical (e.g., Fe-S-C systematics, S and Mo isotopes) and biomarker evidence continues to accumulate in support of low-sulfate (~ 1.5-4.5 mM) stratified Middle Proterozoic ocean basins (Lyons et al., 2000; Shen et al., 2002, 2003; Arnold et al., 2004; Kah et al., 2004; Poulton et al., 2004; Brocks et al., 2005; Johnston et al., 2006) with low dissolved nutrient abundances that may have retarded eukaryotic diversification until the Neoproterozoic (Anbar and Knoll, 2002). Recently, Slack et al. (2007) suggest Middle Proterozoic open-marine deep oceans may have been suboxic (based on Ce anomalies from 1.74-1.71 Ga hematitic chert and iron formation, and association of hematitic chert and/or iron formation with Middle Proterozoic volcanogenic massive sulfide deposits), with euxinic deep waters in intracratonic and silled basins, and possibly upwelling zones on continental margins. Sulfur isotope data (suggesting the onset of active microbial sulfur disproportionation by ~ 1300 Ma; Johnston et al., 2005) and recent constraints on atmospheric pCO_2 and pCH_4 (Kah and Riding, 2007) indicate a protracted and gradual increase in atmosphere and ocean oxygen abundances during the

Mesoproterozoic that accelerated during the Neoproterozoic (Knoll et al., 1986; Derry et al., 1992; Des Marais et al., 1992; Canfield and Teske, 1996; Hurtgen et al., 2005; Fike et al., 2006; Kennedy et al., 2006; Canfield et al., 2007).

Simultaneous application of the recently developed Re-Os radioisotope and Mo and Fe stable isotope systems to black shales has tremendous potential for tracking changes in ocean and atmosphere redox state over geological time. The precision and accuracy of the ^{187}Re-^{187}Os system as a deposition-age geochronometer for black shales has been demonstrated by the excellent agreement (to within ~ 0.2%) of Re-Os black shale and U-Pb zircon age constraints for the Devonian-Carboniferous boundary (Selby and Creaser, 2005a). Precise Re-Os ages have been obtained for several Neoproterozoic shales with low total organic carbon contents (e.g., TOC ~ 0.5-1%), and the Re-Os black shale geochronometer is robust up to the onset of lowermost greenschist facies metamorphism (Kendall et al., 2004, see Chapters 3 and 4). Molybdenum and Fe isotopes in euxinic black shales show excellent promise as ocean paleoredox proxies. Black shales may record the Mo isotope composition of contemporaneous seawater if Mo uptake from the immediately overlying euxinic water column and pore waters is quantitative (Barling et al., 2001; Arnold et al., 2004). Fractionation of seawater Mo isotopes relative to lithogenic/riverine sources occurs predominantly in association with adsorption of isotopically light Mo onto Mn nodules in oxic environments (Barling et al., 2001; Siebert et al., 2003; Barling and Anbar, 2004). A much smaller Mo isotope fractionation occurs during diagenetic Mo sulfide formation in anoxic/non-sulfidic environments (Poulson et al., 2006). Consequently, the ocean Mo isotope budget is sensitive to the redox state (oxic versus euxinic) of the global deep oceans (Barling et al., 2001; Siebert et al., 2003; Arnold et al., 2004). Bulk and pyrite Fe isotope analyses of modern sediments and ancient black shales have shown that Fe isotopes can be used to recognize ancient euxinia within sedimentary basins, and may track the nature of Fe redox cycling within ocean basins over geological time (Matthews et al., 2004; Rouxel et al., 2005; Yamaguchi et al., 2005; Archer and Vance, 2006; Duan et al., 2006, 2007; Severmann et al., 2006a, b, c).

Here, I investigate the Re-Os, Mo, and Fe isotope systematics and trace metal abundances in the 1.73 Ga Wollogorang Formation (Tawallah Group), 1.64 Ga Barney Creek Formation (McArthur Group), and 1.4 Ga Velkerri Formation (Roper Group) black shales from the McArthur Basin, northern Australia. Arnold et al. (2004) have previously presented Mo isotope data for the Velkerri and Wollogorang Formation shales, and suggested the Mo isotope composition ($\delta^{97/95}$Mo) of 1.7-1.4 Ga seawater was ~ 0.8‰ lighter relative to present-day seawater. They interpreted these results to reflect a decreased uptake of isotopically light Mo onto Mn oxides because of expanded Middle Proterozoic deep-sea anoxia. I present new Re-Os ages that better constrain the depositional age of the Velkerri Formation, as well as new precise Mo isotope data that provide a tighter constraint on the Mo isotope composition of global seawater at 1.4 Ga. Trace metal and Re-Os isotope systematics in the Velkerri and Wollogorang Formation black shales are compared to elucidate the nature of elemental partitioning of Re and Os, and thus variations in initial ^{187}Re/^{188}Os isotope ratios, during organic-rich sediment deposition. Post-depositional hydrothermal fluid flow is suggested to have disturbed the Re-Os and Mo isotope systematics in the Wollogorang Formation black shales. New bulk Fe isotope data for the Wollogorang and Velkerri Formation shales suggest that both the nature of Fe redox cycling in suboxic continental margin sediments and the shelf-to-basin transport of isotopically light benthic Fe was not greatly dissimilar in Middle Proterozoic versus Phanerozoic and present-day ocean basins.

5.2 THE WOLLOGORANG, BARNEY CREEK, AND VELKERRI FORMATIONS, McARTHUR BASIN, NORTHERN AUSTRALIA

The intracratonic McArthur Basin of northern Australia preserves a regionally extensive, thick (up to 10 km) succession of essentially unmetamorphosed and weakly-to-mildly deformed sedimentary and subordinate volcanic rocks deposited between 1.8 and 1.4 Ga (Plumb, 1979). Formation and evolution of the McArthur Basin and other intracratonic, continental back-arc regions (e.g., Lawn Hill and Mount Isa) of north-central Australia was shaped by cratonic tilting and intraplate deformation associated with subduction and orogeny at a convergent tectonic zone on the southern margin of the North Australia Craton between 1800 and 1575 Ma (Myers et al., 1996; Scott et al., 2000; Betts et al., 2003). Although McArthur Basin strata have traditionally been subdivided into the Tawallah, McArthur, Nathan, and Roper Groups (Figure 5.1), three main superbasin phases have recently been recognized between 1800 and 1575 Ma (1800-1760

Ma Leichhardt, 1740-1690 Ma Calvert, and 1670-1575 Ma Isa), each separated by ~ 20 M.y. (Page et al., 2000; Scott et al., 2000). Subdivision of the Leichhardt, Calvert, and Isa rock records into second-order supersequences of 10-20 M.y. duration has been interpreted to reflect the interplay of basin dynamics with episodes of intracratonic deformation, some of which resulted in enhanced hydrothermal fluid flow along reactivated faults and the formation of the world-class 1650 Ma Mt Isa, 1640 Ma McArthur River, and 1575 Ma Century Pb-Zn-Ag stratiform ore deposits (Jackson et al., 2000; Page et al., 2000; Southgate et al., 2000). Following basin-wide inversion during the ca. 1575-1500 Ma Isan Orogeny (Lindsay, 2001), development of the intracratonic Roper Superbasin resulted in deposition of up to 5 km of predominantly marine siliciclastic sedimentary rocks (Roper Group). The tectonic controls on Roper deposition are not clear, but may be related to flexural tectonics associated with the Isan Orogeny and ca. 1500-1400 Ma Anmatjira Uplift (Abbott and Sweet, 2000). A final Mesoproterozoic-Neoproterozoic basin inversion event affecting all McArthur Basin and underlying basement rock units was followed by development of the Neoproterozoic to Paleozoic Arafura Basin (Rawlings, 1999). Preservation of nonbiodegraded, fluid inclusion-hosted oils in the Roper Group attest to the stability of the McArthur Basin region since ~ 1 Ga (Dutkiewicz et al., 2003, 2004; Volk et al., 2005).

5.2.1 Wollogorang Formation

The 100-150 m thick, regionally extensive (30,000 km^2 in the southern McArthur Basin), Wollogorang Formation (traditionally part of the Tawallah Group, but recently placed into the Big Supersequence, Calvert Superbasin phase; Southgate et al., 2000) is overlain and underlain by the Settlement Creek and Gold Creek Volcanics, respectively, and is divided into six litho-facies. A basal red siltstone is overlain by stromatolitic to massive dolostone, black shale, and grey dolomitic siltstone (Figure 5.2; Jackson, 1985; Donnelly and Jackson, 1988). A sequence boundary recording a hiatus of up to several million years (Jackson et al., 2000; Page et al., 2000) separates the lower Wollogorang Formation from coarse- and fine-grained dolomitic sandstone and subordinate red dolomitic mudstone of the upper Wollogorang Formation. Although a low-sulfate, lacustrine setting was originally suggested for the Wollogorang Formation (Donnelly and

Jackson, 1988), Shen et al. (2002) have re-interpreted the depositional environment of the Wollogorang Formation as an euxinic, low-sulfate (0.5-2.4 mM), marine intracratonic basin (with at least partial connection to the global ocean) based on sequence stratigraphic studies (Jackson et al., 2000; Page et al., 2000; Southgate et al., 2000), Fe redox proxies (e.g., degree of pyritization [DOP] > 0.45; highly reactive iron to total iron ratios [Fe_{HR}/Fe_T] > 0.38), and uniform pyrite $\delta^{34}S$ isotope compositions (–1.0‰ to +6.3‰).

A ~ 20 m thick unit of dolomitic, pyritic, organic-rich shale (total organic carbon [TOC] up to 6%; Donnelly and Jackson, 1988) occurs within the upper part of the lower Wollogorang Formation, and is characterized by mm- to sub-mm laminations and thin (up to 2 cm) groupings of laminations (microcycles) composed of alternating organic-poor dolomitic mudstone and organic-rich mudstone (Jackson, 1985). The thinnest laminations and microcycles have been interpreted by Jackson (1985) as chemical varves and bundles of varves, respectively. X-ray diffraction (XRD) analysis reveals a mineral assemblage consisting of quartz, feldspar, illite, and minor pyrite and dolomite (Donnelly and Jackson, 1988). Disseminated chalcopyrite, galena, and sphalerite have also been identified from thin sections (Jackson, 1985). Disseminated pyrite within the black shale is typically fine-grained and euhedral with occasional framboidal forms (Shen et al., 2002), although coarse pyrite aggregates are observed within early diagenetic, bituminous dolomite and quartz nodules. Thin dolomite veinlets are also present within the black shale (Donnelly and Jackson, 1988).

Although the Wollogorang Formation is not considered to be mineralized, the presence of high pyrite S to organic C ratios in black shales and dolomitic siltstones, combined with coarse aggregates of pyrite associated with dolomitic nodules and sporadic enrichments in base metal sulfides (Cu, Pb, Zn) at multiple stratigraphic levels, suggests hydrothermal fluids have percolated through the Wollogorang Formation (Jackson, 1985; Donnelly and Jackson, 1988). Primary and overprinted paleomagnetic poles have been identified from the Wollogorang Formation (Idnurm et al., 1995). The overprinted pole plots on a major bend in the apparent polar wander path for Late Paleoproterozoic and Early Mesoproterozoic rocks of northern Australia (Idnurm, 2000) corresponding to a major episode of elevated hydrothermal fluid flow associated with formation of the ca. 1640 Ma stratiform McArthur River (HYC) sedimentary exhalative (SEDEX) ore deposit in the southern McArthur Basin (Idnurm, 2000; Southgate et al., 2000). Mathematical modeling of fault-controlled fluid flow in the southern McArthur Basin associated with ore formation suggests hydrothermal fluids descended to depths of a few kilometers into the upper Tawallah Group (including the Wollogorang Formation) (Garven et al., 2001). The Settlement Creek and Gold Creek Volcanics are suggested to be leached of base metals (Cu, Pb, Zn) by low-temperature (~ 100°C), oxidizing, and saline (> 20 wt. % NaCl equivalent) brines, and have undergone potassic alteration (Cooke et al., 1998). Thermal alteration of the Wollogorang Formation is minimal, with maximum depths of burial corresponding to the overmature zone of hydrocarbon generation (Crick et al., 1988).

The depositional age of the Wollogorang Formation black shale is well-constrained by U-Pb SHRIMP zircon ages of 1729 ± 4 Ma and 1730 ± 3 Ma from tuffaceous green claystone layers in the middle of the black shale (BMR Mount Young 2 drill hole; Page et al., 2000). Given the paleomagnetic, petrological, geochemical, and numerical modeling evidence for a post-depositional hydrothermal influence on the Wollogorang Formation, this rock unit allows a test of the robustness of the Re-Os radioisotope, and Mo and Fe stable isotope systems in black shales during hydrothermal fluid flow.

5.2.2 Barney Creek Formation

In the Batten Fault Zone and Glyde Sub-basin to the south, the Barney Creek Formation (McArthur Group, recently placed into the River Supersequence of the Isa Superbasin phase; Southgate et al., 2000) extends over 25,000 km^2 and comprises up to 700-900 m of laminated, organic-rich dolomitic siltstone and shale that is underlain and overlain by the stromatolitic Teena Dolomite and Reward Dolomite, respectively (Davidson and Dashlooty, 1993; Jackson et al., 1987; Bull, 1998). The Barney Creek Formation can be subdivided into the lower W-Fold (multi-colored dolomitic siltstone and shale) and upper HYC Pyritic Shale (organic-rich, locally pyritic, dolomitic siltstone and shale) Members (Figure 5.3; Jackson et al., 1987; Bull, 1998). The HYC Pyritic Shale Member and overlying Reward Dolomite form one of four depositional cycles whereby the former represents a condensed section deposited during tectonic subsidence and rapid transgression, and the latter represents high stand conditions and declining accommodation space (Southgate et al., 2000). The lower part of the HYC Pyritic Shale Member is the host rock of the world-class McArthur River SEDEX ore deposit, whose mechanism of ore formation and fluid chemistry are still being debated (e.g., Davidson, 1998; Large et al., 1998, 2001; Garven et al., 2001; Chen et al., 2003; Yang et al., 2004). Based on sedimentology (stacked series of flooding surfaces and increasing thickness of organic-rich shale beds upsection in the HYC Pyritic Shale Member) and geochemistry (Mn haloes in the underlying W-Fold Shale Member, and Pb-Zn mineralization in the HYC Pyritic Shale Member), ore formation was likely contemporaneous with deposition in an euxinic basin under water depths of more than several hundred meters (Bull, 1998; Large et al., 1998). A narrow range in pyrite $\delta^{34}S$ of +18.2‰ to +23.4‰ (likely similar to contemporaneous seawater sulfate) and elevated DOP and Fe_{HR}/Fe_T ratios from black shales further suggests deposition in a sulfate-depleted euxinic basin with more restricted connection to the global ocean relative to the Wollogorang Formation (Shen et al., 2002). This is consistent with hydrocarbon biomarkers diagnostic of strongly reducing conditions and the presence of co-existing communities of phototrophic purple sulfur bacteria and green sulfur bacteria (Brocks et al., 2005), with low abundances of steranes suggesting a minor contribution from eukaryotes (Summons et al., 1988). Biomarkers and large filamentous microfossils from the ore deposit also provide evidence for the oldest known sulfide-oxidizing bacteria (Logan et al., 2001).

The HYC Pyritic Shale Member (~ 80 m thick in drillhole DDH BMR McArthur 2 located 23 km southwest of the McArthur River mine; Bull, 1998) is characterized predominantly by thin-bedded grey dolomitic siltstone and fine-grained sandstone interbedded with subordinate organic-rich, dolomitic black shale containing diffuse pyritic bands (with similar morphologies as in the Wollogorang Formation; Shen et al., 2002), and rare dolomitic sandstone. Organic-rich shale beds range in thickness from 0.5 m to 6.5 m, and thin sections reveal a mineral assemblage consisting primarily of quartz + dolomite ± pyrite (Bull, 1998). Typical TOC abundance for the Barney Creek Formation organic-rich shales is between 2% and 4% (Bull, 1998) although values up to ~ 10% are known (Crick et al., 1988; Jackson et al., 1988). Organic matter is predominantly type I (e.g., algal) and is thermally mature except near major fault zones (associated with hydrothermal fluid flow) and in some regions of the Batten Fault Zone (associated with deposition in a complex, tectonically active environment) where it is highly mature to overmature (Crick et al., 1988; Crick, 1992; Logan et al., 2001).

Three U-Pb SHRIMP zircon dates of 1640 ± 3 Ma, 1639 ± 3 Ma, and 1638 ± 7 Ma from tuffaceous beds throughout the Barney Creek Formation provide tight age constraints on its depositional age. The first two ages come from tuffs below the HYC ore horizon, whereas the last age is from a tuff above the ore (Page and Sweet, 1998). Based on paleomagnetic data from the McArthur River deposit, the timing of the mineralization event occurred within 15 million years of deposition of the Barney Creek Formation (Symons, 2006).

5.2.3 Velkerri Formation

Relatively undeformed strata of the Roper Group are subdivided into a cyclic series of formations comprising 200-400 m thick shale and 100-300 m thick quartz arenite that is preserved over an area of 145,000 km^2 within the Roper Superbasin (Jackson and Raiswell, 1991; Abbott and Sweet, 2000). Six third-order progradational sequences comprising lower shale-rich and upper sandstone-rich intervals make up the middle part of the Roper Group in the Roper River district (Abbott and Sweet, 2000) (Figure 5.4). The Velkerri Formation and the overlying Moroak Sandstone Member (McMinn Formation) comprise the Veloak Sequence that is underlain and overlain by sandstones and shales of the Corbess and Shermi sequences, respectively (Abbott and Sweet, 2000). Initial studies suggested deposition of the Roper Group in a passive margin (Jackson et al., 1988) or a barred bay or lake (Donnelly and Crick, 1988), but more recent sedimentological (e.g., presence of glauconite) and sequence stratigraphic studies favor an open-marine, epicratonic basin as the depositional environment (Jackson and Raiswell, 1991; Warren et al., 1998; Abbott and Sweet, 2000). Subsequently, pyrite sulfur isotope and Fe redox proxy data (DOP and Fe_{HR}/Fe_T) along a paleodepth gradient from continental shelf to basin floor suggests deposition of the Roper Group sediments took place in an open-marine, low-sulfate, stratified water column characterized by oxidizing surface waters on the continental shelf (pyrite $\delta^{34}S \geq +10.2‰$) and euxinic, basinal deep waters (pyrite $\delta^{34}S$: –20.7‰ to +25.5‰) (Shen et al., 2003).

Of the mudstone-rich intervals in the Roper Group, the Velkerri Formation (~ 400 m thick) represents the most basinal facies, and has an areal extent of at least 80,000 km^2. It is dominantly composed of grey to black massive, thin-bedded, laminated, or contorted organic-rich, pyritic mudstone with subordinate grey-green, organic-poor glauconitic siltstone (Jackson and Raiswell, 1991; Warren et al., 1998; Abbott and Sweet, 2000). XRD analysis, glycolation, and staining indicate a mineral assemblage composed of quartz, chlorite, illite and mixed-layer illite/smectite, and subordinate albite, calcite, dolomite, pyrite, siderite, kaolin, and calcium phosphate (Warren et al., 1998). Highly organic-rich sections (TOC > 5%) tens of meters thick occur at three levels within the Velkerri Formation and are oil source beds (Jackson and Raiswell, 1991; Warren et al., 1998). Live oil containing prokaryotic biomarkers (Jackson et al., 1986) is documented from drillhole BMR Urapunga-4 at 345.4-346.5 m (Jackson et al., 1986) and 352.1-353.0 m (Crick et al., 1988) depth. Organic matter from lamalginites in the Velkerri Formation is between type I and II (e.g., derived from algae and cyanobacteria; Crick et al., 1988; Summons et al., 1994), and high abundances of monomethyl branched alkanes and low abundances of steranes in thermally immature sections reflect a predominantly prokaryotic organic matter source with a subordinate contribution from eukaryotes (Summons et al., 1988). The latter is consistent with the presence of large spheroidal microfossils (e.g., acritarchs such as *Tappania plana*) in the Roper Group interpreted as eukaryotic marine protists (Javaux et al., 2001, 2004).

Thermal maturity of organic matter in the Velkerri Formation ranges from marginally mature (e.g., maximum burial depth of ~ 2.5 km and ~ 75°C; Jackson et al., 1988) to highly mature except where affected by a dolerite sill intrusion (Crick et al., 1988; Crick, 1992; Summons et al., 1994; George and Ahmed, 2002). Multiple episodes of hydrocarbon migration from the Velkerri Formation occurred prior to ca. 1 Ga. Bitumen in pore spaces of the Bessie Creek Sandstone and in veins cross-cutting a dolerite sill represents the oldest known hydrocarbon migration event and was associated with sill intrusion prior to ca. 1280 Ma. Non-biodegraded fluid inclusion oils preserved in quartz from the Bessie Creek Sandstone, and in partially altered plagioclase feldspar, and calcite and quartz veins within the dolerite sills represent at least one younger episode of hydrocarbon migration associated with late Mesoproterozoic – Early Neoproterozoic McArthur Basin inversion (Dutkiewicz et al., 2003, 2004; Volk et al., 2005). High molecular weight (C_{13+}) hydrocarbons with vitrinite reflectance values of ~ 0.8-1.0 % in the fluid inclusion oils were likely sourced from the Velkerri Formation based on similarities of biomarker chemistry and thermal maturity, and consideration of migration distance. Lower molecular weight hydrocarbons from fluid inclusion oil in dolerite sill plagioclase feldspar may have been sourced from the Barney Creek Formation (Volk et al., 2005).

The depositional age of the Velkerri Formation is not as well-constrained as the Wollogorang Formation. A robust maximum age constraint of 1492 ± 4 Ma is provided by a U-Pb SHRIMP zircon date on tuff from the Wooden Duck Member of the Mainoru Formation, which is over 700 m stratigraphically beneath the Velkerri Formation in the Roper Group (Jackson et al., 1999). A Rb-Sr illite date of 1429 ± 31 Ma from dolomitic siltstone of the Kyalla Member from the overlying McMinn Formation may provide a minimum age constraint (Kralik, 1982), but authigenic and detrital considerations render the interpretation of Rb-Sr dates highly problematic (e.g., Gorokhov et al., 2001). Dolerite sills intruding into the Roper Group (and Velkerri Formation) yield K-Ar dates of ca. 1220 and 1280 Ma from plagioclase, but probable Ar loss suggests these ages are only minimum estimates for dolerite intrusion (McDougall et al., 1965).

5.3 SAMPLES AND ANALYTICAL METHODS

For this study, drillcore samples from the Wollogorang (drill hole BMR Mount Young 2; Plate 5.1), Barney Creek (drill hole BMR McArthur 2; Plate 5.2), and Velkerri (drill hole BMR Urapunga-4; Plates 5.3 and 5.4) Formation black shales were obtained from the drill core repository of Geoscience Australia at Canberra, Australian Capital Territory, Australia. The Mount Young 2 drill hole lies within the deformed Batten Fault Zone and is ~ 100 km from the world-class Pb-Zn-Ag HYC ore deposit at McArthur River (see Figure 5.1). Wollogorang Formation samples were obtained from 74-77 m depth in Mount Young 2, and are several meters below the ca. 1730 Ma tuff horizons dated by the U-Pb SHRIMP zircon method (Page et al., 2000). From the McArthur 2 drill hole, the Barney Creek Formation was sampled from an organic-rich shale bed at 68.11-68.58 m and another stratigraphically lower bed at 83.11-83.44 m depth. The relatively undeformed Velkerri Formation in Urapunga-4 was sampled at 136.9-137.9 m and 325.7-326.7 m depth, which corresponds to the upper-most and lower-most organic-rich intervals (TOC > 5%) of Jackson and Raiswell (1991). For each sample, at least 20 g of shale was processed to fine powder. Smaller samples (5-15 g) of Wollogorang Formation shale adjacent to small dolomite veinlets (Plate 5.5) were also prepared for assessing the robustness of Re-Os, Mo, and Fe isotope systematics during hydrothermal fluid flow.

Protocols for metal-free processing of organic-rich sedimentary rocks (ORS) to produce powdered samples, subsequent chemical digestion, separation, and purification of Re and Os, and isotopic analysis by isotope dilution – negative thermal ionization mass spectrometry (ID-NTIMS) are described in Appendix A. Chemical digestion, separation, purification, and isotopic analysis of Mo and Fe by multiple collector – inductively coupled plasma – mass spectrometry (MC-ICP-MS) was carried out following the methods outlined in Appendix B. In addition, elemental abundances of sample powders were determined by quadrupole – inductively coupled plasma – mass spectrometry (Q-ICP-MS) (Appendix C.1). Sample degree-of-pyritization (DOP) was determined following the protocols outlined in Appendix C.3.

Rhenium and Os abundances and isotope compositions were obtained for all samples, with a subset of these also analyzed for elemental abundances and Mo and Fe isotopes. Total procedural blank abundances of Re and Os based on three 100 g bottles of Fluka Chemika CrO_3 (Lots #447647/1, 1125527, and 1177884) used over the course of this study were 10.7 ± 4.6 pg (1σ, n=12) and 0.38 ± 0.22 pg (1σ, n=12), respectively, with blank $^{187}Os/^{188}Os$ of 0.26 ± 0.10 (1σ, n=9). Procedural blanks for Mo and Fe are generally negligible relative to sample abundance. Molybdenum and Fe isotope data are reported using the conventional per-mil delta (δ) notation:

$$\delta R_{sample}\ (‰) = [R_{sample}/R_{standard} - 1] \times 1000 \qquad (1)$$

where R = isotope ratio ($\delta^{97/95}Mo$ or $\delta^{56/54}Fe$). Sample $\delta^{97/95}Mo$ is reported relative to the Johnson Matthey Specpure® Mo plasma standard (Lot #802309E; RochMo2) which has an identical Mo isotopic composition as the RochMo standard (Lot #7024991) used at the University of Rochester (Anbar et al., 2001; Barling et al., 2001; Arnold et al., 2004).

Iron isotope analyses are reported as $\delta^{56/54}$Fe relative to the IRMM-014 standard (Taylor et al., 1992).

5.4 RESULTS

5.4.1 Elemental Abundances

Elemental abundances were obtained for selected samples of the Wollogorang Formation, Barney Creek Formation, and the upper and lower Velkerri Formation organic-rich intervals, and are presented in Table 5.1. Enrichment factors (EF) were calculated for each element using the following formula:

$$EF = (\text{element/Al})_{\text{sample}} / (\text{element/Al})_{\text{average shale}} \qquad (2)$$

where average shale data are from Wedepohl (1971, 1991). Element EF, Fe_T/Al ratios (Fe_T = total Fe abundance), and DOP data (see section 2.4.2 for a brief summary of the Fe-based redox proxies) are presented in Table 5.2. These data are used to place constraints on the paleoredox state of bottom waters during deposition of the Wollogorang, Barney Creek, and Velkerri Formation black shale intervals studied here.

Recently, the degree of enrichment of certain redox-sensitive metals in open-marine organic-rich shales has been suggested as a possible redox proxy for distinguishing between deposition from anoxic/non-sulfidic and euxinic bottom waters (Algeo and Maynard, 2004; Tribovillard et al., 2006). For example, using trace metal data obtained for Upper Pennsylvanian shales from eastern Kansas, Algeo and Maynard (2004) suggested that highly elevated EF of at least two of four elements of "strong euxinic affinity" (Mo, U, V, and Zn) can be considered diagnostic of euxinic conditions. However, this approach requires caution as such enrichments may not be observed for euxinic sediments deposited in restricted basins or under conditions of widespread global anoxia (e.g., as is postulated for stratified Proterozoic oceans; Anbar and Knoll, 2002) because in these cases, the seawater trace metal inventory may become depleted (Algeo, 2004; Algeo and Lyons, 2006). With this in mind, I compare the EF of the elements of strong euxinic affinity (Mo, U, V, and Zn) with DOP and Fe_T/Al data to assess the redox conditions during deposition of the sampled Wollogorang, Barney Creek, and Velkerri Formation black shale intervals.

Samples from the upper Velkerri Formation interval show high and invariant DOP (0.90-0.92) and elevated Fe_T/Al ratios (1.4-1.9). Rhenium (EF > 100) and Mo (EF > 200) show a high degree of enrichment, whereas moderately elevated EFs are also observed for U (8-10), V (8-12), and Zn (7-16). In contrast, lower DOP (0.43-0.51), Fe_T/Al (0.5-1.4), and EFs for the redox-sensitive metals (Mo: 5-19; Re: 7-24; U: 2-5; V: 1-2; Zn: 3-8) characterize the lower Velkerri Formation interval. These observations are most consistent with deposition of the upper and lower Velkerri Formation intervals from euxinic and anoxic/non-sulfidic bottom waters, respectively.

The bottom water redox state during deposition of the Wollogorang Formation is less clear because of large variation in DOP values (0.58-0.92) and elemental EFs. Although Mo (EF: 45-143) and Re (EF: 23-87) are appreciably enriched in the Wollogorang Formation black shales, U is only moderately enriched (EF: 4-10), whereas V is not (EF < 5), and Zn is anomalously depleted (EF < 0.6). In addition, the Fe_T/Al ratios (0.22-0.73) overlap with the average shale value of ~ 0.55. Based on these observations, the Wollogorang Formation black shale interval may have been deposited from bottom waters that fluctuated between anoxic/non-sulfidic and euxinic redox conditions, and were characterized by variable deep water metal replenishment times associated with variably restricted basin conditions (Algeo and Lyons, 2006). The low Fe_T/Al ratios may reflect high sedimentation rates in an euxinic water column that could also explain some DOP values less than 0.75 (Canfield et al., 1996; Lyons, 1997; Lyons and Severmann, 2006). Alternatively, enhanced reactivity of the detrital fraction may be a possible explanation for the low Fe_T/Al ratios, but generally high DOP values (Anderson and Raiswell, 2004). However, the large variation in Cu abundances (48-278 ppm), combined with depleted Zn abundances (< 20 ppm; average shale: 95 ppm), suggests the ambiguous redox proxy data may result from metal remobilization during hydrothermal fluid flow through the Wollogorang Formation (e.g., Donnelly and Jackson, 1988). Elevated abundances of CaO, MgO, and Mn in some samples [e.g., 74.35-74.38 m, 75.08-75.11 m, 76.91-76.96 (dol) m] reflect a greater proportion of dolomite veinlets in those samples.

Two samples (one from each of the two shale intervals) from the Barney Creek Formation have DOP > 0.75 and Fe_T/Al ratios (0.72 and 1.2) above average shale (~

0.55), but are characterized by lower EF for Re (2.7 and 7.8), Mo (8.8 and 20), and U (3.5 and 3.7) compared to the upper Velkerri and Wollogorang Formations. Vanadium (EF: 1.5 and 2.7) and Zn (EF: 0.71 and 0.38) are not enriched in these shales. Anomalously high abundances of Mn (EF: 6.0 and 6.3), likely associated with dolomite, are probably derived from Mn-enriched bottom waters discharged into the basin from fault systems (Large et al., 1998). These observations are consistent with sulfur isotope (Shen et al., 2002) and biomarker (Brocks et al., 2005) data, and suggest deposition in a markedly restricted euxinic basin where bottom waters were strongly depleted of trace metals (c.f., Algeo and Lyons, 2006).

5.4.2 Re-Os, Mo, and Fe Isotopes

The Re-Os, Mo and Fe abundance and isotope data for the Wollogorang, Barney Creek, and Velkerri Formation black shales are shown in Tables 5.3-5.5. The Wollogorang and Velkerri Formation shales are markedly enriched in Re and Os relative to average present-day eroding upper continental crust (~ 0.2-2 ppb Re and 30-50 ppt Os; Esser and Turekian, 1993; Peucker-Ehrenbrink and Jahn, 2001; Hattori et al., 2003; Sun et al., 2003a, b). The upper Velkerri Formation interval is significantly enriched in Re (39-53 ppb) and Os (972-1286 ppt) relative to the lower interval (4.9-8.1 ppb Re and 123-204 ppt Os), whereas the Wollogorang Formation black shales have intermediate Re (9-30 ppb) and Os (240-729 ppt) abundances. The ^{187}Re/^{188}Os isotope ratios for the upper and lower Velkerri Formation intervals range between 450 and 600, and between 388 and 519, respectively, whereas ^{187}Os/^{188}Os isotope ratios range between 10.6 and 14.0, and between 9.3 and 12.4, respectively. The Wollogorang Formation is characterized by a large spread in ^{187}Re/^{188}Os (475-778) and ^{187}Os/^{188}Os (13.8-20.3) isotope compositions. One replicate analysis of a lower Velkerri Formation sample (137.84-137.89 m) shows excellent reproducibility in Re and Os abundances, and ^{187}Re/^{188}Os and ^{187}Os/^{188}Os isotope ratios. However, replicate analyses of three Wollogorang Formation samples (75.51-75.53 m, 76.00-76.03 m, and 76.03-76.08 m) show poor reproducibility in Re and Os (up to 5% variation) abundances, and ^{187}Re/^{188}Os (up to 17% variation) and ^{187}Os/^{188}Os (up to 15% variation) isotope ratios. The Barney Creek Formation shales have low Re (0.7-3 ppb) but elevated Os (118-550 ppt) abundances, and have a low and narrow range of ^{187}Re/^{188}Os (22-36) and ^{187}Os/^{188}Os (0.85-1.14) isotope ratios.

Regression of the Re-Os isotope data for the upper and lower Velkerri Formation intervals yields Re-Os dates of 1361 ± 21 Ma (2σ, n = 14, Mean Square of Weighted Deviates [MSWD] = 1.3, Model 1, probability of fit = 0.20, initial ^{187}Os/^{188}Os [I_{Os}] = 0.29 ± 0.18; Figure 5.5A) and 1417 ± 29 Ma (n = 12, MSWD = 1.3, Model 1, probability of fit = 0.25, I_{Os} = 0.06 ± 0.22; Figure 5.5B), respectively. If an uncertainty of ± 0.31% (2σ) for λ^{187}Re (Smoliar et al., 1996; Selby et al., 2007a) is propagated together with the uncertainty in the slope of the regression, then the Re-Os dates for the upper and lower Velkerri Formation are 1361 ± 22 Ma and 1417 ± 30 Ma, respectively. In contrast, the Wollogorang Formation Re-Os isotope data show considerable scatter, and yield an imprecise date of 1359 ± 150 Ma with an unusually high I_{Os} value (n = 21, MSWD = 86, Model 3, I_{Os} = 3.5 ± 1.5; Figure 5.5C). The restricted range in ^{187}Re/^{188}Os and ^{187}Os/^{188}Os isotope ratios for the two shale intervals of the Barney Creek Formation do not allow derivation of any age information.

Molybdenum isotope data for the Mo-enriched samples (105-119 ppm) of the upper Velkerri Formation interval overlap within 2σ analytical uncertainties, and have an average $\delta^{97/95}$Mo of 0.72 ± 0.10 ‰ (n = 6). In contrast, a wider variation in Mo abundance (41-58 ppm) and $\delta^{97/95}$Mo (from 0.30‰ to 0.79‰) is observed for nine Wollogorang Formation samples. No correlations are observed among $\delta^{97/95}$Mo, Mo abundance, and DOP for the Wollogorang Formation (Figure 5.6). The new Mo isotope data reported here are generally consistent with previously reported data for the Wollogorang Formation and stratigraphically lower samples of the Velkerri Formation that were obtained using black shales from the same drill cores sampled in this study (Arnold et al., 2004).

The $\delta^{56/54}$Fe values for five Velkerri and nine Wollogorang Formation samples range from –0.31‰ to +0.22‰, and from –0.33‰ to –0.09‰, respectively. A well-correlated inverse trend between DOP and $\delta^{56/54}$Fe (R^2 = 0.97) is observed for the Velkerri Formation samples whereas a weak inverse correlation (R^2 = 0.31) is observed for the Wollogorang Formation samples (Figure 5.7). In contrast, two Barney Creek

Formation samples have markedly heavy $\delta^{56/54}$Fe values (+0.34‰ and +0.39‰), and plot well above the overall trend defined by the Wollogorang and Velkerri Formations.

5.5 DISCUSSION

5.5.1 Implications of the Velkerri Formation Re-Os Ages and Controls on the Initial ^{187}Re/^{188}Os Ratio During Organic-rich Sediment Deposition

5.5.1.1 Re-Os Depositional Ages and the Os Isotope Composition of Middle Proterozoic Seawater

The Re-Os dates of 1361 ± 21 Ma and 1417 ± 29 Ma for the upper and lower organic-rich intervals of the Velkerri Formation, respectively, are internally consistent with stratigraphic position, and consistent with the U-Pb SHRIMP zircon age of 1492 ± 4 Ma from the Mainoru Formation of the lower Roper Group (Jackson et al., 1999). In conjunction with the low degree of scatter associated with both regressions (MSWD = 1.3), the Re-Os dates are interpreted to represent depositional ages for these intervals of the Velkerri Formation. Accordingly, the new Re-Os ages directly constrain the age of biomarkers (Jackson et al., 1986; Summons et al., 1988) in the Velkerri Formation, and the acritarch and microfossil-bearing strata in the Roper Group (Javaux et al., 2001, 2004) are now known to span at least 100 M.y. of geological time. In addition, the multiple episodes of hydrocarbon maturation and migration from the Velkerri Formation prior to ca. 1 Ga (Dutkiewicz et al., 2003, 2004; Volk et al., 2005) do not appear to have affected the Re-Os systematics in these shales, consistent with the previous findings of Creaser et al. (2002), Kendall et al. (2004), and Selby and Creaser (2005a) that collectively suggest the Re-Os black shale geochronometer is robust up to the onset of lower greenschist-facies metamorphism. The oldest hydrocarbon migration event from the Velkerri Formation associated with dolerite sill intrusion (Dutkiewicz et al., 2004; Volk et al., 2005) is now bracketed between the minimum K-Ar plagioclase date of 1280 Ma (McDougall et al., 1965) and the Re-Os shale date of 1361 ± 21 Ma. Finally, the new Re-Os ages for the Velkerri Formation demonstrate the utility of Re-Os geochronology of black shales deposited from both anoxic/non-sulfidic and euxinic bottom water conditions.

Initial Os isotope compositions (hereafter I_{Os}) from Re-Os isochron regressions may record the Os isotope composition of the contemporaneous seawater at the time of sediment deposition (Ravizza and Turekian, 1992). Large uncertainties are associated with the I_{Os} from the Re-Os isochron regressions for the Velkerri Formation (0.29 ± 0.18 and 0.06 ± 0.22 for the upper and lower intervals, respectively) because only samples with radiogenic present-day $^{187}Os/^{188}Os$ isotope ratios (between ~ 9 and 14) were analyzed. However, the values for I_{Os} overlap with the chondritic $^{187}Os/^{188}Os$ isotope composition at ca. 1400 Ma (~ 0.12; Walker et al., 2002a). Based on the similar present-day $^{187}Os/^{188}Os$ isotope compositions (~ 0.13) of the primitive (Meisel et al., 1996, 2001) and convecting (Walker et al., 2002b) upper mantle to carbonaceous, ordinary, and enstatite chondrites (Walker et al., 2002a), the major source of common Os in the Velkerri Formation was likely from volcanism (Alves et al., 2002), weathering of young subduction arc-related crust (Martin et al., 2000), low- and high-temperature hydrothermal metasomatism at mid-ocean spreading centers (Sharma et al., 2000; Cave et al., 2003), and/or dissolution of cosmic dust (Peucker-Ehrenbrink, 1996) rather than radiogenic riverine Os inputs from weathering and erosion of crustal sources (Levasseur et al., 1999). The importance of extraterrestrial versus unradiogenic terrestrial Os sources is difficult to evaluate in the absence of constraints on the meteoritic particulate flux to the Middle Proterozoic Earth relative to the present-day flux. A volcanogenic provenance for middle Velkerri Formation shales is suggested by the presence of silty laminae containing quartz grains and volcanogenic lithic clasts cemented with chlorite (Warren et al., 1998). Thus, the low I_{Os} of the upper Velkerri Formation interval may result at least partly from input of unradiogenic riverine Os derived from weathering of volcanic rocks. Present-day subduction zone lavas, for example, are known to contain unradiogenic Os (Alves et al., 2002). Volcanic activity during deposition of the Velkerri Formation may be associated with ongoing orogenic activity on the southern margin of the North Australia Craton (e.g., Myers et al., 1996).

Modern organic-rich sediments from reducing continental margins have a $^{187}Os/^{188}Os$ isotope composition of ~ 0.98-1.07 (Ravizza and Turekian, 1992), similar to that of present-day global seawater (~ 1.06; Sharma et al., 1997; Levasseur et al., 1998; Woodhouse et al., 1999; Peucker-Ehrenbrink and Ravizza, 2000). However, the Os isotope composition of organic-rich sediments in the semi-restricted Black Sea and the Saanich Inlet fjord have less radiogenic Os isotope compositions relative to global seawater that likely reflects lower dissolved and particulate $^{187}Os/^{188}Os$ derived from weathering of mafic/ultramafic lithologies in riverine drainage basins (Ravizza et al., 1991; Poirier, 2006). Input of unradiogenic riverine Os to the ocean from Papua New Guinea is known to lower the Os isotope composition of ambient seawater in the nearby Coral Sea (Martin et al., 2000). Considering the residence time of Os in the stratified McArthur Basin (Shen et al., 2002, 2003) is likely less than that of today (~ 10^4 years; Oxburgh, 1998, 2001; Levasseur et al., 1999), it is possible the upper Velkerri Formation I_{Os} represents only a minimum value for global seawater $^{187}Os/^{188}Os$. At least moderately radiogenic global seawater $^{187}Os/^{188}Os$ is expected at 1.4 Ga given that oxidative weathering of the upper continental crust was likely well established by this time (Yang and Holland, 2002). This is supported by elevated redox-sensitive metal abundances in the upper Velkerri Formation interval and a moderately radiogenic I_{Os} determination of ~ 0.5 from the 1.54 Ga Douglas Formation (Athabasca Basin, Western Canada; Creaser and Stasiuk, 2007). Although the large uncertainty in the upper Velkerri Formation I_{Os} also permits this possibility, determination of I_{Os} from black shales on different crustal blocks is required to better assess the Os isotope composition of global seawater at 1.4 Ga.

5.5.1.2 Variations in the $^{187}Re/^{188}Os$ Isotope Ratio in Black Shales

As discussed in Chapter 3 (section 3.5.7), the mechanism(s) controlling the range in initial $^{187}Re/^{188}Os$ of ORS is not well understood. Overall, Re and ^{192}Os abundances from the Velkerri and Wollogorang Formation shales are well-correlated ($R^2 = 0.94$) and reflect increased enrichment of these redox-sensitive metals in euxinic relative to anoxic/non-sulfidic black shales (Figure 5.8). On an individual basis, however, the correlation ranges from poor (lower Velkerri Formation interval) to excellent (Wollogorang Formation). Although the Re-Os isotope systematics of the Wollogorang Formation black shales have been altered by hydrothermal fluid flow (see section 5.5.3.1), the Re and Os abundances, and thus $^{187}Re/^{188}Os$ isotope ratios, of the shales likely reflect to a first order approximation the original metal enrichments given the preservation of a good correlation between present-day $^{187}Re/^{188}Os$ and $^{187}Os/^{188}Os$ isotope ratios (see Figure 5.5C). Common Os (represented by ^{192}Os) abundances are not well-correlated with $^{187}Re/^{188}Os$ isotope ratios, but Re does show strong correlations with $^{187}Re/^{188}Os$ isotope ratio for the lower Velkerri Formation interval ($R^2 = 0.88$) and the Wollogorang Formation ($R^2 = 0.74$), but not the upper Velkerri Formation interval ($R^2 = 0.06$) (Figure 5.9A, B). The above observations indicate multiple, but poorly understood, controls on Re and Os elemental partitioning in black shales. Cross-plots of major and trace metal abundances with Re and ^{192}Os abundances, and $^{187}Re/^{188}Os$ isotope ratios, may help pinpoint the dominant control on $^{187}Re/^{188}Os$ isotope variations in organic-rich shales (to avoid the development of spurious correlations, elemental abundances were not normalized to Al; Van der Weijden, 2002).

However, systematic relationships between major and trace metal abundances and Re-Os systematics do not appear to be present (Table 5.6). For example, a strong positive correlation between Mo abundance and $^{187}Re/^{188}Os$ isotope ratio ($R^2 = 0.92$) and between Re and Mo abundance ($R^2 = 0.88$), but no correlation between ^{192}Os and Mo abundance, is observed for the lower Velkerri Formation interval (Figure 5.9C). However, the same relationships are not observed for the other two shale intervals with the exception of a moderately positive correlation between Re and Mo abundance ($R^2 = 0.62$) in the upper Velkerri Formation interval. In addition, some correlations between redox-sensitive trace metal abundance and Re or Os abundance are present for each of the three shale intervals, but a similar relationship is not typically observed with $^{187}Re/^{188}Os$ isotope ratios. The main exceptions are the positive correlation with Mo abundance for the lower Velkerri Formation interval, noted above, and the moderately positive correlation with V abundance for the upper Velkerri Formation interval ($R^2 = 0.52$) and the Wollogorang Formation ($R^2 = 0.58$) (Figure 5.9D). One possible explanation for the first case is that under anoxic/non-sulfidic bottom water conditions, variable Re and Mo fluxes to accumulating organic-rich sediments, together with slow precipitation kinetics for these metals (Crusius and Thomson, 2000; Sundby et al., 2004; Yamashita et al., 2007), resulted in correlated Re and Mo abundances, and dominated variations in $^{187}Re/^{188}Os$ isotope ratio for the lower Velkerri Formation interval. In contrast, the moderate correlations between $^{187}Re/^{188}Os$ isotope ratio and V abundance observed for the upper Velkerri Formation interval and the Wollogorang Formation suggest a different control on Re and Os elemental partitioning that is described below.

Rhenium and Os are present in natural hydrocarbons (Poplavko et al., 1975; Barre et al., 1995; Woodland et al., 2001; Selby and Creaser, 2005b) and bitumens (Selby et al., 2005). Bulk organic matter is known to contain a large fraction of the Re and Os in shale source rocks (Ripley et al., 2001; Selby and Creaser, 2003). Theoretical calculations have suggested that Re and Os should form metalloporphyrin complexes with stability indices greater than those of the most common metalloporphyrin-forming elements vanadium (as VO_2^+) and nickel (as Ni^{2+}) (Buchler, 1975). Miller (2004) showed that a significant proportion of the Re in source rocks is solvent-extractable and likely forms metalloporphyrins (or is bound to some solvent-extractable organic phase) whereas Os does not, thus providing further indirect evidence that Re and Os do not reside in the same organic phase(s). Photosynthesis was well-established by the Middle Proterozoic, and metalloporphyrins in source rocks of this age would be derived from cyanobacteria, algae and protists (e.g., Hardison, 1996; Mauzerall, 1998; Xiong et al., 2000; Douglas et al., 2003). The moderate correlations between $^{187}Re/^{188}Os$ and V content for the upper Velkerri Formation interval and the Wollogorang Formation may thus reflect formation of Re and V metalloporphyrins (e.g., Breit and Wanty, 1991; Wanty and Goldhaber, 1992). A moderate correlation between $^{187}Re/^{188}Os$ and Ni ($R^2 = 0.49$) for the Wollogorang Formation, but absence of such a correlation in the upper Velkerri Formation interval, may reflect sufficient dissolved H_2S during deposition of the latter (consistent with high DOP of ~ 0.9) to inhibit the formation of Ni organic complexes (Breit and Wanty, 1991).

Complexation with metalloporphyrins only represents a minor fraction of the V and Ni budget in hydrocarbons. Significant amounts of these metals are also bound to non-porphyrin metal complexes (Filby, 1975; Yen, 1975; Filby and Branthaver, 1987; Filby and Van Berkel, 1987) that may concentrate in the heavy (asphaltene) fraction of hydrocarbons as heteroatomic (N-, S- or O-containing) species (Filby, 1975; Yen, 1975). Recently, Selby et al. (2007b) observed that Re and Os are partitioned predominantly into the asphaltene fraction of oil (> 83%) whereas only a small proportion (< 14%) of these elements were present in the maltene fraction. Thus, shale source rocks may also be characterized by a similar concentration of Re and Os in non-porphyrin metal complexes.

Direct identification of Re- and Os-bearing organic complexes in shale source rocks and determination of their isotopic composition has not been systematically studied. I suggest variations in black shale ^{187}Re/^{188}Os isotope ratios may result, at least in part, from complexing of Re and Os into separate and/or multiple organic host phases, each possessing its own distinctive ^{187}Re/^{188}Os isotope ratio. If correct, then distinct organic complexes from a single whole rock sample may define a greater range in ^{187}Re/^{188}Os isotope ratio than that defined by multiple whole rock analyses, and thus may potentially yield more precise Re-Os depositional age information. In contrast, a control on ^{187}Re/^{188}Os isotope ratios by differential metal uptake rates may be more significant in organic-poor gray shales (e.g., TOC < 1%; see Chapter 3), or in shales deposited under non-euxinic conditions (e.g., lower Velkerri Formation interval), but this topic ultimately requires further research.

5.5.2 The Mo Isotope Composition of Global Seawater at 1.4 Ga

A brief review of the Mo geochemical cycle in present-day oceans and the utility of Mo isotopes in euxinic black shales as a global ocean paleoredox proxy over geological time (Barling et al., 2001; Arnold et al., 2004) is given in Chapter 2 (section 2.5.4). Arnold et al. (2004) applied the Mo isotope paleoredox proxy to five samples of the Velkerri Formation from the Urapunga-4 drill core (four samples from 156-214 m depth, and one sample from 363 m depth). Their samples are moderately enriched in Mo (11-33 ppm) and had a range in DOP values (0.60-0.84), but overlapped in $\delta^{97/95}$Mo (0.54-0.67‰), albeit with significant 2σ uncertainties on some samples ($\geq$ 0.2‰ for three samples) (see Figure 5.6). Six samples from the upper Velkerri Formation organic-rich interval analyzed in this study have high and invariant DOP (0.90-0.92), elevated Fe$_T$/Al ratios (1.4-1.9), and Mo abundances (105-119 ppm). Given the low degree of scatter associated with the Re-Os isochron regressions for the Velkerri Formation (MSWD = 1.3), and the agreement of the Re-Os ages (1361 ± 21 Ma and 1417 ± 29 Ma) with previous maximum U-Pb zircon age constraints (1492 ± 4 Ma for the Mainoru Formation, lower Roper Group; Jackson et al., 1999), the Mo isotope systematics and

DOP determinations of the Velkerri Formation black shales observed here and by Arnold et al. (2004) should accurately represent sedimentary conditions during deposition.

The lower Mo abundance data for the black shales analyzed by Arnold et al. (2004) compared to the samples analyzed in this study, together with positive pyrite δ^{34}S values in basinal shales from the lower and middle Velkerri Formation (Shen et al., 2003), could reflect significant restriction between the Roper Superbasin and global ocean (cf. Shen et al., 2002). Thus, one possibility for some slightly lower $\delta^{97/95}$Mo values (0.31-0.55‰) in the sample set of Arnold et al. (2004) is minor overprinting of the global seawater signatures by local riverine inputs. Alternatively, the lower Mo abundances and $\delta^{97/95}$Mo could reflect a higher redox potential in the bottom waters during deposition (as evidenced by lower DOP values; Shen et al., 2003). Notwithstanding that much of the Velkerri Formation may have been deposited under euxinic bottom waters based on the Fe redox proxies (DOP and Fe_{HR}/Fe_{T}), those samples from Arnold et al. (2004) with DOP less than 0.75 may indicate anoxic, but non-sulfidic, bottom water conditions during deposition (Raiswell et al., 1988) (although enhanced sedimentation rates in euxinic bottom waters is an alternative explanation; Canfield et al., 1996; Lyons, 1997; Lyons and Severmann, 2006). A small fractionation in Mo isotopes is known to occur in association with diagenetic Mo sulfide formation (e.g., thiomolybdates; $MoO_xS_{4-x}^{2-}$), and results in a lighter Mo isotope composition of anoxic/non-sulfidic sediments ($\Delta^{97/95}Mo_{SW\text{-}anoxic}$ ~ 0.5‰) relative to seawater (Nägler et al., 2005; Poulson et al., 2006; Siebert et al., 2006). Thus, it is possible a small Mo isotope fractionation effect resulting from decreased bottom water sulfide concentrations (e.g., 10 μM < $[H_2S]$ < ~ 100 μM) is preserved in some samples analyzed by Arnold et al. (2004). Taking this into consideration, Arnold et al. (2004) suggested the $\delta^{97/95}$Mo of 1.4 Ga seawater was ~ 0.8‰, or ~ 0.3‰ heavier than the average $\delta^{97/95}$Mo observed for their Velkerri (and Wollogorang) Formation samples.

This suggestion is consistent with the new precise Mo isotope data presented here from the upper Velkerri Formation organic-rich interval that yields an average $\delta^{97/95}$Mo of 0.72 ± 0.10 ‰ (individual 2σ uncertainties between 0.04‰ and 0.12‰). Elevated DOP (0.90-0.92) and Mo abundances, together with the restricted variation in $\delta^{97/95}$Mo observed for my samples, suggests Mo uptake into the upper Velkerri Formation interval was likely quantitative. Thus, the Mo isotope composition from this interval should represent a direct proxy for dissolved $\delta^{97/95}$Mo in the overlying water column. Elevated metal enrichments for the upper Velkerri Formation interval, together with onset of negative pyrite δ^{34}S values (Shen et al., 2003) suggest a significant connection between the Roper seaway and the global ocean during deposition of this interval. Given the long residence time of Mo (i.e., 1-2 orders of magnitude larger than that of Os), the Mo isotope composition of the Roper seawater should also be well-mixed with respect to the global ocean. Thus, the average $\delta^{97/95}$Mo of 0.72 ± 0.10 ‰ derived from the new Mo isotope data for the upper Velkerri Formation represents a more precise estimate for 1.4 Ga global seawater $\delta^{97/95}$Mo, and confirms the original findings and conclusions of Arnold et al. (2004) regarding expanded deep-sea anoxia at 1.4 Ga relative to the present-day. Specifically, the $\delta^{97/95}$Mo of 1.4 Ga seawater is ~ 0.8‰ lighter than present-day seawater (assuming similar global riverine $\delta^{97/95}$Mo at 1.4 Ga and today). It is therefore consistent with decreased uptake of Mo onto Mn oxides associated with the expansion of deep sea euxinia at the expense of oxic, suboxic, and anoxic/non-sulfidic marine deposition.

5.5.3 Re-Os and Mo Isotope Systematics in Black Shales Resulting From Post-Depositional Hydrothermal Fluid Flow

5.5.3.1 Re-Os Isotopes

The imprecise Re-Os date of 1359 ± 150 Ma (MSWD = 86) obtained for the Wollogorang Formation black shales is significantly younger than the U-Pb SHRIMP zircon ages of 1729 ± 4 Ma and 1730 ± 3 Ma obtained for ash beds within the black shale several meters above the sampled interval in the Mount Young 2 drill hole (Page et al., 2000). In addition, the I_{Os} from this regression (3.5 ± 1.5) is significantly more radiogenic than the estimated Os isotope composition of the currently eroding upper continental crust (between ~ 1.0 and 1.4; Esser and Turekian, 1993; Peucker-Ehrenbrink and Jahn, 2001; Hattori et al., 2003) and the average for present-day rivers (~ 1.54; Levasseur et al., 1999). Thus, the Re-Os radioisotope system in the Wollogorang Formation black shales has been strongly disturbed by some post-depositional process(es).

Weathering and metamorphism are unlikely explanations for the scattered Re-Os isotope systematics because drill core material was used for analysis, and the Wollogorang Formation was buried to depths no greater than the overmature zone of hydrocarbon generation (Crick et al., 1988). Alternatively, previous paleomagnetic (overprinted paleomagnetic pole; Idnurm et al., 1995; Idnurm, 2000), geochemical (high pyrite S to organic C ratios in dolomitic siltstones and black shales, and base metal sulfide enrichment at multiple levels), and petrologic evidence (coarse pyrite aggregates within diagenetic nodules and dolomite veinlets) (Jackson, 1985; Donnelly and Jackson, 1988) suggests the Wollogorang Formation has been affected by hydrothermal fluid flow that may be associated with formation of the HYC SEDEX ore deposit at McArthur River (Idnurm, 2000; Southgate et al., 2000). A mathematical modeling study by Garven et al. (2001) suggests that the hydrothermal fluids associated with ore formation passed through the upper Tawallah Group, including the Wollogorang Formation, before returning to the surface as mineralizing fluids. Low-temperature (~ 100°C), oxidizing (low H_2S content), and saline (> 20 wt. % NaCl equivalent) brines are suggested to have leached base metals from the overlying and underlying Settlement Creek and Gold Creek Volcanics (Cooke et al., 1998). Dolomite veinlets within the black shale unit, and the variable Cu (48-278 ppm) and depleted Zn (typically < 20 ppm; average shale has ~ 95 ppm) abundances are consistent with trace metal redistribution by hydrothermal fluids (c.f., Lindsay, 2001).

Deviation of the Re-Os isotope data from a ca. 1730 Ma reference line increases toward the base of the black shale unit (Figure 5.10). Regression of the sample subsets from 74.18-75.53 m and 76.00-76.96 m depth yields Model 3 Re-Os dates of 1781 ± 190 Ma (2σ, $n = 12$, MSWD = 22, $I_{Os} = -0.5 \pm 1.9$) and 1234 ± 370 Ma (2σ, $n = 9$, MSWD = 93, $I_{Os} = 4.8 \pm 4.3$), respectively. Although the first subset yields a Re-Os date within error of the U-Pb zircon ages, the second subset yields an erroneously young Re-Os date with a large degree of scatter. The calculated $I_{Os\ (1730\ Ma)}$ of individual samples from 74.18-75.53 m range between –0.35 and +0.45, but samples from 76.00-76.96 m are all negative (–0.19 to –2.41) (see Table 5.5). Replicate analyses of three samples (75.51-75.53 m, 76.00-76.03 m, and 76.03-76.08 m) show variations in Re and Os abundances (up to 5%), and $^{187}Re/^{188}Os$ (up to 17%) and $^{187}Os/^{188}Os$ (up to 15%) isotope ratios, and wide variations in $I_{Os\ (1730\ Ma)}$ (e.g., –0.19 to –1.24 for sample 76.03-76.08 m). In the absence of post-depositional Re and Os disturbance, replicate analyses of the same powder aliquot should ideally yield reproducible Re-Os abundance and isotope data. If the powder aliquot is not sufficiently homogenized, then a nugget effect can result in coupled variations in $^{187}Re/^{188}Os$ and $^{187}Os/^{188}Os$ isotope ratios, and identical I_{Os} values for replicate analyses, thus introducing additional variation along isochrons (Creaser et al., 2002; Kendall et al., 2004). In the event of post-depositional mobilization of Re and Os in a non-homogenized powder aliquot with a nugget effect, the replicate analyses may scatter on a Re-Os isochron diagram and not have reproducible I_{Os} values. The above observations are thus consistent with post-depositional mobilization of Re and Os in the Wollogorang Formation shales that has affected samples from 76.00-76.96 m to a greater degree relative to samples from 74.18-75.53 m.

To test the effect of hydrothermal fluid alteration on the Re-Os isotope systematics in the Wollogorang Formation shales, I further examined two samples that contain thin (< 1 mm) dolomite veinlets. Specifically, I compared the Re and Os isotope data for dolomite veinlet and immediately surrounding shale versus the adjacent shale material that is ≥ 4 mm from the dolomite veinlet. At 76.91-76.96 m depth, the $^{187}Re/^{188}Os$ isotope composition of the dolomite veinlet and immediately surrounding shale [76.91-76.96 (dol)] is significantly greater (~ 8.5%) than the adjacent shale material (76.91-76.96 and 76.91-76.96-2), and is accompanied by a ~ 2.8% increase in the $^{187}Os/^{188}Os$ isotope ratio (see Figure 5.10). In contrast, the sample at 74.93-74.95 m shows only a modest increase in $^{187}Re/^{188}Os$ (~ 1.4%) and $^{187}Os/^{188}Os$ (~ 2.3%) isotope ratio for the dolomite – shale material relative to the adjacent shale. In both cases, the increase in $^{187}Os/^{188}Os$ isotope ratio is approximately similar. Rhenium and ^{192}Os abundances for dolomite – shale material at 74.93-74.95 m are depleted by ~ 12-13 % relative to adjacent shale material, although this could be explained largely by dolomite dilution. However, the sample at 76.91-76.96 m shows a pronounced depletion in ^{192}Os abundance (up to 16%) relative to Re abundance (up to 8%) that resulted in a higher $^{187}Re/^{188}Os$ isotope ratio and more negative I_{Os} for the dolomite – shale material. These observations are compatible with either preferential mobilization of Os relative to Re, or preferential addition of Re relative to Os. Interestingly, the two other samples (74.35-

74.38 m and 75.08-75.11 m) with abundant dolomite veinlets (reflected in their elevated CaO, MgO and Mn abundances) from the 74.18-75.53 m interval do not show significant disturbance in Re-Os isotope systematics based on their proximity to the ca. 1730 Ma reference line and I_{Os} values near zero. Thus, the re-distribution of Re and Os within the Wollogorang Formation black shales was likely a complex process.

Percolation of hydrothermal fluids into the Wollogorang Formation black shale unit from the underlying dolomitic rocks and/or from along the lithologic contact (located at ~ 80 m depth in Mount Young 2; see Figure 5.2) strongly disturbed the Re-Os systematics in shales between 76.00 and 76.96 m depth, and to a lesser degree, the stratigraphically higher shales between 74.18 m and 75.53 m depth. Caution is thus required when attempting to apply the Re-Os deposition-age geochronometer to ORS from tectonically deformed intracratonic regions flushed by hydrothermal fluids.

5.5.3.2 Mo Isotopes

In addition to the Velkerri Formation, Arnold et al. (2004) also reported Mo isotope analyses for two Wollogorang Formation black shale samples and utilized them in their interpretation of the paleoredox state of Middle Proterozoic deep oceans. Unlike the Velkerri Formation, however, a large range in $\delta^{97/95}$Mo (0.30-0.79 ‰), Mo abundance (41-58 ppm), and DOP values (0.57-0.92) is observed for the Wollogorang Formation samples in this study (see Figure 5.6). Those samples with DOP < 0.75 may reflect non-quantitative Mo sequestration from lower dissolved sulfide ($[H_2S] < \sim 100$ μM) bottom waters. In this case, a Mo isotope fractionation associated with diagenetic Mo sulfide formation would result in lighter $\delta^{97/95}$Mo values in black shales relative to the overlying water column (Nägler et al., 2005; Poulson et al., 2006; Siebert et al., 2006). However, no correlations are observed between $\delta^{97/95}$Mo and DOP, or between $\delta^{97/95}$Mo and Mo abundance, for the Wollogorang Formation. Indeed, some samples (e.g., 74.27-74.29 m and 76.91-76.96 m) have high DOP (> 0.85), but low $\delta^{97/95}$Mo (< 0.6 ‰), which is not consistent with fluctuating redox conditions being the sole control on the observed $\delta^{97/95}$Mo variations.

Given the strong evidence for post-depositional mobilization of Re and Os in the Wollogorang Formation black shales, it is prudent to assess whether hydrothermal fluid flow also disturbed the Mo isotope systematics. As was the case for the Re-Os isotope data, there appears to be a systematic difference in $\delta^{97/95}$Mo with stratigraphic depth. Specifically, samples from 76.00-76.96 m depth (0.30-0.56 ‰) are isotopically lighter relative to the samples from 74.18-75.53 m depth (0.54-0.79 ‰). In addition, sample 76.91-76.96 m shows the lightest $\delta^{97/95}$Mo values (0.35 ± 0.07 ‰ and 0.30 ± 0.06 ‰) although there is no significant difference (within 2σ uncertainties) between the dolomite – shale and adjacent shale material as was observed for Re-Os isotopes. Collectively, these observations suggest that isotopically light hydrothermal fluids have modestly altered the authigenic Mo isotope signatures in the Wollogorang Formation black shales, with the greatest effect again occurring in samples between 76.00 m and 76.96 m. This result is not entirely unexpected, as hydrothermal fluids would intuitively be expected to have $\delta^{97/95}$Mo similar to average lithogenic Mo (e.g., near 0‰) if significant water-rock equilibration has occurred during fluid passage through basement and sedimentary rock cover. Modern warm ridge-flank hydrothermal fluids from the Baby Bare outcrop (~ 100 km east of the Juan de Fuca Ridge) are also characterized by relatively low $\delta^{97/95}$Mo of ~ 0.5‰ that may reflect extensive water-basalt reaction (McManus et al., 2002). An additional, or alternative, possibility is that some Mo isotope fractionation effect occurs during exchange of Mo between the Wollogorang Formation black shales and the hydrothermal fluid. This fractionation would have favored the uptake of lighter isotopes into the shales (e.g., McManus et al., 2002), and enriched the fluid in heavier isotopes although the effect of this process on fluid $\delta^{97/95}$Mo would be small for a large, and constantly replenishing, fluid reservoir.

Four of five samples from 74.18-75.53 m depth have $\delta^{97/95}$Mo values that overlap with the average $\delta^{97/95}$Mo value of 0.72 ± 0.10 ‰ for the Velkerri Formation. Three of these samples have DOP $\geq$ 0.7 that suggests possible quantitative uptake of Mo from euxinic bottom waters. Based on the observed Re-Os and Mo isotope systematics, the degree of hydrothermal alteration of the authigenic $\delta^{97/95}$Mo signature at 74.18-75.53 m depth may have been relatively minor. Accordingly, I suggest the $\delta^{97/95}$Mo values from the samples at 74.18-75.53 m (e.g., between 0.6‰ and 0.8‰) may represent a close approximation of the Mo isotope composition of ca. 1730 Ma global seawater because the McArthur Basin was probably partially connected to the global ocean at this time (Jackson et al., 2000; Page et al., 2000; Southgate et al., 2000; Shen et al., 2002).

5.5.4 Redox Cycling of Fe in the Middle Proterozoic (1.7 – 1.4 Ga) Oceans

Iron isotope data for the McArthur shales place some tentative constraints on the nature of Fe redox cycling in Middle Proterozoic oceans (see Chapter 2, section 2.5.5 for a review). A well-correlated inverse relationship ($R^2 = 0.97$) between bulk $\delta^{56/54}$Fe (–0.31‰ to +0.22‰) and DOP is defined by five samples of the Velkerri Formation, consistent with enrichment of highly reactive iron (and thus elevated DOP) in the euxinic upper organic-rich interval relative to the anoxic/non-sulfidic lower organic-rich interval (see Figure 5.7). The Wollogorang Formation black shales record predominantly negative bulk $\delta^{56/54}$Fe values (–0.33‰ to –0.09‰) that also show a weak negative correlation with DOP ($R^2 = 0.31$). Hydrothermal fluid flow through the Wollogorang Formation may have partially obscured the primary relationships between $\delta^{56/54}$Fe and DOP. Unlike the Re-Os and Mo isotope systematics, however, there is no correlation between $\delta^{56/54}$Fe and stratigraphic depth nor is there any significant difference in Fe isotope composition near dolomite veinlets (e.g., sample 76.91-76.96 m). Thus, the effect of hydrothermal alteration on the Fe isotope systematics of the Wollogorang Formation may be less profound compared to that observed for Re-Os and Mo isotopes. Together, the Wollogorang and Velkerri Formation $\delta^{56/54}$Fe – DOP systematics define a well-correlated inverse trend ($R^2 = 0.73$). The overall range in $\delta^{56/54}$Fe (–0.33‰ to +0.22‰) is similar to that observed for the Devonian Geneseo and Oatka Creek Formations (–0.21‰ to +0.30‰; Duan et al., 2006), the Jurassic Kimmeridge Clay Formation from the United Kingdom (–0.41‰ to +0.33‰; Matthews et al., 2004), and the modern Black Sea (~ –0.3‰ to +0.1‰; Severmann et al., 2006a). Significantly, the negative $\delta^{56/54}$Fe of the euxinic upper Velkerri Formation (–0.31‰ and –0.26‰) and the Wollogorang Formation overlaps the $\delta^{56/54}$Fe of euxinic Phanerozoic black shales and modern Black Sea sediments. Iron sequestration into euxinic sediments can be quantitative (Severmann et al., 2006a). An isotopically light benthic Fe flux (derived from dissimilatory Fe[III] reduction; Severmann et al., 2006b; Staubwasser et al., 2006) generated on suboxic continental shelves can be transported to ocean basin floors via the Fe shuttle (Severmann et al., 2006a, c). Thus, the negative $\delta^{56/54}$Fe for the upper Velkerri Formation is consistent with operation of a Fe shuttle mechanism in Middle Proterozoic oceans in a fashion analogous to the Phanerozoic and modern shuttle. In contrast, the lower Velkerri Formation interval has positive $\delta^{56/54}$Fe (0.12‰ to 0.22‰) and was deposited from basinal anoxic/non-sulfidic bottom waters. Thus, Fe sequestration was likely non-quantitative and the authigenic $\delta^{56/54}$Fe was probably overprinted by Fe isotope fractionations associated with isotope exchange reactions (e.g., between dissolved $Fe(II)_{aq}$ and pyrite Fe; Severmann et al., 2006a, b). Heavy pyrite S isotope data for this interval of the Velkerri Formation may indicate a limited sulfur supply associated with more restricted basin conditions, high bacterial sulfate reduction rates, and/or slow sulfate diffusion rates across the sediment-water interface (Shen et al., 2003). Such conditions may be responsible for the positive $\delta^{56/54}$Fe in the lower Velkerri Formation, but the nature and magnitude of the associated fractionations remains poorly understood (Severmann et al., 2006b).

Two samples of the Barney Creek Formation have positive $\delta^{56/54}$Fe values of +0.34‰ and +0.39‰ despite high DOP (0.77 and 0.88, respectively), and thus do not plot on the $\delta^{56/54}$Fe – DOP trend defined by black shales of the Wollogorang and Velkerri Formations. Instead, the Barney Creek Formation Fe isotope systematics are broadly similar to $\delta^{56/54}$Fe values from Member 4 from the Neoproterozoic Doushantuo Formation (see Chapter 2). Such heavy positive Fe isotope compositions are similar to that of isotopically heavy pore fluids in zones of bacterial sulfate reduction (Severmann et al., 2006b). During deposition of the Barney Creek Formation in the Batten Fault Zone, connection with the global ocean may have been severely restricted based on pyrite sulfur isotope compositions (δ^{34}S values of +18.2‰ to +23.4‰), which may have been similar to contemporaneous seawater sulfate (Shen et al., 2002). Thus, basinal, organic-rich shales in the Batten Fault Zone may have sequestered $Fe(II)_{aq}$ from a water column that had become isotopically heavy as a result of extensive bacterial sulfate reduction.

Highly negative pyrite $\delta^{56/54}$Fe (as low as –3.5‰; in comparison, Black Sea pyrite $\delta^{56/54}$Fe is ~ –1‰; Severmann et al., 2006a) from Archean black shales were interpreted by Rouxel et al. (2005) as evidence for an Archean ocean rich in isotopically light $Fe(II)_{aq}$ because of sequestration of isotopically heavy Fe in Fe oxides (e.g., in banded iron formations). Duan et al. (2007) also invoke Fe oxide precipitation to explain highly negative bulk and pyrite $\delta^{56/54}$Fe in the Mt. McRae shale associated with mild oxygenation in the water column at ca. 2.5 Ga. Widespread Fe redox cycling on continental shelves, and Fe shuttling of the isotopically light benthic iron flux may have been important during the Archean (Severmann et al., 2006a, c). In contrast, Yamaguchi et al. (2005) have interpreted negative bulk $\delta^{56/54}$Fe values (between –2.3‰ and –1.0‰) in 2.9-2.6 Ga Archean magnetite- and organic-rich shales as the products of bacterially-mediated dissimilatory Fe(III) reduction. Archer and Vance (2006) subsequently proposed coupled Fe and S bacterial reduction to explain $\delta^{56/54}$Fe values of –2.7‰ to –0.7‰ in 2.7 Ga sedimentary pyrites from the Belingwe greenstone belt, Zimbabwe. The controlling factors behind Fe redox cycling in the Archean and Paleoproterozoic remains disputed (Rouxel et al., 2006; Yamaguchi and Ohmoto, 2006; Archer and Vance, 2006). In addition, the origin of positive pyrite $\delta^{56/54}$Fe values in Paleoproterozoic black shales older than ~ 1.8 Ga remains enigmatic (Rouxel et al., 2005). Further analysis of bulk and pyrite $\delta^{56/54}$Fe of Archean and Paleoproterozoic black shales coupled with an improved understanding of Fe isotope fractionation factors are required for elucidating the relationship between ocean-atmosphere redox state and Fe marine geochemistry and redox cycling during the Precambrian Eon.

5.6 CONCLUSIONS

Simultaneous application of the Re-Os radioisotope and Mo stable isotope systems to black shales has tremendous potential for tracing the redox evolution of Earth's oceans and atmosphere over geological time. New Re-Os black shale ages of 1361 ± 21 Ma (MSWD = 1.3) and 1417 ± 29 Ma (MSWD = 1.3) constrain the depositional age of biomarkers from the Velkerri Formation, and acritarchs and microfossils in the Roper Group of the McArthur Basin, northern Australia. Trace metal abundance and ^{187}Re/^{188}Os isotope ratio variations in the Wollogorang and Velkerri Formation black shales are consistent with previous data suggesting the presence of multiple and/or separate Re- and Os-bearing organic complexes. In euxinic shales, the formation of these organic complexes may be the dominant control on elemental partitioning of Re and Os, and thus initial ^{187}Re/^{188}Os isotope ratio variations.

New Mo isotope data from the upper Velkerri Formation provides a more precise estimate of the Mo isotope composition of 1.4 Ga seawater ($\delta^{97/95}$Mo = 0.72 ± 0.10 ‰). Consistent with the previous findings and conclusions of Arnold et al. (2004), seawater $\delta^{97/95}$Mo at 1.4 Ga was ~ 0.8‰ lighter than present-day seawater. This is best explained by decreased uptake of Mo onto Mn oxides associated with expansion of deep sea euxinia at the expense of oxic, suboxic, and anoxic/non-sulfidic marine deposition.

An erroneously young Re-Os date of 1359 ± 150 Ma (MSWD = 85) with an anomalously high initial ^{187}Os/^{188}Os isotope composition (3.5 ± 1.5) for the ca. 1730 Ma Wollogorang Formation black shales provides evidence that hydrothermal fluid flow through black shales results in post-depositional remobilization of Re and Os and loss of reliable depositional age information. Molybdenum isotopes in the Wollogorang Formation were also likely modified by isotopically light hydrothermal fluids. In both cases, the greatest degree of disturbance in Re-Os and Mo isotope systematics occurred near the base of the Wollogorang Formation black shale unit. Paleomagnetic data suggest the hydrothermal fluid flow may have been associated with the formation of a world-class Pb-Zn-Ag SEDEX ore deposit (McArthur River) at ca. 1640 Ma. The highest $\delta^{97/95}$Mo values observed for the Wollogorang Formation are consistent with those observed in the Velkerri Formation and may reflect seawater $\delta^{97/95}$Mo at 1.73 Ga.

Bulk $\delta^{56/54}$Fe for the Velkerri and Wollogorang Formations range between −0.3‰ and +0.2‰, and are similar to values observed for present-day organic-rich sediments and Jurassic and Devonian black shales, but are significantly heavier than values observed for Archean black shales. Negative $\delta^{56/54}$Fe for the euxinic upper Velkerri and Wollogorang Formation black shales are generally consistent with operation of a Fe shuttle during the Middle Proterozoic that transported isotopically light Fe from suboxic continental shelf sediments to basinal organic-rich sediments. The nature of Fe redox cycling in stratified Middle Proterozoic and oxygenated Phanerozoic and present-day oceans was thus not greatly dissimilar. In contrast, positive $\delta^{56/54}$Fe for anoxic/non-sulfidic shales of the lower Velkerri Formation may reflect isotopic fractionation during authigenic mineral formation under restricted basin conditions (e.g., limited sulfur supply) with dissolved $Fe(II)_{aq}$ possibly also having $\delta^{56/54}$Fe > 0‰. The highest $\delta^{56/54}$Fe values are observed in the euxinic Barney Creek Formation and may have been generated by extensive bacterial sulfate reduction proximal to, or within, a restricted basin.

Table 5.1. Major and trace element data for selected samples of the Wollogorang, Barney Creek, and Velkerri Formation black shales.

Core Depth (m)	Al_2O_3	TiO_2	Fe_2O_3	MgO	CaO	Na_2O	K_2O	V	Cr	Mn	Co	Ni	Cu	Zn	As	Rb	Sr	Zr	Mo	Ba	Pb	U
Velkerri Fm. (Urapunga-4)																						
136.98-137.05	5.89	0.37	8.07	1.05	0.84	0.13	2.80	378	36	180	36	332	108	379	102	44	33	82	112	293	58	11
137.19-137.26	6.05	0.36	7.24	0.80	0.69	0.11	2.85	442	39	126	30	254	160	576	64	59	40	83	110	364	51	13
137.26-137.33	5.39	0.42	7.56	0.80	0.56	0.14	3.04	499	41	104	32	260	131	485	72	38	29	91	106	347	54	12
137.46-137.52	7.18	0.35	7.78	0.99	0.71	0.10	3.13	458	38	93	30	234	135	379	63	100	43	82	119	390	55	13
137.75-137.79	6.32	0.32	7.96	0.97	0.62	0.09	2.76	408	33	129	29	254	103	253	91	87	39	71	105	353	56	12
137.84-137.89	6.60	0.42	7.46	0.94	0.58	0.15	3.02	559	42	95	31	271	137	497	83	50	33	90	114	344	55	13
325.71-325.78	5.53	0.56	5.70	0.28	0.03	0.14	2.27	106	44	108	14	47	137	244	8.8	23	13	189	8.6	123	71	5.8
326.20-326.28	8.71	0.55	4.77	0.85	0.06	0.14	2.68	97	41	100	13	43	106	185	7.1	30	23	138	8.8	189	52	4.5
326.42-326.48	14.9	0.64	5.09	1.43	0.10	0.17	3.51	97	48	112	11	43	120	233	7.8	98	34	142	6.0	269	55	5.3
326.48-326.55	6.77	0.51	5.01	0.57	0.04	0.13	2.42	86	43	131	10	38	123	226	7.4	52	23	132	6.0	189	56	4.8
326.62-326.69	8.71	0.57	6.04	0.88	0.06	0.16	2.83	106	47	118	13	45	141	263	9.5	70	28	148	7.5	221	59	5.8
Barney Creek Fm. (McArthur 2)																						
68.11-68.15	4.60	0.29	2.51	5.09	10.60	0.05	6.13	54	27	1468	9.5	27	23	19	37	34	24	86	3.2	214	44	3.6
83.11-83.14	5.36	0.37	4.97	2.21	7.17	0.12	7.22	116	38	1622	20	53	37	12	57	77	26	91	8.5	162	75	4.4
Wollogorang Fm. (Mount Young 2)																						
74.27-74.29	6.15	0.35	3.40	0.51	0.46	0.04	5.14	81	34	75	23	38	48	16	66	80	17	72	58	435	21	11
74.35-74.38	5.06	0.26	2.67	0.81	1.14	0.03	4.03	64	26	268	17	33	243	38	86	43	16	55	57	433	18	9.4
75.08-75.11	8.89	0.27	1.86	1.25	1.14	0.03	4.72	70	28	238	15	31	122	12	39	144	23	55	41	494	12	8.7
75.48-75.51	4.96	0.41	2.51	0.35	0.18	0.04	6.35	102	37	16	24	43	58	17	68	61	10	114	57	422	16	11
75.51-75.53	5.48	0.43	2.14	0.42	0.16	0.04	6.47	106	42	20	21	40	278	9.0	49	83	11	88	56	667	15	11
76.00-76.03	7.68	0.46	2.19	0.59	0.46	0.04	7.09	133	51	119	21	47	72	8.2	58	92	19	84	56	804	23	12
76.03-76.08	14.64	0.44	2.47	1.11	0.74	0.04	7.72	127	45	71	25	48	115	10	66	217	38	85	52	1239	19	14
76.91-76.96 (dol)*	5.34	0.37	2.01	0.90	1.47	0.03	5.61	119	38	274	33	47	174	6.8	70	37	14	68	49	594	13	12
76.91-76.96	6.37	0.50	2.22	0.26	0.22	0.04	7.74	161	51	22	45	59	215	7.8	73	93	13	91	56	636	15	14
Average Shale	16.70	0.78	6.90	2.60	2.20	1.60	3.60	130	90	850	19	68	45	95	10	140	300	160	1.3	580	22	3.7

Average shale data from Wedepohl (1971, 1991). Major oxide and trace element abundances in weight % and ppm, respectively.

*"dol" denotes shale adjacent to dolomite veinlet.

Table 5.2. Enrichment factors, Fe_T/Al ratios, and DOP data for the Wollogorang, Barney Creek, and Velkerri Formation black shales.

Core Depth (m)	Ti	Fe	Mg	Ca	Na	K	V	Cr	Mn	Co	Ni	Cu	Zn	As	Rb	Sr	Zr	Mo	Ba	Re	Pb	U	Fe_T/Al	DOP
Velkerri Fm. (Urapunga-4)																								
136.98-137.05	1.4	3.3	1.1	1.1	0.24	2.2	8.1	1.1	0.60	5.5	14	6.8	11	30	0.87	0.31	1.5	240	1.4	111	7.4	8.7	1.8	0.92
137.19-137.26	1.3	2.9	0.83	0.85	0.20	2.2	9.2	1.2	0.41	4.4	10	9.8	16	18	1.2	0.36	1.4	228	1.7	120	6.4	9.7	1.6	0.90
137.26-137.33	1.6	3.4	0.94	0.77	0.29	2.6	12	1.4	0.38	5.3	12	9.0	15	23	0.83	0.29	1.8	248	1.8	128	7.6	10	1.9	0.92
137.46-137.52	1.0	2.6	0.88	0.74	0.15	2.0	8.0	1.0	0.26	3.7	8.0	7.0	9.1	16	1.6	0.34	1.2	209	1.6	123	5.8	8.0	1.4	0.92
137.75-137.79	1.1	3.0	1.0	0.74	0.16	2.0	8.1	1.0	0.40	4.1	9.9	6.0	6.9	25	1.6	0.34	1.2	210	1.6	111	6.8	6.8	1.7	0.91
137.84-137.89	1.4	2.7	0.91	0.66	0.24	2.1	11	1.2	0.28	4.2	10	7.7	13	22	0.90	0.28	1.4	217	1.5	121	6.3	8.9	1.5	0.90
325.71-325.78	2.2	2.5	0.32	0.036	0.28	1.9	2.4	1.5	0.39	2.2	2.1	9.2	7.6	2.7	0.50	0.14	3.6	19	0.64	24	9.7	4.7	1.4	0.43
326.20-326.28	1.4	1.3	0.62	0.055	0.17	1.4	1.4	0.87	0.23	1.3	1.2	4.5	3.6	1.4	0.41	0.15	1.7	13	0.62	14	4.5	2.3	0.72	0.43
326.42-326.48	0.91	0.82	0.61	0.051	0.12	1.1	0.82	0.59	0.15	0.69	0.70	3.0	2.7	0.90	0.78	0.13	1.0	5.1	0.52	6.7	2.8	1.6	0.45	
326.48-326.55	1.6	1.8	0.53	0.049	0.21	1.6	1.6	1.2	0.38	1.4	1.4	6.7	5.7	1.9	0.90	0.19	2.0	11	0.80	14	6.3	3.2	0.98	0.51
326.62-326.69	1.4	1.7	0.64	0.056	0.19	1.5	1.5	1.0	0.27	1.4	1.3	6.0	5.2	1.9	0.95	0.18	1.8	11	0.73	12	5.1	3.0	0.92	
Barney Creek Fm. (McArthur 2)																								
68.11-68.15	1.3	1.3	7.0	17	0.12	6.1	1.5	1.1	6.3	1.9	1.4	1.9	0.71	14	0.87	0.29	2.0	8.8	1.3	2.7	7.2	3.5	0.72	0.77
83.11-83.14	1.5	2.2	2.6	10	0.24	6.2	2.7	1.3	6.0	3.4	2.4	2.6	0.38	18	1.7	0.27	1.8	20	0.86	7.9	11	3.7	1.2	0.88
Wollogorang Fm. (Mount Young 2)																								
74.27-74.29	1.2	1.3	0.53	0.56	0.077	3.9	1.7	1.0	0.24	3.3	1.5	2.9	0.45	18	1.5	0.15	1.2	119	2.0	37	2.6	8.3	0.73	0.86
74.35-74.38	1.1	1.3	1.0	1.7	0.073	3.7	1.6	1.0	1.0	3.0	1.6	18	1.3	29	1.0	0.18	1.1	142	2.5	33	2.7	8.3	0.70	0.77
75.08-75.11	0.65	0.50	0.69	0.96	0.039	2.5	1.0	0.56	0.53	1.5	0.86	5.1	0.22	7.6	1.9	0.14	0.65	58	1.6	27	1.0	4.4	0.28	0.82
75.48-75.51	1.8	1.2	0.45	0.28	0.084	5.9	2.6	1.4	0.062	4.4	2.1	4.3	0.57	23	1.5	0.11	2.4	143	2.4	79	2.4	10	0.67	0.56
75.51-75.53	1.7	0.94	0.49	0.21	0.075	5.4	2.4	1.4	0.071	3.4	1.8	19	0.28	15	1.8	0.11	1.7	130	3.5	62	2.1	8.7	0.52	0.70
76.00-76.03	1.3	0.69	0.48	0.45	0.050	4.3	2.2	1.2	0.31	2.5	1.5	3.5	0.18	13	1.4	0.14	1.2	92	3.0	47	2.2	6.8	0.38	0.57
76.03-76.08	0.65	0.41	0.46	0.38	0.030	2.4	1.1	0.58	0.10	1.6	0.81	2.9	0.11	7.8	1.7	0.14	0.61	45	2.4	23	1.0	4.4	0.22	0.62
76.91-76.96 (dol)*	1.5	0.90	1.1	2.1	0.062	4.9	2.8	1.3	1.0	5.6	2.2	12	0.22	23	0.82	0.15	1.3	117	3.2	87	1.9	10	0.50	0.82
76.91-76.96	1.7	0.84	0.25	0.25	0.075	5.6	3.2	1.5	0.069	6.3	2.3	12	0.21	20	1.7	0.12	1.5	110	2.9	80	1.8	9.7	0.46	0.92

Enrichment factors calculated using average shale data from Wedepohl (1971, 1991), except for Re (1 ppb; Crusius et al., 1996).

Re enrichment factors calculated using the Re abundance data from Tables 5.3, 5,4, and 5.5.

*"dol" denotes shale adjacent to dolomite veinlet.

Table 5.3. Re-Os, Mo, and Fe isotope data for the Velkerri Formation (drill hole Urapunga-4).

Core Depth (m)	Re (ppb)	Os (ppt)	^{192}Os (ppt)	^{187}Re/^{188}Os	^{187}Os/^{188}Os	rho	Os$_i$[*]	Mo (ppm)	δ$^{97/95}$Mo (‰)[†]	n[‡]	Fe (ppm)	δ$^{56/54}$Fe (‰)	n[‡]
136.91-136.98	47.37 ± 0.17	1169.0 ± 12.9	197.0 ± 1.2	478.32 ± 3.49	11.2397 ± 0.1112	0.554	0.27						
136.98-137.05	38.99 ± 0.14	986.8 ± 5.2	172.4 ± 0.3	449.81 ± 1.82	10.5745 ± 0.0281	0.288	0.26	112	0.78 ± 0.09	5			
137.12-137.19	39.81 ± 0.15	990.9 ± 8.6	167.2 ± 0.6	473.74 ± 2.45	11.2216 ± 0.0727	0.401	0.36						
137.19-137.26	43.31 ± 0.16	1081.0 ± 8.0	184.3 ± 0.5	467.45 ± 2.20	11.0256 ± 0.0541	0.380	0.31	110	0.65 ± 0.07	3			
137.26-137.33	41.05 ± 0.15	972.9 ± 6.9	153.1 ± 0.4	533.42 ± 2.44	12.5722 ± 0.0554	0.380	0.34	106	0.75 ± 0.04	4	52677	−0.31 ± 0.02	3
137.40-137.46	42.22 ± 0.15	1051.6 ± 6.3	178.6 ± 0.4	470.34 ± 2.00	11.0990 ± 0.0375	0.331	0.31						
137.46-137.52	52.73 ± 0.19	1285.7 ± 10.6	212.7 ± 0.8	493.27 ± 2.61	11.5943 ± 0.0684	0.469	0.28	119	0.70 ± 0.12	4			
137.52-137.58	48.92 ± 0.18	1192.4 ± 8.8	197.9 ± 0.6	491.78 ± 2.26	11.5336 ± 0.0558	0.349	0.26						
137.63-137.69	47.23 ± 0.17	1161.6 ± 7.0	193.9 ± 0.4	484.66 ± 2.08	11.4248 ± 0.0386	0.353	0.31						
137.75-137.79	41.80 ± 0.15	972.3 ± 5.1	150.1 ± 0.3	554.22 ± 2.24	12.9699 ± 0.0322	0.307	0.26	105	0.75 ± 0.12	4			
137.79-137.84	45.75 ± 0.17	1125.5 ± 6.4	187.8 ± 0.4	484.69 ± 2.03	11.4312 ± 0.0348	0.334	0.32						
137.84-137.89	47.54 ± 0.17	1072.4 ± 11.2	157.6 ± 0.8	600.13 ± 3.65	14.0003 ± 0.1159	0.469	0.24	114	0.69 ± 0.08	6	52204	−0.26 ± 0.01	3
replicate	47.47 ± 0.17	1077.2 ± 6.3	158.6 ± 0.3	595.53 ± 2.46	13.9608 ± 0.0413	0.302	0.30						
137.89-137.95	46.13 ± 0.17	1095.4 ± 6.7	173.3 ± 0.4	529.45 ± 2.24	12.4650 ± 0.0420	0.325	0.32						
325.64-325.71	5.06 ± 0.02	132.0 ± 1.5	23.3 ± 0.2	432.86 ± 3.84	10.4157 ± 0.1198	0.636	0.08						
325.71-325.78	7.85 ± 0.03	192.8 ± 1.7	31.1 ± 0.2	501.47 ± 3.29	12.0571 ± 0.0858	0.631	0.08						
325.85-325.92	8.06 ± 0.03	204.2 ± 1.8	34.9 ± 0.2	459.94 ± 2.95	10.9984 ± 0.0783	0.607	0.01						
325.92-325.99	5.66 ± 0.02	142.2 ± 1.8	23.7 ± 0.2	474.60 ± 4.43	11.4137 ± 0.1445	0.623	0.08				27037	0.22 ± 0.03	3
326.06-326.13	7.13 ± 0.03	172.8 ± 2.5	27.4 ± 0.3	518.00 ± 5.27	12.4285 ± 0.1854	0.592	0.05						
326.13-326.20	4.87 ± 0.02	123.3 ± 0.9	20.8 ± 0.1	465.12 ± 3.00	11.2093 ± 0.0631	0.770	0.10						
326.20-326.28	7.34 ± 0.03	177.4 ± 1.5	28.2 ± 0.1	518.65 ± 3.25	12.3958 ± 0.0784	0.648	0.01				33393	0.12 ± 0.05	3
326.36-326.42	7.68 ± 0.03	192.2 ± 2.0	32.0 ± 0.2	477.41 ± 3.28	11.4653 ± 0.0999	0.562	0.06						
326.42-326.48	5.97 ± 0.02	162.7 ± 1.7	30.6 ± 0.2	387.68 ± 3.10	9.2614 ± 0.0940	0.621	0.00						
326.48-326.55	5.80 ± 0.02	155.7 ± 1.2	28.5 ± 0.1	405.43 ± 2.54	9.7670 ± 0.0597	0.670	0.08				35008	0.14 ± 0.04	3
326.55-326.62	6.74 ± 0.02	177.1 ± 1.9	31.8 ± 0.2	422.23 ± 3.31	10.1019 ± 0.0985	0.627	0.02						
326.62-326.69	6.38 ± 0.02	167.4 ± 1.3	29.8 ± 0.1	425.77 ± 2.45	10.2300 ± 0.0573	0.608	0.06						

Uncertainties are quoted at the 2σ level.

[*] Os$_i$ = initial ^{187}Os/^{188}Os isotope ratio calculated at 1361 Ma (136.91-137.95 m) and 1417 Ma (325.64-326.69 m).

[†] Average includes powder replicate analyses for some samples.

[‡] Number of replicate Mo or Fe isotope mass spectrometer analyses.

Table 5.4. Re-Os and Fe isotope data for the Barney Creek Formation (drill hole McArthur 2).

Core Depth (m)	Re (ppb)	Os (ppt)	^{192}Os (ppt)	^{187}Re/^{188}Os	^{187}Os/^{188}Os	rho	$I_{Os\ (1640\ Ma)}$*	Fe (ppm)	$\delta^{56/54}$Fe (‰)	n†
68.11-68.15	0.74 ± 0.01	118.3 ± 0.8	43.3 ± 0.4	33.94 ± 0.38	1.1058 ± 0.0154	0.62	0.18	17580	0.34 ± 0.02	3
68.55-68.58	1.43 ± 0.01	336.8 ± 2.9	126.6 ± 1.8	22.41 ± 0.33	0.8801 ± 0.0182	0.66	0.19			
83.11-83.14	2.51 ± 0.01	549.7 ± 3.6	207.4 ± 2.0	24.06 ± 0.25	0.8498 ± 0.0116	0.64	0.16	34747	0.39 ± 0.01	3
83.29-83.32	1.33 ± 0.01	290.6 ± 2.0	109.5 ± 1.1	24.21 ± 0.26	0.8570 ± 0.0122	0.63	0.15			
83.36-83.39	2.95 ± 0.01	467.1 ± 4.1	171.0 ± 2.2	34.27 ± 0.46	1.1050 ± 0.0209	0.65	0.17			
83.42-83.44	2.53 ± 0.01	387.0 ± 2.7	141.1 ± 1.3	35.67 ± 0.36	1.1387 ± 0.0151	0.65	0.26			

Uncertainties are quoted at the 2σ level.

*$I_{Os(1640\ Ma)}$ = initial ^{187}Os/^{188}Os isotope ratio calculated at 1640 Ma.

†Number of replicate Fe isotope mass spectrometer analyses.

Table 5.5. Re-Os, Mo, and Fe isotope data for the Wollogorang Formation (drill hole Mount Young 2).

Core Depth (m)	Re (ppb)	Os (ppt)	^{192}Os (ppt)	^{187}Re/^{188}Os	^{187}Os/^{188}Os	rho	I_{Os}*	Mo (ppm)	$\delta^{97/95}$Mo (‰)†	n‡	Fe (ppm)	$\delta^{56/54}$Fe (‰)	n‡
74.18-74.21	10.38 ± 0.04	272.7 ± 3.6	35.5 ± 0.5	581.89 ± 7.99	16.7906 ± 0.2400	0.892	−0.22						
74.27-74.29	13.61 ± 0.05	372.5 ± 3.9	51.0 ± 0.4	531.25 ± 4.34	15.5944 ± 0.1350	0.730	0.06	58	0.54 ± 0.06	3	23769	−0.33 ± 0.06	3
74.35-74.38	10.06 ± 0.04	284.4 ± 3.0	42.2 ± 0.3	474.64 ± 3.65	13.8086 ± 0.1213	0.674	−0.07	57	0.62 ± 0.07	3	18671	−0.15 ± 0.02	3
74.53-74.55	8.69 ± 0.03	240.0 ± 3.2	33.4 ± 0.5	516.67 ± 7.56	15.1755 ± 0.2263	0.919	0.07						
74.93-74.95	15.21 ± 0.06	408.4 ± 4.7	56.7 ± 0.5	533.45 ± 5.10	15.2538 ± 0.1609	0.774	−0.35						
74.93-74.95 (dol)	13.45 ± 0.05	361.5 ± 4.2	49.4 ± 0.5	541.08 ± 5.51	15.6078 ± 0.1704	0.814	−0.21						
75.08-75.11	14.29 ± 0.05	373.8 ± 3.8	46.2 ± 0.3	615.49 ± 4.49	18.0709 ± 0.1450	0.679	0.07	41	0.79 ± 0.07	4	12975	−0.20 ± 0.02	3
75.48-75.51	23.31 ± 0.09	609.4 ± 4.3	77.4 ± 0.2	598.93 ± 2.74	17.3679 ± 0.0707	0.409	−0.15	57	0.60 ± 0.10	4	17575	−0.10 ± 0.02	3
75.51-75.53	20.14 ± 0.07	532.3 ± 3.7	67.5 ± 0.2	593.56 ± 2.74	17.4235 ± 0.0886	0.438	0.07	56	0.78 ± 0.12	4	14976	−0.09 ± 0.01	3
replicate	19.59 ± 0.07	528.6 ± 4.1	66.7 ± 0.3	583.91 ± 3.39	17.5239 ± 0.0892	0.666	0.45						
replicate	20.61 ± 0.08	545.8 ± 5.4	69.9 ± 0.4	587.09 ± 4.19	17.1928 ± 0.1309	0.677	0.03						
replicate	20.60 ± 0.08	536.6 ± 5.7	67.4 ± 0.6	608.31 ± 5.53	17.6733 ± 0.1631	0.820	−0.11						
76.00-76.03	21.77 ± 0.08	528.7 ± 5.0	61.8 ± 0.2	701.08 ± 3.74	19.5470 ± 0.1280	0.431	−0.95	56	0.55 ± 0.06	5	15336	−0.21 ± 0.04	3
replicate	21.63 ± 0.08	536.6 ± 6.0	62.8 ± 0.6	685.75 ± 6.49	19.5254 ± 0.1899	0.823	−0.53						
76.03-76.08	20.79 ± 0.08	503.8 ± 3.9	61.1 ± 0.2	676.61 ± 3.24	18.5481 ± 0.0870	0.424	−1.24	52	0.56 ± 0.03	3	17287	−0.22 ± 0.02	3
replicate	20.09 ± 0.07	529.4 ± 4.3	71.4 ± 0.3	560.03 ± 3.14	15.9399 ± 0.0653	0.568	−0.44						
replicate	20.52 ± 0.08	516.5 ± 6.0	63.2 ± 0.5	645.44 ± 5.31	18.3123 ± 0.1796	0.664	−0.56						
replicate	20.07 ± 0.08	512.0 ± 5.7	61.6 ± 0.6	648.04 ± 6.48	18.7555 ± 0.1878	0.859	−0.19						
76.91-76.96 (dol)	27.68 ± 0.10	623.5 ± 5.0	70.8 ± 0.2	777.51 ± 3.82	20.3256 ± 0.0975	0.458	−2.41	49	0.35 ± 0.07	4	14025	−0.26 ± 0.08	3
76.91-76.96	30.22 ± 0.11	728.9 ± 6.6	84.5 ± 0.4	711.29 ± 4.00	19.7539 ± 0.1217	0.526	−1.05	56	0.30 ± 0.06	3	15550	−0.25 ± 0.04	3
76.91-76.96-2	29.21 ± 0.11	713.0 ± 5.4	82.9 ± 0.3	701.29 ± 3.44	19.6973 ± 0.0873	0.492	−0.81						

Uncertainties are quoted at the 2_σ level.

*I_{Os} = initial ^{187}Os/^{188}Os isotope ratio calculated at 1730 Ma.

†Average includes powder replicate analyses for some samples.

‡Number of replicate Mo or Fe isotope mass spectrometer analyses.

Table 5.6. Coefficients of determination for Re, ^{192}Os, and $^{187}Re/^{188}Os$ plotted against elemental abundances.

	Re			^{192}Os			$^{187}Re/^{188}Os$		
	U. Velkerri*	L. Velkerri*	Wollogorang	U. Velkerri*	L. Velkerri*	Wollogorang	U. Velkerri*	L. Velkerri*	Wollogorang
Al_2O_3	0.78	0.25 (I)	0.00	0.38	0.04	0.01 (I)	0.03	0.30 (I)	0.01 (I)
TiO_2	0.00	0.01 (I)	0.59	0.07 (I)	0.40	0.68	0.10	0.09 (I)	0.30
Fe_2O_3	0.05 (I)	0.03	0.20 (I)	0.00	0.35	0.08 (I)	0.03 (I)	0.00	0.39 (I)
MgO	0.02	0.31 (I)	0.15 (I)	0.04	0.00	0.34 (I)	0.00	0.29 (I)	0.00
CaO	0.02 (I)	0.29 (I)	0.06 (I)	0.27	0.00	0.25 (I)	0.68 (I)	0.27 (I)	0.01
Na_2O	0.07 (I)	0.05 (I)	0.03	0.18 (I)	0.36	0.14	0.06	0.18 (I)	0.03 (I)
K_2O	0.55	0.27 (I)	0.53	0.19	0.05	0.60	0.06	0.32 (I)	0.31
V	0.21	0.36	0.78	0.03 (I)	0.37	0.70	0.52	0.16	0.58
Cr	0.07	0.25 (I)	0.55	0.00	0.41	0.53	0.06	0.52 (I)	0.40
Mn	0.53 (I)	0.54 (I)	0.13 (I)	0.02 (I)	0.02 (I)	0.37 (I)	0.38 (I)	0.53 (I)	0.00
Co	0.29 (I)	0.69	0.71	0.01 (I)	0.12	0.63	0.22 (I)	0.54	0.41
Ni	0.40 (I)	0.50	0.78	0.08 (I)	0.49	0.73	0.12 (I)	0.23	0.49
Cu	0.17	0.00	0.01	0.17	0.38	0.00	0.01 (I)	0.04 (I)	0.00
Zn	0.00	0.05 (I)	0.49 (I)	0.01	0.45	0.35 (I)	0.00	0.23 (I)	0.63 (I)
As	0.35 (I)	0.03	0.00	0.28 (I)	0.42	0.01	0.00	0.00	0.02 (I)
Rb	0.40	0.62 (I)	0.01 (I)	0.28	0.06	0.01 (I)	0.00	0.76 (I)	0.00
Sr	0.36	0.58 (I)	0.05 (I)	0.50	0.00	0.09 (I)	0.07 (I)	0.52 (I)	0.00
Zr	0.02	0.54	0.35	0.00	0.57	0.64	0.04	0.22	0.06
Mo	0.62	0.88	0.00	0.65	0.00	0.06	0.04 (I)	0.92	0.10 (I)
Ba	0.58	0.57 (I)	0.07	0.25	0.00	0.05	0.04	0.52 (I)	0.11
Pb	0.02 (I)	0.28	0.07 (I)	0.05 (I)	0.53	0.04 (I)	0.01	0.07	0.08 (I)
U	0.52	0.03	0.42	0.09	0.72	0.43	0.16	0.02 (I)	0.25

(I) denotes inverse correlation. For samples with Re-Os replicate analyses, the average Re and Os abundance, and $^{187}Re/^{188}Os$ ratio was used. To avoid any spurious correlations, sample elemental abundances were not normalized to Al abundances.
*Upper Velkerri Formation organic-rich interval (136.91-137.95 m). Lower Velkerri Formation organic-rich interval (325.64-326.69 m).

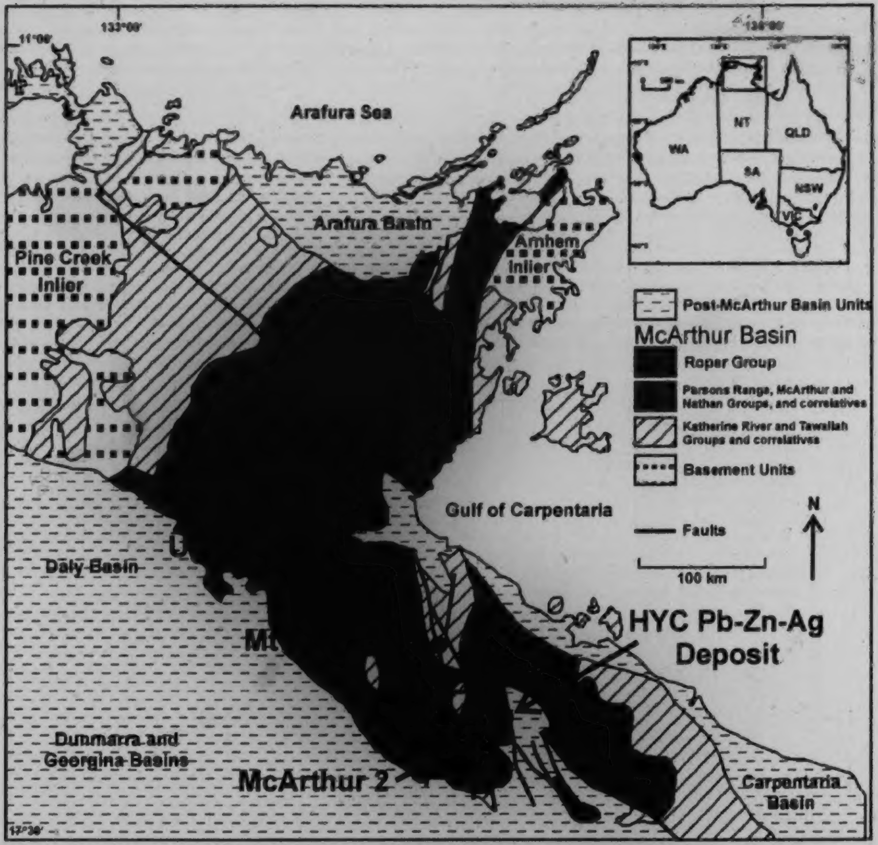
11°00'
133°00'
136°00'
17°30'
Arafura Sea
Arafura Basin
Pine Creek Inlier
Arnhem Inlier
Gulf of Carpentaria
Daly Basin
Dummarra and Georgina Basins
Carpentaria Basin
McArthur 2
HYC Pb-Zn-Ag Deposit
WA
NT
QLD
SA
NSW
VIC
Post-McArthur Basin Units
McArthur Basin
Roper Group
Parsons Range, McArthur and Nathan Groups, and correlatives
Katherine River and Tawallah Groups and correlatives
Basement Units
Faults
100 km
N

Figure 5.1: Regional geological setting of the McArthur Basin, northern Australia. The location of the drill holes Mount Young 2 (Wollogorang Formation), McArthur 2 (Barney Creek Formation), and Urapunga-4 (Velkerri Formation), and the McArthur River (HYC) Pb-Zn-Ag ore deposit are shown. Modified from Volk et al. (2005).

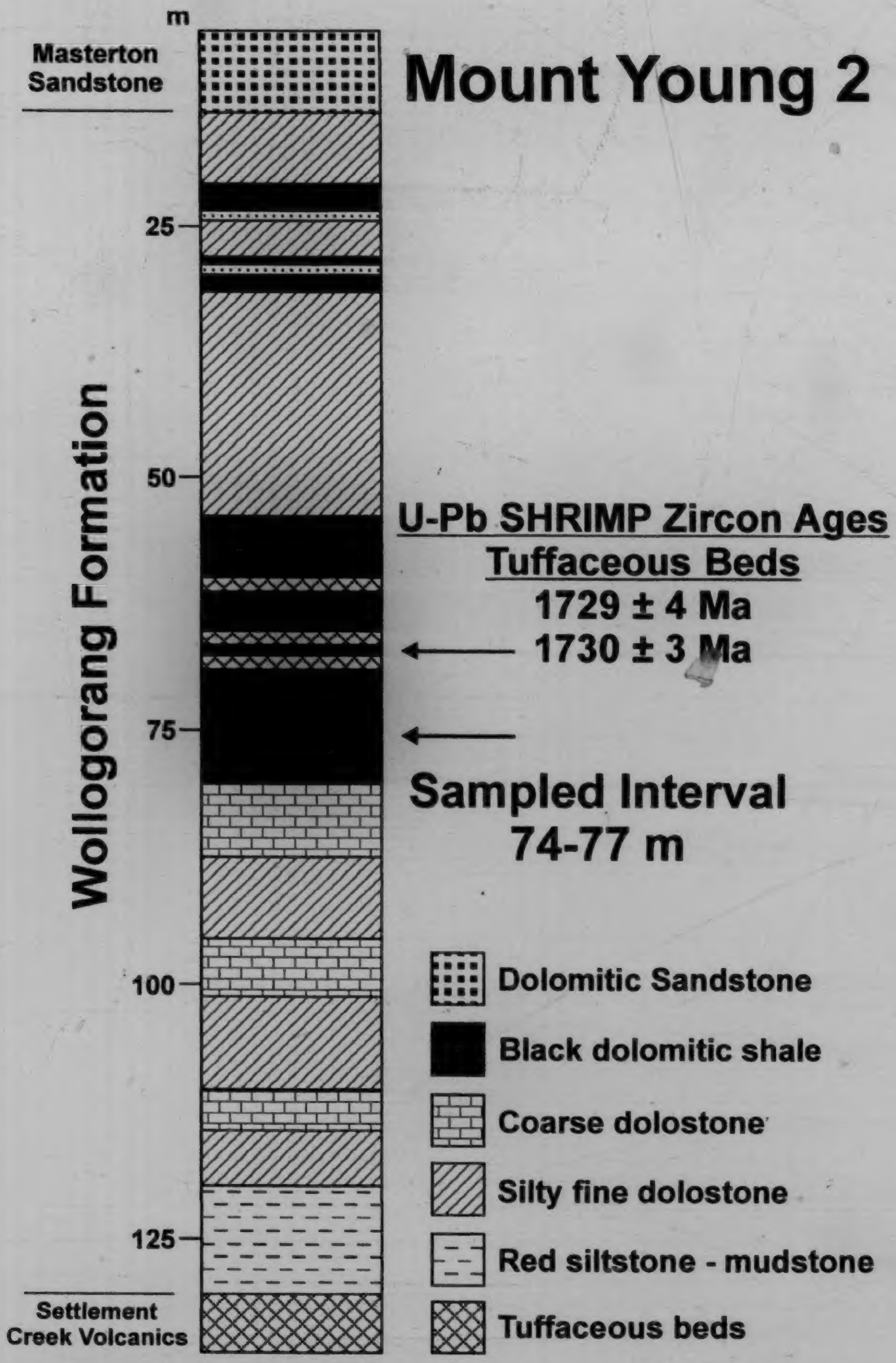
m
Masterton Sandstone
Mount Young 2
25
50
75
100
125
Wollogorang Formation
U-Pb SHRIMP Zircon Ages
Tuffaceous Beds
1729 ± 4 Ma
1730 ± 3 Ma
Sampled Interval
74-77 m
Settlement Creek Volcanics
Dolomitic Sandstone
Black dolomitic shale
Coarse dolostone
Silty fine dolostone
Red siltstone - mudstone
Tuffaceous beds

Figure 5.2: Lithostratigraphic column for the Wollogorang Formation in drill hole Mount Young 2 (modified from Donnelly and Jackson, 1988). U-Pb zircon ages from Page et al. (2000).

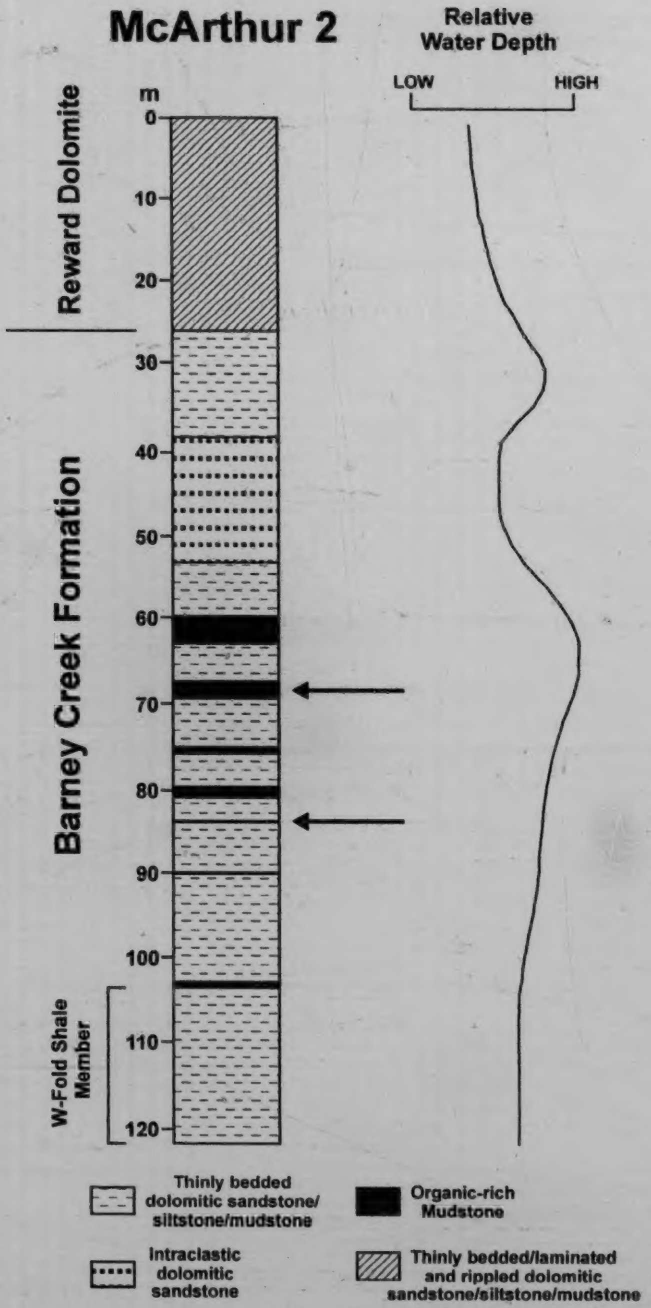
McArthur 2
Relative Water Depth
LOW
HIGH
m
0
10
20
30
40
50
60
70
80
90
100
110
120
Reward Dolomite
Barney Creek Formation
W-Fold Shale Member
Thinly bedded dolomitic sandstone/ siltstone/mudstone
Organic-rich Mudstone
Intraclastic dolomitic sandstone
Thinly bedded/laminated and rippled dolomitic sandstone/siltstone/mudstone

Figure 5.3: Lithostratigraphic column (left) and inferred relative water depth curve (right) for the Barney Creek Formation and Reward Dolomite in drill hole McArthur 2 (modified from Bull, 1998). Arrows show the position of sampled stratigraphic intervals.

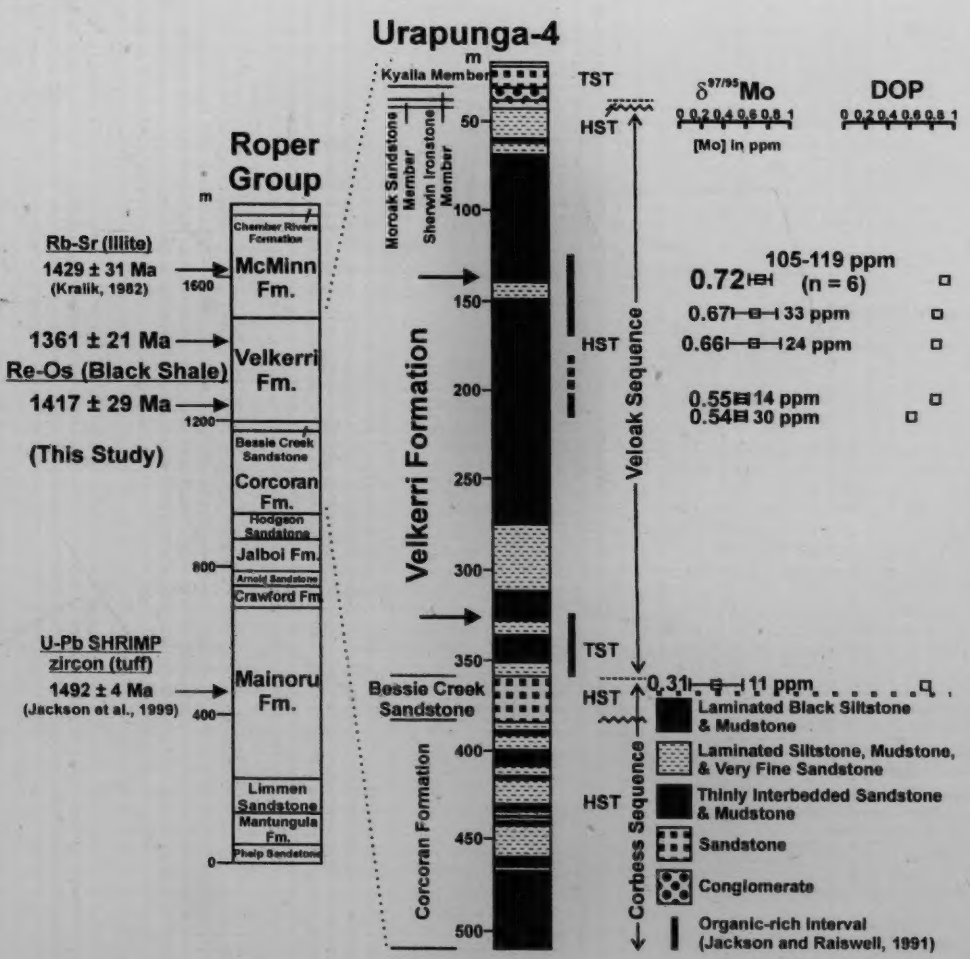
Urapunga-4
m
Kyalla Member
Moroak Sandstone Member
Sherwin Ironstone Member
Velkerri Formation
Bessie Creek Sandstone
Corcoran Formation
50
100
150
200
250
300
350
400
450
500
TST
HST
HST
TST
HST
HST
Veloak Sequence
Corbess Sequence
δ97/95Mo
0 0.2 0.4 0.6 0.8 1
[Mo] in ppm
DOP
0 0.2 0.4 0.6 0.8 1
105-119 ppm
0.72 (n = 6)
0.67 33 ppm
0.66 24 ppm
0.55 14 ppm
0.54 30 ppm
0.31 11 ppm
Laminated Black Siltstone & Mudstone
Laminated Siltstone, Mudstone, & Very Fine Sandstone
Thinly Interbedded Sandstone & Mudstone
Sandstone
Conglomerate
Organic-rich interval (Jackson and Raiswell, 1991)
Roper Group
m
Chamber River Formation
McMinn Fm.
Velkerri Fm.
Bessie Creek Sandstone
Corcoran Fm.
Hodgson Sandstone
Jalboi Fm.
Arnold Sandstone
Crawford Fm.
Mainoru Fm.
Limmen Sandstone
Mantungula Fm.
Phelp Sandstone
1600
1200
800
400
0
Rb-Sr (Illite)
1429 ± 31 Ma
(Kralik, 1982)
1361 ± 21 Ma
Re-Os (Black Shale)
1417 ± 29 Ma
(This Study)
U-Pb SHRIMP zircon (tuff)
1492 ± 4 Ma
(Jackson et al., 1999)

Figure 5.4: Generalized stratigraphic column and age constraints for the Roper Group (left), lithostratigraphic column for the Velkerri Formation in drill hole Urapunga-4 (middle, modified from Abbott and Sweet, 2000), and Mo isotope and DOP data from Arnold et al. (2004) and this study (right). The two arrows correspond to the upper and lower organic-rich intervals sampled in this study. TST and HST refer to Transgressive Systems Tract and Highstand Systems Tract, respectively.

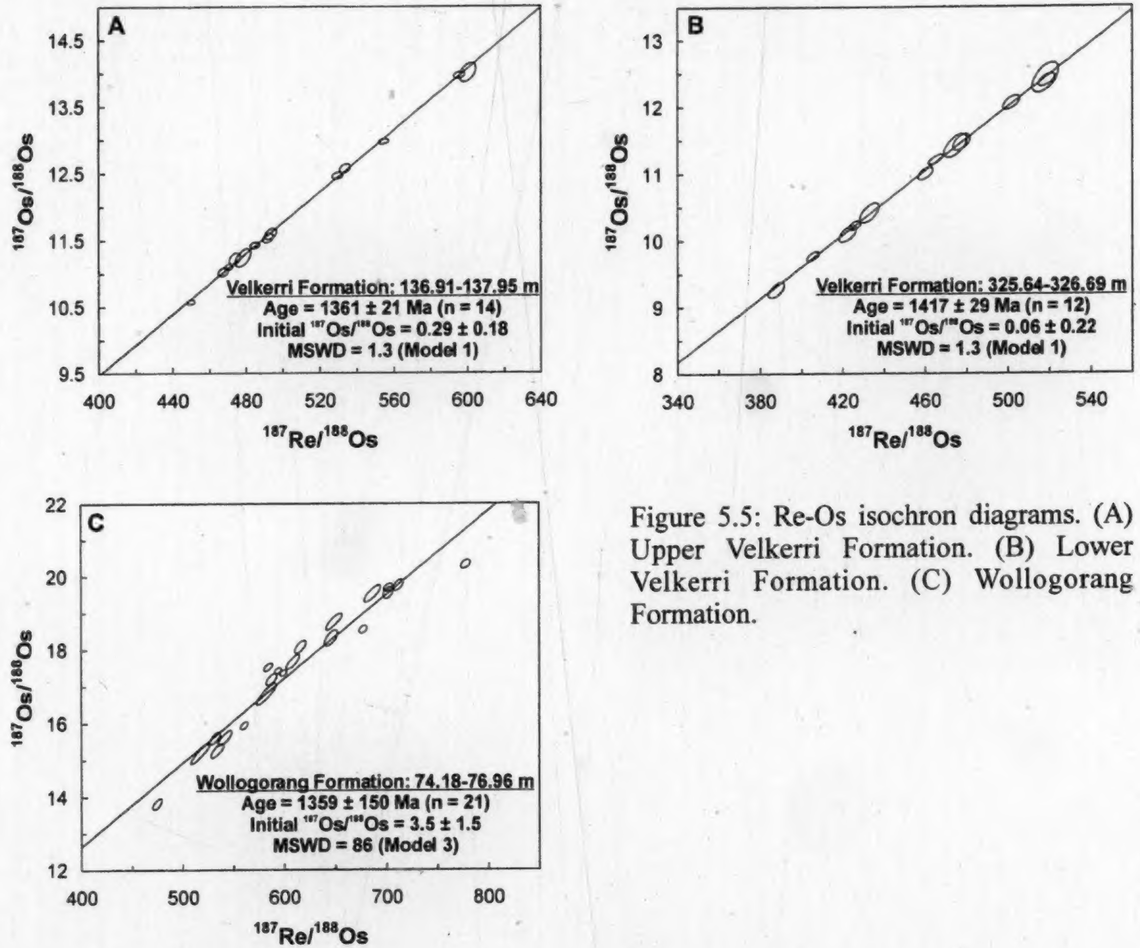

Figure 5.5: Re-Os isochron diagrams. (A) Upper Velkerri Formation. (B) Lower Velkerri Formation. (C) Wollogorang Formation.

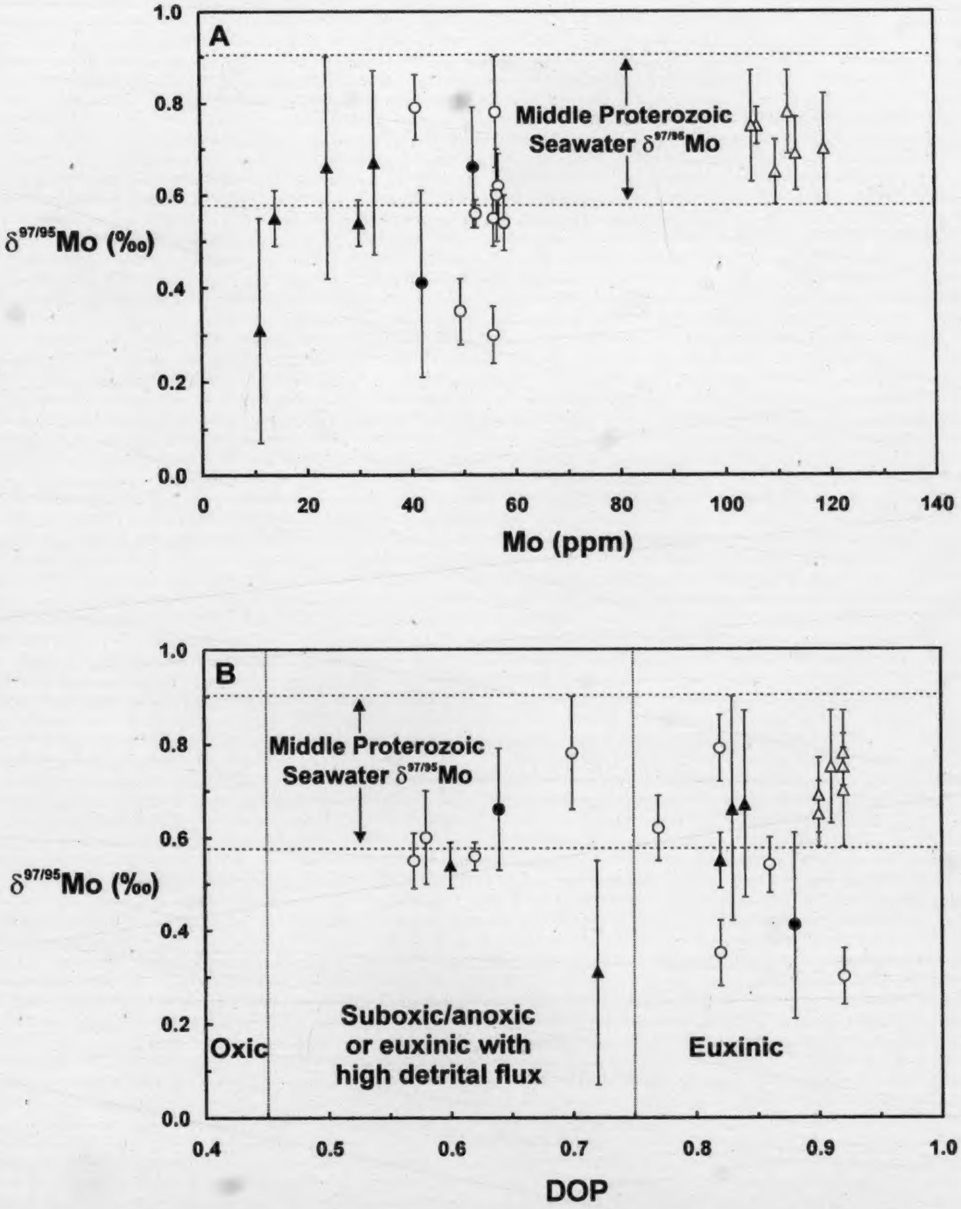

Figure 5.6: Molybdenum isotope compositions of the Velkerri and Wollogorang Formation black shales plotted against (A) Mo abundance and (B) DOP. The enclosed field denotes the most probable seawater $\delta^{97/95}$Mo composition at 1.4 Ga, and possibly at 1.7 Ga. Open triangles: Velkerri Formation (this study); filled triangles: Velkerri Formation (Arnold et al., 2004); open circles: Wollogorang Formation (this study); filled circles: Wollogorang Formation (Arnold et al., 2004).

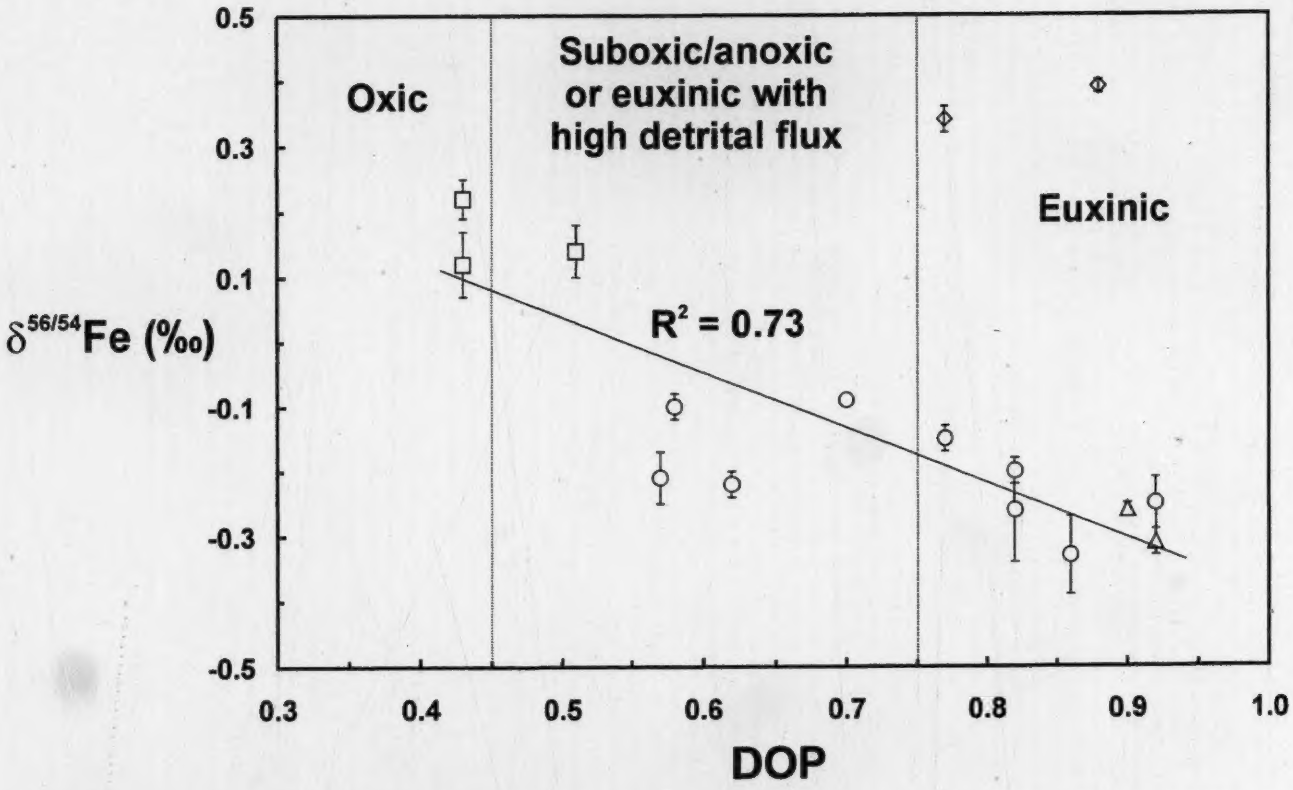

Figure 5.7: Iron isotope compositions plotted against DOP for the upper (triangles) and lower (squares) Velkerri, Wollogorang (circles), and Barney Creek (diamonds) Formations.

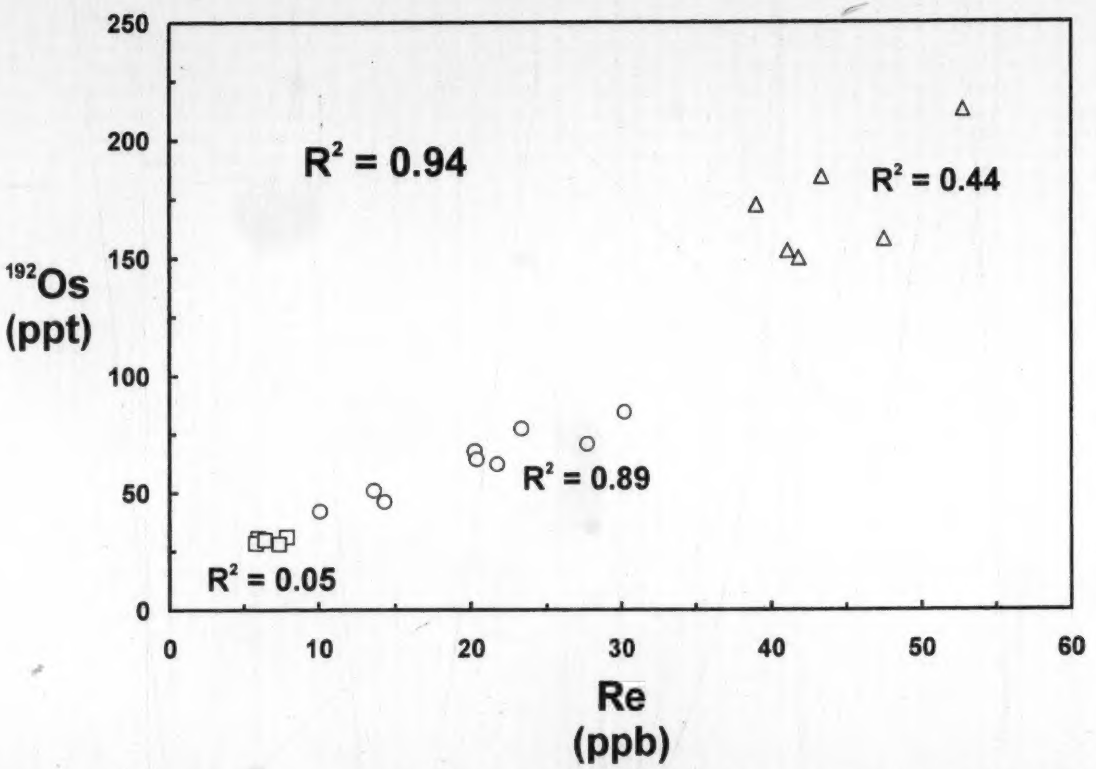

Figure 5.8: Variation in Re and Os abundance in the Velkerri and Wollogorang Formation black shales. The mean Re and Os abundance was used for samples with replicate analyses. Coefficients of determination for individual shale intervals are shown. For the purpose of comparison with trace metal data in Figure 5.9, only those samples with trace metal data were plotted. Triangles: upper Velkerri Formation; squares: lower Velkerri Formation; circles: Wollogorang Formation.

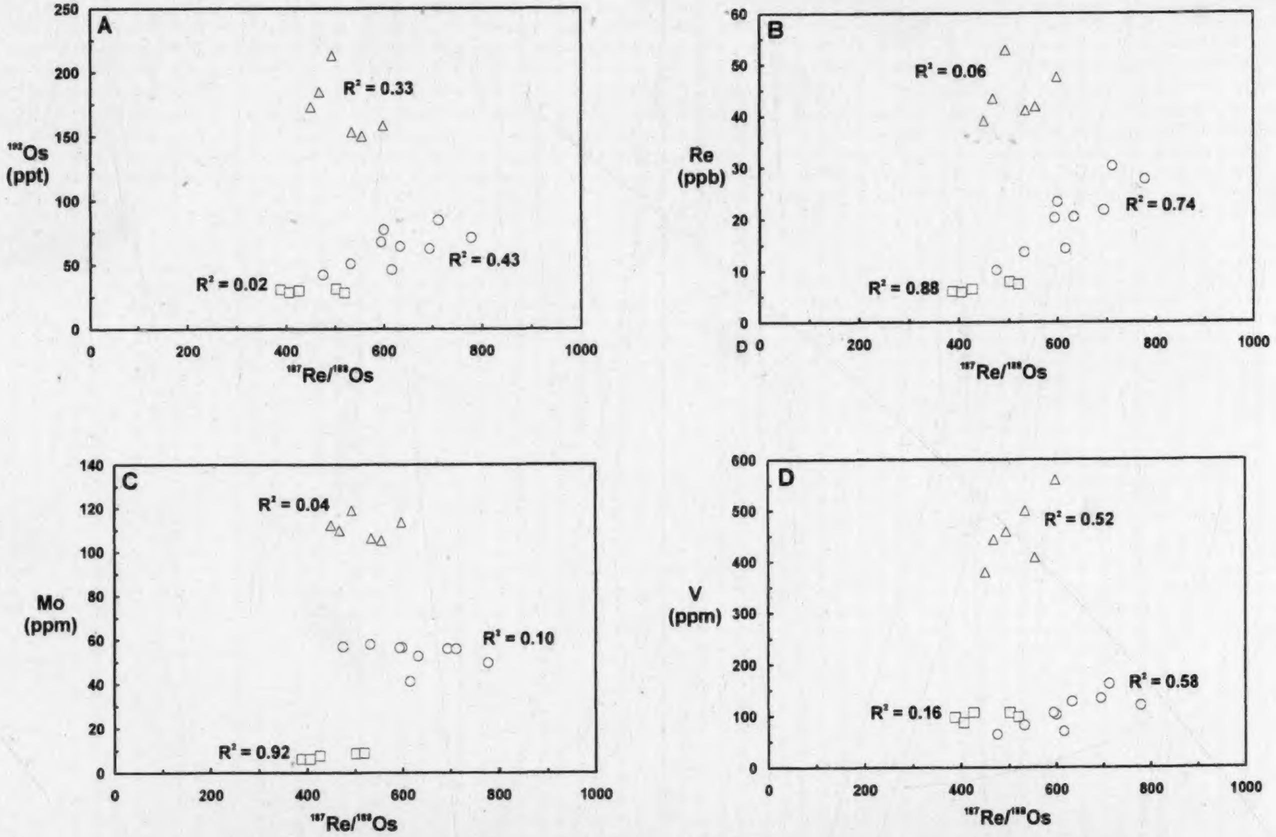

Figure 5.9: Geochemical diagrams illustrating variations in ^{187}Re/^{188}Os isotope ratio plotted against (A) ^{192}Os, (B) Re, (C) Mo, and (D) V abundance for the Velkerri and Wollogorang Formation black shales. Coefficients of determination for individual shale intervals are shown. Symbols as for Figure 5.8.

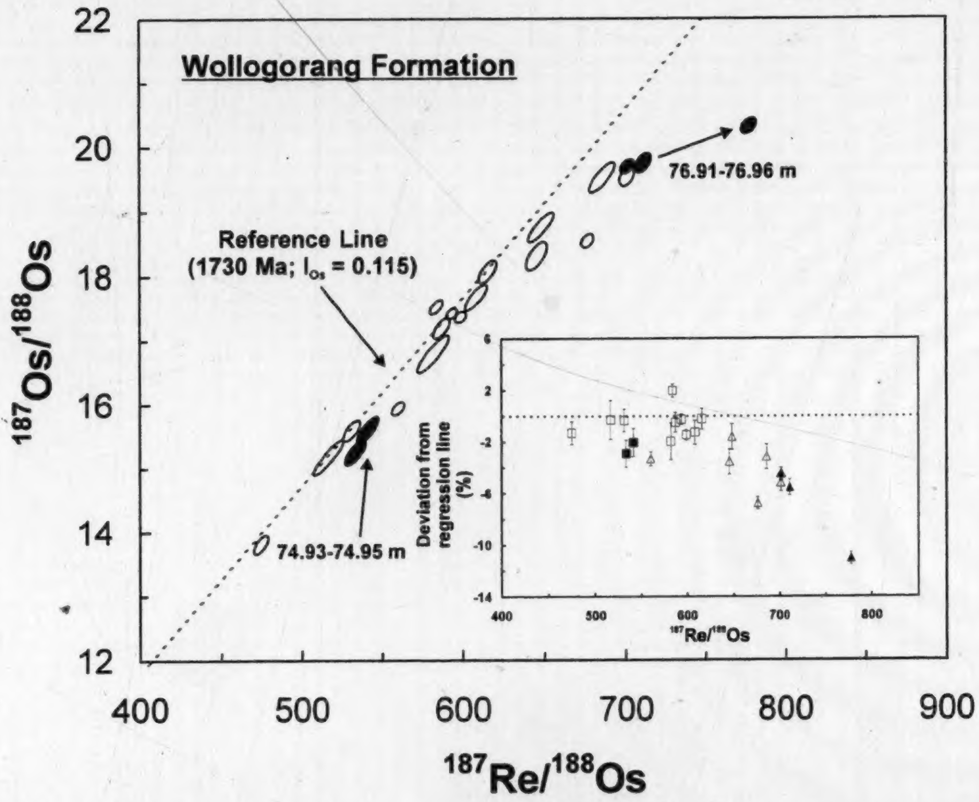

Figure 5.10: Re-Os isochron diagram for the Wollogorang Formation showing an increasing degree of deviation, with stratigraphic depth, from a 1730 Ma reference line (inset diagram) with chondritic initial $^{187}Os/^{188}Os$ isotope composition, and a comparison of the Re-Os isotope systematics of dolomite veinlets plus surrounding shale (black) relative to adjacent shale material ≥ 4 mm from dolomite veinlets (grey). Regression of sample subsets from 74.18-75.53 m and 76.00-76.96 m depth yields Re-Os dates of 1781 ± 190 Ma (n = 12, MSWD = 22, I_{Os} = –0.5 ± 1.9) and 1234 ± 370 Ma (n = 9, MSWD = 93, I_{Os} = 4.8 ± 4.3) (not shown).

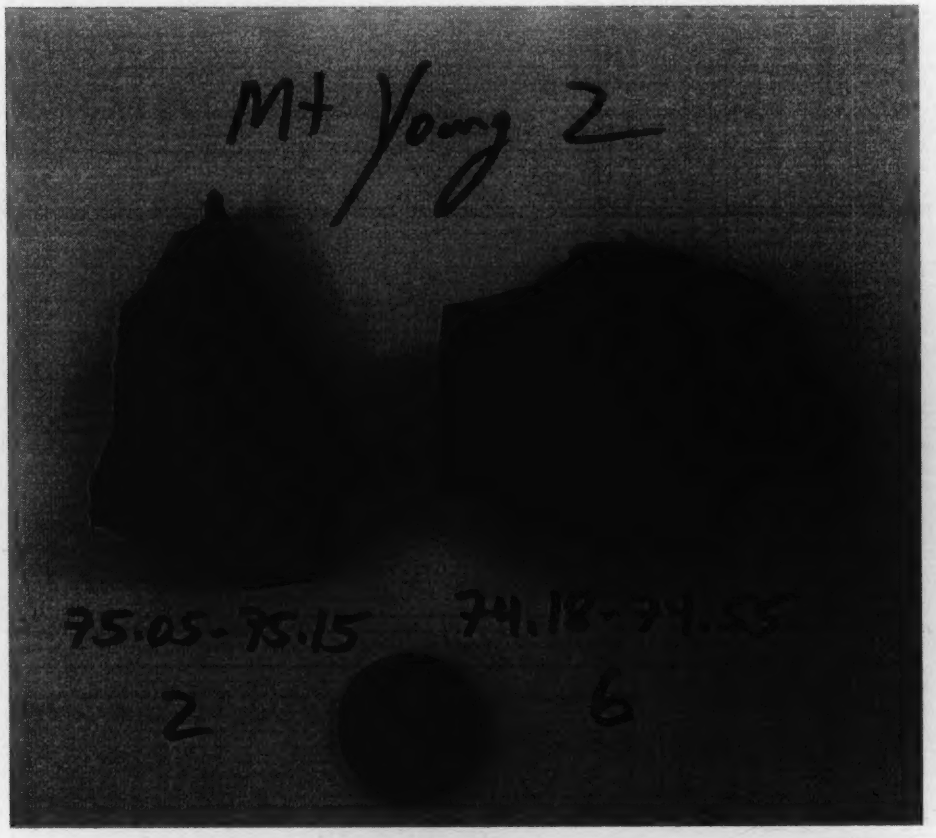

Plate 5.1: Pyritic, dolomitic, thinly laminated black shale from the Late Paleoproterozoic Wollogorang Formation (Tawallah Group, McArthur Basin, northern Australia), drill hole Mount Young 2. Samples shown are from depths 75.08-75.11 m (left) and 74.35-74.38 m (right). Note the abundant dolomite veinlets.

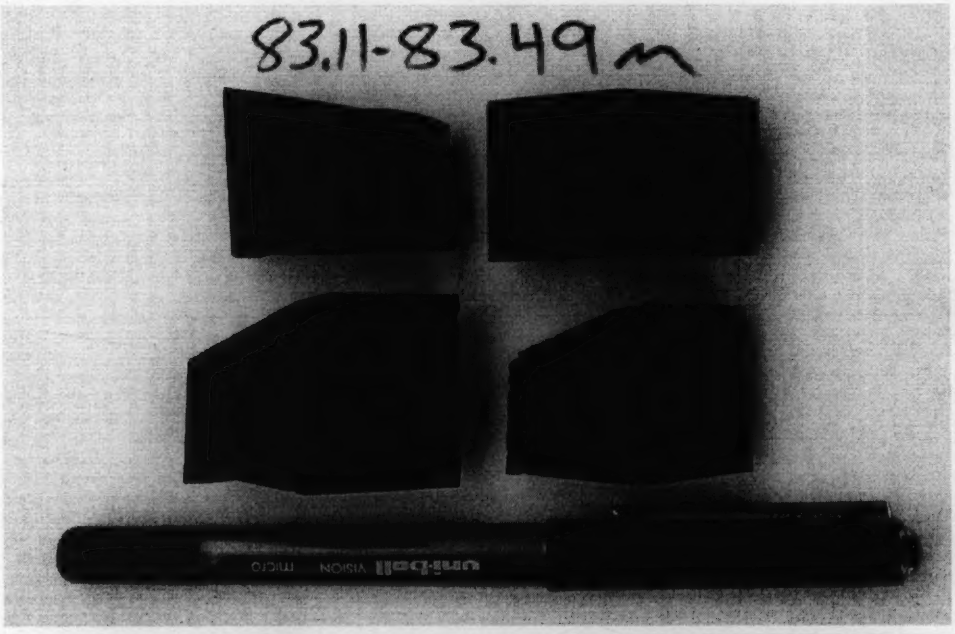
83.11-83.49 m
uni-ball VISION micro

Plate 5.2: Finely laminated and pyritic black shale from the HYC Pyritic Shale Member, Late Paleoproterozoic Barney Creek Formation (McArthur Group, McArthur Basin), drill hole McArthur 2. Samples shown are from depths 83.11-83.14 m (1), 83.29-83.32 m (6), 83.36-83.39 m (10), and 83.42-83.44 m (12).

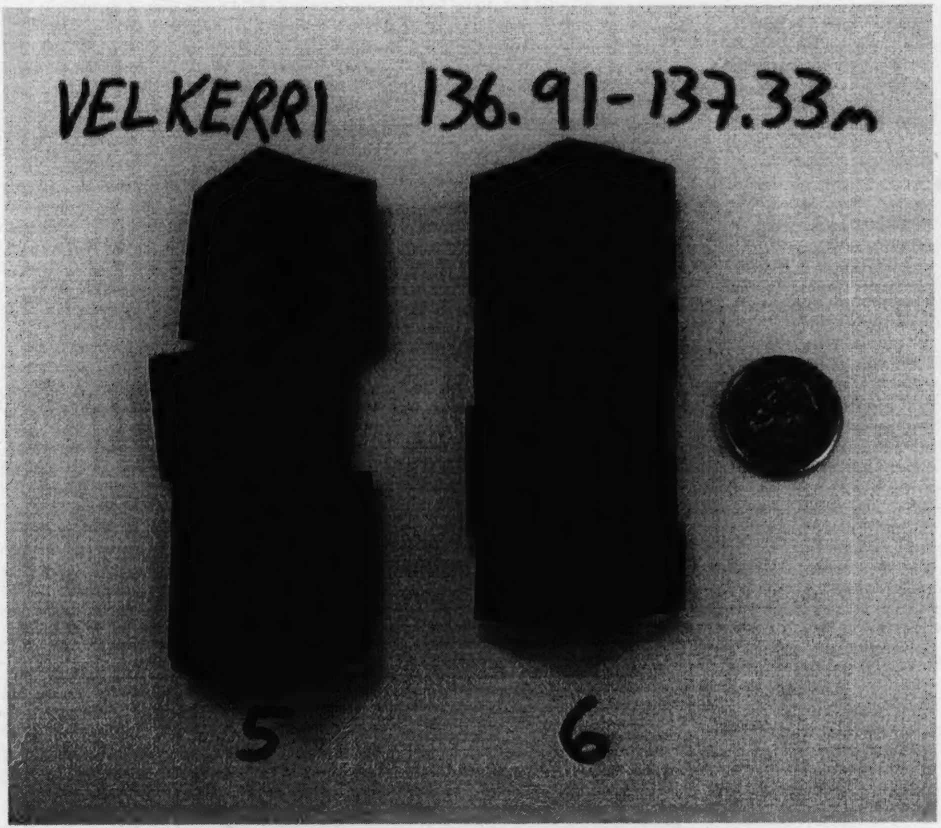

Plate 5.3: Pyritic, finely laminated black shale from the upper organic-rich interval of the Early Mesoproterozoic Velkerri Formation (Roper Group, McArthur Basin), drill hole Urapunga-4. Samples shown are from depths 137.19-137.26 m (left) and 137.26-137.33 m (right).

VELKERR1 325.5-326.2
4
7
10

Plate 5.4: Pyritic, finely laminated black shale from the lower organic-rich interval of the Velkerri Formation, drill hole Urapunga-4. Samples shown are from depths 325.71-325.78 m (4), 325.92-325.99 m (7), and 326.13-326.20 m (10).

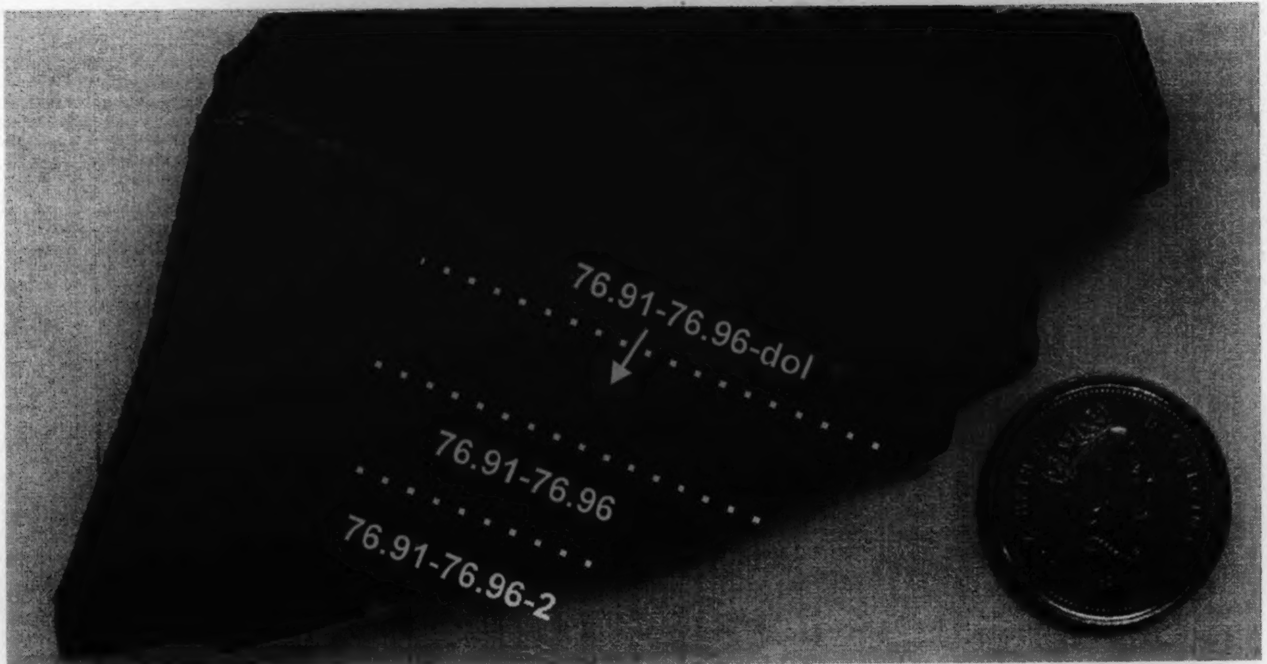
76.91-76.96-dol
76.91-76.96
76.91-76.96-2

Plate 5.5: Wollogorang Formation black shale at 76.91-76.96 m depth with a prominent dolomite veinlet and the three sub-samples from this interval.

REFERENCES

Abbott, S.T., and Sweet, I.P., 2000, Tectonic control on third-order sequences in a siliciclastic ramp-style basin: an example from the Roper Superbasin (Mesoproterozoic), northern Australia: Australian Journal of Earth Sciences, v. 47, p. 637-657.

Algeo, T.J., 2004, Can marine anoxic events draw down the trace-element inventory of seawater?: Geology, v. 32, p. 1057-1060.

Algeo, T.J., and Maynard, J.B., 2004, Trace-element behavior and redox facies in core shales of Upper Pennsylvanian Kansas-type cyclothems: Chemical Geology, v. 206, p. 289-318.

Algeo, T.J., and Lyons, T.W., 2006, Mo – total organic carbon covariation in modern anoxic marine environments: implications for analysis of paleoredox and paleohydrographic conditions: Paleoceanography, v. 21, paper #PA1016.

Alves, S., Schiano, P., Capmas, F., and Allègre, C.J., 2002, Osmium isotope binary mixing arrays in arc volcanism: Earth and Planetary Science Letters, v. 198, p. 355-369.

Anbar, A.D., and Knoll, A.H., 2002, Proterozoic ocean chemistry and evolution: a bioinorganic bridge?: Science, v. 297, p. 1137-1142.

Anbar, A.D., Knab, K.A., and Barling, J., 2001, Precise determination of mass-dependent variations in the isotopic composition of molybdenum using MC-ICPMS: Analytical Chemistry, v. 73, p. 1425-1431.

Anderson, T.F., and Raiswell, R., 2004, Sources and mechanisms for the enrichment of highly reactive iron in euxinic Black Sea sediments: American Journal of Science, v. 304, p. 203-233.

Archer, C., and Vance, D., 2006, Coupled Fe and S isotope evidence for Archean microbial Fe (III) and sulfate reduction: Geology, v. 34, p. 153-156.

Arnold, G.L., Anbar, A.D., Barling, J., and Lyons, T.W., 2004, Molybdenum isotope evidence for widespread anoxia in Mid-Proterozoic oceans: Science, v. 304, p. 87-90.

Barling, J., and Anbar, A.D., 2004, Molybdenum isotope fractionation during adsorption by manganese oxides: Earth and Planetary Science Letters, v. 217, p. 315-329.

Barling, J., Arnold, G.L., and Anbar, A.D., 2001, Natural mass-dependent variations in the isotopic composition of molybdenum: Earth and Planetary Science Letters, v. 193, p. 447-457.

Barre, A.B., Prinzhofer, A., and Allegre, C.J., 1995, Osmium isotopes in the organic matter of crude oil and asphaltenes: Terra Abstracts, v. 7, p. 1999.

Bekker, A., Holland, H.D., Wang, P.-L., Rumble III, D., Stein, H.J., Hannah, J.L., Coetzee, L.L., and Beukes, N.J., 2004, Dating the rise of atmospheric oxygen: Nature, v. 427, p. 117-120.

Betts, P.G., Giles, D., and Lister, G.S., 2003, Tectonic environment of shale-hosted massive sulfide Pb-Zn-Ag deposits of Proterozoic northeastern Australia: Economic Geology, v. 98, p. 557-576.

Breit, G.N., and Wanty, R.B., 1991, Vanadium accumulation in carbonaceous rocks: a review of geochemical controls during deposition and diagenesis: Chemical Geology, v. 91, p. 83-97.

Brocks, J.J., Love, G.D., Summons, R.E., Knoll, A.H., Logan, G.A., and Bowden, S.A., 2005, Biomarker evidence for green and purple sulphur bacteria in a stratified Palaeoproterozoic sea: Nature, v. 437, p. 866-870.

Buchler, J.W., 1975, Static coordination chemistry of metalloporphyrins, *in* Smith K., ed., Porphyrins and Metalloporphyrins: Elsevier, Amsterdam, p. 157-230.

Bull, S.W., 1998, Sedimentology of the Palaeoproterozoic Barney Creek Formation in DDH BMR McArthur 2, southern McArthur Basin, Northern Territory: Australian Journal of Earth Sciences, v. 45, p. 21-31.

Canfield, D.E., 1998, A new model for Proterozoic ocean chemistry: Nature, v. 396, p. 450-453.

Canfield, D.E., and Teske, A., 1996, Late Proterozoic rise in atmospheric oxygen concentration inferred from phylogenetic and sulphur-isotope studies: Nature, v. 382, p. 127-132.

Canfield, D.E., Lyons, T.W., and Raiswell, R., 1996, A model for iron deposition to euxinic Black Sea sediments: American Journal of Science, v. 296, p. 818-834.

Canfield, D.E., Poulton, S.W., and Narbonne, G.M., 2007, Late-Neoproterozoic deep-ocean oxygenation and the rise of animal life: Science, v. 315, p. 92-95.

Cave, R.R., Ravizza, G.E., German, C.R., Thomson, J., and Nesbitt, R.W., 2003, Deposition of osmium and other platinum-group elements beneath the ultramafic-hosted Rainbow hydrothermal plume: Earth and Planetary Science Letters, v. 210, p. 65-79.

Chen, J., Walter, M.R., Logan, G.A., Hinman, M.C., and Summons, R.E., 2003, The Paleoproterozoic McArthur (HYC) Pb/Zn/Ag deposit of northern Australia:

organic geochemistry and ore genesis: Earth and Planetary Science Letters, v. 210, p. 467-479.

Cooke, D.R., Bull, S.W., Donovan, S., and Rogers, J.R., 1998, K-metasomatism and base metal depletion in volcanic rocks from the McArthur Basin, Northern Territory – Implications for base metal mineralization: Economic Geology, v. 93, p. 1237-1263.

Creaser, R.A., and Stasiuk, L.D., 2007, Depositional age of the Douglas Formation, northern Saskatchewan, determined by Re-Os geochronology, *in* Jefferson, C.W., and Delaney, G., eds., EXTECH IV: Geology and Uranium EXploration TECHnology of the Proterozoic Athabasca Basin, Saskatchewan and Alberta: Geological Survey of Canada Bulletin 588, p. 341-346.

Creaser, R.A., Sannigrahi, P., Chacko, T., and Selby, D., 2002, Further evaluation of the Re-Os geochronometer in organic-rich sedimentary rocks: a test of hydrocarbon maturation effects in the Exshaw Formation, Western Canada Sedimentary Basin: Geochimica et Cosmochimica Acta, v. 66, p. 3441-3452.

Crick, I.H., 1992, Petrological and maturation characteristics of organic matter from the Middle Proterozoic McArthur Basin, Australia: Australian Journal of Earth Sciences, v. 39, p. 501-519.

Crick, I.H., Boreham, C.J., Cook, A.C., and Powell, T.G., 1988, Petroleum geology and geochemistry of Middle Proterozoic McArthur Basin, northern Australia II: assessment of source rock potential: American Association of Petroleum Geology Bulletin, v. 72, p. 1495-1514.

Crusius, J., and Thomson, J., 2000, Comparative behavior of authigenic Re, U and Mo during reoxidation and subsequent long-term burial in marine sediments: Geochimica et Cosmochimica Acta, v. 64, p. 2233-2242.

Davidson, G.J., 1998, Alkali alteration styles and mechanisms, and their implications for a 'brine' factory source of base metals in the rift-related McArthur Group, Australia: Australian Journal of Earth Sciences, v. 45, p. 33-49.

Davidson, G.J., and Dashlooty, S.A., 1993, The Glyde Sub-basin: a volcaniclastic-bearing pull-apart basin coeval with the McArthur River base-metal deposit, Northern Territory: Australian Journal of Earth Sciences, v. 40, p. 527-543.

Derry, L.A., Kaufman, A.J., and Jacobsen, S.B., 1992, Sedimentary cycling and environmental change in the Late Proterozoic: evidence from stable and radiogenic isotopes: Geochimica et Cosmochimica Acta, v. 56, p. 1317-1329.

Des Marais, D.J., Strauss, H., Summons, R.E., and Hayes, J.M., 1992, Carbon isotope evidence for the stepwise oxidation of the Proterozoic environment: Nature, v. 359, p. 605-609.

Donnelly, T.H., and Crick, I.H., 1988, Depositional environment of the Middle Proterozoic Velkerri Formation in northern Australia: geochemical evidence: Precambrian Research, v. 42, p. 165-172.

Donnelly, T.H., and Jackson, M.J., 1988, Sedimentology and geochemistry of a Mid-Proterozoic lacustrine unit from northern Australia: Sedimentary Geology, v. 58, p. 145-169.

Douglas, S.E., Larkum, A.W.D., and Raven, J.A., 2003, Photosynthesis in algae: Advances in Photosynthesis and Respiration Volume 14, Kluwer Academic Publishers.

Duan, Y., Anbar, A.D., Gordon, G., Severmann, S., Lyons, T.W., and Sageman, B., 2006, Investigation of iron isotope systematics in Middle Devonian anoxic basins. Astrobiology Science Conference 2006 abstract, Washington, D.C.

Duan, Y., Anbar, A.D., Arnold, G.L., Gordon, G.W., Severmann, S., and Lyons, T.W., 2007, The iron isotope variations in the ~ 2.5 Ga Mt. McRae Shale: Geological Society of America Abstracts With Programs, v. 39 (6), p. 449.

Dutkiewicz, A., Volk, H., Ridley, J., and George, S., 2003, Biomarkers, brines, and oil in the Mesoproterozoic, Roper Superbasin, Australia: Geology, v. 31, p. 981-984.

Dutkiewicz, A., Volk, H., Ridley, J., and George, S.C., 2004, Geochemistry of oil in fluid inclusions in a middle Proterozoic igneous intrusion: implications for the source of hydrocarbons in crystalline rocks: Organic Geochemistry, v. 35, p. 937-957.

Esser, B.K., and Turekian, K.K., 1993, The osmium isotopic composition of the continental crust: Geochimica et Cosmochimica Acta, v. 57, p. 3093-3104.

Farquhar, J., and Wing, B.A., 2003, Multiple sulfur isotopes and the evolution of the atmosphere: Earth and Planetary Science Letters, v. 213, p. 1-13.

Fike, D.A., Grotzinger, J.P., Pratt, L.M., and Summons, R.E., 2006, Oxidation of the Ediacaran Ocean: Nature, v. 444, p. 744-747.

Filby, R.H., 1975, The nature of metals in petroleum, *in* Yen, T.F., ed., The Role of Trace Metals in Petroleum: Ann Arbor Science, Ann Arbor, MI., p. 31-58.

Filby, R.H., and Branthaver, J.F., 1987, Metal complexes in fossil fuels: geochemistry, characterization, and processing: American Chemical Society.

Filby, R.H., and Van Berkel, G.J., 1987, Geochemistry of metal complexes in petroleum, source rocks and coal: an overview, *in* Filby, R.H., and Branthaver, J.F., eds., Metal complexes in fossil fuels: geochemistry, characterization and processing: American Chemical Society, p. 2-39.

Garven, G., Bull, S.W., and Large, R.R., 2001, Hydrothermal fluid flow models of stratiform ore genesis in the McArthur Basin, Northern Territory, Australia: Geofluids, v. 1, p. 289-311.

George, S.C., and Ahmed, M., 2002, Use of aromatic compound distributions to evaluate organic maturity of the Proterozoic Middle Velkerri Formation, McArthur Basin, Australia, *in* Keep, M., and Moss, S.J., eds., The sedimentary basins of western Australia 3: Proceedings of the Petroleum Exploration Society of Australia Symposium, p. 253-270.

Goldblatt, C., Lenton, T.M., and Watson, A.J., 2006, Bistability of atmospheric oxygen and the Great Oxidation: Nature, v. 443, p. 683-686.

Gorokhov, I.M., Siedlecka, A., Roberts, D., Melnikov, N.N., and Turchenko, T.L., 2001, Rb-Sr dating of diagenetic illite in Neoproterozoic shales, Varanger Peninsula, northern Norway: Geological Magazine, v. 138, p. 541-562.

Hardison, R.C., 1996, A brief history of hemoglobins: Plant, animal, protist, and bacteria: Proceedings of the National Academy of Sciences, v. 93, p. 5675-5679.

Hattori, Y., Suzuki, K., Honda, M., and Shimizu, H., 2003, Re-Os isotope systematics of the Taklimakan Desert sands, moraines and river sediments around the Taklimakan Desert, and of Tibetan soils: Geochimica et Cosmochimica Acta, v. 67, p. 1195-1205.

Hurtgen, M.T., Arthur, M.A., and Halverson, G.P., 2005, Neoproterozoic sulfur isotopes, the evolution of microbial sulfur species, and the burial efficiency of sulfide as sedimentary pyrite: Geology, v. 33, 41-44.

Idnurm, M., 2000, Towards a high resolution Late Palaeoproterozoic – earliest Mesoproterozoic apparent polar wander path for northern Australia: Australian Journal of Earth Sciences, v. 47, p. 405-429.

Idnurm, M., Giddings, J.W., and Plumb, K.A., 1995, Apparent polar wander and reversal stratigraphy of the Palaeo-Mesoproterozoic southeastern McArthur Basin, Australia: Precambrian Research, v. 72, p. 1-41.

Jackson, M.J., 1985, Mid-Proterozoic dolomitic varves and microcycles from the McArthur Basin, northern Australia: Sedimentary Geology, v. 44, p. 301-326.

Jackson, M.J., and Raiswell, R., 1991, Sedimentology and carbon-sulphur geochemistry of the Velkerri Formation, a Mid-Proterozoic potential oil source in northern Australia: Precambrian Research, v. 54, p. 81-108.

Jackson, M.J., Powell, T.G., Summons, R.E., and Sweet, I.P., 1986, Hydrocarbon shows and petroleum source rocks in sediments as old as 1.7 x 10^9 years: Nature, v. 322, p. 727-729.

Jackson, M.J., Muir, M.D., and Plumb, K.A., 1987, Geology of the southern McArthur Basin: Bureau of Mineral Resources Bulletin 220.

Jackson, M.J., Sweet, I.P., and Powell, T.G., 1988, Studies on petroleum geology and geochemistry, Middle Proterozoic, McArthur Basin, northern Australia. I: petroleum potential: Australia Petroleum Exploration Association Journal, v. 28, p. 283-302.

Jackson, M.J., Sweet, I.P., Page, R.W., and Bradshaw, B.E., 1999, The South Nicholson and Roper Groups: evidence for the early Mesoproterozoic Roper Superbasin, *in* Integrated basin analysis of the Isa Superbasin using seismic, well-log, and geopotential data: an evaluation of the economic potential of the northern Lawn Hill Platform: Australian Geological Survey Organisation Record 1999/19 (unpaginated).

Jackson, M.J., Scott, D.L., and Rawlings, D.J., 2000, Stratigraphic framework for the Leichhardt and Calvert Superbasins: review and correlations of the pre-1700 Ma successions between Mt Isa and McArthur River: Australian Journal of Earth Sciences, v. 47, p. 381-403.

Javaux, E.J., Knoll, A.H., and Walter, M.R., 2001, Morphological and ecological complexity in early eukaryotic ecosystems: Nature, v. 412, p. 66-69.

Javaux, E.J., Knoll, A.H., and Walter, M.R., 2004, TEM evidence for eukaryotic diversity in mid-Proterozoic oceans: Geobiology, v. 2, p. 121-132.

Johnston, D.T., Wing, B.A., Farquhar, J., Kaufman, A.J., Strauss, H., Lyons, T.W., Kah, L.C., and Canfield, D.E., 2005, Active microbial sulfur disproportionation in the Mesoproterozoic: Science, v. 310, p. 1477-1479.

Johnston, D.T., Poulton, S.W., Fralick, P.W., Wing, B.A., Canfield, D.E., and Farquhar, J., 2006, Evolution of the ocean sulfur cycle at the end of the Paleoproterozoic: Geochimica et Cosmochimica Acta, v. 70, p. 5723-5739.

Kah, L.C., and Riding, R., 2007, Mesoproterozoic carbon dioxide levels inferred from calcified cyanobacteria: Geology, v. 35, p. 799-802.

Kah, L.C., Lyons, T.W., and Frank, T.D., 2004, Low marine sulphate and protracted oxygenation of the Proterozoic biosphere: Nature, v. 431, p. 834-838.

Kendall, B.S., Creaser, R.A., Ross, G.M., and Selby, D., 2004, Constraints on the timing of Marinoan "Snowball Earth" glaciation by ^{187}Re-^{187}Os dating of a Neoproterozoic, post-glacial black shale in Western Canada: Earth and Planetary Science Letters, v. 222, p. 729-740.

Kennedy, M., Droser, M., Mayer, L.M., Pevear, D., Mrofka, D., 2006, Late Precambrian oxygenation; inception of the clay mineral factory: Science, v. 311, p. 1446-1449.

Knoll, A.H., Hayes, J.M., Kaufman, A.J., Swett, K., and Lambert, I.B., 1986, Secular variation in carbon isotope ratios from Upper Proterozoic successions of Svalbard and East Greenland: Nature, v. 321, p. 832-838.

Kralik, M., 1982, Rb-Sr age determinations on Precambrian carbonate rocks of the Carpentarian McArthur Basin, Northern Territories, Australia: Precambian Research, v. 18, p. 157-170.

Large, R.R., Bull, S.W., Cooke, D.R., and McGoldrick, P.J., 1998, A genetic model for the HYC deposit, Australia: based on regional sedimentology, geochemistry, and sulfide-sediment relationships: Economic Geology, v. 93, p. 1345-1368.

Large, R.R., Bull, S.W., and Winefield, P.R., 2001, Carbon and oxygen isotope halo in carbonates related to the McArthur River (HYC) Zn-Pb-Ag deposit, North Australia: Implications for sedimentation, ore genesis, and mineral exploration: Economic Geology, v. 96, p. 1567-1593.

Lasaga, A.C., and Ohmoto, H., 2002, The oxygen geochemical cycle: dynamics and stability: Geochimica et Cosmochimica Acta, v. 66, p. 361-381.

Levasseur, S., Birck, J.-L., and Allègre, C.J., 1998, Direct measurement of femtomoles of osmium and the ^{187}Os/^{186}Os ratio in seawater: Science, v. 282, p. 272-274.

Levasseur, S., Birck, J.-L., and Allègre, C.J., 1999, The osmium riverine flux and the oceanic mass balance of osmium: Earth and Planetary Science Letters, v. 174, p. 7-23.

Lindsay, J.F., 2001, Basin dynamics and mineralization, McArthur Basin, northern Australia: Australian Journal of Earth Sciences, v. 48, p. 703-720.

Logan, G.A., Hinman, M.C., Walter, M.R., and Summons, R.E., 2001, Biogeochemistry of the ca. 1640 Ma McArthur River (HYC) lead-zinc ore and host sediments, Northern Territory, Australia: Geochimica et Cosmochimica Acta, v. 65, p. 2317-2336.

Lyons, T.W., 1997, Sulfur isotope trends and pathways of iron sulfide formation in the upper Holocene sediments of the anoxic Black Sea: Geochimica et Cosmochimica Acta, v. 61, p. 3367-3382.

Lyons, T.W., and Severmann, S., 2006, A critical look at iron paleoredox proxies: New insights from modern euxinic marine basins: Geochimica et Cosmochimica Acta, v. 70, p. 5698-5722.

Lyons, T.W., Luepke, J.J., Schreiber, M.E., and Zieg G.A., 2000, Sulfur geochemical constraints on Mesoproterozoic restricted marine deposition: Lower Belt Supergroup, northwestern United States: Geochimica et Cosmochimica Acta, v. 64, p. 427-437.

Martin, C.E., Peucker-Ehrenbrink, B., Brunskill, G.J., and Szymczak, R., 2000, Sources and sinks of unradiogenic osmium runoff from Papua New Guinea: Earth and Planetary Science Letters, v. 183, p. 261-274.

Matthews, A., Morgans-Bell, H.S., Emmanuel, S., Jenkyns, H.C., Erel, Y., and Halicz, L., 2004, Controls on iron-isotope fractionation in organic-rich sediments (Kimmeridge Clay, Upper Jurassic, southern England): Geochimica et Cosmochimica Acta, v. 68, p. 3107-3123.

Mauzerall, D.C., 1998, Evolution of porphyrins: Clinics in Dermatology, v. 16, p. 195-201.

McDougall, I., Dunn, P.R., Compston, W., Webb, A.W., Richards, J.R., and Bofinger, V.M., 1965, Isotopic age determinations on Precambrian rocks of the Carpentaria region, Northern Territory, Australia: Journal of the Geological Society of Australia, v. 12, p. 67-90.

McManus, J., Nägler, T.F., Siebert, C., Wheat, C.G., and Hammond, D.E., 2002, Oceanic molybdenum isotope fractionation: diagenesis and hydrothermal ridge-flank alteration: Geochemistry, Geophysics, Geosystems, v. 3, Paper 2002GC000356.

Meisel, T., Walker, R.J., and Morgan, J.W., 1996, The osmium isotopic composition of the Earth's primitive upper mantle: Nature, v. 383, p. 517-520.

Meisel, T., Walker, R.J., Irving, A.J., and Lorand, J.-P., 2001, Osmium isotopic compositions of mantle xenoliths: a global perspective: Geochimica et Cosmochimica Acta, v. 65, p. 1311-1323.

Miller, C.A., 2004, Re-Os dating of algal laminites: reduction-enrichment of metals in the sedimentary environment and evidence for new geoporphyrins: M.Sc. Thesis, University of Saskatchewan.

Myers, J.S., Shaw, R.D., and Tyler, I.M., 1996, Tectonic evolution of Proterozoic Australia: Tectonics, v. 15, p. 1431-1446.

Nägler, T.F., Siebert, C., Lüshcen, H., and Böttcher, M.E., 2005, Sedimentary Mo isotope record across the Holocene fresh-brackish water transition of the Black Sea: Chemical Geology, v. 219, p. 283-295.

Ohmoto, H., 2004, Archaean atmosphere, hydrosphere and biosphere, *in* Eriksson, P.G., et al., eds., Developments in Precambrian geology, 12: The Precambrian Earth: tempos and events: Elsevier B.V., p. 361-388.

Ohmoto, H., Watanabe, Y., Ikemi, H., Poulson, S.R., and Taylor, B.E., 2006, Sulphur isotope evidence for an oxic Archaean atmosphere: Nature, v. 442, p. 908-911.

Oxburgh, R., 1998, Variations in the osmium isotope composition of seawater over the past 200,000 years: Earth and Planetary Science Letters, v. 159, p. 183-191.

Oxburgh, R., 2001, Residence time of osmium in the oceans: Geochemistry, Geophysics, Geosystems, v. 2, Paper 2000GC000104.

Page, R.W. and Sweet, I.P., 1998, Geochronology of basin phases in the western Mt Isa Inlier, and correlation with the McArthur Basin: Australian Journal of Earth Sciences, v. 45, p. 219-232.

Page, R.W., Jackson, M.J., and Krassay, A.A., 2000, Constraining sequence stratigraphy in north Australian basins: SHRIMP U-Pb zircon geochronology between Mt Isa and McArthur River: Australian Journal of Earth Sciences, v. 47, p. 431-459.

Pavlov, A.A., and Kasting, J.F., 2002, Mass-independent fractionation of sulfur isotopes in Archean sediments: strong evidence for an anoxic Archean atmosphere: Astrobiology, v. 2, p. 27-41.

Peucker-Ehrenbrink, B., 1996, Accretion of extraterrestrial matter during the last 80 million years and its effect on the marine osmium isotope record: Geochimica et Cosmochimica Acta, v. 60, p. 3187-3196.

Peucker-Ehrenbrink, B., and Ravizza, G., 2000, The marine osmium isotope record: Terra Nova, v. 12, p. 205-219.

Peucker-Ehrenbrink, B., and Jahn, B.-M., 2001, Rhenium-osmium isotope systematics and platinum group element concentrations: loess and the upper continental crust: Geochemistry Geophysics Geosystems, v. 2, Paper 2001GC000172.

Plumb, K.A., 1979, The tectonic evolution of Australia: Earth Science Reviews, v. 14, p. 205-249.

Poirier, A., 2006, Re-Os and Pb isotope systematics in reduced fjord sediments from Saanich Inlet (Western Canada): Earth and Planetary Science Letters, v. 249, p. 119-131.

Poplavko, Y.M., Ivanov, V.V., Karasik, T.G., Miller, A.D., Fadeyeva, V.A., Orekhov, V.S., Taliyev, S.D., and Tarkhov, Y.A., 1975, On the concentration of rhenium in petroleum, petroleum bitumens and oil shales: Geochemistry International, v. 11, p. 969-972.

Poulson, R.L., Siebert, C., McManus, J., and Berelson, W.M., 2006, Authigenic molybdenum isotope signatures in marine sediments: Geology, v. 34, p. 617-620.

Poulton, S.W., Fralick, P.W., and Canfield, D.E., 2004, The transition to a sulphidic ocean ~ 1.84 billion years ago: Nature, v. 431, p. 173-177.

Raiswell, R., Buckley, F., Berner, R.A., and Anderson, T.F., 1988, Degree of pyritization of iron as a paleoenvironmental indicator of bottom-water oxygenation: Journal of Sedimentary Petrology, v. 58, p. 812-819.

Ravizza, G., Turekian, K.K., and Hay, B.J., 1991, The geochemistry of rhenium and osmium in recent sediments from the Black Sea: Geochimica et Cosmochimica Acta, v. 55, p. 3741-3752.

Ravizza, G., and Turekian, K.K., 1992, The osmium isotopic composition of organic-rich marine sediments: Earth and Planetary Science Letters, v. 110, p. 1-6.

Rawlings, D.J., 1999, Stratigraphic resolution of a multiphase intracratonic basin system: the McArthur Basin, northern Australia: Australian Journal of Earth Sciences, v. 46, p. 703-723.

Ripley, E.M., Park, Y.-R., Lambert, D.D., and Frick, L.R., 2001, Re-Os isotopic composition and PGE contents of Proterozoic carbonaceous argillites, Virginia Formation, Northeastern Minnesota: Organic Geochemistry, v. 32, p. 857-866.

Rouxel, O.J., Bekker, A., and Edwards, K.J., 2005, Iron isotope constraints on the Archean and Paleoproterozoic ocean redox state: Science, v. 307, p. 1088-1091.

Rouxel, O.J., Bekker, A., and Edwards, K.J., 2006, Response to comment on "Iron isotope constraints on the Archean and Paleoproterozoic ocean redox state": Science, v. 311, p. 177.

Scott, D.L., Rawlings, D.J., Page, R.W., Tarlowski, C.Z., Idnurm, M., Jackson, M.J., and Southgate, P.N., 2000, Basement framework and geodynamic evolution of the Palaeoproterozoic superbasins of north-central Australia: an integrated review of geochemical, geochronological and geophysical data: Australian Journal of Earth Sciences, v. 47, p. 341-380.

Selby, D., and Creaser, R.A., 2003, Re-Os geochronology of organic-rich sediments: an evaluation of organic matter analysis methods: Chemical Geology, v. 200, p. 225-240.

Selby, D., and Creaser, R.A., 2005a, Direct radiometric dating of the Devonian-Mississippian time-scale boundary using the Re-Os black shale geochronometer: Geology, v. 33, p. 545-548.

Selby, D., and Creaser, R.A., 2005b, Direct radiometric dating of hydrocarbon deposits using rhenium-osmium isotopes: Science, v. 308, p. 1293-1295.

Selby, D., Creaser, R.A., Dewing, K., and Fowler, M., 2005, Evaluation of bitumen as a ^{187}Re-^{187}Os geochronometer for hydrocarbon maturation and migration: a case study from the Polaris MVT deposit, Canada: Earth and Planetary Science Letters, v. 235, p. 1-15.

Selby, D., Creaser, R.A., Stein, H.J., Markey, R.J., and Hannah, J.L., 2007a, Assessment of the ^{187}Re decay constant by cross calibration of Re-Os molybdenite and U-Pb zircon chronometers in magmatic ore systems: Geochimica et Cosmochimica Acta, v.71, p. 1999-2013.

Selby, D., Creaser, R.A., and Fowler, M.G., 2007b, Re-Os elemental and isotopic systematics in crude oils: Geochimica et Cosmochimica Acta, v. 71, p. 378-386.

Severmann, S., Lyons, T., Anbar, A., Gordon, G., and McManus, J., 2006a, The isotopic expression of iron shuttling in the euxinic Black Sea basin and implications for the rise of oxygen in the early atmosphere: Geological Society of America Abstracts With Programs, v. 38 (7), p. 124.

Severmann, S., Johnson, C.M., Beard, B.L., and McManus, J., 2006b, The effect of early diagenesis on the Fe isotope compositions of porewaters and authigenic minerals in continental margin sediments: Geochimica et Cosmochimica Acta, v. 70, p. 2006-2022.

Severmann, S., Lyons, T.W., Duan, Y., Anbar, A., Gordon, G., and McManus, J., 2006c, The isotopic expression of Fe shuttling in modern and ancient euxinic sediments: implications for the rise of oxygen: Geochimica et Cosmochimica Acta, v. 70 (18; supplement 1), p. A572.

Sharma, M., Papanastassiou, D.A., and Wasserburg, G.J., 1997, The concentration and isotopic composition of osmium in the oceans: Geochimica et Cosmochimica Acta, v. 61, p. 3287-3299.

Sharma, M., Wasserburg, G.J., Hofmann, A.W., and Butterfield, D.A., 2000, Osmium isotopes in hydrothermal fluids from the Juan de Fuca Ridge: Earth and Planetary Science Letters, v. 179, p. 139-152.

Shen, Y., Canfield, D.E., and Knoll, A.H., 2002, Middle Proterozoic ocean chemistry: evidence from the McArthur Basin, northern Australia: American Journal of Science, v. 302, p. 81-109.

Shen, Y., Knoll, A.H., and Walter, M.R., 2003, Evidence for low sulphate and anoxia in a mid-Proterozoic marine basin: Nature, v. 423, p. 632-635.

Siebert, C., Nägler, T.F., von Blanckenburg, F., and Kramers, J.D., 2003, Molybdenum isotope records as a potential new proxy for paleoceanography: Earth and Planetary Science Letters, v. 211, p. 159-171.

Siebert, C., McManus, J., Bice, A., Poulson, R., and Berelson, W.M., 2006, Molybdenum isotope signatures in continental margin sediments: Earth and Planetary Science Letters, v. 241, p. 723-733.

Slack, J.F., Grenne, T., Bekker, A., Rouxel, O.J., and Lindberg, P.A., 2007, Suboxic deep seawater in the late Paleoproterozoic: evidence from hematitic chert and iron formation related to seafloor-hydrothermal sulfide deposits, central Arizona, USA: Earth and Planetary Science Letters, v. 255, p. 243-256.

Smoliar, M.I., Walker, R.J., and Morgan, J.W., 1996, Re-Os ages of Group IIA, IIIA, IVA, and IVB iron meteorites: Science, v. 271, p. 1099-1102.

Southgate, P.N., Bradshaw, B.E., Domagala, J., Jackson, M.J., Idnurm, M., Krassay, A.A., Page, R.W., Sami, T.T., Scott, D.L., Lindsay, J.F., McConachie, B.A., and Tarlowski, C., 2000, Chronostratigraphic basin framework for Palaeoproterozoic rocks (1730-1575 Ma) in northern Australia and implications for base-metal mineralization: Australian Journal of Earth Sciences, v. 47, p. 461-483.

Staubwasser, M., Von Blanckenburg, F., and Schoenberg, R., 2006, Iron isotopes in the early marine diagenetic iron cycle: Geology, v. 34, p. 629-632.

Summons, R.E., Powell, T.G., and Boreham, C.J., 1988, Petroleum geology and geochemistry of the Middle Proterozoic McArthur Basin, northern Australia: III. Composition of extractable hydrocarbons: Geochimica et Cosmochimica Acta, v. 52, p. 1747-1763.

Summons, R.E., Taylor, D., and Boreham, C.J., 1994, Geochemical tools for evaluating petroleum generation in Middle Proterozoic sediments of the McArthur Basin, Northern Territory, Australia: Australia Petroleum Exploration Assocation Journal, v. 34, p. 692-706.

Sun, W., Arculus, R.J., Bennett, V.C., Eggins, S.M., and Binns, R.A., 2003a, Evidence for rhenium enrichment in the mantle wedge from submarine arc-like volcanic glasses (Papua New Guinea): Geology, v. 31, p. 845-848.

Sun, W., Bennett, V.C., Eggins, S.M., Kamenetsky, V.S., and Arculus, R.J., 2003b, Enhanced mantle-to-crust rhenium transfer in undegassed arc magmas: Nature, v. 422, p. 294-297.

Sundby, B., Martinez, P., and Gobeil, C., 2004, Comparative geochemistry of cadmium, rhenium, uranium, and molybdenum in continental margin sediments: Geochimica et Cosmochimica Acta, v. 68, p. 2485-2493.

Symons, D.T.A., 2006, HYC (McArthur River) SEDEX deposit, Australia: first paleomagnetic results: Journal of Geochemical Exploration, v. 89, p. 380-383.

Taylor, P.D.P., Maeck, R., and De Bièvre, P., 1992, Determination of the absolute isotopic composition and atomic weight of a reference sample of natural iron: International Journal of Mass Spectrometry and Ion Processes, v. 121, p. 111-125.

Tribovillard, N., Algeo, T.J., Lyons, T., and Riboulleau, A., 2006, Trace metals as paleoredox and paleoproductivity proxies: An update: Chemical Geology, v. 232, p. 12-32.

Van der Weijden, C.H., 2002, Pitfalls of normalization of marine geochemical data using a common divisor: Marine Geology, v. 184, p. 167-187.

Volk, H., George, S.C., Dutkiewicz, A., and Ridley, J., 2005, Characterisation of fluid inclusion oil in a Mid-Proterozoic sandstone and dolerite (Roper Superbasin, Australia): Chemical Geology, v. 223, p. 109-135.

Walker, R.J., Horan, M.F., Morgan, J.W., Becker, H., Grossman, J.N., and Rubin, A.E., 2002a, Comparative ^{187}Re-^{187}Os systematics of chondrites: implications regarding early solar system processes: Geochimica et Cosmochimica Acta, v. 66, p. 4187-4201.

Walker, R.J., Prichard, H.M., Ishiwatari, A., and Pimentel, M., 2002b, The osmium isotopic composition of convecting upper mantle deduced from ophiolite chromites: Geochimica et Cosmochimica Acta, v. 66, p. 329-345.

Wanty, R.B., and Goldhaber, R., 2002, Thermodynamics and kinetics of reactions involving vanadium in natural systems: accumulation of vanadium in sedimentary rock: Geochimica et Cosmochimica Acta, v. 56, p. 171-183.

Warren, J.K., George, S.C., Hamilton, P.J., and Tingate, P., 1998, Proterozoic source rocks: sedimentology and organic characteristics of the Velkerri Formation, Northern Territory, Australia: American Association of Petroleum Geology Bulletin, v. 82, p. 442-463.

Wedepohl, K.H., 1971, Environmental influences on the chemical composition of shales and clays, *in* Ahrens, L.H., et al., eds., Physics and chemistry of the Earth, volume 8: Pergamon, Oxford, UK, p. 305-333.

Wedepohl, K.H., 1991, The composition of the upper Earth's crust and the natural cycles of selected metals. Metals in natural raw materials. Natural resources, *in* Merian, E., ed., Metals and their compounds in the environment: VCH, Weinheim, Germany, p. 3-17.

Woodhouse, O.B., Ravizza, G., Falkner, K.K., Statham, P.J., and Peucker-Ehrenbrink, B., 1999, Osmium in seawater: vertical profiles of concentration and isotopic composition in the eastern Pacific Ocean: Earth and Planetary Science Letters, v. 173, p. 223-233.

Woodland, S.J., Ottley, C.J., Pearson, D.G., and Swarbrick, R.E., 2001, Microwave digestion of oils for analysis of platinum group and rare earth elements by ICP-MS, *in* Plasma Source Mass Spectrometry: Special Publication Royal Society of Chemistry, p. 17-24.

Xiong, J., Fischer, W.M., Inoue, K., Nakahara, M., and Bauer, C.E., 2000, Molecular evidence for the early evolution of photosynthesis: Science, v. 289, p. 1724-1730.

Yamaguchi, K.E., and Ohmoto, H., 2006, Comment on "Iron isotope constraints on the Archean and Paleoproterozoic ocean redox state": Science, v. 311, p. 177.

Yamaguchi, K.E., Johnson, C.M., Beard, B.L., and Ohmoto, H., 2005, Biogeochemical cycling of iron in the Archean-Paleoproterozoic Earth: Constraints from iron isotope variations in sedimentary rocks from the Kaapvaal and Pilbara Cratons: Chemical Geology, v. 218, p. 135-169.

Yamashita, Y., Takahashi, Y., Haba, H., Enomoto, S., and Shimizu, H., 2007, Comparison of reductive accumulation of Re and Os in seawater-sediment systems: Geochimica et Cosmochimica Acta, v. 71, p. 3458-3475.

Yang, J., Bull, S., and Large, R., 2004, Numerical investigation of salinity in controlling ore-forming fluid transport in sedimentary basins: example of the HYC deposit, northern Australia: Mineralium Deposita, v. 39, p. 622-631.

Yang, W., and Holland, H.D., 2002, The redox-sensitive trace elements, Mo, U, and Re in Precambrian carbonaceous shales: Indicators of the Great Oxidation Event: Geological Society of America Abstracts With Programs, v. 34, p. 381.

Yen, T.F., 1975, Chemical aspects of metals in native petroleum, *in* Yen, T.F., ed., The role of trace metals in petroleum: Ann Arbor Science, Ann Arbor, Michigan, p. 1-30.

CHAPTER 6

Re-Os Isotope Systematics of Late Archean and Early Paleoproterozoic Black Shales, the $^{187}Os/^{188}Os$ Isotope Composition of Precambrian Seawater, and the Re-Os Systematics of Organic-rich Sedimentary Rocks over Geological Time

Part of this chapter is published in the following source:

Anbar, A.D., Duan, Y., Lyons, T.W., Arnold, G.L., Kendall, B., Creaser, R.A., Kaufman, A.J., Gordon, G.W., Scott, C., Garvin, J., and Buick, R., 2007, A whiff of oxygen before the Great Oxidation Event?: Science, v. 317, p. 1903-1906.

6.1 INTRODUCTION

Formation of Earth's oceans, evolution of photosynthesis, and the initial oxidation of Earth's atmosphere and surface oceans ultimately led to the evolution of complex eukaryote cell machinery (Acquisti et al., 2007), but the chronology of these events remains poorly constrained. Oxygen and hafnium isotopes, inclusion mineralogy (inclusions of quartz, K-feldspar, monazite, and microdiamonds), and geochemistry (light-rare-earth element enrichment), and low estimated crystallization temperatures of detrital zircons from the Acasta Gneiss Complex (Slave craton, northwestern Canada) and Narryer Gneiss Complex (Yilgarn craton, western Australia) suggest continental crust and water may have existed on Earth's surface by 4.4 – 4.2 Ga, and could in principle have hosted primitive life (e.g., Mojzsis et al., 2001; Wilde et al., 2001; Harrison et al., 2005; Iizuka et al., 2006; Valley et al., 2006; Menneken et al., 2007 and references therein). Low $\delta^{13}C_{org}$ values (to –28‰) from Earth's earliest sedimentary rock record (Isua supracrustal belt and Akilia island, west Greenland) may represent indirect geochemical evidence for the presence of primitive microbial life at ca. 3.8 Ga (Schidlowski, 1988, 2001; Mojzsis et al., 1996; Rosing, 1999; Rosing and Frei, 2004; McKeegan et al., 2007). Earth's oldest known microfossils and stromatolites may be from 3.5 – 3.2 Ga rock units from the Pilbara Craton (western Australia) and Barberton Mountain Land (South Africa), including those from the 3.465 Ga Apex Basalt (Warrawoona Group, western Australia) and 3.5 Ga pillow lavas (Barberton Greenstone Belt) (Walsh and Lowe, 1985; Schopf and Packer, 1987; Schopf, 1993; Hofmann et al., 1999; Kazmierczak and Kremer, 2002; Schopf et al., 2002; Van Kranendonk et al., 2003; Furnes et al., 2004; Schopf, 2004; Banerjee et al., 2007 and references therein). Both the carbon isotope evidence (Brasier et al., 2002; Fedo and Whitehouse, 2002; Van Zuilen et al., 2002) and the biogenicity of some of the earliest microfossils has been challenged (e.g., Brasier et al., 2002; Garcia-Ruiz et al., 2002; Pasteris et al., 2002). However, Schopf et al. (2007) provided additional supporting evidence (e.g., Raman spectroscopic images of cellular structure) for a microbial origin of filamentous fossils in the Apex Basalt and thus the existence of life on Earth as far back as ~ 3500 M.y.

Molecular phylogenetic studies suggest anoxygenic photosynthesis evolved prior to oxygenic photosynthesis (Canfield and Raiswell, 1999; Xiong et al., 2000; Raymond et al., 2002). Biomarker data and limited fossil evidence indicate cyanobacterial oxygenic photosynthesis was established after ca. 2.8 Ga (Buick, 1992; Altermann and Schopf, 1995; Brocks et al., 1999, 2003a, b, c; Summons et al., 1999; Kazmierczak and Altermann, 2002; Dutkiewicz et al., 2006). Molecular and fossil evidence for divergence of more advanced cyanobacterial lineages between 2.45 and 2.10 Ga (Tomitani et al., 2005), and C and Pb isotope (suggesting high U/Th ratios) evidence from > 3.7 Ga metamorphosed shales (Isua supracrustal belt) may suggest a very early evolution for oxygenic photosynthesis (Rosing and Frei, 2004), perhaps closely following the end of Hadean to early Archean asteroid bombardment (Sleep et al., 1989). Alternatively, the mineralogy and geochemistry of microbial mats from the Buck Reef Chert (Barberton Greenstone Belt, South Africa) is more consistent with anoxygenic photosynthesis (using H_2 as an electron donor) at ca. 3.416 Ga (Tice and Lowe, 2004, 2006). In addition, the significance of the biomarker 2-methylhopane as a proxy for oxygenic photosynthesis is questionable in light of a recent discovery that anoxygenic photoautotrophs can produce the same biomarker (Rashby et al., 2007). Oxygenic photosynthesis is the major producer of atmospheric free oxygen (Allen and Martin, 2007). Initial Earth surface oxidation either rapidly followed or lagged significantly behind the evolution of oxygenic photosynthesis. In the latter scenario, possible explanations for a sudden rise in atmospheric oxygen abundances include increased organic carbon burial, and/or a declining oxygen sink associated with loss of molecular hydrogen to space, an increasing oxidation state of volcanic, hydrothermal, and metamorphic fluxes to Earth's surface, and/or a switch from submarine-dominated to subaerial-dominated volcanism (Kasting, 1993, 2001; Godderis and Veizer, 2000; Catling et al., 2001; Holland, 2002; Catling and Claire, 2005; Claire et al., 2006; Hayes and Waldbauer, 2006; Kump and Barley, 2007).

Mass-independent fractionations (MIF) of sulfur isotopes in rocks older than ca. 2.45 Ga (e.g., Farquhar et al., 2000; Bekker et al., 2004; Papineau and Mojzsis, 2006; Papineau et al., 2007) suggest Archean atmospheric pO_2 was less than 10^{-5} present-day atmospheric levels [PAL] (Pavlov and Kasting, 2002; Goldblatt et al., 2006). A large number of geological and geochemical lines of evidence support a "Great Oxidation Event" (GOE) between 2.45 and 2.32 Ga (Bekker et al., 2004). This includes Fe(II) mobility in paleosols (Rye and Holland, 1998) and fluvial placer deposits of redox-sensitive detrital minerals (e.g., pyrite, uraninite; Fleet, 1998; Rasmussen and Buick, 1999; Young et al., 2001; England et al., 2002). A transition from reduced to oxidized shallow-water banded iron formation facies may have occurred at 2.32 Ga (Bekker et al., 2004). Higher dissolved sulfate concentrations (> 200μM) following the GOE may explain stronger sulfur isotope fractionations associated with bacterial sulfate reduction (Goodwin et al., 1976; Schidlowski et al., 1983; Canfield and Raiswell, 1999; Canfield et al., 2000; Habicht et al., 2002; Lyons et al., 2004). Red beds (Eriksson and Cheney, 1992; Young et al., 2001) and calcium sulfate evaporite minerals appear in the geological record (El Tabakh et al., 1999; Bekker et al., 2006) contemporaneously with the 2.20-2.06 Ga Lomagundi – Jatuli positive carbon isotope excursion, whose origin remains enigmatic (e.g., Melezhik et al., 2007). Based on the degree of MIF in post 2.32 Ga rocks, Paleoproterozoic atmospheric oxygen abundances may have been between 10^{-5} and > 10^{-2} PAL (Farquhar and Wing, 2003).

This hypothesis of early Paleoproterozoic Earth surface oxygenation ("Cloud – Walker – Holland – Kasting" hypothesis) is not universally accepted, and the alternative "Dimroth – Ohmoto" hypothesis suggests atmospheric pO_2 between 0.5 and 2 PAL since ~ 3.8 Ga (Ohmoto, 1996, 2004 and references therein; Beukes et al., 2002; Ohmoto et al., 2006). A growing body of evidence suggests the chronology of initial Earth surface oxidation may have been complicated (e.g., Kasting, 2006; Lowe and Tice, 2007). Attenuated MIF of sulfur isotopes in 2.96 to 2.76 Ga shales may reflect a weakly oxygenated atmosphere (e.g., between 10^{-5} and 10^{-2} PAL; Ohmoto et al., 2006; Ono et al., 2006). However, Farquhar et al. (2007) examined sulfur isotope data for Mesoarchean (3.2-2.8 Ga) sedimentary rocks and showed that MIF is present, consistent with an anoxic Mesoarchean atmosphere. Both mass-independent and mass-dependent fractionation of sulfur isotopes are recorded in Late Archean (2.7 – 2.5 Ga) rocks (Ono et al., 2003; Kamber and Whitehouse, 2007; Kaufman et al., 2007). Local oxygenation of isolated shallow ocean regions via photosynthesis may have preceded that of the atmosphere (Hayes, 1983), consistent with possible biomarker evidence for eukaryotic life in shallow oceans prior to the GOE (Brocks et al., 2003a; but see Kirschvink, 2006). Carbon isotope evidence suggests a possible retreat of methane-recycling anaerobe communities to deeper waters concomitant with increasingly oxygenated shallow water environments at

2.72 – 2.57 Ga (Eigenbrode and Freeman, 2006; Hayes and Waldbauer, 2006). Numerical modeling studies suggest a bi-stable atmosphere following the evolution of oxygenic photosynthesis (Goldblatt et al., 2006), and permit possible rapid transitions between an oxic and anoxic atmosphere (Kasting, 2006; Ohmoto et al., 2006).

The abundances of redox-sensitive metals (e.g., Re, Os, Mo, U) in organic-rich sedimentary rocks (ORS) may provide further constraints on initial Earth atmosphere and surface ocean oxygenation. Geochemical evidence for oxidative dissolution of redox-sensitive metals is absent from ca. 3.46 Ga hydrothermally altered basalts (U/Th ratios similar to unaltered magmatic rocks; Nakamura and Kato, 2007), the 3.25 – 3.15 Ga Fig Tree and Moodies Groups (Barberton Greenstone Belt, South Africa), and the 2.7 Ga Ventersdorp Supergroup (predominantly detrital origin for Mo and Re + platinum group elements [PGE] in ORS; Yang and Holland, 2002; Siebert et al., 2005; Wille et al., 2007). Hydrogenous enrichment of Mo and Re, fractionated PGE patterns relative to komatiites, and Mo isotope fractionation in Late Archean (ca. 2.7 – 2.5 Ga) ORS suggest weakly to mildly oxygenated surface ocean waters and a possible transient increase in atmospheric pO_2 prior to the GOE (Siebert et al., 2005; Wille et al., 2007). The clearest evidence for mild oxidation of surface oceans prior to the GOE is represented by a pronounced spike in Mo and Re abundances within the 2.5 Ga Mt. McRae Shale (Hamersley Group, Western Australia) (Anbar et al., 2007).

Rhenium-osmium black shale geochronology has some potential to constrain the timeline of initial Earth surface oxidation by providing precise depositional ages for ORS deposited from a water column with some dissolved oxygen. Further, the initial $^{187}Os/^{188}Os$ ratio from Re-Os isochron regressions of Archean and Proterozoic black shales may provide important insights into the evolution of the Os marine geochemical cycle. Chondritic I_{Os} values (~ 0.11-0.13) from the 2.00 Ga "Productive Formation" (Re-Os black shale age, Pechenga Greenstone Belt, Russia; Hannah et al., 2006) and the 2.32 Ga Rooihoogte and Timeball Hill Formations (Re-Os pyrite age, Transvaal Supergroup, South Africa; Hannah et al., 2004) may suggest a time lag between the GOE and appreciable riverine transport of radiogenic crustal Os to the oceans because of insufficiently oxidizing conditions and/or low Re abundances of uplifted Archean shales (Hannah et al., 2004, 2006). Here, I report new Re-Os data from the 2.5 Ga Mt. McRae

Shale and Late Archean (Monteville Formation, Campbellrand Subgroup) and Early Paleoproterozoic (Klipput Shale Member, lower Nelani Formation, Koegas Subgroup) shales from the Ghaap Group, Transvaal Supergroup. Compilations of seawater Os isotope compositions and the Re-Os isotope systematics of ORS over geological time are presented and interpreted with respect to Earth atmosphere and ocean oxidation.

6.2 SAMPLE DETAILS

6.2.1 Mt. McRae Shale

In the Hamersley Basin, the ca. 2.78 to < 2.45 Ga Mt. Bruce Supergroup is exposed over an area of at least 150,000 km^2 and comprises more than 10 km of volcaniclastic and siliciclastic sediments, banded iron formations, carbonates, and cherts of the Fortescue, Hamersley, and Turee Creek Groups (Figure 6.1; Morris and Horwitz, 1983; Arndt et al., 1991; Barley et al., 1997; Trendall et al., 2004). On the basis of sequence stratigraphy, Blake and Barley (1992) and Blake (1993, 2001) subdivide the Mt. Bruce Supergroup into two mega-sequences, each comprising three supersequences. The 2.77-2.6 Ga Chichester Range Megasequence (Fortescue Group and lower half of the Hamersley Group) is suggested to reflect deposition during rift-related flood basalt volcanism and continental breakup. The unconformably overlying 2.6-2.45 Ga Hamersley Range Megasequence (upper half of the Hamersley Group plus the Turee Creek Group) is interpreted as a continental back-arc basin associated with subduction-related orogenesis (Blake and Barley, 1992; Blake, 1993). At the base of the Hamersley Range Megasequence is the Brockman Supersequence, which includes iron formation (lower Mt. Sylvia Formation and upper Brockman Iron Formation) separated by organic-rich shale (Mt. McRae Shale), and is suggested to represent deposition on a quiet shallow-water, sediment-starved, continental back-arc platform/shelf with a well-established connection to the global ocean (Morris and Horwitz, 1983; Blake and Barley, 1992; Morris, 1993).

The Mt. McRae Shale averages 50 m in thickness and comprises pyritic black shale (TOC = 2-8 %) and subordinate carbonate and chert (Morris, 1993; Kakegawa et al., 1999; Trendall et al., 2004). U-Pb zircon ages bracket the depositional age of the Mt.

McRae shale to between 2561 ± 8 Ma (Bee Gorge Member, uppermost Wittenoom Formation which underlies the Mt. Sylvia Formation; Trendall et al., 1998) and 2481 ± 4 Ma (Dales Gorge Member, Brockman Iron Formation; Trendall et al., 2004) (Figure 6.2A). Impact ejecta layers preserved in the Bee Gorge and Dales Gorge Members attest to significant asteroid impacts around the Archean-Paleoproterozoic boundary (Glikson and Vickers, 2007 and references therein). Disseminated pyrite from the upper Mt. McRae Shale has $\delta^{34}S$ values of –6.3‰ to +7.1‰ that may reflect isotope fractionation associated with bacterial sulfate reduction (original seawater sulfate $\delta^{34}S$ is inferred to be ~ +10‰ to +15‰). If correct, sulfate concentrations in seawater during deposition of the Mt. McRae Shale may have been approximately one-third that of modern seawater (e.g., ~ 10 mM), consistent with some oxygenation of shallow oceans (Kakegawa et al., 1999). Subsequent studies have demonstrated the presence of MIF of sulfur isotopes in sulfides and bulk sedimentary rocks from the Mt. McRae Shale, suggesting low but possibly fluctuating atmospheric O_2 levels ($< 10^{-5}$ PAL). The MIF signal is variably preserved and mixed with isotopic effects from mass-dependant bacterial sulfate reduction and detrital inputs (Ono et al., 2003; Kaufman et al., 2007). Syngenetic molecular fossils from the Mt. McRae Shale include fossil sterane biomarkers, suggesting the presence of eukaryotic life which may require dissolved oxygen levels of > 0.01 PAL (Brocks et al., 2003a, b, c).

In drill hole ABDP-9 (Archean Biosphere Drilling Project, drillhole #9; Anbar et al., 2007) in the western Pilbara Craton, the Mt. McRae Shale is ~ 85 m thick and is essentially undeformed (Figure 6.2B). Metamorphism of mafic and intermediate volcanic rocks in the Fortescue Group at the drill hole site reached the prehnite-pumpellyite facies (prehnite – pumpellyite – epidote zone 2 of Smith et al., 1982) corresponding to metamorphic temperatures between 175°C and 280°C (Frey et al., 1991). Thus, the overlying Hamersley Group is likely of similar (zone 2) or lower (zone 1; prehnite – pumpellyite) metamorphic grade (Smith et al., 1982; Brocks et al., 2003b). Anbar et al. (2007) subdivide the Mt. McRae Shale in ABDP-9 into lower pyritic black shale (S2; 190-173 m; TOC = 2.5-6.3%), middle siderite banded iron formation (173-160 m), transitional facies (160-153 m), upper pyritic black shale (S1; 153-125 m; TOC = 3.9-16.1%), and uppermost shale/carbonate (125-105 m) intervals. They produced a detailed chemostratigraphic profile of redox-sensitive metal (Mo, Re, and U) and TOC and S content. Pyritic, organic-rich samples of the Mt. McRae shale (Plate 6.1) selected for Re-Os analysis are from depths 128.71-129.85 m and 145.22-148.32 m, and occur near the top and base of interval S1. The stratigraphically lower interval occurs within a zone of peak redox-sensitive metal (up to 40 ppm Mo and 37 ppb Re) and TOC (8.7% to 15.2%) enrichment (153-143 m depth), mildly negative sulfide $\delta^{34}S$, and attenuated MIF of S isotopes (lower $\Delta^{33}S$) which is suggested to mark the onset of possible mild shallow-water oxygenation that preceded the GOE (Anbar et al., 2007; Kaufman et al., 2007). The upper stratigraphic level contains lower metal abundances (up to 13 ppm Mo and 29 ppb Re) and TOC contents (5.5% to 6.5%), and represents part of a declining trend to lower redox-sensitive metal abundances (typically < 10 ppm Mo and < 10 ppb Re) above the S1 interval. Rhenium abundances are elevated above average continental crust throughout ABDP-9, suggesting at least some minor dissolved oxygen in the shallow water column during deposition of the Mt. McRae Shale.

6.2.2 Monteville Formation and Klipput Shale Member (Lower Nelani Formation)

The Kaapvaal Craton of South Africa also contains a well-preserved late Archean to early Paleoproterozoic supracrustal succession. Deposition of siliciclastic sedimentary rocks of the 2.72 – 2.67 Ga Ventersdorp Supergroup followed a high-temperature 2.720 – 2.715 Ga melting event (T > 1000°C) in the lower crust (Schmitz and Bowring, 2003) associated with flood basalt volcanism and crustal extension (Armstrong et al., 1991; Barton et al., 1995; Catuneanu and Eriksson, 1999; Tinker et al., 2002; Poujol et al., 2003; Sumner and Beukes, 2006). Unconformably overlying Transvaal Supergroup sedimentary rocks are preserved in the western Griqualand West and eastern Transvaal sub-basins (Figure 6.3). Sequence stratigraphic studies suggest cyclic deposition of ramp-platform marine siliciclastic and carbonate rocks following thermal subsidence associated with Ventersdorp rifting (Altermann and Nelson, 1998; Catuneanu and Eriksson, 1999; Schmitz and Bowring, 2003; Sumner and Beukes, 2006). In the Griqualand West sub-basin, the lower to middle Transvaal Supergroup is represented by the 2.67 – 2.42 Ga Ghaap Group (Figure 6.4), whose basal section comprises ramp deposits (< 250 m thick Schmidtsdrif Subgroup) that record initial flooding of the Kaapvaal Craton (Beukes, 1977; Schröder et al., 2006; Sumner and Beukes, 2006). These are conformably overlain by carbonates of the Campbellrand Subgroup that, together with the correlative Malmani Subgroup from the Transvaal sub-basin, formed one of Earth's earliest extensive (> 600,000 km^2) carbonate platforms (Beukes, 1987; Sumner, 1997; Eriksson et al., 2001; Sumner and Grotzinger, 2004; Sumner and Beukes, 2006). Campbellrand Subgroup strata can be subdivided into a southwestern basinal Prieska facies (up to 650 m of organic-rich mudstone, carbonate, chert, and ironstone) and a northeastern proximal Ghaap Plateau facies (up to 1700 m of predominantly stromatolitic dolomite) (Beukes, 1987). Subsequently, a cycle of marine transgression and regression resulted in deposition of conformably overlying deep- and shallow-water micro-banded and granular iron formation of the Kuruman and Griquatown Formations, respectively (≤ 1000 m thick Asbestos Hills Subgroup; Beukes, 1984, 1987; Klein and Beukes, 1989; Beukes and Klein, 1990). In the Prieska facies, the overlying Koegas Subgroup (up to 600 m thick) comprises predominantly coarse- and fine-grained siliciclastics with subordinate banded iron formation (Beukes, 1983). The Ghaap Group is conformably or unconformably overlain by glacial diamictites of the Makganyene Formation (lowermost Postmasburg Group; Polteau et al., 2006).

Most of the lower Transvaal Supergroup is largely undeformed and unmetamorphosed (sub-greenschist facies) except near the ~ 2.06 Ga Bushveld Complex (Walraven et al., 1990) and the western margin of the Kaapvaal Craton (Beukes, 1987; Sumner and Grotzinger, 2004 and references therein). A number of geological and geochemical lines of evidence for increasing atmospheric pO_2 between 2.45 and 2.32 Ga (Bekker et al., 2004; Hannah et al., 2004) have been documented for the Transvaal Supergroup. These include 1) detrital pyrite and uraninite grains in the ≥ 2.6 Ga Black Reef Quartzite (basal unit of the Chuniespoort Group in the Transvaal sub-basin; Martin et al., 1998; England et al., 2002), 2) a strong MIF signal from sedimentary pyrite (Farquhar et al., 2000; Kamber and Whitehouse, 2007) in the 2.52 Ga Gamohan Formation (upper Campbellrand Subgroup; Sumner and Bowring, 1996; Altermann and Nelson, 1998), and disappearance of this signal in the 2.32 Ga Rooihoogte and Timeball Hill Formations (Transvaal sub-basin) (see Figure 6.4; Bekker et al., 2004; Hannah et al., 2004), 3) magnetite-rich (reduced) Kuruman-Griquatown shallow-water iron formation at

2.46 Ga (Beukes and Klein, 1990; Pickard, 2003) and hematite-rich (oxidized) shallow-water iron ores in the Timeball Hill Formation at ~ 2.32 Ga (Bekker et al., 2004), and 4) a restricted range in pyrite $\delta^{34}S$ values for Ghaap Group correlatives in the Transvaal sub-basin (Chuniespoort Group), but strongly ^{34}S depleted pyrite in the Timeball Hill and Rooihoogte Formations (Cameron, 1982; Bekker et al., 2004). However, elevated Mo (up to 7 ppm), Re (typically up to 13 ppb), and Os abundances (typically up to 0.73 ppb), together with variably fractionated Mo isotope compositions (relative to average crustal material) of ORS suggests the presence of some dissolved oxygen in shallow-water environments during deposition of the Ghaap Group (Wille et al., 2007). In addition, the sulfide S isotope record from the Gamohan and Kuruman Formations is remarkably similar to that observed in the Mt. McRae Shale, including the interval of mildly negative $\delta^{34}S$ and smaller $\Delta^{33}S$ associated with mild surface ocean oxygenation (Kaufman et al., 2007).

Black shales from the Monteville Formation and the Klipput Shale Member (lower Nelani Formation) have been selected for a preliminary Re-Os isotope study. The Monteville Formation forms the lowermost unit of the ca. 2588 – 2520 Ma Campbellrand Subgroup in the Prieska facies (Altermann and Nelson, 1998; Sumner and Bowring, 1996) and conformably overlies and underlies fine-grained mudrocks of the Lokammona Formation (upper Schmidtsdrif Subgroup) and thick microbialites of the lower Nauga Formation, respectively (Schröder et al., 2006). In drill hole GKP01 (Figure 6.5A), the Monteville Formation comprises ~ 100 m of predominantly grainy to muddy dolostones with subordinate interbedded mudstone and thin microbialites arranged as meter-scale parasequences. Occurrences of turbiditic dolarenites and the lack of wave- and storm-generated sedimentary structures suggest the Monteville Formation was deposited below storm wave base on the continental slope. Near the base of the Monteville Formation in the more proximal drill hole GKF01 (located 24 km to the northeast of GKP01) is a tektite impact ejecta layer (Schröder et al., 2006) that may be correlative with the 2630 ± 6 Ma Carawine mega-breccia spherule layer (Rasmussen et al., 2005) and the 2629 ± 5 Ma Jeerinah Formation impact ejecta horizon (Trendall et al., 2004) in the Hamersley Basin (Simonson et al., 2006; Glikson and Vickers, 2007). A number of U-Pb SHRIMP zircon dates between 2717 ± 26 Ma and 2455 ± 32 Ma have been reported for tuffaceous sediments in the Monteville Formation. Their accuracy is questionable because some analyses were likely derived from reworked (e.g., detrital) zircons and/or zircons with significant post-depositional lead loss (Sumner and Beukes, 2006), but an age of 2555 ± 19 Ma from two zircon grains within a tuffaceous horizon in the upper Monteville Formation has been interpreted as a depositional age constraint (Altermann and Nelson, 1998). Other age constraints include a maximum age of 2642.2 ± 2.3 Ma (unpublished U-Pb TIMS zircon age for the Vryburg Formation, lower Schmidtsdrif Subgroup; quoted by Walvaren and Martini, 1995) a U-Pb SHRIMP zircon age of 2588 ± 6 Ma from tuff in the overlying and partially correlative Nauga Formation (Altermann and Nelson, 1998), and a probable minimum age of 2549 ± 7 Ma (U-Pb SHRIMP zircon age from a tuffaceous horizon near the top of the Nauga Formation (Altermann and Nelson, 1998).

The Koegas Subgroup comprises, in stratigraphic order, the Pannetjie (sandstone and shale), Doradale (banded iron formation), Kwakwas (riebeckitic slate), Naragas (siliciclastics and banded iron formation), Rooinekke (banded iron formation, mudstone and carbonate), and Nelani (banded iron formation, siliciclastics, and carbonate) Formations (Beukes, 1983; Polteau et al., 2006). The Klipput Shale Member occurs at the base of the Nelani Formation, and is ~ 35 m thick in drill hole GEC01 (Figure 6.5B; the stratigraphy of GEC01 is not yet available in the literature). An unpublished Pb-Pb age of 2415 ± 6 Ma has been reported for the Rooinekke Formation (quoted by Kirschvink et al., 2000; and cited by Polteau et al., 2006) that is in general agreement with a diagenetic Pb-Pb carbonate age of 2394 ± 26 Ma for the younger Mooidraai Dolomite Formation (upper Postmasburg Group), a Re-Os pyrite depositional age of 2316 ± 7 Ma for black shales of the Rooihoogte and Timeball Hill Formations (Transvaal sub-basin; Hannah et al., 2004), a U-Pb SHRIMP zircon age of 2460 ± 5 Ma for the Kuruman Formation (Pickard, 2003), and various unpublished U-Pb ages between 2489 ± 33 Ma and 2432 ± 31 Ma for the Kuruman and Griquatown Formations (summarized by Nelson et al., 1999).

Finely laminated, organic-rich (TOC ~ 2%; Wille et al., 2007), and pyritic black shale of the Monteville Formation (Plate 6.2) was sampled from depths 1019.76-1020.20 m in GKP01. The black shale interval is associated with a well-defined spike in the gamma ray profile for GKP01 (Schröder et al., 2006). Lighter-colored, finely laminated shale with rare disseminated pyrite from the Klipput Shale Member (Plate 6.3) was sampled at depths 174.53-174.83 m and 176.06-176.35 m in drill hole GEC01.

6.2.3 Analytical Methods

Powder aliquots of ORS from the Mt. McRae Shale, Monteville Formation, and Klipput Shale Member comprise between 14 and 52 g. Protocols for metal-free processing of ORS to produce powdered samples, subsequent chemical digestion, separation, and purification of Re and Os, and isotopic analysis by isotope dilution – negative thermal ionization mass spectrometry (ID-NTIMS) are described in Appendix A. Average total procedural blanks of Re and Os based on Cr^{VI}-H_2SO_4 solutions prepared from Fluka Chemika CrO_3 (Lot #1177884) were 10.4 ± 1.7 pg and 0.24 ± 0.22 pg, respectively, with blank $^{187}Os/^{188}Os$ of 0.21 ± 0.06 (1σ, n = 9).

6.3 RESULTS

6.3.1 Mt. McRae Shale

Rhenium (11-39 ppb) and Os (467-1148 ppt) are markedly enriched in the Mt. McRae Shale compared to average present-day upper continental crust (Esser and Turekian, 1993; Peucker-Ehrenbrink and Jahn, 2001; Hattori et al., 2003; Sun et al., 2003a, b), especially the shales from the 145.22-148.32 m interval (22-39 ppb Re and 681-1148 ppt Os) (Table 6.1). The $^{187}Re/^{188}Os$ and $^{187}Os/^{188}Os$ isotope ratios range between 173 and 1743, and between 7.4 and 74.0, respectively. Separate regressions of the 128.71-129.85 m and 145.22-148.32 m subsets yield Re-Os dates of 2495 ± 18 Ma (2σ, n = 5, MSWD = 0.95, Model 1, probability of fit = 0.42, I_{Os} = 0.06 ± 0.09; Figure 6.6A) and 2464 ± 41 Ma (n = 4, MSWD = 0.48, Model 1, probability of fit = 0.62, I_{Os} = 0.86 ± 0.86; Figure 6.6B), respectively. Regression of all Re-Os isotope data for the Mt. McRae Shale yields a Re-Os date of 2501.1 ± 8.2 Ma (n = 9, MSWD = 1.1, Model 1, probability of fit = 0.33, I_{Os} = 0.04 ± 0.06; Figure 6.6C), or a Re-Os age of 2501 ± 12 Ma if an uncertainty of ± 0.31% (2σ) for $\lambda^{187}Re$ (Smoliar et al., 1996; Selby et al., 2007) is propagated together with the uncertainty in the slope of the regression.

6.3.2 Monteville Formation and Klipput Shale Member (Lower Nelani Formation)

In contrast to the Mt. McRae Shale, the black shale intervals from the Monteville Formation and Klipput Shale Member have significantly lower Re (0.4-1.5 ppb) and Os (34-415 ppt) abundances, and $^{187}Re/^{188}Os$ (15-84) and $^{187}Os/^{188}Os$ (0.75-3.66) isotope ratios. Both intervals have Re abundances broadly similar to present-day eroding upper continental crust, but Os abundances show marked (approximately an order of magnitude) and minor (up to a factor of ~ 3-4) or negligible enrichment in the Monteville Formation and Klipput Shale Member, respectively. Regression of the Re-Os isotope data for the Monteville Formation yields a Re-Os date of 2901 ± 210 Ma (n = 6, MSWD = 9.2, Model 3, $I_{Os} = 0.07 \pm 0.09$; Figure 6.7A). All samples of the Klipput Shale Member define a Model 3 regression with a Re-Os date of 2465 ± 53 Ma (n = 9, MSWD = 8.8, $I_{Os} = 0.14 \pm 0.03$; Figure 6.7B). Separate regressions of the 174.50-174.98 m and 176.06-176.35 m subsets for the Klipput Shale Member yield Re-Os dates of 2483 ± 980 Ma (n = 4, MSWD = 11.7, Model 3, $I_{Os} = 0.14 \pm 0.46$; Figure 6.7C) and 2479 ± 20 Ma (n = 5, MSWD = 0.01, Model 1, probability of fit = 0.998, $I_{Os} = 0.12 \pm 0.01$; Figure 6.7D).

6.4 DISCUSSION

6.4.1 Utility of the Re-Os Deposition-Age Geochronometer for Late Archean to Early Paleoproterozoic Black Shales

Prior to this study, the oldest whole-rock black shale Re-Os age determination was a 2006 ± 26 Ma date (MSWD = 4.3) from the "Productive" Formation (Pechenga Greenstone Belt, Kola Peninsula, Russia). This Re-Os date agrees well with both a Re-Os date of 2004 ± 20 Ma (MSWD = 17) for syn-sedimentary sulfides within the "Productive Formation" and a previous radiometric age determination of 1988 ± 39 Ma from approximately coeval ultramafic flows and intrusions. The whole-rock and sulfide fractions together yield a precise Re-Os age of 2004 ± 9 Ma (MSWD = 7.0, $I_{Os} = 0.13 \pm 0.02$) that suggests the Re-Os isotope system in the "Productive" Formation was not significantly disturbed since the time of deposition (Hannah et al., 2006). The precise Re-Os date of 2501.1 ± 8.2 Ma (MSWD = 1.1) for the Mt. McRae Shale is consistent with previous U-Pb zircon age constraints bracketing the depositional age of this rock unit to between 2561 ± 8 Ma (Bee Gorge Member, uppermost Wittenoom Formation; Trendall et al., 1998) and 2481 ± 4 Ma (Dales Gorge Member, Brockman Iron Formation; Trendall et al., 2004). Thus, the utility of the Re-Os deposition-age geochronometer for ORS can be confidently extended back in time to the Archean-Paleoproterozoic boundary.

Interpretation of the Re-Os ages from the Monteville Formation and Klipput Shale Member requires caution because low Re and Os abundances in these shales suggests the presence of a significant detrital component. The Re-Os age of 2901 ± 210 Ma for the Monteville Formation is older than U-Pb zircon age constraints bracketing this rock unit between 2642.2 ± 2.3 Ma (Vryburg Formation, lower Schmidtsdrif Subgroup; Walvaren and Martini, 1995) and 2549 ± 7 Ma (Nauga Formation, Campbellrand Subgroup; Altermann and Nelson, 1998). Although the poor precision (± 7.2%) and elevated MSWD value of 9.2 suggests possible post-depositional mobility of Re and/or Os in the Monteville Formation, there is no obvious evidence of secondary alteration (e.g., such as veinlets) visible in the GKP01 core samples, and metamorphism is reported to be sub-greenschist facies (Sumner and Grotzinger, 2004 and references therein). Excluding sample GKP01-1020-1 from the Monteville Formation regression yields a younger Re-Os age of 2789 ± 210 Ma (Model 3, MSWD = 5.2, I_{Os} = 0.11 ± 0.09) that marginally overlaps the age constraints for the Monteville Formation given above. In this case, the Re-Os isotope systematics of the excluded sample may have been affected by post-depositional mobility or this sample has a different I_{Os}. Interpretation of the Monteville Formation Re-Os isotope systematics is hampered by the narrow range in ^{187}Re/^{188}Os (19-30) and ^{187}Os/^{188}Os (1.03-1.58) isotope ratios.

Fine-grained siliciclastics from the Monteville Formation have elemental abundances broadly similar to average Archean crust ("Schmidtsdrif" pattern of Schröder et al., 2006). One analysis at 1019.9 m depth (which lies within the stratigraphic interval sampled in this study) is characterized by a high Al abundance of ~ 25 wt. %, thus indicating the likely presence of a significant detrital component despite somewhat elevated TOC contents (~ 2%; Wille et al., 2007). Total Os (255-415 ppt) and ^{192}Os (89-154 ppt) abundances are mildly enriched above present-day average crustal values and probably reflects some hydrogenous enrichment of Os, but a large fraction of the Re (1.1-

1.5 ppb) may be of detrital origin. Calculated sample I_{Os} values (using reasonable minimum and maximum age constraints of 2549 and 2642 Ma, respectively) range between 0.16 and 0.27. These values could be taken as evidence for oxidative weathering and limited release of radiogenic crustal Os into a Late Archean ocean dominated by magmatic/hydrothermal Os inputs (and dissolution of cosmic dust). Alternatively, low Re abundances imply an absence of significant oxidative weathering (in the absence of reservoir effects), and the significant detrital component inferred for the sample at 1019.9 m depth (Schröder et al., 2006) suggests the elevated I_{Os} can just as easily be explained by a component of radiogenic detrital Os.

Recently, Wille et al. (2007) report Re and Os abundance and isotope data for Ghaap Group black shales throughout the GKP01 core. Their Re and Os isotope data (obtained by less precise quadrupole ICP-MS) generally plot near a 2550 Ma reference line (these workers used a I_{Os} value of 0.1296 representing the present-day primitive upper mantle composition [Meisel et al., 2001] although at 2550 Ma, the appropriate value would be ~ 0.111 assuming a chondritic present-day ^{187}Re/^{188}Os ratio [Walker et al., 2002]) except for one sample with the highest ^{187}Re/^{188}Os and ^{187}Os/^{188}Os isotope ratios. Given that these data is derived from black shales spanning over 1000 m of stratigraphy, the well-correlated Re-Os isotope systematics suggests minor to negligible post-depositional disturbance of Re and Os. Some intervals in the Nauga Formation (Campbellrand Subgroup) are clearly enriched in Re (to > 10 ppb) and Os (to > 500 ppt), and black shale from one horizon (depth 385 m) has a highly elevated Re and Os abundance of 270 ppb and 57 ppb, respectively. Thus, these Re- and Os-rich intervals represent more promising targets for Re-Os geochronological studies with potential for higher precision calibration of the sequence stratigraphy of the Ghaap Group (Sumner and Beukes, 2006), improved estimates of sedimentation rates (Altermann and Nelson, 1998), and precise determinations of the Os isotope composition of contemporaneous Late Archean seawater. Identification of a suitable black shale interval in the lower part of the Monteville Formation may also provide a more rigorous test of correlations between the impact ejecta horizon in drill hole GKF01 and the ca. 2.63 Ga Carawine and Jeerinah Formation ejecta horizons (Trendall et al., 2004; Rasmussen et al., 2005; Simonson et al., 2006).

The Klipput Shale Member has lower Re (< 1 ppb) and Os abundances (< 200 ppt) relative to the Monteville Formation interval, but is characterized by a significantly greater spread in $^{187}Re/^{188}Os$ and $^{187}Os/^{188}Os$ isotope ratios, particularly for the 176.06-176.35 m depth interval. The latter subset yields a precise Re-Os date of 2479 ± 20 Ma that is broadly consistent with previous age constraints of between 2489 ± 33 Ma and 2432 ± 31 Ma (including a U-Pb zircon age of 2460 ± 5 Ma) for the Kuruman and Griquatown Formations of the older Asbestos Hills Subgroup (Nelson et al., 1999; Pickard, 2003), but is at odds with a Pb-Pb age of 2415 ± 6 Ma for the immediately underlying Rooinekke Formation (Kirschvink et al., 2000). Given the precision (0.8%) and very low MSWD (0.01) of the 2479 ± 20 Ma regression, post-depositional mobility of Re and Os is not a likely explanation for this discrepancy.

If hydrogenous enrichment of Re and Os is minimal, then a detrital fraction of Re and Os is expected to influence the Re-Os isotope systematics of ORS. The Cr^{VI}-H_2SO_4 dissolution medium minimizes dissolution of detrital Re and Os during high-temperature (240°C) digestion (Selby and Creaser, 2003; Kendall et al., 2004; see Chapter 3), but does not quantitatively exclude it (Ravizza et al., 1991). One possible interpretation is that the detrital component in the shales between 176.06 m and 176.35 m had a homogeneous Os isotope composition (I_{Os} = 0.12 ± 0.01) dominated by ultramafic and extraterrestrial particulates, and that any hydrogenous Re and Os component likewise also had a similar Os isotope composition derived from hydrothermal sources and the dissolution of chondritic cosmic dust (Meisel et al., 2001; Walker et al., 2002a, b). In this interpretation, the scatter in the 2465 ± 53 Ma age (derived from all analyses) results from the presence of a more radiogenic detrital component in the samples from the 174.50-174.98 m interval (see Table 6.2). If the Re-Os age of 2479 ± 20 Ma does represent the depositional age of the Klipput Shale Member, then the Pb-Pb age of 2415 ± 6 Ma is incorrect. However, this discrepancy between the Re-Os and Pb-Pb ages cannot be directly evaluated because the analytical and sampling details concerning the Pb-Pb age quoted by Kirschvink et al. (2000) is apparently not published.

On the other hand, if the Pb-Pb age accurately represents the depositional age for the Rooinekke Formation (and of the overlying Klipput Shale Member), the Re-Os age of 2479 ± 20 Ma is erroneously old. This is the preferred interpretation, and is explained by a positive correlation between ^{187}Re/^{188}Os and ^{187}Os/^{188}Os at the time of deposition (e.g., Ravizza et al., 1991). Both present-day ^{187}Re/^{188}Os and ^{192}Os abundance are well-correlated with $I_{Os\ (2415\ Ma)}$ (Figure 6.8) whereas no correlation is present between Re abundance and $I_{Os\ (2415\ Ma)}$. These observations suggest mixing of a hydrogenous end-member with lower Re/Os, lower I_{Os}, and higher Os content with a detrital end-member with higher Re/Os, higher I_{Os}, and lower Os content. The calculated $I_{Os\ (2415\ Ma)}$ of the samples from the 174.50-174.98 m interval defines a much narrower range (0.16 and 0.19), and may reflect a more constant detrital Os flux compared to the 176.06-176.35 m interval. Thus, attempts at Re-Os geochronology of late Archean to early Paleoproterozoic black shales with limited hydrogenous enrichment of Re and Os should be approached with caution. In a predominantly anoxic water column (such as that suggested for much of the Archean; Pavlov and Kasting, 2002; Farquhar and Wing, 2003; Goldblatt et al., 2006), the fundamental basis behind the Re-Os black shale geochronometer (reductive capture of dissolved Re and Os from an oxygenated water column into reducing ORS) breaks down and depositional age determinations for Archean shales are not likely to be feasible.

Siebert et al. (2005) report significant scatter in ^{187}Re/^{188}Os and ^{187}Os/^{188}Os isotope ratios for several middle Archean to early Paleoproterozoic black shales, and could not derive any useful geochronological information for any individual sample suite. Considering the well-known evidence for post-depositional mobility of Re in surface environments, they suggest the scatter resulted from sub-recent gain or loss of Re, and proceeded to estimate the original Re abundances from measured ^{187}Os/^{188}Os isotope ratios, an assumed depositional age, and an I_{Os} value equivalent to the estimated minimum composition for the primitive upper mantle at the time of deposition (present-day value is 0.1296; Meisel et al., 2001). Some samples, notably those from the 2.7 Ga Manjeri Formation, yield negative I_{Os} (using the published Re-Os data), and may have been affected by post-depositional addition of Re (or loss of Os). Other samples have positive I_{Os} well above the mantle/extraterrestrial baseline. In this case, Re- and Os-rich (e.g., Manjeri Formation) samples could conceivably have suffered some Re loss (or Os gain), but as discussed above, samples with low abundances of Re and Os (e.g., Fig Tree Group) may have a significant radiogenic detrital component and may not have been affected by post-depositional processes. Metamorphism of the Manjeri Formation is typically at the sub-greenschist facies (T = 200-300°C), and petrological and mineralogical characteristics suggest hydrothermal fluid flow was not extensive (e.g., Bolhar et al., 2002). Thus, the report of post-depositional mobility of Re and Os in the Manjeri Formation is somewhat surprising, and warrants further investigation because this rock unit represents a potential candidate for obtaining Late Archean depositional age and seawater Os isotope information.

6.4.2 The Redox State of Late Archean to Paleoproterozoic Seawater: Implications of the I_{Os} from Re-Os Black Shale Isochron Regressions

The present-day $^{187}Os/^{188}Os$ isotope composition of seawater (~ 1.06; Sharma et al., 1997; Levasseur et al., 1998; Woodhouse et al., 1999; Peucker-Ehrenbrink and Ravizza, 2000) is controlled by a mass balance dominated by a radiogenic riverine input flux (average $^{187}Os/^{188}Os$ of ~ 1.5; Levasseur et al., 1999) relative to unradiogenic hydrothermal/magmatic and cosmic dust inputs ($^{187}Os/^{188}Os$ ~ 0.11-0.13; Peucker-Ehrenbrink, 1996; Ravizza et al., 1996; Shirey and Walker, 1998; Sharma et al., 2000; Meisel et al., 2001; Walker et al., 2002a, b; Cave et al., 2003). Oxidative weathering of the eroding upper continental crust (average $^{187}Os/^{188}Os$ ~ 1.0-1.4; Esser and Turekian, 1993; Peucker-Ehrenbrink and Jahn, 2001; Hattori et al., 2003) is required to generate a large dissolved radiogenic Os riverine flux to the oceans. Weathering of ORS is known to be a major source of radiogenic Os to present-day and Phanerozoic oceans (Peucker-Ehrenbrink and Hannigan, 2000; Peucker-Ehrenbrink and Ravizza, 2000; Dalai et al., 2002; Jaffe et al., 2002; Pierson-Wickmann et al., 2002; Huh et al., 2004). Other crustal sources include radiogenic Os from Precambrian shields and Phanerozoic platforms (Peucker-Ehrenbrink and Ravizza, 1996; Peucker-Ehrenbrink and Blum, 1998; Huh et al., 2004) and relatively unradiogenic Os inputs from volcanism (Alves et al., 2002) and weathering of subduction arc-related crust (Martin et al., 2000).

The value of I_{Os} from a Re-Os ORS isochron regression may record the $^{187}Os/^{188}Os$ isotope composition of the contemporaneous seawater at the time of sediment deposition assuming the hydrogenous Os fraction has swamped the terrestrial and meteoritic particulate Os fraction (Ravizza and Turekian 1989, 1992; Ravizza et al., 1991). This hypothesis is supported by the similar Os isotope composition of recent organic-rich sediments ($^{187}Os/^{188}Os$ = 0.98-1.07 based on data from three localities in the Pacific and Atlantic Oceans) compared to present-day seawater (Ravizza and Turekian 1992). Based on the relatively long present-day seawater residence time of Os (~ 10^4 years; Oxburgh 1998, 2001; Levasseur et al., 1999) compared to the ocean mixing time of 2-3 k.y., large global variations in the $^{187}Os/^{188}Os$ isotope composition of seawater are suggested to have occurred during the Cenozoic and Mesozoic (Figure 6.9). These variations result from major changes in the proportion of radiogenic crustal Os and unradiogenic mantle/extraterrestrial Os in the oceans (e.g., Peucker-Ehrenbrink et al., 1995; Pegram and Turekian 1999; Ravizza et al., 2001; Cohen and Coe, 2002, 2007; Ravizza and Peucker-Ehrenbrink, 2003a; Cohen, 2004; Cohen et al., 2004).

In an anoxic Archean weathering regime, riverine transport of soluble Re and radiogenic Os from weathering and erosion of crustal rocks would be negligible, resulting in deposition of Archean shales with low Re abundances (Yang and Holland, 2002; Siebert et al., 2005; Wille et al., 2007), and $^{187}Re/^{188}Os$ and $^{187}Os/^{188}Os$ isotope ratios (Wille et al., 2007; this thesis). There may have been a time lag between the GOE (between 2.45 and 2.32 Ga; Bekker et al., 2004) and appreciable riverine transport of radiogenic crustal Os to the oceans because of the low Re abundances in uplifted Archean shales and/or insufficiently oxidizing conditions (Hannah et al., 2004). Either tenet is supported by chondritic I_{Os} values from black shales post-dating the GOE, including a value of 0.1121 ± 0.0012 from the 2316 ± 7 Ma Rooihoogte and Timeball Hill Formations (Transvaal Supergroup; Hannah et al., 2004) and 0.133 ± 0.020 from the 2004 ± 9 Ma "Productive Formation" (Pechenga Greenstone Belt, Russia; Hannah et al., 2006). The pre-GOE 2.5 Ga Mt. McRae Shale has a I_{Os} value of 0.06 ± 0.09 (from the 128.71-129.85 m depth interval in ABDP-9). These observations hint towards predominance of mantle and cosmic input fluxes over radiogenic crustal material as sources of Os to the late Archean and early and middle Paleoproterozoic oceans. Chondritic or near-chondritic I_{Os} compositions are intuitively expected for marine shales deposited under an anoxic weathering regime or under the conditions of a weakly oxygenated atmosphere (e.g., < 10^{-5} to 10^{-2} PAL) with stratified oceans containing anoxic or euxinic deep waters (Canfield, 1998; Farquhar et al., 2000; Pavlov and Kasting, 2002; Farquhar and Wing, 2003; Goldblatt et al., 2006).

A relatively small increase in pO_2 in the shallow oceans and atmosphere may have occurred prior to the GOE at ~ 2.5 Ga (Anbar et al., 2007; Kaufman et al., 2007). Molybdenum and Re abundance data from a high-resolution chemostratigraphic profile through the Mt. McRae Shale in drill hole ABDP-9 show a major peak within the S1 interval (~ 143-153 m depth) (Anbar et al., 2007) that correlates with an excursion to negative $\delta^{34}S$ values in pyrite and weaker MIF of sulfur isotopes (Kaufman et al., 2007), thus implying a rise in pO_2 (but still $\leq 10^{-5}$ PAL). Authigenic enrichment of Mo and Re during this interval is inferred from a strong correlation with TOC, and highly elevated enrichment factors (up to 55 and 75, respectively). Positive correlations between Re and ^{192}Os with TOC are known for Re- and Os-rich black shales younger than ~ 1.6 Ga (Cohen et al., 1999; Singh et al., 1999; Peucker-Ehrenbrink and Hannigan, 2000; Creaser et al., 2002; Jaffe et al., 2002; Yang and Holland, 2002). The enrichment cannot be ascribed to post-depositional processes because the Re-Os isotope data from two separate intervals in ABDP-9 (128.71-129.85 m and 145.22-148.32 m) yield identical Re-Os ages within 2σ uncertainties, and together yield a precise Model 1 age of 2501.1 ± 8.2 Ma that is in excellent agreement with previous U-Pb age constraints for the Mt. McRae Shale. A hydrothermal origin for the peak Mo and Re enrichment is not consistent with relative depletions in Fe and Mn abundance within the S1 interval compared to pyritic black shales from the stratigraphically lower interval S2 in ABDP-9 (Anbar et al., 2007). Any large influx of unradiogenic Os from an asteroid impact > 50 M.y. earlier (recorded in the Bee Gorge Member spherule marker bed; Trendall et al., 1998, 2004) would likely have been removed from the oceans in less than a few to several hundred thousand years after the impact event because of the low seawater residence time of Os (as suggested by the rapid recovery of seawater Os isotope compositions to moderately radiogenic values following the K-T boundary impact; Burton, 2005; Klemm et al., 2005 and references therein). On the other hand, an origin for the Mo and Re enrichment by oxidative weathering of crustal material would be consistent with inferences of mild shallow water oxygenation (perhaps > 0.01 PAL allowing aerobic respiration) based on the presence of eukaryotic sterane biomarkers (Brocks et al., 2003a, b, c) and negative $\delta^{34}S$ of pyrites that reflects appreciable mass-dependant sulfur isotope fractionation during bacterial sulfate reduction (Kakegawa et al., 1999; Ono et al., 2003; Kaufman et al., 2007).

This raises the question of whether the seawater Os isotope composition increased above the mantle/extraterrestrial baseline in association with mild shallow water oxygenation during deposition of the S1 interval. The Re-Os age of 2501.1 ± 8.2 Ma derived from the entire Re-Os isotope dataset for the Mt. McRae Shale yields a sub-chondritic I_{Os} value of 0.04 ± 0.06. Recently, the sedimentation rate for the Mt. McRae Shale was estimated at 4.5 m/Ma (Trendall et al., 2004), and thus the 128.71-129.85 m and 145.22-148.32 m intervals may be separated by ~ 3.5 M.y. The residence time of Os in 2.5 Ga Archean seawater was probably less than ~ 10^4 years, and the seawater Os isotope composition could have changed between the two intervals. The 128.71-129.85 m interval, deposited during a declining trend of metal enrichment following the S1 peak, has an I_{Os} of 0.06 ± 0.09 (see Figure 6.6). Using the present-day average riverine ^{187}Os/^{188}Os of 1.54 as a maximum for 2.5 Ga rivers (Levasseur et al., 1999) and chondritic ^{187}Os/^{188}Os of ~ 0.11 at 2.5 Ga (Walker et al., 2002a), the uncertainty in this I_{Os} determination permits a seawater Os budget containing up to 3% of radiogenic crustal Os. The 145.22-148.32 m interval, deposited during the pO_2 rise, has an I_{Os} of 0.86 ± 0.86. Despite the marginal overlap of the I_{Os} determinations from the two subsets, it is possible that seawater Os isotope compositions could have evolved to more radiogenic values during the 145.22-148.32 m interval. Because of the highly elevated present-day ^{187}Re/^{188}Os and ^{187}Os/^{188}Os isotope ratios (and associated uncertainties) of the samples from the 145.22-148.32 m interval, individual sample I_{Os} determinations are associated with significant uncertainties that precludes a meaningful comparison with individual sample I_{Os} values of the 128.71-129.85 m interval.

The eroding upper continental crust at 2.5 Ga may have been smaller in volume and less radiogenic if hypotheses of continental crust growth over geological time, including a major growth event at ca. 2.7 Ga, are correct (Arndt, 2004). Most of the Mo and Re during the S1 oxygenation event was probably derived from crustal sulfides in igneous and metamorphic rocks. Pyrite will rapidly dissolve into solution even under conditions of low pO_2 (Williamson and Rimstidt, 1994; Anbar et al., 2007). Low U abundances throughout the ABDP-9 core are consistent with limited oxidative weathering of silicate and phosphate minerals (Anbar et al., 2007), suggesting minimal weathering of silicate minerals known to contain radiogenic Os (e.g., such as biotite, pyroxene, olivine, plagioclase; Peucker-Ehrenbrink and Blum, 1998; Gannoun et al., 2004, 2006). Organic matter also weathers rapidly in the presence of oxygen (Petsch et al., 2000). However, oxidative weathering of exhumed Archean organic-rich shales may not have represented a significant source of Re and Mo because these rocks probably contained predominantly low abundances of these metals (Yang and Holland, 2002; Siebert et al., 2005).

Archean molybdenites are known to contain ppb to hundreds of ppm Re (Stein et al., 1998, 2001, 2004; Selby and Creaser, 2004; Selby et al., 2007) whereas Archean and Phanerozoic pyrites contain tens to hundreds of ppb Re (Stein et al., 1998; Mathur et al., 1999; Morelli et al., 2004). Archean molybdenites with high Re abundances will quickly acquire abundant radiogenic ^{187}Os through radioactive decay of ^{187}Re (e.g., 1 ppm Re, negligible initial ^{187}Os at molybdenite formation, and 200 M.y. of radiogenic in-growth will result in 3.33 ppb ^{187}Os). Thus, oxidative weathering of sulfides may have been sufficient to elevate seawater Os isotope compositions above the mantle/extraterrestrial baseline. I note that a more radiogenic I_{Os} for the samples from the 145.22-148.32 m interval would result in a slightly steeper slope of the 2501 Ma isochron, thereby explaining the sub-chondritic I_{Os} determination (0.04 ± 0.06) of the combined regression. The large range in present-day ^{187}Re/^{188}Os and ^{187}Os/^{188}Os isotope ratios for the entire Mt. McRae Shale Re-Os dataset was apparently sufficient to drown out any I_{Os} heterogeneity and yield a Model 1 result (e.g., Ravizza et al., 1991). Thus, the Re-Os isotope data are consistent with dominance of the 2.5 Ga seawater Os budget by magmatic/hydrothermal/extraterrestrial sources, but do not rule out some small contribution of radiogenic Os from crustal sulfides.

6.4.3 Progress Towards a Precambrian Seawater ^{187}Os/^{188}Os Curve

Interpretations of I_{Os} from Re-Os isochron regressions of Precambrian ORS with regards to global seawater ^{187}Os/^{188}Os are complicated by the likelihood of a significantly reduced seawater residence time for Os (and other redox-sensitive elements like Mo; Anbar and Knoll, 2002) under conditions of a predominantly anoxic Archean atmosphere and ocean prior to the GOE (Farquhar et al., 2000; Pavlov and Kasting, 2002; Goldblatt et al., 2006), or in a stratified Proterozoic ocean with oxidizing surface waters and suboxic, anoxic or euxinic deep waters following the GOE (Canfield, 1998; Farquhar and Wing, 2003; Slack et al., 2007). The deep ocean may not have become fully oxygenated until the Neoproterozoic (e.g., Fike et al., 2006; Kennedy et al., 2006; Canfield et al., 2007). A restricted or semi-restricted (e.g., intracratonic) depositional environment can lead to preservation of I_{Os} in ORS that does not reflect the contemporaneous global seawater Os isotope composition (Ravizza et al., 1991; Martin et al., 2000; Poirer, 2006; see Chapter 5). A shorter residence time of Os in Precambrian seawater could in principle allow rapid fluctuations in the Os isotope composition of even regional water masses derived from changes in the flux and/or isotopic composition of input sources.

Despite these complications, the I_{Os} from ORS isochron regressions holds potential for tracking relative changes in the Os mass balance of Precambrian seawater resulting from shifts in the flux and/or isotopic composition of radiogenic crustal and unradiogenic magmatic/hydrothermal/extraterrestrial sources. Of particular interest is a precise determination of the time when pO_2 in the atmosphere rose sufficiently to allow oxidative weathering of continental crust and the development of a significant radiogenic riverine Os flux to the oceans. The limited information available for the Os isotope composition of Precambrian seawater does not yet provide this information (see Figure 6.9). A chondritic $^{187}Os/^{188}Os$ isotope composition of 0.133 ± 0.020 for ca. 2.0 Ga seawater ("Productive Formation", Pechenga Greenstone Belt, Russia) may reflect a minimal riverine flux of radiogenic Os during the middle Paleoproterozoic and/or dominance of mantle inputs in a rift-related environment (Hannah et al., 2006). A large time gap in the seawater Os isotope curve exists until 1.54 Ga, where a precise I_{Os} determination of 0.51 ± 0.03 for the Douglas Formation (Athabasca Basin, western Canada) clearly indicates that crustal weathering and transport of radiogenic Os to seawater was possible during the Mesoproterozoic (Creaser and Stasiuk, 2007). Two Re-Os isochron ages from the Velkerri Formation (McArthur Basin, northern Australia) yield I_{Os} values of 0.29 ± 0.18 and 0.06 ± 0.22 (see Chapter 5) that also permit some contribution of dissolved radiogenic crustal Os to the 1.4 Ga oceans. By late Neoproterozoic time, however, crustal Os inputs exerted a significant control on the $^{187}Os/^{188}Os$ isotope composition of seawater, as evidenced by predominantly radiogenic

I_{Os} from the ca. 657 Ma Aralka Formation, central Australia (0.82 ± 0.03), ca. 643 Ma Tindelpina Shale Member, Tapley Hill Formation, southern Australia (0.95 ± 0.01) and correlative black shales from northwestern Tasmania (1.00 ± 0.05) (see Chapter 3), ca. 608 Ma Old Fort Point Formation, western Canada (0.62 ± 0.03) (Kendall et al., 2004), and the ca. 551 Ma Miaohe Member, Doushantuo Formation, South China (1.26 ± 0.22) (see Chapter 2). Delineation of the broad features of the Proterozoic seawater $^{187}Os/^{188}Os$ curve will depend upon determination of further I_{Os} values from precise Re-Os age determinations of ORS. Some similarities in the marine geochemical cycle of Os in the Proterozoic and Phanerozoic are apparent from the available dataset. For example, ORS deposited during deglaciation (e.g., Aralka Formation, Tindelpina Shale Member) record elevated seawater Os isotope compositions that were likely derived from enhanced post-glacial weathering and transport of eroded crustal material to the oceans in a fashion similar to that observed for Cenozoic post-glacial/inter-glacial intervals (Peucker-Ehrenbrink and Blum, 1998; Ravizza and Peucker-Ehrenbrink, 2003b; Williams and Turekian, 2004; Dalai et al., 2005, 2006).

6.4.4 Re-Os Systematics in Organic-Rich Shales Over Geological Time

To provide a fresh perspective regarding first-order variations in the redox state of Earth's atmosphere and oceans over geological time, the available Re and Os (using ^{192}Os to eliminate variations resulting from radioactive isotope decay) abundance and $^{187}Re/^{188}Os$ isotope data of ORS from the literature and presented in this thesis has been compiled and presented in Table 6.3. The Re and Os data presented in this compilation has been obtained using a variety of analytical methodologies (e.g., bulk versus organic-selective whole-rock dissolution protocols). Some rock units are affected to some degree by post-depositional processes (e.g., Wollogorang and Lapa Formations). Although the degree of preservation of primary Re-Os abundance and isotope systematics of some shales in the compilation have not been evaluated by the use of isochron diagrams, the average Re and Os abundances, and $^{187}Re/^{188}Os$ isotope ratios for each rock unit should generally reflect to first order the paleoenvironmental conditions (e.g., seawater metal abundances, local and/or global redox conditions) at the time of sediment deposition. Analyses with spuriously high or low Re and ^{192}Os abundances and/or $^{187}Re/^{188}Os$ isotope ratios relative to other samples within a rock unit are listed separately where applicable (e.g., Nauga and Silverton Formations). Using the average values from Table 6.3 (highlighted in bold), scatter plots of Re abundance versus ^{192}Os abundance (Figure 6.10), and Re or ^{192}Os abundance versus ^{187}Re/^{188}Os (Figure 6.11) have been constructed in an attempt to discern major differences in Re and Os marine geochemical cycles over geological time.

The Re and ^{192}Os abundances of ORS are well-correlated over geological time ($R^2 = 0.71$; Figure 6.10A). However, distinctive relationships among these parameters emerge when the data are grouped into three age categories: Phanerozoic-Recent, Mesoproterozoic-Neoproterozoic, and Archean-Paleoproterozoic. Relative to Recent organic-rich sediments, there is a large range in Re and ^{192}Os abundances for Phanerozoic ORS. Both subsets show a generally good correlation between Re and ^{192}Os abundance, albeit with significant scatter (Figure 6.10B). The scatter is not unexpected because hydrogenous Re and Os sequestration into organic-rich sediments in predominantly oxygenated Recent and Phanerozoic oceans is undoubtedly a function of several factors, including redox conditions, nature and abundance of organic matter content, precipitation rate kinetics, sediment accumulation rates, and seawater Re and Os abundances (Ravizza et al., 1991; Cohen et al., 1999; Sundby et al., 2004; Yamashita et al., 2007). Seawater Re and Os abundances are controlled by input fluxes from rivers and magmatic/extraterrestrial inputs and global burial fluxes (e.g., areal extent of suboxic, anoxic, and euxinic sediment deposition), which determine the residence time of Re and Os in seawater (Cohen et al., 1999). In the case of restricted or semi-restricted basins, paleohydrographic conditions (e.g., reservoir effects related to the degree of restriction of the overlying water column and associated renewal time of deep water masses) probably exerts a strong control on the Re and Os abundances of local seawater, as has been documented for Mo (Algeo and Lyons, 2006). The marine budgets of Re and Os are also dissimilar in some respects, including seawater residence times (Re: 7.5×10^5 years, Os: $\sim 10^4$ years; Colodner et al., 1993; Oxburgh 1998, 2001; Levasseur et al., 1999) and the importance of metalliferous sediments (e.g., ppb to hundreds of ppt Os are known from ferromanganese oxides, metalliferous pelagic clays and carbonates; Palmer and Turekian, 1986; Palmer et al., 1988; Esser and Turekian, 1988; Peucker-Ehrenbrink et al., 1995;

Oxburgh, 1998; Reusch et al., 1998; Burton et al., 1999; Yamashita et al., 2007) as a marine sink for Os, but not Re.

A surprisingly good correlation emerges for the dataset of both the Neoproterozoic and Mesoproterozoic Eras ($R^2 = 0.99$; Figure 6.10C), and remains excellent if Paleoproterozoic ORS are included ($R^2 = 0.97$). It is tempting to speculate on the significance of these well-correlated trends with regards to hypotheses concerning Proterozoic ocean chemistry. Following mild shallow water ocean oxygenation by 2.5 Ga (Anbar et al., 2007), but prior to the development of pervasive deep ocean oxygenation (possibly after ca. 580 Ma; Fike et al., 2006; Canfield et al., 2007), Paleoproterozoic, Mesoproterozoic and Neoproterozoic oceans may have been stratified, with oxidizing surface waters and oxic, suboxic, or sulfidic deep waters (Canfield, 1998; Siebert et al., 2005; Anbar et al., 2007; Slack et al., 2007; Wille et al., 2007). For example, recent Mo isotope evidence suggest the areal extent of euxinic sediment deposition was significantly expanded at ca. 1.7 Ga and 1.4 Ga relative to Phanerozoic and present-day oceans (Arnold et al., 2004; see Chapter 5). Abundant organic-rich sediment deposition in O_2-depleted deep waters between ca. 2.5 Ga and 0.6 Ga may have resulted in tight coupling of the marine geochemical cycles of Re and Os because ORS represented the primary marine sink for both metals. The number of Re- and Os-rich ORS (e.g., > 25 ppb and 0.1 ppb, respectively) from this time interval relative to younger shales is markedly limited. This is consistent with a diminished Re and Os seawater inventory in stratified Proterozoic oceans, similar to that suggested for Mo (Anbar and Knoll, 2002; Anbar et al., 2007).

The absence of a correlation between average Re and ^{192}Os abundance for Paleoproterozoic and Archean ORS (Figure 6.10D) stands in marked contrast to the trends defined by younger ORS. The most significant observation is the clustering of the Archean dataset along the ^{192}Os-axis. With the exception of the Manjeri Formation and Mt. McRae Shale, Archean ORS are characterized by low Re abundances, but have ^{192}Os abundances generally comparable to that of Proterozoic and Phanerozoic ORS. Unlike Re, the seawater Os inventory was apparently not depleted significantly in predominantly reducing oceans prior to the GOE. This reason for this is not clear. Osmium may have been continuously replenished through hydrothermal inputs (Ravizza et al., 1996; Sharma et al., 2000; Cave et al., 2003) at a rate faster than burial in ORS because of more vigorous hydrothermal circulation systems on a younger, hotter Earth. In contrast, hydrothermal fluids are not a significant source of Re to the oceans (Colodner et al., 1993; Ravizza et al., 1996). Enhanced magmatic inputs to Archean seawater from alteration of recently emplaced igneous provinces (e.g., during plume or superplume events; Condie, 2004; Ernst et al., 2004) may be significant sources of both Os and Re (e.g., Cohen and Coe, 2002; Cohen, 2004). Extreme enrichment in Re (270 ppb) and Os (57 ppb) observed in a sample from the Nauga Formation could be explained by this process (rather than oxidative weathering as suggested by Wille et al., 2007). In a Re-poor anoxic or weakly oxygenated, stratified ocean, the additional Re may have been quickly removed from solution into reducing sediments. Bolide impact rates on the Earth and Moon were likely twice as high at ca. 3 Ga as the present-day (Ryder, 2003). A number of impact ejecta horizons have been identified in the Archean to early Paleoproterozoic rock record (Simonson et al., 2004). Thus, extraterrestrial Os likely had a more important role on the Os budget of ORS during the Archean and Paleoproterozoic compared to younger times.

Another method for examining the Re-Os systematics in ORS over geological time is to consider the relationship between average Re or ^{192}Os abundance with average ^{187}Re/^{188}Os isotope ratio. For Mesoproterozoic to Recent units, this correlation is poor ($R^2 \leq 0.4$; Figure 6.11A, B) and likely reflects multiple controlling factors on variations in ^{187}Re/^{188}Os for ORS deposited in moderately to fully oxygenated oceans. These include redox conditions, precipitation rate kinetics, variations in the flux of Re and Os to ORS, and the nature of Re and Os complexation with organic matter. In contrast, a well-correlated trend is observed between average ^{187}Re/^{188}Os and Re abundance ($R^2 > 0.95$; Figure 6.11C), but not between average ^{187}Re/^{188}Os and ^{192}Os abundance ($R^2 < 0.10$; Figure 6.11D) for Archean and Paleoproterozoic ORS. A similar relationship between Re abundance and ^{187}Re/^{188}Os ($R^2 = 0.80$) is observed when considering the Mt. McRae Shale data alone. Under the conditions of a weakly oxygenated to anoxic atmosphere, the development of sufficiently oxidizing conditions in the shallow water column for oxidative weathering of Re from crustal sulfides was probably the dominant control for increasing the average ^{187}Re/^{188}Os ratio in seawater, and thus of Archean and Paleoproterozoic ORS.

6.5 CONCLUSIONS

The excellent agreement between the Re-Os age of 2501.1 ± 8.2 Ma and previous U-Pb age constraints for the Mt. McRae Shale suggests the Re-Os deposition-age geochronometer is applicable to well-preserved ORS as old as the Archean-Paleoproterozoic boundary. Depositional age determinations may also be possible for Late Archean shales deposited from a water column with a weakly oxygenated shallow layer if there is appreciable hydrogenous Re and Os enrichment. In contrast, ORS deposited in an anoxic water column or containing minimal reductive metal enrichment are not suitable targets for Re-Os geochronology because they can yield meaningless dates that reflect mixing of hydrogenous and detrital Os at the time of sediment deposition (e.g., Monteville Formation and Klipput Shale Member, lower Nelani Formation). Chondritic initial ^{187}Os/^{188}Os determinations from isochron regressions of Re- and Os-rich shales prior to, during, and following the GOE are consistent with the principal source of Os to seawater being unradiogenic magmatic/hydrothermal/extraterrestrial Os rather than weathering and erosion of radiogenic crustal Os. However, consideration of the Mt. McRae Shale Re-Os isotope systematics suggests that increases in the Os isotope composition of Late Archean to early Paleoproterozoic seawater above the magmatic/extraterrestrial baseline are possible, and would likely result from oxidative weathering of highly radiogenic crustal sulfides. The Re and ^{192}Os abundances, and ^{187}Re/^{188}Os isotope systematics of ORS over geological time is generally consistent with the presently popular hypothesis of a multi-stage evolution in the redox state of Earth's oceans and atmosphere. Specifically, low Re abundances and ^{187}Re/^{188}Os ratios in Archean shales reflects a predominantly anoxic atmosphere and oceans (e.g., atmospheric $pO_2 < 10^{-5}$ PAL; Pavlov and Kasting, 2002; Goldblatt et al., 2006), with Recent/Phanerozoic-like ^{192}Os abundances being maintained by enhanced magmatic/hydrothermal/extraterrestrial inputs. The onset of initial Earth surface oxidation in the Late Archean is marked by a coupled increase in Re abundance and ^{187}Re/^{188}Os. Early Paleoproterozoic to Neoproterozoic ORS are characterized by lowered Re and ^{192}Os abundances that likely reflects reduced seawater metal inventories associated with the development of stratified oceans and the expansion of reducing depositional environments (Canfield, 1998; Arnold et al., 2004; Siebert et al., 2005; Anbar et al., 2007; Slack et al., 2007; Wille et al., 2007). Phanerozoic and Recent ORS have a wide range in Re and ^{192}Os abundances that are only moderately correlated, and the highest and most variable ^{187}Re/^{188}Os isotope ratios, consistent with a wide range in paleoenvironmental controls on Re and Os accumulation in ORS deposited in restricted or productive, upwelling regions of predominantly oxygenated oceans.

Table 6.1. Re-Os Data for the Mt. McRae Shale (drill hole ABDP-9), Hamersley Group, Western Australia.

Sample (depths in m)	Re (ppb)	Os (ppt)	^{192}Os (ppt)	^{187}Re/^{188}Os	^{187}Os/^{188}Os	rho	$I_{Os\,(2500\,Ma)}$*
ABDP9-128.71	11.59 ± 0.04	628.8 ± 5.9	133.2 ± 1.0	173.11 ± 1.42	7.3989 ± 0.0675	0.717	0.04
ABDP9-128.84	11.49 ± 0.04	513.8 ± 6.3	86.1 ± 1.0	265.57 ± 3.12	11.3592 ± 0.1463	0.822	0.06
ABDP9-129.15	13.32 ± 0.05	467.3 ± 7.9	47.4 ± 0.9	558.35 ± 10.44	23.6301 ± 0.4745	0.895	–0.12
ABDP9-129.36	20.94 ± 0.08	792.7 ± 9.3	96.8 ± 1.0	430.21 ± 4.44	18.3693 ± 0.1997	0.830	0.07
ABDP9-129.85	21.04 ± 0.08	761.0 ± 9.7	83.4 ± 0.9	501.84 ± 5.43	21.3396 ± 0.2533	0.808	0.00
ABDP9-145.22	39.06 ± 0.14	1148.2 ± 18.2	44.6 ± 0.6	1742.85 ± 23.25	73.9781 ± 1.0922	0.836	–0.14
ABDP9-146.08	27.20 ± 0.10	820.3 ± 11.8	39.2 ± 0.6	1381.41 ± 19.89	58.7478 ± 0.8446	0.937	0.00
ABDP9-147.10	28.60 ± 0.10	911.3 ± 12.8	58.8 ± 0.6	967.45 ± 10.94	41.5033 ± 0.5201	0.809	0.36
ABDP9-148.32	21.94 ± 0.08	681.0 ± 9.6	39.2 ± 0.6	1113.77 ± 16.10	47.4586 ± 0.6796	0.945	0.09

Uncertainties are quoted at the 2σ level.

*I_{Os} = initial ^{187}Os/^{188}Os ratio calculated using the age indicated in brackets.

Table 6.2. Re-Os Data for the Monteville Formation (drill hole GKP01) and Klipput Shale Member (drill hole GEC01), Transvaal Supergroup, South Africa.

Sample	Depth (m)	Re (ppb)	Os (ppt)	^{192}Os (ppt)	^{187}Re/^{188}Os	^{187}Os/^{188}Os	rho	I_{Os} [illegible]*	I_{Os} [illegible]*	I_{Os} [illegible]*	I_{Os} [illegible]*
Monteville Formation											
GKP01-1020-1	1019.76-1019.79	1.35 ± 0.01	255.4 ± 1.2	88.7 ± 0.3	30.23 ± 0.18	1.5772 ± 0.0090	0.453	0.22	0.27		
GKP01-1020-4	1019.88-1019.90	1.10 ± 0.01	260.0 ± 1.1	93.9 ± 0.4	23.34 ± 0.15	1.2285 ± 0.0068	0.416	0.18	0.22		
GKP01-1020-6	1019.94-1019.96	1.31 ± 0.01	330.9 ± 1.2	120.8 ± 0.4	21.52 ± 0.12	1.1272 ± 0.0047	0.373	0.16	0.19		
GKP01-1020-10	1020.05-1020.08	1.35 ± 0.01	316.4 ± 1.2	114.1 ± 0.4	23.60 ± 0.13	1.2375 ± 0.0057	0.394	0.18	0.21		
GKP01-1020-11B	1020.12-1020.14	1.49 ± 0.01	415.4 ± 1.5	153.5 ± 0.5	19.35 ± 0.10	1.0288 ± 0.0047	0.377	0.16	0.19		
GKP01-1020-12B	1020.18-1020.20	1.43 ± 0.01	284.8 ± 1.1	100.2 ± 0.3	28.41 ± 0.15	1.4552 ± 0.0068	0.409	0.18	0.22		
Klipput Shale Member, lower Nelani Formation											
GEC-174.50-174.98-2	174.53-174.57	0.737 ± 0.004	136.8 ± 0.6	48.3 ± 0.2	30.33 ± 0.20	1.4191 ± 0.0083	0.398			0.14	0.17
GEC-174.50-174.98-4	174.61-174.65	0.723 ± 0.004	153.1 ± 1.0	55.0 ± 0.4	26.15 ± 0.25	1.2661 ± 0.0144	0.597			0.16	0.19
GEC-174.50-174.98-6	174.69-174.72	0.758 ± 0.004	162.7 ± 0.8	58.9 ± 0.3	25.62 ± 0.18	1.2083 ± 0.0089	0.454			0.13	0.16
GEC-174.50-174.98-9	174.79-174.83	0.766 ± 0.004	172.2 ± 0.8	62.6 ± 0.2	24.33 ± 0.16	1.1665 ± 0.0072	0.368			0.14	0.17
GEC-176.06-176.35-1	176.06-176.09	0.767 ± 0.004	100.6 ± 0.5	33.2 ± 0.1	46.00 ± 0.28	2.0591 ± 0.0095	0.386			0.12	0.17
GEC-176.06-176.35-3	176.12-176.16	0.465 ± 0.003	73.0 ± 0.6	25.1 ± 0.2	36.88 ± 0.40	1.6745 ± 0.0214	0.569			0.12	0.16
GEC-176.06-176.35-6	176.20-176.23	0.404 ± 0.003	33.9 ± 0.4	9.6 ± 0.1	83.84 ± 1.02	3.6571 ± 0.0528	0.580			0.12	0.22
GEC-176.06-176.35-8	176.26-176.29	0.452 ± 0.003	156.9 ± 0.5	59.9 ± 0.2	15.01 ± 0.13	0.7526 ± 0.0041	0.272			0.12	0.14
GEC-176.06-176.35-10	176.32-176.35	0.408 ± 0.003	78.0 ± 0.6	27.8 ± 0.2	29.18 ± 0.32	1.3513 ± 0.0176	0.511			0.12	0.15

Uncertainties are quoted at the 2σ level.

*I_{Os} = initial ^{187}Os/^{188}Os isotope ratio calculated using the age in brackets.

Table 6.3. Re, Os abundances and ^{187}Re/^{188}Os ratios [minimum / maximum (average)] of organic-rich sedimentary rocks over geological time.

Age	Locality/Lithological Unit/Stage	Number of analyses	Re (ppb)	^{187}Re/^{188}Os
Recent	Black Sea[1,2]	21 (Re), 11 (Os, ^{187}Re/^{188}Os)	20.9 / 184.4 **(48.9)**	447 / 1368 **(723)**
	Saanich Inlet[2,3,4]	40 (Re), 19 (Os, ^{187}Re/^{188}Os)	1.8 / 42.1 **(7.4)**	62 / 1053 **(349)**
	Chilean Margin[2]	6 (Re)	62 / 127 (96.0)	
	Peru Margin[2]	14 (Re)	6.2 / 42 (22.7)	
	Mazatlan, Mexico[2]	1 (Re)	44.4	
	Soledad Basin, Mexico[2]	2 (Re)	25.2 / 30.3 (27.8)	
	Whites Point, Los Angeles, California[2]	4 (Re)	28 / 48 (40.0)	
	San Pedro Martir Basin (Gulf of California)[2,5,6]	2 (Re), 1 (Os, ^{187}Re/^{188}Os)	15.3 / 17 **(16.2)**	**546**
	Carmen Basin (Gulf of California)[5,6]	4	26.3 / 31.2 **(28.7)**	664 / 1005 **(891)**
	Walvis Bay (Eastern South Atlantic)[5,6]	1	**15.9**	**1002**
	Jelly Fish Lake (Western Equatorial Pacific)[5,6]	1	**34.6**	**1083**
	Arabian Sea[3,7]	34 (Re)	0.9 / 41.5 (15.8)	
	Northwest U.S.A. Margin[7,8]	6 (Re)	1.8 / 15.8 (8.2)	
	Northwest African Margin[7]	4 (Re)	3.1 / 12.5 (8.8)	
	California Borderlands[8]	3 (Re)	8.8 / 22.7 (14.6)	
	Santa Barbara Basin[7,9]	3 (Data from different samples)	5.8 / 14.5 (8.8)	
	Cariaco Basin[10]			
	Sea of Japan (TL-1 & TL-2 intervals)[11]	6	2.8 / 20.8 **(13.3)**	40 / 645 **(386)**
Cretaceous	Cenomanian/Turonian (OAE2)[12]			
Jurassic	Kimmeridgian[13]	19	11.0 / 96.0 **(48.4)**	126 / 1264 **(567)**
	Oxfordian-Kimmeridgian Boundary[14]	8	13.2 / 49.8 **(33.1)**	374 / 902 **(634)**
	Callovian[15]	2	66.1 / 66.3 **(66.2)**	814 / 830 **(822)**
	Toarcian[13,16]	27	7.3 / 57.2 **(21.7)**	212 / 2167 **(700)**
	Sinemurian[13]	4	60.1 / 203.1 **(114.8)**	673 / 1388 **(1064)**
	Hettangian[13]	13	64.5 / 455.7 **(267.6)**	318 / 1571 **(729)**
Triassic/Jurassic	Rhaetian/Hettangian Boundary[17]	20 (Re), 19 (Os, ^{187}Re/^{188}Os)	0.7 / 101.2 **(30.3)**	28 / 611 **(209)**
Mississippian	Bakken Shale[18]	7	55.0 / 285.0 **(162.1)**	397 / 689 **(524)**
Devonian/Mississippian	Exshaw Formation[19-21]	21	15.2 / 128.7 **(38.7)**	165 / 894 **(354)**
Devonian	Ohio Shale[22]	5	74.8 / 115.6 **(88.1)**	1002 / 1786 **(1340)**
	Frasnian-Famennian Boundary[23]	32	3.3 / 40.9 **(18.2)**	121 / 777 **(472)**
	Lower Earn Group[24]	3	50.3 / 507.0 **(232.3)**	324 / 2104 **(1029)**

Table 6.3. Continued.

Locality/Lithological Unit/Stage	Os (ppb)	^{192}Os (ppb)	TOC
Black Sea[1,2]	0.232 / 0.685 (0.358)	0.088 / 0.258 **(0.136)**	3.3 / 17 (7.8)
Saanich Inlet[2,3,4]	0.052 / 0.265 (0.073)	0.021 / 0.108 **(0.028)**	2.1 / 2.7 (2.4)
Chilean Margin[2]			
Peru Margin[2]			
Mazatlan, Mexico[2]			
Soledad Basin, Mexico[2]			
Whites Point, Los Angeles, California[2]			
San Pedro Martir Basin (Gulf of California)[2,5,6]	0.149	**0.055**	12.5
Carmen Basin (Gulf of California)[5,6]	0.152 / 0.212 (0.175)	0.056 / 0.078 **(0.065)**	11.7 / 12.3 (11.9)
Walvis Bay (Eastern South Atlantic)[5,6]	0.095	**0.035**	24.9
Jelly Fish Lake (Western Equatorial Pacific)[5,6]	0.172	**0.063**	60
Arabian Sea[3,7]			
Northwest U.S.A. Margin[7,8]			
Northwest African Margin[7]			
California Borderlands[8]			
Santa Barbara Basin[2,9]	0.129 / 0.179 (0.158)	0.049 / 0.069 (0.060)	
Cariaco Basin[10]	~ 0.09 to 0.31		~ 0.2 to 5.6
Sea of Japan (TL-1 & TL-2 intervals)[11]	0.159 / 0.371 (0.211)	0.059 / 0.137 **(0.078)**	
Cenomanian/Turonian (OAE2)[12]	< 0.1 to 25		
Kimmeridgian[13]	0.212 / 0.999 (0.545)	0.061 / 0.324 **(0.179)**	6.4 / 54.2 (22.1)
Oxfordian-Kimmeridgian Boundary[14]	0.194 / 0.490 (0.308)	0.068 / 0.161 **(0.100)**	
Callovian[15]	0.502 / 0.513 (0.507)	0.156 / 0.160 **(0.158)**	
Toarcian[13,16]	0.130 / 0.288 (0.224)	0.041 / 0.096 **(0.070)**	~ 5 to 15
Sinemurian[13]	0.470 / 1.224 (0.740)	0.134 / 0.311 **(0.202)**	5.3 / 9.1 (6.6)
Hettangian[13]	1.113 / 3.172 (2.289)	0.348 / 0.876 **(0.701)**	7.4 / 13.6 (9.2)
Rhaetian/Hettangian Boundary[17]	0.085 / 2.004 (0.714)	0.032 / 0.748 **(0.264)**	1.0 / 9.5 (4.8)
Bakken Shale[18]	0.910 / 3.690 (2.084)	0.270 / 1.050 **(0.587)**	
Exshaw Formation[19-21]	0.230 / 1.708 (0.675)	0.070 / 0.509 **(0.214)**	1.4 / 12.6 (5.0)
Ohio Shale[22]	0.488 / 0.654 (0.586)	0.107 / 0.149 **(0.132)**	6.0 / 7.8 (7.0)
Frasnian-Famennian Boundary[23]	0.088 / 0.454 (0.249)	0.028 / 0.121 **(0.071)**	~ 0.4 to 4
Lower Earn Group[24]	0.939 / 2.553 (1.718)	0.350 / 0.509 **(0.440)**	

Table 6.3. Continued.

Age	Locality/Lithological Unit/Stage	Number of analyses	Re (ppb)	^{187}Re/^{188}Os
Ordovician	Utica Shale[25]	4	1.3 / 8.2 **(4.5)**	36 / 231 **(107)**
Cambrian	Tal Formation[26]	22 (Re), 23 (Os), 21 (^{187}Re/^{188}Os)	0.2 / 264.0 **(37.5)**	50 / 522 **(145)**
Neoproterozoic (Ediacaran)	Upper Krol Formation[26]	3 (Re), 3 (Os), 1 (^{187}Re/^{188}Os)	3.5 / 6.4 **(5.0)**	**447**
	Doushantuo Formation (Member 4)[27]	14	32.6 / 566.0 **(227.3)**	178 / 612 **(470)**
	Doushantuo Formation (Member 2)[27]	12	2.6 / 5.3 **(3.5)**	117 / 236 **(202)**
	Upper Miette Group[28]	6	7.0 / 12.5 **(9.1)**	362 / 615 **(450)**
	Old Fort Point Formation[29]	5	6.3 / 15.4 **(10.0)**	267 / 570 **(417)**
	Pertatataka Formation[27]	4	0.9 / 1.1 **(1.0)**	68 / 69 **(68)**
	Brachina Formation[27]	4	2.0 / 5.5 **(3.6)**	115 / 325 **(213)**
	Yarra Creek Shale[27]	11	11.9 / 15.8 **(13.9)**	284 / 462 **(370)**
Neoproterozoic (pre-Ediacaran)	Shali Formation (age uncertain)[26]	3 (Re, ^{187}Re/^{188}Os), 4 (Os)	0.9 / 13.1 **(5.0)**	104 / 868 **(375)**
	Tindelpina Shale Member (0.64 Ga)[27]	12	1.7 / 10.0 **(4.6)**	102 / 1010 **(328)**
	Upper Black River Dolomite (0.64 Ga)[27]	5	93.8 / 101.5 **(97.9)**	479 / 499 **(487)**
	Upper Black River Dolomite (0.64 Ga)[27]	10	19.5 / 39.2 **(29.9)**	534 / 832 **(723)**
	Araka Formation (0.66 Ga)[27,30]	17 (Re), 16 (Os, ^{187}Re/^{188}Os)	2.0 / 7.0 **(4.7)**	143 / 601 **(319)**
	Horsethief Creek Group (age uncertain)[27]	3	25.1 / 32.6 **(28.0)**	621 / 715 **(674)**
Mesoproterozoic	Lapa Formation (1.0-1.1 Ga?)[27]	14	0.1 / 16.9 **(4.4)**	21 / 281 **(153)**
	Upper Velkerri Formation (1.36 Ga)[27]	13	39.0 / 52.7 **(44.8)**	450 / 596 **(501)**
	Lower Velkerri Formation (1.42 Ga)[27]	13	4.7 / 8.1 **(6.4)**	388 / 519 **(461)**
	Douglas Formation (1.54 Ga)[31]	5	1.6 / 4.4 **(2.9)**	92 / 744 **(302)**
Paleoproterozoic	Barney Creek Formation (1.64 Ga)[27]	6	0.7 / 3.0 **(1.9)**	
	Wollogorang Formation (1.73 Ga)[27]	11	8.7 / 29.7 **(17.1)**	
	Virginia Formation (1.80 Ga)[32]	8	0.6 / 12.0 **(6.1)**	22 / 36 **(29)**
	Silverton Formation (2.15 Ga)[33]	2	0.2 / 2.6 **(1.4)**	475 / 706 **(589)**
	Silverton Formation (2.15 Ga)[33]	1	90	43 / 400 **(203)**
	Timeball Hill Formation (2.32 Ga)[33]	1 (Re)	17	9 / 175 **(92)**
	Klipput Shale (2.42 Ga)[27]	9	0.4 / 0.8 **(0.6)**	56344
	Kuruman Formation (2.46 Ga)[33]	1	**2.8**	
				15 / 84 **(35)**
Archean	pre-S1 of Mount McRae Shale (2.50 Ga)[34]	22 (Re)	0.3 / 39.0 **(6.1)**	**121**
	S-1 of Mount McRae Shale (2.50 Ga)[27,34]	58 (Re), 10 (Os, ^{187}Re/^{188}Os)	5.8 / 40.9 **(21.6)**	
	Siderite BIF of Mount McRae Shale (2.50 Ga)[34]	17 (Re)	1.6 / 11.0 **(4.0)**	
	S2 of Mount McRae Shale (2.50 Ga)[34]	17 (Re)	1.2 / 10.7 **(6.0)**	173 / 1743 **(778)**

Table 6.3. Continued.

Locality/Lithological Unit/Stage	Os (ppb)	^{192}Os (ppb)	TOC
Utica Shale[25]	0.126 / 0.451 (0.296)	0.046 / 0.157 **(0.103)**	4.2 / 7.8 (6.1)
Tal Formation[26]	0.020 / 13.500 (1.490)	0.007 / 4.402 **(0.466)**	0.2 / 7.3 (3.2)
Upper Krol Formation[26]	0.040 / 0.510 (0.210)	0.020 / 0.150 **(0.063)**	0.8 / 5.9 (2.8)
Doushantuo Formation (Member 4)[27]	1.151 / 8.235 (3.662)	0.364 / 1.839 **(0.863)**	up to 10
Doushantuo Formation (Member 2)[27]	0.078 / 0.157 (0.111)	0.025 / 0.050 **(0.035)**	
Upper Miette Group[28]	0.143 / 0.178 (0.159)	0.037 / 0.043 **(0.040)**	~ 1.8 to 2.1
Old Fort Point Formation[29]	0.133 / 0.240 (0.188)	0.033 / 0.054 **(0.047)**	~ 0.5
Pertatataka Formation[27]*	0.075 / 0.098 (0.085)	0.025 / 0.033 **(0.029)**	up to 0.7
Brachina Formation[27]*	0.107 / 0.130 (0.118)	0.033 / 0.035 **(0.034)**	up to 0.3
Yarra Creek Shale[27]*	0.294 / 0.330 (0.304)	0.068 / 0.089 **(0.075)**	
Shali Formation (age uncertain)[26]	0.050 / 0.180 (0.095)	0.015 / 0.030 **(0.020)**	0.7 / 4.0 (1.9)
Tindelpina Shale Member (0.64 Ga)[27]	0.093 / 0.145 (0.118)	0.020 / 0.042 **(0.032)**	~ 0.5 to 1
Upper Black River Dolomite (0.64 Ga)[27]	1.675 / 1.800 (1.723)	0.390 / 0.418 **(0.399)**	
Upper Black River Dolomite (0.64 Ga)[27]	0.329 / 0.525 (0.422)	0.073 / 0.096 **(0.082)**	
Aralka Formation (0.66 Ga)[27,30]	0.082 / 0.151 (0.117)	0.020 / 0.043 **(0.032)**	0.6 / 0.9 (0.7)
Horsethief Creek Group (age uncertain)[27]	0.367 / 0.465 (0.404)	0.073 / 0.095 **(0.083)**	
Lapa Formation (1.0-1.1 Ga?)[27]	0.026 / 0.490 (0.153)	0.009 / 0.119 **(0.040)**	
Upper Velkerri Formation (1.36 Ga)[27]	0.972 / 1.286 (1.089)	0.150 / 0.213 **(0.179)**	up to 9
Lower Velkerri Formation (1.42 Ga)[27]	0.114 / 0.204 (0.163)	0.019 / 0.035 **(0.028)**	up to 9
Douglas Formation (1.54 Ga)[31]	0.095 / 0.125 (0.110)	0.012 / 0.035 **(0.025)**	up to 3.6
Barney Creek Formation (1.64 Ga)[27]	0.118 / 0.550 (0.358)	0.043 / 0.207 **(0.133)**	~ 2 to 4
Wollogorang Formation (1.73 Ga)[27]	0.240 / 0.721 (0.442)	0.033 / 0.084 **(0.056)**	up to 6
Virginia Formation (1.80 Ga)[32]	0.092 / 0.798 (0.313)	0.023 / 0.281 **(0.084)**	0.4 / 1.6 (0.9)
Silverton Formation (2.15 Ga)[33]	0.110 / 0.140 (0.125)	0.030 / 0.043 **(0.037)**	0.4 / 0.5 (0.4)
Silverton Formation (2.15 Ga)[33]	0.008	0.003	0.4
Timeball Hill Formation (2.32 Ga)[33]			5.2
Klipput Shale (2.42 Ga)[27]	0.034 / 0.172 (0.119)	0.010 / 0.063 **(0.042)**	
Kuruman Formation (2.46 Ga)[33]	0.190	**0.048**	0.2
pre-S1 of Mount McRae Shale (2.50 Ga)[34]			1.9 / 5.8 (3.0)
S-1 of Mount McRae Shale (2.50 Ga)[27,34]	0.467 / 1.148 (0.748)	0.039 / 0.133 **(0.070)**	3.9 / 16.1 (8.8)
Siderite BIF of Mount McRae Shale (2.50 Ga)[34]			1.8 / 5.8 (2.7)
S2 of Mount McRae Shale (2.50 Ga)[34]			2.5 / 6.3 (3.9)

Table 6.3. Continued.

Age	Locality/Lithological Unit/Stage	Number of analyses	Re (ppb)	^{187}Re/^{188}Os
	Klein Naute Formation (2.50 Ga?)[33]	3 (Re), 2 (Os, ^{187}Re/^{188}Os)	0.6 / 3.2 **(1.8)**	321 / 983 (652)
	Nauga Formation (2.58-2.52 Ga)[33]	8 (Re), 5 (Os, ^{187}Re/^{188}Os)	0.1 / 13.0 **(6.1)**	73 / 172 **(138)**
	Nauga Formation (2.58-2.52 Ga)[33]	1	270	**25**
	Black Reef Quartzite (~ 2.6-2.5 Ga)[33]	2	< 0.1 / 0.1 **(0.1)**	**< 1**
	Monteville Formation (~ 2.6 Ga)[27,33]	7	1.1 / 1.5 **(1.3)**	19 / 30 **(24)**
	Vryburg Formation (~ 2.6 Ga)[33]	1	**4.2**	**126**
	Chesire Formation (~ 2.6 Ga)[35]	1	**4.8**	**67**
	Kameeldorings Formation (~ 2.7-2.6 Ga)[35]	1	**1.4**	**13**
	Manjeri Formation (~ 2.7 Ga)[35]	5	2.2 / 27.3 **(10.9)**	31 / 859 **(247)**
	Coronation Shale Member (2.95 Ga)[35]	1	**2.2**	**3**
	Moodies Group (3.15 Ga)[35]	1	**0.3**	**4**
	Fig Tree Group (3.23 Ga)[33,35]	6	0.1 / 2.3 **(0.7)**	< 1 / 12 **(6)**

Table 6.3. Continued.

Locality/Lithological Unit/Stage	Os (ppb)	^{192}Os (ppb)	TOC
Klein Naute Formation (2.50 Ga?)[33]	0.020 / 0.070 (0.044)	0.004 / 0.007 **(0.006)**	0.4 / 1.5 (0.9)
Nauga Formation (2.58-2.52 Ga)[33]	0.010 / 0.730 (0.484)	0.003 / 0.159 **(0.104)**	1.1 / 4.9 (2.3)
Nauga Formation (2.58-2.52 Ga)[33]	57.000	22.193	2.5
Black Reef Quartzite (~ 2.6-2.5 Ga)[33]	0.510 / 0.620 (0.565)	0.197 / 0.240 **(0.219)**	
Monteville Formation (~ 2.6 Ga)[27,33]	0.255 / 0.415 (0.308)	0.089 / 0.154 **(0.111)**	~ 2
Vryburg Formation (~ 2.6 Ga)[33]	0.290	**0.067**	0.8
Chesire Formation (~ 2.6 Ga)[35]	0.470	**0.140**	
Kameeldorings Formation (~ 2.7-2.6 Ga)[35]	0.550	**0.210**	
Manjeri Formation (~ 2.7 Ga)[35]	0.062 / 1.830 (0.722)	0.009 / 0.668 **(0.238)**	
Coronation Shale Member (2.95 Ga)[35]	4.070	**1.646**	
Moodies Group (3.15 Ga)[35]	0.336	**0.136**	
Fig Tree Group (3.23 Ga)[33,35]	0.200 / 1.600 (0.705)	0.077 / 0.624 **(0.276)**	

Where necessary, ^{192}Os and ^{187}Re/^{188}Os isotope ratios were calculated from literature data using Os abundances and ^{187}Os/^{188}Os isotope ratios. Replicate analyses of individual samples were averaged. Published tabulations of Re-Os data for the Cariaco Basin and Cenomanian-Turonian boundary are not available. Pyrite Re-Os analyses from black shales of the Timeball Hill and Rooihoogte Formations from Hannah et al. (2004) were not included in this compilation. Sources of data: 1 - Ravizza et al. (1991), 2 - Koide et al. (1986), 3 - Crusius et al. (1996), 4 - Poirier (2006), 5 - Ravizza and Turekian (1992), 6 - Colodner et al. (1993), 7 - Morford and Emerson (1999), 8 - Morford et al. (2005), 9 - Williams and Turekian (2004), 10 - Oxburgh (2001), 11 - Dalai et al. (2005), 12 - Turgeon and Creaser (2007), 13 - Cohen et al. (1999), 14 - Selby (in press), 15 - Cohen (2004), 16 - Cohen et al. (2004), 17 - Cohen and Coe (2002), 18 - Ravizza and Turekian (1989), 19 - Creaser et al. (2002), 20 - Selby and Creaser (2003), 21 - Selby and Creaser (2005), 22- Jaffe et al. (2002), 23 - Turgeon et al. (2007), 24 - Horan et al. (1994), 25 - Peucker-Ehrenbrink and Hannigan (2000), 26 - Singh et al. (1999), 27 - This Thesis, 28 - Kendall (2003), 29 - Kendall et al. (2004), 30 - Schaefer and Burgess (2003), 31 - Creaser and Stasiuk (2007), 32 - Ripley et al. (2001), 33 - Wille et al. (2007), 34 - Anbar et al. (in press), 35 - Siebert et al. (2005).

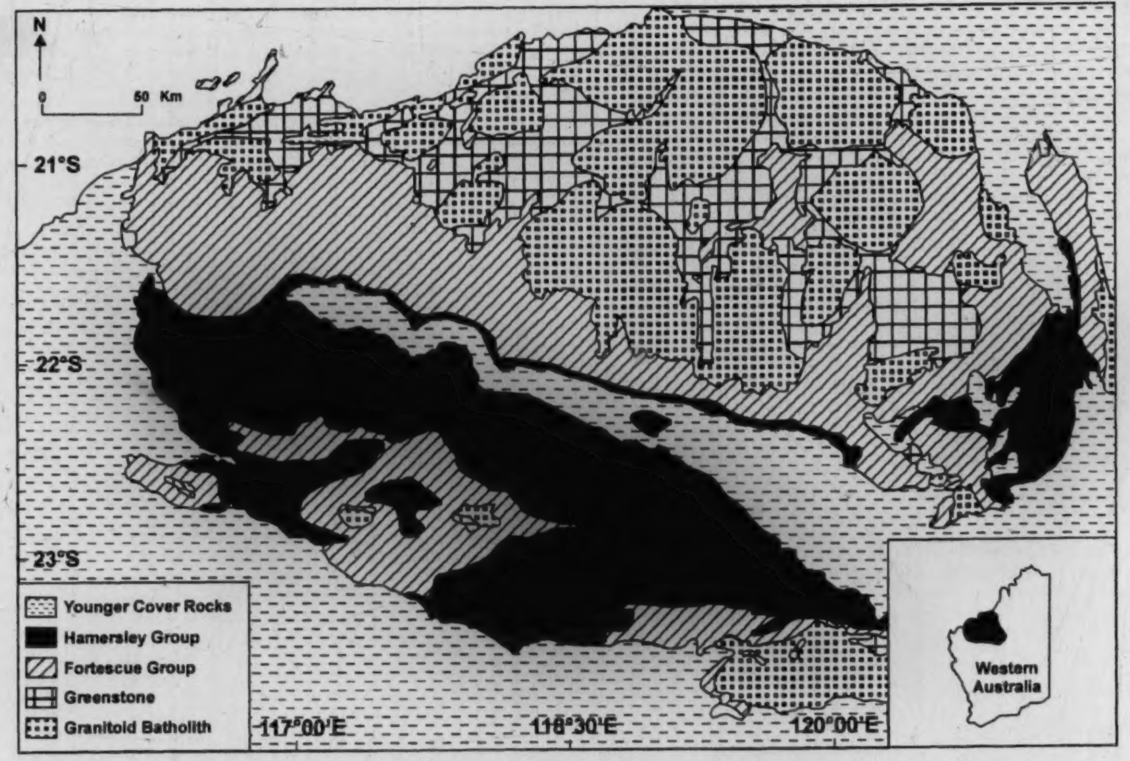
N
0
50 Km
21°S
22°S
23°S
Younger Cover Rocks
Hamersley Group
Fortescue Group
Greenstone
Granitoid Batholith
117°00'E
118°30'E
120°00'E
Western Australia

Figure 6.1: Simplified geological map of the Pilbara Craton showing the extent of the Hamersley Group. Asterisk denotes the location of drill hole ABDP-9 (Anbar et al., 2007). Modified after Glikson and Vickers (2007).

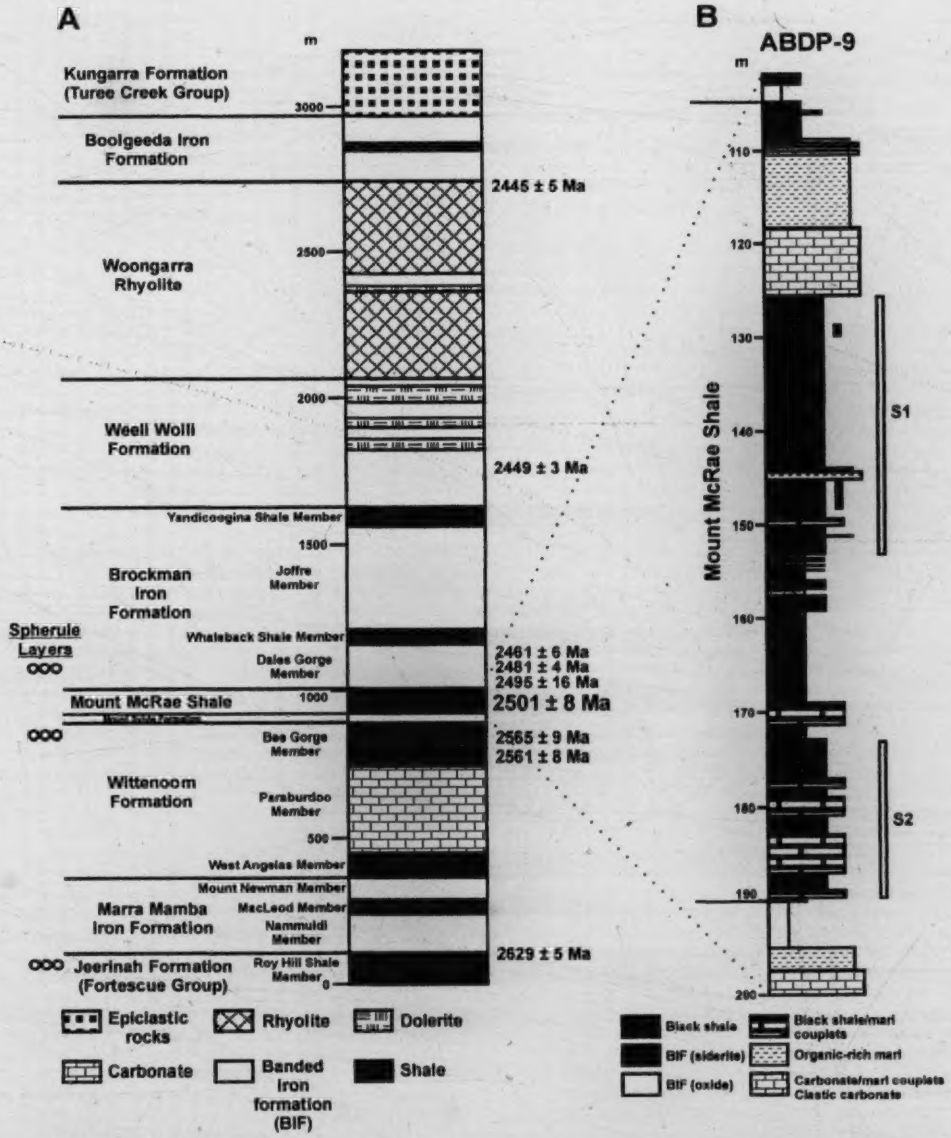
A
m
Kungarra Formation (Turee Creek Group)
3000
Boolgeeda Iron Formation
2445 ± 5 Ma
2500
Woongarra Rhyolite
2000
Weeli Wolli Formation
2449 ± 3 Ma
Yandicoogina Shale Member
1500
Brockman Iron Formation
Joffre Member
Whaleback Shale Member
Spherule Layers
Dales Gorge Member
2461 ± 6 Ma
2481 ± 4 Ma
2495 ± 16 Ma
Mount McRae Shale
1000
2501 ± 8 Ma
Bee Gorge Member
2565 ± 9 Ma
2561 ± 8 Ma
Wittenoom Formation
Paraburdoo Member
500
West Angelas Member
Mount Newman Member
Marra Mamba Iron Formation
MacLeod Member
Nammuldi Member
2629 ± 5 Ma
Jeerinah Formation (Fortescue Group)
Roy Hill Shale Member
0
Epiclastic rocks
Rhyolite
Dolerite
Carbonate
Banded Iron formation (BIF)
Shale
B
ABDP-9
m
110
120
130
140
150
160
170
180
190
200
Mount McRae Shale
S1
S2
Black shale
BIF (siderite)
BIF (oxide)
Black shale/marl couplets
Organic-rich marl
Carbonate/marl couplets
Clastic carbonate

Figure 6.2: (A) Generalized stratigraphic column for the Hamersley Group (modified after Trendall et al., 2004). Age constraints in small type are from Trendall et al. (2004) and references therein. Re-Os age constraint for the Mt. McRae Shale is shown in large type. (B) Stratigraphy of the Mt. McRae Shale in drill hole ABDP-9 (modified after Anbar et al., 2007). Vertical black bars within interval S1 denote the stratigraphic intervals sampled for Re-Os isotope analysis.

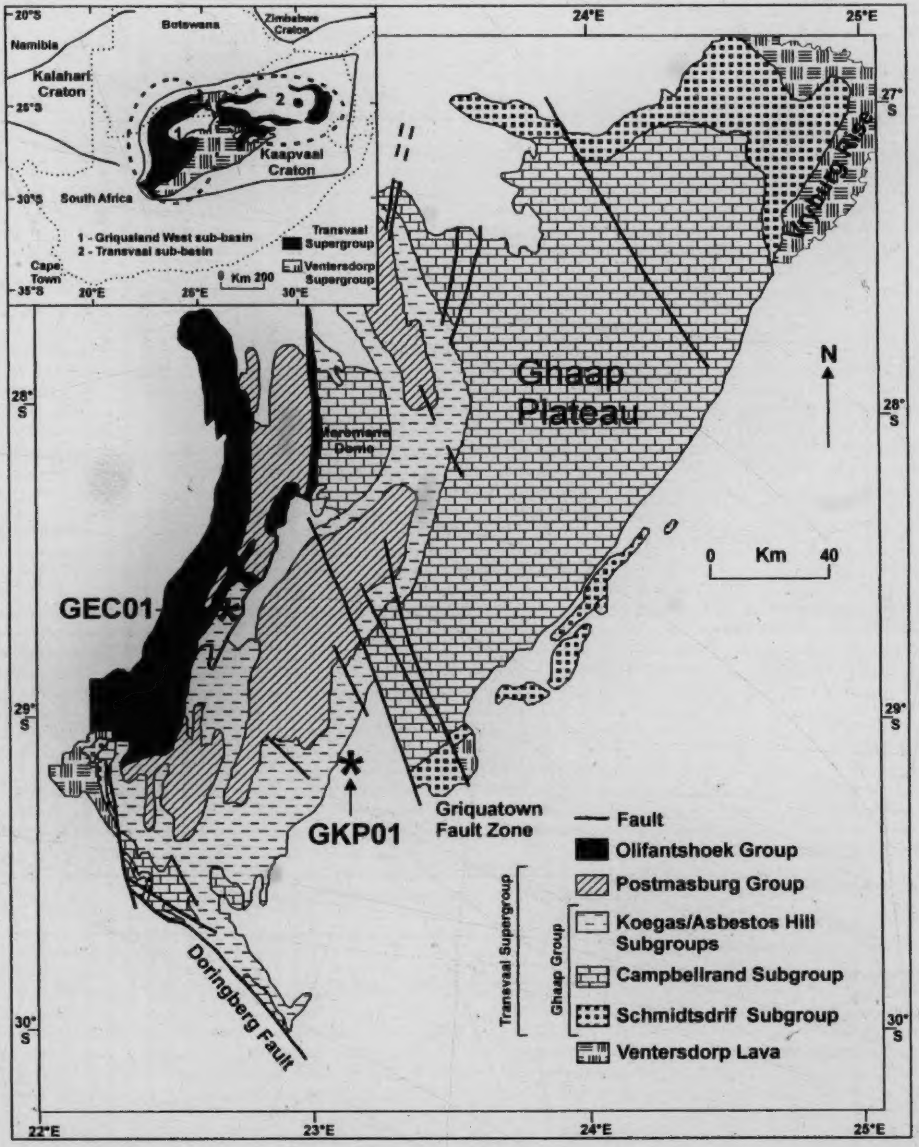
20°S
Namibia
Botswana
Zimbabwe Craton
Kalahari Craton
25°S
2
1
Kaapvaal Craton
30°S
South Africa
1 - Griqualand West sub-basin
2 - Transvaal sub-basin
Transvaal Supergroup
Ventersdorp Supergroup
Cape Town
0 Km 200
35°S
20°E
25°E
30°E
24°E
25°E
27° S
Vryburg Rise
Ghaap Plateau
N
28° S
Maremane Dome
0 Km 40
GEC01
29° S
GKP01
Griquatown Fault Zone
Fault
Olifantshoek Group
Postmasburg Group
Koegas/Asbestos Hill Subgroups
Campbellrand Subgroup
Schmidtsdrif Subgroup
Ventersdorp Lava
Transvaal Supergroup
Ghaap Group
Doringberg Fault
30° S
22°E
23°E
24°E
25°E

Figure 6.3: Geology of the Griqualand West sub-basin and its position within the Kaapvaal Craton (inset). Modified after Altermann and Nelson (1998) and Schröder et al. (2006).

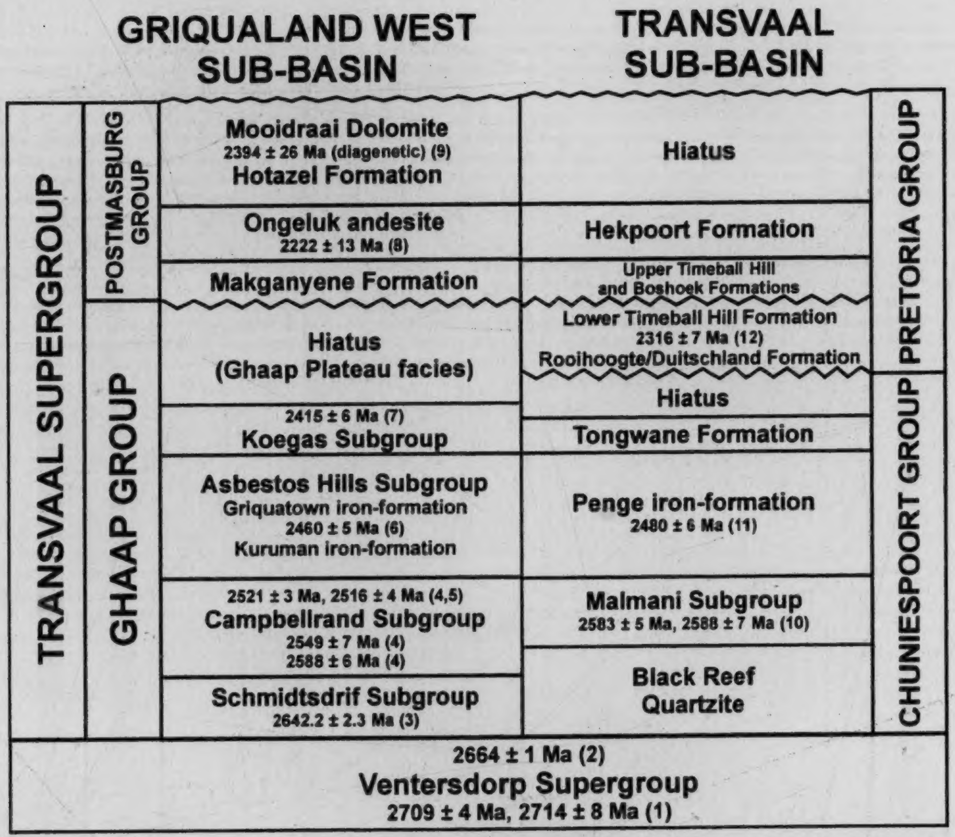
GRIQUALAND WEST SUB-BASIN
TRANSVAAL SUB-BASIN
TRANSVAAL SUPERGROUP
POSTMASBURG GROUP
GHAAP GROUP
PRETORIA GROUP
CHUNIESPOORT GROUP
Mooidraai Dolomite
2394 ± 26 Ma (diagenetic) (9)
Hotazel Formation
Hiatus
Ongeluk andesite
2222 ± 13 Ma (8)
Hekpoort Formation
Makganyene Formation
Upper Timeball Hill and Boshoek Formations
Hiatus
(Ghaap Plateau facies)
Lower Timeball Hill Formation
2316 ± 7 Ma (12)
Rooihoogte/Duitschland Formation
Hiatus
2415 ± 6 Ma (7)
Koegas Subgroup
Tongwane Formation
Asbestos Hills Subgroup
Griquatown iron-formation
2460 ± 5 Ma (6)
Kuruman iron-formation
Penge iron-formation
2480 ± 6 Ma (11)
2521 ± 3 Ma, 2516 ± 4 Ma (4,5)
Campbellrand Subgroup
2549 ± 7 Ma (4)
2588 ± 6 Ma (4)
Malmani Subgroup
2583 ± 5 Ma, 2588 ± 7 Ma (10)
Schmidtsdrif Subgroup
2642.2 ± 2.3 Ma (3)
Black Reef Quartzite
2664 ± 1 Ma (2)
Ventersdorp Supergroup
2709 ± 4 Ma, 2714 ± 8 Ma (1)

Figure 6.4: Correlations between Transvaal Supergroup strata in the Griqualand West and Transvaal sub-basins (modified after Bekker et al., 2001). Age constraints: 1 – Armstrong et al. (1991), 2 – Barton et al. (1995), 3 – Walraven and Martini (1995), 4 – Altermann and Nelson (1998), 5 – Sumner and Bowring (1996), 6 – Pickard (2003), 7 – Kirschvink et al. (2000), 8 – Cornell et al. (1996), 9 – Bau et al. (1999), 10 – Martin et al. (1998), 11 – cited in Nelson et al. (1999), 12 – Hannah et al. (2004).

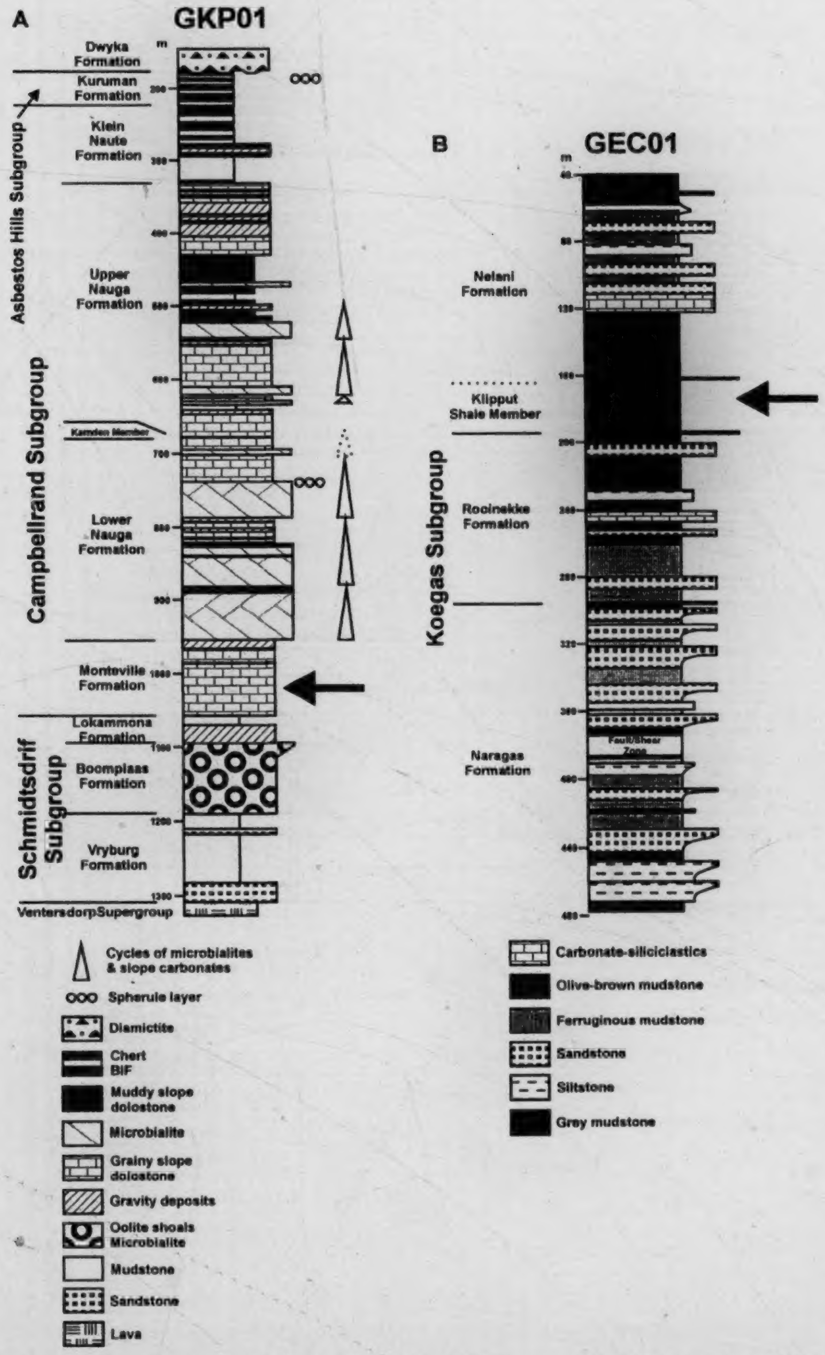
A
GKP01
m
Dwyka Formation
Kuruman Formation
Klein Naute Formation
Upper Nauga Formation
Asbestos Hills Subgroup
Campbellrand Subgroup
Kamden Member
Lower Nauga Formation
Monteville Formation
Lokammona Formation
Boomplaas Formation
Vryburg Formation
Schmidtsdrif Subgroup
VentersdorpSupergroup
200
300
400
500
600
700
800
900
1000
1100
1200
1300
Cycles of microbialites & slope carbonates
Spherule layer
Diamictite
Chert
BIF
Muddy slope dolostone
Microbialite
Grainy slope dolostone
Gravity deposits
Oolite shoals
Microbialite
Mudstone
Sandstone
Lava
B
GEC01
m
Nelani Formation
Klipput Shale Member
Rooinekke Formation
Koegas Subgroup
Naragas Formation
Fault/Shear Zone
40
80
120
160
200
240
280
320
360
400
440
480
Carbonate-siliciclastics
Olive-brown mudstone
Ferruginous mudstone
Sandstone
Siltstone
Grey mudstone

Figure 6.5: Stratigraphic columns for drill holes (A) GKP01 (modified after Schröder et al., 2006) and (B) GEC01 (modified after Schröder, unpublished), Ghaap Group, Transvaal Supergroup. Arrows denote the position of stratigraphic intervals sampled for Re-Os isotope analysis.

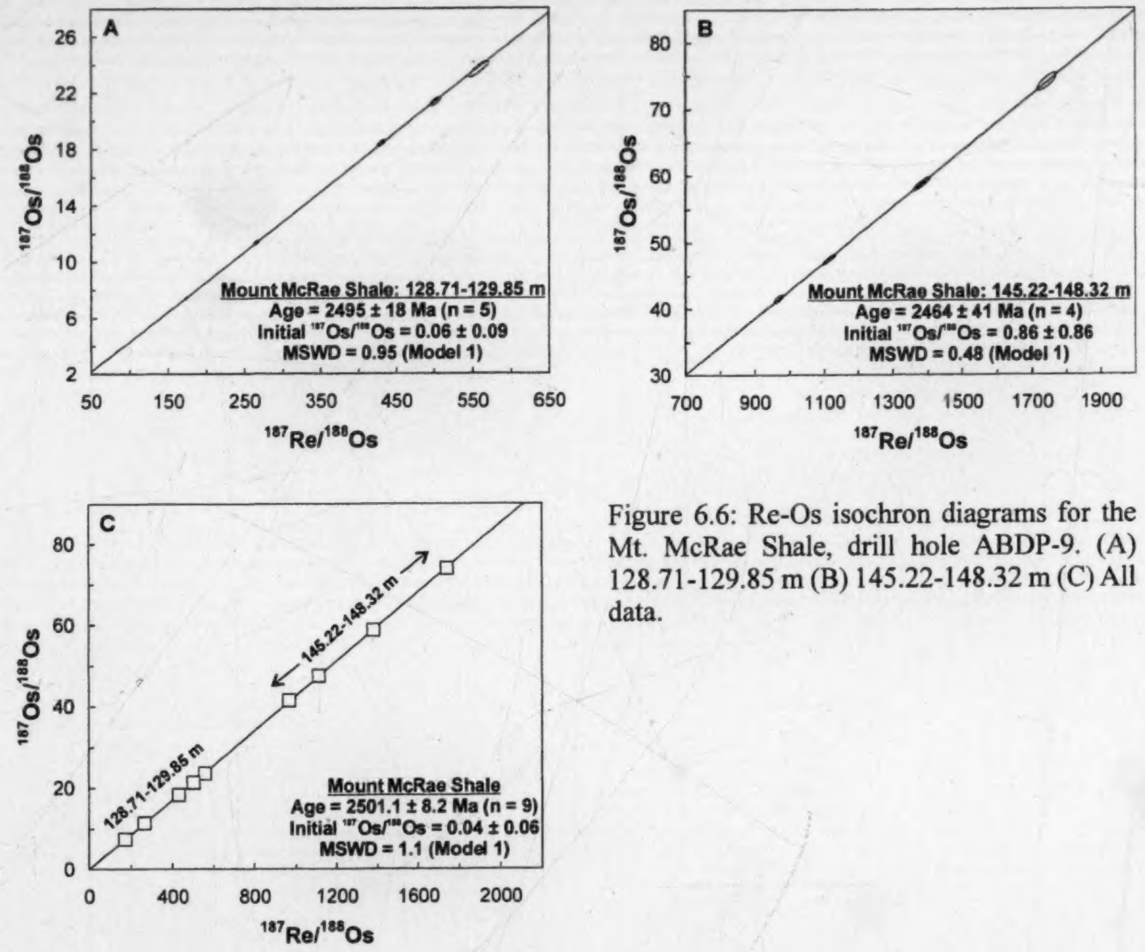

Figure 6.6: Re-Os isochron diagrams for the Mt. McRae Shale, drill hole ABDP-9. (A) 128.71-129.85 m (B) 145.22-148.32 m (C) All data.

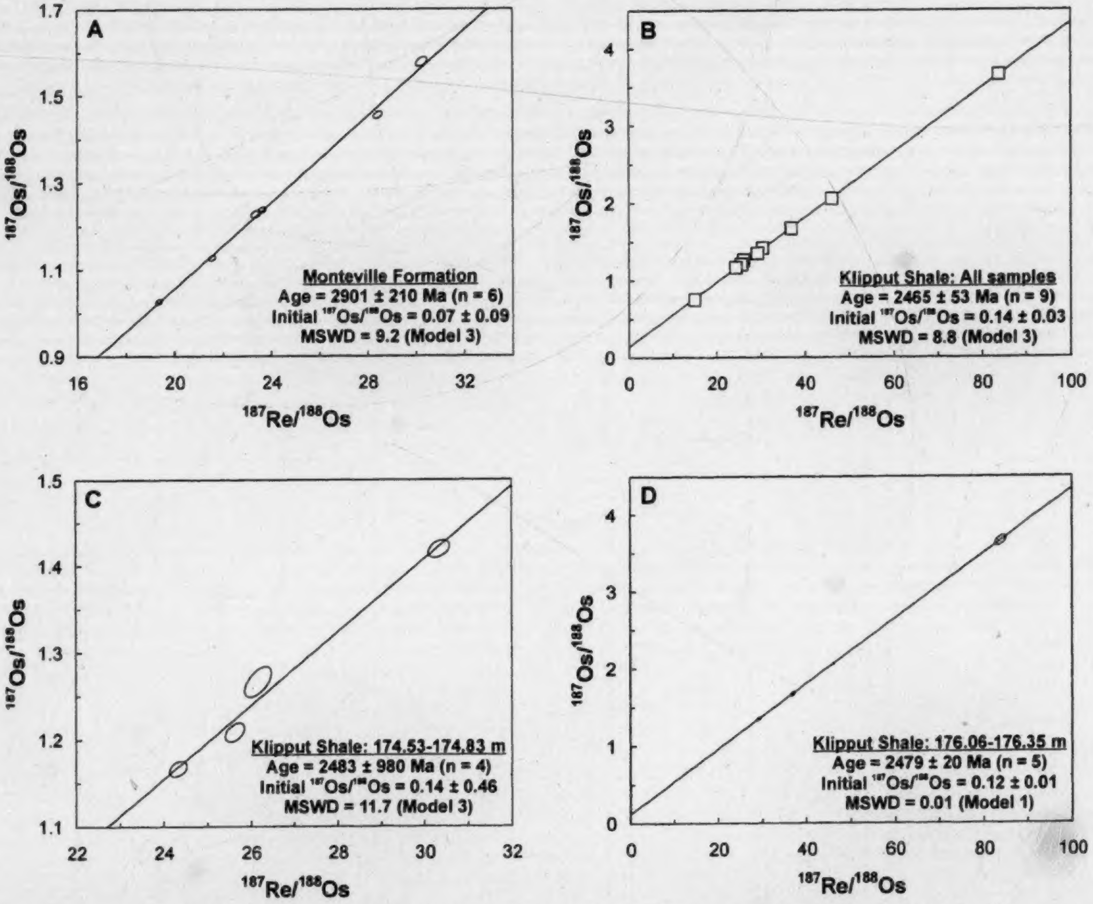

Figure 6.7: Re-Os isochron diagrams. (A) Monteville Formation, drill hole GKP01 (B) Klipput Shale Member, drill hole GEC01, all samples (C) Klipput Shale Member, 174.53-174.83 m (D) Klipput Shale Member, 176.06-176.35 m.

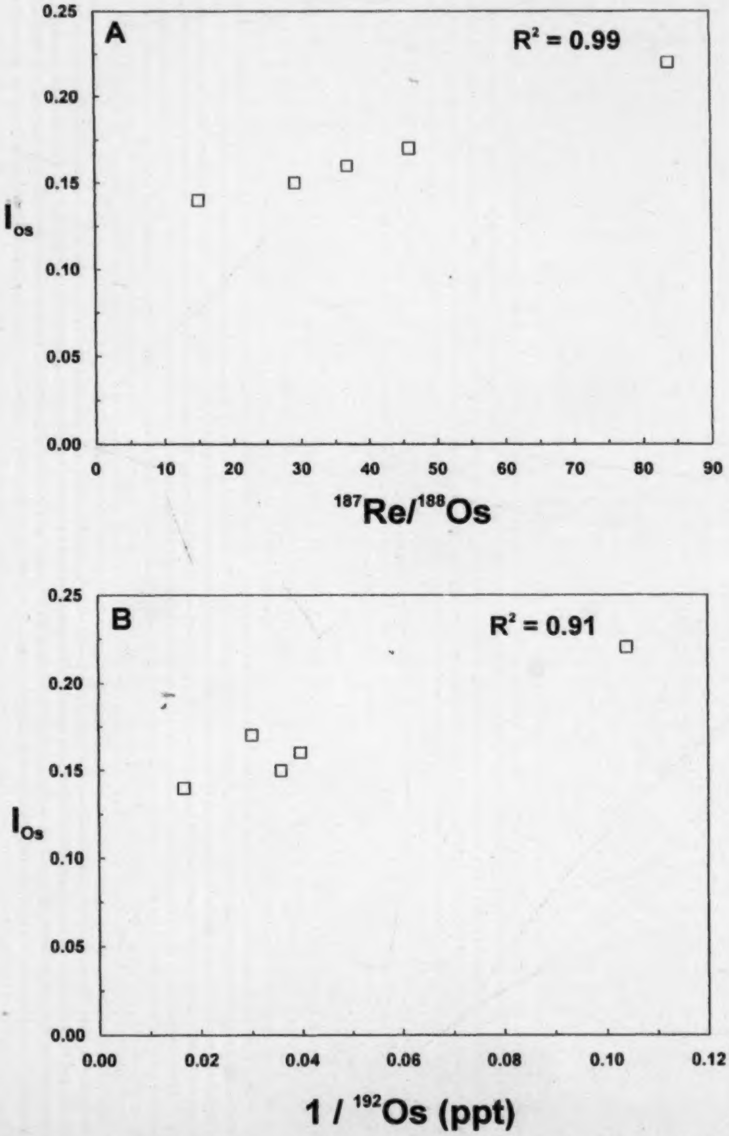

Figure 6.8: Geochemical diagrams illustrating well-correlated trends between (A) calculated individual sample I_{Os} and $^{187}Re/^{188}Os$ isotope ratio and (B) calculated individual sample I_{Os} and ^{192}Os abundance for the Klipput Shale Member (176.06-176.35 m depth). I_{Os} was calculated using an age of 2415 Ma (Pb-Pb age for the Rooinekke Formation; quoted by Kirschvink et al., 2000). These relationships may be construed as evidence of mixing between hydrogenous (high Os, low I_{Os}, low Re/Os) and detrital (low Os, high I_{Os}, high Re/Os) Os at the time of deposition. The y-intercept in (B) may correspond to the Os isotope composition of the hydrogenous end-member ($I_{Os} = 0.128$), which reflects dominance of the ca. 2.4 Ga seawater Os budget by magmatic/extraterrestrial inputs.

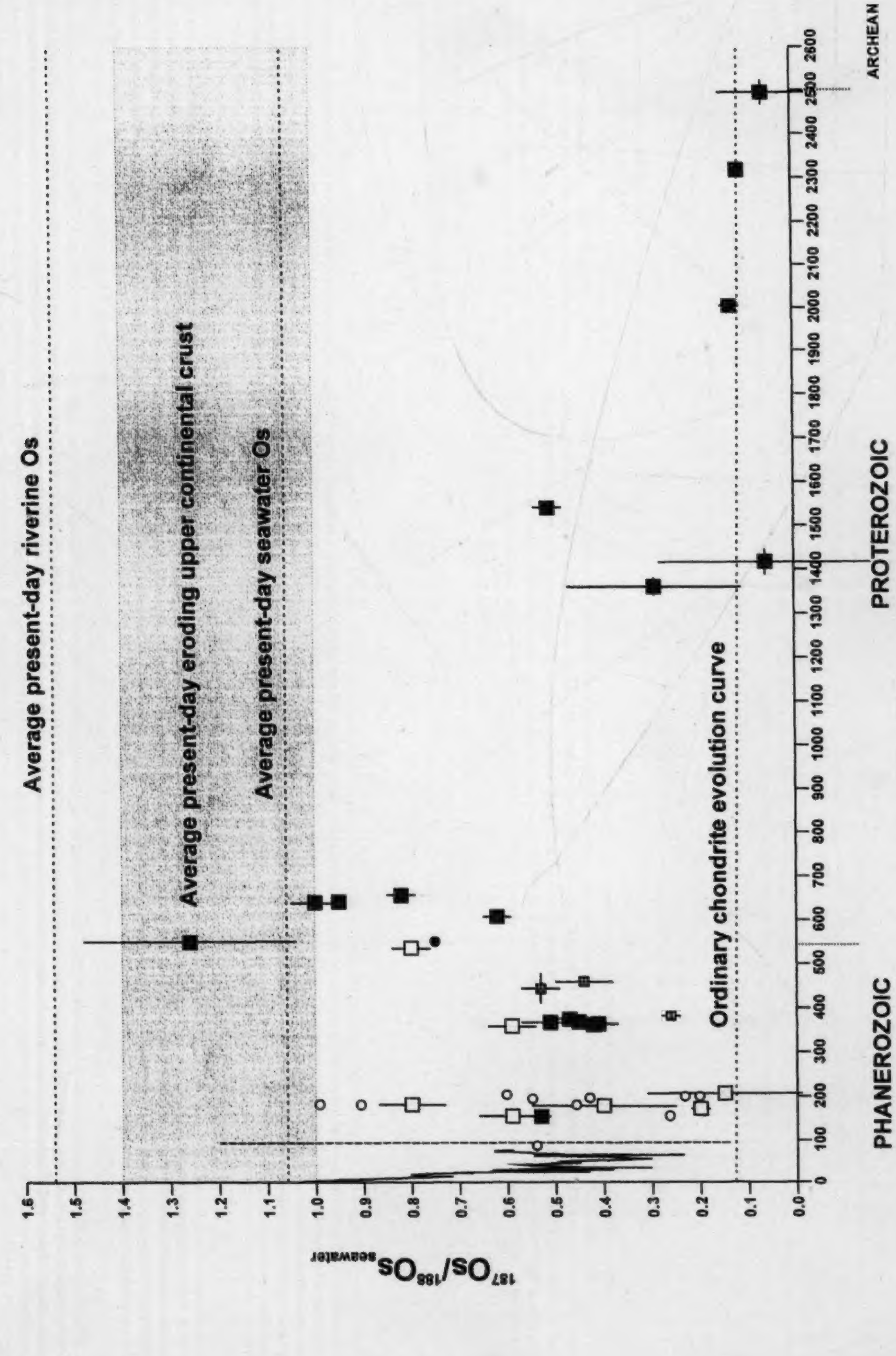Average present-day riverine Os
Average present-day eroding upper continental crust
Average present-day seawater Os
Ordinary chondrite evolution curve
$^{187}Os/^{188}Os_{seawater}$
1.6
1.5
1.4
1.3
1.2
1.1
1.0
0.9
0.8
0.7
0.6
0.5
0.4
0.3
0.2
0.1
0.0
0
100
200
300
400
500
600
700
800
900
1000
1100
1200
1300
1400
1500
1600
1700
1800
1900
2000
2100
2200
2300
2400
2500
2600
PHANEROZOIC
PROTEROZOIC
ARCHEAN
Age (Ma)

Figure 6.9: Seawater Os isotope composition over geological time. See text for discussion. Solid line (Cenozoic – Mesozoic) – ferromanganese crust data (Burton, 2005; Klemm et al., 2005), Dashed line – range in calculated individual sample I_{Os} from Cr^{VI}-H_2SO_4 digestions of organic-rich shale (Cenomanian-Turonian Oceanic Anoxic Event 2; Turgeon and Creaser, 2007), open circles – calculated individual sample I_{Os} from inverse *aqua regia* digestions of organic-rich shale (Ravizza et al., 1999; Cohen et al., 1999, 2004; Cohen and Coe, 2002; Cohen, 2004), grey circles – calculated individual sample I_{Os} from Cr^{VI}-H_2SO_4 digestions of organic-rich shale (this thesis), small light grey squares – isochron regression I_{Os} from algal laminites (Miller, 2004) and carbonate leachates (Widom et al., 2004), large open squares – isochron regression I_{Os} from inverse *aqua regia* digestions of organic-rich shale (Cohen et al., 1999, 2004; Creaser et al., 2002; Graham et al., 2006; Yang et al., 2006), large grey squares - isochron regression I_{Os} from Cr^{VI}-H_2SO_4 digestions of organic-rich shale (Selby and Creaser, 2003, 2005; Kendall et al., 2004; Creaser and Stasiuk, 2007; Selby, in press; Turgeon et al., in press; this thesis), large grey/black square - isochron regression I_{Os} from syn-sedimentary to early diagenetic pyrite plus Cr^{VI}-H_2SO_4 digestions of organic-rich shale (Hannah et al., 2006), large black square - isochron regression I_{Os} derived from syn-sedimentary to early diagenetic pyrite from organic-rich shale (Hannah et al., 2004).

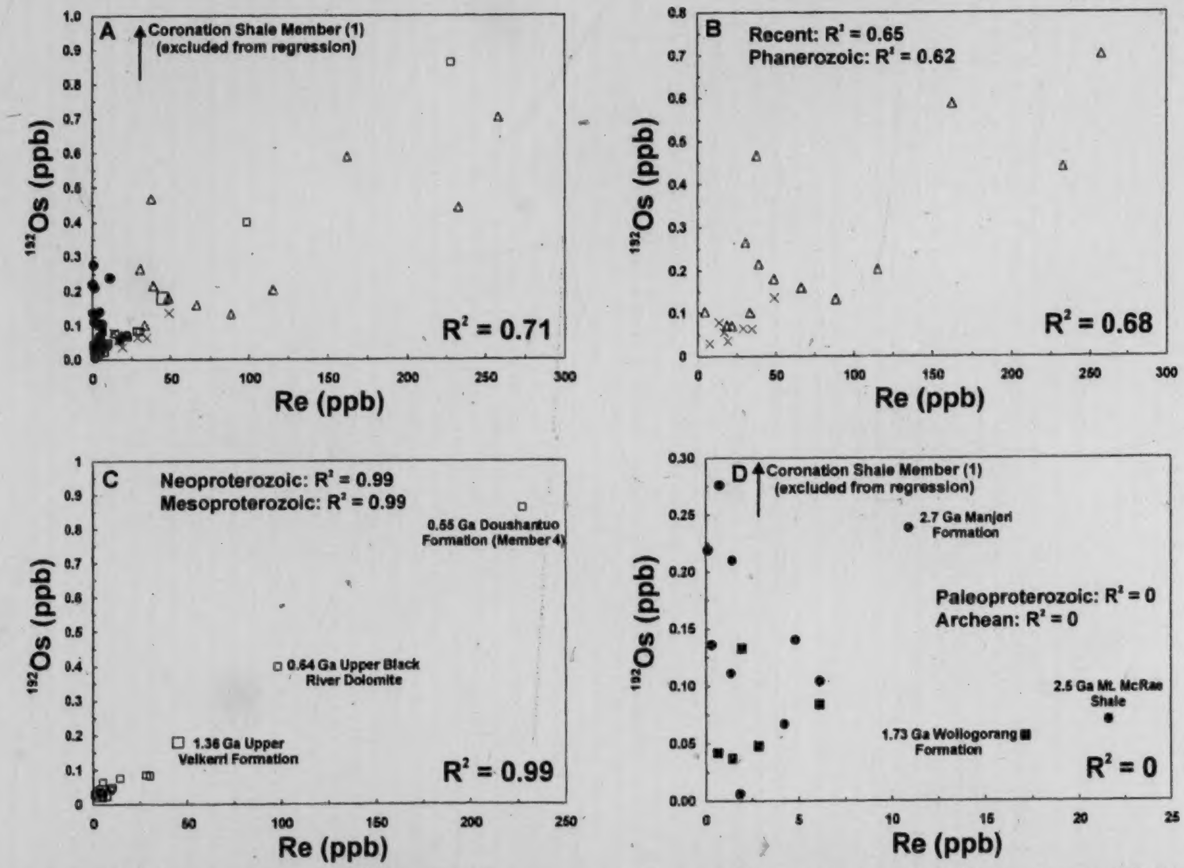

Figure 6.10: Trends between Re and ^{192}Os abundance over geological time. See text for discussion and Table 6.3 for sources of data. (A) All data (B) Recent and Phanerozoic ORS (C) Neoproterozoic and Mesoproterozoic ORS (D) Paleoproterozoic and Archean ORS. Crosses – Recent, triangles – Phanerozoic, small squares – Neoproterozoic, large squares – Mesoproterozoic, filled squares – Paleoproterozoic, shaded circles – Archean.

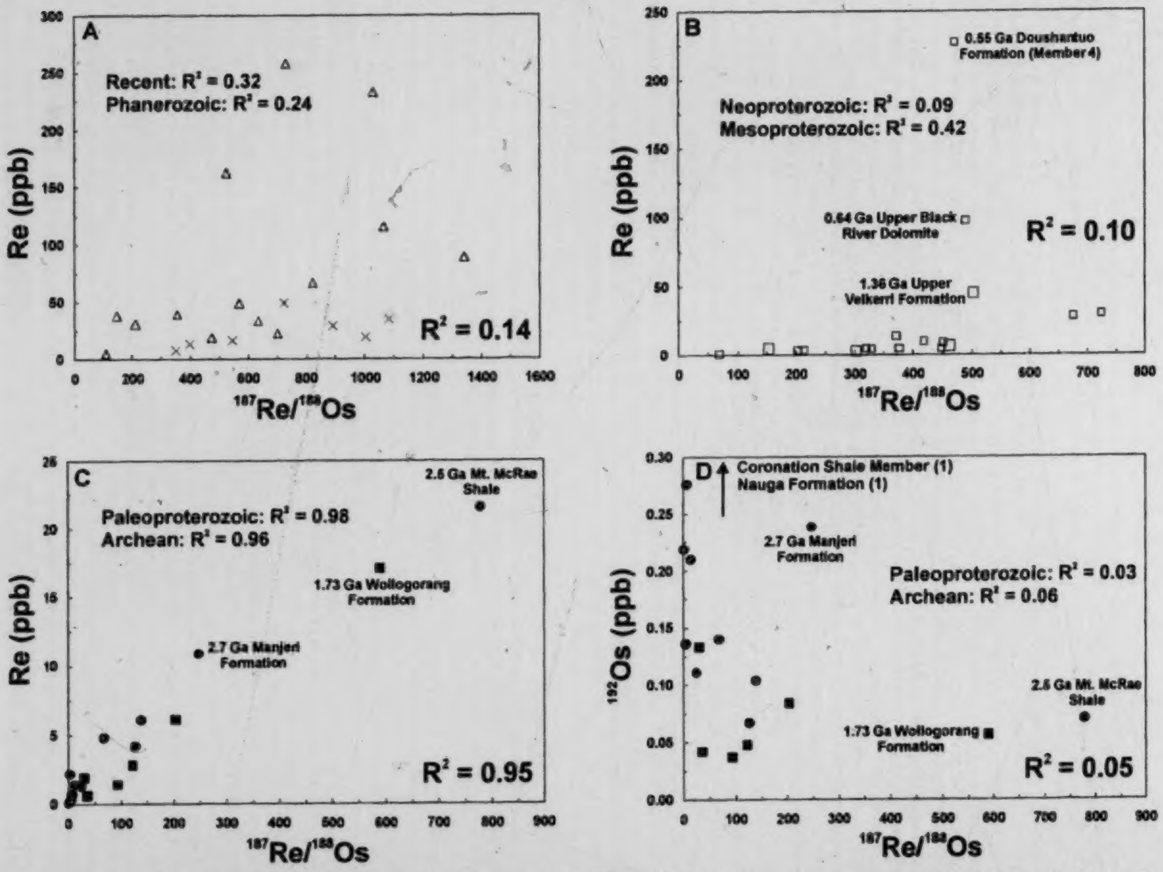

Figure 6.11: Trends between Re or ^{192}Os abundance with ^{187}Re/^{188}Os isotope ratio over geological time. See text for discussion and Table 6.3 for sources of data. (A) Re versus ^{187}Re/^{188}Os for Recent and Phanerozoic ORS (B) Re versus ^{187}Re/^{188}Os for Neoproterozoic and Mesoproterozoic ORS (C) Re versus ^{187}Re/^{188}Os for Paleoproterozoic and Archean ORS (D) ^{192}Os versus ^{187}Re/^{188}Os for Paleoproterozoic and Archean ORS. Symbols as for Figure 6.10.

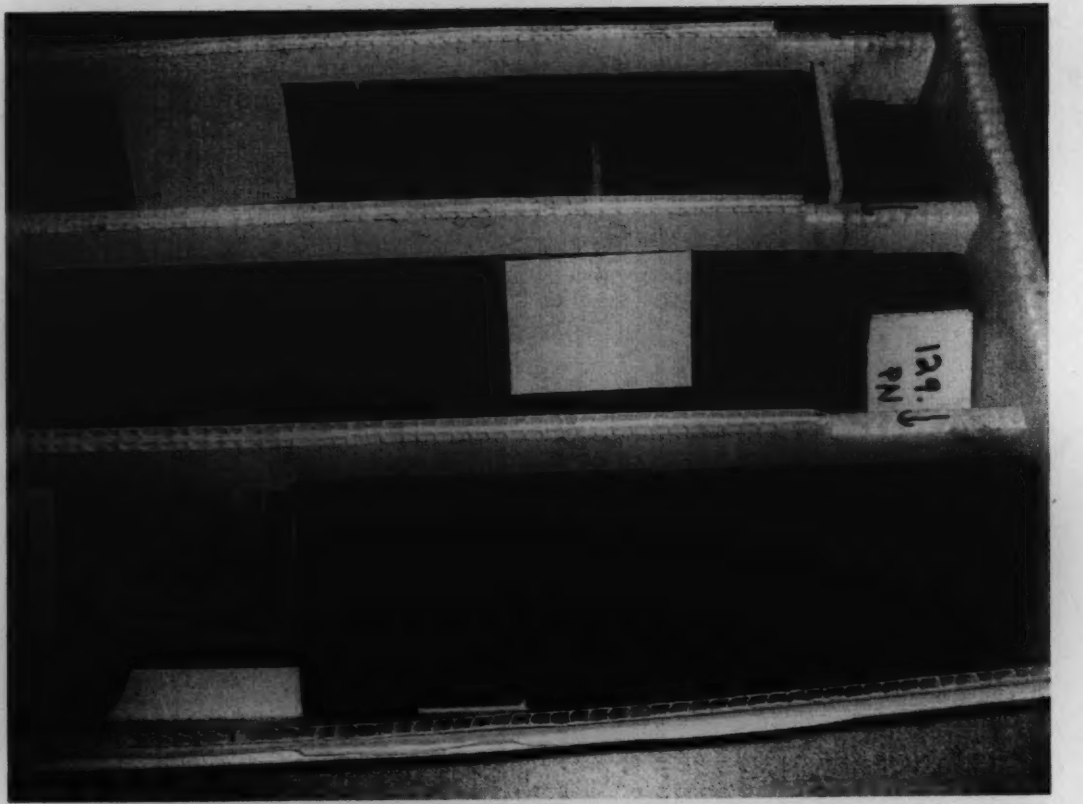

Plate 6.1: Finely laminated, pyritic black shale from the Late Archean Mt. McRae Shale (drill hole ABDP-9), Hamersley Group, Mt. Bruce Supergroup, Western Australia.

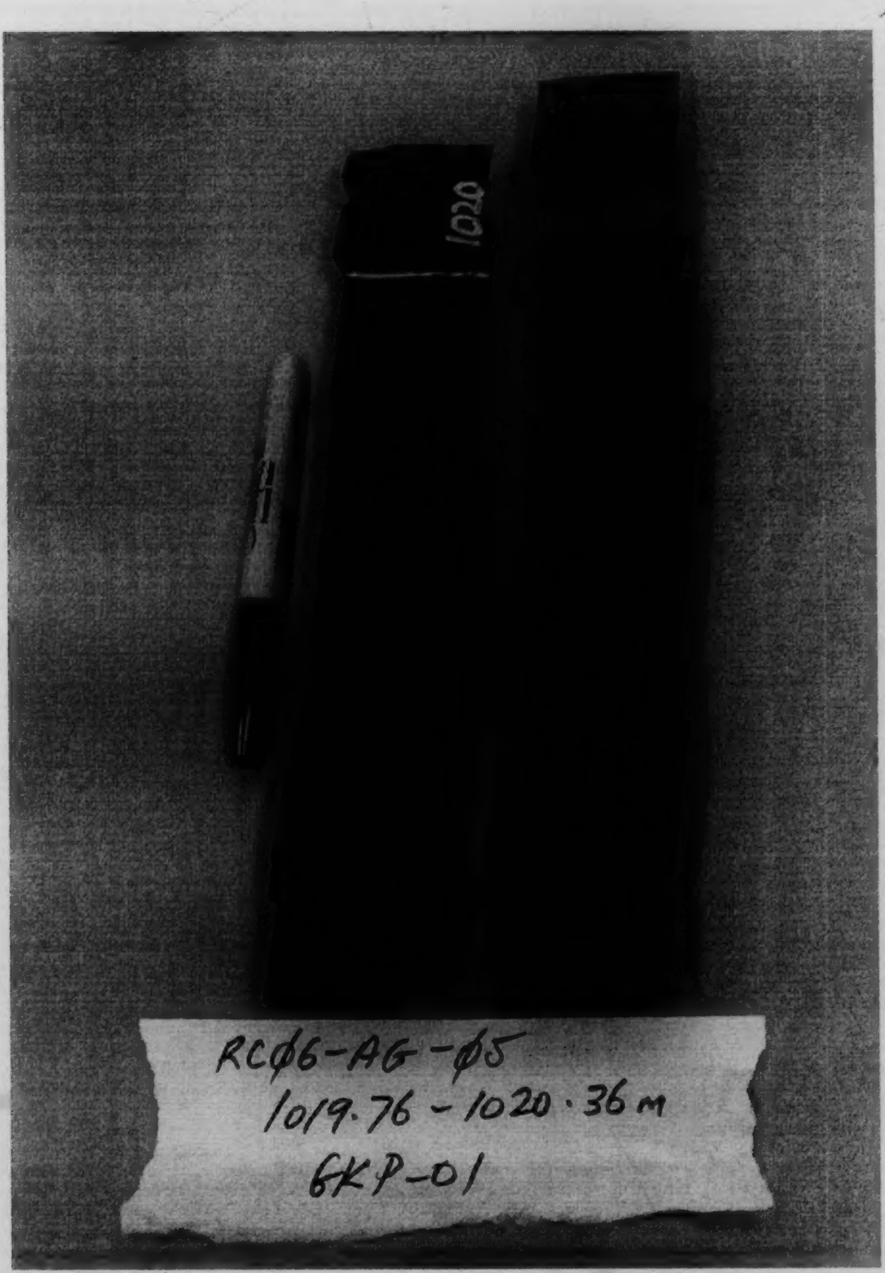
1020
RC06-AG-05
1019.76 - 1020.36 m
GKP-01

Plate 6.2: Finely laminated, pyritic black shale from the Late Archean Monteville Formation (drill hole GKP01), Campbellrand Subgroup, Ghaap Group, Transvaal Supergroup, South Africa. The carbonate-rich interval was avoided during sampling.

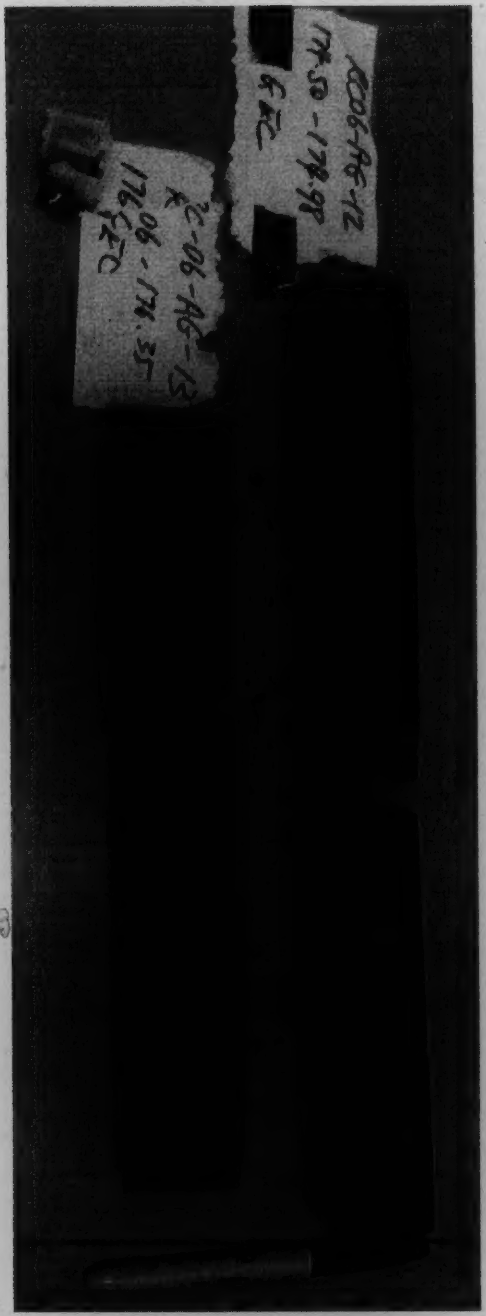
KC06-AG-12
177.50 - 178.98
GEC
KC-06-AG-13
K 06 - 176.35
176 GEC

Plate 6.3: Finely laminated dark grey shale of the Early Paleoproterozoic Klipput Shale Member, lower Nelani Formation (drill hole GEC01), Koegas Subgroup, Ghaap Group, South Africa.

REFERENCES

Acquisti, C., Kleffe, J., and Collins, S., 2007, Oxygen content of transmembrane proteins over macroevolutionary timescales: Nature, v. 445, p. 47-52.

Algeo, T.J., and Lyons, T.W., 2006, Mo – total organic carbon covariation in modern anoxic marine environments: implications for analysis of paleoredox and paleohydrographic conditions: Paleoceanography, v. 21, paper #PA1016.

Allen, J.F., and Martin, W., 2007, Out of thin air: Nature, v. 445, p. 610-612.

Altermann, W., and Nelson, D.R., 1998, Sedimentation rates, basin analysis and regional correlations of three Neoarchean and Paleoproterozoic sub-basins of the Kaapvaal craton as inferred from precise U-Pb zircon ages from volcaniclastic sediments: Precambrian Research, v. 120, p. 225-256.

Altermann, W., and Schopf, J.W., 1995, Microfossils from the Neoarchean Campbell Group, Griqualand West Sequence of the Transvaal Supergroup, and their paleoenvironmental and evolutionary implications: Precambrian Research, v. 75, p. 65-90.

Alves, S., Schiano, P., Capmas, F., and Allègre, C.J., 2002, Osmium isotope binary mixing arrays in arc volcanism: Earth and Planetary Science Letters, v. 198, p. 355-369.

Anbar, A.D., and Knoll, A.H., 2002, Proterozoic ocean chemistry and evolution: A bioinorganic bridge?: Science, v. 297, p. 1137-1142.

Anbar, A.D., Duan, Y., Lyons, T.W., Arnold, G.L., Kendall, B., Creaser, R.A., Kaufman, A.J., Gordon, G.W., Scott, C., Garvin, J., and Buick, R., 2007, A whiff of oxygen before the Great Oxidation Event?: Science, v. 317, p. 1903-1906.

Armstrong, R.A., Compston, W., Retief, E.A., Williams, I.S., and Welke, H.J., 1991, Zircon ion microprobe studies bearing on the age and evolution of the Witwatersrand triad: Precambrian Research, v. 53, p. 243-266.

Arndt, N.T., 2004, Crustal growth rates, *in* Eriksson, P.G., et al., eds., The Precambrian Earth: Tempos and events: Developments in Precambrian Geology 12, Elsevier Amsterdam, p. 155-159.

Arndt, N.T., Nelson, D.R., Compston, W., Trendall, A.F., and Thorne, A.M., 1991, The age of the Fortescue Group, Hamersley Basin, Western Australia, from ion microprobe zircon U-Pb results: Australian Journal of Earth Sciences, v. 38, p. 261-281.

Arnold, G.L., Anbar, A.D., Barling, J., and Lyons, T.W., 2004, Molybdenum isotope evidence for widespread anoxia in Mid-Proterozoic oceans: Science, v. 304, p. 87-90.

Banerjee, N.R., Simonetti, A., Furnes, H., Muehlenbachs, K., Staudigel, H., Heaman, L., and Van Kranendonk, M.J., 2007, Direct dating of Archean microbial ichnofossils: Geology, v. 35, p. 487-490.

Barley, M.E., Pickard, A.L., and Sylvester, P.J., 1997, Emplacement of a large igneous province as a possible cause of banded iron formation 2.45 billion years ago: Nature, v. 385, p. 55-58.

Barton, J.M., Jr., Blignaut, E., Salnikova, E.G., and Kotov, A.B., 1995, The stratigraphical position of the Buffelsfontein Group based on field relationships and chemical and geochronological data: South African Journal of Geology, v. 98, p. 386-392.

Bau, M.,. Romer, R.L., Lüders, V., and Beukes, N.J., 1999, Pb, O, and C isotopes in silicified Mooidraai dolomite (Transvaal Supergroup, South Africa): Implications for the composition of Paleoproterozoic seawater and 'dating' the increase of oxygen in the Precambrian atmosphere: Earth and Planetary Science Letters, v. 174, p. 43-57.

Bekker, A., Holland, H.D., Wang, P.-L., Rumble III, D., Stein, H.J., Hannah, J.L., Coetzee, L.L., and Beukes, N.J., 2004, Dating the rise of atmospheric oxygen: Nature, v. 427, p. 117-120.

Bekker, A., Karhu, J.A., and Kaufman, A.J., 2006, Carbon isotope record for the onset of the Lomagundi carbon isotope excursion in the Great Lakes area, North America: Precambrian Research, v. 148, p. 145-180.

Beukes, N.J., 1977, Transition from siliciclastic to carbonate sedimentation near the base of the Transvaal Supergroup, northern Cape Province, South Africa: Sedimentary Geology, v. 18, p. 201-221.

Beukes, N.J., 1983, Palaeoenvironmental setting of iron-formations in the depositional basin of the Transvaal Supergroup, South Africa, *in* Trendall, A.F., and Morris, S.C., eds., Iron-formations, facts, and problems: Elsevier, Amsterdam, p. 131-209.

Beukes, N.J., 1984, Sedimentology of the Kuruman and Griquatown Iron Formations, Transvaal Supergroup, Griqualand West, South Africa: Precambrian Research, v. 24, p. 47-84.

Beukes, N.J., 1987, Facies relations, depositional environments and diagenesis in a major Early Proterozoic stromatolitic carbonate platform to basinal sequence, Campbellrand Subgroup, Transvaal Supergroup, South Africa: Sedimentary Geology, v. 54, p. 1-46.

Beukes, N.J., and Klein, C., 1990, Geochemistry and sedimentology of a facies transition – from microbanded to granular iron-formation – in the early Proterozoic Transvaal Supergroup, South Africa: Precambrian Research, v. 47, p. 99-139.

Beukes, N.J., Dorland, H., Gutzmer, J., Nedachi, M., and Ohmoto, H., 2002, Tropical laterites, life on land, and the history of atmospheric oxygen in the Paleoproterozoic: Geology, v. 30, p. 491-494.

Blake, T.S., 1993, Late Archaean crustal extension, sedimentary basin formation, flood basalt volcanism and continental rifting: The Nullagine and Mount Jope Supersequences, Western Australia: Precambrian Research, v. 60, p. 185-241.

Blake, T.S., 2001, Cyclic continental mafic tuff and flood basalt volcanism in the Late Archaean Nullagine and Mount Jope Supersequences in the eastern Pilbara, Western Australia: Precambrian Research, v. 107, p. 139-177.

Blake, T.S., and Barley, M.E., 1992, Tectonic evolution of the late Archaean to early Proterozoic Mount Bruce Megasequence Set, Western Australia: Tectonics, v. 11, p. 1415-1425.

Bolhar, R., Hofmann, A., Woodhead, J., Hergt, J., and Dirks, P., 2002, Pb- and Nd-isotope systematics of stromatolitic limestones from the 2.7 Ga Ngezi Group of the Belingwe Greenstone Belt: Constraints on timing of deposition and provenance: Precambrian Research, v. 114, p. 277-294.

Brasier, M.D., Green, O.R., Jephcoat, A.P., Kleppe, A.K., Van Kranendonk, M.J., Lindsay, J.F., Steele, A., and Grassineau, N.V., 2002, Questioning the evidence for Earth's oldest fossils: Nature, v. 416, p. 76-81.

Brocks, J.J., Logan, G.A., Buick, R., and Summons, R.E., 1999, Archean molecular fossils and the early rise of eukaryotes: Science, v. 285, p. 1033-1036.

Brocks, J.J., Buick, R., Summons, R.E., and Logan, G.A., 2003a, A reconstruction of Archean biological diversity based on molecular fossils from the 2.78 to 2.45 billion-year-old Mount Bruce Supergroup, Hamersley basin, western Australia: Geochimica et Cosmochimica Acta, v. 67, p. 4321-4335.

Brocks, J.J., Buick, R., Logan, G.A., and Summons, R.E., 2003b, Composition and syngeneity of molecular fossils from the 2.78 to 2.45 billion-year-old Mount Bruce Supergroup, Pilbara Craton, Western Australia: Geochimica et Cosmochimica Acta, v. 67, p. 4289-4319.

Brocks, J.J., Love, G.D., Snape, C.E., Logan, G.A., Summons, R.E., and Buick, R., 2003c, Release of bound aromatic hydrocarbons from late Archean and Mesoproterozoic kerogens via hydropyrolysis: Geochimica et Cosmochimica Acta, v. 67, p. 1521-1530.

Buick, R., 1992, The antiquity of oxygenic photosynthesis: Evidence from stromatolites in sulphate-deficient Archaean lakes: Science, v. 255, p. 74-77.

Burton, K.W., 2005, Global weathering variations inferred from marine radiogenic isotope records: Journal of Geochemical Exploration, v. 88, p. 262-265.

Burton, K.W., Bourdon, B., Birck, J.-L., Allègre, C.J., and Hein, J.R., 1999, Osmium isotope variations in the oceans recorded by Fe-Mn crusts: Earth and Planetary Science Letters, v. 171, p. 185-197.

Cameron, E.M., 1982, Sulphate and sulphate reduction in early Precambrian oceans: Nature, v. 296, p. 145-148.

Canfield, D.E., 1998, A new model for Proterozoic ocean chemistry: Nature, v. 396, p. 450-453.

Canfield, D.E., and Raiswell, R., 1999, The evolution of the sulfur cycle: American Journal of Science, v. 299, p. 697-723.

Canfield, D.E., Habicht, K.S., and Thamdrup, B., 2000, The Archean sulfur cycle and the early history of atmospheric oxygen: Science, v. 288, p. 658-661.

Canfield, D.E., Poulton, S.W., and Narbonne, G.M., 2007, Late-Neoproterozoic deep-ocean oxygenation and the rise of animal life: Science, v. 315, p. 92-95.

Catling, D.C., and Claire, M.W., 2005, How Earth's atmosphere evolved to an oxic state: A status report: Earth and Planetary Science Letters, v. 237, p. 1-20.

Catling, D.C., Zahnle, K.J., and McKay, C.P., 2001, Biogenic methane, hydrogen escape, and the irreversible oxidation of early Earth: Science, v. 293, p. 839-843.

Catuneanu, O., and Eriksson, P.G., 1999, The sequence stratigraphic concept and the Precambrian rock record: An example from the 2.7-2.1 Ga Transvaal Supergroup, Kaapvaal craton: Precambrian Research, v. 97, p. 215-251.

Cave, R.R., Ravizza, G.E., German, C.R., Thomson, J., and Nesbitt, R.W., 2003, Deposition of osmium and other platinum-group elements beneath the ultramafic-hosted Rainbow hydrothermal plume: Earth and Planetary Science Letters, v. 210, p. 65-79.

Claire, M.W., Catling, D.C., and Zahnle, K.J., 2006, Biogeochemical modelling of the rise in atmospheric oxygen: Geobiology, v. 4, p. 239-269.

Cohen, A.S., 2004, The rhenium-osmium isotope system: applications to geochronological and paleoenvironmental problems: Journal of the Geological Society, London, v. 161, p. 729-734.

Cohen, A.S., and Coe, A.L., 2002, New geochemical evidence for the onset of volcanism in the Central Atlantic magmatic province and environmental change at the Triassic-Jurassic boundary: Geology, v. 30, p. 267-270.

Cohen, A.S., and Coe, A.L., 2007, The impact of the Central Atlantic Magmatic Province on climate and on the Sr- and Os-isotope evolution of seawater: Palaeogeography, Palaeoclimatology, Palaeoecology, v. 244, p. 374-390.

Cohen, A.S., Coe, A.L., Bartlett, J.M., and Hawkesworth, C.J., 1999, Precise Re-Os ages of organic-rich mudrocks and the Os isotope composition of Jurassic seawater: Earth and Planetary Science Letters, v. 167, p. 159-173.

Cohen, A.S., Coe, A.L., Harding, S.M., and Schwark, L., 2004, Osmium isotope evidence for the regulation of atmospheric CO_2 by continental weathering: Geology, v. 32, p. 157-160.

Colodner, D., Sachs, J., Ravizza, G., Turekian, K., Edmond, J., and Boyle, E. 1993, The geochemical cycle of rhenium: a reconnaissance: Earth and Planetary Science Letters, v. 117, p. 205-221.

Condie, K.C., 2004, Precambrian superplume events, *in* Eriksson, P.G., et al., eds., The Precambrian Earth: Tempos and events: Developments in Precambrian Geology 12, Elsevier Amsterdam, p. 163-173.

Cornell, D.H., Schütte, S.S., and Eglington, B.L., 1996, The Ongeluk basaltic andesite formation in Griqualand West, South Africa: Submarine alteration in a 2222 Ma Proterozoic sea: Precambrian Research, v. 79, p. 101-123.

Creaser, R.A., and Stasiuk, L.D., 2007, Depositional age of the Douglas Formation, northern Saskatchewan, determined by Re-Os geochronology, *in* Jefferson, C.W., and Delaney, G., eds., EXTECH IV: Geology and Uranium EXploration TECHnology of the Proterozoic Athabasca Basin, Saskatchewan and Alberta: Geological Survey of Canada Bulletin 588, p. 341-346.

Creaser, R.A., Sannigrahi, P., Chacko, T., and Selby, D. 2002, Further evaluation of the Re-Os geochronometer in organic-rich sedimentary rocks: a test of hydrocarbon maturation effects in the Exshaw Formation, Western Canada Sedimentary Basin: Geochimica et Cosmochimica Acta, v. 66, p. 3441-3452.

Crusius, J., Calvert, S., Pedersen, T., and Sage, D., 1996, Rhenium and molybdenum enrichments in sediments as indicators of oxic, suboxic, and sulfidic conditions of deposition: Earth and Planetary Science Letters, v. 145, p. 65-78.

Dalai, T.K., Singh, S.K., Trivedi, J.R., and Krishnaswami, S., 2002, Dissolved Re in the Yamuna river system and the Ganga in the Himalaya: Role of black shale weathering in the budgets of Re, Os, and U in rivers and CO_2 in the atmosphere: Geochimica et Cosmochimica Acta, v. 66, p. 29-43.

Dalai, T.K., Suzuki, K., Minagawa, M., and Nozaki, Y., 2005, Variations in seawater osmium isotope composition since the last glacial maximum: A case study from the Japan Sea: Chemical Geology, v. 220, p. 303-314.

Dalai, T.K., Ravizza, G.E., and Peucker-Ehrenbrink, B., 2006, The Late Eocene $^{187}Os/^{188}Os$ excursion: Chemostratigraphy, cosmic dust flux and the Early Oligocene glaciation: Earth and Planetary Science Letters, v. 241, p. 477-492.

Dutkiewicz, A., Volk, H., George, S.C., Ridley, J., and Buick, R., 2006, Biomarkers from Huronian oil-bearing fluid inclusions: An uncontaminated record of life before the Great Oxidation Event: Geology, v. 34, p. 437-440.

Eigenbrode, J.L., and Freeman, K.H., 2006, Late Archean rise of aerobic microbial ecosystems: Proceedings of the National Academy of Sciences, v. 103, p. 15759-15764.

El Tabakh, M., Grey, K., Pirajno, F., and Schreiber, B.C., 1999, Pseudomorphs after evaporitic minerals interbedded with 2.2 Ga stromatolites of the Yerrida Basin, Western Australia: Origin and significance: Geology, v. 27, p. 871-874.

England, G.L., Rasmussen, B., Krapez, B., and Groves, D.I., 2002, Palaeoenvironmental significance of rounded pyrite in siliciclastic sequences of the Late Archaean Witwatersrand Basin: Oxygen-deficient atmosphere or hydrothermal alteration: Sedimentology, v. 49, p. 1133-1156.

Eriksson, P.G., and Cheney, E.S., 1992, Evidence for the transition to an oxygen-rich atmosphere during the evolution of red beds in the lower Proterozoic sequences of southern Africa: Precambrian Research, v. 54, p. 257-269.

Eriksson, P.G., Altermann, W., Catuneanu, O., Van der Merwe, R., and Bumby, A.J., 2001, Major influences on the evolution of the 2.67-2.1 Ga Transvaal basin, Kaapvaal craton: Sedimentary Geology, v. 141-142, p. 205-231.

Ernst, R.E., Buchan, K.L., and Prokoph, A., 2004, Large igneous province record through time, *in* Eriksson, P.G., et al., eds., The Precambrian Earth: Tempos and events: Developments in Precambrian Geology 12, Elsevier Amsterdam, p. 173-180.

Esser, B.K., and Turekian, K.K., 1988, Accretion rate of extraterrestrial particles determined from osmium isotope systematics of Pacific pelagic clay and manganese nodules: Geochimica et Cosmochimica Acta, v. 52, p. 1383-1388.

Esser, B.K., and Turekian, K.K., 1993, The osmium isotopic composition of the continental crust: Geochimica et Cosmochimica Acta, v. 57, p. 3093-3104.

Farquhar, J., and Wing, B.A., 2003, Multiple sulfur isotopes and the evolution of the atmosphere: Earth and Planetary Science Letters, v. 213, p. 1-13.

Farquhar, J., Bao, H., and Thiemens, M., 2000, Atmospheric influence of Earth's earliest sulfur cycle: Science, v. 289, p. 756-758.

Farquhar, J., Peters, M., Johnston, D.T., Strauss, H., Masterson, A., Wiechert, U., and Kaufman, A.J., 2007, Isotopic evidence for Mesoarchaean anoxia and changing atmospheric sulphur chemistry: Nature, v. 449, p. 706-709.

Fedo, C.M., and Whitehouse, M.J., 2002, Metasomatic origin of quartz-pyroxene rock, Akilia, Greenland, and implications for Earth's earliest life: Science, v. 296, p. 1448-1452.

Fike, D.A., Grotzinger, J.P., Pratt, L.M., and Summons, R.E., 2006, Oxidation of the Ediacaran Ocean: Nature, v. 444, p. 744-747.

Fleet, M.E., 1998, Detrital pyrite in Witwatersrand gold reefs: X-ray diffraction evidence and implications for atmospheric evolution: Terra Nova, v. 10, p. 302-306.

Frey, M., de Capitani, C., and Liou, J.G., 1991, A new petrogenetic grid for low-grade metabasites: Journal of Metamorphic Geology, v. 9, p. 497-509.

Furnes, H., Banerjee, N.R., Muehlenbachs, K., Staudigel, H., and de Wit, M., 2004, Early life recorded in Archean pillow lavas: Science, v. 304, p. 578-581.

Gannoun, A., Burton, K.W., Thomas, L.E., Parkinson, I.J., van Calsteren, P., and Schiano, P., 2004, Osmium isotope heterogeneity in the constituent phases of mid-ocean ridge basalts: Science, v. 303, p. 70-72.

Gannoun, A., Burton, K.W., Vigier, N., Gíslason, S.R., Rogers, N., Mokadem, F., and Sigfússon, B., 2006, The influence of weathering process on riverine osmium isotopes in a basaltic terrain: Earth and Planetary Science Letters, v. 243, p. 732-748.

García-Ruiz, J.M., Hyde, S.T., Carnerup, A.M., Christy, A.G., Van Kranendonk, M.J., and Welham, N.J., 2002, Self-assembled silica-carbonate structures and detection of ancient microfossils: Science, v. 302, p. 1194-1197.

Glickson, A., and Vickers, J., 2007, Asteroid mega-impacts and Precambrian banded iron formations: 2.63 Ga and 2.56 Ga impact ejecta/fallout at the base of BIF/argillite units, Hamersley Basin, Pilbara Craton, Western Australia: Earth and Planetary Science Letters, v. 254, p. 214-226.

Godderis, Y., and Veizer, J., 2000, Tectonic control of chemical and isotopic composition of ancient oceans: The impact of continental growth: American Journal of Science, v. 300, p. 434-461.

Goldblatt, C., Lenton, T.M., and Watson, A.J., 2006, Bistability of atmospheric oxygen and the Great Oxidation: Nature, v. 443, p. 683-686.

Goodwin, A.M., Monster, J., and Thode, H.G., 1976, Carbon and sulfur isotope abundances in Archean iron-formations and early Precambrian life: Economic Geology, v. 71, p. 870-891.

Graham, S., Karlsen, D.A., Dypvik, H., Andersen, T., and Backer-Owe, K., 2006, Re-Os variations in North Sea shales and oils: Geochimica et Cosmochimica Acta, v. 70 (18; supplement 1), p. A211.

Habicht, K.S., Gade, M., Thamdrup, B., Berg, P., and Canfield, D.E., 2002, Calibration of sulfate levels in the Archean ocean: Science, v. 298, p. 2372-2374.

Hannah, J.L., Bekker, A., Stein, H.J., Markey, R.J., and Holland, H.D., 2004, Primitive Os and 2316 Ma age for marine shale: Implications for Paleoproterozoic glacial events and the rise of atmospheric oxygen: Earth and Planetary Science Letters, v. 225, p. 43-52.

Hannah, J.L., Stein, H.J., Zimmerman, A., Yang, G., Markey, R.J., and Melezhik, V.A., 2006, Precise 2004 ± 9 Ma Re-Os age for the Pechenga black shale: Comparison of sulfides and organic material: Geochimica et Cosmochimica Acta, v. 70 (18; supplement 1), p. A228.

Harrison, T.M., Blichert-Toft, J., Müller, W., Albarede, F., Holden, P., and Mojzsis, S.J., 2005, Heterogeneous Hadean hafnium: evidence of continental crust at 4.4 to 4.5 Ga: Science, v. 310, p. 1947-1950.

Hattori, Y., Suzuki, K., Honda, M., and Shimizu, H., 2003, Re-Os isotope systematics of the Taklimakan Desert sands, moraines and river sediments around the Taklimakan Desert, and of Tibetan soils: Geochimica et Cosmochimica Acta, v. 67, p. 1195-1205.

Hayes, J.M., 1983, Geochemical evidence bearing on the origin of aerobiosis, a speculative hypothesis, *in* Schopf, J.W., ed., Earth's earliest biosphere: Its origin and evolution: Princeton University Press, Princeton, p. 291-301.

Hayes, J.M., and Waldbauer, J.R., 2006, The carbon cycle and associated redox processes through time: Philosophical Transactions of the Royal Society B, v. 361, p. 931-950.

Huh, Y., Birck, J.-L., and Allègre, C.J., 2004, Osmium isotope geochemistry in the Mackenzie River basin: Earth and Planetary Science Letters, v. 222, p. 115-129.

Hofmann, H.J., Grey, K., Hickman, A.H., and Thorpe, R.I., 1999, Origin of 3.45 Ga coniform stromatolites in Warrawoona Group, western Australia: Geological Society of America Bulletin, v. 111, p. 1256-1262.

Holland, H.D., 2002, Volcanic gases, black smokers, and the Great Oxidation Event: Geochimica et Cosmochimica Acta, v. 66, p. 3811-3826.

Horan, M.F., Morgan, J.W., Grauch, R.I., Coveney, R.M., Jr., Murowchick, J.B., and Hulbert, L.J., 1994, Rhenium and osmium isotopes in black shales and Ni-Mo-PGE-rich sulfide layers, Yukon Territory, Canada, and Hunan and Guizhou provinces, China: Geochimica et Cosmochimica Acta, v. 58, p. 257-265.

Iizuka, T., Horie, K., Komiya, T., Maruyama, S., Hirata, T., Hidaka, H., and Windley, B.F., 2006, 4.2 Ga zircon xenocryst in an Acasta gneiss from northwestern Canada: Evidence for early continental crust: Geology, v. 34, p. 245-248.

Jaffe, L.A., Peucker-Ehrenbrink, B., and Petsch, S.T., 2002, Mobility of rhenium, platinum group elements and organic carbon during black shale weathering: Earth and Planetary Science Letters, v. 198, p. 339-353.

Kakegawa, T., Kawai, H., and Ohmoto, H., 1999, Origins of pyrites in the ~ 2.5 Ga Mt. McRae Shale, the Hamersley District, Western Australia: Geochimica et Cosmochimica Acta, v. 62, p. 3205-3220.

Kamber, B.S., and Whitehouse, M.J., 2007, Micro-scale sulphur isotope evidence for sulphur cycling in the late Archean shallow ocean: Geobiology, v. 5, p. 5-17.

Kasting, J.F., 1993, Earth's early atmosphere: Science, v. 259, p. 920-926.

Kasting, J.F., 2001, The rise of atmospheric oxygen: Science, v. 293, p. 819-820.

Kasting, J.F., 2006, Ups and downs of ancient oxygen: Nature, v. 443, p. 643-645.

Kaufman, A.J., Johnston, D.T., Farquhar, J., Masterson, A.L., Lyons, T.W., Bates, S., Anbar, A.D., Arnold, G.L., Garvin, J., and Buick, R., 2007, Late Archean biospheric oxygenation and atmospheric evolution: Science, v. 317, p. 1900-1903.

Kazmierczak, J., and Altermann, W., 2002, Neoarchean biomineralization by benthic cyanobacteria: Science, v. 298, p. 2351.

Kazmierczak, J., and Kremer, B., 2002, Thermal alteration of the Earth's oldest fossils: Nature, v. 420, p. 477-478.

Kendall, B.S., 2003, Evaluation of the Re-Os geochronometer in organic-rich mudrocks as a method for constraining the absolute ages of Neoproterozoic glaciogenic deposits: Unpublished M.Sc. Thesis, University of Alberta.

Kendall, B.S., Creaser, R.A., Ross, G.M., and Selby, D., 2004, Constraints on the timing of Marinoan "Snowball Earth" glaciation by ^{187}Re-^{187}Os dating of a Neoproterozoic, post-glacial black shale in Western Canada: Earth and Planetary Science Letters, v. 222, p. 729-740.

Kennedy, M., Droser, M., Mayer, L.M., Pevear, D., Mrofka, D., 2006, Late Precambrian oxygenation; inception of the clay mineral factory: Science, v. 311, p. 1446-1449.

Kirschvink, J.L., 2006, Archean sterol biomarkers do not prove oxygenic photosynthesis: Geochimica et Cosmochimica Acta, v. 70 (18), p. A320.

Kirschvink, J.L., Gaidos, E.J., Bertani, L.E., Beukes, N.J., Gutzmer, J., Maepa, L.N., and Steinberger, R.E., 2000, Paleoproterozoic snowball Earth: Extreme climatic and geochemical global change and its biological consequences: Proceedings of the National Academy of Sciences, v. 97, p. 1400-1405.

Klein, C., and Beukes, N.J., 1989, Geochemistry and sedimentology of a facies transition from limestone to iron-formation deposition in the Early Proterozoic Transvaal Supergroup, South Africa: Economic Geology, v. 84, p. 1733-1742.

Klemm, V., Levasseur, S., Frank, M., Hein, J.R., and Halliday, A.N., 2005, Osmium isotope stratigraphy of a marine ferromanganese crust: Earth and Planetary Science Letters, v. 238, p. 42-48.

Koide, M., Hodge, V.F., Yang, J.S., Stallard, M., and Goldberg, E.G., 1986, Some comparative marine chemistries of rhenium, gold, silver and molybdenum: Applied Geochemistry, v. 1, p. 705-714.

Kump, L.R., and Barley, M.E., 2007, Increased subaerial volcanism and the rise of atmospheric oxygen 2.5 billion years ago: Nature, v. 448, p. 1033-1036.

Levasseur, S., Birck, J.-L., and Allègre, C.J., 1998, Direct measurement of femtomoles of osmium and the ^{187}Os/^{186}Os ratio in seawater: Science, v. 282, p. 272-274.

Levasseur, S., Birck, J.-L., and Allègre, C.J., 1999, The osmium riverine flux and the oceanic mass balance of osmium: Earth and Planetary Science Letters, v. 174, p. 7-23.

Lowe, D.R., and Tice, M.M., 2007, Tectonic controls on atmospheric, climatic, and biological evolution 3.5-2.4 Ga: Precambrian Research, v. 158, p. 177-197.

Lyons, T.W., Kah, L.C., and Gellatly, A.M., 2004, The Precambrian sulphur isotope record of evolving atmospheric oxygen, *in* Eriksson, P.G., et al., eds., Developments in Precambrian geology 12, The Precambrian Earth: Tempos and events, Elsevier B.V., p. 421-440.

Martin, C.E., Peucker-Ehrenbrink, B., Brunskill, G.J., and Szymczak, R., 2000, Sources and sinks of unradiogenic osmium runoff from Papua New Guinea: Earth and Planetary Science Letters, v. 183, p. 261-274.

Martin, D.M., Clendenin, C.W., Krapez, B., and McNaughton, N.J., 1998, Tectonic and geochronological constraints on late Archaean and Palaeoproterozoic stratigraphic correlation within and between the Kaapvaal and Pilbara Cratons: Geological Society [London] Journal, v. 155, p. 311-322.

Mathur, R., Ruiz, J., and Tornos, F., 1999, Age and sources of the ore at Tharsis and Rio Tinto, Iberian Pyrite Belt, from Re-Os isotopes: Mineralium Deposita, v. 34, p. 790-793.

McKeegan, K.D., Kudryavtsev, A.B., and Schopf, J.W., 2007, Raman and ion microscopic imagery of graphitic inclusions in apatite from older than 3830 Ma Akilia supracrustal rocks, west Greenland: Geology, v.35, p. 591-594.

Meisel, T., Walker, R.J., Irving, A.J., and Lorand, J.-P., 2001, Osmium isotopic compositions of mantle xenoliths: a global perspective: Geochimica et Cosmochimica Acta, v. 65, p. 1311-1323.

Melezhik, V.A., Huhma, H., Condon, D.J., Fallick, A.E., and Whitehouse, M.J., 2007, Temporal constraints on the Paleoproterozoic Lomagundi-Jatuli carbon isotopic event: Geology, v. 35, p. 655-658.

Menneken, M., Nemchin, A.A., Geisler, T., Pidgeon, R.T., and Wilde, S.A., 2007, Hadean diamonds in zircon from Jack Hills, Western Australia: Nature, v. 448, p. 917-920.

Miller, C.A., 2004. Re-Os dating of algal laminites: Reduction-enrichment of metals in the sedimentary environment and evidence of new geoporphyrins. Unpublished M.Sc. thesis, University of Saskatchewan.

Mojzsis, S.J., Arrhenius, G., McKeegan, K.D., Harrison, T.M., Nutman, A.P., and Friend, C.R.L., 1996, Evidence for life on Earth before 3,800 million years ago: Nature, v. 384, p. 55-59.

Mojzsis, S.J., Harrison, T.M., and Pidgeon, R.T., 2001, Oxygen-isotope evidence from ancient zircons for liquid water at the Earth's surface 4,300 Myr ago: Nature, v. 409, p. 178-181.

Morelli, R.M., Creaser, R.A., Selby, D., Kelley, K.D., Leach, D.L., and King, A.R., 2004, Re-Os sulfide geochronology of the Red Dog sediment-hosted Zn-Pb-Ag deposit, Brooks Range, Alaska: Economic Geology, v. 99, p. 1569-1576.

Morford, J.L., and Emerson, S., 1999, The geochemistry of redox sensitive trace metals in sediments: Geochimica et Cosmochimica Acta, v. 63, p. 1735-1750.

Morford, J.L., Emerson, S.R., Breckel, E.J., and Kim, S.H., 2005, Diagenesis of oxyanions (V, U, Re, and Mo) in pore waters and sediments from a continental margin: Geochimica et Cosmochimica Acta, v. 69, p. 5021-5032.

Morris, R.C., 1993, Genetic modeling for banded iron-formation of the Hamersley Group, Pilbara Craton, Western Australia: Precambrian Research, v. 60, p. 243-286.

Morris, R.C., and Horowitz, R.C., 1983, The origin of the iron-formation-rich Hamersley Group of Western Australia – Deposition on a platform: Precambrian Research, v. 21, p. 273-297.

Nakamura, K., and Kato, Y., 2007, A new geochemical approach for constraining a marine redox condition of Early Archean: Earth and Planetary Science Letters, v. 261, p.296-302.

Nelson, D.R., Trendall, A.F., and Altermann, W., 1999, Chronological correlations between the Pilbara and Kaapvaal cratons: Precambrian Research, v. 97, p. 165-189.

Ohmoto, H., 1996, Evidence in pre-2.2 Ga paleosols for the early evolution of atmospheric oxygen and terrestrial biota: Geology, v. 24, p. 1135-1138.

Ohmoto, H., 2004, Archaean atmosphere, hydrosphere and biosphere, *in* Eriksson, P.G., et al., eds., Developments in Precambrian geology, 12, The Precambrian Earth: Tempos and events, Elsevier B.V., p. 361-388.

Ohmoto, H., Watanabe, Y., Ikemi, H., Poulson, S.R., and Taylor, B.E., 2006, Sulphur isotope evidence for an oxic Archaean atmosphere: Nature, v. 442, p. 908-911.

Ono, S., Eigenbrode, J.L., Pavlov, A.A., Kharecha, P., Rumble III, D., Kasting, J.F., and Freeman, K.H., 2003, New insights into Archean sulfur cycle from mass-independent sulfur isotope records from the Hamersley Basin, Australia: Earth and Planetary Science Letters, v. 213, p. 15-30.

Ono, S., Beukes, N.J., Rumble, D., and Fogel, M.L., 2006, Early evolution of atmospheric oxygen from multiple-sulfur and carbon isotope records of the 2.9 Ga Mozaan Group of the Pongola Supergroup, southern Africa: South African Journal of Geology, v. 109, p. 97-108.

Oxburgh, R., 1998, Variations in the osmium isotope composition of seawater over the past 200,000 years: Earth and Planetary Science Letters, v. 159, p. 183-191.

Oxburgh, R., 2001, Residence time of osmium in the oceans: Geochemistry, Geophysics, Geosystems, Paper #2000GC000104.

Palmer, M.R., and Turekian, K.K., 1986, $^{187}Os/^{186}Os$ in marine manganese nodules and the constraints on the crustal geochemistries of rhenium and osmium: Nature, v. 319, p. 216-220.

Palmer, M.R., Falkner, K.K., Turekian, K.K., and Calvert, S.E., 1988, Sources of osmium isotopes in manganese nodules: Geochimica et Cosmochimica Acta, v. 52, p. 1197-1202.

Papineau, D., and Mojzsis, S.J., 2006, Mass-independent fractionation of sulfur isotopes in sulfides from the pre-3770 Ma Isua Supracrustal Belt, West Greenland: Geobiology, v. 4, p. 227-238.

Papineau, D., Mojzsis, S.J., and Schmitt, A.K., 2007, Multiple sulfur isotopes from Paleoproterozoic Huronian interglacial sediments and the rise of atmospheric oxygen: Earth and Planetary Science Letters, v. 255, p. 188-212.

Pasteris, J.D., Wopenka, B., Schopf, J.W., Kudryavtsev, A.B., Agresti, D.G., Wdowiak, T.J., and Czaja, A.D., 2002, Images of the Earth's earliest fossils?: Nature, v. 420, p. 476-477.

Pavlov, A.A., and Kasting, J.F., 2002, Mass-independent fractionation of sulfur isotopes in Archean sediments: strong evidence for an anoxic Archean atmosphere: Astrobiology, v. 2, p. 27-41.

Pegram, W.J., and Turekian, K.K., 1999, The osmium isotopic composition change of Cenozoic sea water as inferred from a deep-sea core corrected for meteoritic contributions: Geochimica et Cosmochimica Acta, v. 63, p. 4053-4058.

Petsch, S.T., Berner, R.A., and Eglinton, T.I., 2000, A field study of the chemical weathering of ancient sedimentary organic matter: Organic Geochemistry, v. 31, p. 475-487.

Peucker-Ehrenbrink, B., 1996, Accretion of extraterrestrial matter during the last 80 million years and its effect on the marine osmium isotope record: Geochimica et Cosmochimica Acta, v. 60, p. 3187-3196.

Peucker-Ehrenbrink, B., and Blum, J.D., 1998, Re-Os isotope systematics and weathering of Precambrian crustal rocks: Implications for the marine osmium isotope record: Geochimica et Cosmochimica Acta, v. 62, p. 3193-3203.

Peucker-Ehrenbrink, B., and Hannigan, R.E., 2000, Effects of black shale weathering on the mobility of rhenium and platinum group elements: Geology, v. 28, p. 475-478.

Peucker-Ehrenbrink, B., and Ravizza, G., 1996, Continental runoff of osmium into the Baltic Sea: Geology, v. 24, p. 327-330.

Peucker-Ehrenbrink, B., and Ravizza, G., 2000, The marine osmium isotope record: Terra Nova, v. 12, p. 205-219.

Peucker-Ehrenbrink, B., and Jahn, B.-M., 2001, Rhenium-osmium isotope systematics and platinum group element concentrations: loess and the upper continental crust: Geochemistry Geophysics Geosystems, v. 2, Paper 2001GC000172.

Peucker-Ehrenbrink, B., Ravizza, G., and Hofmann, A.W., 1995, The marine $^{187}Os/^{186}Os$ record of the past 80 million years: Earth and Planetary Science Letters, v. 130, p. 155-167.

Pickard, A.L., 2003, SHRIMP U-Pb zircon ages for the Palaeoproterozoic Kuruman Iron Formation, Northern Cape Province, South Africa: Evidence for simultaneous BIF deposition on Kaapvaal and Pilbara Cratons: Precambrian Research, v. 125, p. 275-315.

Pierson-Wickmann, A.-C., Reisberg, L., and France-Lanord, C., 2002, Behavior of Re and Os during low-temperature alteration: results from Himalayan soils and altered black shales: Geochimica et Cosmochimica Acta, v. 66, p. 1539-1548.

Poirier, A., 2006, Re-Os and Pb isotope systematics in reduced fjord sediments from Saanich Inlet (Western Canada): Earth and Planetary Science Letters, v. 249, p. 119-131.

Polteau, S., Moore, J.M., and Tsikos, H., 2006, The geology and geochemistry of the Palaeoproterozoic Makganyene diamictite: Precambrian Research, v. 148, p. 257-274.

Poujol, M., Robb, L.J., Anhaeusser, C.R., Gericke, B., 2003, A review of the geochronological constraints on the evolution of the Kaapvaal Craton, South Africa: Precambrian Research, v. 127, p. 181-213.

Rashby, S.E., Sessions, A.L., Summons, R.E., and Newman, D.K., 2007, Biosynthesis of 2-methylbacteriohopanepolyols by an anoxygenic phototroph: Proceedings of the National Academy of Sciences, v. 104, p. 15099-15104.

Rasmussen, B., and Buick, R., 1999, Redox state of the Archean atmosphere: Evidence from detrital heavy minerals in ca. 3250-2750 Ma sandstones from the Pilbara craton, Australia: Geology, v. 27, p. 115-118.

Rasmussen, B., Blake, T.S., and Fletcher, I.R., 2005, U-Pb zircon age constraints on the Hamersley spherule beds: Evidence for a single 2.63 Ga Jeerinah-Carawine impact ejecta layer: Geology, v. 33, p. 725-728.

Ravizza, G., and Peucker-Ehrenbrink, B., 2003a, Chemostratigraphic evidence of Deccan volcanism from the marine osmium isotope record: Science, v. 302, p. 1392-1395.

Ravizza, G., and Peucker-Ehrenbrink, B., 2003b, The ^{187}Os/^{188}Os record of the Eocene-Oligocene transition: The interplay of weathering and glaciation: Earth and Planetary Science Letters, v. 210, p. 151-165.

Ravizza, G., and Turekian, K.K., 1989, Application of the ^{187}Re-^{187}Os system to black shale geochronometry: Geochimica et Cosmochimica Acta, v. 53, p. 3257-3262.

Ravizza, G., and Turekian, K.K., 1992, The osmium isotopic composition of organic-rich marine sediments: Earth and Planetary Science Letters, v. 110, p. 1-6.

Ravizza, G., Turekian, K.K., and Hay, B.J., 1991, The geochemistry of rhenium and osmium in recent sediments from the Black Sea: Geochimica et Cosmochimica Acta, v. 55, p. 3741-3752.

Ravizza, G., Martin, C.E., German, C.R., and Thompson, G., 1996, Os isotopes as tracers in seafloor hydrothermal systems: Metalliferous deposits from the TAG hydrothermal area, 26°N Mid-Atlantic Ridge: Earth and Planetary Science Letters, v. 138, p. 105-119.

Ravizza, G., Sherrell, R.M., Field, M.P., and Pickett, E.A., 1999, Geochemistry of the Margi umbers, Cyprus, and the Os isotope composition of Cretaceous seawater: Geology, v. 27, p. 971-974.

Ravizza, G., Norris, R.N., Blusztajn, J., and Aubry, M.-P., 2001, An osmium isotope excursion associated with the late Paleocene thermal maximum: Evidence of intensified chemical weathering: Paleoceanography, v. 16, p. 155-163.

Raymond, J., Zhaxybayeva, O., Gogarten, J.P., Gerdes, S.Y., and Blankenship, R.E., 2002, Whole-genome analysis of photosynthetic prokaryotes: Science, v. 298, p. 1616-1620.

Reusch, D.N., Ravizza, G., Maasch, K.A., and Wright, J.D., 1998, Miocene seawater ^{187}Os/^{188}Os ratios inferred from metalliferous carbonates: Earth and Planetary Science Letters, v. 160, p. 163-178.

Ripley, E.M., Park, Y.-R., Lambert, D.D., and Frick, L.R., 2001, Re-Os isotopic composition and PGE contents of Proterozoic carbonaceous argillites, Virginia Formation, Northeastern Minnesota: Organic Geochemistry, v. 32, p. 857-866.

Rosing, M.T., 1999, ^{13}C-depleted carbon microparticles in > 3700-Ma sea-floor sedimentary rocks from West Greenland: Science, v. 283, p. 674-676.

Rosing, M.T., and Frei, R., 2004, U-rich Archaean sea-floor sediments from Greenland – Indications of > 3700 Ma oxygenic photosynthesis: Earth and Planetary Science Letters, v. 217, p. 237-244.

Ryder, G., 2003, Bombardment of the Hadean Earth: Wholesome or deleterious?: Astrobiology, v. 3, p. 3-6.

Rye, R., and Holland, H.D., 1998, Paleosols and the evolution of atmospheric oxygen: A critical review: American Journal of Science, v. 298, p. 621-672.

Schaefer, B.F., and Burgess, J.M., 2003, Re-Os isotopic age constraints on deposition in the Neoproterozoic Amadeus Basin: Implications for the 'Snowball Earth': Geological Society (London) Journal, v. 160, p. 825-828.

Schidlowski, M., 1988, A 3,800-million-year isotopic record of life from carbon in sedimentary rocks: Nature, v. 333, p. 313-318.

Schidlowski, M., 2001, Carbon isotopes as biogeochemical recorders of life over 3.8 Ga of Earth history: Evolution of a concept: Precambrian Research, v. 106, p. 117-134.

Schidlowski, M., Hayes, J.M., and Kaplan, I.R., 1983, Isotopic inferences of ancient biogeochemistries: Carbon, sulfur, hydrogen, and nitrogen, *in* Schopf, J.W., ed., Earth's earliest biosphere: Its origin and evolution: Princeton University Press, Princeton, p. 149-186.

Schmitz, M.D., and Bowring, S.A., 2003, Ultra-high temperature metamorphism in the lower crust during Neoarchean Ventersdorp rifting and magmatism, Kaapvaal Craton, southern Africa: Geological Society of America Bulletin, v. 115, p. 533-548.

Schopf, J.W., 1993, Microfossils of the early Archean Apex Chert: New evidence of the antiquity of life: Science, v. 260, p. 640-646.

Schopf, J.W., 2004, Earth's earliest biosphere: Status of the hunt, *in* Eriksson, P.G., et al., eds., Developments in Precambrian geology 12, The Precambrian Earth: Tempos and events, Elsevier B.V., p. 516-539.

Schopf, J.W., and Packer, B.M., 1987, Early Archean (3.3-billion to 3.5-billion-year-old) microfossils from Warrawoona Group, Australia: Science, v. 237, p. 70-73.

Schopf, J.W., Kudryavtsev, A.B., Agresti, D.G., Wdowiak, T.J., and Czaja, A.D., 2002, Laser-Raman imagery of Earth's earliest fossils: Nature, v. 416, p. 73-76.

Schopf, J.W., Kudryavtsev, A.B., Czaja, A.D., and Tripathi, A.B., 2007, Evidence of Archean life: Stromatolites and microfossils: Precambrian Research, v. 158, p. 141-155.

Schröder, S., Lacassie, J.P., and Beukes, N.J., 2006, Stratigraphic and geochemical framework of the Agouron drill cores, Transvaal Supergroup (Neoarchean-Paleoproterozoic, South Africa): South African Journal of Geology, v. 109, p. 23-54.

Selby, D., Direct rhenium-osmium age of the Oxfordian-Kimmeridgian boundary, Staffin Bay, Isle of Skye, UK and the Late Jurassic timescale: Norwegian Journal of Geology, in press.

Selby, D., and Creaser, R.A., 2003, Re-Os geochronology of organic-rich sediments: an evaluation of organic matter analysis methods: Chemical Geology, v. 200, p. 225-240.

Selby, D., and Creaser, R.A., 2004, Macroscale NTIMS and microscale LA-MC-ICP-MS Re-Os isotopic analysis of molybdenite: Testing spatial restrictions for reliable Re-Os age determinations, and implications for the decoupling of Re and Os within molybdenite: Geochimica et Cosmochimica Acta, v. 68, p. 3897-3908.

Selby, D., and Creaser, R.A., 2005, Direct radiometric dating of the Devonian-Mississippian time-scale boundary using the Re-Os black shale geochronometer: Geology, v. 33, p. 545-548.

Selby, D., Creaser, R.A., Stein, H.J., Markey, R.J., and Hannah, J.L., 2007, Assessment of the ^{187}Re decay constant by cross calibration of Re-Os molybdenite and U-Pb zircon chronometers in magmatic ore systems: Geochimica et Cosmochimica Acta, v.71, p. 1999-2013.

Sharma, M., Papanastassiou, D.A., and Wasserburg, G.J., 1997, The concentration and isotopic composition of osmium in the oceans: Geochimica et Cosmochimica Acta, v. 61, p. 3287-3299.

Sharma, M., Wasserburg, G.J., Hofmann, A.W., and Butterfield, D.A., 2000, Osmium isotopes in hydrothermal fluids from the Juan de Fuca Ridge: Earth and Planetary Science Letters, v. 179, p. 139-152.

Shirey, S.B., and Walker, R.J., 1998, The Re-Os isotope system in cosmochemistry and high temperature geochemistry: Annual Reviews of Earth and Planetary Sciences, v. 26, p. 423-500.

Siebert, C., Kramers, J.D., Meisel, T., Morel, P., and Nägler, T.F., 2005, PGE, Re-Os, and Mo isotope systematics in Archean and early Proterozoic sedimentary systems as proxies for redox conditions of the early Earth: Geochimica et Cosmochimica Acta, v. 69, p. 1787-1801.

Simonson, B.M., Byerly, G.R., and Lowe, D.R., 2004, The early Precambrian stratigraphic record of large extraterrestrial impacts, *in* Eriksson, P.G., et al., eds., The Precambrian Earth: Tempos and events: Developments in Precambrian Geology 12, Elsevier Amsterdam, p. 27-45.

Simonson, B.M., Sumner, D.Y., Beukes, N.J., Hassler, S., Kohl, I., Jones-Zimberlin, S., Johnson, S., Scally, A., and Gutzmer, J., 2006, Correlating multiple Neoarchean-Paleoproterozoic impact spherule layers between South Africa and Western Australia: Lunar and Planetary Science XXXVII 1489.pdf.

Singh, S.K., Trivedi, J.R., and Krishnaswami, S., 1999, Re-Os isotope systematics in black shales from the Lesser Himalaya: their chronology and role in the ^{187}Os/^{188}Os evolution of seawater: Geochimica et Cosmochimica Acta, v. 63, p. 2381-2392.

Slack, J.F., Grenne, T., Bekker, A., Rouxel, O.J., and Lindberg, P.A., 2007, Suboxic deep seawater in the late Paleoproterozoic: evidence from hematitic chert and iron formation related to seafloor-hydrothermal sulfide deposits, central Arizona, USA: Earth and Planetary Science Letters, v. 255, p. 243-256.

Sleep, N.H., Zahnle, K.J., Kasting, J.F., and Morowitz, H.J., 1989, Annihilation of ecosystems by large asteroid impacts on the early Earth: Nature, v. 342, p. 139-142.

Smith, R.E., Perdrix, J.L., and Parks, T.C., 1982, Burial metamorphism in the Hamersley Basin, Western Australia: Journal of Petrology, v. 23, p. 75-102.

Smoliar, M.I., Walker, R.J., and Morgan, J.W., 1996, Re-Os ages of Group IIA, IIIA, IVA, and IVB iron meteorites: Science, v. 271, p. 1099-1102.

Stein, H.J., Sundblad, K., Markey, R.J., Morgan, J.W., and Motuza, G., 1998, Re-Os ages for Archean molybdenite and pyrite, Kuittila-Kivisuo, Finland and Proterozoic molybdenite, Kabeliai, Lithuania: Testing the chronometer in a metamorphic and metasomatic setting: Mineralium Deposita, v. 33, p. 329-345.

Stein, H.J., Markey, R.J., Morgan, J.W., Hannah, J.L., and Scherstén, A., 2001, The remarkable Re-Os chronometer in molybdenite: How and why it works: Terra Nova, v. 13, p. 479-486.

Stein, H.J., Hannah, J.L., Zimmerman, A., Markey, R.J., Sarkar, S.C., and Pal, A.B., 2004, A 2.5 Ga porphyry Cu-Mo-Au deposit at Malanjkhand, central India: Implications for Late Archean continental assembly: Precambrian Research, v. 134, p. 189-226.

Summons, R.E., Jahnke, L.L., Hope, J.M., and Logan, G.A., 1999, 2-Methylhopanoids as biomarkers for cyanobacterial oxygenic photosynthesis: Nature, v. 400, p. 554-557.

Sumner, D.Y., 1997, Carbonate precipitation and oxygen stratification in late Archean seawater as deduced from facies and stratigraphy of the Gamohaan and Frisco Formations, Transvaal Supergroup, South Africa: American Journal of Science, v. 297, p. 455-487.

Sumner, D.Y., and Bowring, S.A., 1996, U-Pb geochronologic constraints on deposition of the Campbellrand Subgroup, Transvaal Supergroup, South Africa: Precambrian Research, v. 79, p. 25-35.

Sumner, D.Y., and Grotzinger, J.P., 2004, Implications for Neoarchaean ocean chemistry from primary carbonate mineralogy of the Campbellrand-Malmani Platform, South Africa: Sedimentology, v. 51, p. 1273-1299.

Sumner, D.Y., and Beukes, N.J., 2006, Sequence stratigraphic development of the Neoarchean Transvaal carbonate platform, Kaapvaal Craton, South Africa: South African Journal of Geology, v. 109, p. 11-22.

Sun, W., Arculus, R.J., Bennett, V.C., Eggins, S.M., and Binns, R.A., 2003a, Evidence for rhenium enrichment in the mantle wedge from submarine arc-like volcanic glasses (Papua New Guinea): Geology, v. 31, p. 845-848.

Sun, W., Bennett, V.C., Eggins, S.M., Kamenetsky, V.S., and Arculus, R.J., 2003b, Enhanced mantle-to-crust rhenium transfer in undegassed arc magmas: Nature, v. 422, p. 294-297.

Sundby, B., Martinez, P., and Gobeil, C., 2004, Comparative geochemistry of cadmium, rhenium, uranium, and molybdenum in continental margin sediments: Geochimica et Cosmochimica Acta, v. 68, p. 2485-2493.

Tice, M.M., and Lowe, D.R., 2004, Photosynthetic microbial mats in the 3,416-Myr-old ocean: Nature, v. 431, p. 549-552.

Tice, M.M., and Lowe, D.R., 2006, Hydrogen-based carbon fixation in the earliest known photosynthetic organisms: Geology, v. 34, p. 37-40.

Tinker, J., de Wit, M., and Grotzinger, J., 2002, Seismic stratigraphic constraints on Neoarchean – Paleoproterozoic evolution of the western margin of the Kaapvaal Craton, South Africa: South African Journal of Geology, v. 105, p. 107-134.

Tomitani, A., Knoll, A.H., Cavanaugh, C.M., and Ohno, T., 2005, The evolutionary diversification of cyanobacteria: Molecular-phylogenetic and paleontological perspectives: Proceedings of the National Academy of Sciences, v. 103, p. 5442-5447.

Trendall, A.F., Nelson, D.R., De Laeter, J.R., and Hassler, S.W., 1998, Precise zircon U-Pb ages from the Marra Mamba Iron Formation and Wittenoom Formation, Hamersley Group, Western Australia: Australian Journal of Earth Sciences, v. 45, p. 137-142.

Trendall, A.F., Compston, W., Nelson, D.R., De Laeter, J.R., and Bennett, V.C., 2004, SHRIMP zircon ages constraining the depositional chronology of the Hamersley Group, Western Australia: Australian Journal of Earth Sciences, v. 51, p. 621-644.

Turgeon, S.C., and Creaser, R.A., 2007, Widespread Os isotope evidence for a magmatic pulse at the onset of Oceanic Anoxic Event 2: Geochimica et Cosmochimica Acta, v. 71 (15; supplement 1), p. A1042.

Turgeon, S.C., Creaser, R.A., and Algeo, T.J., Re-Os depositional ages and seawater Os estimates for the Frasnian-Famennian boundary: Implications for weathering rates, land plant evolution, and extinction mechanisms: Earth and Planetary Science Letters, in press.

Valley, J.W., Cavosie, A.J., Fu, B., Peck, W.H., and Wilde, S.A., 2006, Comment on "Heterogeneous Hadean hafnium: Evidence of continental crust at 4.4 to 4.5 Ga: Science, v. 312, p. 1139a.

Van Kranendonk, M.J., Webb, G.E., and Kamber, B.S., 2003, Geological and trace element evidence for a marine sedimentary environment of deposition and biogenicity of 3.45 Ga stromatolitic carbonates in the Pilbara Craton, and support for a reducing Archaean ocean: Geobiology, v. 1, p. 91-108.

Van Zuilen, M.A., Lepland, A., and Arrhenius, G., 2002, Reassessing the evidence for the earliest traces of life: Nature, v. 418, p. 627-630.

Walker, R.J., Horan, M.F., Morgan, J.W., Becker, H., Grossman, J.N., and Rubin, A.E., 2002a, Comparative ^{187}Re-^{187}Os systematics of chondrites: implications regarding early solar system processes: Geochimica et Cosmochimica Acta, v. 66, p. 4187-4201.

Walker, R.J., Prichard, H.M., Ishiwatari, A., and Pimentel, M., 2002b, The osmium isotopic composition of convecting upper mantle deduced from ophiolite chromites: Geochimica et Cosmochimica Acta, v. 66, p. 329-345.

Walraven, F., Armstrong, R.A., and Kruger, F.J., 1990, A chronostratigraphic framework for the north-central Kaapvaal craton, the Bushveld Complex and the Vredefort structure: Tectonophysics, v. 171, p. 23-48.

Walraven, F., and Martini, J., 1995, Zircon Pb-evaporation age determinations of the Oak Tree Formation, Chuniespoort Group, Transvaal Sequence: Implications for Transvaal-Griqualand West Basin correlations: South African Journal of Geology, v. 98, p. 58-67.

Walsh, M.M., and Lowe, D.R., 1985, Filamentous microfossils from the 3,500-Myr-old Onverwacht Group, Barberton Mountain Land, South Africa: Nature, v. 314, p. 530-532.

Widom, E., Gaddis, S.J., and Wells, N.E., Jr., 2004, Re-Os isotope systematics in carbonates from Serpent Mound, Ohio: Implications for Re-Os dating of crustal rocks and the osmium isotopic composition of Ordovician seawater: Geochemistry, Geophysics, Geosystems, v. 5, Paper #2002GC000444.

Wilde, S.A., Valley, J.W., Peck, W.H., and Graham, C.M., 2001, Evidence from detrital zircons for the existence of continental crust and oceans on the Earth 4.4 Gyr ago: Nature, v. 409, p. 175-178.

Wille, M., Kramers, J.D., Nägler, T.F., Beukes, N.J., Schröder, S., Meisel, Th., Lacassie, J.P., and Voegelin, A.R., 2007, Evidence for a gradual rise of oxygen between 2.6 and 2.5 Ga from Mo isotopes and Re-PGE signatures in shales: Geochimica et Cosmochimica Acta, v. 71, p. 2417-2435.

Williams, G.A., and Turekian, K.K., 2004, The glacial-interglacial variation of seawater osmium isotopes as recorded in Santa Barbara Basin: Earth and Planetary Science Letters, v. 228, p. 379-389.

Williamson, M.A., and Rimstidt, J.D., 1994, The kinetics and electrochemical rate-determining step of aqueous pyrite oxidation: Geochimica et Cosmochimica Acta, v. 58, p. 5443-5454.

Woodhouse, O.B., Ravizza, G., Falkner, K.K., Statham, P.J., and Peucker-Ehrenbrink, B., 1999, Osmium in seawater: vertical profiles of concentration and isotopic composition in the eastern Pacific Ocean: Earth and Planetary Science Letters, v. 173, p. 223-233.

Xiong, J., Fischer, W.M., Inoue, K., Nakahara, M., and Bauer, C.E., 2000, Molecular evidence for the early evolution of photosynthesis: Science, v. 289, p. 1724-1730.

Yamashita, Y., Takahashi, Y., Haba, H., Enomoto, S., and Shimizu, H., 2007, Comparison of reductive accumulation of Re and Os in seawater-sediment systems: Geochimica et Cosmochimica Acta, v. 71, p. 3458-3475.

Yang, W., and Holland, H.D., 2002, The redox-sensitive trace elements, Mo, U, and Re in Precambrian carbonaceous shales: Indicators of the Great Oxidation Event: Geological Society of America Abstracts With Programs, v. 34, p. 381.

Yang, J.-H., Jiang, S.-Y., Ling, H.-F., Chen, Y.-Q., and Pu, W., 2006, Re-Os dating of the Lower Cambrian black shales in Guizhou province of South China: Geochimica et Cosmochimica Acta, v. 70 (18; supplement 1), p. A719.

Young, G.M., Long, D.G.F., Fedo, C.M., and Nesbitt, H.W., 2001, Paleoproterozoic Huronian basin: Product of a Wilson cycle punctuated by glaciations and a meteorite impact: Sedimentary Geology, v. 141-142, p. 233-254.

CHAPTER 7

Conclusions

7.1 ACCURACY AND PRECISION OF THE Re-Os DEPOSITION-AGE GEOCHRONOMETER FOR ORGANIC-RICH SHALES

Interpretation of Re-Os isochron dates as depositional ages for a sample set of organic-rich sedimentary rocks (ORS) requires that 1) Re and Os were predominantly hydrogenous in origin (minimal to negligible contributions from terrestrial/meteoritic particulates), 2) post-depositional mobility of Re and Os was negligible, 3) the initial $^{187}Os/^{188}Os$ isotope composition of all samples was homogeneous, and 4) the decay constant of ^{187}Re ($\lambda^{187}Re$) is known accurately. These conditions have been met for the Devonian-Mississippian Exshaw Formation (Western Canada Sedimentary Basin; Selby and Creaser, 2005), and $\lambda^{187}Re$ is generally well-constrained by cross-calibration of the Re-Os molybdenite and U-Pb zircon chronometers on magmatic-hydrothermal ore deposits (Selby et al., 2007a). Multiple examples are now known where Precambrian Re-Os organic-rich (TOC ≥ 0.5%) shale ages are consistent with U-Pb zircon age constraints for that rock unit: 1) The Mt. McRae Shale Re-Os age of 2501.1 ± 8.2 Ma is consistent with bounding U-Pb age constraints of 2561 ± 8 Ma and 2481 ± 4 Ma from underlying and overlying rock units (Trendall et al., 1998, 2004), 2) The Re-Os age of 643.0 ± 2.4 Ma for the Tindelpina Shale Member (basal Tapley Hill Formation, Adelaide Rift Complex, southern Australia) is consistent with a maximum U-Pb age constraint (from tuffaceous bed within stratigraphically underlying glaciogenic diamictites) of ca. 658 Ma for the waxing phase of Sturtian glaciation (Fanning and Link, 2006), and 3) Two Re-Os age determinations of 1361 ± 21 and 1417 ± 29 Ma from the Velkerri Formation (Roper Group, McArthur Basin, northern Australia) are stratigraphically consistent with each other and with a U-Pb age of 1492 ± 4 Ma from a tuffaceous bed 700 m stratigraphically lower in the Roper Group (Jackson et al., 1999). With rigorous sampling and analytical methodologies (including organic-selective Cr^{VI}-H_2SO_4 whole-rock dissolution; Selby and Creaser, 2003), precise (e.g., < 1% age uncertainty, 2σ) and accurate Re-Os ages may be obtained from well-preserved Precambrian organic-rich shales deposited from suboxic or anoxic/non-sulfidic (e.g., Tindelpina Shale Member, Aralka Formation, and lower Velkerri Formation) and euxinic (e.g., upper Black River Dolomite, upper Velkerri Formation, Mt. McRae Shale) bottom waters. Accordingly, the Re-Os deposition-age geochronometer should find widespread utility for Precambrian geological timescale calibration and sedimentary basin analysis, especially since Precambrian stratigraphic successions usually have no biostratigraphic control and sparse U-Pb zircon age constraints. The lower limit of hydrogenous Re and Os enrichment in ORS required for accurate age determinations is not well-constrained, but is probably below ~ 2 ppb Re and ~ 75 ppt Os (minimum abundances of these metals in the Blinman-2 drill core, Tindelpina Shale Member). Shales lacking appreciable hydrogenous metal enrichment may have heterogeneous initial Os isotope compositions (I_{Os}) as a result of mixing between particulate and hydrogenous Os. This may generate a non-zero slope on an isochron diagram at the time of deposition, resulting in erroneously young or old Re-Os dates relative to the true depositional age (e.g., Early Paleoproterozoic Klipput Shale Member, Transvaal Supergroup, South Africa; cf. Ravizza et al., 1991).

7.2 LIMITATIONS OF THE Re-Os ORS GEOCHRONOMETER

Inaccurate and/or imprecise Re-Os ages may result if appropriate sampling strategies are not utilized for geochronology (e.g., Neoproterozoic Doushantuo Formation, South China). Small-scale post-depositional mobilization and/or decoupling of Re and Os may occur within a sufficiently small shale powder aliquot (e.g., ≤ 10 g). In addition, narrow stratigraphic sampling intervals (≤ 1-2 m depending on sediment accumulation rates and the rate of change in seawater Os isotope composition) are required to minimize variations in I_{Os} resulting from temporal evolution of seawater Os isotope compositions. Large-scale disturbance to Re-Os isotope systematics in ORS is known to occur during oxidative subaerial weathering (Peucker-Ehrenbrink and Hannigan, 2000; Jaffe et al., 2002; Pierson-Wickmann et al., 2002). An erroneously young Re-Os date of 1359 ± 150 Ma for the ca. 1730 Ma Wollogorang Formation provides evidence that hydrothermal fluid flow through black shales results in post-depositional remobilization of Re and Os and loss of reliable depositional age information. The complex Re-Os isotope systematics observed in the Late Mesoproterozoic to Early Neoproterozoic Lapa Formation (Vazante Group, Brazil) and Neoproterozoic Horsethief Creek Group (lower Windermere Supergroup, Western Canada) may also result from fluid flow and/or chlorite-grade metamorphism. The robustness of the Re-Os isotope system in ORS during prograde metamorphism remains poorly constrained. Precise Re-Os ages have been obtained from Precambrian organic-rich shales that have undergone hydrocarbon maturation (Velkerri Formation) and thermal alteration up to the onset of lowermost greenschist facies metamorphism (607.8 ± 4.7 Ma Old Fort Point Formation, Windermere Supergroup, Western Canada; Kendall et al., 2004).

Because of their generally low Re and Os abundances (e.g., Ediacaran Dengying Formation, South China, and Horsethief Creek Group), and susceptibility to diagenesis, organic-rich carbonates may not be reliable geochronometers. Shale-hosted benthic microbial mats from basal Ediacaran successions in Australia (Brachina and Pertatataka Formations) and southeastern King Island (Yarra Creek Shale) yield scattered Re-Os isotope systematics, probably as a result of diagenetic remobilization of Re and Os by subaqueous oxidative weathering. On the other hand, carbonate-hosted algal laminites may have some utility for geochronology (Miller, 2004).

7.3 CONTROLS ON INITIAL ^{187}Re/^{188}Os ISOTOPE RATIOS IN ORGANIC-RICH SHALES DURING SEDIMENT DEPOSITION

The fractionation mechanism(s) responsible for variable ^{187}Re/^{188}Os isotope ratios over limited lateral and/or stratigraphic intervals within ancient ORS remains poorly understood. Consideration of variations between Re and ^{192}Os abundances and ^{187}Re/^{188}Os isotope ratios with trace metal abundances suggests multiple controlling factors. In the case of euxinic sediments (e.g., upper Velkerri and Wollogorang Formations), elemental partitioning of Re and Os during organic complexation likely exerts a significant control on initial ^{187}Re/^{188}Os during sediment deposition, consistent with previous data that suggested multiple and/or separate organic complexes as host phases for Re and Os in hydrocarbons and shale source rocks (Selby and Creaser, 2003; Miller, 2004; Selby et al., 2007b). In contrast, gray and black shales deposited from suboxic to anoxic/non-sulfidic bottom waters (e.g., Aralka Formation, Tindelpina Shale Member, lower Velkerri Formation) may have initial ^{187}Re/^{188}Os variations controlled by differential Re and Os uptake rates to accumulating organic-rich sediments that in turn results from a temporal shift in seawater concentration, precipitation rate kinetics (Re), and/or changes in organic matter flux (Os, but possibly also Re).

7.4 APPLICATIONS TO PRECAMBRIAN ORGANIC-RICH SHALES

7.4.1 Timing of Neoproterozoic Glaciation and Rodinia Breakup

The end of Sturtian glaciation in the Adelaide Rift Complex is constrained by a Re-Os date of 643.0 ± 2.4 Ma from the overlying Tindelpina Shale Member. A Re-Os date of 657.2 ± 5.4 Ma for the basal Aralka Formation constrains the age of the underlying Areyonga glacial deposits in the Amadeus Basin. The Re-Os ages show that the Sturtian and Areyonga glacial deposits are younger than other radiometrically dated (ca. 685-750 Ma; Trindade and Macouin, 2007) Neoproterozoic glacial intervals previously regarded as possible correlatives. Thus, the "Sturtian" ice age was markedly diachronous, and/or there were multiple glaciations between ca. 750 and 643 Ma. Some Neoproterozoic glacial deposits may represent the products of regional and diachronous glaciation associated with (or following) regional tectonic uplift or protracted breakup of the supercontinent Rodinia rather than "snowball" (Hoffman and Schrag, 2002) or "slushball" (Hyde et al., 2000) Earth ice ages. Although glaciogenic diamictites of the basal Lapa Formation and upper Vazante Group have been attributed to the "Sturtian" ice age (Azmy et al., 2006), a Re-Os age estimate of 1100 ± 77 Ma suggests instead a regional late Mesoproterozoic to Early Neoproterozoic glaciation. The new Re-Os ages presented here suggest diamictite – cap carbonate pairs cannot be used as chronostratigraphic marker horizons for Neoproterozoic global correlation schemes (as suggested by Corsetti and Lorentz, 2006), and warns against the utility of carbon isotope chemostratigraphy as a correlation tool in the absence of supporting radiometric and biostratigraphic information. Significantly, a tripartite subdivision of all Neoproterozoic glacial deposits ("Sturtian" – "Marinoan" – "Gaskiers") is incorrect in light of the present Neoproterozoic geochronologic database.

Black shales overlying diamictites of the Julius River Member (upper Black River Dolomite, Togari Group, northwestern Tasmania) yield a Re-Os date of 640.7 ± 4.7 Ma that is identical to the Re-Os age of 643.0 ± 2.4 Ma for the Tindelpina Shale Member. Sturtian glacial and post-glacial deposition (ca. 658-643 Ma) significantly post-dates ca. 827-777 Ma magmatic activity in the Adelaide Rift Complex associated with Rodinia supercontinent breakup. Thus, marine inundation associated with the onset of continental separation and passive margin formation may pre-date Sturtian glaciation, and may be represented by sandstone and fine-grained siliciclastic and carbonate strata in the underlying Burra Group. Sturtian glaciation itself may have been associated with an episode of crustal extension and uplift that did not result in a major phase of continental breakup.

7.4.2 Joint Applications of Re-Os Geochronology, and Mo and Fe Stable Isotope – and Trace Metal – based Redox Proxies

Joint application of the Re-Os deposition-age geochronometer and the Mo isotope paleoredox proxy to euxinic black shales has tremendous potential for tracing the evolution of ocean and atmosphere redox chemistry over geological time. New Re-Os ages of 1361 ± 21 Ma and 1417 ± 29 Ma constrain the depositional age of the Velkerri Formation and its contained biomarkers, as well as acritarchs and microfossils from the Roper Group. Black shales from the upper Velkerri Formation have high Mo abundances, degree-of-pyritization (DOP) values, and a restricted range in $\delta^{97/95}$Mo consistent with quantitative sequestration of Mo from overlying seawater. Consistent with previous Mo isotope data (Arnold et al., 2004), the average $\delta^{97/95}$Mo (0.72 ± 0.10 ‰; 2σ) of these shales represents global seawater $\delta^{97/95}$Mo at 1.4 Ga being lighter than present-day seawater by ~ 0.8‰. This reflects decreased uptake of Mo onto Mn oxides associated with expansion of deep sea euxinia at the expense of oxic, suboxic, and anoxic/non-sulfidic marine deposition. Wollogorang Formation black shales are enriched in Mo, but are characterized by variable DOP and $\delta^{97/95}$Mo (0.3-0.8‰). Although isotopically light hydrothermal fluids have likely overprinted the authigenic $\delta^{97/95}$Mo signature in the Wollogorang Formation, the heaviest $\delta^{97/95}$Mo values are similar to those observed for the Velkerri Formation, and may reflect seawater $\delta^{97/95}$Mo at 1.73 Ga.

A high-resolution chemostratigraphic profile through the Mt. McRae Shale reveals an interval of redox-sensitive (Re and Mo) metal enrichment associated with mild oxygenation of shallow ocean waters prior to the 2.45-2.32 Ga Great Oxidation Event (GOE) (Anbar et al., 2007). The age of the Mt. McRae Shale is directly constrained by a Re-Os age of 2501.1 ± 8.2 Ma. In conjunction with other studies (Siebert et al., 2005;

Wille et al., 2007), the Mt. McRae Shale excursion indicates a complex history of initial Earth surface and shallow ocean oxidation prior to the GOE.

Iron isotopes may have utility as a redox proxy and for elucidating the nature of Fe redox cycling in ancient Earth surface environments, but an understanding of Fe isotope fractionation mechanisms is in its infancy. Negative $\delta^{56/54}$Fe (down to –0.3‰) in the Velkerri and Wollogorang Formation euxinic shales are generally consistent with operation of a Fe shuttle that transported isotopically light Fe from suboxic continental shelf sediments to basin floors in a manner analogous to that observed in the Black Sea (Severmann et al., 2006a). Heavy $\delta^{56/54}$Fe (up to +0.4‰) in euxinic shales of the Doushantuo Formation and 1.64 Ga Barney Creek Formation (McArthur Basin, northern Australia) are similar to $\delta^{56/54}$Fe of pore fluids released during bacterial sulfate reduction (Severmann et al., 2006b), and may indicate the widespread activity of sulfate reducing bacteria in contemporaneous continental margin or intracratonic basin environments. Moderately positive $\delta^{56/54}$Fe (~ 0.1-0.2 ‰) for anoxic/non-sulfidic shales of the lower Velkerri Formation may reflect Fe isotope fractionation during authigenic mineral formation under conditions of limited sulfur input fluxes in a restricted basin. Ultimately, additional Fe isotope data (e.g., sequential extraction of Fe-bearing phases) are required for further interpretation of the whole-rock Fe isotope data.

7.5 PRECAMBRIAN SEAWATER Os ISOTOPE COMPOSITIONS AND Re-Os SYSTEMATICS IN ORS OVER GEOLOGICAL TIME

The record of secular change in the Os isotope composition of Precambrian seawater is limited to handful of I_{Os} determinations of precise Re-Os regressions of Proterozoic and latest Archean ORS. Chondritic I_{Os} values (e.g., ≤ 0.15) diagnostic of a magmatic/extraterrestrial origin for seawater Os are known from ORS that predate (2.50 Ga Mt. McRae Shale) and postdate (2.32 Ga Rooihoogte and Timeball Hill Formations, Transvaal Supergroup, South Africa, and the 2.00 Ga "Productive" Formation, Pechenga Greenstone Belt, Russia; Hannah et al., 2004, 2006) the GOE. This may be explained by insufficiently oxidizing conditions for weathering and erosion of Os from crustal rocks and/or a time lag between the GOE and appreciable riverine transport of crustal Os to the oceans because of low Re abundances in uplifted Archean shales (Hannah et al., 2004, 2006). By Mesoproterozoic times (1.54 Ga Douglas Formation and 1.4 Ga Velkerri Formation), however, Earth surface oxygenation was sufficient to generate at least moderately radiogenic seawater Os isotope compositions (I_{Os} up to 0.5) (Creaser and Stasiuk, 2007). Crustal Os inputs exerted a significant control on the Os isotope composition of Late Neoproterozoic seawater, as evidenced by moderate or radiogenic I_{Os} (~ 0.6-1.2) from the ca. 657 Ma Aralka Formation, ca. 643 Ma Tindelpina Shale Member and upper Black River Dolomite, ca. 608 Ma Old Fort Point Formation, and ca. 551 Ma Doushantuo Formation (Member 4).

A synthesis of Re and ^{192}Os abundances and ^{187}Re/^{188}Os isotope ratios for ORS revealed a number of trends that are consistent with a multi-stage evolution of ocean and atmosphere oxygenation. Low Re abundances and ^{187}Re/^{188}Os isotope ratios in Late Archean ORS are consistent with a predominantly anoxic atmosphere and oceans (Farquhar et al., 2000; Pavlov and Kasting, 2002; Goldblatt et al., 2006). Interestingly, the Os abundance of Late Archean ORS is not depleted relative to Proterozoic and Phanerozoic ORS, suggesting magmatic/extraterrestrial Os input fluxes to seawater on the Archean Earth were greater than output fluxes to organic-rich sediments. The onset of initial Earth surface oxidation in the Late Archean is marked by a coupled increase in Re abundance and ^{187}Re/^{188}Os isotope ratio. Low Re and ^{192}Os abundances and well-correlated trends between these metals for Paleoproterozoic to Neoproterozoic ORS may reflect reduced seawater metal inventories associated with the development of stratified oceans and the expansion of reducing depositional environments (Canfield, 1998; Siebert et al., 2005; Anbar et al., 2007; Slack et al., 2007; Wille et al., 2007). Phanerozoic and Recent ORS have a wide range in Re and ^{192}Os abundances that are only moderately correlated, and the highest and most variable ^{187}Re/^{188}Os isotope ratios, consistent with a wide range in paleoenvironmental controls on Re and Os accumulation in ORS deposited in restricted or productive, upwelling regions of predominantly oxygenated oceans.

REFERENCES

Anbar, A.D., Duan, Y., Lyons, T.W., Arnold, G.L., Kendall, B., Creaser, R.A., Kaufman, A.J., Gordon, G.W., Scott, C., Garvin, J., and Buick, R., 2007, A whiff of oxygen before the Great Oxidation Event?: Science, v. 317, p. 1903-1906.

Arnold, G.L., Anbar, A.D., Barling, J., and Lyons, T.W., 2004, Molybdenum isotope evidence for widespread anoxia in Mid-Proterozoic oceans: Science, v. 304, p. 87-90.

Azmy, K., Kaufman, A.J., Misi, A., and de Oliveira, T.F., 2006, Isotope stratigraphy of the Lapa Formation, São Francisco Basin, Brazil: Implications for Late Neoproterozoic glacial events in South America: Precambrian Research, v. 149, p. 231-248.

Canfield, D.E., 1998, A new model for Proterozoic ocean chemistry: Nature, v. 396, p. 450-453.

Corsetti, F.A., and Lorentz, N.J., 2006, On Neoproterozoic cap carbonates as chronostratigraphic markers, *in* Xiao, S., and Kaufman, A.J., eds., Neoproterozoic Geobiology and Paleobiology: Springer, New York, p. 273-294.

Creaser, R.A., and Stasiuk, L.D., 2007, Depositional age of the Douglas Formation, northern Saskatchewan, determined by Re-Os geochronology, *in* Jefferson, C.W., and Delaney, G., eds., EXTECH IV: Geology and Uranium EXploration TECHnology of the Proterozoic Athabasca Basin, Saskatchewan and Alberta: Geological Survey of Canada Bulletin 588, p. 341-346.

Fanning, C.M., and Link, P., 2006, Constraints on the timing of the Sturtian glaciation from southern Australia; i.e. for the true Sturtian: Geological Society of America Abstracts With Programs, v. 38 (7), p. 115.

Farquhar, J., Bao, H., and Thiemens, M., 2000, Atmospheric influence of Earth's earliest sulfur cycle: Science, v. 289, p. 756-758Goldblatt, C., Lenton, T.M., and Watson, A.J., 2006, Bistability of atmospheric oxygen and the Great Oxidation: Nature, v. 443, p. 683-686.

Hannah, J.L., Bekker, A., Stein, H.J., Markey, R.J., and Holland, H.D., 2004, Primitive Os and 2316 Ma age for marine shale: Implications for Paleoproterozoic glacial events and the rise of atmospheric oxygen: Earth and Planetary Science Letters, v. 225, p. 43-52.

Hannah, J.L., Stein, H.J., Zimmerman, A., Yang, G., Markey, R.J., and Melezhik, V.A., 2006, Precise 2004 ± 9 Ma Re-Os age for the Pechenga black shale: Comparison of sulfides and organic material: Geochimica et Cosmochimica Acta, v. 70 (18; supplement 1), p. A228.

Jackson, M.J., Sweet, I.P., Page, R.W., and Bradshaw, B.E., 1999, The South Nicholson and Roper Groups: evidence for the early Mesoproterozoic Roper Superbasin, *in* Integrated basin analysis of the Isa Superbasin using seismic, well-log, and geopotential data: an evaluation of the economic potential of the northern Lawn Hill Platform: Australian Geological Survey Organisation Record 1999/19 (unpaginated).

Jaffe, L.A., Peucker-Ehrenbrink, B., and Petsch, S.T., 2002, Mobility of rhenium, platinum group elements and organic carbon during black shale weathering: Earth and Planetary Science Letters, v. 198, p. 339-353.

Kendall, B.S., Creaser, R.A., Ross, G.M., and Selby, D., 2004, Constraints on the timing of Marinoan "Snowball Earth" glaciation by ^{187}Re-^{187}Os dating of a Neoproterozoic, post-glacial black shale in Western Canada: Earth and Planetary Science Letters, v. 222, p. 729-740.

Hoffman, P.F., and Schrag, D.P., 2002, The snowball Earth hypothesis: Testing the limits of global change: Terra Nova, v. 14, p. 129-155.

Hyde, W.T., Crowley, T.J., Baum, S.K., and Peltier, W.R., 2000, Neoproterozoic 'snowball Earth' simulations with a coupled climate/ice-sheet model: Nature, v. 405, p. 425-429.

Miller, C.A., 2004, Re-Os dating of algal laminites: Reduction-enrichment of metals in the sedimentary environment and evidence of new geoporphyrins: M.Sc. Thesis, University of Saskatchewan.

Pavlov, A.A., and Kasting, J.F., 2002, Mass-independent fractionation of sulfur isotopes in Archean sediments: strong evidence for an anoxic Archean atmosphere: Astrobiology, v. 2, p. 27-41.

Peucker-Ehrenbrink, B., and Hannigan, R.E., 2000, Effects of black shale weathering on the mobility of rhenium and platinum group elements: Geology, v. 28, p. 475-478.Ravizza, G., Turekian, K.K., and Hay, B.J., 1991, The geochemistry of rhenium and osmium in recent sediments from the Black Sea: Geochimica et Cosmochimica Acta, v. 55, p. 3741-3752.

Pierson-Wickmann, A.-C., Reisberg, L., and France-Lanord, C., 2002, Behavior of Re and Os during low-temperature alteration: results from Himalayan soils and altered black shales: Geochimica et Cosmochimica Acta, v. 66, p. 1539-1548.

Selby, D., and Creaser, R.A., 2003, Re-Os geochronology of organic-rich sediments: an evaluation of organic matter analysis methods: Chemical Geology, v. 200, p. 225-240.

Selby, D., and Creaser, R.A., 2005, Direct radiometric dating of the Devonian-Mississippian time-scale boundary using the Re-Os black shale geochronometer: Geology, v. 33, p. 545-548.

Selby, D., Creaser, R.A., Stein, H.J., Markey, R.J., and Hannah, J.L., 2007a, Assessment of the ^{187}Re decay constant by cross calibration of Re-Os molybdenite and U-Pb zircon chronometers in magmatic ore systems: Geochimica et Cosmochimica Acta, v.71, p. 1999-2013.

Selby, D., Creaser, R.A., and Fowler, M.G., 2007b, Re-Os elemental and isotopic systematics in crude oils: Geochimica et Cosmochimica Acta, v. 71, p. 378-386.

Severmann, S., Lyons, T., Anbar, A., Gordon, G., and McManus, J., 2006a, The isotopic expression of iron shuttling in the euxinic Black Sea basin and implications for the rise of oxygen in the early atmosphere: Geological Society of America Abstracts With Programs, v. 38 (7), p. 124.

Severmann, S., Johnson, C.M., Beard, B.L., and McManus, J., 2006b, The effect of early diagenesis on the Fe isotope compositions of porewaters and authigenic minerals in continental margin sediments: Geochimica et Cosmochimica Acta, v. 70, p. 2006-2022.

Siebert, C., Kramers, J.D., Meisel, T., Morel, P., and Nägler, T.F., 2005, PGE, Re-Os, and Mo isotope systematics in Archean and early Proterozoic sedimentary systems as proxies for redox conditions of the early Earth: Geochimica et Cosmochimica Acta, v. 69, p. 1787-1801.

Slack, J.F., Grenne, T., Bekker, A., Rouxel, O.J., and Lindberg, P.A., 2007, Suboxic deep seawater in the late Paleoproterozoic: evidence from hematitic chert and iron formation related to seafloor-hydrothermal sulfide deposits, central Arizona, USA: Earth and Planetary Science Letters, v. 255, p. 243-256.

Trendall, A.F., Nelson, D.R., De Laeter, J.R., and Hassler, S.W., 1998, Precise zircon U-Pb ages from the Marra Mamba Iron Formation and Wittenoom Formation, Hamersley Group, Western Australia: Australian Journal of Earth Sciences, v. 45, p. 137-142.

Trendall, A.F., Compston, W., Nelson, D.R., De Laeter, J.R., and Bennett, V.C., 2004, SHRIMP zircon ages constraining the depositional chronology of the Hamersley Group, Western Australia: Australian Journal of Earth Sciences, v. 51, p. 621-644.

Trindade, R.I.F., and Macouin, M., 2007, Palaeolatitude of glacial deposits and palaeogeography of Neoproterozoic ice ages: Comptes Rendus Geoscience, v. 339, p. 200-211.

Wille, M., Kramers, J.D., Nägler, T.F., Beukes, N.J., Schröder, S., Meisel, Th., Lacassie, J.P., and Voegelin, A.R., 2007, Evidence for a gradual rise of oxygen between 2.6 and 2.5 Ga from Mo isotopes and Re-PGE signatures in shales: Geochimica et Cosmochimica Acta, v. 71, p. 2417-2435.

APPENDICES

Appendix A: Analytical Protocols for Re-Os Isotope Analysis

Rhenium and Os isotope analyses were carried out at the Radiogenic Isotope Facility of the Department of Earth and Atmospheric Sciences, University of Alberta, using chemical digestion, separation, and purification, and mass spectrometry (isotope dilution – negative thermal ionization mass spectrometry; ID-NTIMS) protocols modified from Selby and Creaser (2001, 2003), Creaser et al. (2002), and Kendall et al. (2004).

A.1 Sample Collection and Preparation

Roadcut sampling is typically carried out laterally along a single thin horizon (e.g,, ≤ 50 cm) (Kendall et al., 2004; Selby and Creaser, 2005). Because a significant fraction of the original Re, Os, and TOC budgets in organic-rich sedimentary rocks (ORS) are lost during oxidative weathering (Peucker-Ehrenbrink and Hannigan, 2000; Jaffe et al., 2002; Pierson-Wickmann et al., 2002), the outermost surface of the outcrop is removed to obtain pristine material. Using drill core avoids the issue of weathering altogether, but may require a larger stratigraphic sampling interval (≤ 1-2 m) to obtain a suitable spread in present-day ^{187}Re/^{188}Os and ^{187}Os/^{188}Os isotope ratios. Black shales containing veinlets and/or sheared surfaces should be avoided because of the detrimental effects of post-depositional fluid flow on Re-Os isotope systematics (see Chapter 5). Samples selected for analysis ideally will have finely disseminated and/or framboidal pyrite, thin (mm-scale) laminations, and contain negligible to minimal organic-poor material. Each powder aliquot should comprise over 20 g of material to avoid small-scale post-depositional mobility and/or decoupling of Re and Os isotope systematics (see Chapter 2).

Because Re and Os are siderophile elements, sample processing requires metal-free methods, and thus conventional rock-crushing equipment such as jaw-crushers and steel mills cannot be used (Creaser et al., 2002). Material is extracted from the central sections of outcrop samples, ground to remove cutting and drilling marks, wrapped in plastic bags, and broken into small chips using a hammer covered by duct tape. Final processing to fine powder (~ 30 μm) is carried out in an automated agate mill. Between samples, the agate mill is cleaned using ethanol and by crushing pure quartz sand.

A.2 Purification of Chemical Reagents of Re and Os

Some chemical reagents, including 9N HBr and 12N HCl (Baseline, distilled by sub-boiling in quartz), CCl_4 (Sigma-Aldrich HPLC grade), $CHCl_3$ (Fisher Scientific HPLC grade, pentene stabilized), and SO_2 gas (Praxair) have acceptable Re and Os blank levels and do not require further purification. However, direct use of Trace Metal grade 16N HNO_3 for inverse *aqua regia* digestions can result in procedural Os blank levels of several pg. Procedural Os blanks were reduced to the fg level by reacting 1000 mL of cold concentrated HNO_3 with 50 mL of cold 30% H_2O_2 to volatize Os. After the initial violent reaction, which typically occurs 12-15 minutes after reagent mixing, the mixture is heated at 120°C for 2 h (Ryan Morelli, personal communication).

Shen et al. (1996) reported that commercially available chromium trioxide (CrO_3) displays a wide range in Re (20-170 pg/g) and Os (60-4000 pg/g) abundances. Efficient removal of Re from CrO_3 was attempted during the course of this study, but remains an elusive and challenging problem. An initial attempt to purify CrO_3 of Re used a solvent extraction procedure that employs TPAI (tetra propyl ammonium iodide) as a chelating agent for Re (Maeck et al., 1961; Shen et al., 1996). For this purpose, 10 mL of 2% TPAI in 4N H_2SO_4 and 50 mL of $CHCl_3$ were added to 200 mL of a solution containing 0.25 g of CrO_3 per 1 mL 4N H_2SO_4. After shaking the solution vigorously in a separatory glass funnel for several minutes, the $CHCl_3$ was decanted from solution, and additional 50 mL extractions of $CHCl_3$ were carried out until the $CHCl_3$ became pale yellow to colorless. Using this method, Shen et al. (1996) reported a minor reduction in the Re content of a Cr^{VI}-H_2SO_4 solution (from 20 to 13 pg/g) prepared from E. Merck® CrO_3 powder. Selby and Creaser (2003) also reported a low Re blank of 2.3 pg/g for E. Merck® CrO_3 after treatment with TPAI, but did not determine the Re blank before purification. Subsequently, Re blank abundances of 35-40 pg/g were obtained for a Cr^{VI}-H_2SO_4 solution prepared from Fisher Scientific CrO_3 (Lot #004749) that had been cleaned with TPAI. To evaluate whether or not the TPAI was chelating Re from the Cr^{VI}-H_2SO_4 solution, a more detailed experiment was performed using Fluka Chemika CrO_3 (Lot

#365032/1; Re abundance of 23 pg/g). Approximately 15 g of CrO_3 was dissolved in 15 mL of 0.1N H_2SO_4 followed by direct addition of TPAI (2% by weight of H_2SO_4). After shaking vigorously for five minutes in a sealed 60 mL Teflon vial, 5 mL of $CHCl_3$ was added and the mixture shaken for an additional five minutes, prior to decanting the $CHCl_3$. Three additional extractions with 5 mL of $CHCl_3$ were carried out (the final color of the chloroform was pale yellow), and the 0.1N H_2SO_4 – CrO_3 solution was then evaporated to dryness at > 80°C. The measured Re abundance of the cleaned CrO_3 was 27 pg/g, suggesting that TPAI does not chelate Re from a Cr^{VI}-H_2SO_4 solution. This probably reflects a greater affinity of Re for CrO_3 relative to TPAI.

A second attempt to remove Re from Cr^{VI}-H_2SO_4 by solvent extraction was carried out using tribenzylamine (TBA) in chloroform. This method has previously been employed for Re solvent extraction from H_2SO_4 (Colodner et al., 1993; Horan et al., 1994). Unfortunately, TBA also does not appear to chelate Re from Cr^{VI}-H_2SO_4 because a Re abundance of 870 pg/g was determined for TBA-cleaned CrO_3 (Aldrich Lot #05917MA) that had an original Re content of 765 pg/g. Anion exchange chromatography can purify Cr^{VI}-H_2SO_4 of Re (e.g., 23 pg/g to 3.2 pg/g for Fluka Chemika Lot #365032/1; 765 pg/g to 5.0 pg/g for Aldrich Lot #05917MA), but this method requires reducing the oxidation state of the chromium from +6 to +3 (see below), and it is necessary to re-oxidize chromium back to the hexavalent state for Carius tube digestions. Unfortunately, trivalent chromium proved to be extremely resistant to re-oxidation even when the Cr^{III}-H_2SO_4 solution was bubbled in ozone gas.

Consequently, a search was made for commercially available CrO_3 that already had an acceptably low Re abundance, and did not require further purification. A wide range in Re content was observed (from < 5 to > 500 pg/g), with the lowest levels of Re found in some batches of CrO_3 from Fluka Chemika (Table A.1). The 4N H_2SO_4 (prepared from 36N Seastar H_2SO_4) is purified of Re using anion exchange chromatography and then added to an appropriate amount of CrO_3 to make a solution containing 0.25 g CrO_3 per 1 mL 4N H_2SO_4. Osmium can readily be removed from this solution by bubbling through N_2 gas at ~ 120 °C for 4-6 h.

A.3 Re-Os Chemistry

Rhenium and Os abundances are measured by isotope dilution using a mixed ^{185}Re-^{190}Os tracer solution calibrated against Re (AB-1) and Os (AB-2, lot #H25H35) standard solutions prepared from 99.999% pure Re metal and 99.999% (metal-basis) ammonium hexachloro-osmate, respectively (Selby and Creaser, 2001). The Os content in ammonium hexachloro-osmate can be non-stoichiometric at levels of ± 1% (Papanstassiou et al., 1994; Morgan et al., 1995; Shen et al., 1996; Yin et al., 2001) and can introduce systematic errors into absolute spike calibrations if stoichiometry is assumed. However, gravimetric reduction of Os to the metallic state in a gas furnace (in 98% N_2 and 2% H_2 at ~ 500°C for 2 h) allows precise and reproducible gravimetric determinations of the Os abundance in this salt (Selby and Creaser, 2001; Markey et al., 2007). The direct gravimetric determination (0.4326 ± 0.0003 %; n = 5) was found to be slightly lower than the stoichiometric value (0.4333%) (Selby and Creaser, 2001; also see Yin et al., 2001). Thus, the gravimetric determination was used for spike solution calibrations. Triplicate calibrations of the ^{185}Re abundance in the spike solution agreed to within ± 0.13%, and duplicate calibrations of the ^{190}Os abundance agreed to within ± 0.03% (Creaser et al., 2002).

To avoid memory effects, all Carius Tubes, sample vials, and chromatography columns were used once during chemistry, and then discarded. An accurately weighed amount of whole rock powder and mixed ^{185}Re-^{190}Os tracer, and either 8 mL of a Cr^{VI}-H_2SO_4 solution or 9 mL of inverse *aqua regia* (3 mL of 12N HCl and 6 mL of 16N HNO_3) were sequentially loaded into thick-walled, borosilicate Carius tubes frozen in a dry ice – methanol slurry (Shirey and Walker, 1995). Carius tubes were sealed with an oxygen-propane flame. Samples were digested at 240°C for 48 h, except for some Cr^{VI}-H_2SO_4 digestions carried out at 80°C (see Chapter 3) during the latter part of the thesis research. A green color for the Cr^{VI}-H_2SO_4 solution (normally reddish purple) indicates the oxidizing power of the CrO_3 was consumed during digestion, and requires a new digestion using either a smaller sample aliquant or a larger volume of Cr^{VI}-H_2SO_4 solution.

Osmium was separated from the Cr^{VI}-H_2SO_4 solution by solvent extraction using chloroform. Initially, CCl_4 was used instead of $CHCl_3$ for solvent extraction during the earliest phase of this study. Cohen and Waters (1996) favored the use of CCl_4 over $CHCl_3$ because of higher Os yields and the lower volatility and wetting characteristics of CCl_4. However, a comparison of Re-Os data obtained for the same shale powder using both organic solvents suggests the choice of $CHCl_3$ as the solvent does not significantly impact the uncertainties of Os abundances or isotope ratios (Table A.2). Consequently, $CHCl_3$ was adopted for Os solvent extraction because this organic solvent is much less toxic than CCl_4. After freezing in liquid N_2 or a dry-ice methanol slurry, the Carius tubes are opened and 3.5 mL of $CHCl_3$ are added to each tube. Upon thawing, the contents of each tube are transferred to 50 mL polypropylene centrifuge tubes, shaken vigorously, and placed in a water bath (T = 25°C) for 15 min. Each solution is then agitated for 1 min followed by gravity settling (or centrifuging) to separate the Re-bearing *aqua regia* or Cr^{VI}-H_2SO_4 solutions from the Os-bearing $CHCl_3$. The $CHCl_3$ is then transferred to 22 mL glass vials with Teflon-lined caps each containing 3 mL of 9N HBr, followed by two additional solvent extractions with 3.5 mL of $CHCl_3$. Back-extraction of Os from $CHCl_3$ into HBr is carried out at ~ 70°C for > 12 h. After decanting the $CHCl_3$ to waste, the Os-bearing HBr is evaporated to ~ 30 μL on pyrex watch glasses (covered with adhesive Teflon tape), then transferred to the Teflon inner surface of the 22 mL vial caps, and evaporated to dryness at ~ 70°C. Micro-distillation is used for further purification (Birck et al., 1997) whereby Os is oxidized by 30 μL of a Cr^{VI}-H_2SO_4 solution (containing 0.2 g CrO_3 per 1 mL 7N H_2SO_4) and captured by 20 μL of 9N HBr in sealed, inverted conical Savillex Teflon vials placed on a heating block (T = 80°C). A second micro-distillation step may be used to improve the quality of sample purity and ion beam stability during mass spectrometry. Final dry-down of the Os fraction is carried out under a N_2 atmosphere at 60°C.

Following Os solvent extraction, Re is purified by anion exchange chromatography (using disposable polyethylene columns, quartz wool plugs, and Eichrom 1X8 100-200 mesh anion resin). The *aqua regia* solutions are first evaporated to dryness and then re-dissolved in 3 mL of 0.2N HNO_3 for 2 h at ~ 70°C. The resin is cleaned with 4 mL of 8N HNO_3 and equilibrated with 4 mL of 0.2N HNO_3. Sample solutions are centrifuged to filter out residues, loaded drop-wise onto the column, and washed with 4 * 0.25 mL 0.2N HNO_3, 2 * 1 mL 0.2N HNO_3, 2 * 1 mL 0.2N HCl, and 2 mL 6N HNO_3. Rhenium is eluted from the column in 4 mL 6N HNO_3 and evaporated to dryness at ~ 70°C in a polymethylpentene (PMP) beaker. For Cr^{VI}-H_2SO_4 solutions, the oxidation state of chromium must be reduced completely from +6 to +3 to ensure efficient separation of Cr from Re during anion exchange chromatography. Selby and Creaser (2003) and Kendall et al. (2004) carried out the Cr-reduction step by taking 1 mL of the Cr^{VI}-H_2SO_4 solution following solvent extraction and adding two aliquots of 2 mL H_2SO_3 (Fisher Scientific). Subsequently, it was discovered that new batches of H_2SO_3 contained unacceptably high Re blank levels (e.g., > 2 pg/mL of H_2SO_3). Attempts to purify the H_2SO_3 by anion exchange chromatography resulted in significant evaporation of SO_2 and loss of reduction power. Consequently, a new reduction step was adopted whereby 1 mL of the sample Cr^{VI}-H_2SO_4 solution was diluted with 1 mL of ultrapure, deionized H_2O, and bubbled with SO_2 gas until the solution changed from dark purple to dark green. For accurate measurement of procedural Re blanks, the entire 8 mL of Cr^{VI}-H_2SO_4 solution was diluted to 16 mL with ultrapure, deionized H_2O prior to SO_2 reduction. The resin is cleaned with 4 mL 8N HNO_3 and equilibrated with 4 mL 0.2N HCl. Reduced Cr^{III}-H_2SO_4 solutions are loaded drop-wise onto the resin. Columns are then washed with 4 * 1 mL 1N HCl (to remove the Cr^{III}), 1 mL 0.2N HNO_3 and 1.5 mL 6N HNO_3, followed by elution of Re in 4 mL 6N HNO_3.

Single bead anion exchange chemistry was used for final purification of Re fractions. The Re cut is re-dissolved in 200 μL 0.05N HNO_3 and absorbed by a single DOWEX AGI-X8 < 20 mesh anion bead in a 1.5 mL centrifuge tube placed overnight on a rotator. Rhenium is then released from the anion bead into 1 mL 6N HNO_3 while rotating overnight in a new 1.5 mL centrifuge tube. After removal of the anion bead, the solution is evaporated to dryness (T ~ 70°C) either on a watch glass covered with Teflon tape or in a PMP beaker.

A.4 Negative Thermal Ionization Mass Spectrometry (NTIMS)

Rhenium cuts are re-dissolved in 16N HNO_3, loaded onto Ni filaments, and covered with a $Ba(NO_3)_2$ activator solution. Osmium is taken up in 9N HBr, loaded onto Pt filaments, and covered with a NaOH-$Ba(OH)_2$ activator solution. A fresh batch of NaOH-$Ba(OH)_2$ activator solution was made for each mass spectrometry session because the solution appears to degrade rapidly even when kept under vacuum. Prior to sample loading, the central portions of the Pt and Ni filaments are gently flattened with a XuroGrip crimper and glowed in air at 2.5-3.0 A for 30 min to decrease filament loading blanks. This Pt filament preparation protocol resulted in improved ion beam longevity and stability compared to samples loaded on Pt ribbons with wider loading surfaces. Johnson Matthey Ni wire (99% purity) has Re filament loading blanks of < 0.2 pg (Shen et al., 1996) whereas high purity (99.999%) Pt wire from Williams Advanced Materials yields Os filament blanks of typically < 30 fg, with blank ^{187}Os/^{188}Os of 0.11-0.16.

Rhenium and Os concentrations and isotopic compositions were measured by ID-NTIMS (Creaser et al., 1991; Völkening et al., 1991; Walczyk et al., 1991) on a Micromass Sector 54 mass spectrometer using Faraday collectors in static mode (Re) and a pulse-counting electron multiplier in single collector peak-hopping mode (Os). Metal isotope ratios were obtained by correcting raw Re and Os oxide isotopic ratios for isobaric oxygen interferences. Isobaric interference of $^{187}ReO_3^-$ on $^{187}OsO_3^-$ at mass number 235 was monitored using mass number 233 ($^{185}ReO_3^-$), but was typically determined to be negligible. Further corrections are made for instrumental mass fractionation (using ^{185}Re/^{187}Re = 0.59738 and ^{192}Os/^{188}Os = 3.08261; Nier, 1937 Gramlich et al., 1973), and blank and spike contributions. As there is no internationally accepted standard for Re and Os, in-house standard solutions of Re (AB-1) and Os (AB-2) were repeatedly analyzed over the course of this study to monitor long-term mass spectrometer reproducibility (Table A.3).

Regressions were performed with the program *Isoplot V.3.0* (a Microsoft Excel add-on program available at http://www.bgc.org/klprogrammenu.html; Ludwig, 2003) using a ^{187}Re decay constant of 1.666×10^{-11} year^{-1} (Smoliar et al., 1996; Selby et al., 2007), 2σ uncertainties for ^{187}Re/^{188}Os and ^{187}Os/^{188}Os isotope ratios, and the error correlation function (rho; ρ) (Kendall et al., 2004). Use of the latter in Re-Os isochron regressions is justified by the significant error correlations (typically between 0.2 and 0.9) between ^{187}Re/^{188}Os and ^{187}Os/^{188}Os observed for shales containing a relatively wide variation in Re and Os abundance and ^{187}Re/^{188}Os and ^{187}Os/^{188}Os isotope ratios (Kendall et al., 2004; Selby and Creaser, 2005; this thesis). Uncertainties for ^{187}Re/^{188}Os and ^{187}Os/^{188}Os isotope ratios were calculated by numerical error propagation and includes uncertainties in the spike calibration, spike and sample weighing (for Re, Os abundances only), mass spectrometric analysis, in-house Re standard bias (relative to $^{185}Re/^{187}Re$ = 0.59738; Gramlich et al., 1973), oxygen, spike, and blank isotopic composition and blank abundance.

Appendix B: Analytical Protocols for Mo and Fe Isotope Analysis

Molybdenum and Fe stable isotope analyses were carried out at the W.M. Keck Foundation Laboratory for Environmental Biogeochemistry (School of Earth and Space Exploration, Arizona State University) using analytical protocols modified after Anbar et al. (2001), Barling et al. (2001), and Arnold et al. (2004a, b).

B.1 Mo and Fe Isotope Chemistry

Between 0.05 g and 0.15 g of sample powder was ashed overnight at 550°C to remove organic matter. Residues were transferred to 22 mL Savillex Teflon vials and digested in 5 mL of concentrated HNO_3 and 1 mL of concentrated HF for 10 h at 200°C. Samples were evaporated to near-dryness, and then digested in 1-2 mL of concentrated HCl for at least 2 h at 200°C. Care was taken to avoid evaporating solutions completely as this could result in the formation of insoluble fluorides and adsorption of Mo by the Teflon. A second HF-HNO_3-HCl digestion step was performed if total dissolution was not achieved by the first acid attack. After evaporation to near-dryness, samples were reconstituted in 6N HCl (Mo chemistry) or 7N HCl (Fe chemistry).

Separation and purification of Mo was carried out following a two-step anion and cation exchange chromatography protocol (Barling et al., 2001; Arnold et al., 2004a). Columns are loaded with 2 mL of BioRad AG1X-8 100-200 mesh anion resin and cleaned with 2 * 10 mL 1N HCl and conditioned with 2 * 10 mL 6N HCl. Sample solutions are loaded drop-wise onto the resin, and washed with 3 * 10 mL 6N HCl to remove most matrix elements. Iron and Mo are eluted together in 40 mL of 1 mL HCl. Sample solutions are evaporated to near-dryness and re-constituted in 1 mL 0.5N HCl. For cation exchange chromatography, 2 mL BioRad AG50WX-8 200-400 mesh cation resin was loaded into a column, washed with 10 mL 0.5N HCl, sealed from the atmosphere, and conditioned overnight in ~ 8 mL 0.5N HCl. Columns were further conditioned/cleaned with 10 mL 0.5N HCl containing 10 μL 0.1% H_2O_2 per mL 0.5N HCl (used to ensure Mo is efficiently removed in the hexavalent state; Arnold et al., 2004a). After loading samples drop-wise onto the resin, Mo is eluted in 40 mL 0.5N HCl with 0.1% H_2O_2 while Fe is retained on the column.

Approximately 0.5 mL of the 7N HCl solutions (containing ~ 300 μg/g Fe) was taken for separation and purification of Fe by double anion exchange chromatography using the method of Arnold et al. (2004b). Columns are loaded with 0.5 mL AGMP-1M anion resin, cleaned with 5 mL 0.5N HCl and conditioned with 5 mL 7N HCl. Iron solutions are loaded drop-wise onto the column, and washed with 5 mL 7N HCl, followed by Fe elution in 5 mL 0.5N HCl. After evaporation of solutions to near-dryness and re-constitution in 0.5 mL 7N HCl, the anion exchange column chemistry was repeated a second time.

Following evaporation of the final purified Mo and Fe fractions to near-dryness, Mo and Fe cuts were re-constituted in 0.3N HNO_3 stock solutions of ~ 2 ppm and ~ 30 ppm, respectively, with a few drops of 0.3N HF added to Mo solutions to ensure sample stability. The Mo and Fe chemical yields from column chromatography were required to be $\geq$ 95% to avoid laboratory-induced mass fractionation of Mo and Fe isotopes (Anbar et al., 2000, 2001). Molybdenum chemical yields were verified by isotope dilution – quadrupole inductively coupled plasma mass spectrometry (Q-ICP-MS) analysis of pre- and post-chromatography aliquots (see Appendix C.1). Iron chemical yields were determined either by Q-ICP-MS analysis or by UV-vis spectrophotometry (see Appendix C.3). Procedural blanks for Mo and Fe were insignificant relative to sample abundances.

B.2 Multiple Collector Inductively Coupled Plasma Mass Spectrometry (MC-ICP-MS)

Molybdenum and Fe isotopes were measured on a Thermo-Finnigan Neptune MC-ICP-MS. Standard and sample 0.3N HNO_3 stock solutions were diluted to 200 ppb and 3 ppm for Mo and Fe solutions, respectively, and analyzed using a combination of standard-sample bracketing and the element spike method to correct for instrumental mass fractionation (e.g., Anbar et al., 2001; Arnold et al., 2004b). Bracketing compensates for drift in instrumental mass fractionation during analysis, while the element spike corrects for differences in instrumental mass fractionation between samples and standards arising from minor differences in sample matrix. In the element spike method, a Zr spike (diluted to 100 ppb from a 1 ppm Johnson Matthey Specpure® Zr plasma standard solution; Lot #700193E) and Cu spike (diluted to 3 ppm from a 30 ppm JMC-ICP Specpure® Cu standard solution; Lot #200536E) were added to Mo and Fe sample/standard solutions, respectively. The Zr standard solution was assumed to have a $^{90}\text{Zr}/^{91}\text{Zr}$ isotope ratio of 4.58421 whereas the Cu standard solution was assumed to have a $^{63}\text{Cu}/^{65}\text{Cu}$ isotope ratio of 0.44563. These values were used to correct for instrumental mass fractionation of Mo and Fe isotopes, but it is important to stress that the absolute accuracy of these values do not affect δ determinations, which are all relative.

Molybdenum isotope data are corrected for Zr isobaric interferences at masses 92 and 96. Iron isotopes were measured in high mass resolution mode (Weyer and Schwieters, 2003; Arnold et al., 2004b). Polyatomic argide interferences on Fe isotopes were monitored and determined to be negligible, and $^{53}\text{Cr}^+$ and $^{60}\text{Ni}^+$ were used to correct for any isobaric interference from $^{54}\text{Cr}^+$ and $^{58}\text{Ni}^+$ on $^{54}\text{Fe}^+$ and $^{58}\text{Fe}^+$, respectively (Arnold et al., 2004b).

Molybdenum and Fe isotope data are reported using the conventional δ notation:

$$\delta^{97/95}\text{Mo}_{\text{sample}}\,(‰) = [^{97/95}\text{Mo}_{\text{sample}}/^{97/95}\text{Mo}_{\text{standard}} - 1] \times 1000 \qquad (1)$$

$$\delta^{56/54}\text{Fe}_{\text{sample}}\,(‰) = [^{56/54}\text{Fe}_{\text{sample}}/^{56/54}\text{Fe}_{\text{standard}} - 1] \times 1000 \qquad (2)$$

Sample $\delta^{97/95}\text{Mo}$ is reported relative to the Johnson Matthey Specpure® Mo plasma standard (Lot #802309E; RochMo2) which has an identical Mo isotopic composition as the RochMo standard (Lot #7024991) used at the University of Rochester (Anbar et al., 2001; Barling et al., 2001; Arnold et al., 2004a). Iron isotope analyses are reported relative to the IRMM-014 standard (Taylor et al., 1992).

To ensure a high quality of data, the mass fractionation of Mo and Fe isotopes per atomic mass unit [e.g., $\delta^{9x/95}\text{Mo/amu} = \delta^{9x/95}\text{Mo} / (M_{95} - M_{9x})$; $\delta^{5x/54}\text{Fe/amu} = \delta^{5x/54}\text{Fe} / (M_{54} - M_{5x})$; where M = isotopic mass] were compared for both samples and standards. Molybdenum samples that pass this test have $\delta^{9x/95}\text{Mo/amu} < 0.05‰/\text{amu}$ for ^{97}Mo, ^{98}Mo, and ^{100}Mo, and $\delta^{9x/95}\text{Mo/amu} < 0.10‰/\text{amu}$ for ^{92}Mo and ^{96}Mo (e.g., Barling et al., 2001). Similarly, $\delta^{5x/54}\text{Fe}$ must be $< 0.05‰/\text{amu}$ for ^{56}Fe and ^{57}Fe. Over the course of this study, external 2σ standard reproducibilities were 0.08-0.09‰ and 0.03-0.04‰ for

$\delta^{97/95}$Mo and $\delta^{56/54}$Fe, respectively. Samples were typically analyzed at least in triplicate during different mass spectrometry sessions.

Appendix C: Analytical Protocols for Element Abundance and DOP Determinations

C.1 Element Abundance Determinations at Arizona State University (Chapter 2, 5)

Elemental abundances were determined from a small aliquot that was set aside for this purpose following HF-HNO_3-HCl digestions for Mo isotope analysis. Protocols for whole-rock digestion of shale samples at Arizona State University are described in Appendix B.1. Elemental abundances were measured on a Thermo Scientific X Series Q-ICP-MS against multiple element calibration standards. Signal intensities for each trace metal were typically bracketed by the highest and lowest standard concentration. Elements Ge, In, Y and Bi were used as internal standards to correct for signal drift. Analyte concentration reproducibilities were typically better than 5%. Measurement accuracy was verified by analysis of USGS reference material SDO-1 (Devonian organic-rich shale).

C.2 Elemental Abundance Determinations at the University of Alberta (Chapter 3)

Approximately 0.1 g of sample was weighed into a 15 mL Savillex Teflon vial and digested in 10 mL of concentrated HF and HNO_3 (1:1 mixture) for 24 h at 120°C. Samples were evaporated to dryness and subjected to a second HF/HNO_3 acid attack. After taking the samples to dryness, a final digestion using inverse *aqua regia* (2 mL concentrated HCl and 4 mL concentrated HNO_3) was carried out overnight at 120°C. Samples were evaporated, re-constituted in 10 mL of 0.5N HNO_3, and placed in an ultrasonic bath for ~ 1-2 h to dissolve residue material. Elemental abundances were determined on a Perkin Elmer Elan 6000 Q-ICP-MS against multiple element calibration standards, with elements Sc, In, and Bi used to correct for signal drift. Analyte concentration reproducibilities were typically better than 5%.

C.3 DOP Determinations at Arizona State University

For calculation of sample DOP, the 1 minute boiling HCl technique was used to approximate the fraction of Fe remaining in the sample that was still reactive towards H_2S (Fe_{HCl}), although this method is known to extract poorly reactive, silicate-bound Fe (Canfield et al., 1992; Raiswell and Canfield, 1996). Following the boiling HCl extraction, Fe abundances were determined by UV-vis spectrophotometry ($\lambda = 562$ nm) using a reducing ferrozine reagent in HEPES buffer (adjusted to $pH = 8$ with concentrated ammonium hydroxide) with hydroxylamine (modified from Stookey, 1970).

Pyrite-bound Fe (Fe_P) was determined using a modified version of the Cr-reduction method for liberation of total reducible inorganic sulfur (Canfield et al., 1986). Between 0.10 g and 0.15 g of sample together with 10 mL of ethanol were boiled for 2 h with a 1:2 solution of 20 mL concentrated HCl and 40 mL $CrCl_2$ (in 1N HCl) in a vacuum system flushed with N_2 gas. Total reducible sulfur was trapped in 30 mL of a zinc acetate solution that was subsequently titrated with potassium iodate to determine the weight percent pyrite sulfur, and thus weight percent pyrite Fe. Sample DOP was calculated using the standard formula $DOP = Fe_P / (Fe_P + Fe_{HCl})$ (Berner, 1970).

Appendix D: Thesis Collection

Table D.1 represents a listing of the sample collection for this thesis.

Table A.1. Blank Re abundances for CrO_3 powders.

Manufacturer*	Lot Number	Total Re blank (pg)[†]	n[‡]
Aldrich Ammonium dichromate 45013-8	04219LN	10255	1
Aldrich 207829	05917MA	1601	1
Aldrich 232653	12922CO	1527	1
EM Science CX1615-3	40005314	149	1
Fisher Scientific A100-100	(00)4749	82.2	1
	025374A	107	1
Fluka Chemika 27081	449174/1	207	1
Fluka Chemika 27083	365032/1	60.1 ± 5.2	3
	447647/1	8.89 ± 2.96	11
	1125527	16.4 ± 1.1	4
	1126082	150 ± 23	2
	1177884	10.4 ± 1.7	9
J.T. Baker 1638-04	Y03614	1542	1

Uncertainties are quoted at the 1σ level.

*All brands are CrO_3 powders unless otherwise noted.

[†] For 2 g of powder.

[‡] Number of analyses.

Table A.2. Comparison of Re-Os data obtained using $CHCl_3$ and CCl_4 as organic solvents during Os solvent extraction.

Sample	Organic Solvent	Aliquant Mass (g)*	Re (ppb)	Os (ppt)	^{192}Os (ppt)	$^{187}Re/^{188}Os$	$^{187}Os/^{188}Os$
Doushantuo Formation							
H_1O_1-1	CCl_4	1.50	0.32 ± 0.01	48.3 ± 1.0	18.1 ± 0.7	35.55 ± 1.52	0.9142 ± 0.0523
	$CHCl_3$	1.47	0.30 ± 0.01	46.8 ± 0.9	17.5 ± 0.7	33.68 ± 1.46	0.9149 ± 0.0524
H_1O_{16}-A-1	CCl_4	1.19	3.70 ± 0.02	120.8 ± 0.8	37.7 ± 0.2	195.01 ± 1.38	2.5974 ± 0.0191
	$CHCl_3$	1.19	3.80 ± 0.02	122.3 ± 0.8	38.2 ± 0.2	198.04 ± 1.39	2.5984 ± 0.0189
Horsethief Creek Group							
BK-HG-02-50A	CCl_4	1.02	32.87 ± 0.11	468.6 ± 2.3	96.1 ± 0.2	680.64 ± 2.57	7.8976 ± 0.0203
	$CHCl_3$	0.98	32.94 ± 0.11	470.5 ± 2.4	96.5 ± 0.2	678.84 ± 2.61	7.8861 ± 0.0229
BK-HG-02-51A	CCl_4	1.31	1.88 ± 0.01	38.4 ± 0.4	9.7 ± 0.1	386.81 ± 5.42	5.0492 ± 0.0785
	$CHCl_3$	1.32	1.89 ± 0.01	37.4 ± 0.5	9.3 ± 0.1	404.79 ± 5.91	5.2180 ± 0.0861

Uncertainties are quoted at the 2σ level. Data are from Chapter 2 (Doushantuo Formation) and Chapter 4 (Horsethief Creek Group).

*Used for individual Re-Os analysis.

Table A.3. Average standard isotope ratios for AB-1 (Re) and AB-2 (Os).

Study	AB-1 (Re)			AB-2 (Os)		
	$^{185}Re/^{187}Re$	1σ	n*	$^{187}Os/^{188}Os$	1σ	n*
Chapter 2	0.59832	0.00064	51	0.1068	0.0002	43
Chapter 3 (Pertatataka, Brachina, Aralka Formations, Tindelpina Shale Member)	0.59869	0.00055	28	0.1069	0.0002	27
Chapter 4 (Horsethief Creek Group)	0.59808	0.00042	28	0.1067	0.0001	21
Chapter 5	0.59902	0.00054	39	0.1069	0.0002	53
Chapter 4 (Lapa Formation), and Chapter 6 (Mt. McRae Shale)	0.59896	0.00053	51	0.1068	0.0002	68
Chapter 3 (Black River Dolomite, Yarra Creek Shale), and Chapter 6 (Monteville Formation, Klipput Shale)	0.59889	0.00044	43	0.1069	0.0001	46

*Number of analyses.

Table D.1. Thesis Collection

Lithostratigraphic Unit	Sample	Drill hole Depth (m)	Aliquot Mass (g)	Description
SOUTH CHINA	H_1O_1 - 1		17.8	Black, finely-laminated shaly limestone
Neoproterozoic	H_1O_1 - 2		15.9	
Doushantuo Formation	H_1O_1 - 3		10.3	
Member 2	H_1O_1 - 4		17.5	
(Outcrop)	H_1O_4 - 1		11.1	Finely laminated black shale
	H_1O_4 - 2		14.1	
	H_1O_9 - 1		3.6	
	H_1O_9 - 2		42.2	
	H_1O_{14} - 1		41.4	
	H_1O_{16} - A - 1		17.6	Finely laminated black shale with abundant disseminated pyrite
	H_1O_{16} - A - 2		11.1	
	H_1O_{16} - A - 3		10.1	
	H_1O_{16} - A - 4		6.6	
	H_1O_{16} - A - 5		8.1	
	H_1O_{16} - A - 6		6.1	
	H_1O_{16} - A - 7		5.1	
	H_1O_{16} - B - 1		9.7	
	H_1O_{16} - B - 2		5.7	
	H_1O_{16} - B - 3		4.1	
Member 4	H_1O_{18} - 1		7.0	Very black, finely-laminated shale with disseminated and framboidal pyrite
(Outcrop)	H_1O_{18} - 2		10.4	
	H_1O_{18} - 3		39.8	
	H_1O_{19} - 1		7.8	
	H_1O_{19} - 2		6.6	
	H_1O_{19} - 3		20.5	
	H_1O_{20} - 1		4.8	

Table D.1. Continued.

Lithostratigraphic Unit	Sample	Drill hole Depth (m)	Aliquot Mass (g)	Description
	H_1O_{20} - 2		5.9	
	H_1O_{20} - 3		5.5	
	H_1O_{20} - 4		22.0	
	H_1O_{20} - 5		32.8	
	H_1O_{21} - 1		8.9	Highly organic-rich black shale
	H_1O_{21} - 2		4.6	
	H_1O_{21} - 3		32.2	
Dengying Formation	H_1O_{28} - 1		17.2	Bituminous gray to dark gray limestone; some hand samples contain diagenetic carbonate veinlets
(Outcrop)	H_1O_{32} - 1		22.4	
	H_1O_{33} - 1		11.2	
	H_1O_{36} - 1		5.5	
CENTRAL AUSTRALIA	BK-04-WALLARA-1A	1298.20-1298.25	51.0	Dark grey, dolomitic, organic-rich siltstones
Neoproterozoic	BK-04-WALLARA-1B	1298.20-1298.25	62.0	
Araika Formation	BK-04-WALLARA-2A	1299.00-1299.05	64.9	
(Wallara-1)	BK-04-WALLARA-2B	1299.00-1299.05	72.9	
	BK-04-WALLARA-3	1299.50-1299.60	75.9	
	BK-04-WALLARA-4A	1300.10-1300.15	69.7	
	BK-04-WALLARA-4B	1300.10-1300.15	62.9	
	BK-04-WALLARA-5A	1300.20-1300.25	104.4	
Pertatataka Formation	BK-04-WP-2	1175.93-1175.95	61.1	Dark grey organic-rich shale representing benthic microbial mat material; interbedded and interlaminated with organic-poor grey shale in hand sample
(Wallara-1)	BK-04-WP-7	1176.11-1176.12	62.0	
	BK-04-WP-8	1177.25-1177.27	108.7	
	BK-04-WP-11	1177.36-1177.40	76.2	

Table D.1. Continued.

Lithostratigraphic Unit	Sample	Drill hole Depth (m)	Aliquot Mass (g)	Description
SOUTH AUSTRALIA	BK-04-BLINMAN-1	1609.98-1610.01	35.3	Grey to dark grey, finely laminated, dolomitic, organic-rich shale
Neoproterozoic	BK-04-BLINMAN 3	1610.05-1610.06	30.5	
Tindelpina Shale Member,	BK-04-BLINMAN 4	1610.07-1610.08	33.9	
Tapley Hill Formation	BK-04-BLINMAN-5	1610.10-1610.12	36.7	
(Blinman-2)	BK-04-BLINMAN-6	1610.13-1610.14	30.9	
	BK-04-BLINMAN-7	1610.76-1610.77	25.6	
	BK-04-BLINMAN-9	1610.80-1610.82	20.8	
	BK-04-BLINMAN-10	1610.84-1610.87	23.1	
	BK-04-BLINMAN-11	1610.88-1610.90	25.8	
(SCYW-1a)	BK-04-SCYW1a-1-3-4	1369.33-1369.42	27.7	Dark grey, finely laminated, organic-rich shale
	BK-04-SCYW1a-1-5	1370.00-1370.05	20.6	
	BK-04-SCYW1a-1-6-7	1370.06-1370.14	33.1	
Brachina Formation	BK-04-BWM1a-1-1	157.37-157.40	24.7	Dark grey organic-rich shale representing benthic microbial mat material; interbedded and interlaminated with organic-poor grey shale in hand sample
(BWM1a-1)	BK-04-BWM1a-1-2	157.43-157.46	19.8	
	BK-04-BWM1a-1-4	158.29-158.31	22.1	
	BK-04-BWM1a-1-5	158.32-158.35	26.4	
NORTHWEST TASMANIA	RC06-FOR-01-A	835.84-835.87	31.8	Finely laminated and pyritic black shale; RC06-FOR-02 samples are more organic-rich
Neoproterozoic	RC06-FOR-01-B	835.77-835.79	25.6	
Black River Dolomite	RC06-FOR-01-B2	835.79-835.84	50.7	
(Forest-1)	RC06-FOR-01-C	835.70-835.72	32.1	
	RC06-FOR-01-C2	835.72-835.74	31.8	
	RC06-FOR-01-C3	835.74-835.77	29.1	
	RC06-FOR-01-D	835.65-835.68	30.5	
	RC06-FOR-01-D_2	835.68-835.70	29.0	

Table D.1. Continued.

Lithostratigraphic Unit	Sample	Drill hole Depth (m)	Aliquot Mass (g)	Description
	RC06-FOR-01-E	835.58-835.62	39.2	
	RC06-FOR-01-E2	835.62-835.65	35.4	
	RC06-FOR-02-B	828.11-828.15	39.2	
	RC06-FOR-02-D	828.23-828.27	54.9	
	RC06-FOR-02-G	828.37-828.40	40.4	
	RC06-FOR-02-H	828.48-828.50	33.3	
	RC06-FOR-02-I	828.55-828.58	43.0	
SOUTHEAST KING ISLAND	RC06-KI-01-A		52.2	Black shale with abundant disseminated pyrite; represents benthic microbial mat material and is interbedded with organic-poor, grey-green shale in hand sample
Neoproterozoic	RC06-KI-01-A2		78.6	
Yarra Creek Shale	RC06-KI-01-B		30.9	
(Outcrop)	RC06-KI-01-C		44.5	
	RC06-KI-01-D		43.2	
	RC06-KI-01-E			
	RC06-KI-01-E2		76.0	
	RC06-KI-01-F		83.2	
	RC06-KI-01-G		25.1	
	RC06-KI-01-G2		44.4	
	RC06-KI-01-H		48.1	
WESTERN CANADA	BK-HG-02-50A		49.7	Fine-grained organic-bearing argillaceous carbonate (50C, E, and 51A, B, C) and pyritic organic-rich shale (50A, B, D); carbonate veinlets present in many hand samples
Neoproterozoic	BK-HG-02-50B		20.9	
Horsethief Creek Group	BK-HG-02-50C		44.2	
(Outcrop)	BK-HG-02-50D		6.3	
	BK-HG-02-50E		24.8	
	BK-HG-02-51A		78.9	
	BK-HG-02-51B		192.1	
	BK-HG-02-51C		79.7	

Table D.1. Continued.

Lithostratigraphic Unit	Sample	Drill hole Depth (m)	Aliquot Mass (g)	Description
BRAZIL	MASW01-211-213-1	211.00-213.00	41.8	Dark grey shale
Late Mesoproterozoic to	MASW01-213-215-1	213.00-215.00	32.7	
Early Neoproterozoic	MASW01-215-217-1	215.00-217.00	45.0	
Lapa Formation	MASW01-924.00-930.35-1	924.00-930.35	42.4	Pyritic organic-rich shale containing abundant carbonate ± pyrite veinlets in hand sample; small-scale folds are evident in some samples; pyrite present as disseminations, framboids, and aggregates within veinlets
(MASW01)	MASW01-930.35-932.35-1	930.35-932.35	23.7	
	MASW01-930.35-932.35-2	930.35-932.35	26.4	
	MASW01-930.35-932.35-3	930.35-932.35	17.6	
	MASW01-933.10-935.10-1	933.10-935.10	66.4	
	MASW01-934.35-936.35-1	934.35-936.35	53.2	
	MASW01-935.10-937.10-1a	935.10-937.10	42.0	
	MASW01-935.10-937.10-1b	935.10-937.10	41.7	
	MASW01-935.10-937.10-2	935.10-937.10	68.0	
	MASW01-935.10-937.10-3	935.10-937.10	38.3	
	MASW01-937.10-939.10-1	937.10-939.10		
NORTH AUSTRALIA	BK-05-URAPUNGA4-136.91-137.33-1	136.91-136.98	49.0	Black finely-laminated and pyritic (disseminated and framboidal) shale; 325.64-326.69 m interval is darker in color
Early Mesoproterozoic	BK-05-URAPUNGA4-136.91-137.33-2	136.98-137.05	46.9	
Velkerri Formation	BK-05-URAPUNGA4-136.91-137.33-4	137.12-137.19	51.9	
(Urapunga-4)	BK-05-URAPUNGA4-136.91-137.33-5	137.19-137.26	53.3	
	BK-05-URAPUNGA4-136.91-137.33-6	137.26-137.33	54.0	
	BK-05-URAPUNGA4-137.40-137.95-1	137.40-137.46	45.1	
	BK-05-URAPUNGA4-137.40-137.95-2	137.46-137.52	41.6	
	BK-05-URAPUNGA4-137.40-137.95-3	137.52-137.58	49.6	
	BK-05-URAPUNGA4-137.40-137.95-5	137.63-137.69	35.1	
	BK-05-URAPUNGA4-137.40-137.95-7	137.75-137.79	35.9	
	BK-05-URAPUNGA4-137.40-137.95-8	137.79-137.84	37.6	
	BK-05-URAPUNGA4-137.40-137.95-9	137.84-137.89	32.9	

Table D.1. Continued.

Lithostratigraphic Unit	Sample	Drill hole Depth (m)	Aliquot Mass (g)	Description
	BK-05-URAPUNGA4-137.40-137.95-10	137.89-137.95	49.6	
	BK-05-URAPUNGA4-325.5-326.2-3	325.64-325.71	36.7	
	BK-05-URAPUNGA4-325.5-326.2-4	325.71-325.78	45.4	
	BK-05-URAPUNGA4-325.5-326.2-6	325.85-325.92	50.6	
	BK-05-URAPUNGA4-325.5-326.2-7	325.92-325.99	66.6	
	BK-05-URAPUNGA4-325.5-326.2-9	326.06-326.13	32.8	
	BK-05-URAPUNGA4-325.5-326.2-10	326.13-326.20	45.6	
	BK-05-URAPUNGA4-326.2-326.75-1	326.20-326.28	46.3	
	BK-05-URAPUNGA4-326.2-326.75-3	326.36-326.42	43.4	
	BK-05-URAPUNGA4-326.2-326.75-4	326.42-326.48	52.2	
	BK-05-URAPUNGA4-326.2-326.75-5	326.48-326.55	52.0	
	BK-05-URAPUNGA4-326.2-326.75-6	326.55-326.62	48.3	
	BK-05-URAPUNGA4-326.2-326.75-7	326.62-326.69	39.5	
Late Paleoproterozoic	BK-05-MCA2-68.00-68.58-4	68.11-68.15	46.7	Dark grey to black finely-laminated dolomitic shale with diffuse pyritic bands
Barney Creek Formation	BK-05-MCA2-68.00-68.58-15	68.55-68.58	46.9	
(McArthur River 2)	BK-05-MCA2-83.11-83.49-1	83.11-83.14	26.9	
(also called McArthur 2)	BK-05-MCA2-83.11-83.49-6	83.29-83.32	44.8	
	BK-05-MCA2-83.11-83.49-10	83.36-83.39	45.8	
	BK-05-MCA2-83.11-83.49-12	83.42-83.44	31.1	
Wollogorang Formation	BK-05-MTYOUNG2-74.18-74.55-1	74.18-74.21	53.4	Laminated to thinly-laminated black shale with disseminated and occassional framboidal pyrite; many samples contain thin dolomite veinlets; bituminous quartz and carbonate nodules
(Mount Young 2)	BK-05-MTYOUNG2-74.18-74.55-4	74.27-74.29	38.7	
	BK-05-MTYOUNG2-74.18-74.55-6	74.35-74.38	46.7	
	BK-05-MTYOUNG2-74.18-74.55-10	74.53-74.55	28.1	
	BK-05-MTYOUNG2-74.90-74.95-3	74.93-74.95	27.8	

Table D.1. Continued.

Lithostratigraphic Unit	Sample	Drill hole Depth (m)	Aliquot Mass (g)	Description
	BK-05-MTYOUNG2-74.90-74.95-3-Dol	74.93-74.95 (dol)	4.7	containing coarse pyrite aggregates present in a few hand samples
	BK-05-MTYOUNG2-75.05-75.15-2	75.08-75.11	22.2	
	BK-05-MTYOUNG2-75.45-75.55-2	75.48-75.51	32.0	
	BK-05-MTYOUNG2-75.45-75.55-3	75.51-75.53	36.0	
	BK-05-MTYOUNG2-76.0-76.3-1	76.00-76.03	19.0	
	BK-05-MTYOUNG2-76.0-76.3-2	76.03-76.08	31.1	
	BK-05-MTYOUNG2-76.86-76.98-2-Dol	76.91-76.96 (dol)	13.5	
	BK-05-MTYOUNG2-76.86-76.98-2	76.91-76.96	12.9	
	BK-05-MTYOUNG2-76.86-76.98-2	76.91-76.96-2	5.2	
SOUTH AFRICA	GEC-174.50-174.98-2	174.53-174.57	52.4	Grey to dark grey thinly-laminated shale with rare disseminated pyrite
Early Paleoproterozoic	GEC-174.50-174.98-4	174.61-174.65	41.7	
	GEC-174.50-174.98-6	174.69-174.72	40.5	
	GEC-174.50-174.98-9	174.79-174.83	42.5	
	GEC-176.06-176.35-1	176.06-176.09	48.2	
	GEC-176.06-176.35-3	176.12-176.16	49.4	
	GEC-176.06-176.35-6	176.20-176.23	36.9	
	GEC-176.06-176.35-8	176.26-176.29	46.8	
	GEC-176.06-176.35-10	176.32-176.35	43.8	
Late Archean	GKP-01-1020-1	1019.76-1019.79	43.9	Pyritic, finely-laminated black shale
Monteville Formation	GKP-01-1020-4	1019.88-1019.90	29.6	
(GKP01)	GKP-01-1020-6	1019.94-1019.96	30.4	
	GKP-01-1020-10	1020.05-1020.08	39.2	
	GKP-01-1020-11B	1020.12-1020.14	33.0	
	GKP-01-1020-12B	1020.18-1020.20	23.4	

Table D.1. Continued.

Lithostratigraphic Unit	Sample	Drill hole Depth (m)	Aliquot Mass (g)	Description
WESTERN AUSTRALIA **Late Archean** Mount McRae Shale (ABDP-9)	ABDP 9 - 128.71	128.71	32.7	Finely laminated black shale containing abundant disseminated and framboidal pyrite, and pyrite bands; 145.22-148.32 m interval is more organic-rich
	ABDP 9 - 128.84	128.84	38.7	
	ABDP 9 - 129.15	129.15	38.0	
	ABDP 9 - 129.36	129.36	39.1	
	ABDP 9 - 129.85	129.85	35.5	
	ABDP 9 - 145.22	145.22	19.0	
	ABDP 9 - 146.08	146.08	21.5	
	ABDP 9 - 147.10	147.10	14.2	
	ABDP 9 - 148.32	148.32	24.5	

Drill hole names are given in brackets. Original powder aliquot masses are listed.

References

Anbar, A.D., Roe, J.E., Barling, J., and Nealson, K.H., 2000, Nonbiological fractionation of iron isotopes: Science, v. 288, p. 126-128.

Anbar, A.D., Knab, K.A., and Barling, J., 2001, Precise determination of mass-dependent variations in the isotopic composition of molybdenum using MC-ICPMS: Analytical Chemistry, v. 73, p. 1425-1431.

Arnold, G.L., Anbar, A.D., Barling, J., and Lyons, T.W., 2004a, Molybdenum isotope evidence for widespread anoxia in Mid-Proterozoic oceans: Science, v. 304, p. 87-90.

Arnold, G.L., Weyer, S., and Anbar, A.D., 2004b, Fe isotope variations in natural materials measured using high mass resolution multiple collector ICPMS: Analytical Chemistry, v. 76, p. 322-327.

Barling, J., Arnold, G.L., and Anbar, A.D., 2001, Natural mass-dependent variations in the isotopic composition of molybdenum: Earth and Planetary Science Letters, v. 193, p. 447-457.

Berner, R.A., 1970, Sedimentary pyrite formation: American Journal of Science, v. 268, p. 1-23.

Birck, J.L., Roy Barman, M., and Capmas, F., 1997, Re-Os isotopic measurements at the femtomole level in natural samples: Geostandards Newsletter, v. 20, p. 19-27.

Canfield, D.E., Raiswell, R., Westrich, J.T., Reaves, C.M., and Berner, R.A., 1986, The use of chromium reduction in the analysis of reduced inorganic sulfur in sediments and shales: Chemical Geology, v. 54, p. 149-155.

Canfield, D.E., Raiswell, R., and Bottrell, S.H., 1992, The reactivity of sedimentary iron minerals toward sulfide: American Journal of Science, v. 292, p. 659-683.

Cohen, A.S., and Waters, F.G., 1996, Separation of osmium from geological materials by solvent extraction for analysis by thermal ionization mass spectrometry: Analytical Chimica Acta, v. 332, p. 269-375.

Colodner, D., Sachs, J., Ravizza, G., Turekian, K., Edmond, J., and Boyle, E. 1993, The geochemical cycle of rhenium: a reconnaissance: Earth and Planetary Science Letters, v. 117, p. 205-221.

Creaser, R.A., Papanastassiou, D.A., and Wasserburg, G.J., 1991, Negative thermal ion mass spectrometry of osmium, rhenium, and iridium: Geochimica et Cosmochimica Acta, v. 55, p. 397-401.

Creaser, R.A., Sannigrahi, P., Chacko, T., and Selby, D. 2002, Further evaluation of the Re-Os geochronometer in organic-rich sedimentary rocks: a test of hydrocarbon maturation effects in the Exshaw Formation, Western Canada Sedimentary Basin: Geochimica et Cosmochimica Acta, v. 66, p. 3441-3452.

Gramlich, J.W., Murphy, T.J., Garner, E.L., and Shields, W.R., 1973, Absolute isotopic abundance ratio and atomic weight of a reference sample of rhenium: Journal of Research of the National Bureau of Standards, v. 77A, p. 691-698.

Horan, M.F., Morgan, J.W., Grauch, R.I., Coveney, R.M., Jr., Murowchick, J.B., and Hulbert, L.J., 1994, Rhenium and osmium isotopes in black shales and Ni-Mo-PGE-rich sulfide layers, Yukon Territory, Canada, and Hunan and Guizhou provinces, China: Geochimica et Cosmochimica Acta, v. 58, p. 257-265.

Jaffe, L.A., Peucker-Ehrenbrink, B., and Petsch, S.T., 2002, Mobility of rhenium, platinum group elements and organic carbon during black shale weathering: Earth and Planetary Science Letters, v. 198, p. 339-353.

Kendall, B.S., Creaser, R.A., Ross, G.M., and Selby, D., 2004, Constraints on the timing of Marinoan "Snowball Earth" glaciation by ^{187}Re-^{187}Os dating of a Neoproterozoic, post-glacial black shale in Western Canada: Earth and Planetary Science Letters, v. 222, p. 729-740.

Ludwig, K., 2003, Isoplot/Ex, version 3: A geochronological toolkit for Microsoft Excel: Geochronology Center Berkeley.

Maeck, W.J., Booman, G.L., Kussy, M.E., and Rein, J.E., 1961, Extraction of the elements as Quaternary (propyl, butyl, and hexyl) amine complexes: Analytical Chemistry, v. 33, p. 1755-1780.

Markey, R., Stein, H.J., Hannah, J.L., Zimmerman, A., Selby, D., and Creaser, R.A., 2007, Standardizing Re-Os geochronology: A new molybdenite Reference Material (Henderson, USA) and the stoichiometry of Os salts: Chemical Geology, v. 244, p. 74-87.

Morgan, J.W., Horan, M.F., Walker, R.J., and Grossman, J.N., 1995, Rhenium-osmium concentration and isotope systematics in group IIAB iron meteorites: Geochimica et Cosmochimica Acta, v. 59, p. 2331-2344.

Nier, A.O., 1937, The isotopic constitution of osmium: Physics Reviews, v. 52, p. 885.

Papanastassiou, D.A., Ngo, H.H., and Wasserburg, G.J., 1994, Re-Os calibration for isochron determinations: Lunar and Planetary Science XX, p. 1041-1042.

Peucker-Ehrenbrink, B., and Hannigan, R.E., 2000, Effects of black shale weathering on the mobility of rhenium and platinum group elements: Geology, v. 28, p. 475-478.

Pierson-Wickmann, A.-C., Reisberg, L., and France-Lanord, C., 2002, Behavior of Re and Os during low-temperature alteration: results from Himalayan soils and altered black shales: Geochimica et Cosmochimica Acta, v. 66, p. 1539-1548.

Raiswell, R., and Canfield, D.E., 1996, Rates of reaction between silicate iron and dissolved sulfide in Peru Margin sediments: Geochimica et Cosmochimica Acta, v. 60, p. 2777-2787.

Selby, D., and Creaser, R.A., 2001, Re-Os geochronology and systematics in molybdenite from the Endako porphyry molybdenum deposit, British Columbia, Canada: Economic Geology, v. 96, p. 197-204.

Selby, D., and Creaser, R.A., 2003, Re-Os geochronology of organic-rich sediments: an evaluation of organic matter analysis methods: Chemical Geology, v. 200, p. 225-240.

Selby, D., and Creaser, R.A., 2005, Direct radiometric dating of the Devonian-Mississippian time-scale boundary using the Re-Os black shale geochronometer: Geology, v. 33, p. 545-548.

Selby, D., Creaser, R.A., Stein, H.J., Markey, R.J., and Hannah, J.L., 2007, Assessment of the ^{187}Re decay constant by cross calibration of Re-Os molybdenite and U-Pb zircon chronometers in magmatic ore systems: Geochimica et Cosmochimica Acta, v. 71, p. 1999-2013.

Shen, J.J., Papanastassiou, D.A., and Wasserburg, G.J., 1996, Precise Re-Os determinations and systematics of iron meteorites: Geochimica et Cosmochimica Acta, v. 60, p. 2887-2900.

Shirey, S.B., and Walker, R.J., 1995, Carius tube digestion for low-blank rhenium-osmium analysis: Analytical Chemistry, v. 67, p. 2136-2141.

Smoliar, M.I., Walker, R.J., and Morgan, J.W., 1996, Re-Os ages of Group IIA, IIIA, IVA, and IVB iron meteorites: Science, v. 271, p. 1099-1102.

Stookey, L.L., 1970, Ferrozine – A new spectrophotometric reagent for iron: Analytical Chemistry, v. 42, p. 779-781.

Taylor, P.D.P., Maeck, R., and De Bièvre, P., 1992, Determination of the absolute isotopic composition and Atomic Weight of a reference sample of natural iron: International Journal of Mass Spectrometry and Ion Processes, v. 121, p. 111-125.

Völkening, J., Walczyk, T., and Heumann, K.G., 1991, Osmium isotope ratio determinations by negative thermal ionization mass spectrometry: International Journal of Mass Spectrometry and Ion Processes, v. 105, p. 147-159.

Walczyk, T., Hebeda, E.H., and Heumann, K.G., 1991, Osmium isotope ratio measurements by negative thermal ionization mass spectrometry (NTI-MS): Improvement in precision and enhancement in emission by introducing oxygen or Freon into the ion source: Fresenius' Journal of Analytical Chemistry, v. 341, p. 537-541.

Weyer, S., and Schwieters, J.B., 2003, High precision Fe isotope measurements with high mass resolution MC-ICPMS: International Journal of Mass Spectrometry, v. 226, p. 355-368.

Yin, Q.Z., Jacobsen, S.B., Lee, C.T., McDonough, W.F., Rudnick, R.L., and Horn, I., 2001, A gravimetric K_2OsCl_6 standard: Application to precise and accurate Os spike calibration: Geochimica et Cosmochimica Acta, v. 65, p. 2113-2127.